FLEET TECHNOLOGY LIMITED
A FLEET AEROSPACE COMPANY

FLEET TECHNOLOGY LIMITED E62522C

FINAL REPORT

EVALUATION OF HEAT AFFECTED ZONE AND WELD METAL TOUGHNESS IN SELECTED STEELS (PHASE II)

VOLUME I: SUBMERGED ARC WELDING PROGRAM

By

C. Chiu
L. Malik

Work on this project was jointly funded by AMCA International Limited, and by Metals Technology Laboratories (CANMET, EMR) under the auspices of the Program for Energy R&D (PERD).

CANMET Scientific Authority: Dr. J.E.M. Braid
DSS File No. 06SQ.23440-4-9056-1
DSS Contract Serial No. 0SQ85-00137

Prepared by:

MATERIALS TECHNOLOGY CENTRE
A Division of Fleet Technology Limited
311 Legget Drive
Kanata, Ontario, K2K 1Z8

310 pp

March 1989

MICROMEDIA

ABSTRACT

A series of submerged arc welds has been prepared using two different wire-flux combinations giving weld metals alloyed with Ti-B, and Mo respectively. Procedural variables such as heat input, post weld heat treatment, interpass temperature and joint restraint were systematically changed, and their effect on weld metal toughness (CVN and CTOD) assessed.

The results showed that the Ti-B weld metal had excellent CVN and CTOD toughness which changed marginally with the variables studied in the program. This excellent toughness, and insensitivity to welding procedural variables is attributed to:

(i) reduced susceptibility to strain aging damage on account of low total and free nitrogen content;

(ii) presence of boron which suppresses the formation of grain boundary ferrite, and facilitates formation of acicular ferrite; and

(ii) inclusions which contain Ti, and presumably have an optimum size distribution to nucleate acicular ferrite.

In comparison, the Mo containing weld metal had relatively inferior toughness caused primarily by its:

(i) higher nitrogen content, and smaller unbalance factor;

(ii) higher hardness; and

(iii) higher number density of inclusions greater than 1μm.

It has also been demonstrated that changes in the macrostructure distribution at the notch of a CVN specimen can lead to substantial changes in the transition temperature - larger than those due to procedural variables.

RÉSUMÉ

On a réalisé une série de soudures à l'arc submergé en utilisant deux combinaisons de fil-flux différentes qui ont donné des alliages de métaux d'apport avec du Ti-B et du Mo respectivement. Les variables de l'opération, par exemple l'apport calorifique, le traitement thermique après soudure, la température d'interpasse et le bridage du joint, ont été modifiées systématiquement, et leur effet sur la résilience du métal d'apport a été évalué (par essai Charpy et par essai de déplacement d'ouverture de la pointe de fissure).

Les résultats ont montré que la soudure réalisée avec le Ti-B avait une excellente résilience, déterminée par essai Charpy et par essai de déplacement d'ouverture de la pointe de fissure, qui variait peu avec les variables étudiées dans le programme. Cette excellente résilience et l'absence de sensibilité aux variables de l'opération de soudure sont attribuées aux facteurs suivants:

i) réduction de la susceptibilité au vieillissement par écrouissage en raison de la faible teneur en azote total et en azote libre;

ii) présence de bore qui supprime la formation de ferrite à la limite des grains et facilite la formation de ferrite aciculaire; et

iii) inclusions qui contiennent du Ti et ont supposément une distribution granulométrique optimale pour produire la germination de la ferrite aciculaire.

Par comparaison, l'alliage obtenu avec du Mo avait une résilience relativement inférieure en raison principalement des facteurs suivants:

i) plus grande teneur en azote et plus petit facteur de déséquilibre;

ii) plus grande dureté; et

iii) plus grande densité d'inclusions supérieures à 1μm.

On a aussi démontré que les variations de distribution de la macrostructure à l'entaille d'une éprouvette Charpy peuvent entrainer des variations importantes de la température de transition, supérieures à celles qui sont dues aux variables de l'opération.

TABLE OF CONTENTS

VOLUME I: SUBMERGED ARC WELDING PROGRAM

Page

Abstract (i)

1.0 INTRODUCTION 1

1.1 Objectives of the Present Study 4

2.0 EXPERIMENTAL DESCRIPTIONS AND METHODOLOGY 5

2.1 Materials and Consumables 5
    2.1.1 Base Plate 5
    2.1.2 Submerged Arc Welding Consumables 5
2.2 Welding Procedure and Joint Preparation 6
    2.2.1 Groove Preparation 6
    2.2.2 Welding Fixture 6
    2.2.3 Preheat and Interpass Temperature 7
    2.2.4 Welding Procedure and Parameters 7
    2.2.5 Post Weld Heat Treatment 7
2.3 Lateral Shrinkage Measurements 8
2.4 Specimen Preparation 8
2.5 Chemical Analysis 9
2.6 Inclusion Analysis 9
2.7 Quantitative Metallography 9
    2.7.1 Macrostructure Along the Centreline 9
    2.7.2 Microstructure in the Last Bead 9
2.8 Mechanical Testing 10
    2.8.1 Hardness Testing 10
    2.8.2 CVN Testing 10
    2.8.3 Tensile Testing 10
    2.8.4 Drop Weight Testing 10
    2.8.5 CTOD Testing 10
2.9 Gapped Bead On Plate (GBOP) Testing 11
2.10 Weld Metal Diffusible Hydrogen 11

3.0 EXPERIMENTAL RESULTS AND OBSERVATIONS 12

3.1 Weld Metal Composition 12
    3.1.1 Effect of Heat Input 12
    3.1.2 Effect of Through Thickness Location 13
3.2 Inclusion Analysis 13
3.3 Quantitative Metallography 16
    3.3.1 Macrostructures 16
    3.3.2 Microstructural Characterization 17
3.4 Lateral Shrinkage Measurements 18
    3.4.1 Weld of Reference Restraint Condition (S4A) 19
    3.4.2 High Lateral Restraint and High Angular Restraint (S10A) 19
    3.4.3 Low Angular Restraint and Low Lateral Restraint (S11A) 19
    3.4.4 Low Lateral Restraint and High Angular Restraint (S11B) 20

TABLE OF CONTENTS (Cont'd)

Page

3.5 Tensile Properties and Hardness Results 20
3.6 Drop Weight Testings 21
3.7 CVN Notch Toughness 22
  3.7.1 Effect of Heat Input 22
  3.7.2 Effect of Stress Relief Heat Treatment 22
  3.7.3 Effect of Through Thickness Variation 22
  3.7.4 Effect of Interpass Temperature 23
  3.7.5 Effect of Restraint Condition 23
3.8 CTOD Toughness 24
3.9 SEM Fractography on Selected CTOD Specimens 24
3.10 Weld Metal Diffusible Hydrogen Content 25
3.11 Gapped Bead On Plate (GBOP) Testings 25

4.0 DISCUSSION 26

4.1 Effect of Procedural Parameters on Toughness of Ti-B Weld Consumable A 26
4.2 Effect of Heat Input and Stress Relief on Toughness of C-Mn-Mo Weld 28
4.3 Toughness Comparison Between Ti-B Welds and C-Mn-Mo Welds 28

5.0 CONCLUDING SUMMARY 30

6.0 REFERENCES 32

TABLES

FIGURES

APPENDIX A - Inclusion Analysis

APPENDIX B - Drop Weight Test Results

APPENDIX C - CVN Test Results

APPENDIX D - CTOD Test Results

1.0 INTRODUCTION

In the last decade, extensive research efforts have focused on furthering the fundamental understandings of weld metal toughness. However, the more severe environmental conditions found in the Canadian arctic and offshore applications place a more stringent demand on the toughness of materials. Thus, it is necessary to appraise the structural steel and welding technologies in the context of the Canadian environment, i.e. assurance of sound integrity at low ambient temperatures.

The present project is an integral part of an overall study intended for evaluation of low temperature toughness in the heat affected zone of structural steel[1.1]; and weld metals prepared with various conventional welding processes, viz. shielded metal arc (SMAW)[1.2], submerged arc (SAW), gas metal arc (GMAW), and gas shielded flux cored arc welds (FCAW). For each welding process, the objectives are to study the role of procedural parameters on the low temperature toughness of weld metal.

For each welding process investigated, weld metal toughness can be optimized via many variables which can be classified into two categories, viz.

(i) welding procedural parameters, e.g. heat input, stress relief, etc.; and
(ii) consumable and weld metal compositions.

The traditional route to obtain good toughness is by alloy addition to achieve an optimized balance of hardenability and microstructural refinement. Unlike the popular and deterministic composition/microstructure approach, the effects of procedural parameters on weld metal toughness do not receive similar emphasis. These procedural parameters may be heat input, external restraint, preheat and interpass temperatures, post weld heat treatment, joint geometry, etc.

A higher interpass temperature effectively lowers the cooling rate in the weld metal, especially in the 800-500°C range, leading to microstructural coarsening and reduced strength. As the interpass temperature increases, the slower cooling rate implies more widely spaced temperature isotherms, resulting in a wider reheated region and grain coarsening in the previous deposited weld metal. Hence, the overall proportion of reheated region in multipass weldments increase with higher interpass temperature. Although the reduced proportion of as-deposited columnar region may imply improved toughness, the coarser microstructure due to the higher interpass temperature may partially offset the gain. In addition to overall coarsening in all microstructural phases of C-Mn welds, Evans[1.3] also noted a reduced acicular ferrite content with higher interpass temperature. Summarized in the following table, his results suggest improved CVN notch toughness by increased reheated region at higher interpass temperature despite reduced acicular ferrite content and overall grain coarsening.

Interpass Temperature (°C)	% of Reheated Region at CVN Notch	Hardness (5kg)	Acicular Ferrite (%)	40J Transition Temperature (°C)
20	55	240	80	-55
150	70	243	75	-60
240	85	216	70	-70
300	90	208	65	<-80

Although it is generally perceived that welds have better CVN notch toughness than its vertical counterpart, a brief literature survey[1.4-1.5] indicates that a meaningful comparison made in the flat position among different welding positions is difficult because of complications in discerning the roles of heat input, stringer versus weaving technique, which are intrinsic characteristics to common practice. Nevertheless, the role of welding position will be studied in detail in the flux cored arc welding program. Flat and vertical-up welds will be prepared with the same heat input and stringer bead technique such that the effect of solidification pattern due to gravity pull in vertical welds can be studied.

The use of external restraint is a common fabrication practice to accommodate fit-up and minimize distortion. Two aspects of external restraint are particularly relevant to the resultant weld toughness, viz.

(i) lateral contraction, and
(ii) angular distortion.

Although there are disagreements in the published literature as to whether higher external restraint may improve toughness[1.6-1.8], the disagreement could be due to complications in discerning the roles of various parameters, e.g. effect of dilution, double V versus single V joint geometries, percentage of reheated region at the notched samples, size and length of weld, number of weld passes and thermal history and heat input, etc. Hence, in order to assess the effect of external restraint on weld metal toughness, a systematic comparative study is necessary to isolate these independent variables and examine them individually. In the submerged arc welding and flux cored arc welding programs, an attempt has been made to study the effect of lateral restraint on weld metal toughness, while keeping the angular restraint high (low angular distortion).

Heat input is a procedural parameter comprised of different variables, viz. arc efficiency, current, voltage and travel speed. It is generally agreed that the use of lower heat input welds would provide improved CTOD and CVN toughnesses although it is accompanied with the economic price of lower productivity. The lower fracture toughness in higher heat input welds is due to a combination of the following:

(i) higher proportions of columnar as-deposited macrostructure resulting from larger bead size and deeper penetration;

(ii) overall grain coarsening in both microstructural and macrostructural scale due to the large heat built up and the slow cooling rate; and

(iii) less desirable microstructure because the slower cooling rate may retard acicular ferrite formation.

In addition, to reduce residual stresses, stress relief heat treatment has different effects on CVN toughness depending on composition of weld deposits. In the absence of carbide or (carbo) nitride formers, stress relief of a low alloy deposit leads to improved toughness. Various reports[1.9-1.12] have attributed the benefit deriving from several effects, e.g. lower strength and hardness by softening, removal of strain aging damage, tempering of martensite-retained austenite aggregates, etc. However, in the presence of significant alloy additions, e.g. V and Nb, precipitation of carbides or carbonitrides at the grain boundary leads to reduced toughness. Hence, the merit of stress relief heat treatment on toughness depends on the weld metal composition.

1.1 Objectives of the Present Study

For each welding process, the consumables were selected, usually on the basis of the excellent weld metal toughness they yielded in previous programs at MTL[1.13] and AMCA/MTC[1.14-1.15]. One of the consumables for each process provided weld metal alloyed with Ti and B, whereas the others were alloyed with Mo or Ni.

Welds have been made with the selected consumables with the objectives to study the effects of heat input, stress relief heat treatment and interpass temperature on the following:

(i) weld metal composition;
(ii) weld metal macrostructure;
(iii) weld metal microstructure; and
(iv) inclusion distribution.

Attempts are then made to rationalize the effects of these procedural parameters on fracture toughness on the basis of observed changes in (i)-(iv) above.

Results and discussion are presented in three parts by classifying according to welding processes, viz.

Volume I : Submerged Arc Welding Program
Volume II : Gas Metal Arc Welding Program
Volume III : Flux Cored Arc Welding Program

CONFIDENTIAL

Consumable	Trade Name		Manufacturer
	Wire	Flux	
A	US-36	PFH-55LT	Kobe
B	OK Autrod 12.34	OK Flux 10.62	ESAB

This page can be removed at the discretion of the Scientific Authority.

2.0 EXPERIMENTAL DESCRIPTIONS AND METHODOLOGY

2.1 Materials and Consumables

2.1.1 Base Plate

The base plate used for all welds was 50mm thick normalized C-Mn microalloyed steel conforming to CSA G40.21 Grade 350 WT requirements. The chemical composition and mechanical properties, as per mill report, are included in Table 2.1.

2.1.2 Submerged Arc Welding Consumables

Two consumables (subsequently designated as A and B) were selected for the experiments with the objective to study the low temperature fracture toughness of weld metal in two families represented by these consumables, viz. Ti-B (consumable A) and C-Mn-Mo (consumable B). The selection of these consumables was made on the basis of CVN and CTOD data provided by the consumable manufacturers, and by the courtesy of MTL/EMR. Both of these consumables are designed for multipass welds in Al-killed steel plates for low temperature applications. The CVN and CTOD data are summarized as follows:

Consumable Type	CVN Toughness	CTOD (mm)	Reference
A	40J transition temp. is lower than -75°C	At -50°C, as welded condition, avg. = 0.72, min. = 0.22	[2.1]
B	60J at -60°C	Unavailable	[2.2]
	35J transition temp. is lower than -60°C	At -30°C, as welded condition, avg. = 0.49, min. = 0.23mm	[2.3]

For consumable A, the 4mm diameter wire is Mn-Si alloyed and copper coated, meeting the AWS A5.17 EH14 classification. The flux is a Ti-B treated basic agglomerated type with basicity index of ~2.3 (AWS 5.23: F7A8-EH14, F7P8-EH14). The flux was reconditioned at 250-300°C for 1 hour prior to use.

For consumable B, the 4mm wire is Mn-Mo alloyed and copper coated, meeting the AWS A5.23-80:EA4 classification. The flux is a non-alloying basic flux of basicity index of ~3.4 and the consumable combination is designated as F9A10-EA4-A4.

2.2 Welding Procedure and Joint Preparation

2.2.1 Groove Preparation

A single joint geometry was used throughout the entire submerged arc welding program. The welded assembly was nominally 915mm (36") long X 610mm (24") wide with double V geometry of 2/3 (60° included angle) and 1/3 (80° included angle) (Figure 2.1). The welding direction was transverse to the rolling direction of base plate.

In order to ensure consistency between welds, the groove surfaces were machine finished to the desired dimensions and angles. Prior to the submerged arc welding of root passes on the first side, three passes of shielded metal arc weld using low hydrogen covered electrodes of E48018-1 were deposited on the root of the second side to prevent burnthrough, particularly in the high heat input welds.

2.2.2 Welding Fixture

The same welding fixture was used for the first nine welds (S1-S9, Table 2.2). It is designed to control both the angular distortion and lateral shrinkage transverse to welding direction. In addition, they serve as a reference restraint condition for the subsequent welds where changes in restraint condition were attempted. A schematic representation of the welding fixture is included in Figure 2.2.

Different modifications to the welding jig were used for the three remaining welds intended for restraint studies. They are designed for the following purposes:

(i) High angular restraint and high lateral restraint - in addition to the clamps and fixture used in the reference welds, additional restraint was provided by butt welded restraint blocks on both ends, and the entire assembly was fillet welded to the welding table (Figure 2.3);

(ii) Low angular restraint and low lateral restraint - the normal stress under the clamping bolt was intended to be reduced by using spacer blocks with larger surface area under the bolt near the plate edges. It was hoped that the lower normal stress would enable relatively free lateral movement without reducing the angular restraint. Friction was minimized by covering all contact surfaces with 1.6mm (1/16") thick Teflon sheet such that all surfaces are in Teflon/Teflon contact. Teflon sheets were applied to ground and degreased surfaces with special adhesive that can withstand temperature higher than 200°C in continuous use. However, the resultant angular restraint was judged to be low since Teflon sheets between the spacer blocks and plate surface were crushed to next to nothing on account of Teflons low compressive strength (Figure 2.4).

(iii) High angular restraint and low lateral restraint - the setup was similar to (ii) but instead of Teflon/Teflon contact, all contact surfaces were covered with Mo disulphide grease that can provide low friction and tolerance to high temperature (Figure 2.5).

2.2.3 Preheat and Interpass Temperature

With the exception of one weld prepared with consumable A, the preheat and interpass temperatures were 150°C which satisfies the CSA W59 requirements for 65°C minimum for 50mm thick 350WT steel. The preheat was applied by an oxy-fuel rosebud heating torch. Appropriate Templesticks were used to monitor the preheat and interpass temperatures during the course of welding.

An additional weld of consumable A was prepared with interpass temperature of 232°C. The preheat temperature of 150°C remained the same.

2.2.4 Welding Procedure and Parameters

A total of 12 welds were made with different combinations of consumables, post weld heat treatment conditions, heat inputs, interpass temperatures and restraint conditions. Each of these welds comprised two lengths of 0.9m (3′) each. The first eight welds were made with the two selected consumables at two heat inputs, and in both as-welded and stress relieved conditions. The ninth weld was prepared with a higher interpass temperature. The remaining three welds were the "restraint welds" for the evaluation of different external restraint conditions on toughness. The eleventh and twelfth welds were only 0.9m (3′) each in length. The experimental matrix for the program is included in Table 2.2. Backgouging was undertaken at the root pass of side one to completely remove the SMAW backing passes and the majority of the first SAW bead, and subsequently widened by grinding to provide a wider groove (Figure 2.6).

In order to maintain consistency and meaningful comparisons among different welds, the sequence and positioning of the bead depositions were the same for all welds. Relative to side 1, the welding direction was reversed on side 2. Run-on and run-off tabs (75mm long) were attached to each weld assembly.

2.2.5 Post Weld Heat Treatment

The thermal cycles for stress relieving for the selected welds were as per CSA W59 (1984), Clause 5.1.2. The welded assemblies were placed in an electric furnace at room temperature; heated at a rate of 50°C/hour; soaked at 600°C for 2 hours; and furnace cooled at a rate of 50°C/hour to room temperature.

2.3 Lateral Shrinkage Measurements

For the welds selected for studying external restraint as a variable on toughness, lateral shrinkage measurements were taken on the plate surface at 1/4, 1/2 and 3/4 weld length positions. At each location, a pair of shallow holes, 80mm apart and located on either side of the weld, were drilled and tapped into which short bolts were inserted. The purpose of the bolts was to provide rigid reference points for shrinkage measurements. The setup is schematically illustrated in Figure 2.7.

After the backing passes were deposited and prior to deposition of first root pass on side 1, spacing between the bolts at all locations was measured under full restraint. After the first root pass was deposited, the weld was allowed to cool to room temperature, then the spacings were measured again. The same procedure was repeated after completion of side 1. After the plate was backgouged, a new set of bolts was tapped into the plate surface of side 2. Then the measurements were repeated before and after first root pass on side 2, and the completion of side 2. The measurements after the completion of side 1 and side 2 were taken with the plate remaining under full restraint. Since the effect of strain aging is one of the prime considerations in the restraint welds, the additional cooling time of 4-6 hours for the root pass of side 1 should be taken into consideration. However, the relative short cooling time is similar to the overnight interruption during production. In addition, the backing passes on side 2 also provide additional restraint. Hence, the additional cooling time should not have a significant effect on toughness.

2.4 Specimen Preparation

For welds S1-S10 (Table 2.2), Charpy (CVN), tensile, drop weight and crack tip opening displacement (CTOD) specimens were machined as per ASTM E23, ASTM A370, ASTM E208 (1984a), and BS 5762, respectively. For the shorter welds of S11A and S11B, only CVN and CTOD specimens were extracted.

The standard size (10mm X 10mm) CVN specimens were taken from two locations, viz. subsurface and root. Prior to extraction, the cross section of the full thickness weldment was first surface ground and then etched with 10% Nital to reveal the macrostructure. The subsurface locations corresponded to 2mm below the plate surface on side 2, whereas the root location specimens were extracted from side 1, but located at 2mm from the root pass of side 2 (Figure 2.8). For both subsurface and root locations, the notch coincided with the weld centreline which is determined by the mid-point of the narrowest portion of root.

The P-2 type drop weight specimens were taken from 2mm below the plate surface of side 2 (Figure 2.9). The crack starter bead was deposited transverse to the welding direction with hard facing consumable at 180-200A and slow travel speed of 150-170mm/min. The two bead technique was used with start position at each end and stop positions overlapping at the center.

The all weld metal 6.25mm diameter round tensile specimens with 25mm gauge length were taken longitudinally with the tensile axis located at 8mm from the plate surface of side 1 (Figure 2.10).

Although the plate thickness was 50mm, the thickness in Bx2B CTOD specimens was reduced to 48mm to avoid any lack of reinforcement in the capping layer. The notch root coincided with the weld centreline (Figure 2.11).

2.5 Chemical Analysis

Four welds in as welded condition were selected for chemical analysis. For each selected weld, all weld metal samples were machined from corresponding subsurface and root CVN notch locations, and sent to ORTECH International for chemical analysis for the following elements, viz. C, Mn, Si, S, P, Mo, Ni, Cr, Cu, Nb, V, O, N, Ti, B, Zr and Al. C and S are analyzed by Leco methods, O and N by vacuum fusion and the balance by D.C. plasma spectrometry.

2.6 Inclusion Analysis

Since the inclusions are high temperature transformation products, the post weld heat treatment and different interpass temperature should not affect the inclusion characteristics. Hence, the inclusion analysis was undertaken for the same as welded joints as those selected for chemical analysis. The exact description of methodology is included in Appendix A. Briefly, an area of 2mm (parallel to weld centreline) X 0.5mm at the T/2 location is selected for analysis. Each inclusion is identified by shape, composition and size. The presence of an element in an inclusion is defined by either having a K_α peak of at least 5% relative intensity. For each weld, the inclusions are classified according to size and composition.

2.7 Quantitative Metallography

Welds in the as-welded condition were selected for metallographic characterization. The transverse sections were polished to a 1 micron diamond finish and subsequently etched with 2% Nital for metallographic examination.

2.7.1 Macrostructure Along the Centreline

For each weld, the macrostructure along the weld centreline was characterized as columnar region, coarse grain reheated zone, and fine grain reheated zone. The percentage distribution of each structure was calculated by the linear intercept method.

2.7.2 Microstructure in the Last Bead

For each reference weld (S1-S9) in the as-welded condition, the as-deposited microstructure in the final bead on side 2 was characterized by point counting as per IIW designations[2.4]. The point counting was carried out in 100 x 10 grids at a magnification of 500X.

The X-intervals and Y-intervals for the grid were 0.05mm and 0.2mm respectively. The microstructural characterization was not carried out for any of the "restraint welds" because of their same thermal history and cooling rate as the corresponding reference weld (S3).

2.8 Mechanical Testing

2.8.1 Hardness Testing

For each weld, Vickers (10kg load) hardness traverses were taken along the weld centreline perpendicular to plate surface and at mid-thickness of both CVN locations (parallel to plate surface). Readings were taken every 5mm intervals along the centreline from cap to cap, and every 3mm along the mid-thickness at each CVN location.

2.8.2 CVN Testing

For each weld, 16 CVN specimens were extracted from each of the root and subsurface locations. The notch profiles were checked frequently for adherence to ASTM E23 Standard. The test temperature ranged from 20°C to -120°C.

2.8.3 Tensile Testing

For welds S1-S10, tensile specimens were tested at 20°C. The tests were carried out at a strain rate of 0.02/min with an extensometer.

2.8.4 Drop Weight Testing

For each weld, up to 8 drop weight P-2 specimens were tested at temperatures ranging from -20° to -70°C. Although an impact energy of 400J is intended for all tests, some of the specimens were inadvertently tested with 540J. After the impact, a break or no break condition was prescribed for each specimen, depending on whether the crack had reached at least one side of the specimen. A nil ductility transition (NDT) temperature was determined as the highest temperature at and below which all tests yield break condition.

2.8.5 CTOD Testing

The specimen geometry for the machined specimens is included in Figure 2.11.

In order to ensure a smooth fatigue crack front, local compression was carried out for all specimens in the as-welded condition, as per the procedure outlined by Towers and Robinson[2.5]. The ligament below the notch is locally compressed from both sides by circular indentors of 25mm diameter. The indented area extended from 5mm overlapping the notch root to at least 5mm from the side to avoid bulging. Local compression is not required for stress relieved welds.

The fatigue precracking was carried out in two stages, i.e. a higher fatigue load range was used for accelerated crack initiation and propagation initially, then it was reduced to meet the stress intensity specification in BS 5762. The maximum load range for each stage is

$$P_f = \text{Peak load during precracking} = \frac{\beta \sigma_y B^{3/2} W^{1/2}}{Y}$$

where β = 0.6 for the first 1mm of precracking
β = 0.4 for the next 3mm of precracking
Y = stress intensity
σ_y = yield strength

The test temperature was monitored by a thermocouple attached to the specimen and maintained within 2°C of the specified temperature. At each temperature, three CTOD specimens prepared from each weld were tested as per BS 5762. After the tests, the specimens were broken to measure the effective crack sizes.

2.9 Gapped Bead On Plate (GBOP) Testing

In order to assess the cold cracking susceptibility of the weld metals deposited by the respective wires, the GBOP tests were carried out for the consumables with the test blocks machined from the same 350WT steel used in this program. The dimension of the test blocks for the GBOP tests are included in Figure 2.12. The test assembly consists of two blocks of the same dimensions except one has a machined recess of 0.75mm. At a predetermined preheat, the assembly is pneumatically clamped together with 10 MPa pressure. A weld bead is deposited across the machined recess using the respective consumables under investigation. The welded blocks are left under pressure for 24 hours, then left for another 24 hours without pressure. Subsequently, the welded blocks are heated to dull red heat in the vicinity of the gap and allowed to cool to room temperature. The weld bead is snapped open and the extent of cold cracking is determined by the presence/ absence of the blue-colour oxide layer.

The weld beads were deposited at 530A, 28V and 4.2mm/sec. The preheat temperatures were room temperature, 75°C, and 150°C.

2.10 Weld Metal Diffusible Hydrogen

For each consumable, the diffusible hydrogen in weld metal was measured by a single pass weld deposited on degassed A36 steel blocks held together in a copper jig. The welding parameters of 30V, 450A, and 8.9mm/sec. were used. Once the weld bead was deposited, it was released from the copper jig and quenched in liquid nitrogen. The diffusible hydrogen content in weld metal was determined over mercury using the ISO 3690 method.

3.0 EXPERIMENTAL RESULTS AND OBSERVATIONS

3.1 Weld Metal Composition

The compositions of weld metals in the as-welded condition for both subsurface and root locations and different heat inputs are tabulated in Table 3.1. In addition, the calculated carbon equivalents (IIW) and Pcm values are also included in Table 3.2.

3.1.1 Effect of Heat Input

Except for some lowering of weld metal oxygen content for both deposits, and of Mo in deposit B, heat input seems to have a negligible effect on weld metal composition. Although both consumables experience a decrease in oxygen content with heat input, the relative decrease in consumable A is larger, especially when subsurface locations are compared (Figure 3.1). The welds of consumable B have lower oxygen contents than the welds of consumable A because of higher basicity in the flux. Furthermore, since all weld metals share similar sulphur contents which are unaffected by heat input, the sum of oxygen and sulphur contents (subsequently abbreviated as O+S) also decreases with heat input. The decrease in oxygen or O+S contents implies that lower inclusion contents should be found in the higher heat input welds. This hypothesis will be studied in more detail in Section 3.2.

Although the overall weld metal compositions of the Ti-B type consumable A are insensitive to changing heat input, the Ti-Al-B-N-O balance seems to be affected by heat input. Fehervari and Rittinger[3.1] have developed the unbalance factor (BF) as an indication of free nitrogen content in the presence of nitriding alloying additions in gas metal arc welds. It is defined as:

$$BF = 14(Ti/48 + Al/27 + V/51 + Nb/93) - N$$

Optimum CVN toughness coincides with BF=0 because these elements are assumed to preferentially interact with N to reduce free nitrogen. Excessive hardenability occurs when BF>0, whereas insufficient nitride fixers are present in weld metal if BF<0. Hence, when BF is greater or smaller than zero, a lower CVN toughness is due to either excessive hardenability or excessive free nitrogen. However, since the deoxidation process is in constant competition with the nitriding process in weld metal, additional microalloying additions are required such that an optimum BF is found to be 100ppm instead. In the present project, the unbalance factors of consumable A are close to this optimum value and they remain relatively unchanged with heat input (Table 3.2).

The molybdenum content in the weld metals of consumable B decreases with higher heat input (Figure 3.2). Apart from Mo and oxygen contents, there is no significant change in weld metal composition with heat input. In the absence of significant Ti or Al additions, the unbalance factors in weld metals of consumable B are primarily attributed to the dilutions of V and Nb from base plate such that the BF values are consistently below 100ppm (with one exception), thus implying insufficient additions of nitriding elements and the possibility of free nitrogen. Given the slightly higher nitrogen contents found in consumable B than consumable A, then the weld metals of consumable B may be more susceptible to strain aging and subsequently lower toughness.

There is a lack of a discernible trend in the calculated values of carbon equivalent and Pcm with heat input. In comparison, the welds of consumable B have higher carbon equivalents than consumable A.

3.1.2 Effect of Through Thickness Location

Since the root CVN specimens are located at the 2nd-3rd passes on the first side, the dilution may be higher at the root than subsurface location, therefore weld metal compositions from both locations are analyzed to study the effect of dilution on composition in the through thickness dimension. Examination of the tabulated weld metal compositions indicates that for both consumables, the only significant variation in composition among the subsurface and root locations are found in silicon contents. However, the higher Si content in the root location may be due to the dilution from the backing passes deposited with E48018-1 electrodes, which typically have ~0.4w/o Si. The higher Si content may have a deleterious effect on CVN toughness at root location which will be discussed in further detail in Section 4.1.

Kohno et al[3.2] have reported experimental results showing that the molybdenum content decreases with the number of weld passes in the Mo-Ti-B submerged arc weld at 4.0 kJ/mm, i.e. the subsurface molybdenum content is smaller than that at the root location. They have rationalized the observations of through thickness variation in composition by modelling based on partition coefficient calculations. In the present study, the weld metals of consumable B show a conflicting trend with regard to this conjecture, viz. the 3.5 kJ/mm weld is in agreement whereas the 5.0 kJ/mm weld shows an opposite trend (Figure 3.2).

3.2 Inclusion Analysis

The results of the inclusion analysis are tabulated in Tables 3.3 to 3.5. The inclusions characteristics are discussed in terms of overall distribution and individual size groupings, viz.

(i) $0.2\mu \leq$ inclusion diameter $< 0.5\mu m$;
(ii) $0.5\mu m \leq$ inclusion diameter $< 1.0\mu m$; and
(iii) inclusion diameter $\geq 1.0\mu m$.

The full documentation of the inclusion analysis is attached in Appendix A.

Although the dominant inclusion types found in the weld metals of both consumables contain varying amounts of Al and Mn, the analysis suggests that a higher heat input results in a lower Mn content and a concurrent increased Al content in the dominant inclusions. Similar observations with oxygen contents are reported by Ohkita et al as quoted by Abson[3.3]. Since the higher heat input welds have lower oxygen contents, the observed trends on relative Al and Mn contents with heat input may be a manifestation of oxygen effects. Although all welds share similar total Al contents in bulk weld metal, the Al contents in the dominant inclusions in weld metal of consumable A decreases with increased heat input. Furthermore, when the average diameters for each dominant inclusion types are plotted with the relative contents of Al, Mn and Ti (in the case of consumable A only), the changes in relative Ti, Al and Mn contents in inclusion do not correlate to inclusion diameter (Figures 3.3 and 3.4). However, consumable B yields a strong correlation in inclusion diameter with the relative amounts of Al and Mn in the inclusions.

The individual inclusions are most likely to be in complex shapes, however attempts are made to understand the physical meanings of the shape factor. Since the shape factor (SF) for each inclusion is determined by the relationship

$$SF = \frac{4\pi\,(\text{surface area})}{(\text{perimeter})^2}$$

the shape factors for the simple geometries of a rectangle and an ellipse then become:

$$SF = \frac{4\pi ab}{[2(a+b)]^2}$$ for a rectangle, where a, b = length, width

$$SF = \frac{4\pi(\pi ab)}{(\pi[1.5(a+b)-\sqrt{ab}])^2}$$ for an ellipse, where a, b = major and minor axis

Defining length/width aspect ratio as $n = a/b$, and substituting in the equations for shape factor:

$$SF = \frac{\pi n}{(n+1)^2}$$ for rectangle

$$SF = \frac{4n}{[1.5(n+1)-\sqrt{n}]^2}$$ for ellipse

The aspect ratio versus shape factor is plotted in Figure 3.5. In terms of inclusion shapes, it is interesting to note that higher heat input, i.e. lower oxygen, leads to a more equiaxed inclusion morphology for weld metals of both consumables. In addition to the effects of Al and Mn on the average diameter of dominant inclusions of consumable B, a similar correlation can be found for the shape factor (Figures 3.6-3.7). In summary, the larger relative Mn content in the inclusions of lower heat input weld of consumable B has resulted in larger diameter but less equiaxed inclusions. No such correlation can be observed for consumable A.

For consumable B (C-Mn-Mo), the average diameter and inclusion density increase significantly with heat input (Figure 3.8). Since the average spacing is inversely proportional to the inclusion density, it is not surprising that the average inclusion spacing decreases with heat input. However, the inclusions are approximately 10 average diameters apart. Despite the lower oxygen or O+S contents at higher heat input (Figure 3.1), the area fractions remain unaffected by the heat input.

In the three size groupings, the inclusions found in the weld metal of consumable B show an increase in the number density of inclusions with a diameter larger than 0.5μm, with the more significant change occurring in the intermediate group, i.e. the inclusions with a diameter between 0.5-1.0μm (Figures 3.8 and 3.9). Since the proportional increase in these larger size groupings may be at the expense of the smaller inclusions, there is a concomitant decrease in the density of small inclusions with a diameter between 0.2-0.5μm. The higher proportion of larger inclusions would imply a larger average inclusion diameter which is in accordance with the experimental findings in overall distribution. Inclusion densities in the small and intermediate size groupings also vary with higher heat input in the same manner as the proportion.

For consumable B, the dominant inclusions have much higher relative Al contents (as suggested by larger peak intensity) than the inclusions found in the weld metal of consumable A. Considering the total Al contents in weld metal are similar in all four welds regardless of heat input and oxygen contents, the higher Al content found in inclusions of the weld metal of consumable B coincided with a lower oxygen content.

For consumable A, the area fraction and average diameter has negligible change with heat input, whereas the inclusion density decreases significantly, and there is also a corresponding increase in average inclusion spacing with higher heat input. In addition, the area fractions for both consumables are significantly lower than the predicted volume fraction suggested by Widgery[3.4]:

$$V/o = 5.5\ (O+S)$$

The volume fraction is estimated by the following equations:

$$V/o = (100\pi/6)N_s[(D_{avg})^2 + (D_{std})^2]$$

where D_{avg} = average diameter in micron
D_{std} = standard deviation in diameter
N_s = number of inclusions per micron^2

The estimated volume fractions are tabulated in Table 3.6. Although the estimate volume fraction seems to obey the trend of higher fraction with increasing O+S, the estimated fractions remain below the predicted values (Figure 3.10). Nevertheless, the estimate volume fractions for both consumables increases with higher O+S contents.

For each inclusion size grouping, there is no change in relative distribution with higher heat input. This observation is in agreement with the overall distribution wherein the average diameter is unaffected by heat input. Although the inclusion density in each size grouping decreases with higher heat input, the smallest size grouping with a diameter between 0.2-0.5µm has the most significant decrease, i.e. the decrease in overall inclusion density is largely due to the decreasing density of small inclusions (Figures 3.8 and 3.9).

3.3 Quantitative Metallography

3.3.1 Macrostructures

The macrostructural distributions along the weld centreline in the through thickness dimension are tabulated in Table 3.7. The representative macrographs are included in Figures 3.11 to 3.19 for reference.

Effect of Heat Input

For the centreline distribution, the higher heat input weld metal of consumable A has a moderate increase in columnar as-deposited region at the expense of fine grain reheated region (Figure 3.20). In contrast, the weld metals of consumable B show the coarse grain reheated region increases at the expense of columnar as-deposited and fine grain reheated regions. For repeatability, the macrostructures are also characterized on the stress relieved counterparts. In general, a similar trend of changing macrostructure with heat input is also observed despite some scatter due to experimental uncertainties. At 3.5 kJ/mm at least, the weld metals of consumable A have a much lower proportion of columnar as-deposited region than consumable B.

Due to the multipass nature for the majority of layers, the centreline macrostructure distributions are characterized by a high percentage of reheated regions, particularly on the first side (refer to macrographs). In the case of higher heat input, the completion of the weld requires a fewer number of passes, each of which is larger in size, and has deeper penetration. A larger bead size may increase the columnar region whereas the deeper penetration provides a wider reheated zone adjacent to each bead. Thus, the resultant macrostructural distribution depends on the sum of these two opposing forces. Furthermore, the selection of current, voltage, travel speed and electrode stickout also affect the bead size and penetration characteristics[3.5]. As well, the macrostructural distribution along the centreline of the same heat input weld is very much dependent on the sequence and positioning of weld passes. Figure 3.21 schematically illustrates the effect of bead sequence on the macrostructure distribution found along the centreline.

Effect of Interpass Temperature

For the weld metals deposited at 3.5 kJ/mm with consumable A, the higher interpass temperature has a minor effect on macrostructural distribution along the centreline, such that the fine grain reheated regions increase moderately at the expense of both columnar and the reheated coarse grain region (Figure 3.22). With C-Mn SMAW welds, Evans has reported increases in fine grain reheated region at the expense of columnar region with higher interpass temperature[3.6]. His results were further reinforced by the bead on plate welds which show that the higher interpass temperature does not affect the fused metal area, but it increases the width of the heat affected zone associated with the bead on plate welds. Extrapolating these observations to the multipass weldments, then it would be expected that the reheated zone proportion would increase with interpass temperature.

3.3.2 Microstructural Characterization

The microstructural characterizations on the last deposited bead are tabulated in Table 3.8. The representative micrographs are included in Figures 3.23 to 3.32.

Effect of Heat Input

The weld metals of both consumables show higher acicular ferrite contents at the lower heat input. Although both weld metals have a similar acicular ferrite proportion at 3.5 kJ/mm, 67.6% vs. 70.4% for A and B respectively, the weld metal of consumable A (Ti-B) shows a better tolerance to higher heat input by maintaining a lower rate of decrease in acicular ferrite than consumable B (C-Mn-Mo) (Figure 3.33). The lower acicular ferrite implies gains in the coarse ferrite phases (grain boundary ferrite and intragranular polygonal ferrite) and/or the ferrite with second phases (both aligned and non-aligned). For both consumables, the ferrite with aligned second phase remains insensitive to the effect of heat input (Figure 3.34). The ferrite with non-aligned second phases increases with heat input, particularly for welds of consumable B. In the case of coarse ferrite, the weld metals of consumable A only show moderate increases in both grain boundary ferrites and polygonal ferrite with higher heat input, whereas the increase in both phases is significant in consumable B, thus suggesting the welds of consumable B are more susceptible to the grain coarsening effect of a slower cooling rate with higher heat input.

Effect of Interpass Temperature

Owing to the slower cooling rate in the weld metal prepared using a higher interpass temperature, it is expected to have a lower acicular ferrite content with a coarser ferrite size.

With a higher interpass temperature, the slower cooling rate retards the nucleation of acicular ferrite and enhances grain coarsening. The change in acicular ferrite and polygonal ferrite contents are in accordance with this expectation (Figures 3.35 and 3.36). It is of interest to note that the acicular ferrite content at 5.0 kJ/mm is higher than that for the 3.5 kJ/mm weld with interpass temperature of 232°C. In terms of other microstructures, the bulk of the decrease in the acicular ferrite is taken up by increases in polygonal ferrite and ferrite with non-aligned second phase, whereas the ferrite with aligned second phase and grain boundary ferrite show minor changes. These observations are in agreement with the reported results of SMAW experiments with C-Mn consumables by Evans[3.6]. However, the drastic increase in the ferrite with aligned second phase in his C-Mn deposits and the absence of the same observation in the present study is indicative of the ability of Ti-B alloyed weld metals to nucleate acicular ferrite under a wider range of welding procedural variables affecting the cooling rate.

3.4 Lateral Shrinkage Measurements

The lateral shrinkage measurements across the weld are indicative of the restraint condition and resultant plastic deformation (Table 3.9). Under high angular and low lateral restraint condition (S11B), the plates are relatively free to move in response to weld shrinkage so that the transverse shrinkage is accommodated by both weld deformation and plate movement. Because of the plate movement, the plastic deformation in the weld metal is small. Hence, the CVN toughness may not be affected significantly by the low lateral restraint.

Under high angular and high lateral restraint conditions (S10A), the plate movement is limited by the rigid set up, therefore the transverse shrinkage is primarily accommodated by plastic deformation in the weld metal. However, because of the rigid restraint, the distribution of plastic strain in the through thickness dimension should be uniform, leading to uniform reduction in CVN toughness than that obtained in low lateral and high angular restraint condition (S11B).

Similarly, under low lateral and low angular restraint condition (S11A), although the plastic deformation in the weld metal should be minimized because of free plate movement, large plastic deformation persists in the root region due to the bending deformation from large angular distortion. Hence the localization of large plastic strain at the root pass should result in a variation of CVN toughness in the through thickness dimension, i.e. greater degradation in root toughness. Although the high lateral and low angular restraint condition is not attempted in the present study, it is surmised that the localization of plastic deformation from angular distortion will lead to larger reduction in root toughness.

In summary, it is believed that the magnitude of restraint can be qualitatively assessed by the extent of transverse shrinkage across the weld, e.g. low transverse shrinkage corresponds to a high lateral restraint; therefore the data on shrinkage measurements is discussed in terms of angular and lateral restraint conditions for each weld.

3.4.1 Weld of Reference Restraint Condition (S4A)

The objective of measurements in this weld was to provide representative restraint condition for the welds S1-S9. Even though a balance welding technique (alternate passes on each side) was not followed, the observations of relatively little angular distortion and the similar transverse shrinkage as that of weld S10A suggest that the restraint condition can be qualified as high angular restraint and moderate lateral restraint.

3.4.2 High Lateral Restraint and High Angular Restraint (S10A)

Compared to the reference weld S4A, it was decided to increase the lateral restraint while keeping angular restraint at a similar level. The higher lateral restraint was facilitated by the use of end blocks and fillet welding of the test plate to the welding table. Although it was anticipated that the lateral shrinkage would decrease significantly with the use of a rigid restraint setup, such an effect is observed only after the completion of side 1. There is no significant change in measurements after deposition of root passes on either side, or completion of side 2 because a difference of 0.2mm is within the scatter among individual measurements. The lack of response to a high restraint in the root pass of side 1 is rationalized as follows. Since the transverse shrinkage measurements are taken on the plate surface of side 1 after the deposition of root pass on side 1, the measuring technique may not be sensitive enough to detect the actual transverse shrinkage across the bead surface. Furthermore, the fillet welds intended to increase restraint are located on the table surface which is closer to the root than the plate surface of side 1. The lack of change in transverse shrinkage in response to the intended increase in lateral restraint could therefore be due to insensitivity in the measuring technique and underestimation of the actual shrinkage across the surface of root bead.

3.4.3 Low Angular Restraint and Low Lateral Restraint (S11A)

Originally this weld was intended to simulate the restraint condition of lower lateral restraint and similar angular restraint as that of the reference welds. The lateral restraint is lowered by allowing easier transverse movement with the lower coefficient of friction in the Teflon/Teflon contact surfaces and lower clamping force by enlarging the contact surface areas of the fixture. However, the resultant angular restraint was deemed to be low because of the low compressive strength of Teflon. There is angular distortion of approximately 1° after the completion of each side. Hence, it is classified as a low angular and low lateral restraint condition.

Consistent with this suggestion, the transverse shrinkage measurements are the largest among all welds. The exceptionally large transverse shrinkage after the completion of side 2 may include the angular distortion from side 1.

3.4.4 Low Lateral Restraint and High Angular Restraint (S11B)

With the use of Mo disulphide grease and spacers, the angular restraint is maintained and relatively free transverse movement is allowed. In comparison with other welds, the transverse shrinkage is the largest in the root pass of side 1. Although the transverse shrinkage of S11B is similar to that of S11A, the shrinkage after completion of side 1 is larger in S11A. However the shrinkage measurements in S11A have included the effect of angular distortion which would give a large value. The angular distortion in S11B is much smaller, i.e. 0.2-0.3°. Hence, the shrinkage measurements for S11B are more reliable.

3.5 Tensile Properties and Hardness Results

The tensile properties and Vickers hardness (10 kg load) measurements are summarized in Tables 3.10 to 3.12. Due to the hardenability of molybdenum and higher carbon contents, the weld metals of consumable B have higher yield strengths and hardnesses than consumable A for all corresponding conditions.

For the weld metals of both consumables in the as-welded condition, higher heat input has minor softening effects on both tensile strengths and yield strengths. However, hardnesses show a moderate increase with heat input for the weld metals of consumable A, in both as-welded and stress relieved conditions. For the weld metal of consumable B in both as-welded and stress relieved conditions, the higher heat input brings about a negligible change in average Vickers hardnesses in all transverse profiles.

Regarding the effect of stress relief, except for the consumable B weld at 5.0 kJ/mm, the treatment leads to a slight reduction in the average hardness for the remaining three cases. In the case of the exception (consumable B, 5.0 kJ/mm) there is no significant change in hardness.

It should also be noted that, in general, for the weld metals of both consumables, the root locations in general, have similar hardness as the subsurface locations, particularly in the as welded conditions. It is uncertain whether the small difference in hardness is due to dilution or strain aging in the root location.

In comparison, the weld metals of consumable B exhibit a more uniform hardness value, whereas the weld metals of consumable A have a wider range in hardness measurements at different locations.

3.5.4 Effect of Interpass Temperature

Considering the slower cooling rate and possible grain coarsening in the higher interpass temperature weld, a general softening trend would be expected.

Evans[3.6] has shown that increasing interpass temperature from 150-240°C in SMAW welds leads to lower yield strength due to larger grain size, however the ultimate tensile strength also decreases due to accompanying compositional effects (lower Mn contents in the C-Mn consumables). The lower strength in his report is also consistent with the lower hardnesses at the higher interpass temperature observed here.

In the present program, the average hardness measurements have shown that the effect of higher interpass temperature is negligible in the root location but is moderate in the subsurface location. The through thickness variation can be rationalized as follows. Since the root location is located at the 2nd-3rd passes of side 1, the small weld metal volume relative to a large heat sink offered by the base plate implies that the cooling rate may not be unduly affected despite higher interpass temperatures. Hence, the hardness remains relatively the same. However, at the subsurface location, which would have required a lot more passes, the effect of slower cooling rate as allowed by higher interpass temperature is attained, i.e. softening occurs.

3.6 Drop Weight Testing

The full documentation of drop weight test results are tabulated in Appendix B. The nil ductility temperature is summarized in Table 3.13.

The NDT temperature for weld metals of consumable A are consistently below -60°C. The use of either larger heat input, higher interpass temperature, or more rigid lateral restraint all lead to 5-10°C increase in NDT temperature. The stress relief heat treatment appears to be beneficial, at least for the larger heat input weld. For consumable B in the as-welded condition, a large heat input leads to a higher NDT temperature. However, it is difficult to judge the effect of stress relief due to incorrect impact energy used for some specimens.

3.7 CVN Notch Toughness

The full documentation of CVN data and individual transition curves are included in Appendix C. The transition temperatures and comparative transition curves are included in Table 3.14 and Figures 3.37-3.42, respectively. In summary, the weld metals of consumable A have better CVN notch toughness than consumable B in all corresponding conditions.

3.7.1 Effect of Heat Input

For the weld metals of consumable A, the comparative transition curves demonstrate that heat input has a negligible effect on the stress relieved welds, regardless of CVN locations (Figure 3.37). For the as welded condition and the subsurface Charpy locations, the upper shelf region extends to lower temperature for the lower heat input weld. The effect is reversed at the root location though the magnitude is smaller. In terms of transition temperatures, the observed changes of ≈5°C with changes in heat input, post weld heat treatment, etc. are of small magnitude, and are similar to the uncertainty caused by scatter in the data points for any series of specimens.

For the transition curves for weld metals of consumable B, the effect of heat input is relatively small (Figure 3.38) except for the root location of stress relieved welds, where the 40J transition temperature for the 5.0 kJ/mm weld is higher by ≈18°C. The CVN transition curves for the two heat inputs virtually coincide for the as-welded root location and the stress relieved subsurface location. For the as-welded subsurface location, the upper shelf energy is slightly lower at the higher heat input.

3.7.2 Effect of Stress Relief Heat Treatment

For the same heat input welds of consumable A (Ti-B), the stress relief heat treatment has moderately deleterious effect on the CVN transition curves regardless of heat input or location (Figure 3.39). In terms of transition temperatures, the stress relief heat treatment has negligible effects at root locations, whereas it raises the transition temperatures at subsurface location by 5 to 7°C. This slight deleterious effect of stress relief on CVN toughness may be due to the precipitation of small carbides.

For the same heat input welds of consumable B (C-Mn-Mo), the stress relief heat treatment has a beneficial effect on CVN toughness regardless of heat input with only one exception, i.e. the root location in the 5.0 kJ/mm weld deposit (Figure 3.40).

3.7.3 Effect of Through Thickness Variation

From the comparative CVN transition curves (Figures 3.41-3.42), it can be surmised that for the welds of consumable A, the CVN notch toughness is largely unaffected by the location in the through thickness dimension as long as the proportion of various macrostructures is comparable among the specimens extracted from different locations. The welds of consumable B give conflicting results due primarily, it is believed, to larger variation in macrostructure at the notch.

Thus, to illustrate the role of macrostructure distribution along the notch on CVN toughness, subsurface CVN specimens of consumable B have been extracted from:

(i) the weld centreline where the columnar structure at the notch location is much higher (~90%); and

(ii) the notch location has been shifted to yield ~50% columnar region.

A higher percentage of columnar region at the CVN notch leads to reduced CVN toughness by shifting the entire CVN transition curve to higher temperature (Figure 3.43 and Table 3.15). Amongst all the variables discussed so far, viz. the through thickness location, heat input, and stress relief, it is of value to note that the effect of macrostructure on the CVN transition curves is most distinct and dramatic. In summary, the often reported through thickness variation in CVN toughness, or for that matter, those due to heat input, post weld heat treatment, etc., need to be reviewed carefully to ensure that the reported variation in toughness is not due to a variation in macrostructure distribution at notch location.

3.7.4 Effect of Interpass Temperature

For the weld metals of consumable A in the as-welded condition, increasing the interpass temperature from 150°C to 232°C has a negligible effect on the root location and a moderate deleterious effect on the CVN transition curve (Figure 3.44). The transition temperature follows the same trend. Again, Evans[3.6] reported an improvement in CVN toughness with higher interpass temperature. However, the improvement is only due to the stated higher proportion of fine grain reheated region found at the CVN notch. Hence, the present report may offer a more unbiased effect of the interpass temperature from the macrostructural influence.

3.7.5 Effect of Restraint Condition

In the brief discussion on shrinkage measurements, it was proposed that both higher angular restraint and higher lateral restraint would lead to more uniform toughness with respect to the thickness direction, whereas lower angular restraint would more adversely affect the toughness in the root region. Thus it is of value to seek a correlation, if any, between the different restraint conditions and the observed CVN toughness (Table 3.16 and Figures 3.45-3.46).

In comparison with S3A, S10A has higher lateral restraint with similar angular restraint, thus it is expected that overall CVN toughness would deteriorate somewhat. Although qualitatively, the trend is correct, the observed deterioration in transition temperature is 1 to 5°C, i.e. of the same order of magnitude as the experimental scatter. The high angular restraint and the lower lateral restraint in S11B would imply an improvement in CVN toughness over S3A. However, the experimental observations of transition temperatures suggest otherwise, with 40J transition temperature increasing by up to 5°C. Thus, under the high angular restraint with which the angular distortion is minimized, varying lateral restraint would not necessarily result in significant degradation in CVN toughness. When the low angular restraint is accompanied by low lateral restraint, S11A vs. S11B, the 40J transition temperature for the root location increases, as anticipated, from -75 to -65°C, therefore implying the angular restraint is the dominant factor in determining CVN toughness.

3.8 CTOD Toughness

The full documentation of the individual CTOD test data is included in Appendix D. The average CTOD values are summarized in Tables 3.17 and 3.18. In summary, the weld metals of consumable A (Ti-B) consistently have higher CTOD values than consumable B in all corresponding conditions.

The CTOD values for weld deposits made with consumable A are excellent, even down to -50°C, irrespective of the heat input, post weld heat treatment condition, interpass temperature or restraint.

The lowest values recorded are at -50°C for the as-welded 5 kJ/mm weld with 0.38mm average and 0.21mm minimum respectively. Otherwise, the CTOD values are usually 2mm or above. For the welds with joint restraint as a variable, the highest CTOD value would have been anticipated for weld S11B (high angular restraint, low lateral restraint). Instead, at -50°C, it has one of the lower CTOD values (.78mm average, .58mm minimum) for welds made with consumable A. Similarly, weld S11A would have been expected to give poorer CTOD values because of the low angular restraint, however, no such effect is evident.

For welds made with consumable B, higher heat inputs are accompanied by lower CTOD values in general, and the stress relief heat treatment consistently leads to an improvement in the CTOD toughness.

3.9 SEM Fractography on Selected CTOD Specimens

Fifteen CTOD specimens were selected for detailed fractography analysis, viz. 3 and 12 for weld metals of consumable A and consumable B respectively. The emphasis is placed on the welds of consumable B because of their lower CTOD values. The three specimens from the welds of consumable A are selected on the basis of its decrease in CTOD values relative to other specimens taken from the same weld.

Out of these 15 specimens, attempts to locate the cleavage initiation site are successful on only 7 samples, all of them from consumable B welds. For specimens with consumable A, there was a large ductile tearing zone at the crack tip.

The selected fractographic micrographs are included in Figures 3.47-3.56. In summary, these micrographs demonstrate the following:

(i) Inclusions acting as cleavage initiation site.

(ii) The inclusions consistently have diameters >1μm.

(iii) Although the relative compositions of the cleavage initiating inclusion do not always agree with the dominant inclusion types (Tables 3.5-3.6), there is a general agreement such that cleavage initiating inclusions are Ti-rich for consumables A and B respectively. Even though some of these detected inclusions are not dominant inclusion types, their role in cleavage initiation may be a case of coincidence of large inclusions located at the crack front.

3.10 Weld Metal Diffusible Hydrogen Content

The diffusible hydrogen content in the weld metals was 3.26 and 3.19ml/100g for consumables A and B respectively. These wire/flux combinations can be classified as low hydrogen consumables.

3.11 Gapped Bead On Plate (GBOP) Testings

The GBOP test results are given in Table 3.19. For both consumables, the 10% cracking preheat temperature is somewhere between room temperature and 75°C.

4.0 DISCUSSION

The results and observations presented in the previous section indicate the following:

(i) Among the two selected consumables, the C-Mn-Mo weld metals consistently have lower toughness than Ti-B welds, in all corresponding conditions.

(ii) For the Ti-B weld deposits, the procedural parameters, viz. heat input, stress relief, interpass temperature and restraint condition, do not significantly effect the CVN or the CTOD toughness.

(iii) For C-Mn-Mo weld deposits, the stress relief heat treatment leads to improved CVN and CTOD toughness. The CTOD toughness decreases with higher heat input, whereas the CVN toughness is affected marginally.

These main observations are discussed in the following sections.

4.1 Effect of Procedural Parameters on Toughness of Ti-B Weld Consumable A

Since the 800° to 500°C cooling time, (t_{8-5}) at 5.0 kJ/mm, is about 1.5 times greater than 3.5 kJ/mm (Table 4.1), the acicular ferrite content is expected to decrease at higher heat inputs because of the slower cooling. Although welds with both consumables have undergone the same increase in heat input, the in Ti-B weld metal has exhibited a better tolerance to heat input as it maintains a higher acicular ferrite content. The phase transformation in a weldment may be influenced by composition, cooling rate and inclusion populations. The subsequent discussion focuses primarily on composition and inclusions.

It has been widely reported that inclusions can serve as nucleation sites for acicular ferrite. However, the efficacy for its nucleation role requires an optimum combination of size, shape, composition, inter or intragranular locations, surface energy, crystallography, etc.[4.1]. Although the exact mechanisms of nucleation and optimum combinations are still a subject of research, a few qualitative observations have been made in literature, viz.:

(i) Effectiveness in nucleation role varies among inclusion types.

(ii) Efficacy is enhanced by the presence of Mn, Al or Ti in the inclusions. TiO or TiO_2 is surmised to be more beneficial in this regard.

(iii) Increased availability of intermediate size inclusions (0.5 to 1.0μm) tends to increase acicular ferrite contents.

(iv) Electron microscopy shows that spherical inclusions participate in the nucleation of acicular ferrite.

In the present report, all dominant inclusions (Table 3.5) contain significant amounts of Mn, Al and Ti. The relative contents of these elements are not affected significantly by the changing heat input. Furthermore, the proportion and density of intermediate size inclusions also remains unchanged with heat input. The shape factors for both the overall inclusion populations on individual dominant types increase with higher heat input, i.e. the inclusions are becoming more equiaxed. The ability shown by Ti-B weld metal to maintain the acicular ferrite at higher heat input could partly be due to the retention of the favourable inclusion characteristics the higher heat input, though the primary effect must be related to the effect of boron in inhibiting nucleation of grain boundary ferrite.

During the brief discussion on the influence of the unbalance factor on CVN toughness (Section 3.1.1), it was indicated that optimum CVN toughness coincides with the critical value of BF = 100ppm. At such a critical value, the nitrogen in weld metal is stabilized without incurring excessive hardenability. Since the unbalance factors in the Ti-B weld of consumable A remains unchanged with heat input and they are slightly larger than the optimum value by 10-20ppm, it is surmised that there are sufficient alloy additions to minimize free nitrogen, i.e. the weld metals are least susceptible to strain aging effects.

In summary, the lack of response by the Ti-B weld to changing heat input is due to its ability to retain a relatively high proportion of acicular ferrite, and minimal free nitrogen content.

Raising the interpass temperature from 150° to 242°C at 3.5 kJ/mm is equivalent to an increase in heat input to 5.0 kJ/mm at 150°C preheat (Table 4.1). There may also be an increase in the soaking time in the range of 200-250°C. Both of these factors, especially if there is sufficient free nitrogen in weld metal, would lead to lower toughness, more so in the root region. However, it can be reasonably assumed that composition and unbalance factor would not change as a result of different interpass temperatures, and therefore, the free nitrogen content would be similarly minimal. Hence, no significant adverse effect of higher interpass temperature on toughness should be expected, which indeed is the case, with the transition temperature increasing by 5°C only. It should be noted that the 3.5 kJ/mm - 232°C welds have the lowest acicular ferrite proportion (≈47%) compared to 3.5 and 5.0 kJ/mm welds at 150°C interpass temperature (67 and 56% respectively). Yet there is no corresponding deleterious effect on toughness.

The beneficial role of stress relief heat treatment is generally attributed to microstructural softening and at least partial removal of the strain aging damage. However, stress relief heat treatment may also have an adverse effect on toughness if carbides are precipitated at grain boundaries from the transformation of martensite-retained austenite aggregates, or if fine nitrocarbide precipitation leads to an increase in weld metal hardness.

In the Ti-B weld metal, it has been argued that little strain aging damage, if any, would have occurred, therefore no appreciable improvement in toughness is to be expected by removal of strain aging damage. There is a slight softening as indicated by reduction in hardness on stress relieving. However, any potential improvement in toughness on this count is perhaps slightly over compensated by precipitation of carbides at grain boundaries which in itself is probably not of significant magnitude because of the small proportion of the ferrite with aligned second phase in the microstructure (<5%).

4.2 Effect of Heat Input and Stress Relief on Toughness of C-Mn-Mo Weld

The experimental observations have shown that CVN toughness in the as-welded condition is relatively unaffected by the higher heat input, whereas the stress relief heat treatment has improved the toughness.

In addition to slower cooling rate at higher heat input, the drastic decrease in acicular ferrite may be rationalized by lower Mo recovery and larger inclusion size, both of which imply a less favourable condition for acicular ferrite formation. In addition, the absence of significant Ti contents in the inclusions also reduced their overall efficacy in the ferrite nucleation role. The increase in coarse ferrite phases of polygonal and grain boundary ferrite also implies microstructural softening. However, a similar reduction in the CVN toughness in the as-welded condition is not observed with the less desirable microstructure.

Since the unbalance factor in C-Mn-Mo welds is smaller than the optimum value of 100ppm, the presence of free nitrogen in weld metal implies the susceptibility to strain aging effects. However, the unbalance factor increases with higher heat input. Thus, the expected reduction in CVN toughness due to a less desirable microstructure is offset by reduced susceptibility to strain aging effects.

In addition to the hardenability influence, the beneficial role of stress relief on toughness is due to removal of strain age effect and microstructural softening.

4.3 Toughness Comparison Between Ti-B Welds and C-Mn-Mo Welds

The experimental results have shown that Ti-B welds have superior toughness than C-Mn-Mo welds in all corresponding conditions (Figures 4.1-4.2). The different toughness can be rationalized by the combined influence of hardenability, free nitrogen content and microstructure.

Because of the significant Mo addition, the larger carbon equivalents in C-Mn-Mo welds lead to higher hardness. Higher hardness/ tensile strength leads to lower toughness. At 3.5 kJ/mm, although both welds share similar acicular ferrite, the much improved toughness in the Ti-B welds is because of its lower hardness. At 5.0 kJ/mm, the superior toughness in the Ti-B welds is due to its ability to retain acicular ferrite at the higher heat inputs, thus offering a better resistance to cleavage fracture. Furthermore, the reduced susceptibility to strain aging in Ti-B welds also contributes to its superior toughness.

Despite the beneficial effect of stress relief heat treatments, the lower CTOD toughness in C-Mn-Mo welds is due to the much higher density (2-3 times) of large inclusions which provide more cleavage initiation sites, leading to a lower CTOD toughness. At 5.0 kJ/mm, the combined influence of lower acicular ferrite and high density of large inclusions contributes to the low CTOD toughness.

5.0 CONCLUDING SUMMARY

The main conclusions are summarized as follows:

(A) For the procedural parameters investigated in the present study, viz. heat input, interpass temperature, and stress relief heat treatment, restraint conditions, the Ti-B alloyed weld deposits have shown good toughness characteristics which are relatively insensitive to the changing parameters. Regardless of the procedural parameters and post weld conditions, the 40J transition temperature is within the range of -65 and -80°C, whereas the minimum CTOD values are 0.21mm at -50°C. The excellent toughness observed in the Ti-B deposit is attributed to the following:

(i) reduced susceptibility to strain aging damage by both low total nitrogen and free nitrogen contents.

(ii) desirable microstructure - the proportions of grain boundary ferrite and ferrite with aligned second phase are small. The relatively high proportions of acicular ferrite offer improved resistance to cleavage fracture. These effects are related to the presence of boron.

(iii) desirable inclusion distribution - despite higher oxygen contents than C-Mn-Mo deposits, the abundance of Ti-bearing inclusions are of a size range which are effective for nucleation of acicular ferrite but not large enough to incur cleavage fracture.

(B) In comparison with Ti-B deposits, C-Mn-Mo weld metals consistently show lower toughness. Regardless of heat inputs and post weld conditions, the 40J CVN transition temperatures are in the range of -48 to -66°C, whereas the minimum CTOD value is 0.07mm at -30°C. The lower toughness observed in C-Mn-Mo deposits is attributed to the following:

(i) Susceptibility to strain aging damage due to the higher total nitrogen content and small unbalanced factor.

(ii) Large Mo and Mn additions have introduced excessive hardening in the deposits.

(iii) At higher heat input, the smaller proportions of acicular ferrite offer reduced resistance to cleavage fracture. The lower acicular ferrite contents in the larger heat input is due to combined effects of reduced Mo recovery and heat input. In the absence of adequate acicular ferrite contents, the higher proportions of grain boundary ferrite, accompanied by coarsening, leads to reduced resistance of cleavage.

(iv) Despite smaller O+S contents, the inclusion distribution is characterized by larger inclusion sizes and higher densities of large inclusions (>1μm) which leads to lower resistance to cleavage.

(C) The effects of procedural parameters on CVN toughness are investigated with the intrinsic condition of controlled macrostructure (50% reheated region) on the CVN notch location. In the limited study on the effect of macrostructure on CVN toughness, it is shown that the macrostructure found at the notch location has far more influence on CVN toughness than procedural parameters. Varying the macrostructure at the notch has led to an increase in 30°C in 40J transition which far exceeds the ~20°C range produced by procedural parameters.

6.0 REFERENCES

• Section 1.0 - Introduction

[1.1] Bala, S.R. and Santyr, S., "Evaluation of Heat Affected Zone and Weld Metal Toughness in Selected Steels - Phase I". AMCA International Ltd. Report 7-184-071-099 (1986).

[1.2] Bala, S.R., Chiu, C. and Morrison, K., "Evaluation of Heat Affected Zone and Weld Metal Toughness in Selected Steels - Phase II". AMCA International Ltd. Report 7-185-141-099 (1986).

[1.3] Evans, G.M., "Effect of Interpass Temperature on the Microstructure and Properties of C-Mn All Weld Metal Deposits". Welding Research Abroad, 29, 24-35 (1983).

[1.4] Evans, G.M., "Effect of Welding Position on the Microstructure and Properties of C-Mn All Weld Metal Deposits". Welding Research Abroad, 29, 58-69 (1983).

[1.5] Dawes, M.G., "Fracture Initiation in Weld Metals". 40, 95-103 (1972).

[1.6] Robinson, J.L., "A Study of the Factors Controlling Root Toughness in Multipass Manual Metal Arc Welds in C-Mn Steels". WI Research Report 41/1977/M (1977).

[1.7] Dawson, G.W. and Judson, P., "Procedural Guidelines for the Achievement of Tough Welded Joints in Structural Steels for Offshore Applications". Proceedings of Second International Conference on Offshore Welded Structures, Welding Institute (1983).

[1.8] Leggatt, R.H., "Studies on the Dependence of Weld Metal Toughness on the Level of Test Panel Restraint: Final Report". WI Report 255/1984 (1984).

[1.9] Nicholson, S. and Rogers, P.F., "Controlling Weld Metal Toughness in Manual Metal Arc Welds". Paper 11, Proceedings of Welding in Offshore Construction, Welding Institute (UK) (1974).

[1.10] Entrekin, C.H., "Effect of Stress Relief on Microalloyed Weld Metal Impact Propereties". Welding Journal, 62, 197s-203s, (1983).

[1.11] Braid, J.E.M. and Gianetto, J.A., "Effects of PWHT on the Toughness of Shielded Metal Arc Weld Metals for Use in Canadian Offshore Structure Fabrication". IIW Doc. IX-1385-86 (1986).

[1.12] Evans, G.M., "Effect of Stress Relieving on the Microstructure and Properties of C-Mn All Weld Metal Deposits". Welding Journal, 65, 326s-334s, (1986).

[1.13] Braid, J.E.M. and Gianetto, J.A., "Toughness of Weld Metals for Fabrication of Cold Marine Structures and Vessels, Part 2: Submerged Aec Welding". MTL Report 8825-25(TR).

[1.14] Chiu, C. and Malik, L., "Toughness Evaluation of GMA Welding Consumables for Offshore and Petrochemical Application: Interim Report". Arctec/FTL Report (1987).

[1.15] Bala, S.R. and Santyr, S., "Evaluation of Flux Cored Arc Welding Consumables for Offshore and Arctic Structures Fabrication". AMCA International Ltd. Report 7-184-096 (1986).

- **Section 2.0 - Experimental Descriptions and Methodology**

[2.1] Technical References 0782-186, "Submerged Arc Welding Consumables for Low Temperature Service Steel". Welding Division, Kobe Steel Ltd. (1982).

[2.2] "ESAB Welding Handbook", 4th Edition.

[2.3] Braid, J.E.M. and Gianetto, J.A., "Toughness of Weld Metals for Fabrication of Cold Marine Structures and Vessels - Part 2: Submerged Arc Welding". MTL Report MTL-88-25.

[2.4] Pargeter, R.J. and Dolby, R.E., "Identification and Quantitative Description for Ferritic Steel Weld Metal Microstructure". IIW Doc. IX-1323-84 (1984).

[2.5] Towers, O.L. and Robinson, P., "Procedures for Fatigue Cracking Fracture Toughness Test Pieces, With Particular Reference to Weldments". WI Research Bulletin, 23, 112-120 (1982).

- **Section 3.0 - Experimental Results and Observations**

[3.1] Fehervari, A. and Rittinger, J., "Effect of Titanium on Transition Temperature of CO_2 Weld". IIW Doc. XII-B-98-71 (1971).

[3.2] Kohno, R., Takami, T., Mori, N. and Nagano, K., "New Fluxes of Improved Weld Metal Toughness for HSLA Steels". Welding Journal, 12, 373s-380s, (1982).

[3.3] Abson, D.J., "Non-Metallic Inclusions in Ferritic Steel Weld Metals - A Review". IIW Doc. IX-1486-87, (1987).

[3.4] Widgery, D.J., "Deoxidation Practice for Mild Steel Weld Metal". Welding Journal, 55, 57s-68s, (1976).

[3.5] Chai, C.S. and Eagar, T.W., "Effect of SAW Parameters on Weld Metal Chemistry". Welding Journal, 59, 93s-98s, (1980).

[3.6] Evans, G.M., "Effect of Interpass Temperature on the Microstructure and Properties of C-Mn All Weld Metal Deposits". Welding Research Abroad, 29, 24-35 (1983).

- **Section 4.0 - Discussion**

[4.1] Abson, D.J., "Non-Metallic Inclusions in Ferritic Steel Weld Metals - A Review". IIW Doc. IX-1486-87, (1987).

TABLES

Table 2.1

Characterizations of the Base Plate

C	Mn	S	P	Si	Cr	Ni	Al	Nb	V	Cu
0.14	1.27	0.01	.017	0.29	0.03	0.17	0.04	0.032	0.043	0.2

Yield Strength (MPa)	Ultimate Tensile Strength (MPa)	% Elongation	CVN Impact Energy @ -60°C (J)	
			Transverse	Longitudinal
364	510	29	66	129

Table 2.2
Experimental Matrix for Submerged Arc Weld Program

Restraint Condition	Interpass Temp (°C)	Consumable	Heat Input kJ/mm	Voltage (V)	Current (Amps)	Travel Speed mm/sec	Post Weld Cond'n	I.D.
Reference:	150	A	3.5	28	530	4.2	AW	S3A, S3B
							SR	S4A, S4B
Angular Restraint: High			5.0	31	610	3.8	AW	S1A, S1B
							SR	S2A, S2B
Lateral Restraint: Moderate		B	3.5	28	530	4.2	AW	S7A, S7B
							SR	S8A, S8B
			5.0	31	610	3.8	AW	S5A, S5B
							SR	S6A, S6B
	232	A	3.5	28	530	4.2	AW	S9A, S9B
Angular Restraint: High Lateral Rest.: High	150	A	3.5	28	530	4.2	AW	S10A, S10B
Angular Restraint: Low Lateral Rest.: Low	150	A	3.5	28	530	4.2	AW	S11A
Angular Restraint: High Lateral Rest.: Low	150	A	3.5	28	530	4.2	AW	S11B

All welds were made of 4mm wire; DCEP and electrode stickout of 32mm (1.25 in.), except at the root pass which is 35mm (1.38 in.)

AW - As Welded
SR - Stress Relieved

CONSUMABLE	HEAT INPUT (KJ/mm)	POST WELD CONDITION	INTERPASS TEMPERATURE (°C)	PLATE ID	LOCATION	C (W/O)	Mn (W/O)	Si (W/O)	S (W/O)	P (W/O)	Ti (W/O)	Mo (W/O)	Al (W/O)	Zr (W/O)	O (W/O)	N (W/O)	Cr (W/O)	Ni (W/O)	Cu (W/O)	V (W/O)	B (W/O)	Nb (W/O)
A	3.5	AW	150	S3	SUBSURFACE	0.07	1.74	0.300	0.005	0.010	0.015	0.002	0.010	0.002	0.0340	0.0040	0.027	0.050	0.124	0.010	0.004	0.007
A	3.5	AW	150	S3	ROOT	0.07	1.73	0.319	0.005	0.012	0.010	0.001	0.010	0.002	0.0328	0.0040	0.023	0.071	0.130	0.020	0.004	0.009
A	5.0	AW	150	S1	SUBSURFACE	0.08	1.66	0.270	0.006	0.017	0.012	0.002	0.010	0.002	0.0288	0.0052	0.024	0.087	0.145	0.022	0.002	0.013
A	5.0	AW	150	S1	ROOT	0.08	1.63	0.300	0.005	0.024	0.014	0.001	0.007	0.002	0.0272	0.0041	0.023	0.103	0.157	0.027	0.003	0.011
B	3.5	AW	150	S7	SUBSURFACE	0.09	1.60	0.367	0.004	0.076	0.002	0.436	0.010	0.001	0.0294	0.0070	0.060	0.096	0.217	0.010	0.001	0.007
B	3.5	AW	150	S7	ROOT	0.09	1.60	0.370	0.004	0.016	0.003	0.343	0.016	0.003	0.0264	0.0057	0.051	0.130	0.205	0.028	0.001	0.007
B	5.0	AW	150	S5	SUBSURFACE	0.10	1.59	0.313	0.005	0.021	0.002	0.329	0.007	0.001	0.0170	0.0063	0.044	0.123	0.213	0.025	0.001	0.011
B	5.0	AW	150	S5	ROOT	0.10	1.67	0.355	0.004	0.025	0.003	0.301	0.007	0.002	0.0154	0.0063	0.052	0.100	0.163	0.016	0.001	0.012
WIRE A						0.13	1.57	0.014	0.007	0.015	<0.001	0.002	0.001	N/A	0.0096	0.0085	0.015	0.012	0.060	0.002	<0.005	0.002
WIRE B						0.10	1.3	0.020	0.007	0.010	0.001	0.500	0.023	--	0.0110	0.0084	0.054	0.040	0.180	0.001	<0.005	0.002

Table 3.1

Summary of Weld Metal Composition
Submerged Arc Welds

HEAT INPUT (KJ/mm)	LOCATION	O+S (w/o)	UNBALANCE FACTOR	CE (IIW) (w/o)	Pcm (w/o)	Al/(O^2) (w/o)	B/N (w/o)	Ti/Al (w/o)	Ti/B (w/o)
3.5	SUBSURFACE	0.0390	0.0101	0.3800	0.1950	8.65	0.82	--	--
3.5	ROOT	0.0378	0.0127	0.3811	0.1964	9.30	1.00	--	--
5.0	SUBSURFACE	0.0349	0.0115	0.3817	0.1923	11.97	0.38	--	--
5.0	ROOT	0.0322	0.0127	0.3792	0.1976	9.46	0.73	--	--
3.5	SUBSURFACE	0.0244	0.0042	0.4953	0.2364	24.03	0.14	0.20	2.00
3.5	ROOT	0.0304	0.0122	0.4784	0.2297	22.96	0.18	0.19	3.00
5.0	SUBSURFACE	0.0229	0.0085	0.4670	0.2318	21.85	0.16	0.29	2.00
5.0	ROOT	0.0194	0.0059	0.4894	0.2398	29.52	0.16	0.43	3.00

Table 3.2

Summary of Carbon Equivalents

Table 3.3

Summary of Inclusion Distribution
(Submerged Arc Welds)

Consumable	Heat Input kJ/mm	Overall Inclusion Distribution					Individual Size Grouping					
		Area Fraction (%)	Average Shape Factor	Average Diameter (micron)	Number Density $(X10^5/cm^2)$	Average Spacing (micron)	$0.2 \leq$ dia < 0.5 micron		$0.5 \leq$ dia < 1.0 micron		dia ≥ 1.0 micron	
							% of all inclusions	Density $(X10^5/cm^2)$	% of all inclusions	Density $(X10^5/cm^2)$	% of all inclusions	Density $(X10^5/cm^2)$
A	3.5	0.10	0.57	0.51	7.8	5.7	58.4	4.57	37.1	2.90	4.5	0.35
	5.0	0.11	0.74	0.50	5.8	6.5	58.4	3.41	38.1	2.35	3.5	0.20
B	3.5	0.08	0.61	0.41	5.1	7.0	79.3	4.04	19.3	0.98	1.4	0.73
	5.0	(0.10)	0.75	0.62	7.0	6.0	40.1	2.83	49.5	3.48	10.4	0.73

TABLE 3.4

Summary of Predominant Inclusion Types in Consumable B
Submerged Arc Welds

Inclusion Type	Average Inclusion Diameter (micron)	% Distribution of** Diameter (%)		Average Relative Peak Intensities (%)					Percent* Distribution of Inclusion	Shape Factor
		$0.2 \leq d \leq 0.5$	$0.5 < d \leq 1.0$	Ti	Mn	Al	S	Si		
Al-Ti-Si-Mn-S	0.51 (0.40)$^+$	54.8 (80.4)	41.9 (19.6)	7 (7)	21 (27)	56 (44)	6 (11)	7 (8)	44.4 (49.3)	0.74 (0.60)
Al-Ti-Si-Mn	0.62 (0.59)	30.2 (52.9)	67.4 (35.3)	7 (8)	18 (23)	66 (58)	1 (1)	6 (8)	15.4 (6.1)	0.80 (0.69)
Al-Ti-Mn-S	0.69 (0.45)	29.7 (63.6)	59.5 (36.4)	5 (7)	19 (29)	64 (47)	9 (13)	0 (1)	13.3 (7.9)	0.76 (0.65)
Al-Ti-Mn	0.99 (N/D)	0 (N/D)	51.7 (N/D)	4 (N/D)	13 (N/D)	80 (N/D)	0 (N/D)	0 (N/D)	10.4 (N/D)	0.84 (N/D)
Al-Mn-S	0.59 (0.48)	35.3 (80.0)	58.8 (13.3)	0 (1)	13 (25)	79 (58)	4 (12)	0 (1)	6.1 (5.4)	0.64 (0.69)
Al-Si-Mn-S	0.47 (0.37)	70.0 (88.1)	30.0 (10.2)	0 (1)	22 (29)	58 (43)	10 (14)	6 (10)	3.6 (21.1)	0.79 (0.58)
Overall	0.62 (0.41)	40.1 (79.3)	49.5 (19.3)	--	--	--	--	--	---	0.75 (0.61)

$^+$The unbracketed value is at 5.0 kJ/mm, whereas the bracketed value is at 3.5 kJ/mm.
*Percent distributions in all the inclusions, regardless of type.
**Percent of inclusions within the same type.
N/D - Not defined as dominant types.

TABLE 3.5

Summary of Predominant Inclusion Types in Consumable A Submerged Arc Welds

Inclusion Type	Average Inclusion Diameter (micron)	% Distribution of** Diameter (%)		Average Relative Peak Intensities (%)					Percent* Distribution of Inclusion	Shape Factor
		$0.2 \le d \le 0.5$	$0.5 < d \le 1.0$	Ti	Mn	Al	S	Si		
Al-Ti-Si-Mn-S	0.49 $(0.48)^{+}$	60.7 (62.6)	34.8 (34.3)	23 (21)	32 (30)	22 (29)	10 (8)	9 (9)	77.1 (74.2)	0.74 (0.56)
Al-Ti-Si-Mn	0.63 (0.50)	38.1 (60.5)	47.6 (34.2)	25 (24)	31 (28)	32 (36)	0 (0)	9 (8)	9.1 (12.3)	0.76 (0.53)
Al-Ti-Mn-S	0.48 (0.68)	56.3 (22.2)	43.8 (72.2)	26 (22)	34 (27)	24 (38)	11 (9)	1 (1)	6.9 (5.8)	0.70 (0.68)
Overall	0.50 (0.51)	58.4 (58.4)	38.1 (37.1)	--	--	--	--	--	---	0.74 (0.57)

$^{+}$The unbracketed value is at 5.0 kJ/mm, whereas the bracketed value is at 3.5 kJ/mm.

*Percent distributions in all the inclusions, regardless of type.

**Percent of inclusions within the same type.

Table 3.6

Summary of Estimated Inclusion Volume Fraction

Consumable	Heat Input kJ/mm	Average Diameter (μm)	Standard Deviation in Average Diameter (μm)	Number Density ($X10^{-3}/\mu m^2$)	Calculation Volume Fraction (%)	O+S at Root (w/o)	Predicted Volume Fraction (%)
A	3.5	0.50	0.23	7.8	0.12	0.0378	0.21
	5.0	0.51	0.25	5.8	0.10	0.0322	0.18
B	3.5	0.62	0.29	5.1	0.12	0.0304	0.17
	5.0	0.41	0.17	7.0	0.07	0.0194	0.11

Table 3.7

Summary of Macrostructural Characterization Submerged Arc Welds

Consumable	Heat Input kJ/mm	Post Weld Condition	Macrostructure Distribution Along Centreline (%)		
			Columnar Grains	Coarse Grain Reheated Zone	Fine Grain Reheated Zone
A	3.5	AW	29.3	17.6	53.1
		SR	28.4	17.3	54.3
	5.0	AW	34.6	16.2	49.2
		SR	45.0	18.5	36.5
B	3.5	AW	47.6	11.4	41.0
		SR	45.1	19.3	35.6
	5.0	AW	41.5	25.9	32.6
		SR	34.0	20.6	45.4
A	3.5*	AW	24.6	14.2	61.2

*Interpass temperature = 232°C

TABLE 3.8

Summary of Microstructure Characterization of Submerged Arc Welds

Consumable	Heat Input (kJ/mm)	Polygonal Ferrite	Grain Boundary Ferrite	Ferrite with Non-Aligned Second Phase	Ferrite with Aligned Second Phase	Accicular Ferrite	Average Inclusion Diameter (micron)	Oxygen at Subsurface Location (v/o)
A	3.5	6.2±1.5 (4.8±1.9)⁺	9.6±1.8 (10.8±2.7)	15.0±2.2 (20.4±3.5)	1.6±0.8 (1.2±1.0)	67.6±2.0 (62.8±4.2)	0.51	0.0340
	5.0	7.5±1.6 (7.1±1.6)	11.9±2.0 (13.6±2.1)	21.9±2.6 (20.6±2.5)	2.4±1.0 (1.4±0.7)	56.3±3.1 (57.3±3.1)	0.50	0.0289
B	3.5	6.4±2.1 (6.7±1.5)	6.2±2.1 (9.1±1.8)	12.6±2.9 (13.2±2.1)	4.4±1.8 (0.8±0.6)	70.4±4.0 (70.2±2.8)	0.41	0.0264
	5.0	12.7±2.1 (13.0±1.5)	13.2±2.1 (13.2±1.5)	20.3±2.5 (24.4±4.3)	5.0±1.4 (2.8±0.7)	48.3±3.1 (46.6±2.2)	0.62	0.0179
A	3.5*	16.2	9.2	23.8	3.6	47.2	---	---

*Interpass temperature of 150°C

⁺Repeating the microstructure characterization on B plates.

Table 3.9

Summary of Transverse Shrinkage Measurements

Plate I.D.	Restraint Condition	Weld Passes	Average* (mm)
S4A	Lateral: Moderate Angular: High	root pass, side 1	0.60
		completion of side 1	2.75
		root pass, side 2	0.51
		completion of side 2	0.89
S10A	Lateral: High Angular: High	root pass, side 1	0.61
		completion of side 1	1.94
		root pass, side 2	0.49
		completion of side 2	0.92
S11A	Lateral: Low Angular: Low	root pass, side 1	0.69
		completion of side 1	2.37
		root pass, side 2	0.52
		completion of side 2	1.20
S11B	Lateral: Low Angular: High	root pass, side 1	0.69
		completion of side 1	1.91
		root pass, side 2	0.46
		completion of side 2	0.87

*Average transverse shrinkage from Locations A, B and C

Table 3.10

Summary of Tensile Properties of Submerged Arc Welds As Welded Condition

Consumable	Heat Input (kJ/mm)	Yield Strength (MPa)	Ultimate Tensile Strength (MPa)	% Elongation
A	3.5	456	543	35.6
	5.0	440	545	33.4
B	3.5	586	698	27.6
	5.0	573	693	21.5

Table 3.11

Summary of Hardness Measurements Submerged Arc Welds

Consumable	Heat Input kJ/mm	Location	Post Weld Condition	
			As Welded	Stress Relieved
A	3.5	Centreline	188 (168-207)*	184 (160-209)
		Subsurface	198 (179-219)	181 (160-212)
		Root	205 (193-216)	197 (167-232)
	5.0	Centreline	210 (189-227)	198 (167-224)
		Subsurface	212 (203-221)	204 (183-242)
		Root	221 (205-232)	198 (180-207)
B	3.5	Centreline	250 (236-256)	242 (232-253)
		Subsurface	248 (242-251)	232 (199-245)
		Root	250 (243-256)	241 (233-249)
	5.0	Centreline	242 (232-264)	245 (236-254)
		Subsurface	244 (232-266)	245 (233-254)
		Root	248 (240-256)	244 (236-249)
A+	3.5	Centreline	196 (173-243)	Not Applicable
		Subsurface	188 (177-202)	
		Root	202 (183-221)	

*The value in parentheses denotes the range of hardness measurements.

+232°C interpass temperature.

Table 3.12

Summary of Hardness Measurements for the Restraint Welds

Plate I.D.	Angular Restraint	Lateral Restraint	Average Vickers Hardness (10kg)		
			Centreline	Subsurface	Root
S10A	High	High	199 (172-215)	195 (181-210)	201 (191-225)
S3A	High	Moderate	188 (168-207)	198 (179-219)	205 (193-216)
S11B	High	Low	196 (181-228)	194 (180-201)	209 (199-221)
S11A	Low	Low	192 (165-219)	193 (177-212)	207 (188-213)

Table 3.13

Summary of NDT Temperature (°C) for Submerged Arc Welds

Consumable	Heat Input kJ/mm	As Welded	Stress Relieved
A	3.5	-75	(-65)
	5.0	-60	(-75)
B	3.5	-60	(-50)
	5.0	-65	(-45)
A	3.5	-65*	Not Applicable
		(-60[+])	

The values in parentheses are tested with 540J impact energy, and correct NDT temperatures (with 450J impact energy) would be the same or even lower.
*Interpass temperature of 232°C.
*Interpass temperature of 232°C.

[+] High lateral and high angular restraint conditions.

—

Table 3.14

Summary of CVN Data of Submerged Arc Welds

Consumable	Heat Input (kJ/mm)	Post Weld Heat Treatment	CVN Location	Transition Temp. (°C)		CVN Impact Energy @ (J)				
				40J	27J	0°C	-20°C	-30°C	-40°C	-60°C
A	3.5	AW*	Subsurface	-80	-84	156	155	153	151	135
			Root	-74	-78	158	154	149	143	116
		SR	Subsurface	-75	-80	154	148	144	137	116
			Root	-75	-80	155	144	140	132	102
	5.0	AW	Subsurface	-80	-86	159	157	145	135	103
			Root	-74	-76	155	155	155	155	136
		SR	Subsurface	-73	-77	153	149	146	136	102
			Root	-70	-76	153	149	146	136	95
B	3.5	AW	Subsurface	-49	-62	106	93	80	55	29
			Root	-49	-62	143	109	82	55	29
		SR	Subsurface	-57	-70	134	113	96	73	37
			Root	-66	-73	150	140	131	118	57
	5.0	AW	Subsurface	-48	-65	97	66	55	46	31
			Root	-52	-62	132	110	89	63	29
		SR	Subsurface	-61	-70	114	101	91	78	41
			Root	-48	-60	114	92	75	54	27
A	3.5**	AW	Subsurface	-78	-83	155	155	155	153	143
			Root	-69	-73	155	154	152	145	102

*AW = As Welded; SR = Stress Relieved.

**Interpass temperature of 232°C.

Table 3.15

Summary of CVN Properties for Different Macrostructure at the Notch

% Columnar Region at CVN Notch	Transition Temp. (°C)		CVN Impact Energy @ (J)				
	40J	27J	0°	-20°	-30°	-40°	-60°
50	-48	-65	97	66	55	46	31
90	-19	-31	64	40	28	19	--

Table 3.16

Summary of CVN Impact Properties of Submerged Arc elds in Various Restraint Conditions (3.5 kJ/mm, As Welded)

Restraint Condition	CVN Location	Transition Temperature (°C)		CVN Impact Energy @ (J)				
		40J	27J	0°C	-20°C	-30°C	-40°C	-60°C
S3A High Angular Moderate Lateral	Subsurface	-80	-84	156	155	153	151	135
	Root	-74	-78	158	154	149	143	116
S10A High Angular High Lateral	Subsurface	-79	-83	161	159	157	152	135
	Root	-69	-75	162	162	160	157	135
S11A Low Angular Low Lateral	Subsurface	-80	-86	159	156	152	145	106
	Root	-65	-68	162	158	154	147	115
S11B High Angular Low Lateral	Subsurface	-75	-77	162	157	152	145	120
	Root	-75	-79	163	158	155	147	122

Table 3.17

Summary of CTOD Values for Submerged Arc Welds

Consumable	Heat Input (KJ/mm)	Temperature (°C)	Average CTOD (mm)	
			As Welded	Stress Relieved
A	3.5	-30	2.46 (2.23 - 2.76)*	3.58 min. (3.55 - 3.61)+
		-50	1.92 (0.70 - 2.56)	2.81 (1.25 - 3.67)+
	5.0	-30	2.75 (2.73 - 2.77)	1.98 (1.17 - 3.05)
		-50	0.38 (0.21 - 0.53)	1.98 (1.27 - 2.94)
B	3.5	-10	0.30 (0.21 - 0.46)	0.90 (0.78 - 1.46)
		-30	0.14 (0.094 - 0.17)	0.30 (0.20 - 0.40)
	5.0	-10	0.11 (0.072 - 0.14)	0.47 (0.29 - 0.72)
		-30	0.11 (0.071 - 0.15)	0.33 (0.036 - 0.51)
A	3.5**	-30	2.58 (2.40 - 2.90)	N/A
		-50	1.84 (1.16 - 2.86)	N/A

* The range of CTOD values were given in brackets.

** Interpass temperature of 232°C

+ All three tests exceeded the maximum clip gauge displacement of 12.5 mm.

Table 3.18

Summary of CTOD Values for Submerged Arc Weld in Different Restraint Conditions
Consumable A, 3.5 kJ/mm, As Welded

Angular Restraint	Lateral Restraint	Plate I.D.	Average CTOD (mm)	
			-30°C	-50°C
High	High	S10A	2.48 (2.26-2.66)	2.42 (2.33-2.49)
	Moderate	S3A	2.46 (2.23-2.76)	1.93 (0.71-2.56)
	Low	S11B	2.76 (2.61-2.93)	0.78 (0.58-0.95)
Low	Low	S11A	2.44 (2.22-2.63)	2.17 (0.88-3.08)

Table 3.19

Summary of G-BOP Tests for Submerged Arc Welds

Preheat Temperature (°C)	Consumable A	Consumable B
20	40-45%	40-45%
75	0-5%	0-5%
150	0-5%	0-5%

Table 4.1

Estimated Cooling Rate

Heat Input (kJ/mm)	Interpass Temp. (°C)	$t_{800-500}$* (Sec)
3.5	150	28
	232	40
5.0	150	42

*Estimated with Bibby's model[1]

[1] Bibby, M., "Weld Quality Software for the HP71B Hand Held Computer". Dept. of Mechanical and Aeronautical Engineering, Carleton University Report, January 1987.

FIGURES

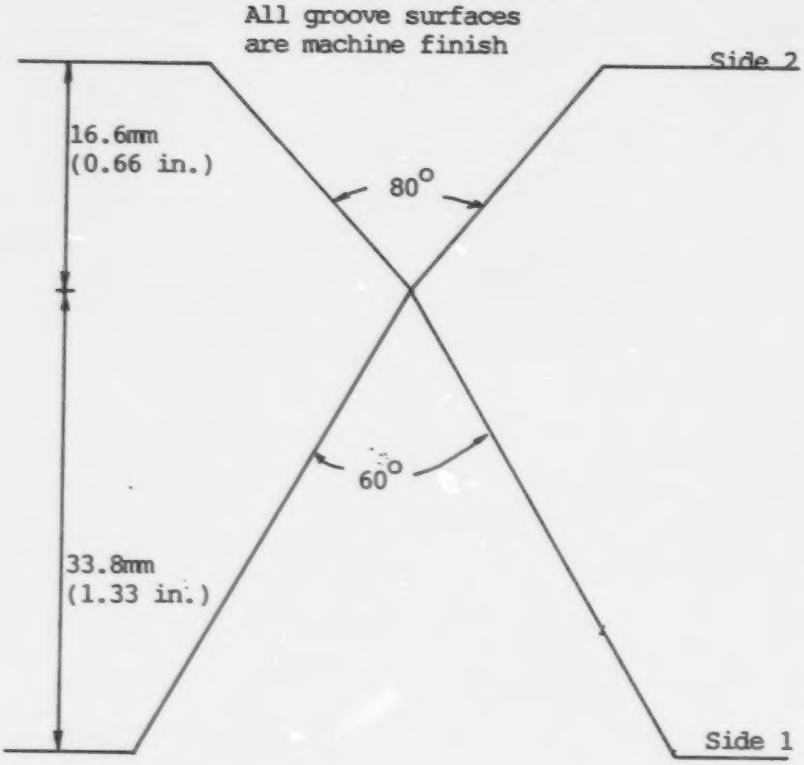
All groove surfaces
are machine finish
Side 2
16.6mm
(0.66 in.)
80°
60°
33.8mm
(1.33 in.)
Side 1

Figure 2.1 Joint Geometry

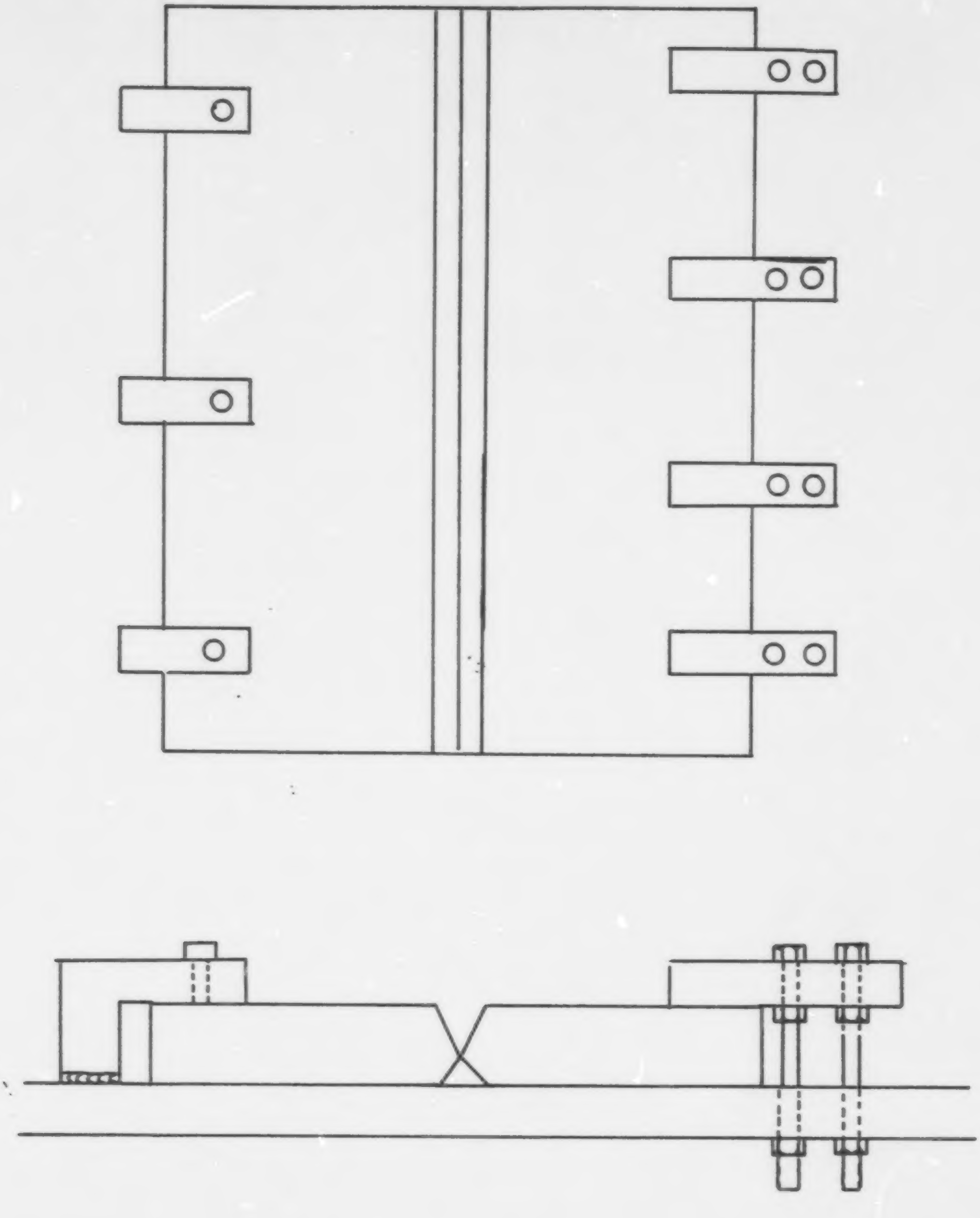

Figure 2.2 Schematic illustration of restraint set up for welds S1-S9

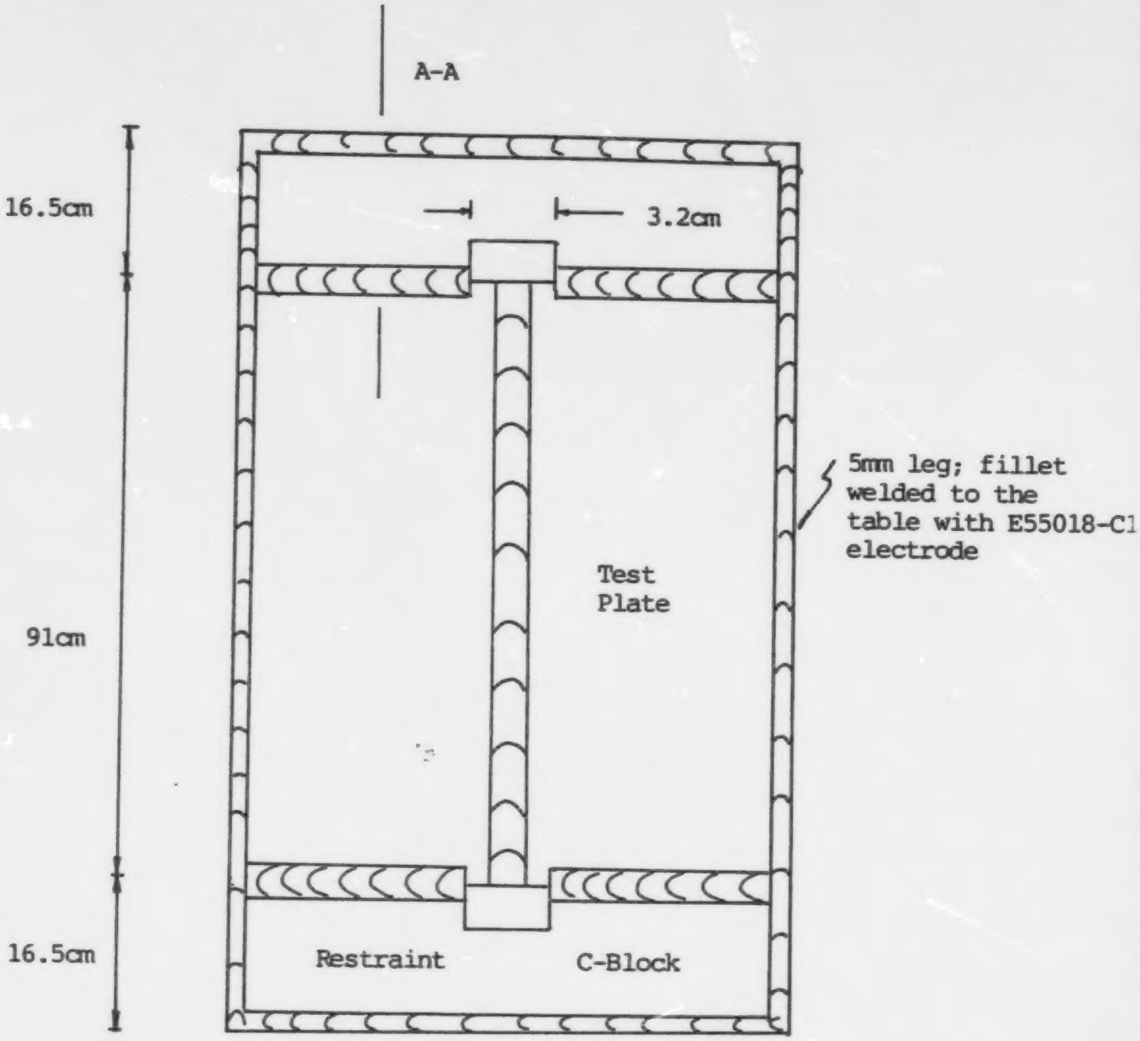
A-A
16.5cm
3.2cm
91cm
16.5cm
Test
Plate
Restraint
C-Block
5mm leg; fillet
welded to the
table with E55018-C1
electrode

(a) Top view

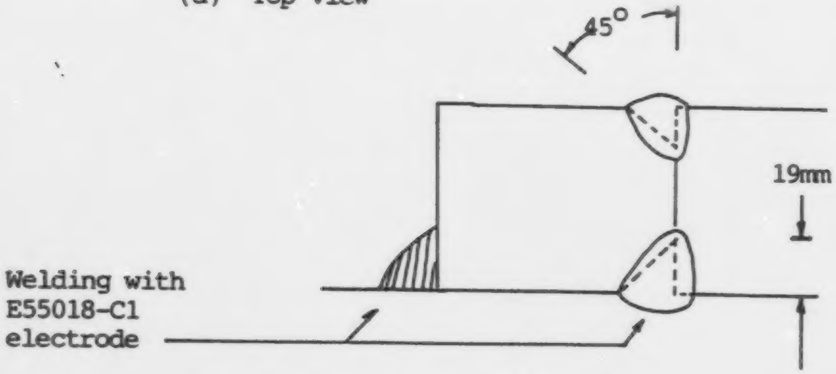
45°
19mm
Welding with
E55018-C1
electrode

(b) Cross section at A-A

Figure 2.3 High angular restraint and high lateral restraint set up for S10

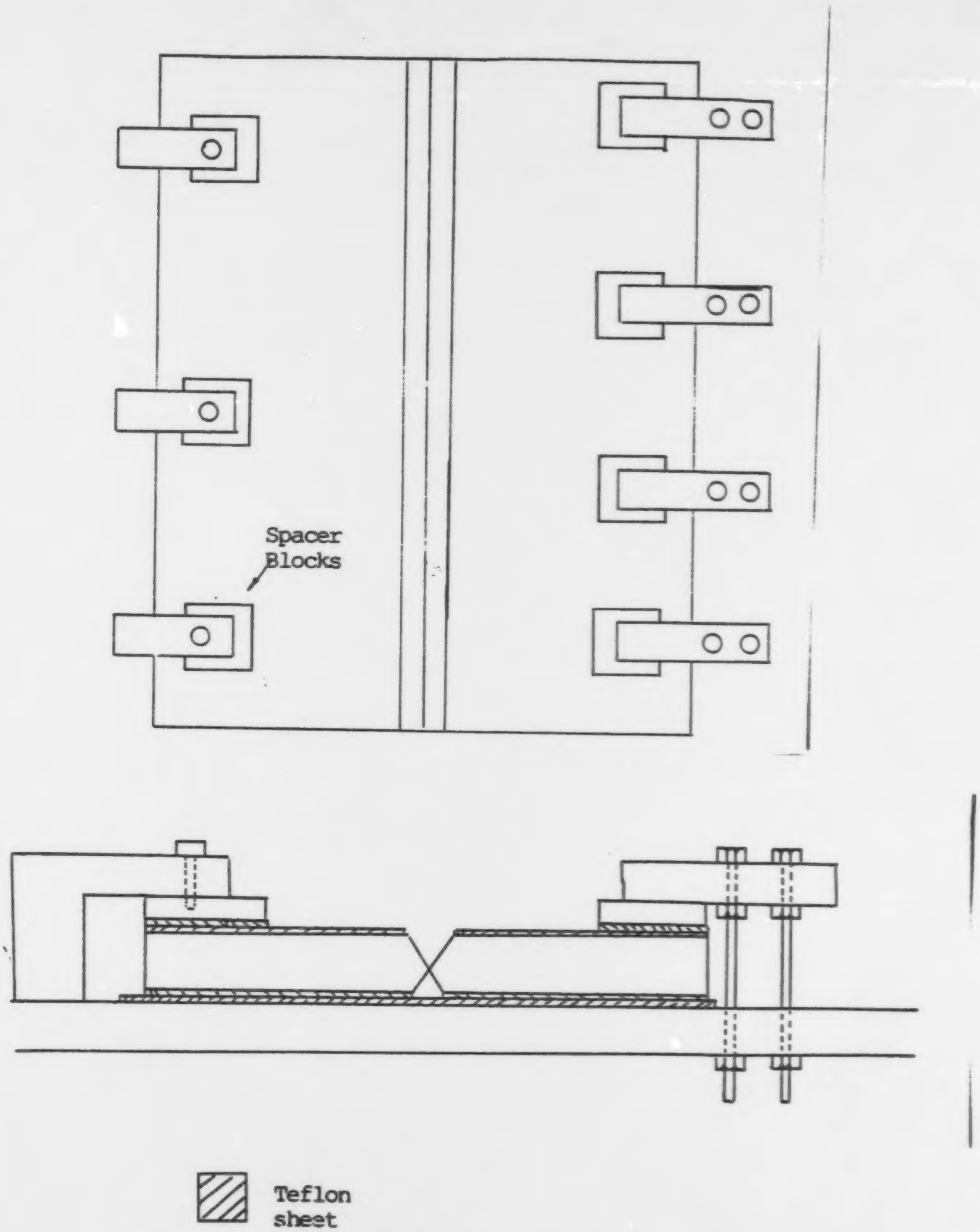
Spacer
Blocks
Teflon
sheet

Figure 2.4 Restraint set up for low lateral and low angular restraint (S11A)

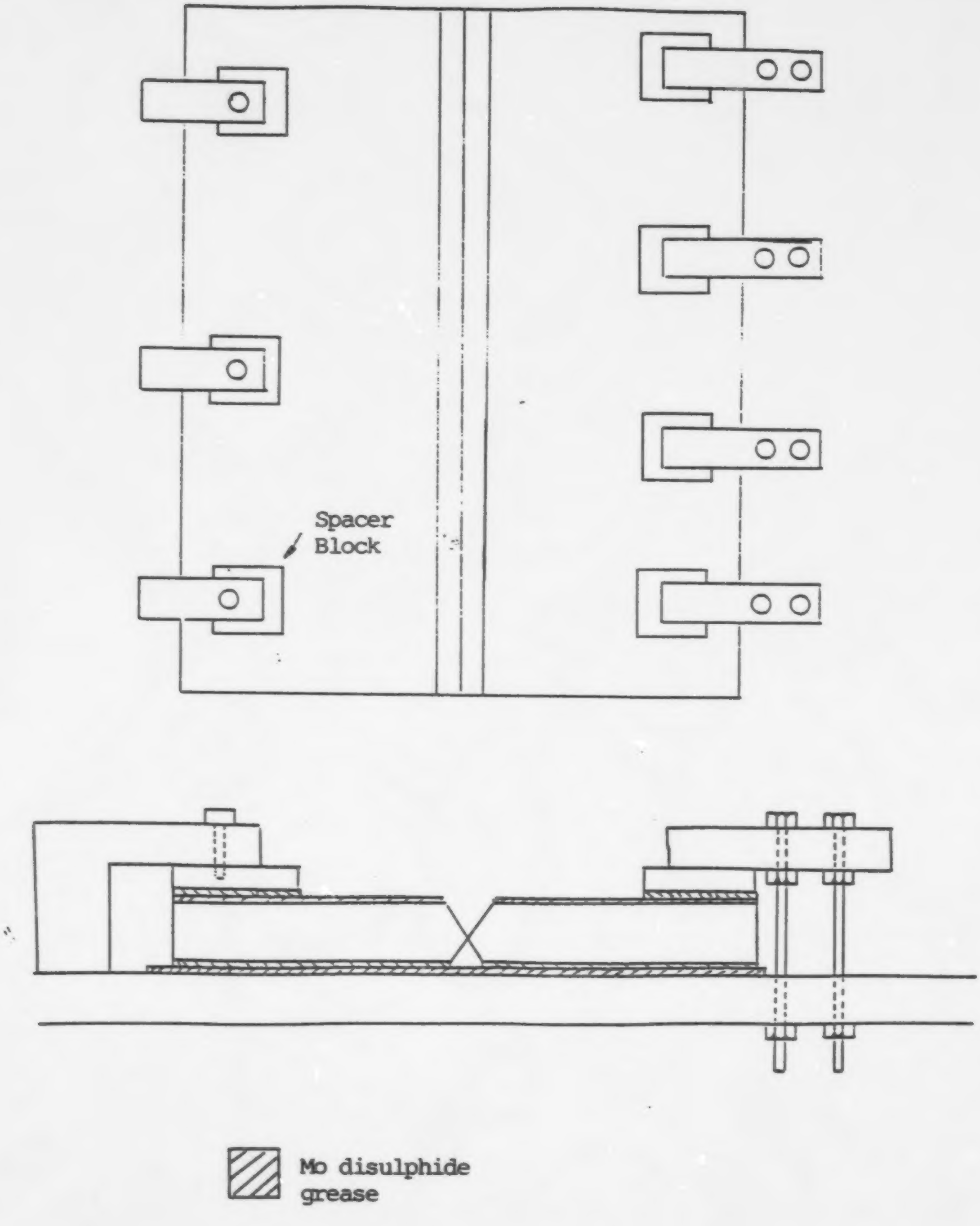
Spacer
Block
▨ Mo disulphide
grease

Figure 2.5 Restraint set up for high angular and low lateral restraint condition (S11B)

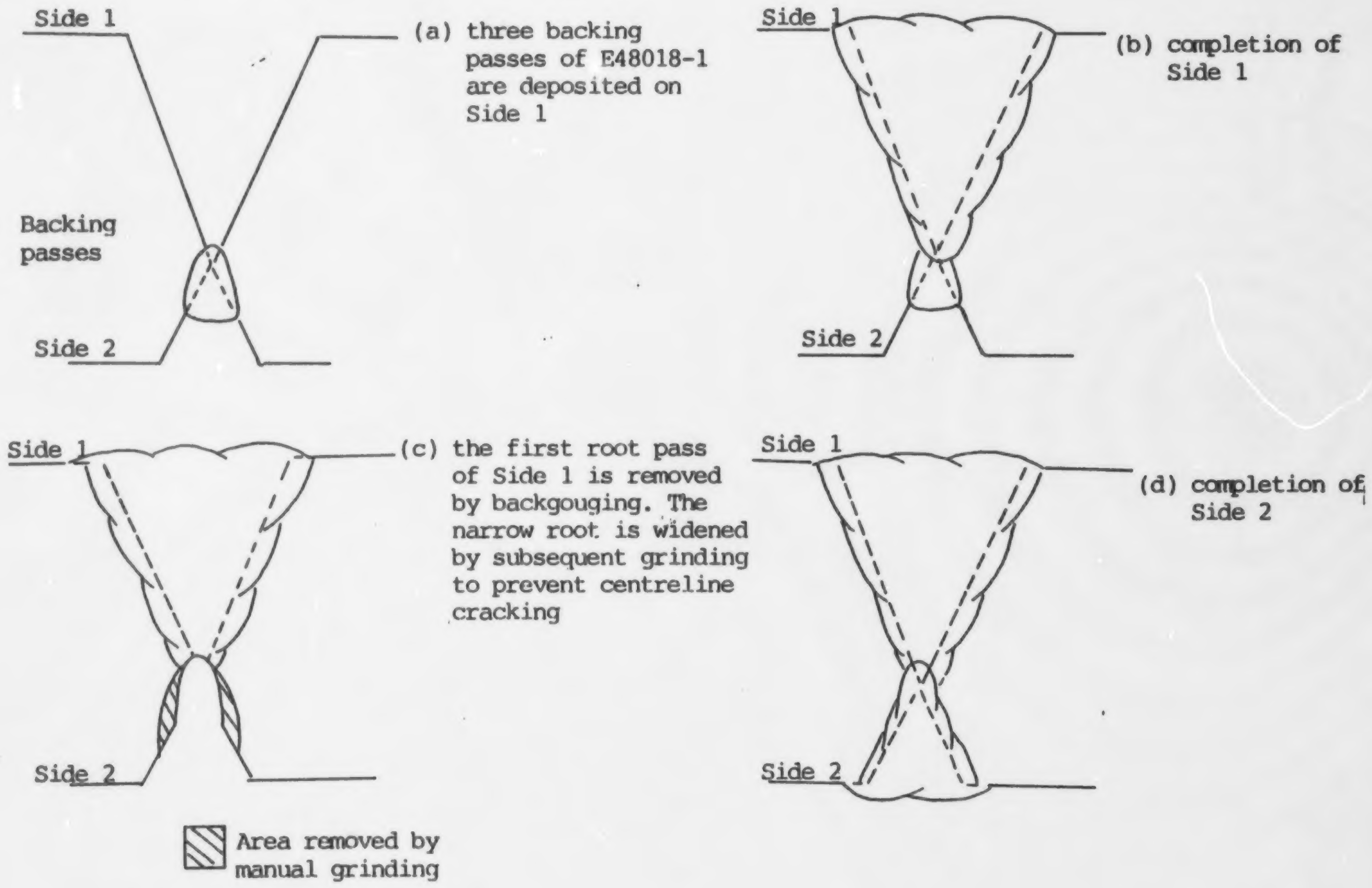

(a) three backing passes of E48018-1 are deposited on Side 1

(b) completion of Side 1

(c) the first root pass of Side 1 is removed by backgouging. The narrow root is widened by subsequent grinding to prevent centreline cracking

(d) completion of Side 2

Side 1
Side 2
Backing passes
Side 1
Side 2
Side 1
Side 2
Side 1
Side 2
▨ Area removed by manual grinding

Figure 2.6 Schematic representation of welding sequence

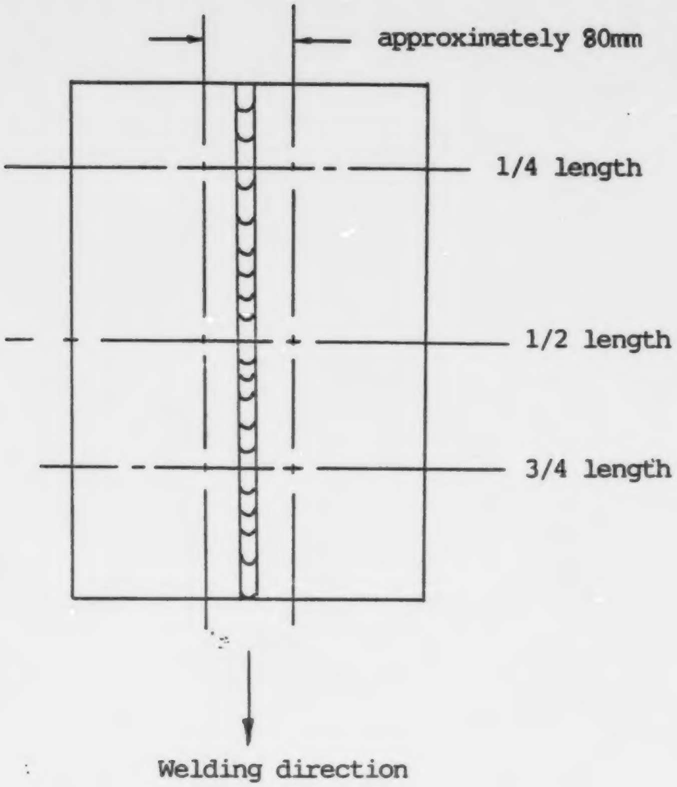
approximately 80mm
1/4 length
1/2 length
3/4 length
Welding direction

(a) Top View

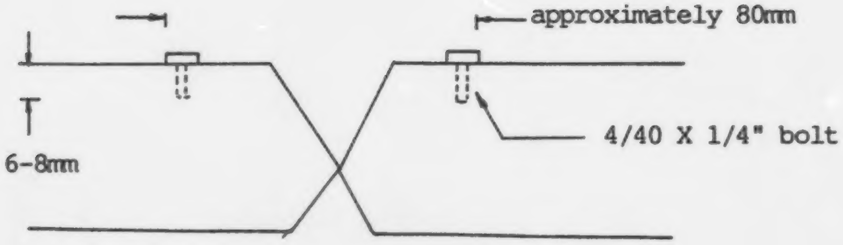
approximately 80mm
4/40 X 1/4" bolt
6-8mm

(b) Side View

Figure 2.7 Reference points for shrinkage measurements

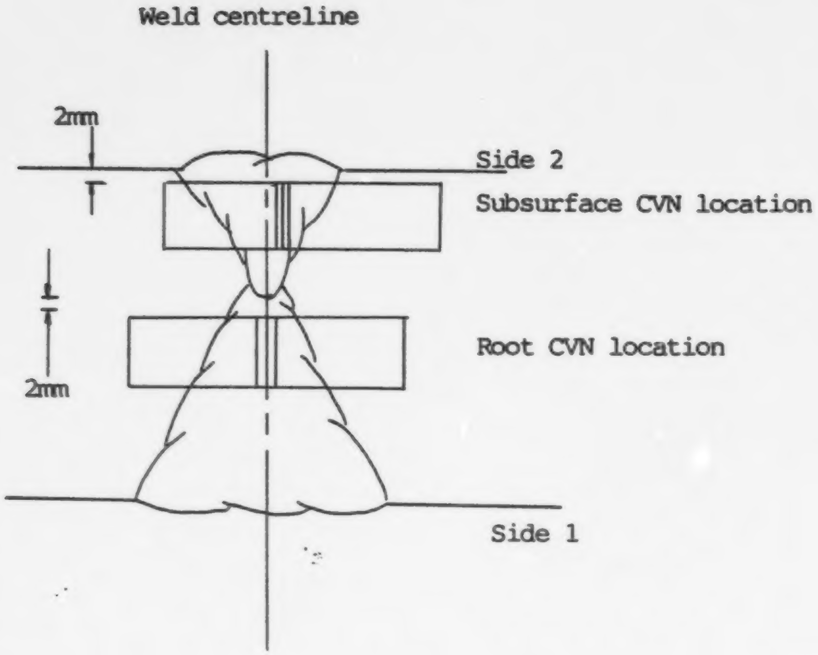
Weld centreline
2mm
Side 2
Subsurface CVN location
Root CVN location
2mm
Side 1

Figure 2.8 Extraction of CVN specimens

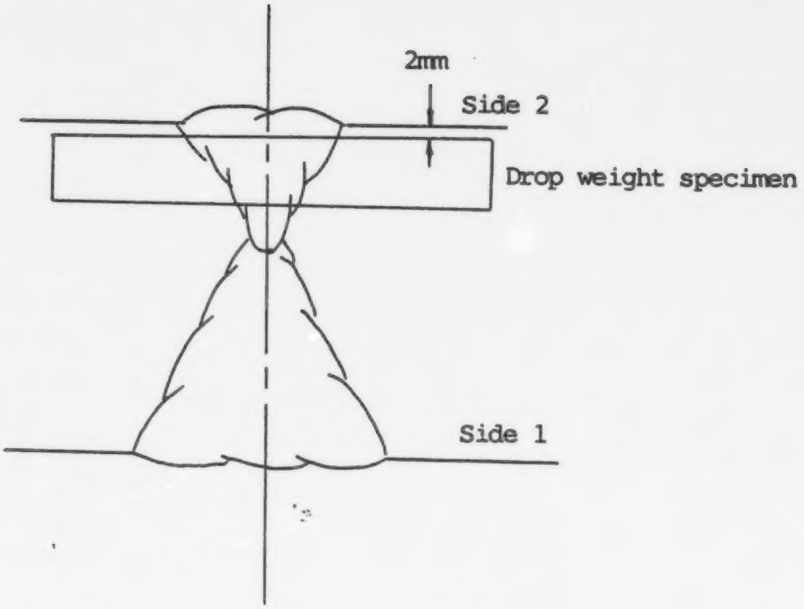
2mm
Side 2
Drop weight specimen
Side 1

Figure 2.9 Location of extraction of drop weight P-2 Specimens

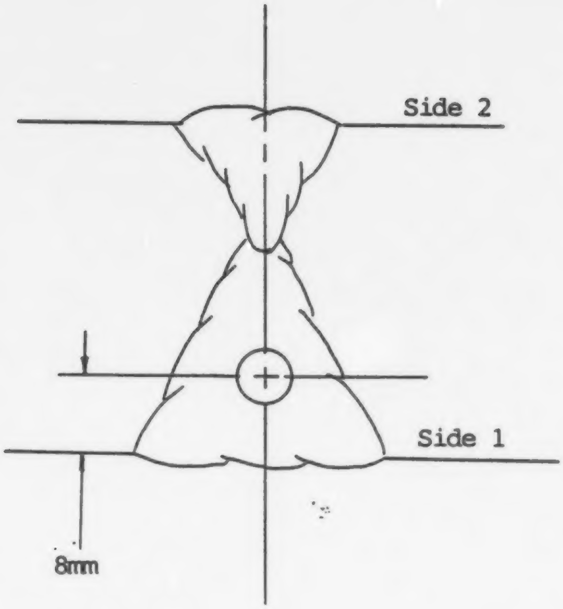
Side 2
Side 1
8mm

Figure 2.10 All weld metal round tensile specimens

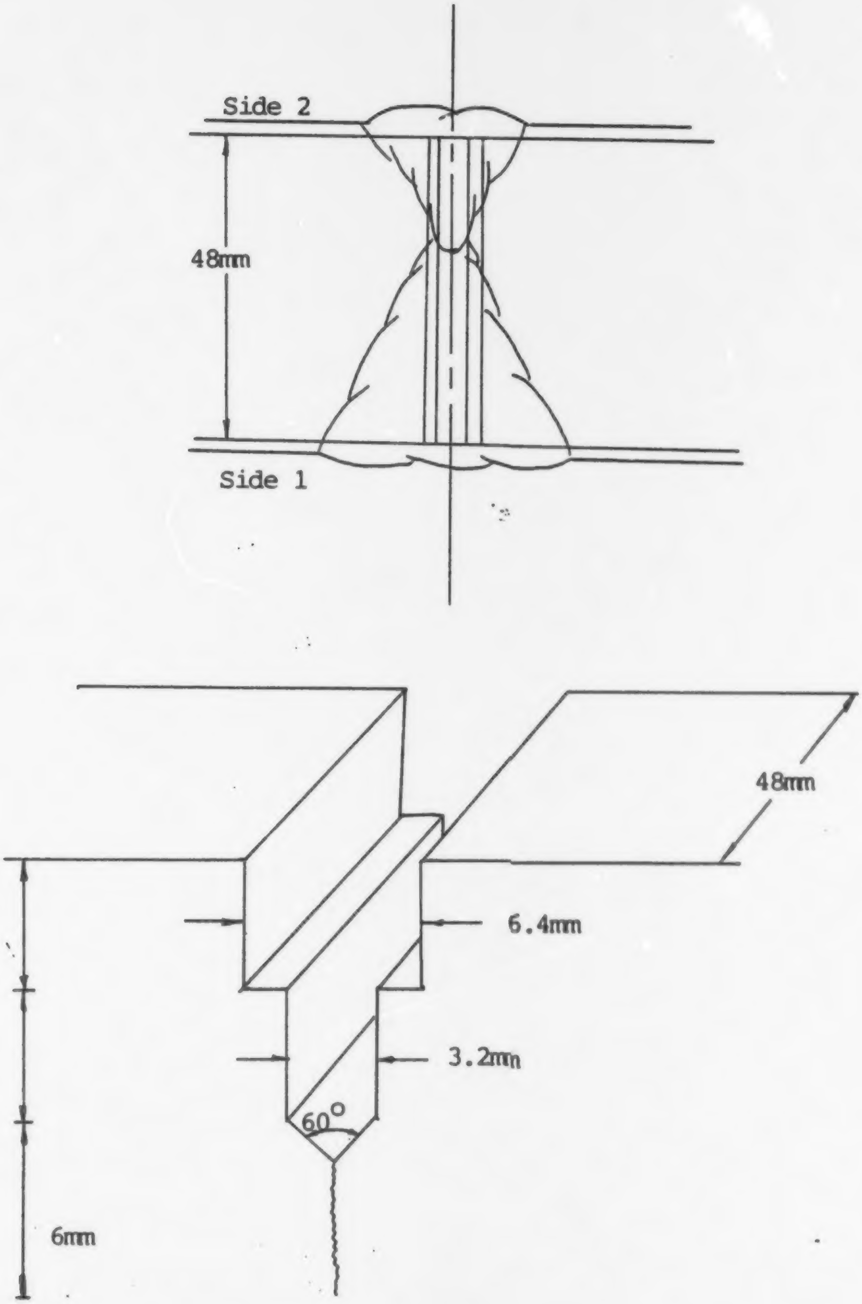
Side 2
48mm
Side 1
48mm
6.4mm
3.2mm
60°
6mm

Figure 2.11 CTOD specimens

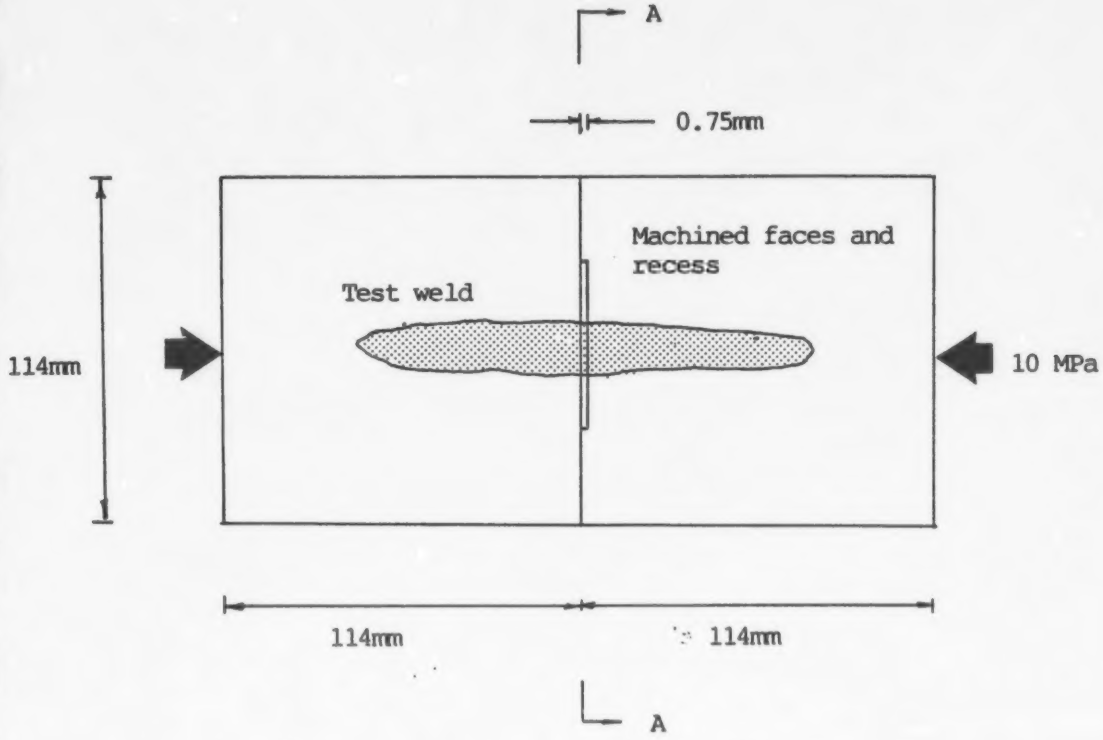
A
0.75mm
Machined faces and recess
Test weld
114mm
10 MPa
114mm
114mm
A

(a) Top view

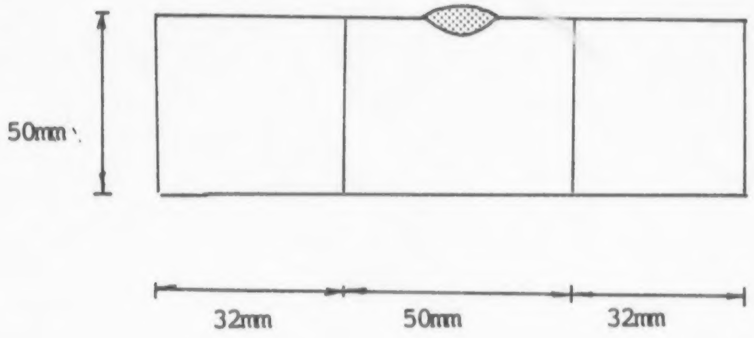
50mm
32mm
50mm
32mm

(b) Section A-A

Figure 2.12 G-BOP test specimens

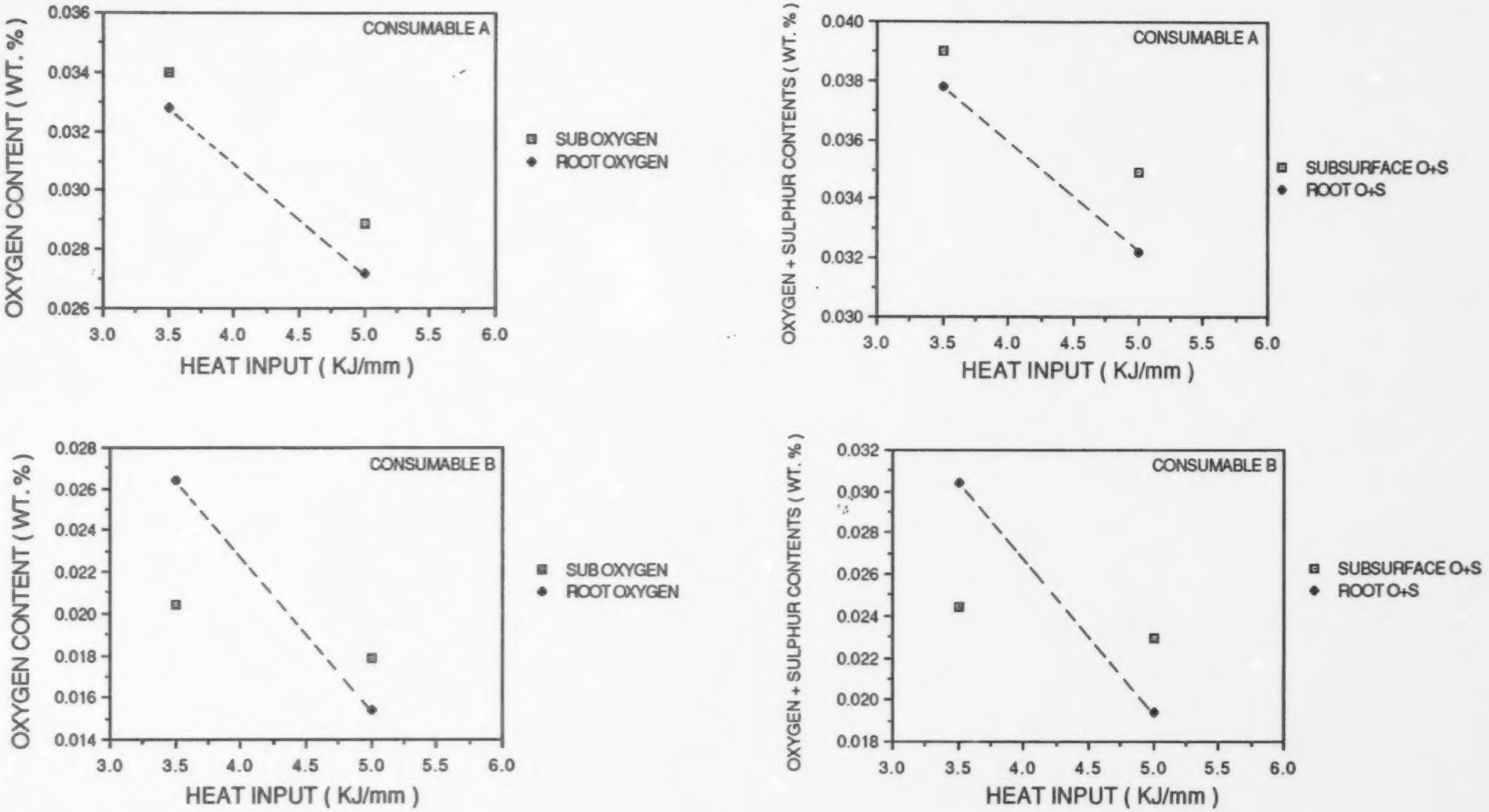

Figures 3.1 Effect of heat input on oxygen and O+S contents for both consumables

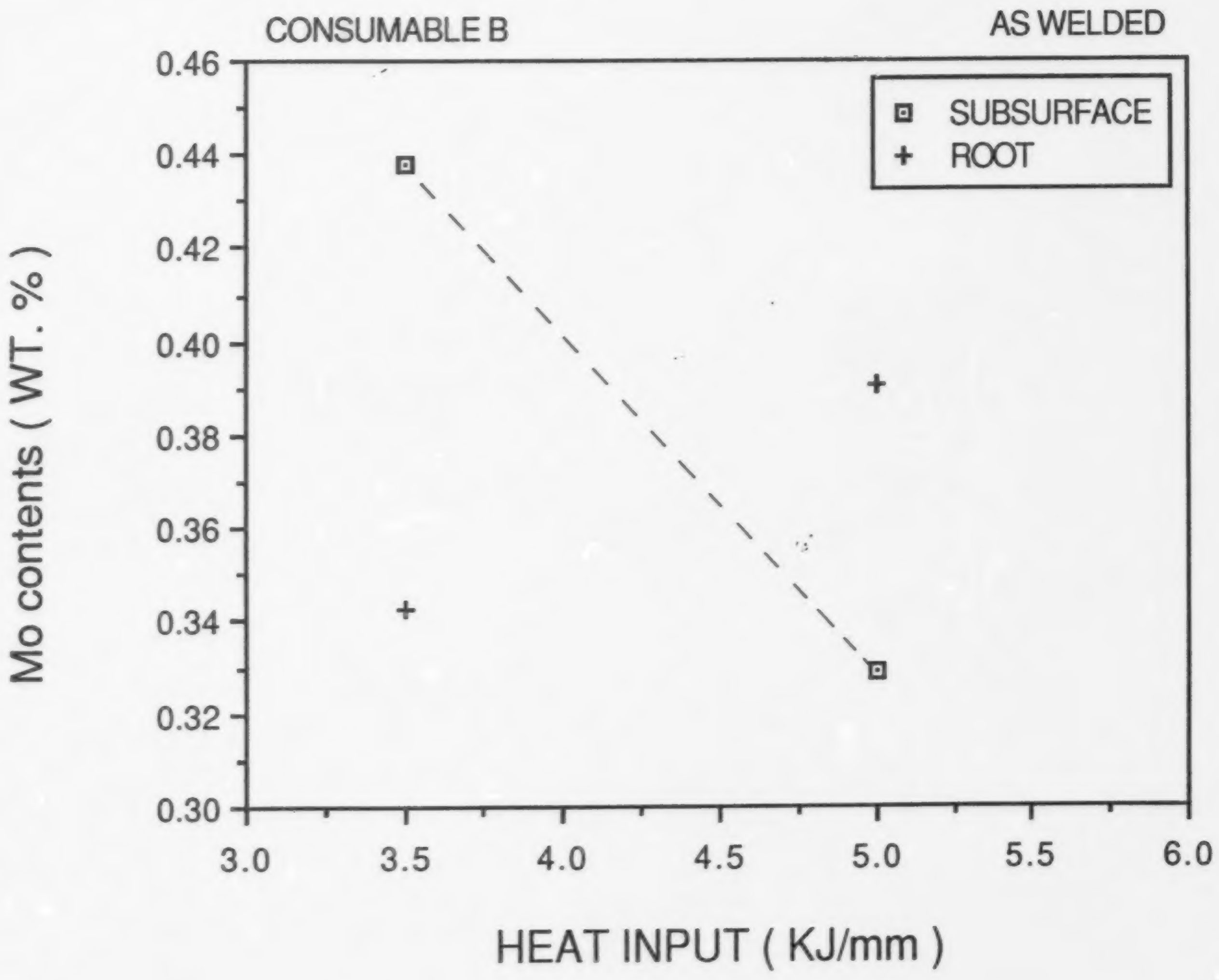

Figure 3.2 Effect of heat input on Mo contents of Consumable B

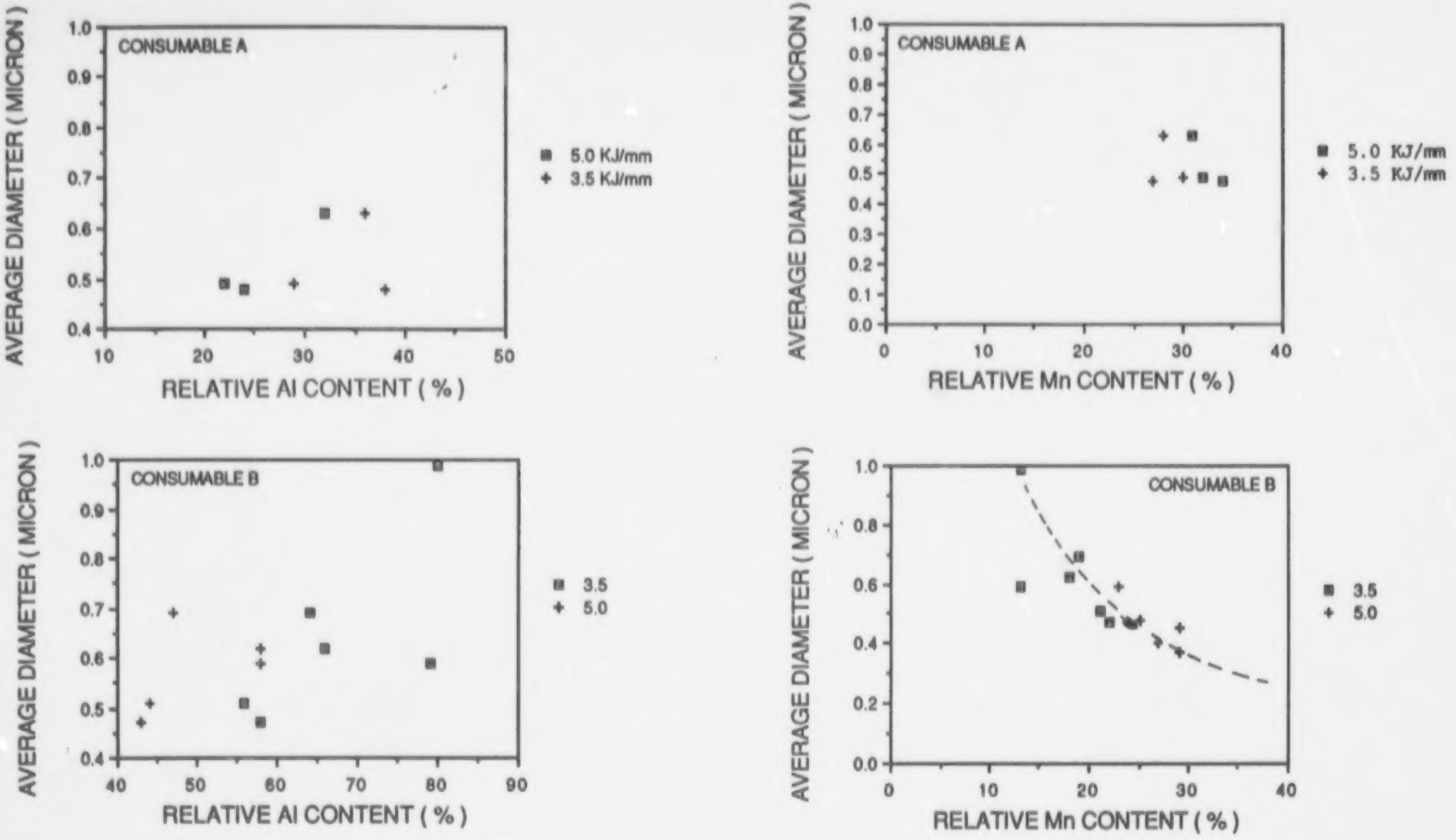

Figure 3.3 The effect of relative contents of Al and Mn in inclusions on the average diameter of dominant inclusions

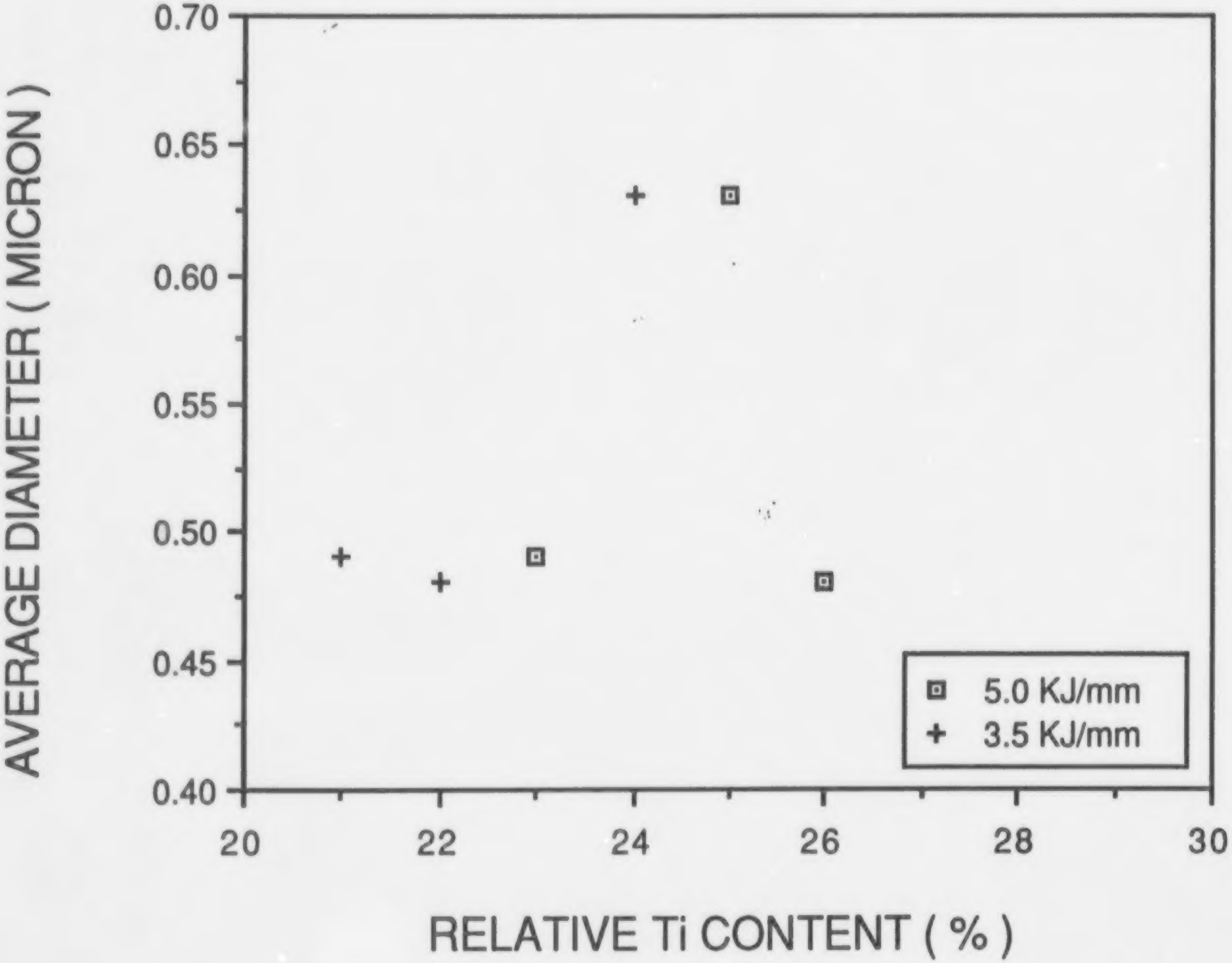

Figure 3.4 For the dominant inclusions found in welds of Consumable A, although the relative Ti content increases with larger heat input, there is little change in inclusion diameter

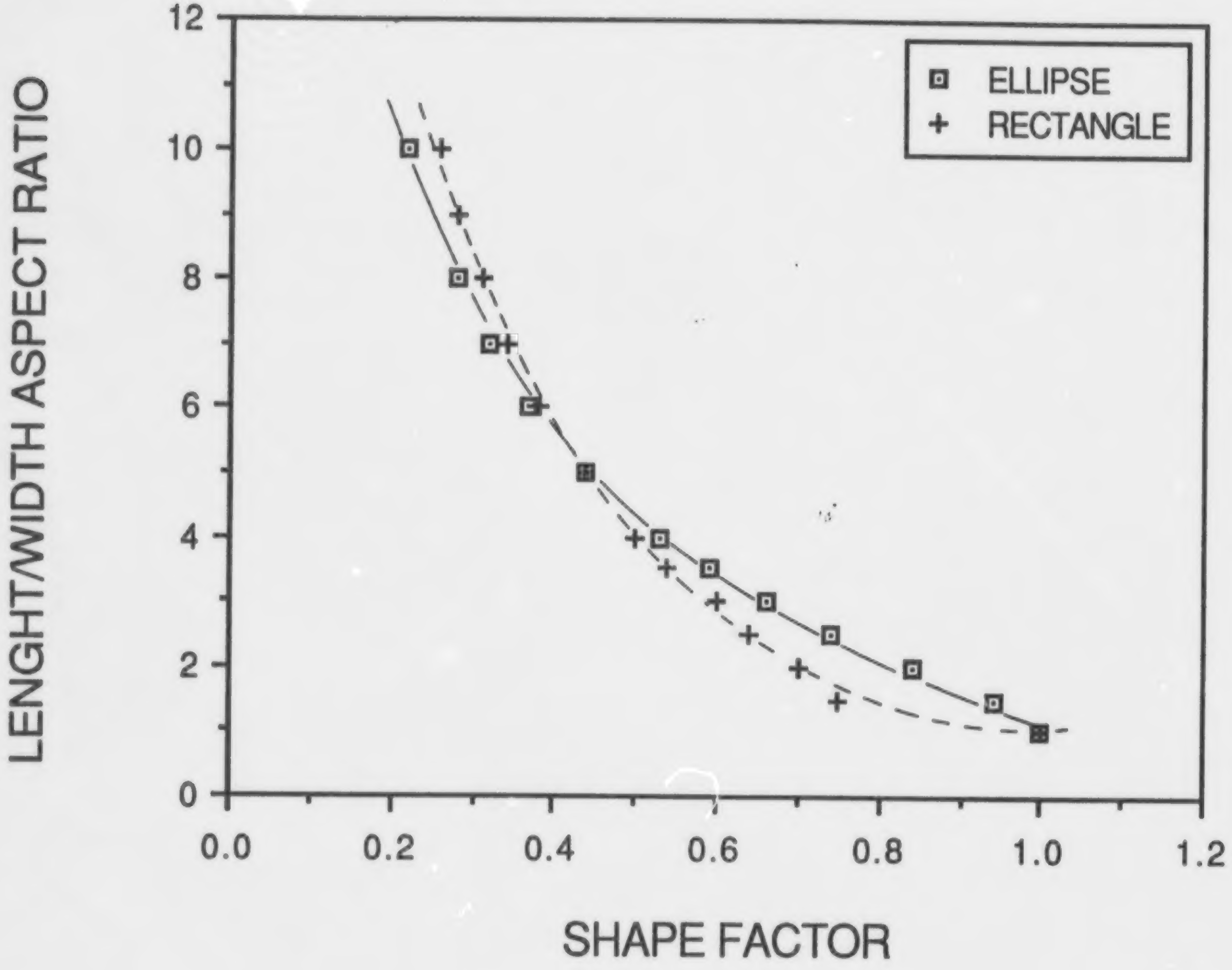

Figure 3.5 The length/width aspect ratio developed from shape factor

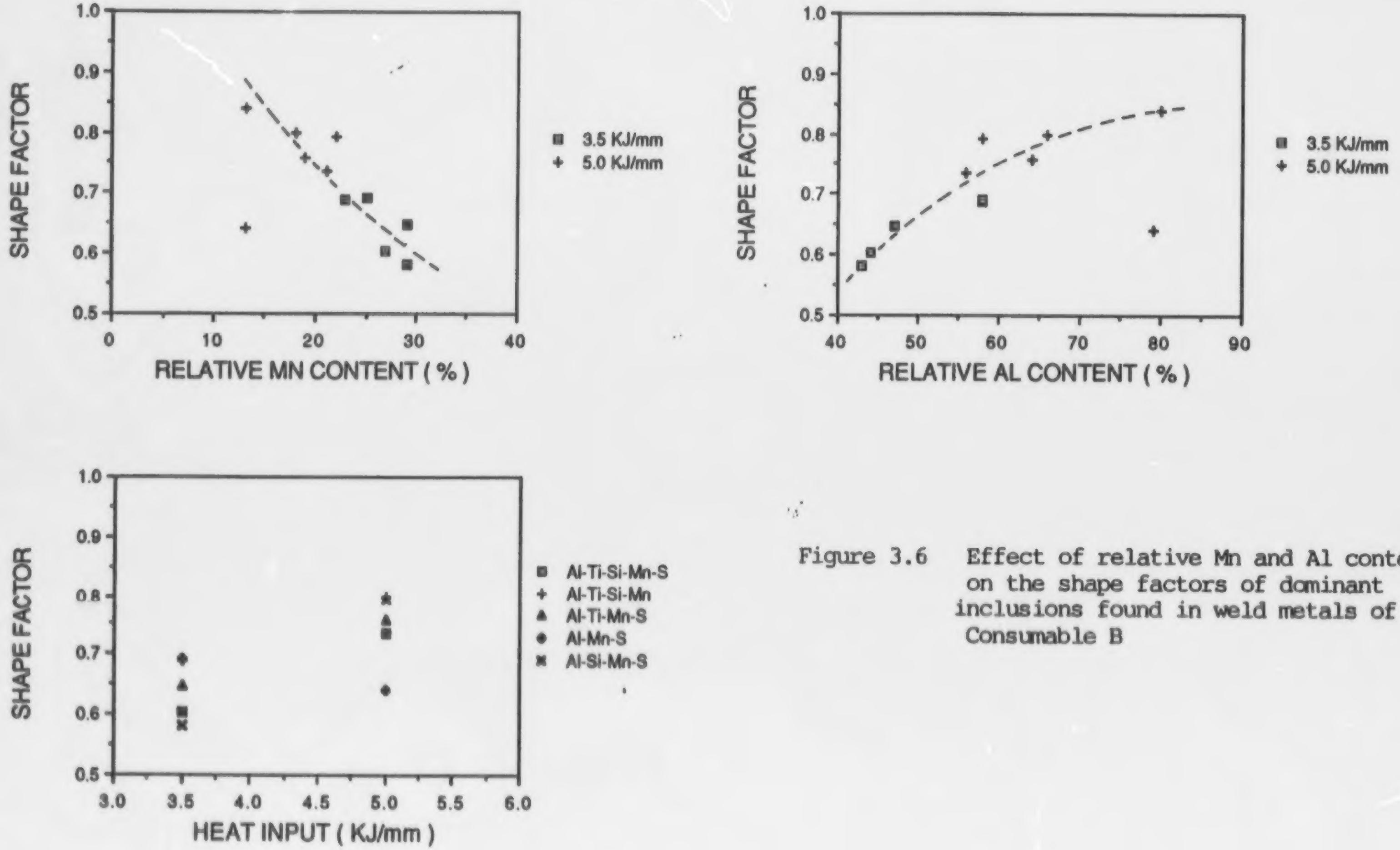

Figure 3.6 Effect of relative Mn and Al contents on the shape factors of dominant inclusions found in weld metals of Consumable B

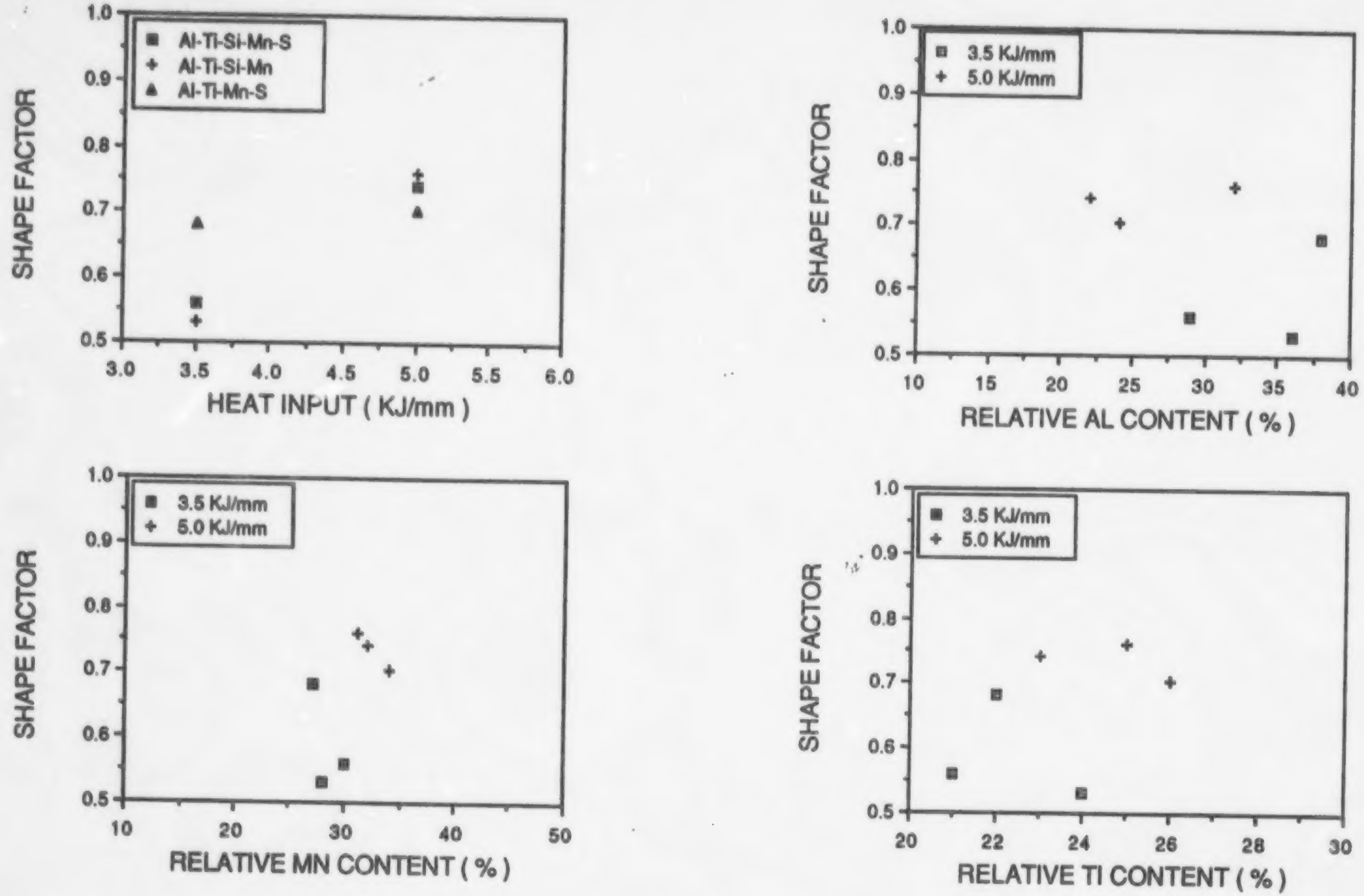

Figure 3.7 For Consumable A, there is no trend relating the relative alloy contents with the inclusion shape factor

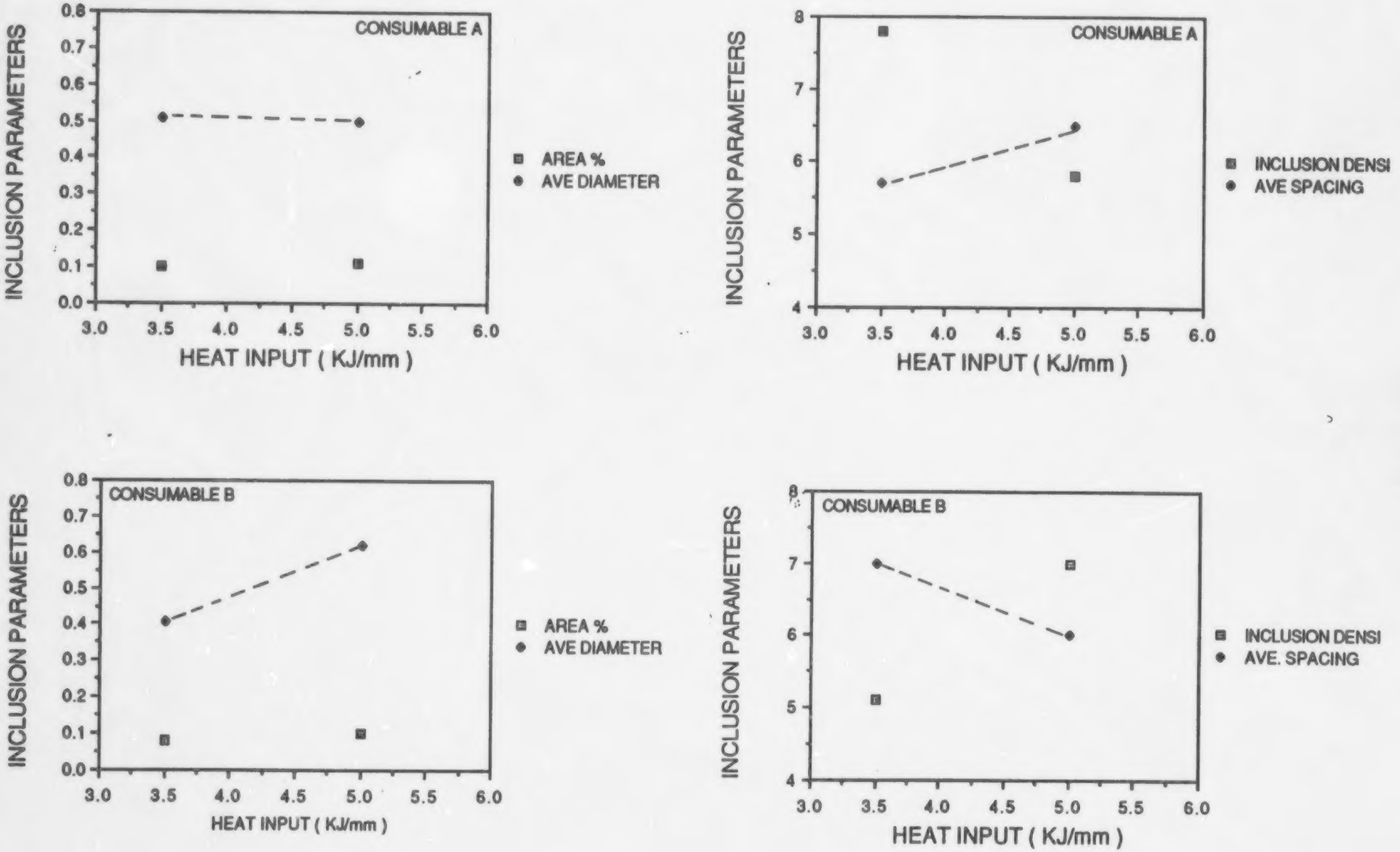

Figure 3.8 The effect of heat input on inclusion characteristics (the units for area fraction are %; microns for average diameter and spacings; and X $10^5/cm^2$ for density)

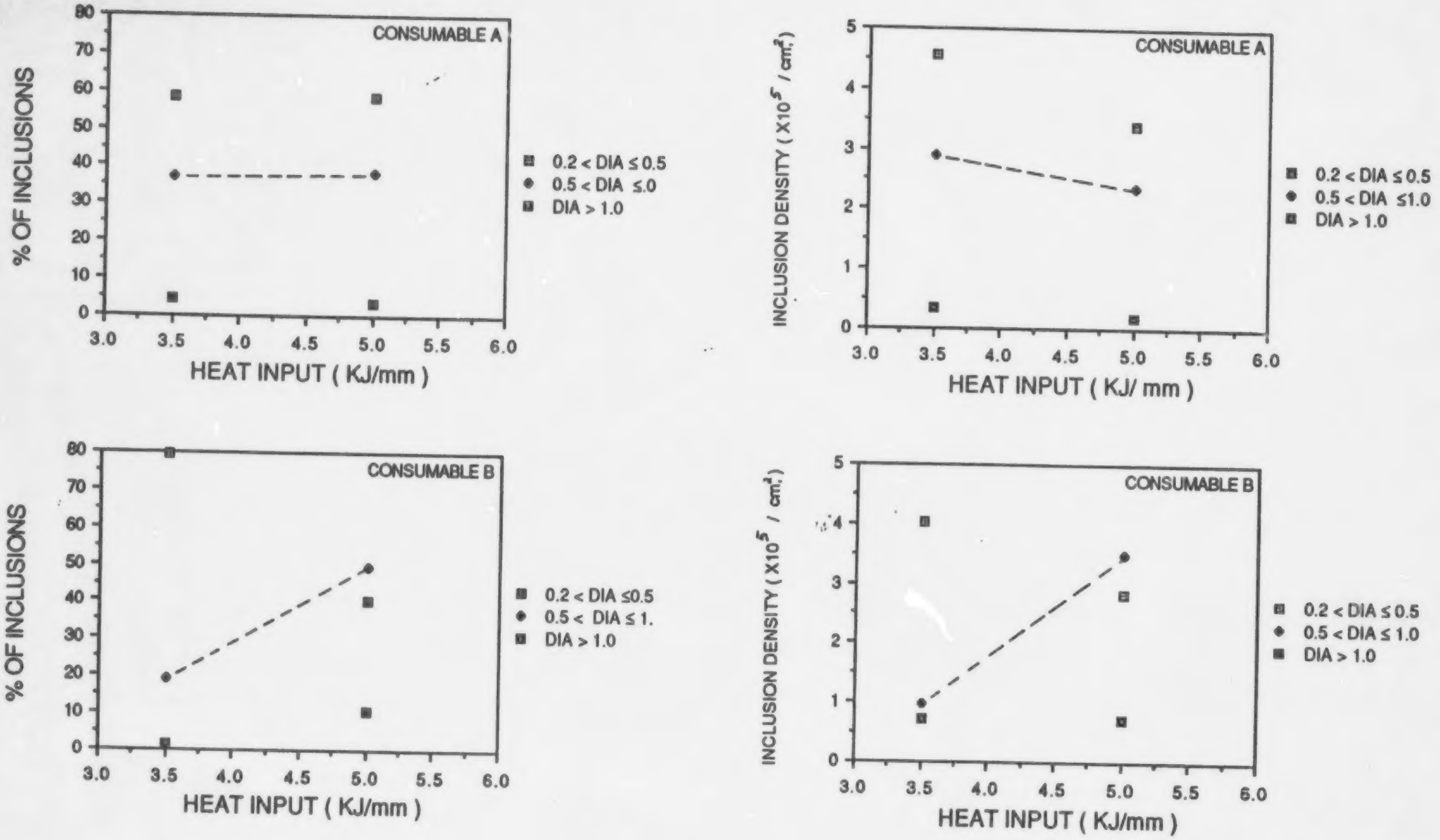

Figure 3.9 Variation of inclusion size grouping with heat input

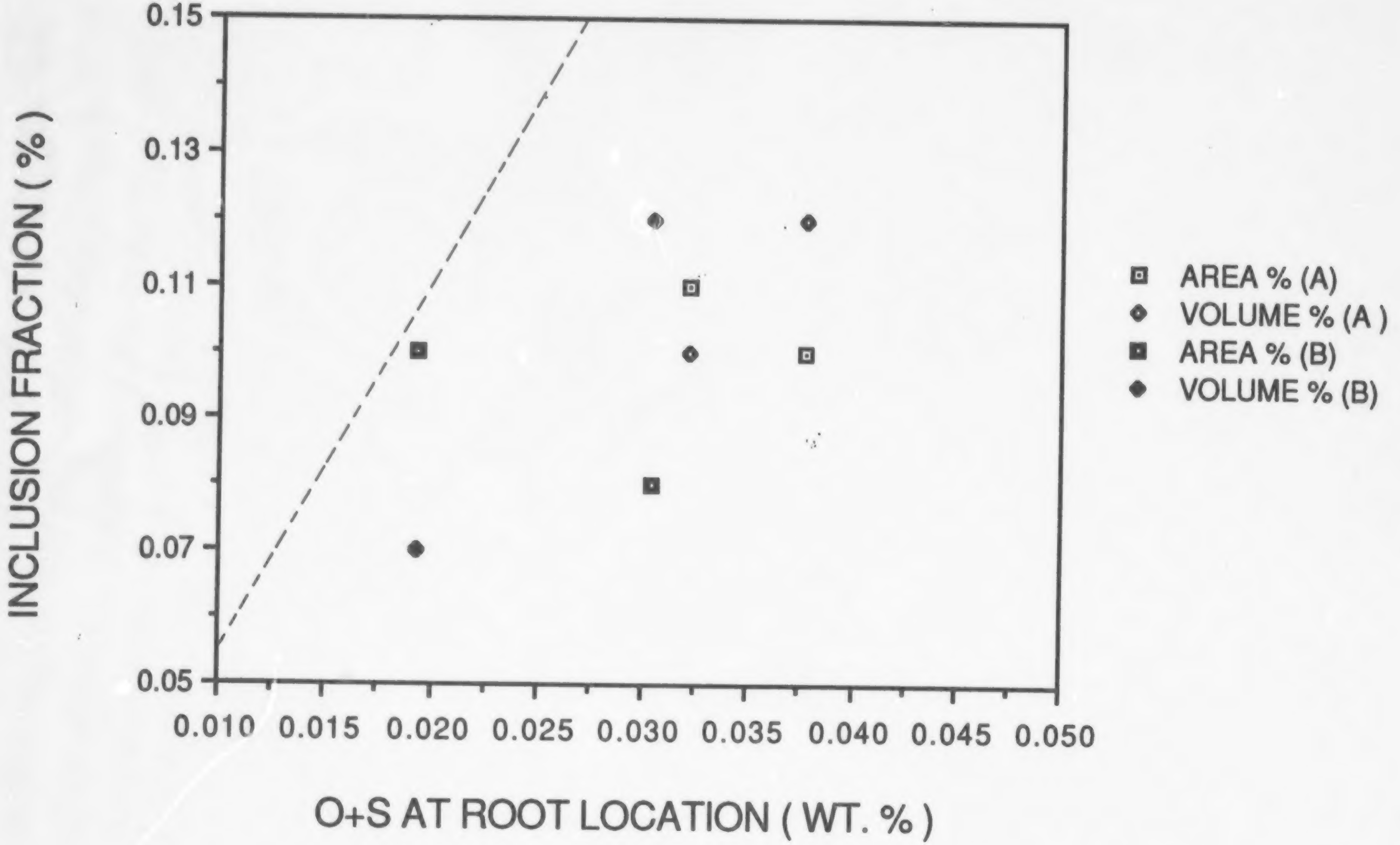

Figure 3.10 Effect of O+S on inclusion volume and area fractions

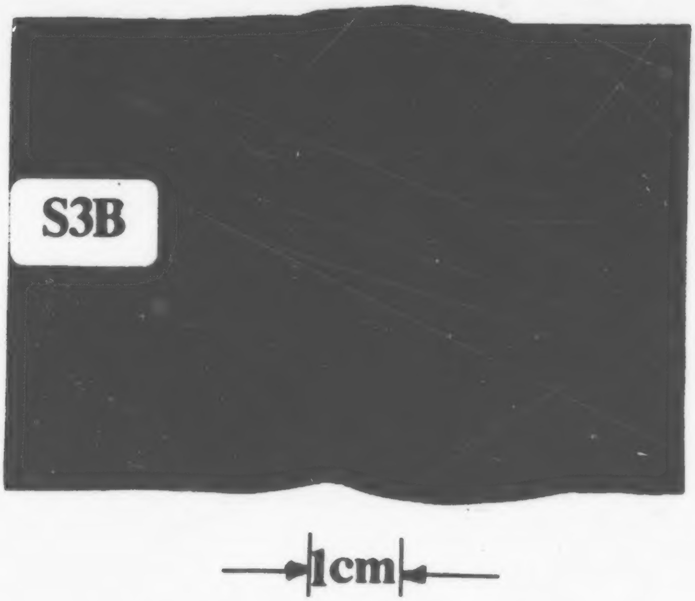

Figure 3.11 Macrograph of 3.5 kJ/mm weld of Consumable A in as-welded condition (S3B) (1.3X, Neg. 9974)

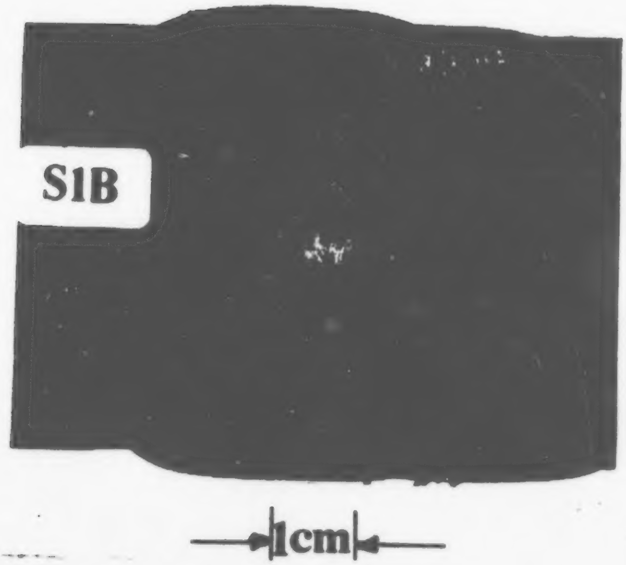

Figure 3.12 Macrograph of 5.0 kJ/mm weld of Consumable A in as-welded condition (S1B) (1.3X, Neg. 9951)

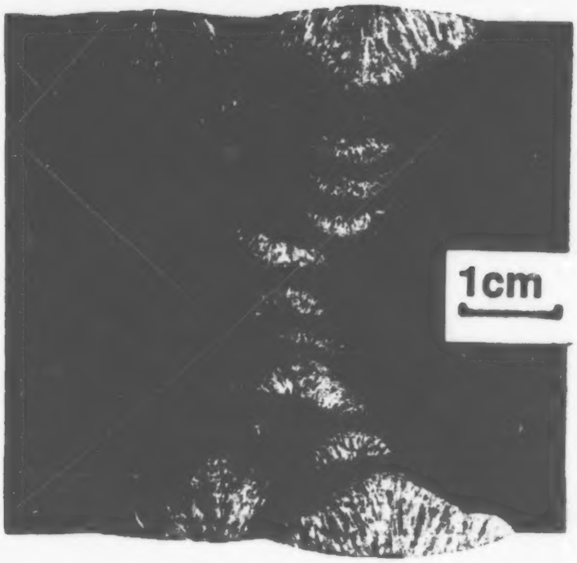

Figure 3.13 Macrograph of 3.5 kJ/mm weld of Consumable A in stress relieved condition (S4A) (1.5X, Neg. 11162)

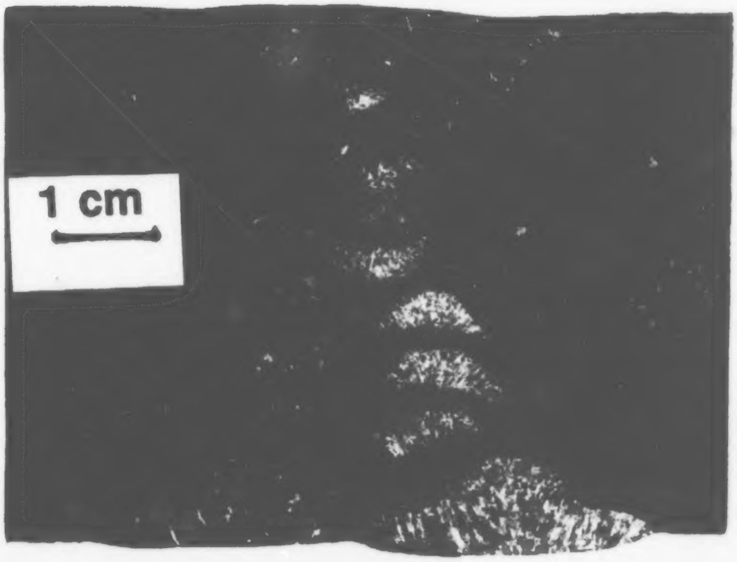

Figure 3.14 Macrograph of 5.0 kJ/mm weld of Consumable A in stress relieved condition (S2A) (1.5X, Neg. 11164)

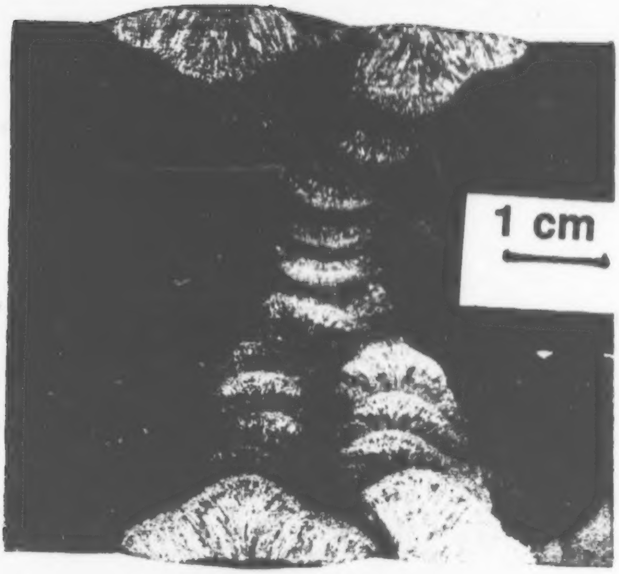

Figure 3.15 Macrograph of 3.5 kJ/mm of Consumable A, with interpass temperature of 232°C, in as-welded condition (S9A) (1.5X, Neg. 11165)

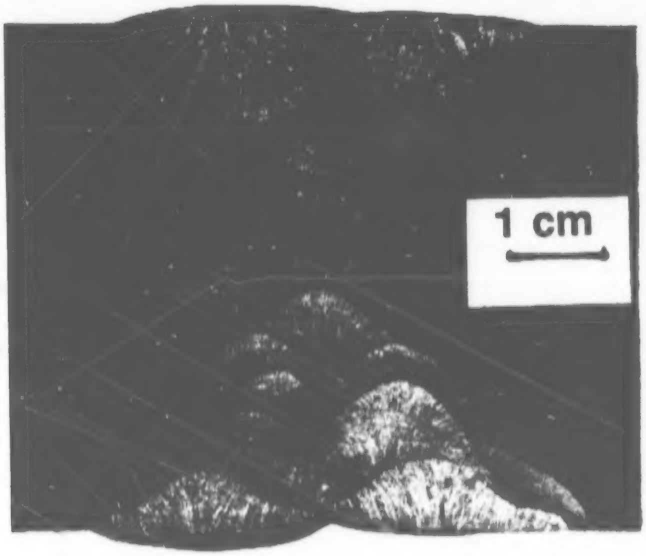

Figure 3.16 Macrograph of 3.5 kJ/mm weld of Consumable B in as-welded condition (S7A) (1.5X, Neg. 11167)

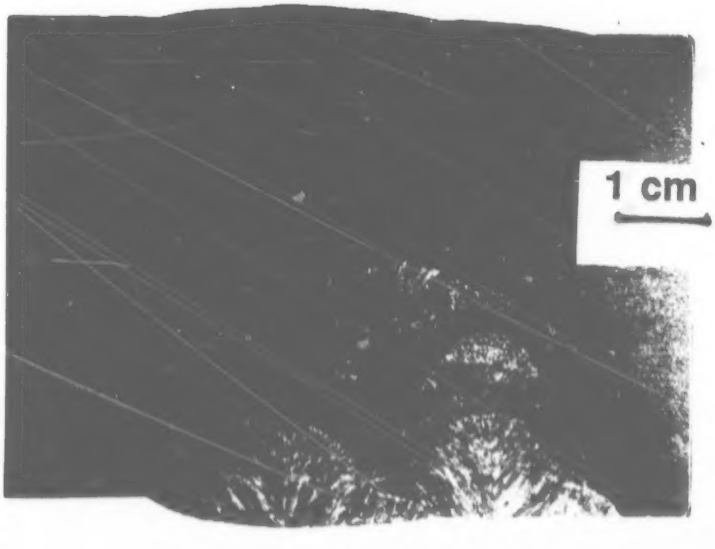

Figure 3.17 Macrograph of 5.0 kJ/mm weld of Consumable B in as-welded condition (S5A) (1.5X, Neg. 11161)

Figure 3.18 Macrograph of 3.5 kJ/mm weld of Consumable B in stress relieved condition (S8A) (1.5X, Neg. 11166)

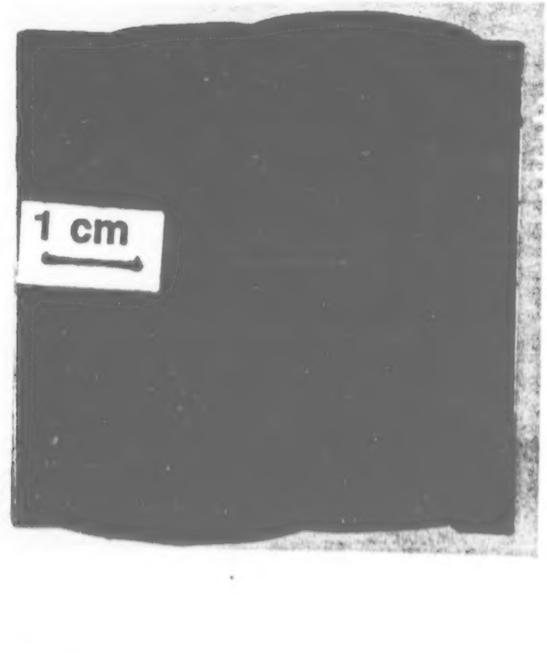

Figure 3.19 Macrograph of 5.0 kJ/mm weld of Consumable B in stress relieved condition (S6A) (1.5X, Neg. 11270)

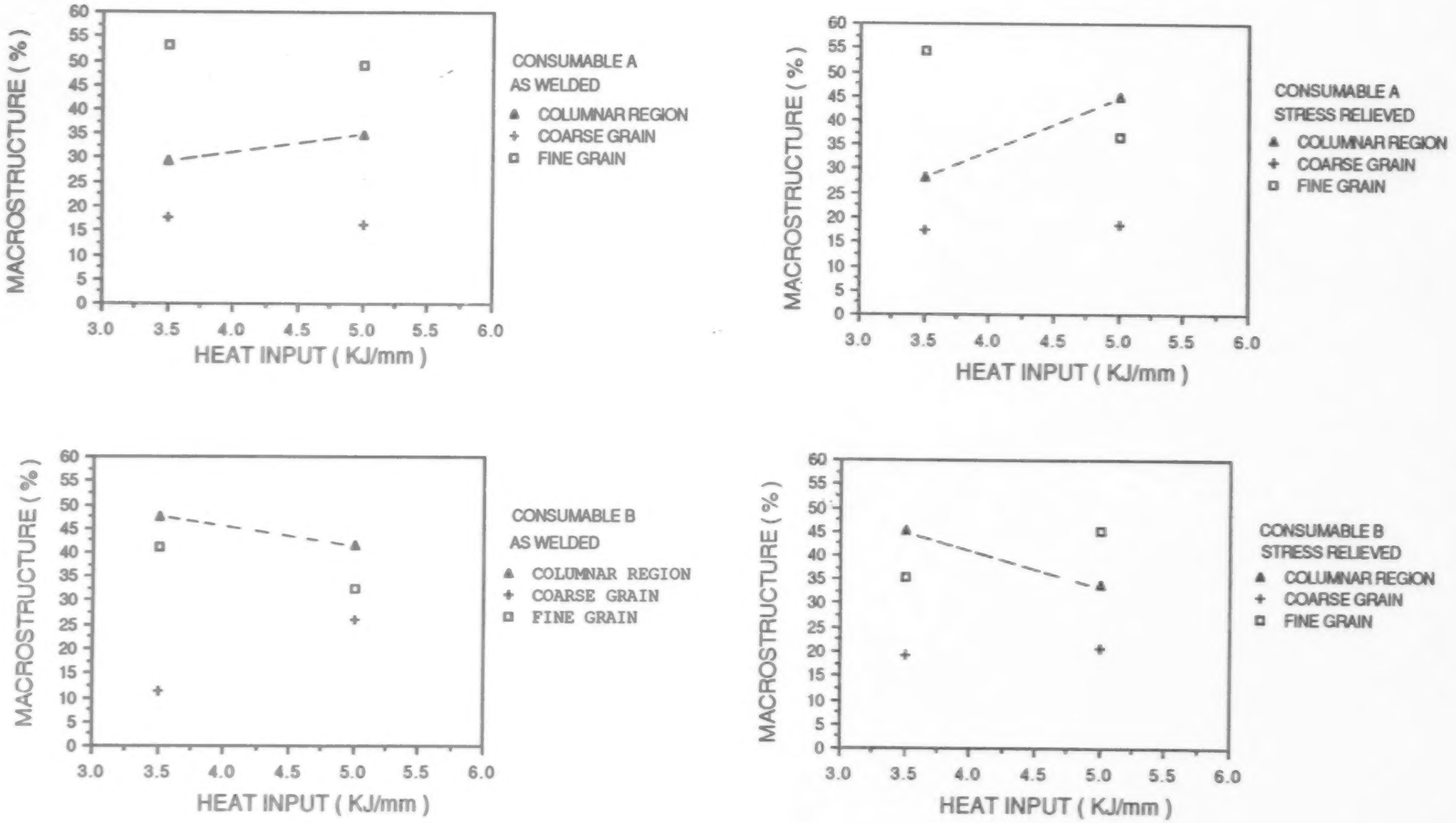

Figure 3.20 Variation of centreline macrostructure with heat input

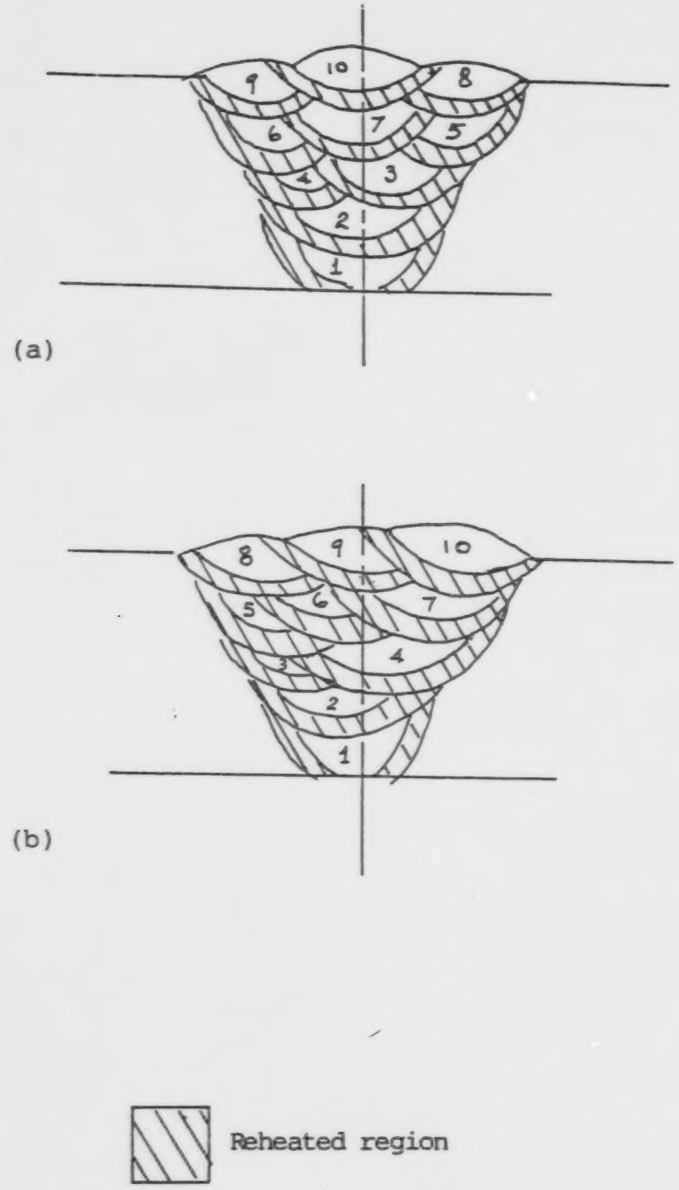
10
9
8
7
6
5
4
3
2
1
(a)
8
9
10
5
6
7
3
4
2
1
(b)
▨ Reheated region

Figure 3.21 Different bead position and sequence can lead to higher proportions of as deposited columnar macrostructure in (a)

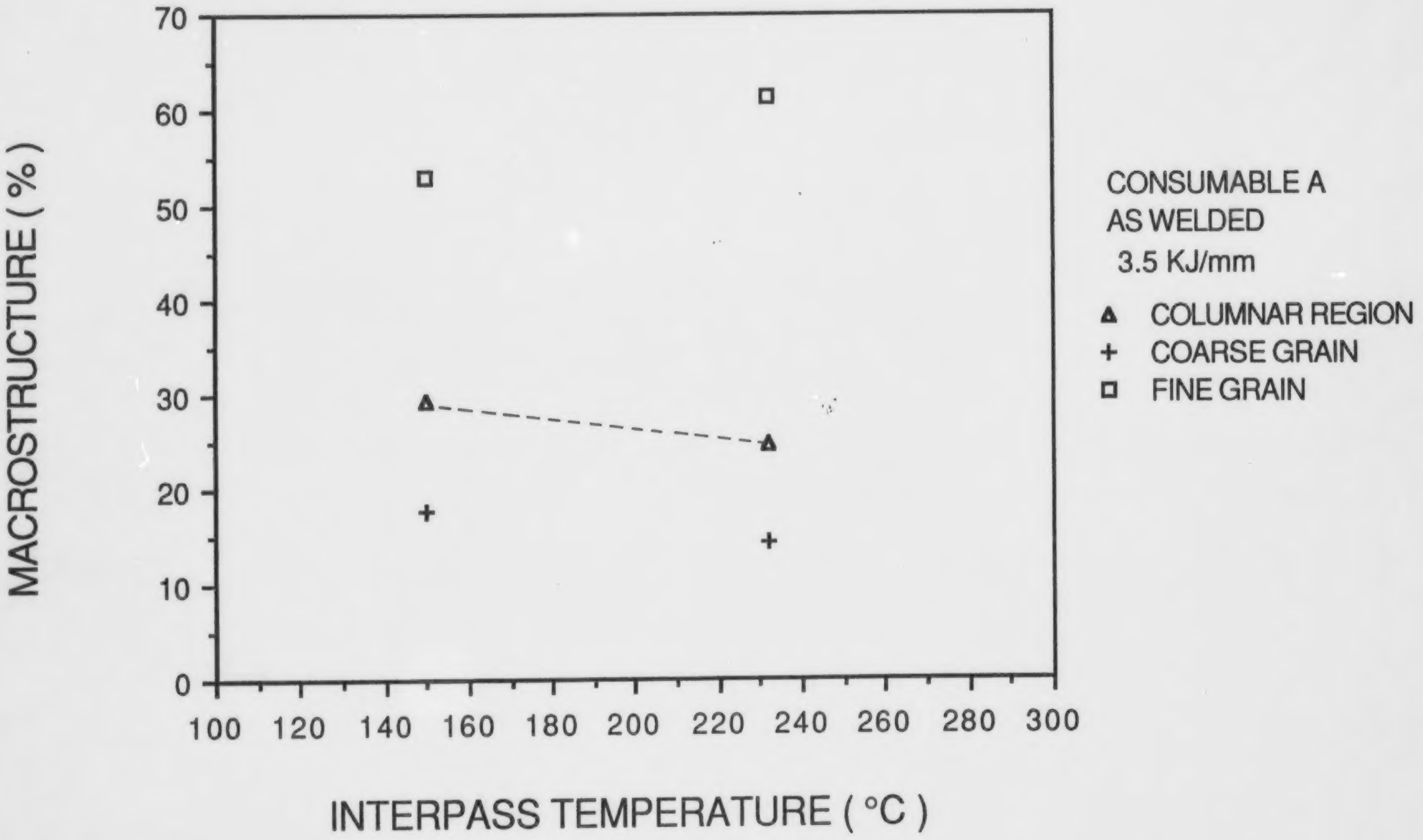

Figure 3.22 Effect of interpass temperature on centreline macrostructure distribution

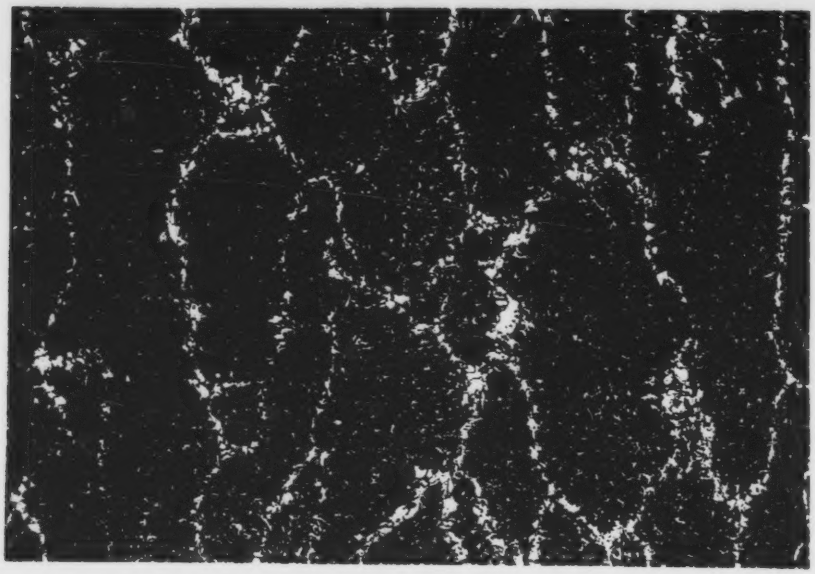

Figure 3.23 Micrograph of last deposited bead in as-welded 3.5 kJ/mm weld of Consumable A (S3A) (100X, Neg. 9954)

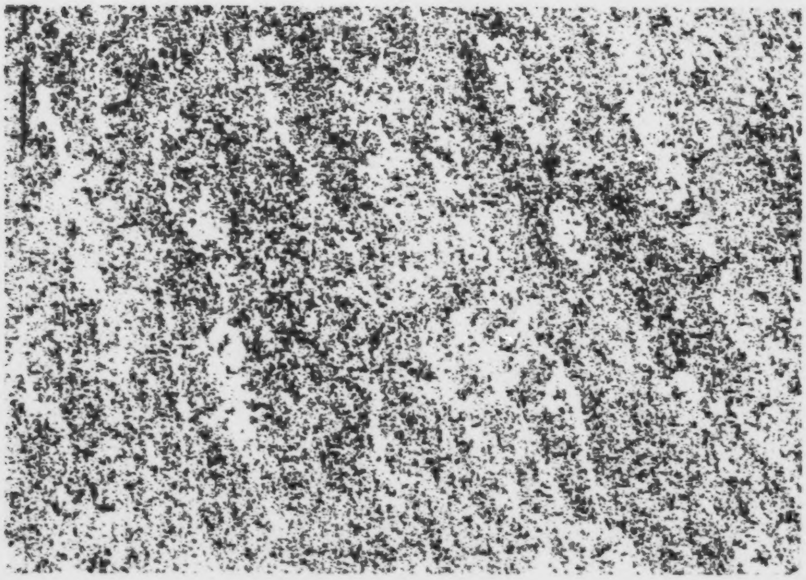

Figure 3.24 Micrograph of last deposited bead in as-welded 5.0 kJ/mm weld of Consumable A (S1A) (100X, Neg. 9956)

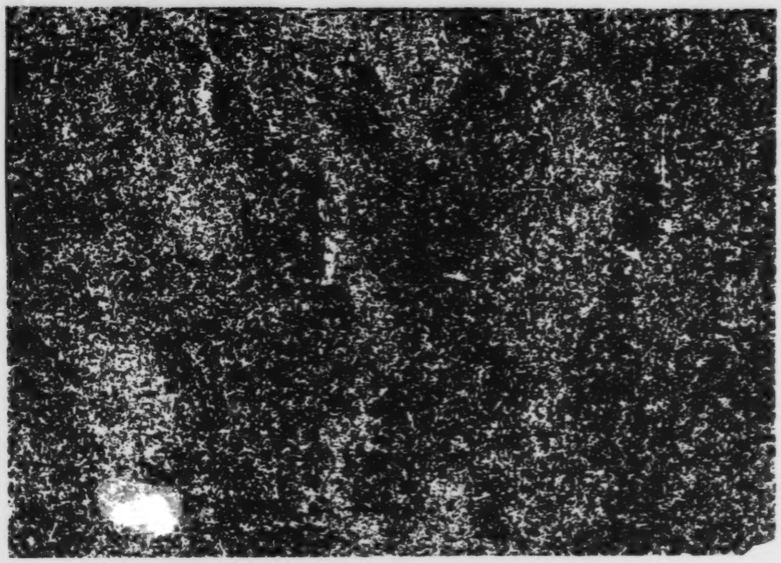

Figure 3.25 Micrograph of as-welded 3.5 kJ/mm weld of Consumable B depicts the lack of grain boundary ferrite (S7A) (100X, Neg. 9941)

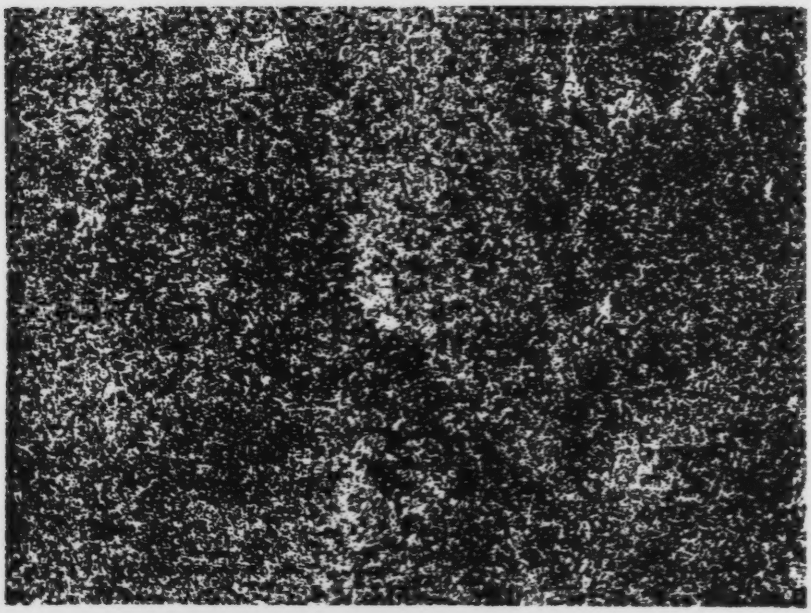

Figure 3.26 Micrograph of last deposited bead in as-welded 5.0 kJ/mm weld of Consumable B depicts the lack of grain boundary ferrite (S5A) (100X, Neg. 9933)

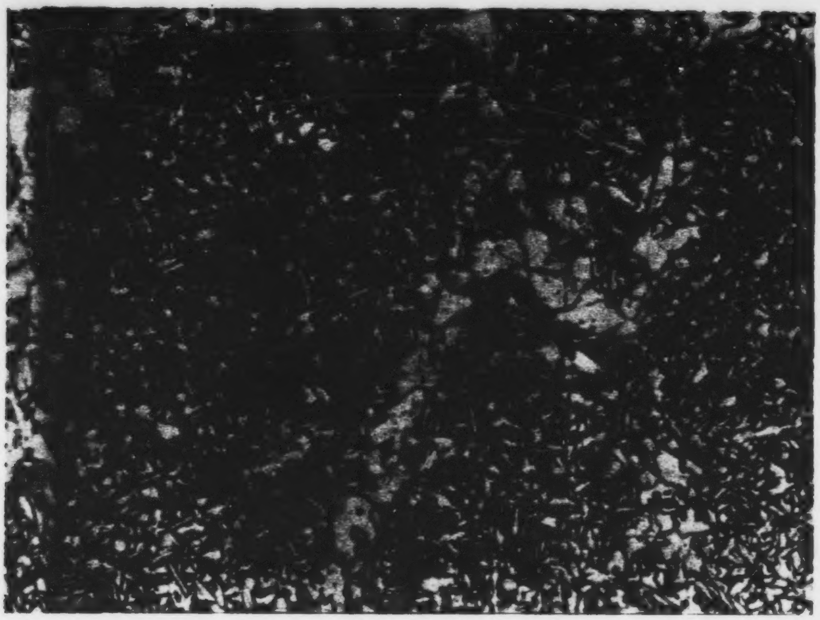

Figure 3.27 Representative microstructure in the last deposited bead of as-welded 3.5 kJ/mm weld of Consumable A (S3A) (500X, Neg. 9955)

Figure 3.28 Representative microstructure in the last deposited bead of as-welded 5.0 kJ/mm weld of Consumable A (S1A) (500X, Neg. 9957)

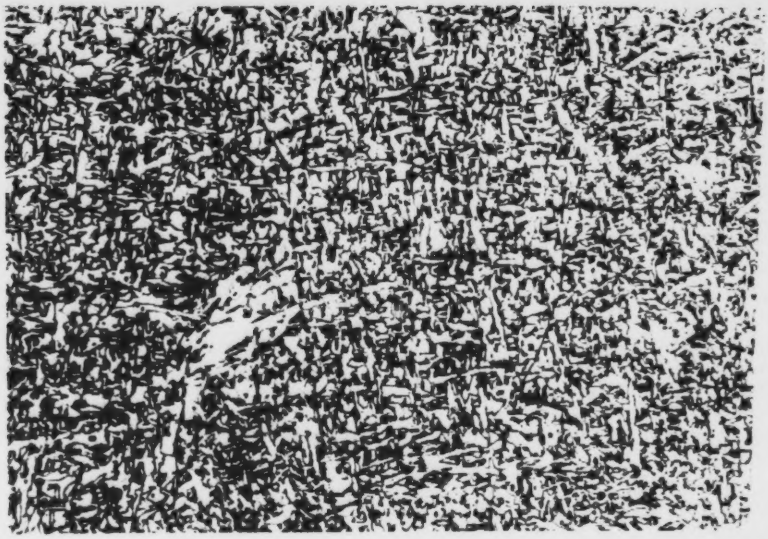

Figure 3.29 Representative microstructure in the last deposited bead of as-welded 3.5 kJ/mm weld of Consumable B. The arrows indicate the lack of growth in grain boundary ferrite from columnar grains (S7B) (500X, Neg. 9959)

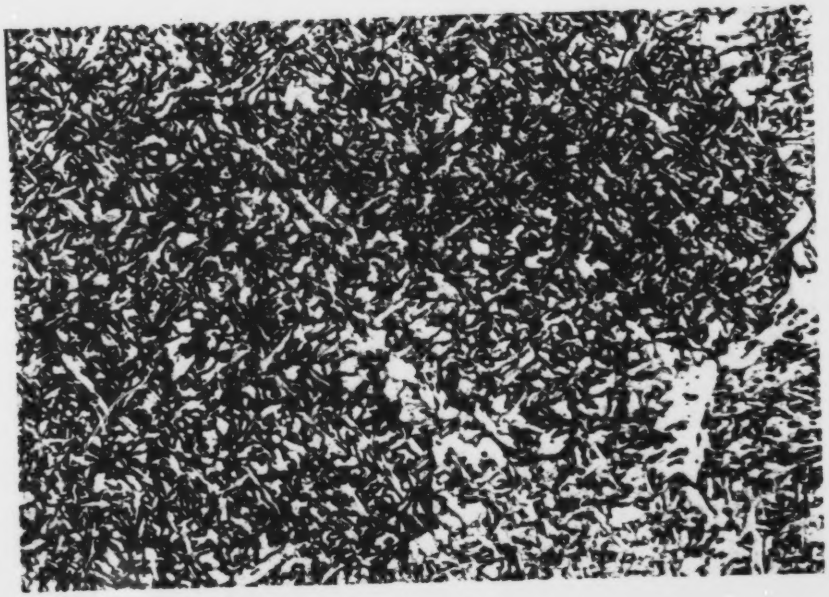

Figure 3.30 Representative microstructure in the last deposited bead of as-welded 3.5 kJ/mm weld of Consumable B. The arrows indicate the coarser grain boundary ferrite from columnar grains (S5A) (500X, Neg. 9934)

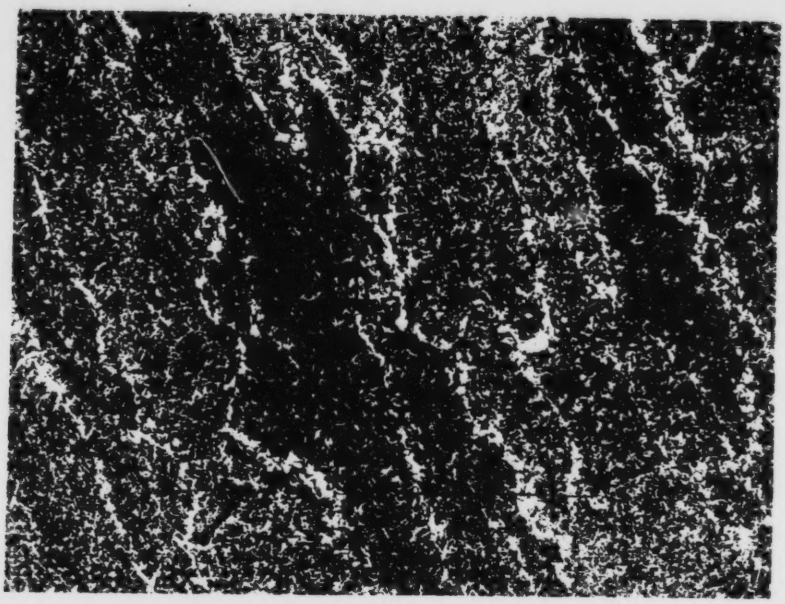

Figure 3.31 Micrograph of as-welded 3.5 kJ/mm of Consumable A; interpass temperature of 232°C (S9A) (100X, Neg. 11169)

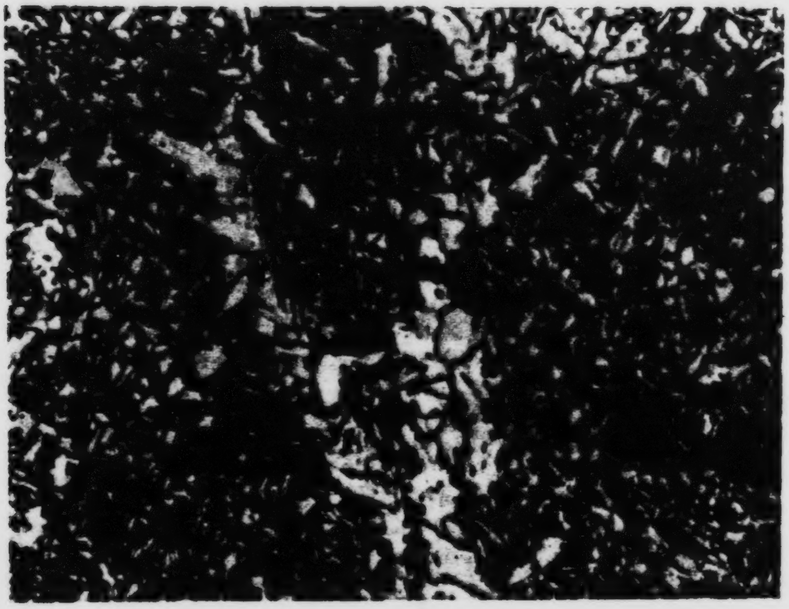

Figure 3.32 Representative microstructure in the last deposited bead of as-welded 3.5 kJ/mm weld of Consumable A; interpass temperature of 232°C (S9A) (500X, Neg. 11171)

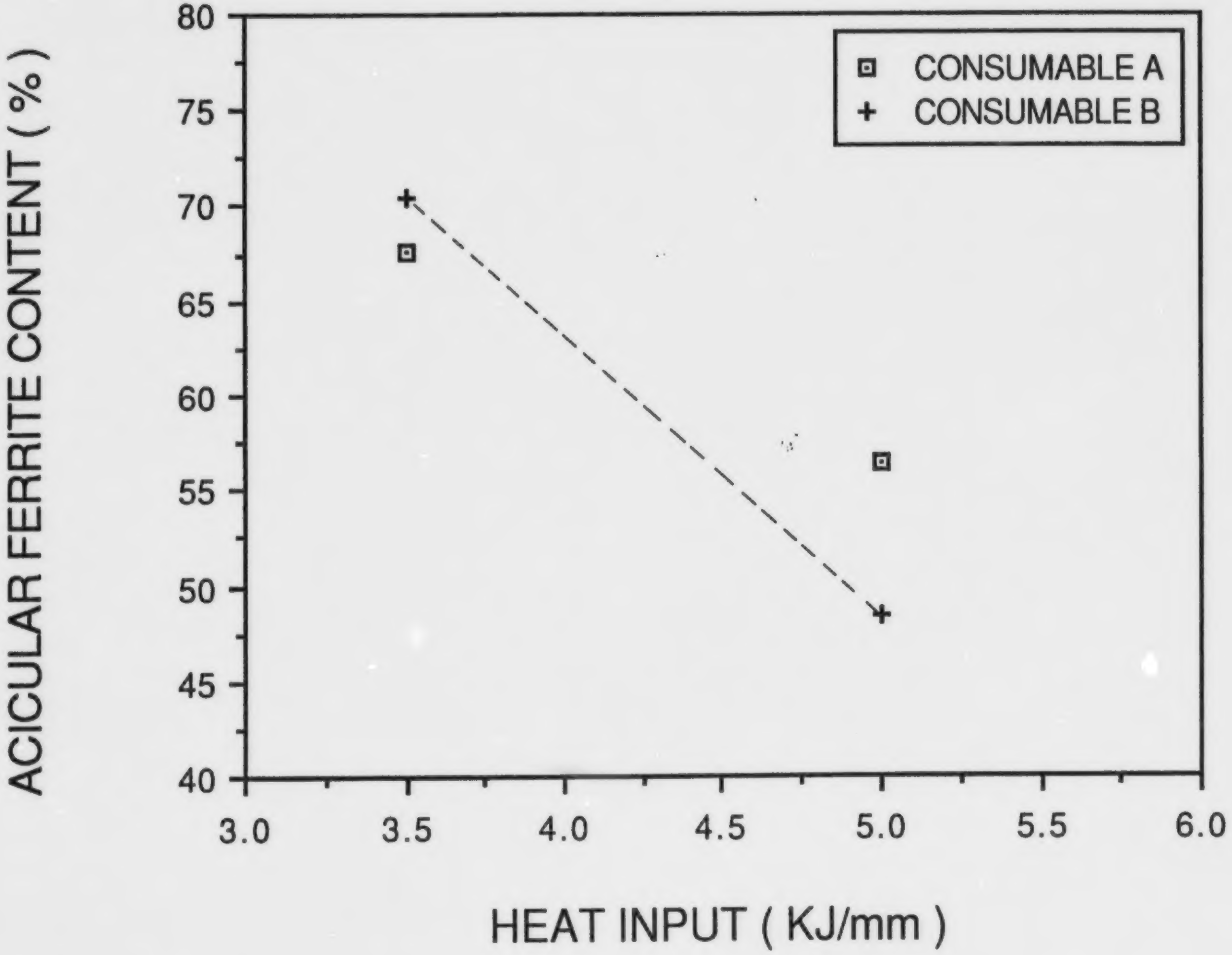

Figure 3.33 Effect of heat input on acicular ferrite contents

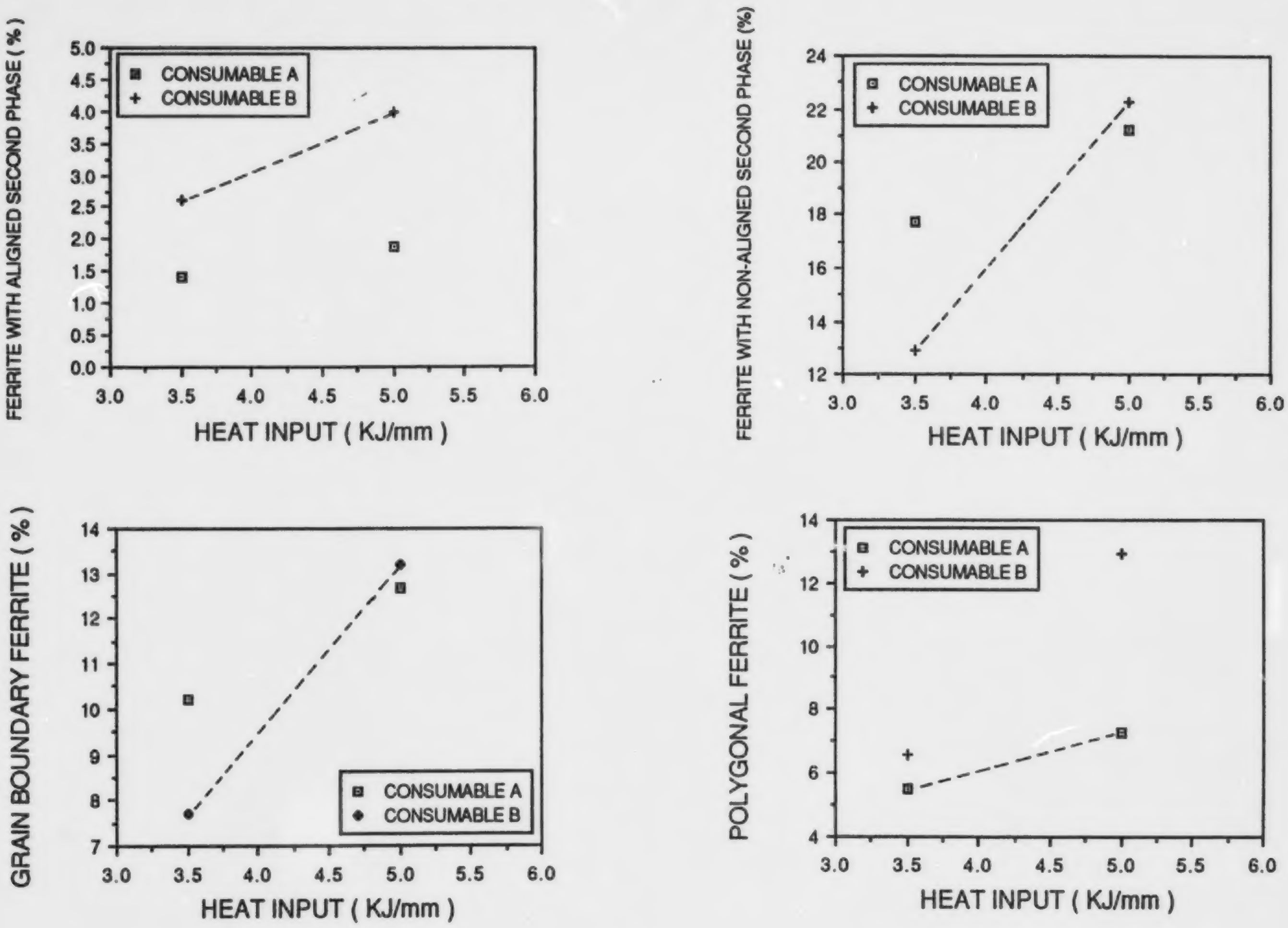

Figure 3.34 Effect of heat input on microstructures other than acicular ferrite

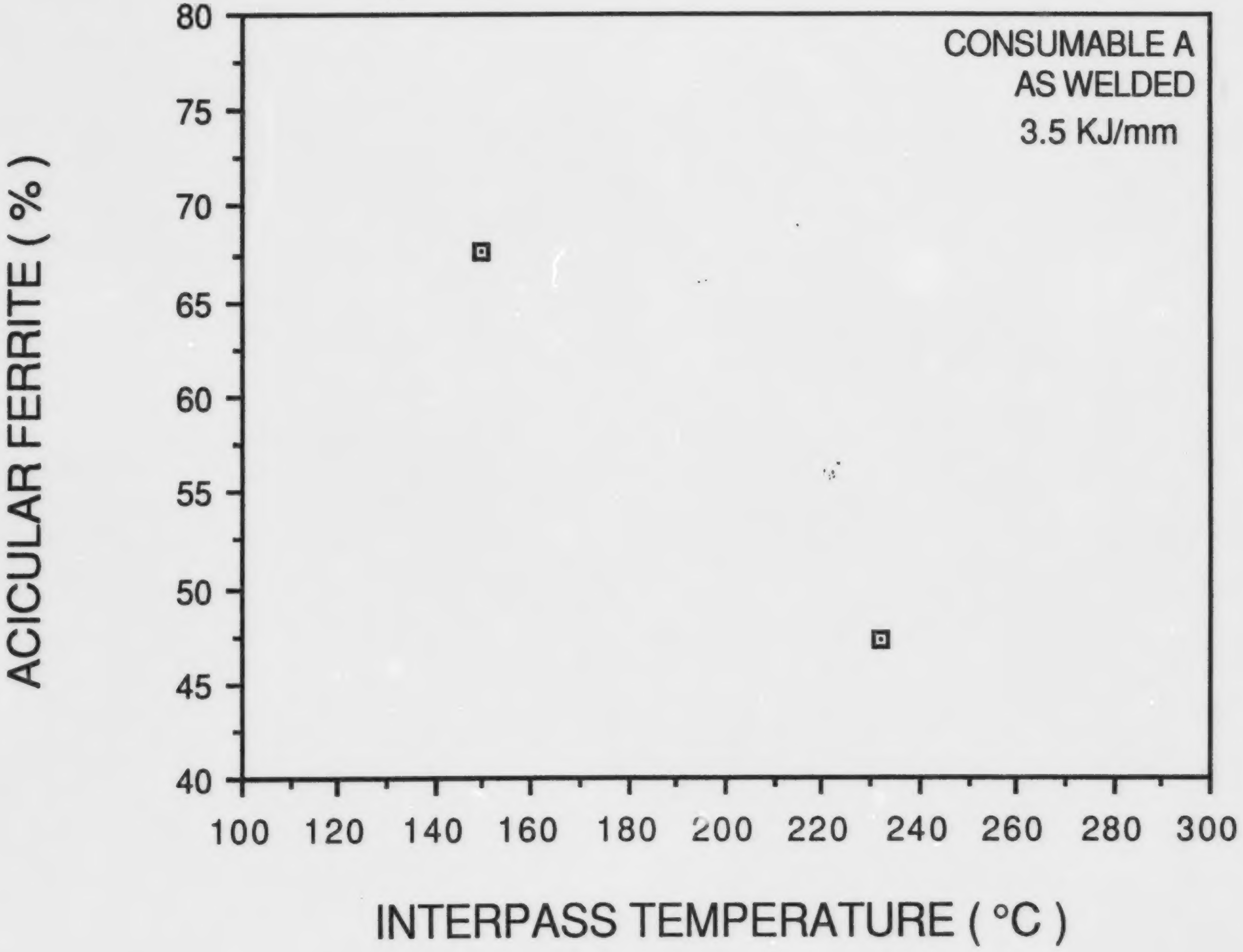

Figure 3.35 Effect of higher interpass temperature on acicular ferrite

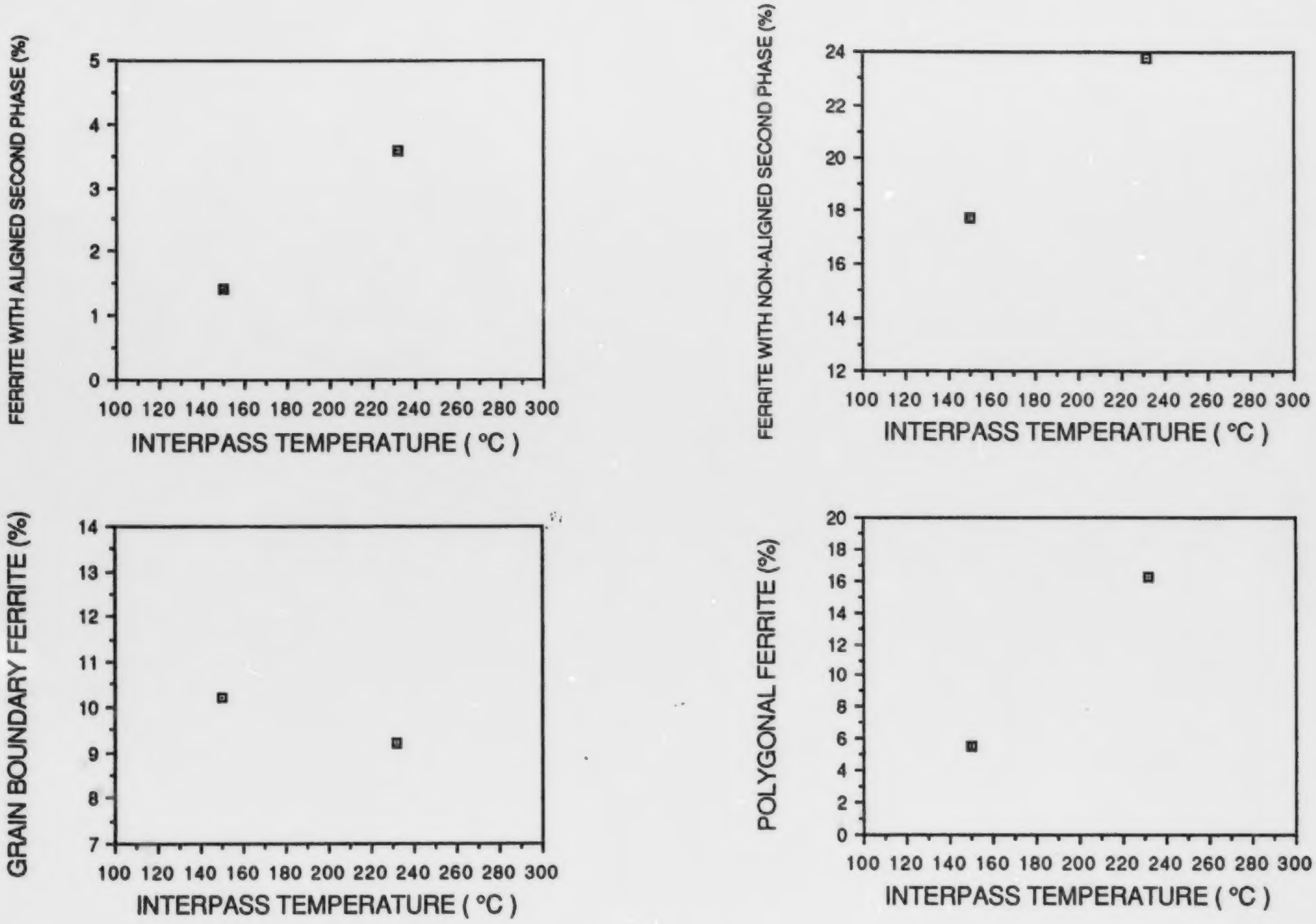

Figure 3.36 Effect of interpass temperature on microstructure other than acicular ferrite

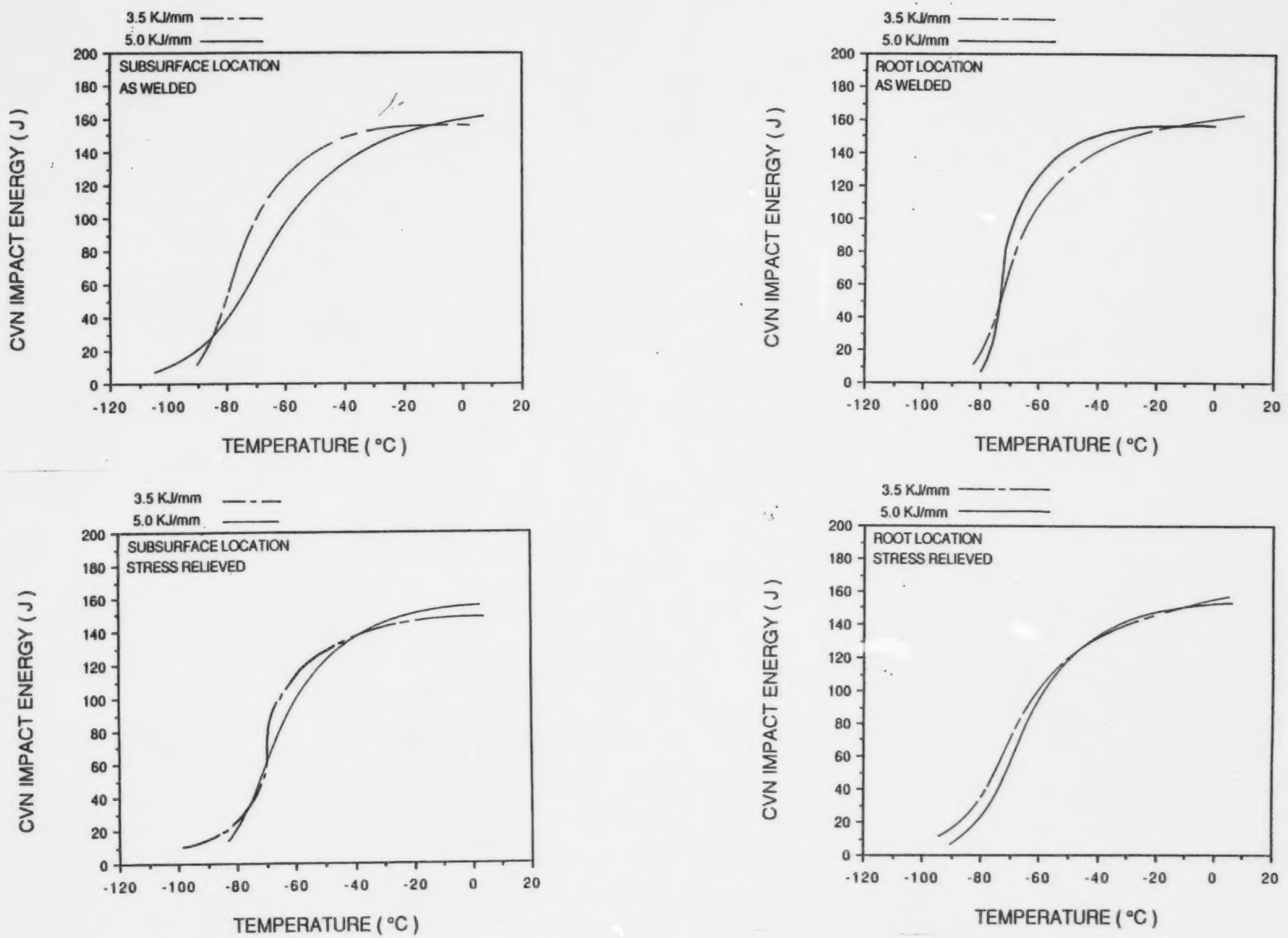

Figure 3.37 Effect of heat input on CVN transition curves of Consumable A

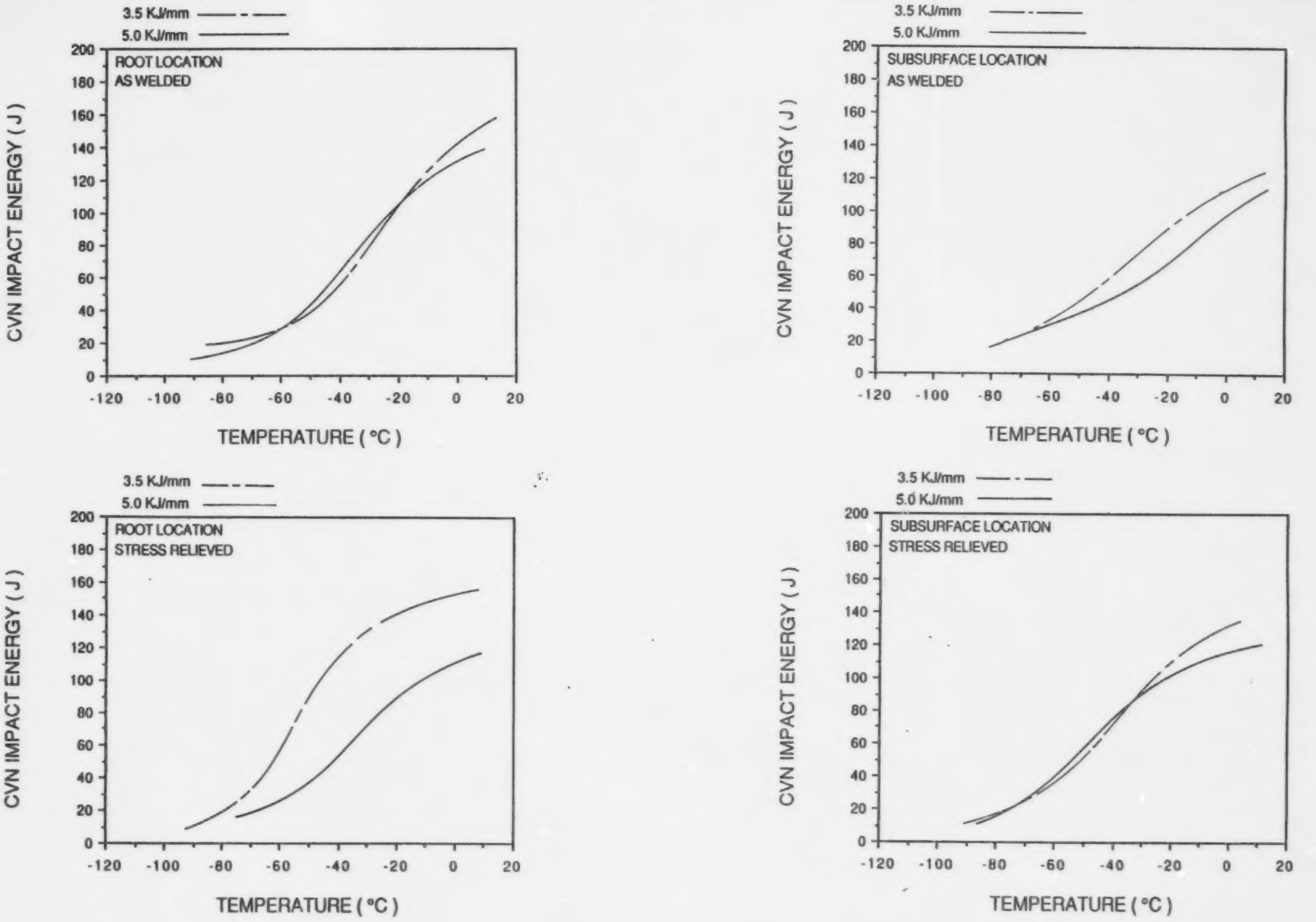

Figure 3.38 Effect on heat input on CVN transition curves for Consumable B

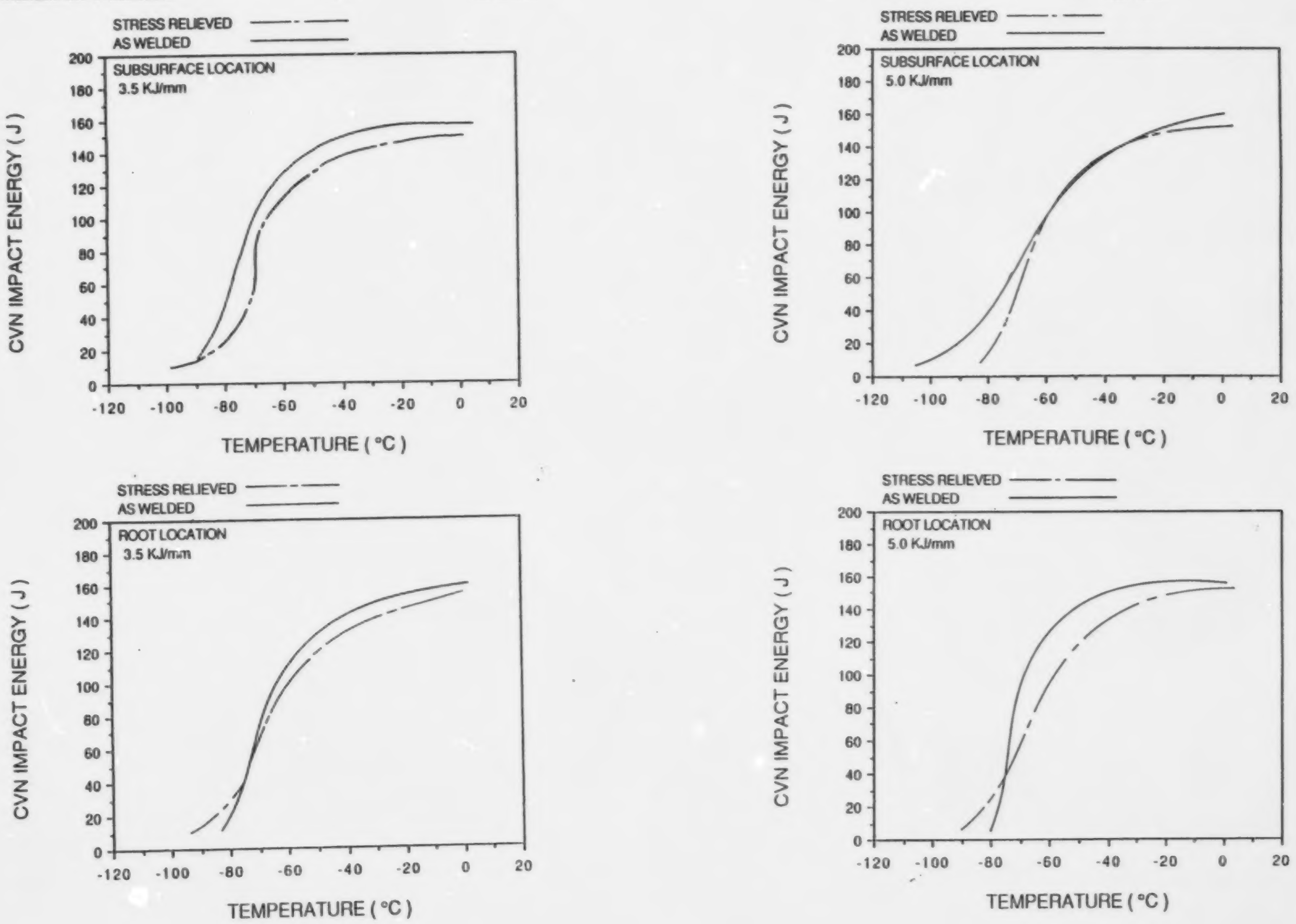

Figure 3.39 Effect of stress relief on CVN transition curves of Consumable A

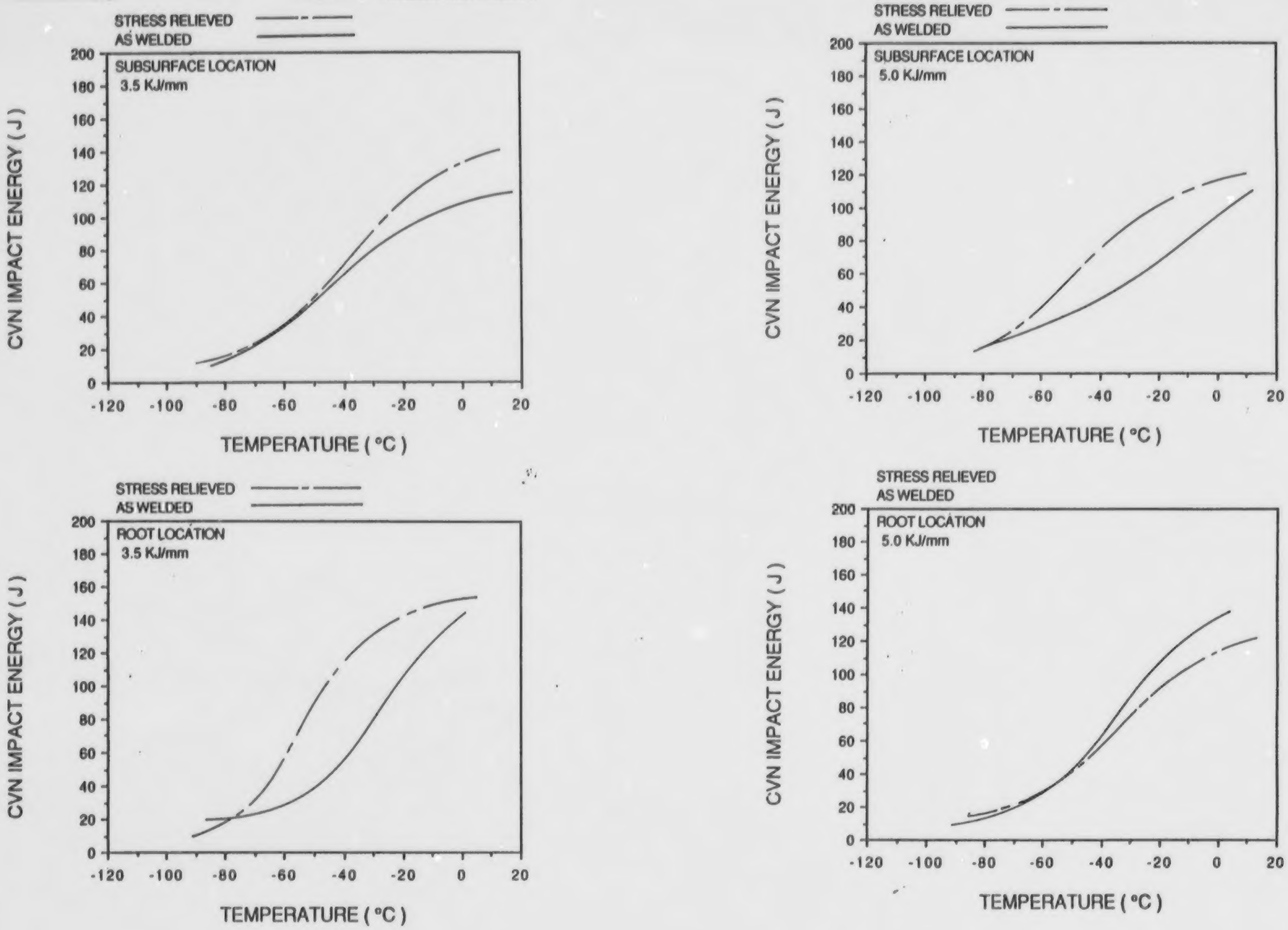

Figure 3.40 Effect of stress relief on CVN transition curves of Consumable B

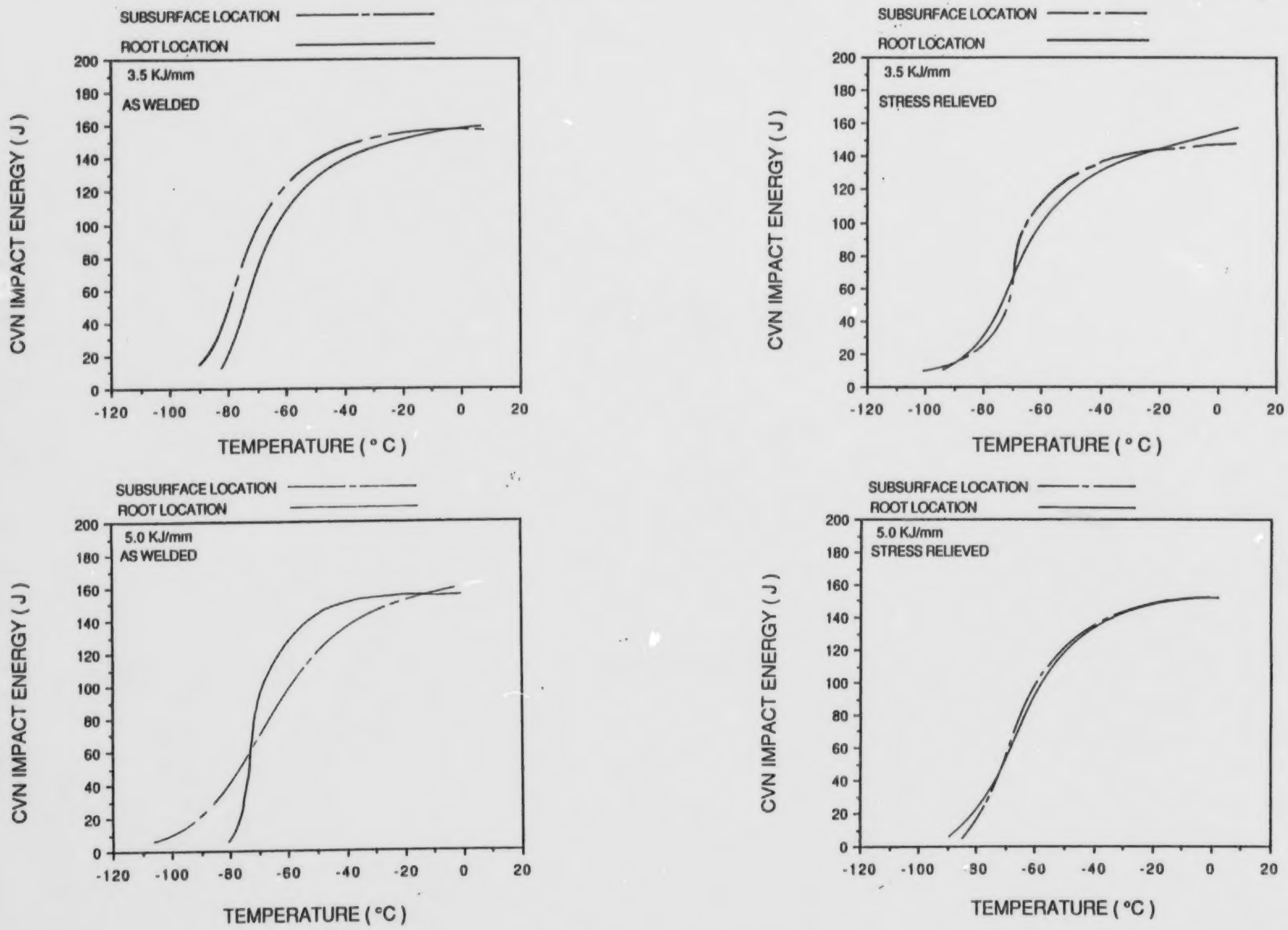

Figure 3.41 Through thickness variation on CVN transition curves of Consumable A

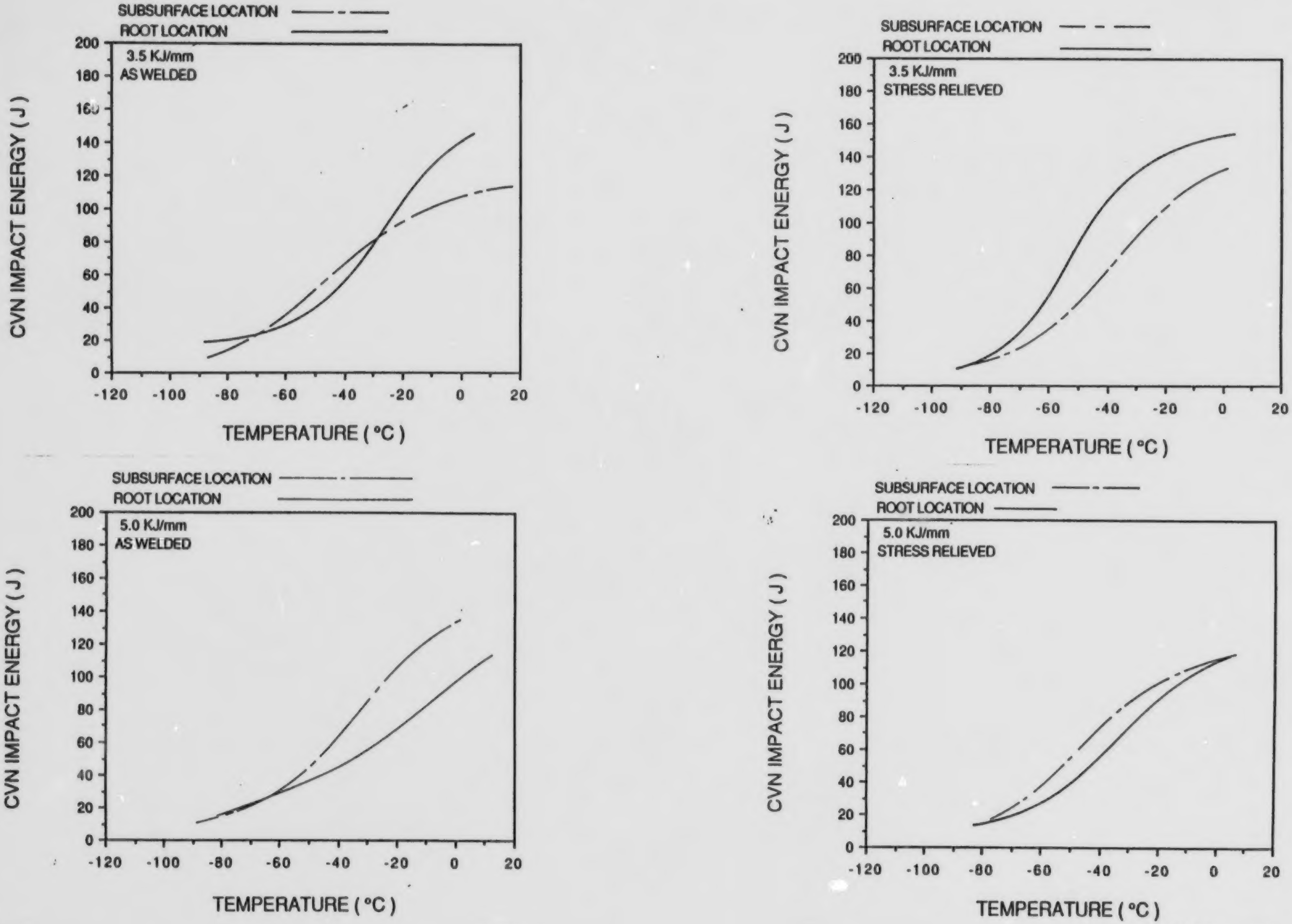

Figure 3.42 Through thickness variation on CVN transition curves of Consumable B

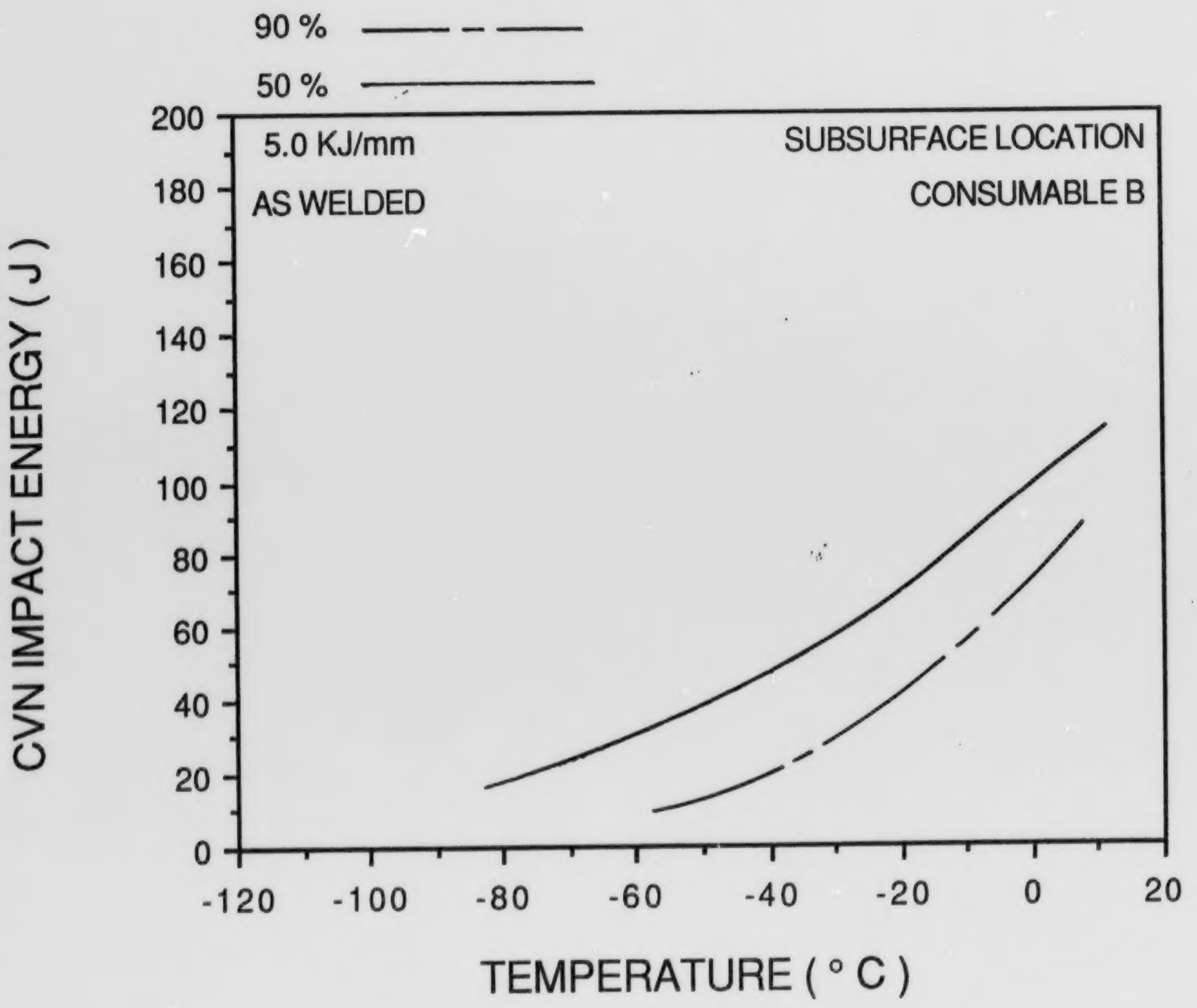

Figure 3.43 The effect of increasing columnar region on CVN toughness of Consumable B

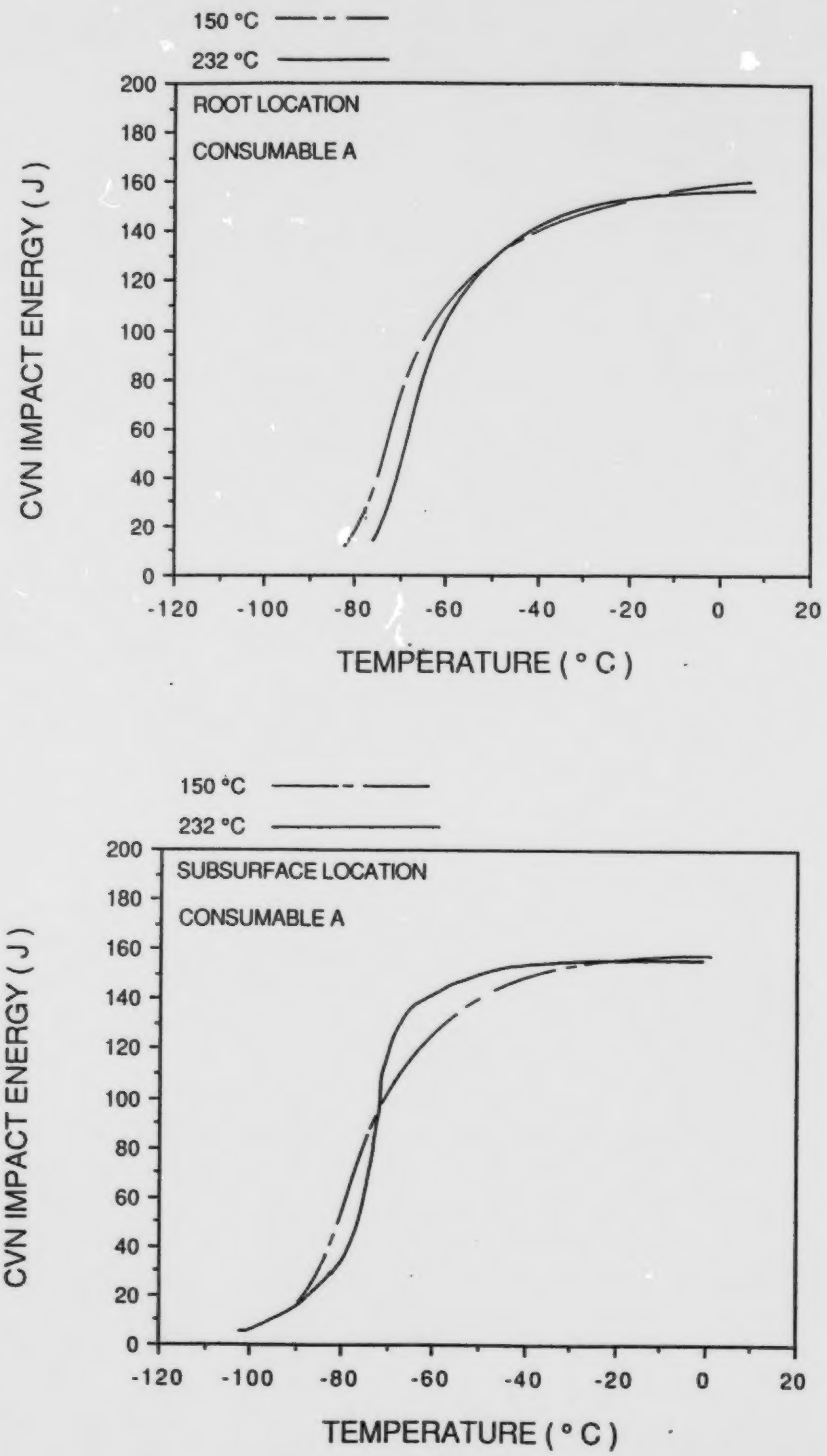

Figure 3.44 Effect of interpass temperature on CVN toughness

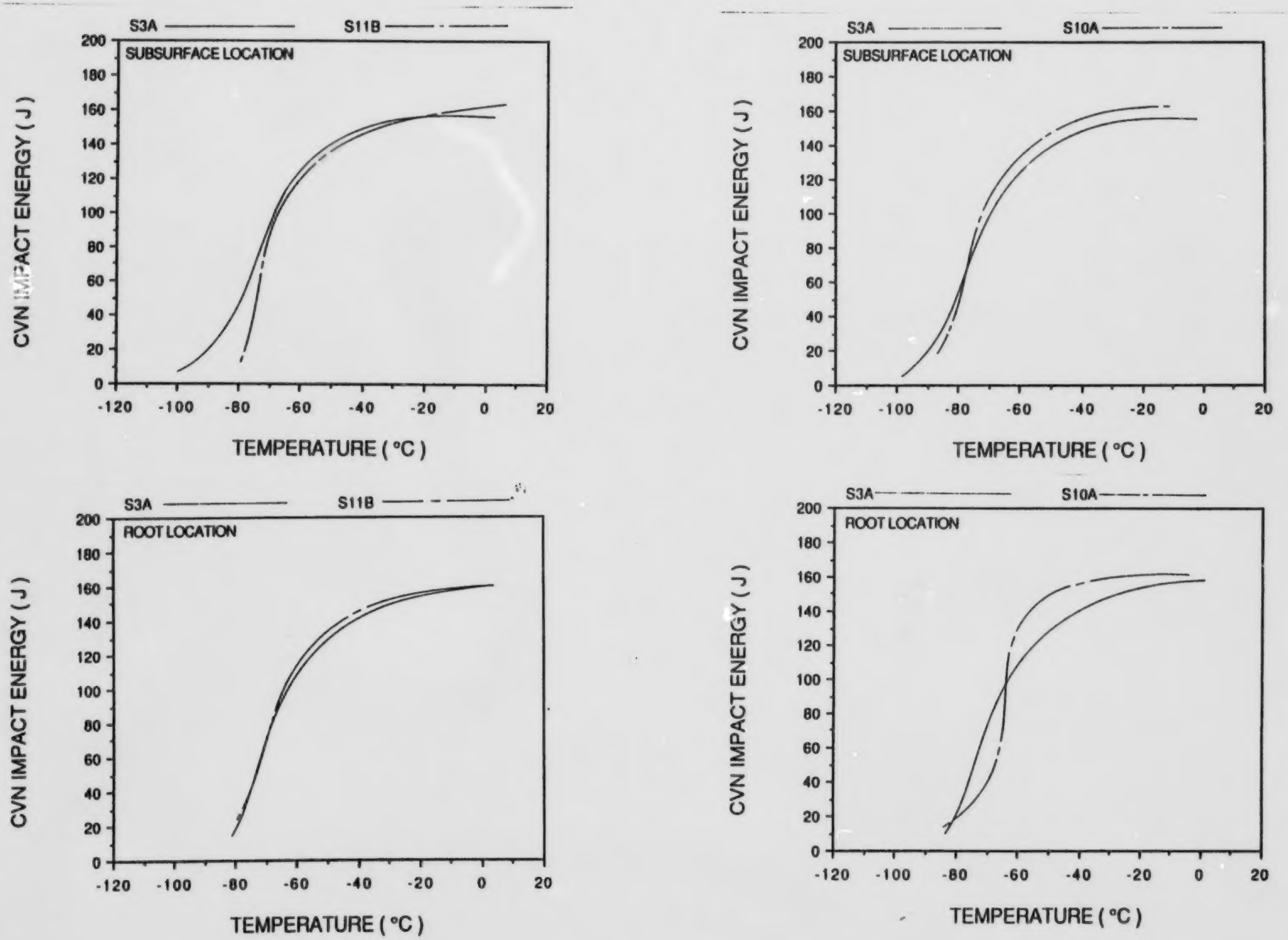

Figure 3.45 Under high angular restraint, the effect of varying lateral restraint on toughness

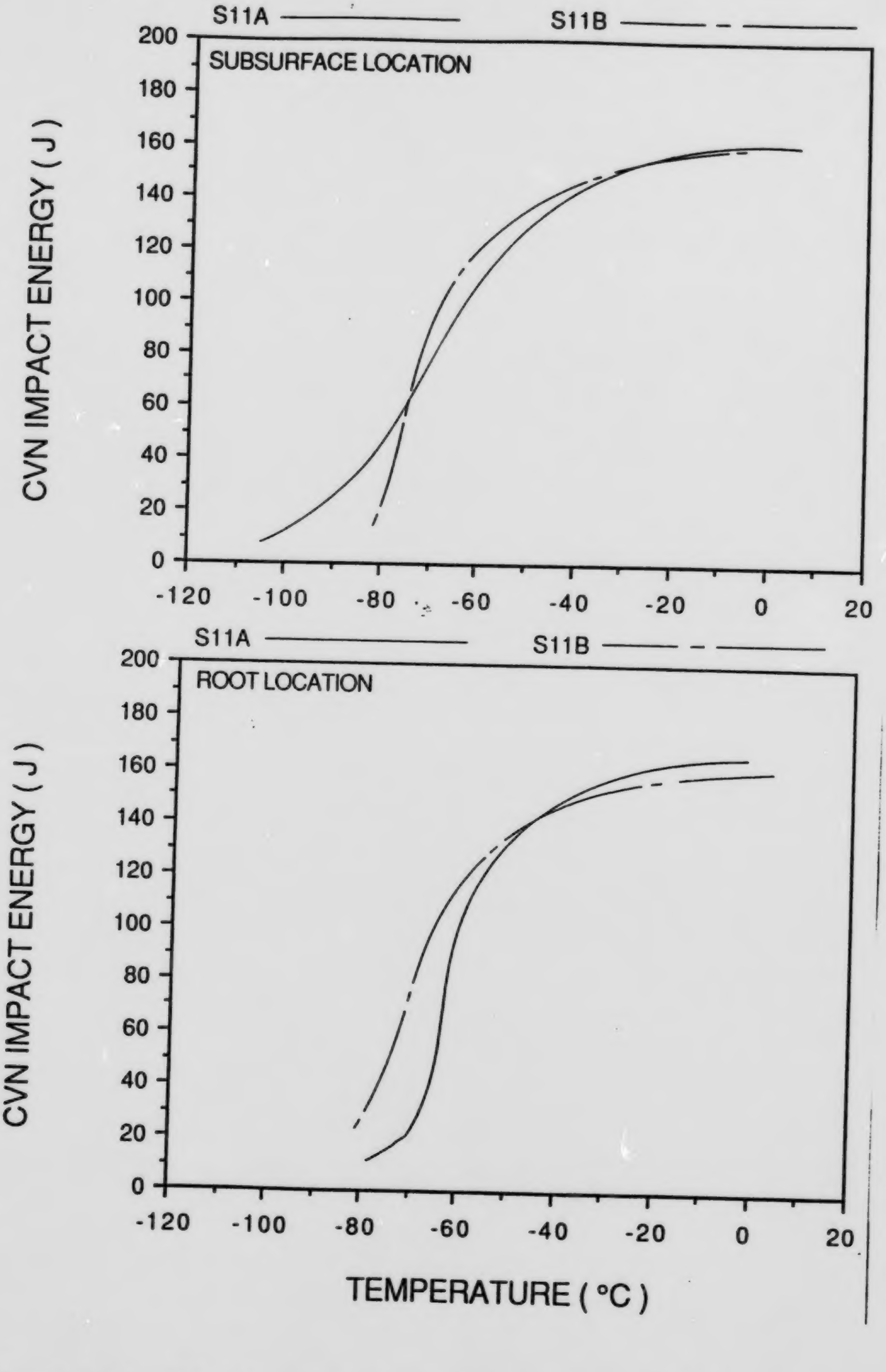

Figure 3.46 Under low restraint condition, the effect of varying angular restraint on toughness

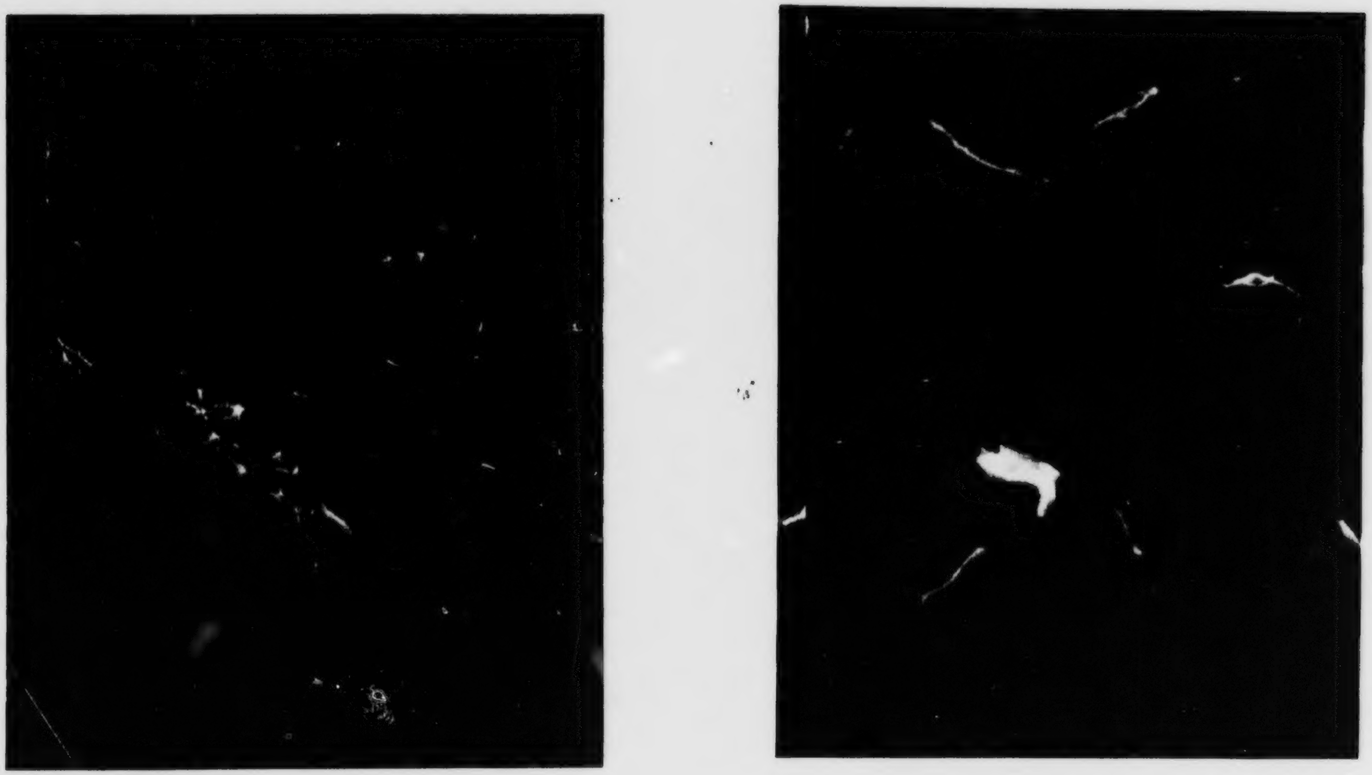

(a) (1000X, Neg. 717) (b) (5000X, Neg. 716)

Figure 3.47 SEM fractography indicates a cleavage initiation found in stress relieved 3.5 kJ/mm weld of Consumable A at -30^{o}C (S4A-1)

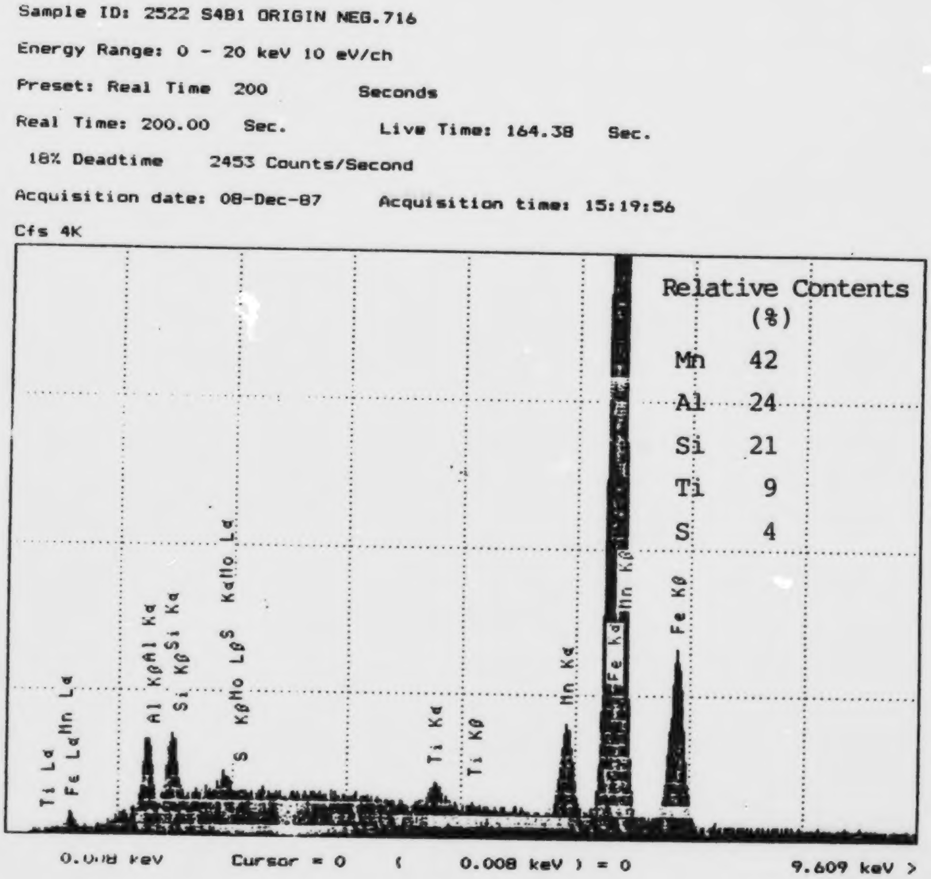

```
Sample ID: 2522 S4B1 ORIGIN NEG.716
Energy Range: 0 - 20 keV 10 eV/ch
Preset: Real Time  200        Seconds
Real Time: 200.00   Sec.       Live Time: 164.38   Sec.
 18% Deadtime     2453 Counts/Second
Acquisition date: 08-Dec-87    Acquisition time: 15:19:56
Cfs 4K
```

Relative Contents (%)

Mn	42
Al	24
Si	21
Ti	9
S	4

```
0.008 keV        Cursor = 0    (    0.008 keV ) = 0                9.609 keV >
```

Figure 3.48 The EDX spectrum of the cleavage initiation site (found in Figure 3.47) suggested that it is an inclusion

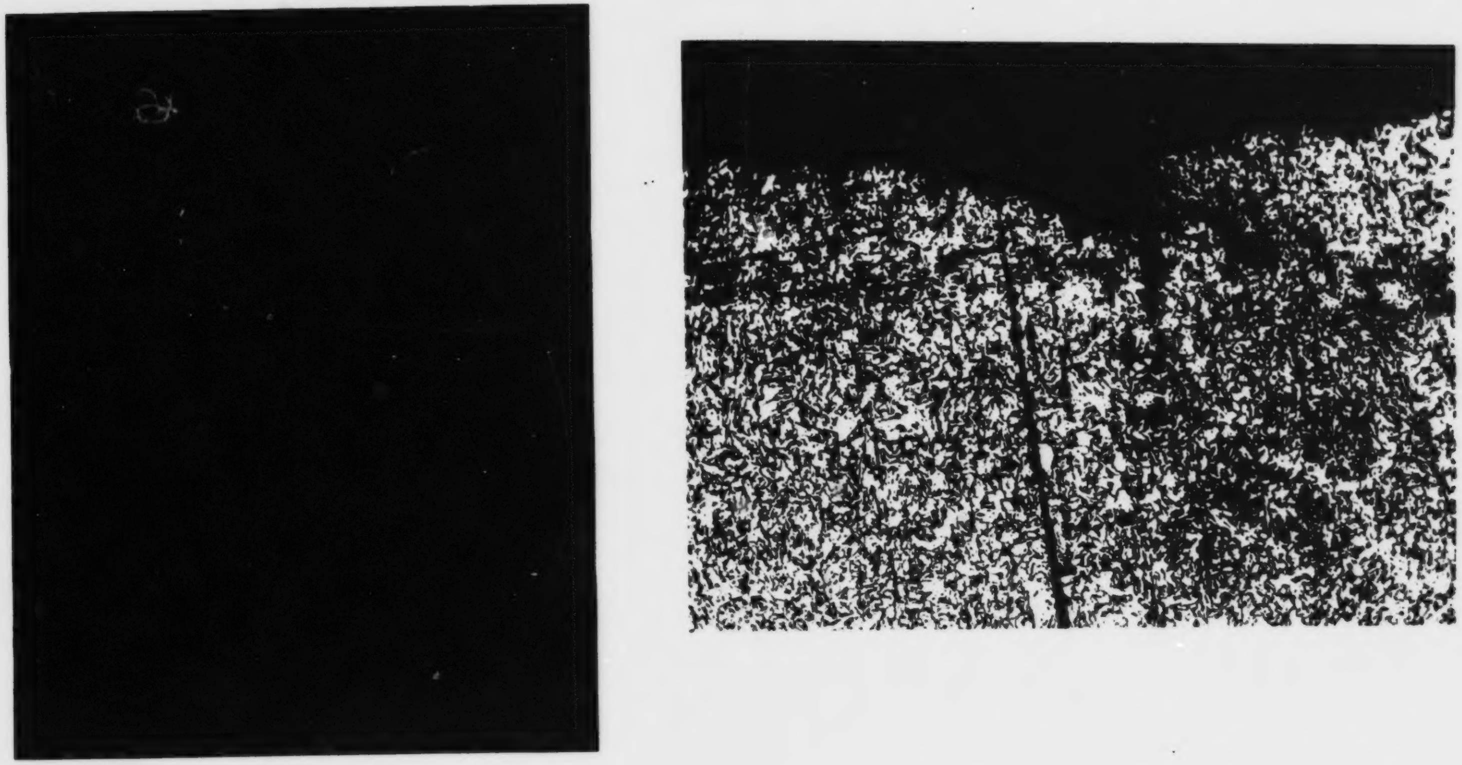

(a) (5000X, Neg. 713)

(b) (200X, Neg. 11238)

Figure 3.49 SEM fractography indicates a cleavage initiation found in the fine grain reheated zone of first root pass of side 2 in stress relieved 5.0 kJ/mm weld of Consumable A (S2B-1)

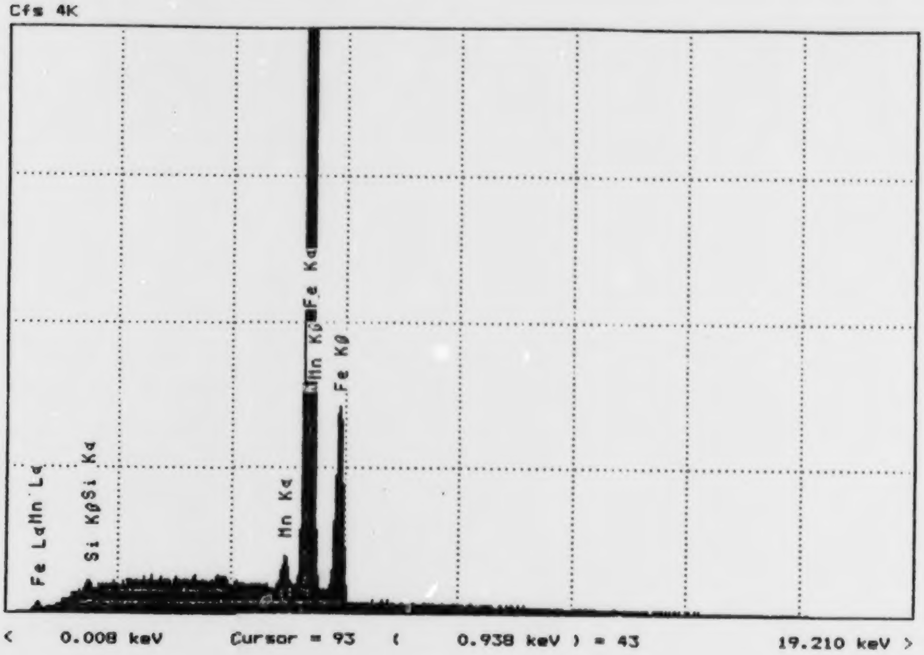

(a) Surrounding Matrix

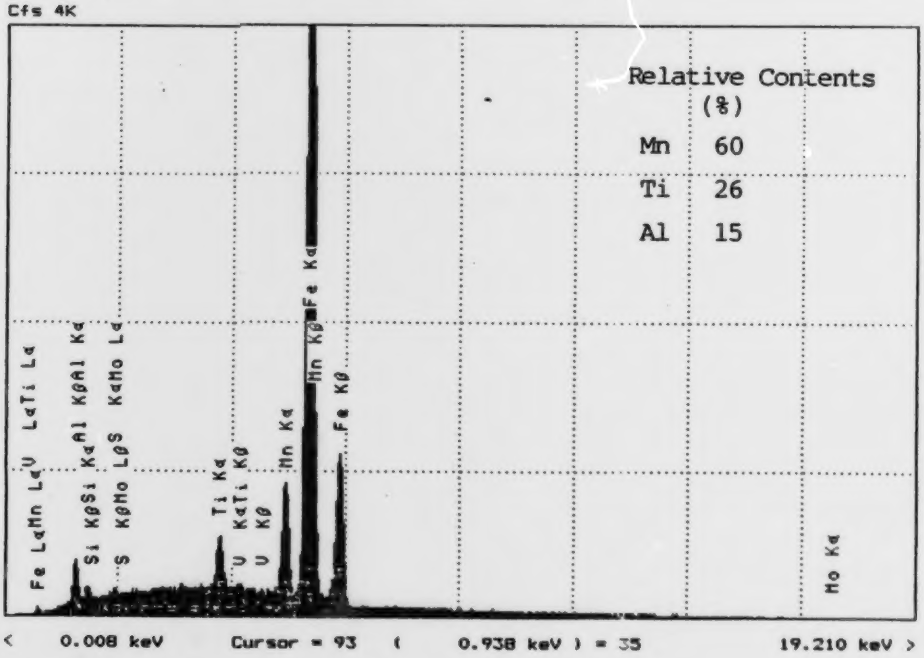

Relative Contents (%)	
Mn	60
Ti	26
Al	15

(b) Cleavage initiation site

Figure 3.50 The difference in EDX spectrums confirms the role of inclusion acting as cleavage initiation site found in Figure 3.49 (S2B-1)

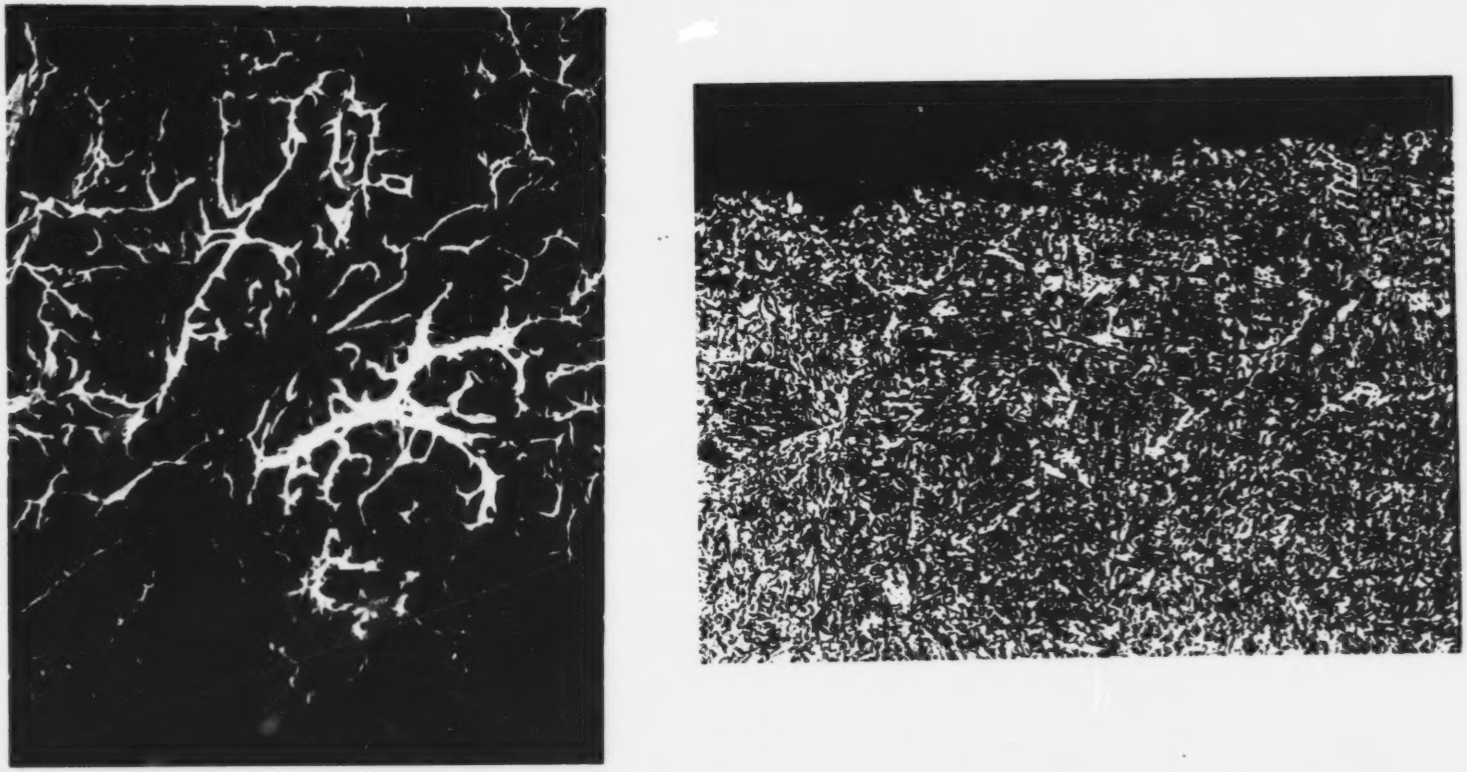

(a) (100X, Neg. 720)

(b) (250X, Neg. 11239)

Figure 3.51 SEM fractography indicates a cleavage initiation found in the grain boundary ferrite of columnar region of stress relieved 5.0 kJ/mm veld of Consumable B (S6A-2)

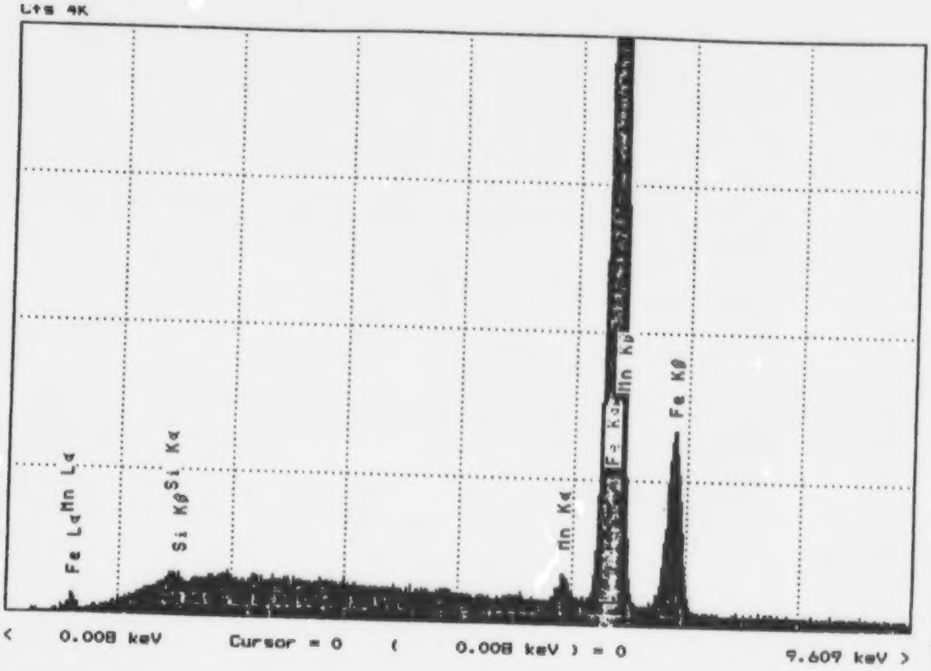

(a) Surrounding Matrix

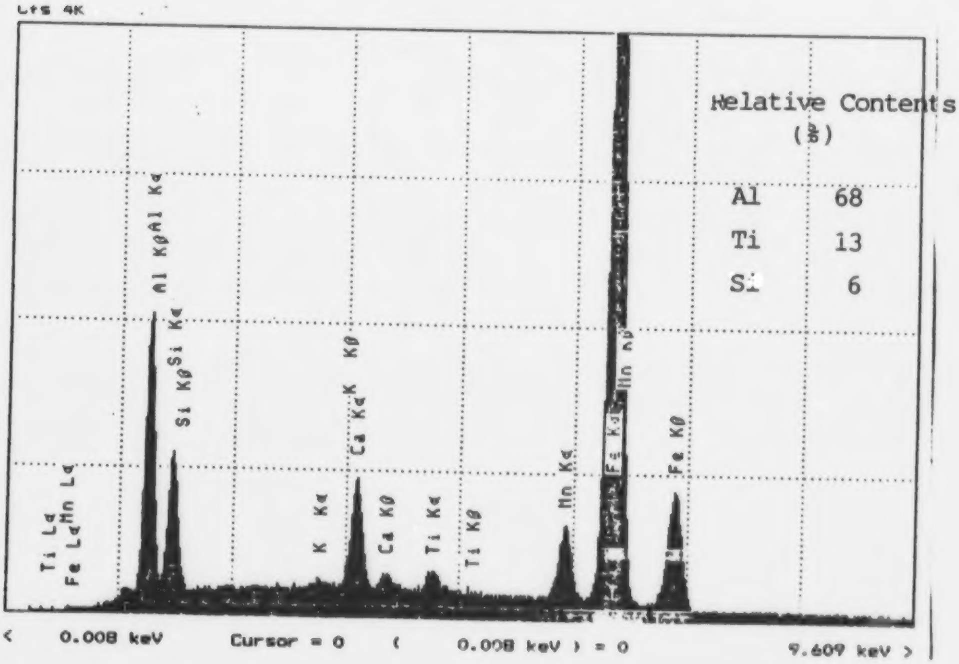

Relative Contents (%)	
Al	68
Ti	13
Si	6

(b) Cleavage initiation site

Figure 3.52 The difference in EDX spectrums confirms the role of inclusion acting as cleavage initiation site found in Figure 3.51 (S6A-2)

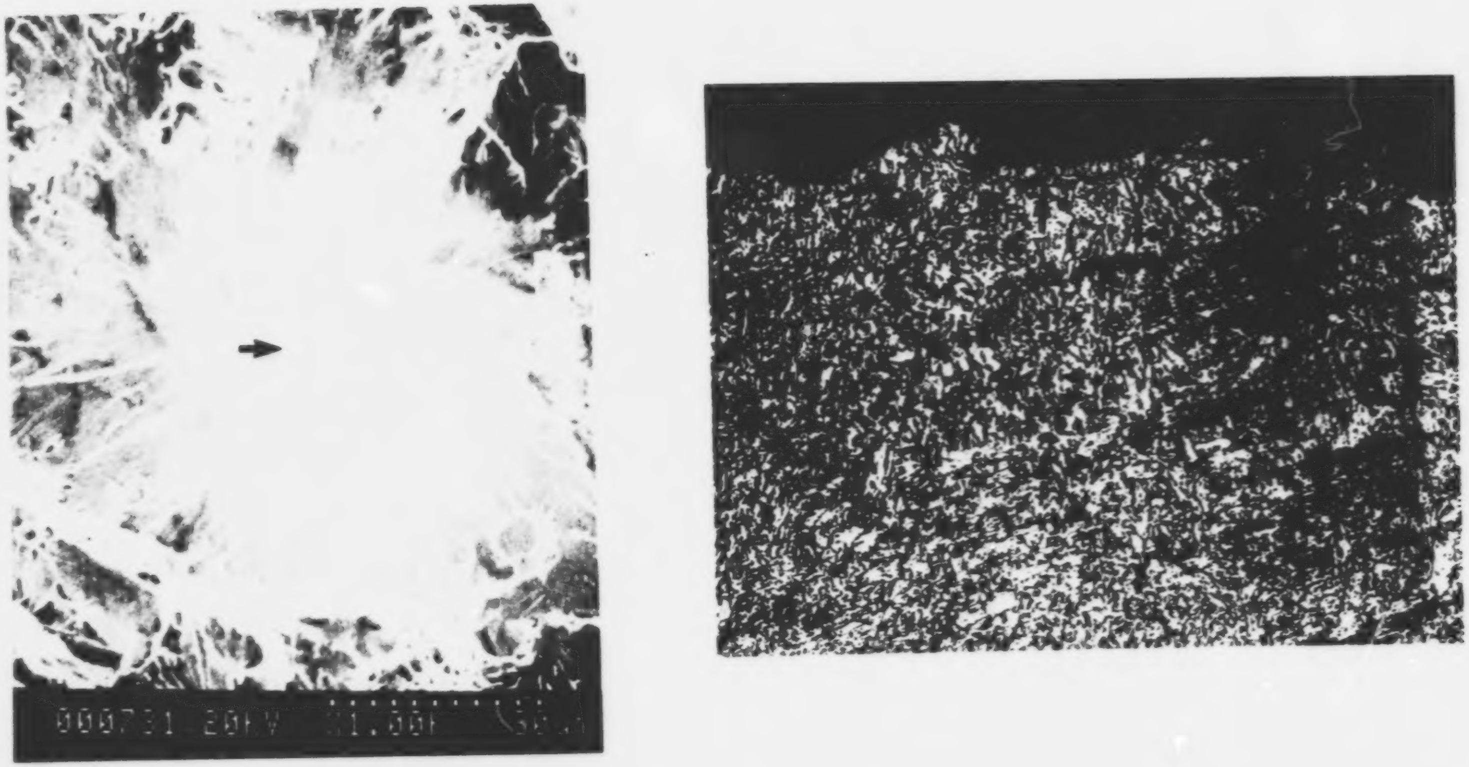

(a) (1000X, Neg. 731)

(b) (200X, Neg. 11237)

Figure 3.53 SEM fractography indicates a cleavage initiation found in fine grain reheated region of as-velded 5.0 kJ/mm veld of Consumable B (S5B-2)

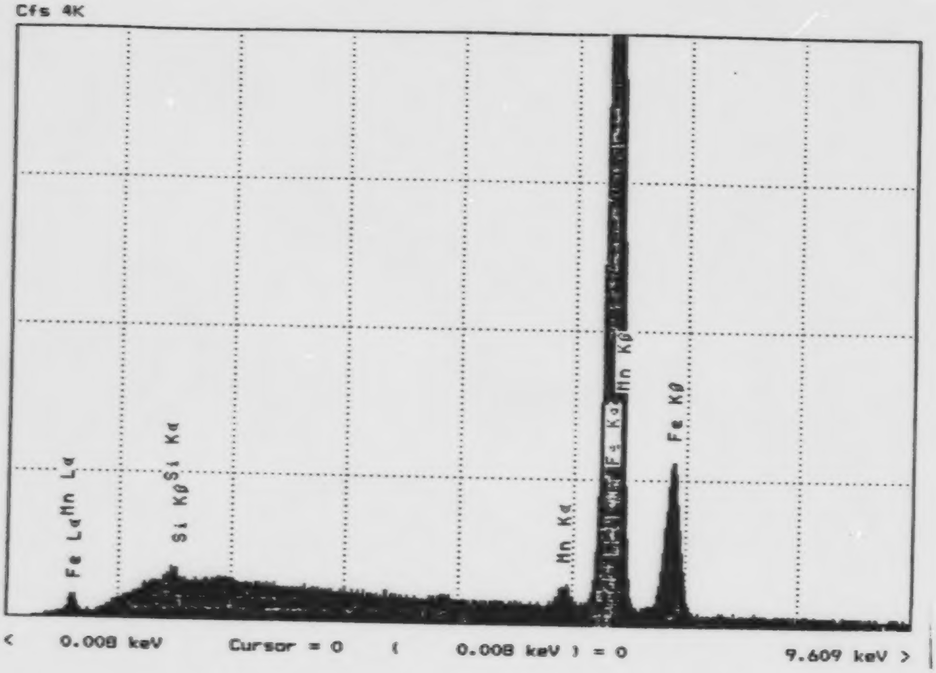

(a) Surrounding Matrix

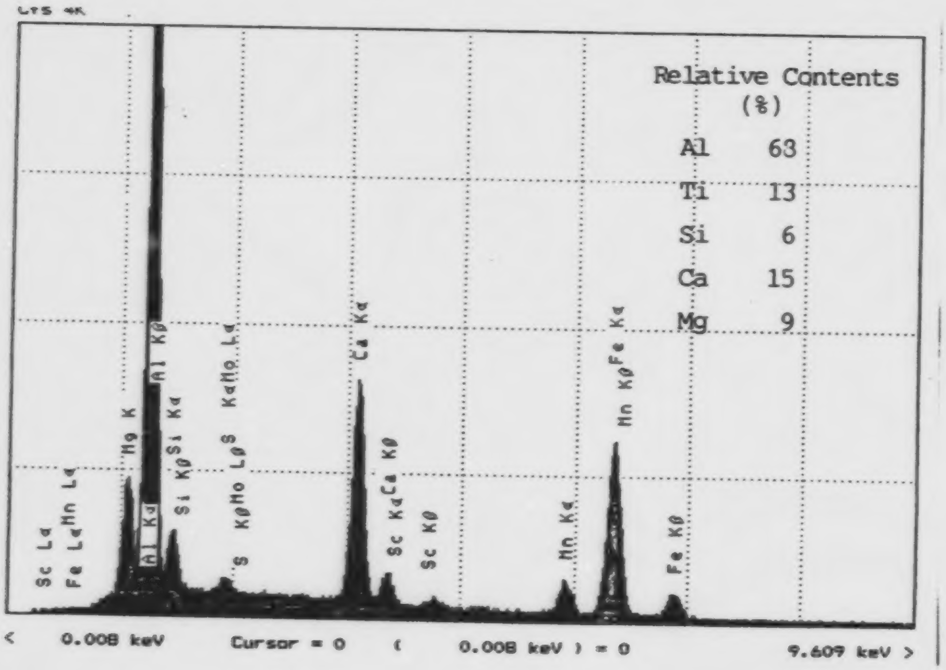

Relative Contents	(%)
Al	63
Ti	13
Si	6
Ca	15
Mg	9

(b) Cleavage initiation site

Figure 3.54 Difference in EDX spectrums confirms the role of inclusion acting as cleavage initiation site found in Figure 3.53 (S5B-2)

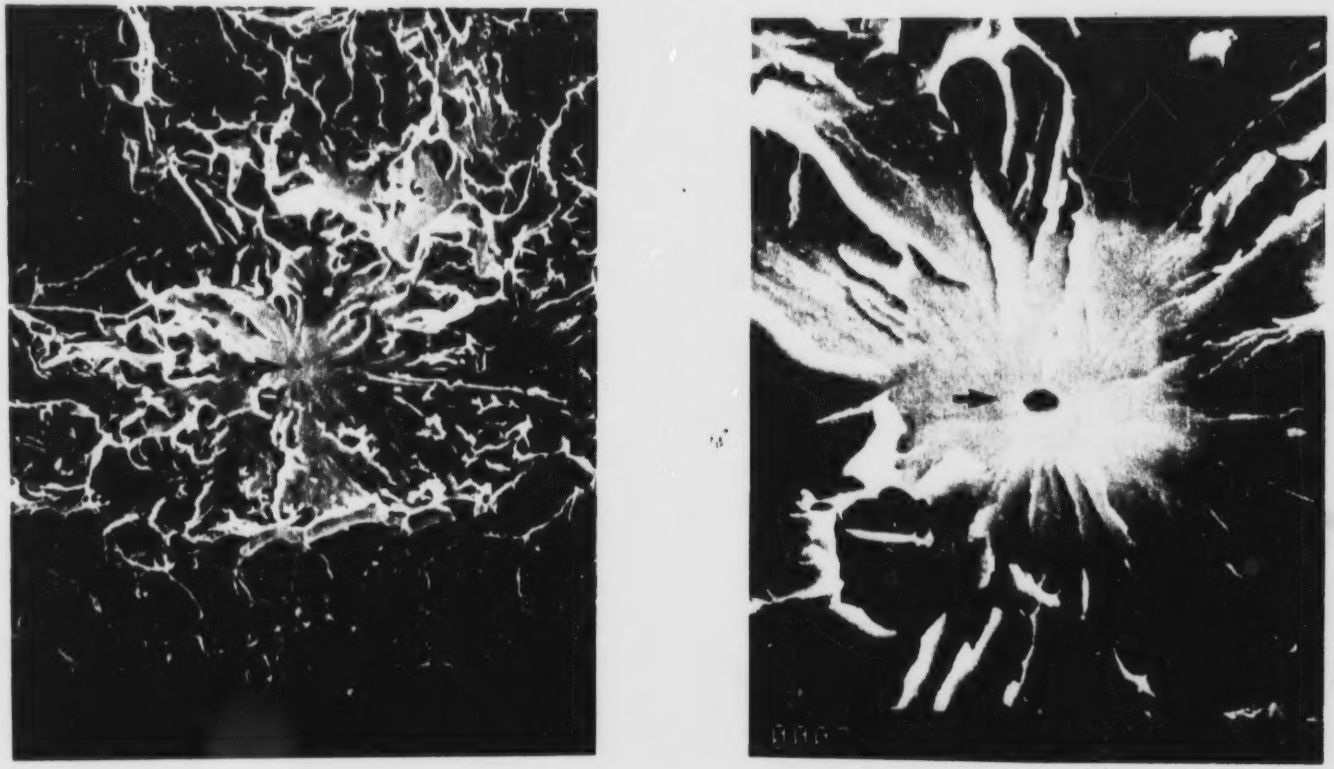

(a) (1000X, Neg. 723) (b) (5000X, Neg. 722)

Figure 3.55 SEM fractography indicates a cleavage initiation found in stress relieved 5.0 kJ/mm weld of Consumable B at -30°C (S8A-2)

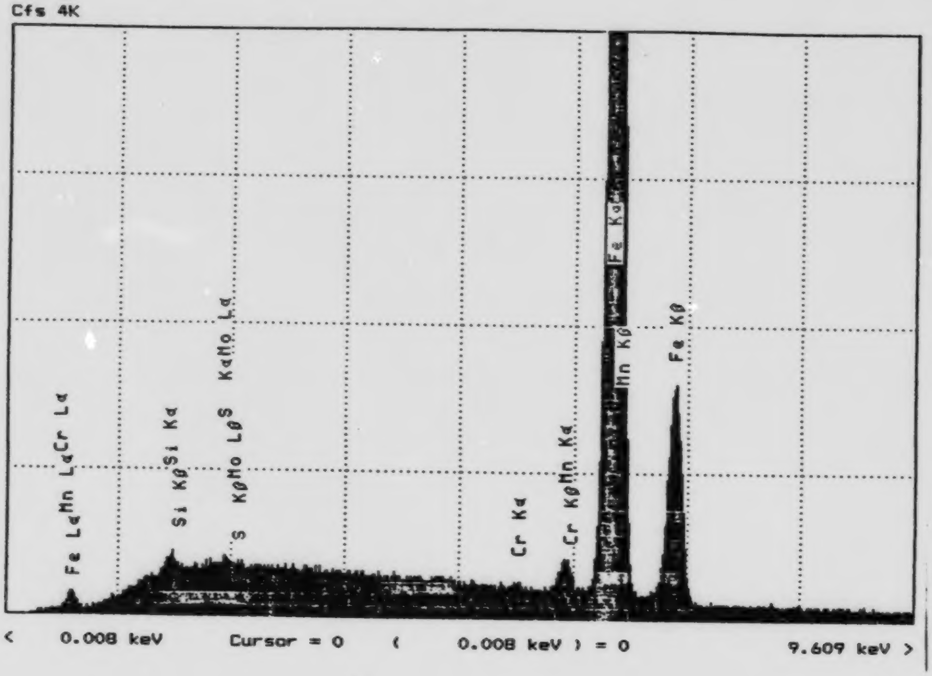

(a) Surrounding Matrix

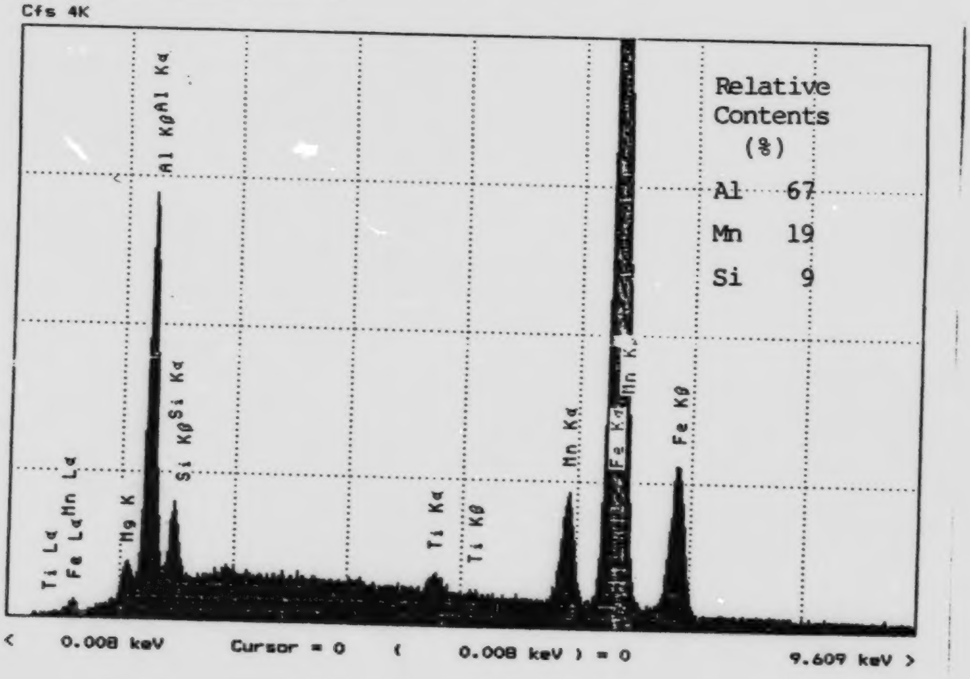

(b) Cleavage initiation site

Figure 3.56 The difference in EDX spectrums confirms the role of inclusion acting as cleavage initiation site found in Figure 3.55 (S8A-2)

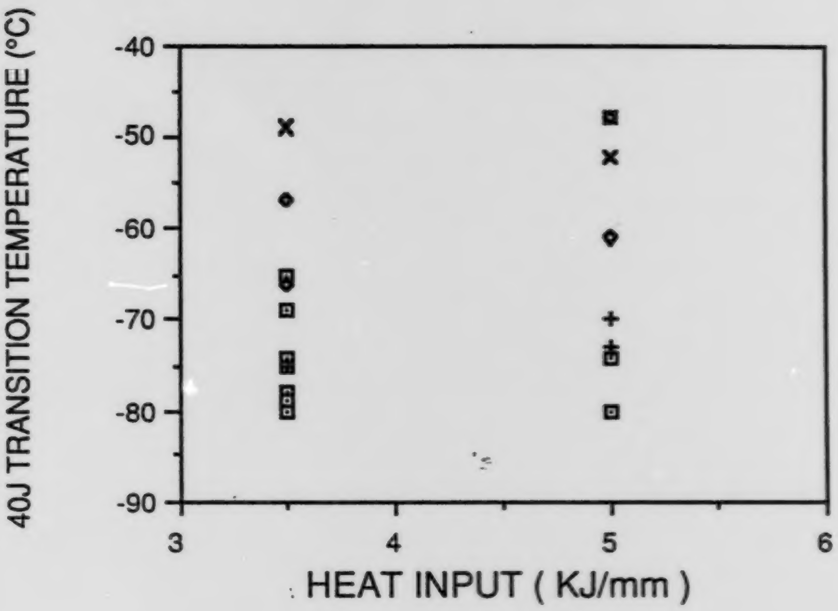

HEAT INPUT	AS WELDED	STRESS RELIEVED
3.5	□	+
5.0	□	+
3.5	x	◇
5.0	x	◇

Figure 4.1: Summary of 40J transition temperatures

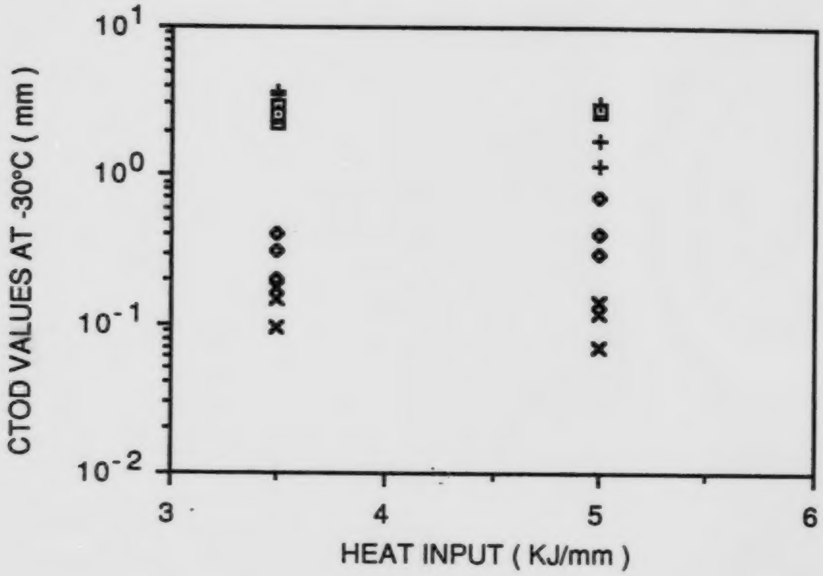

type	heat input	as welded	stress relieved
A	3.5	□	+
A	5.0	□	+
B	3.5	X	◇
B	5.0	X	◇

Figure 4.2: Summary of CTOD values

APPENDIX A

Inclusion Analysis

REPORT

QUANTITATIVE ANALYSIS BY COMPUTER CONTROLLED SCANNING ELECTRON MICROSCOPY OF INCLUSIONS IN SAW SAMPLES

prepared for:

Materials Technology Centre
ARCTEC CANADA LIMITED
Kanta, Ontario
K2K 1Z8

July 1987

Projet CDT-P919

CDT
Centre de
Développement
Technologique
École Polytechnique
de Montréal

CDT PROJECT-P919

REPORT

QUANTITATIVE ANALYSIS BY COMPUTER CONTROLLED SCANNING ELECTRON MICROSCOPY OF INCLUSION IN SAW SAMPLES

prepared for:

Materials Technology Centre
ARCTEC CANADA LIMITED
311 Lettet Drive
Kanta, Ontario
K2K 1Z8

by:

Lawrence R. Cutler, Ph.D.
Gilles L'Espérance, Ph.D.
Department of Metallurgical Engineering
ECOLE POLYTECHNIQUE DE MONTREAL

submitted by:

LE CENTRE DE DÉVELOPPEMENT TECHNOLOGIQUE
DE L'ECOLE POLYTECHNIQUE DE MONTREAL
Campus de l'Université de Montréal
Case postale 6079, Succursale A
Montréal, Québec H3C 3A7

July 1987

Lawrence R. Cutler
Lawrence R. Cutler, Ph.D.
Researcher LCM^2

TABLE OF CONTENTS

Page

A. INTRODUCTION 1

B. METHODOLOGY 3
  1. Specimen Preparation and Observation 3
  2. Operation of the PRC Program 3
  3. Setup of PRC 4
  4. Limitations of PRC 6

C. RESULTS 7
  1. Size Classification 7
  2. Chemical Composition Classification 7
  3. Combined Chemical Composition and Size Classification 8
  4. Area Fraction and Nearest Neighbour Distances 8

D. CONCLUSIONS 8

APPENDIX A: SIZE DISTRIBUTIONS 14

APPENDIX B: TYPE DISTRIBUTIONS FOR THE MAJOR CHEMICAL TYPES 19

APPENDIX C: SIZE DISTRIBUTIONS FOR THE MAJOR CHEMICAL TYPES 25

* * * * * *

Report on Quantitative Analysis by Computer Controlled Scanning Electron Microscopy of Inclusion in SAW Samples

by

Lawrence R. Cutler Ph.D. and Gilles L'Espérance Ph.D.
Département de Génie Métallurgique
Ecole Polytechnique

A: INTRODUCTION

Mr. Chris Chiu of the Materials Technology Center of Arctec Canada Limited asked the Laboratory for Characterization and Microscopy of Materials (LCM^2) of the Metallurgical Engineering Department of Ecole Polytechnique to characterize the inclusions in the as-deposited weld metal of four Submerged Arc Welds (SAW). A characterization of the chemical composition and size distribution of the inclusions was requested.

This was accomplished with the aid of the Particle Recognition and Characterization (PRC) which runs on the Tracor-Northern Model TN-2000 Energy Dispersive X-ray analyzer equipped with a digital scan generator. This system combines three powerful tools, namely:

- Scanning Electron Microscope (SEM) with high resolution and multiple image display modes

- Energy Dispersive X-ray spectroscopy with the ability to detect elements with atomic numbers greater than 10

- Digital Scan Generator which allows computer control of the electron beam in the SEM and digitization of the resultant video signal or the acquisition of X-ray data from specific locations.

This combination forms the basis of a Scanning Electron Microscope based automatic image analysis system (SEM-AIA). This setup gives great flexibility since the type of data collected can be easily modified just by changing the data acquisition or data reduction programs. In the case of PRC, the program controls the electron beam in the (SEM) and digitizes the resultant video signal thereby allowing the acquisition of information based on the local variations in contrast. In the present study, inclusions were detected by variations in the signal level of the backscattered electron image (BEI) which is related to the average atomic weight, Z. Areas with larger values of Z appear brighter in the BEI.

The particle recognition and characterization program (PRC) was developed to characterize the size, shape and chemical composition of particles. The data can be classed according to the average diameter and/or the chemical composition of the individual particles. Specific inclusion types can be further classed by the relative abundance or ratios of the elements present.

This report presents the results of a characterization by the PRC programs of the inclusions in the samples supplied by Mr. Chiu. Classification of the inclusions according to size, chemical composition and shape factor was achieved. The significance and the limitations of the data and techniques are also discussed.

B: METHODOLOGY

1- Specimen Preparation and Observation

The four welds were received from ARCTEC in the polished state. In order to identify the zones in the weld sample, these samples were lightly etched to reveal the weld metal zone. Scratches were made to indicate the centerline of the weld and the half thickness location in order to be able to accurately locate the region of analysis. The specimens were then polished using only diamond polishing compound in order to not introduce Al into the sample surface which enables the accurate analysis of Al in the inclusions. Analysis of the inclusion size and chemical type was done within a zone 2mm by 0.5 mm as requested. Observations and measurements were done using the JEOL 840 SEM in the BEI inverse and normal observation modes.

2- Operation of the PRC Program

The inclusions can be differentiated from the matrix due to variations in the BEI signal levels. Since the inclusions are lighter than the matrix ($Z<Fe$), the inverse BEI was used so that the inclusions will have a higher video signal level than the matrix.

For the PRC program, a window of analysis was then selected so that the lower threshold was just above the BEI signal level of the matrix.

This adjustment was critical since the small inclusions could be lost due to the small difference in contrast between them and the matrix. The upper threshold was left at its maximum value.

The PRC program sweeps the electron beam across the specimen until the resultant video signal level exceeds the lower threshold. The center of the particle is then located. The size, area and shape factor of the inclusion is measured by tracing a series of eight diameters through the center. At this point, a X-ray spectrum is obtained from the center of the inclusion and the intensities of selected peaks are recorded along with the size information of the particle. This process is repeated for the entire field of view. Multiple fields can also be measured during the analysis of a specimen.

The data recorded includes the shape factor which is the surface area of the inclusion times 4 pi divided by the perimeter squared . The shape factor for a sphere is 1, for a square 0.78 and a particle with a length to width ratio of five to one, 0.43. This measure of the shape factor is quite accurate for convex particles but can be in error for highly elongated irregular inclusion.

3- Setup of PRC

Considerable care was exercised in the setup of the elemental classifications in the PRC program. Initially, the specimens were scanned using the BEI mode to determine the size and type of inclusion present. Representative X- ray spectra were taken from various regions to determine the range of elements present in the inclusions. The elemental types then formed to reflect these observations. Trial analysis were done using these elements in order to be sure that no other elements were present in the inclusions.

In most specimens, Mn, S, Ti, Al and Si were the principle elements found in inclusions, although the relative amounts of each varied. Mn, Al and Ti are the major elements found in the inclusions although the relative abundance of each varied from sample to sample. Since all the inclusions had an average diameter under 3 µm, the inclusions were grouped into 0,1 µm bins in the histograms.

In order to have a good resolution of the smaller inclusions as well as to include as many inclusions as possible into each field, a magnification of 4000 was used. An accelerating voltage of 13 kV was used to reduce the size of the X-ray generation zone in order to increase the relative intensities of the light element Kα peaks as compared to the Fe peak which is emitted from the matrix. This is especially important for analysis of the smaller inclusions.

All analysis were done using exactly the same experimental conditions, (i.e. accelerating voltage, working distance, beam current) in order to be able to compare the data from sample to sample. If this is not done, the relative peak height can vary which does not reflect changes in the specimen composition.

The data for the relative intensities of the elements, size, shape factor, maximum and minimum diameter, average diameter and perimeter were saved to disk for each of the inclusions. This data was transferred over to the IBM personal computer. A database manager was used to find the type classification for each of the inclusions. If an element was present in more than 2 percent relative weight, that element appears in the type classification for that inclusion. For example, a type TiMnS contains at least 3 percent relative weight of Ti, Mn and S. After classification, the inclusions were counted according to their size and type classification.

The area fraction of occupation , the average size and the nearest neighbour distance was calculated for each of the samples. The nearest neighbour distance is calculated from 0.5/square root of the number of inclusions per unit area. The average diameter and average relative intensities of each of the major inclusion types were calculated.

4 - Limitations of PRC

PRC was designed to characterize the size, shape and chemical composition of individual particles of regular convex shape. It cannot deal very well with multi-phase or irregularly shaped inclusions such as highly elongated stringers. Possible difficulties include:

- the chemical composition measured will be the average value near the center of the inclusion which will not reflect the variations in composition in complex inclusions.

- irregularly shaped inclusions may be treated as multiple inclusions

- the low contrast of the small inclusions may mean that they may not be found

The relative abundance of the elements measured can in no way be considered a measure of the chemical composition of the inclusions. A large proportion of the X-ray signal comes from the iron matrix but if the solubilities of the elements in the inclusions are low in Fe, as is usually is the case, the spectra recorded reflect changes in the relative composition of the inclusions. Absorption effects can reduce the intensities of the various elements which can change the relative intensities of the peaks somewhat. No matrix corrections (ZAF) were performed and not all of the possible elements present such as oxygen can be measured by the X-ray detector. Still, these measures give valuable data concerning the elements present and the relative abundance of each. These data are indispensable for the understanding of the relationship of processing history and composition to the inclusion characteristics. At this time, there is no other way to obtain such detailed information.

C: RESULTS

1- Size Classification

The size distributions for the four specimens are presented in Appendix A. For all the specimens most of the inclusions are under 2,0 µm in diameter. The most numerous size classification is the 0.3 to 0.4 or the 0.4 to 0.5 micron range.

2- Chemical Composition Classification

The major inclusion type is AlTiSiMnS. The relative abundance of Mn are nearly constant for all of the major inclusion types. It is the level of Al and Ti in the inclusions which change the most from sample to sample. In general, when the Al level is high the Ti level is low and vice-versa. S, when present, is occupies usually only about 10 percent of the inclusion. These results are summarized in Table 1 to 4 which are a summary of the results of the inclusion characterization and includes the numbers for each size and inclusion type as well as the average intensities of the elements for each class of inclusion along with the average diameter of the inclusions. Histograms of the major inclusion types are presented in Appendix B.

3- Combined Chemical Composition and Size Classification

The results for the size classifications for the major chemical types are presented in Tables 1 to 4.

The data can be broken down even further. Histograms of size groupings for an individual inclusion type can be plotted and compared . This is done for the most numerous inclusion types for the four specimens and are presented in Appendix C.

4 Area Fraction and Nearest Neighbour Distances

The results of the volume fraction, inclusion density and nearest neighbour distance is presented in Table 5. There is no large differences in the inclusion density, area fraction (i.e. volume fraction) or nearest neighbour distance for the four welds.

D: CONCLUSIONS

1- The major inclusion type in these specimens is AlTiSiMnS.

2- The most numerous size is either in the 0.3 to 0.4 or the 0.4 to the 0.5 micron range.

3- The relative proportions of Mn remain almost constant throughout the major inclusion types whereas the Ti and Al levels vary. S is usually less than 10 percent of the inclusions.

TABLE 1

SUMMARY OF RESULTS FOR THE S1B WELD

SPECIMEN NAME: ARCTEC S1B
NUMBER OF
INCLUSIONS: 231

CHEMICAL TYPE	SIZE RANGE OF INCLUSIONS																			AVERAGE RELATIVE PEAK INTENSITIES (PERCENT)						AVERAGE DIAMETER (um)	TOTAL NUMBER	PERCENTAGE
From	0.2	0.3	0.4	0.5	0.6	0.7	0.8	0.9	1	1.1	1.2	1.3	1.4	1.5	1.6	1.7	1.8	1.9	2									
To	0.3	0.4	0.5	0.6	0.7	0.8	0.9	1	1.1	1.2	1.3	1.4	1.5	1.6	1.7	1.8	1.9	2	2.1	Si	S	Ti	Mn	Al	Mg			
AlTiSiMnS	32	45	31	24	17	13	8	3	1	2	1	0	1	0	0	0	0	0	0	9	10	23	32	22	0	0.49	178	77.1
AlTiSiMn	3	4	1	2	4	1	2	1	2	0	0	0	1	0	0	0	0	0	0	9	0	25	31	33	0	0.63	21	9.1
AlTiMnS	3	2	4	3	3	0	0	1	0	0	0	0	0	0	0	0	0	0	0	1	11	26	34	24	0	0.48	16	6.9
MgAlTiSiMnS	2	3	1	0	0	0	0	0	0	0	0	0	0	0	0	0	0	0	0	12	8	23	32	20	2	0.34	6	2.6
TiMnS	1	0	0	2	0	0	0	0	0	0	0	0	0	0	0	0	0	0	0	1	46	6	43	1	0	0.44	3	1.3
AlTiMn	0	0	0	1	0	0	1	0	0	0	0	0	0	0	0	0	0	0	0	1	0	20	36	50	0	0.71	2	0.9
TiSiMnS	0	1	0	1	0	0	0	0	0	0	0	0	0	0	0	0	0	0	0	12	35	12	36	1	0	0.47	2	0.9
MgAlSiMn	1	0	0	0	0	0	0	0	0	0	0	0	0	0	0	0	0	0	0	33	0	0	54	9	2	0.28	1	0.4
SiMnS	0	0	0	0	0	1	0	0	0	0	0	0	0	0	0	0	0	0	0	7	30	0	60	0	0	0.76	1	0.4
MgAlTiMnS	0	0	1	0	0	0	0	0	0	0	0	0	0	0	0	0	0	0	0	2	4	3	18	68	2	0.45	1	0.4
TOTAL NUMBER	43	55	38	33	24	15	11	5	3	2	1	0	2	0	0	0	0	0	0									

TABLE 4

SUMMARY OF RESULTS FOR THE 7B WELD

SPECIMEN NAME: ARCTEC 7B
NUMBER OF
INCLUSIONS: 280

CHEMICAL TYPE	SIZE RANGE OF INCLUSIONS																			AVERAGE RELATIVE PEAK INTENSITIES (PERCENT)								
From	0.2	0.3	0.4	0.5	0.6	0.7	0.8	0.9	1	1.1	1.2	1.3	1.4	1.5	1.6	1.7	1.8	1.9	2							AVERAGE DIAMETER	TOTAL	PERCENTAGE
To	0.3	0.4	0.5	0.6	0.7	0.8	0.9	1	1.1	1.2	1.3	1.4	1.5	1.6	1.7	1.8	1.9	2	2.1	Si	S	Ti	Mn	Al	Mg	(um)	NUMBER	
AlTiSiMnS	31	44	36	16	6	3	0	2	0	0	0	0	0	0	0	0	0	0	0	8	11	7	27	44	0	0.40	138	49.3
AlSiMnS	19	20	13	5	1	0	0	0	0	1	0	0	0	0	0	0	0	0	0	10	14	1	29	43	0	0.37	59	21.1
AlTiMnS	3	5	6	5	1	2	0	0	0	0	0	0	0	0	0	0	0	0	0	1	13	7	29	47	0	0.45	22	7.9
AlTiSiMn	3	2	4	1	1	0	3	1	1	1	0	0	0	0	0	0	0	0	0	8	1	8	23	58	0	0.59	17	6.1
AlMnS	0	6	6	1	0	0	1	0	0	1	0	0	0	0	0	0	0	0	0	1	12	1	25	58	0	0.48	15	5.4
NiAlTiSiMnS	6	2	3	0	0	0	0	0	0	0	0	0	0	0	0	0	0	0	0	9	14	7	26	38	3	0.32	11	3.9
NiAlSiMnS	3	5	0	0	0	1	0	0	0	0	0	0	0	0	0	0	0	0	0	11	14	0	31	37	4	0.34	9	3.2
AlSiMn	0	0	3	0	0	0	0	0	0	0	0	0	0	0	0	0	0	0	0	7	1	1	23	65	0	0.45	3	1.1
AlMn	0	0	0	1	0	0	0	1	0	0	0	0	0	0	0	0	0	0	0	0	2	1	24	71	0	0.75	2	0.7
SiMnS	0	0	0	1	0	0	0	1	0	0	0	0	0	0	0	0	0	0	0	6	42	0	50	0	0	0.74	2	0.7
NiAlTiSiMn	0	1	0	0	0	0	0	0	0	0	0	0	0	0	0	0	0	0	0	9	0	6	33	47	3	0.32	1	0.4
NiTiSiMnS	0	1	0	0	0	0	0	0	0	0	0	0	0	0	0	0	0	0	0	18	4	10	47	0	18	0.36	1	0.4
TOTAL NUMBER	65	86	71	30	9	6	4	5	1	3	0	0	0	0	0	0	0	0	0									

TABLE 3

SUMMARY OF RESULTS FOR THE 5B WELD

SPECIMEN NAME: ARCTEC 5B
NUMBER OF
INCLUSIONS: 279

CHEMICAL TYPE	SIZE RANGE OF INCLUSIONS																			AVERAGE RELATIVE PEAK INTENSITIES (PERCENT)						AVERAGE DIAMETER (um)	TOTAL NUMBER	PERCENTAGE
From	0.2	0.3	0.4	0.5	0.6	0.7	0.8	0.9	1	1.1	1.2	1.3	1.4	1.5	1.6	1.7	1.8	1.9	2									
To	0.3	0.4	0.5	0.6	0.7	0.8	0.9	1	1.1	1.2	1.3	1.4	1.5	1.6	1.7	1.8	1.9	2	2.1	Si	S	Ti	Mn	Al	Mg			
AlTiSiMnS	12	27	29	22	19	4	5	2	4	0	0	0	0	0	0	0	0	0	0	7	6	7	21	56	0	0.81	124	44.4
AlTiSiMn	1	7	5	6	10	6	2	5	0	1	0	0	0	0	0	0	0	0	0	6	1	7	18	66	0	0.62	43	15.4
AlTiMnS	0	3	8	8	4	3	3	4	1	0	0	1	1	1	0	0	0	0	0	0	9	5	19	64	0	0.69	37	13.3
AlTiMn	0	0	0	6	4	3	1	1	3	1	6	1	1	2	0	0	0	0	0	0	0	4	13	80	0	0.99	29	10.4
AlMnS	1	3	2	4	3	0	1	2	1	0	0	0	0	0	0	0	0	0	0	0	4	0	13	79	0	0.59	17	6.1
AlMn	0	2	0	3	0	1	0	1	3	1	0	0	0	0	0	0	0	0	0	0	0	1	10	86	0	0.75	11	3.9
AlSiMnS	1	3	3	0	0	2	1	0	0	0	0	0	0	0	0	0	0	0	0	6	10	0	22	58	0	0.47	10	3.6
AlSiMn	1	0	2	0	0	0	0	0	0	0	0	0	0	0	0	0	0	0	0	6	1	1	18	71	0	0.40	3	1.1
MgAlSiMnS	0	1	0	1	0	0	0	0	0	0	0	0	0	0	0	0	0	0	0	30	12	0	24	30	2	0.44	2	0.7
MgAlTiMn	0	0	0	0	0	0	0	0	0	1	0	0	0	0	0	0	0	0	0	0	0	2	11	82	2	1.18	1	0.4
SiMnS	0	0	0	0	0	0	0	1	0	0	0	0	0	0	0	0	0	0	0	47	18	1	30	0	0	0.94	1	0.4
TiSiMnS	0	1	0	0	0	0	0	0	0	0	0	0	0	0	0	0	0	0	0	3	4	87	4	0	0	0.38	1	0.4
TOTAL NUMBER	16	47	49	50	40	19	13	16	12	4	6	2	2	3	0	0	0	0	0									
PERCENTAGE	5.7	16.8	17.6	17.9	14.3	6.8	4.7	5.7	4.3	1.4	2.2	0.7	0.7	1.1	0.0	0.0	0.0	0.0	0.0									

TABLE 2

SUMMARY OF RESULTS FOR THE 3B WELD

SPECIMEN NAME: ARCTEC 3B
NUMBER OF
INCLUSIONS: 310

CHEMICAL TYPE	SIZE RANGE OF INCLUSIONS																			AVERAGE RELATIVE PEAK INTENSITIES (PERCENT)						AVERAGE DIAMETER (um)	TOTAL NUMBER	PERCENTAGE
From	0.2	0.3	0.4	0.5	0.6	0.7	0.8	0.9	1	1.1	1.2	1.3	1.4	1.5	1.6	1.7	1.8	1.9	2									
To	0.3	0.4	0.5	0.6	0.7	0.8	0.9	1	1.1	1.2	1.3	1.4	1.5	1.6	1.7	1.8	1.9	2	2.1	Si	S	Ti	Mn	Al	Mg			
AlTiSiMnS	38	68	38	35	21	14	5	4	3	2	1	0	0	1	0	0	0	0	0	9	8	21	30	29	0	0.48	230	74.2
AlTiSiMn	4	12	7	5	3	3	1	1	0	1	0	1	0	0	0	0	0	0	0	8	0	24	28	36	0	0.50	38	12.3
AlTiMnS	1	1	2	3	2	3	2	3	1	0	0	0	0	0	0	0	0	0	0	1	9	22	27	38	0	0.68	18	5.8
AlTiMn	0	0	0	2	2	1	0	0	0	0	1	1	0	0	1	1	0	0	0	1	0	16	20	60	0	1.03	9	2.9
TiSiMnS	1	1	2	0	1	0	0	0	0	0	0	0	0	0	0	0	0	0	0	26	11	44	16	0	0	0.44	5	1.6
AlSiMnS	0	0	1	1	0	0	1	0	0	0	0	0	0	0	0	0	0	0	0	43	13	0	15	26	0	0.59	3	1.0
MgAlTiSiMnS	0	1	1	0	0	0	0	0	0	0	0	0	0	0	0	0	0	0	0	8	12	22	30	24	2	0.40	2	0.6
MgAlSiMnS	0	0	1	0	0	0	0	0	0	0	0	0	0	0	0	0	0	0	0	24	6	0	51	14	4	0.41	1	0.3
MgAlTiSiMn	0	1	0	0	0	0	0	0	0	0	0	0	0	0	0	0	0	0	0	11	0	21	17	47	2	0.38	1	0.3
SiMnS	1	0	0	0	0	0	0	0	0	0	0	0	0	0	0	0	0	0	0	90	2	1	4	1	0	0.24	1	0.3
TiSiMn	0	0	0	0	1	0	0	0	0	0	0	0	0	0	0	0	0	0	0	8	0	88	2	0	0	0.65	1	0.3
AlMn	0	0	0	0	1	0	0	0	0	0	0	0	0	0	0	0	0	0	0	8	0	0	8	90	0	0.61	1	0.3
TOTAL NUMBER	45	84	52	46	31	21	9	8	4	3	2	2	0	1	1	1	0	0	0									
PERCENTAGE	14.5	27.1	16.8	14.8	10.0	6.8	2.9	2.6	1.3	1.0	0.6	0.6	0.0	0.3	0.3	0.3	0.0	0.0	0.0									

TABLE 5

SUMMARY OF THE AREA FRACTION AND NEAREST NEIGHBOUR DISTANCE

Sample Name	Number of Inclusions	Number of Fields	Total Area cm^2	Number of Inclusions per cm^2	Area Fraction Percent	Nearest-Neighbour Distance microns	Dominant Inclusion Type
S1B	231	18	3.96E-04	5.8E+05	0.11	6.5	AlTiSiMnS
3B	310	18	3.96E-04	7.8E+05	0.10	5.7	AlTiSiMnS
5B	279	18	3.96E-04	7.0E+05	0.10	6.0	AlTiSiMnS
7B	280	25	5.50E-04	5.1E+05	0.08	7.0	AlTiSiMnS

APPENDIX A

SIZE DISTRIBUTIONS

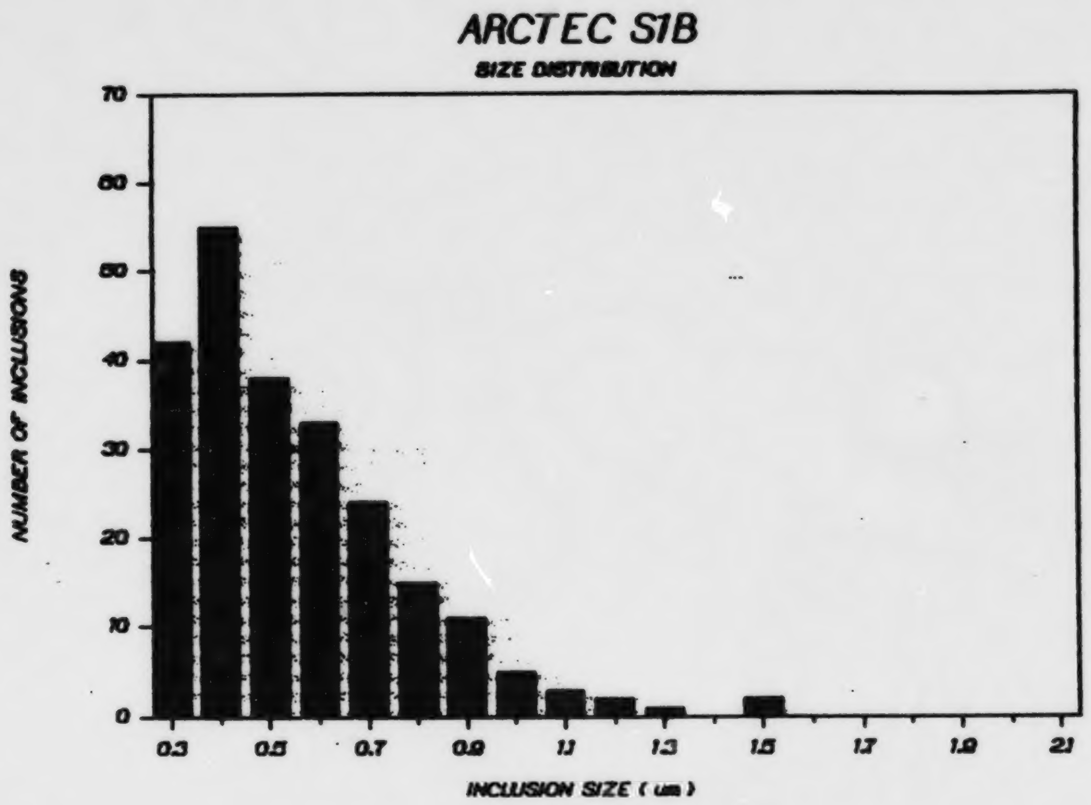
ARCTEC S1B
SIZE DISTRIBUTION
NUMBER OF INCLUSIONS
70
60
50
40
30
20
10
0
0.3
0.5
0.7
0.9
1.1
1.3
1.5
1.7
1.9
2.1
INCLUSION SIZE (um)

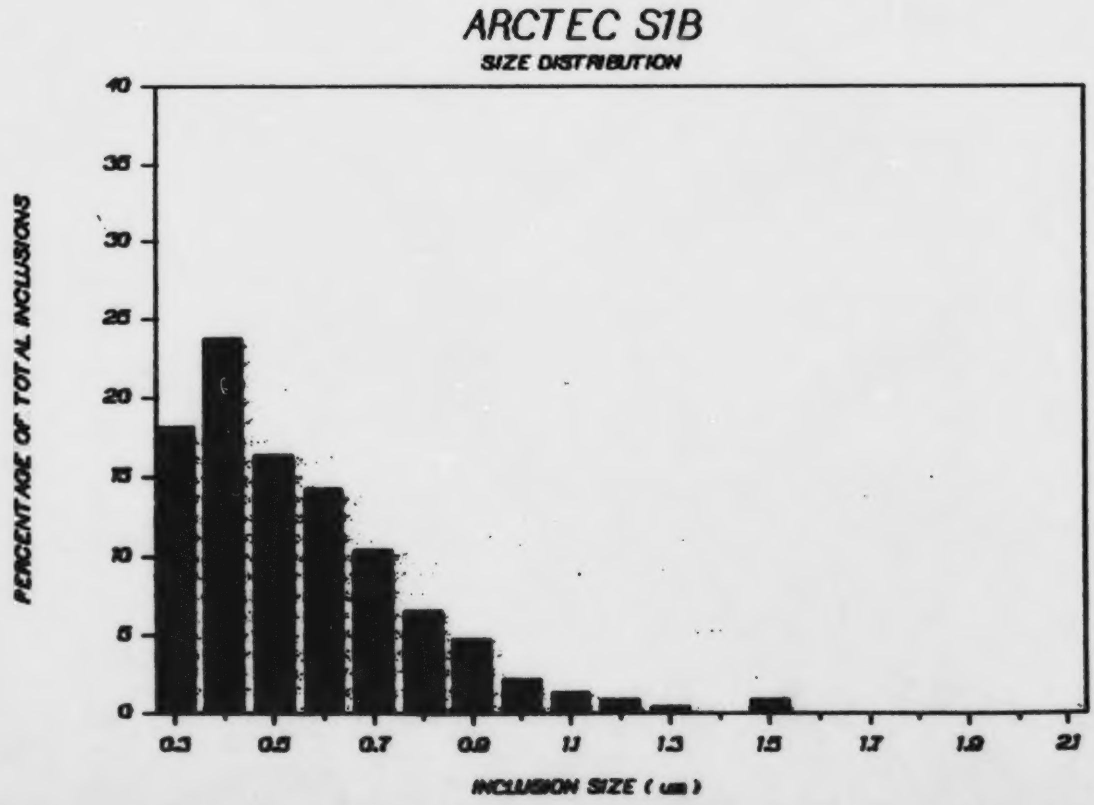
ARCTEC S1B
SIZE DISTRIBUTION
PERCENTAGE OF TOTAL INCLUSIONS
40
35
30
25
20
15
10
5
0
0.3
0.5
0.7
0.9
1.1
1.3
1.5
1.7
1.9
2.1
INCLUSION SIZE (um)

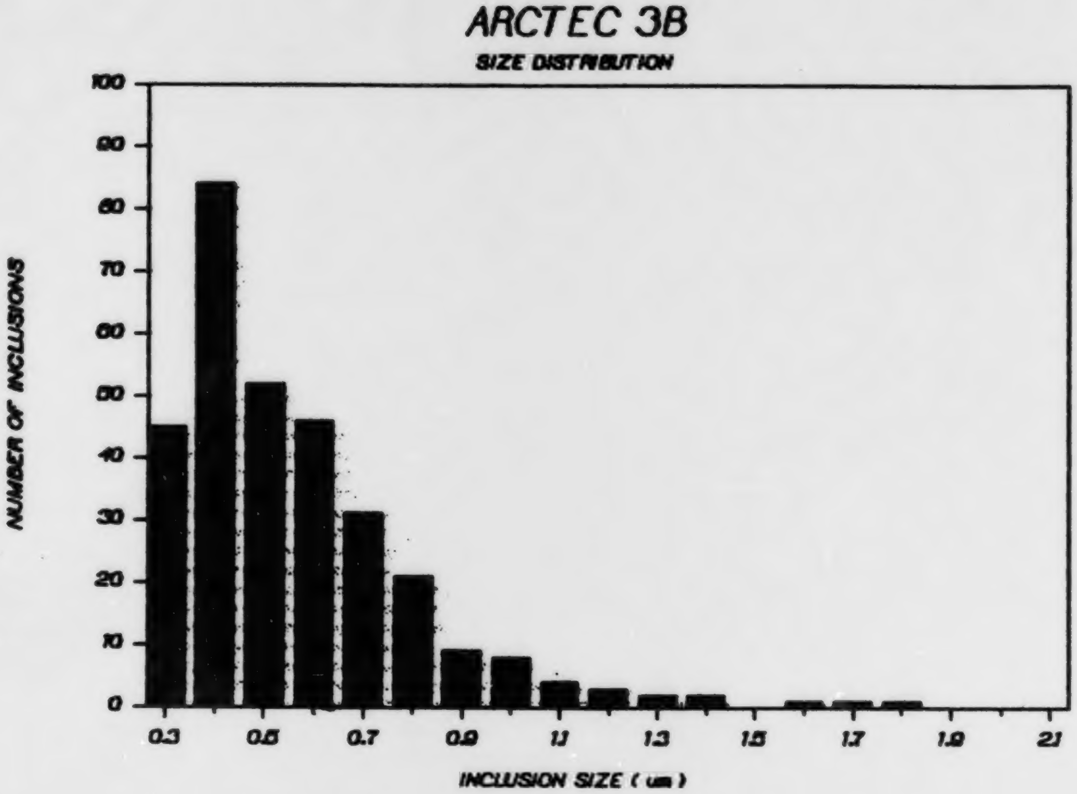
ARCTEC 3B
SIZE DISTRIBUTION
NUMBER OF INCLUSIONS
100
90
80
70
60
50
40
30
20
10
0
0.3
0.5
0.7
0.9
1.1
1.3
1.5
1.7
1.9
2.1
INCLUSION SIZE (um)

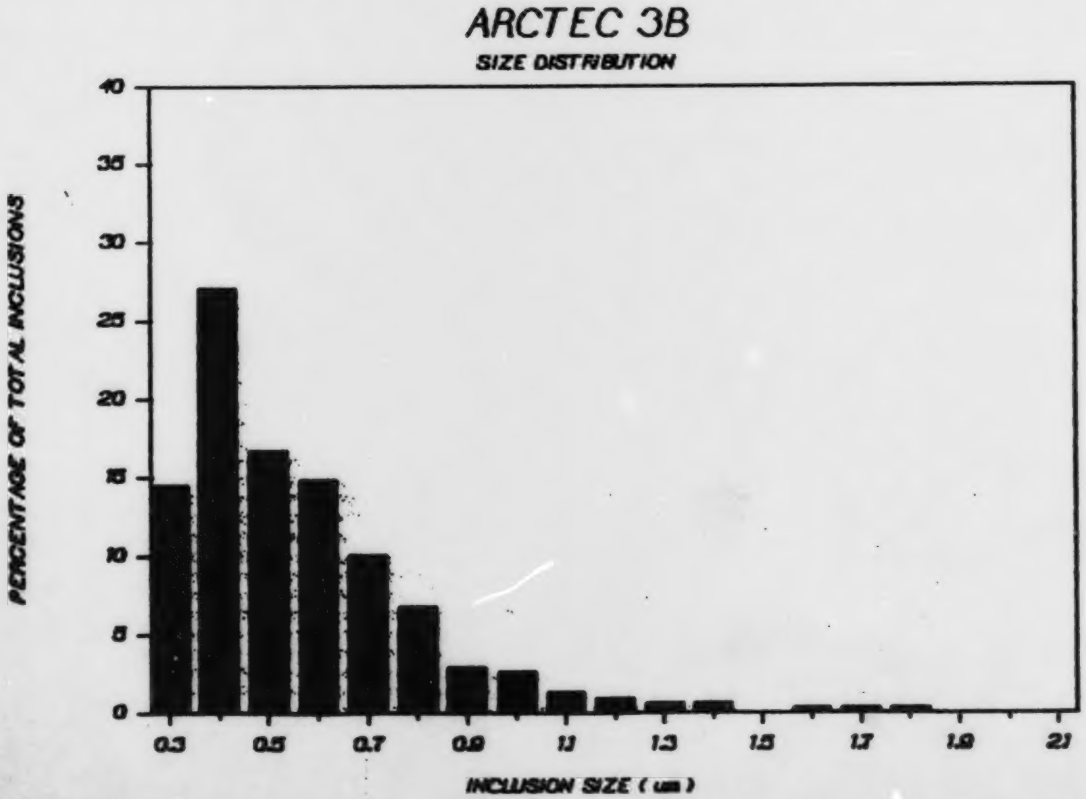
ARCTEC 3B
SIZE DISTRIBUTION
PERCENTAGE OF TOTAL INCLUSIONS
40
35
30
25
20
15
10
5
0
0.3
0.5
0.7
0.9
1.1
1.3
1.5
1.7
1.9
2.1
INCLUSION SIZE (um)

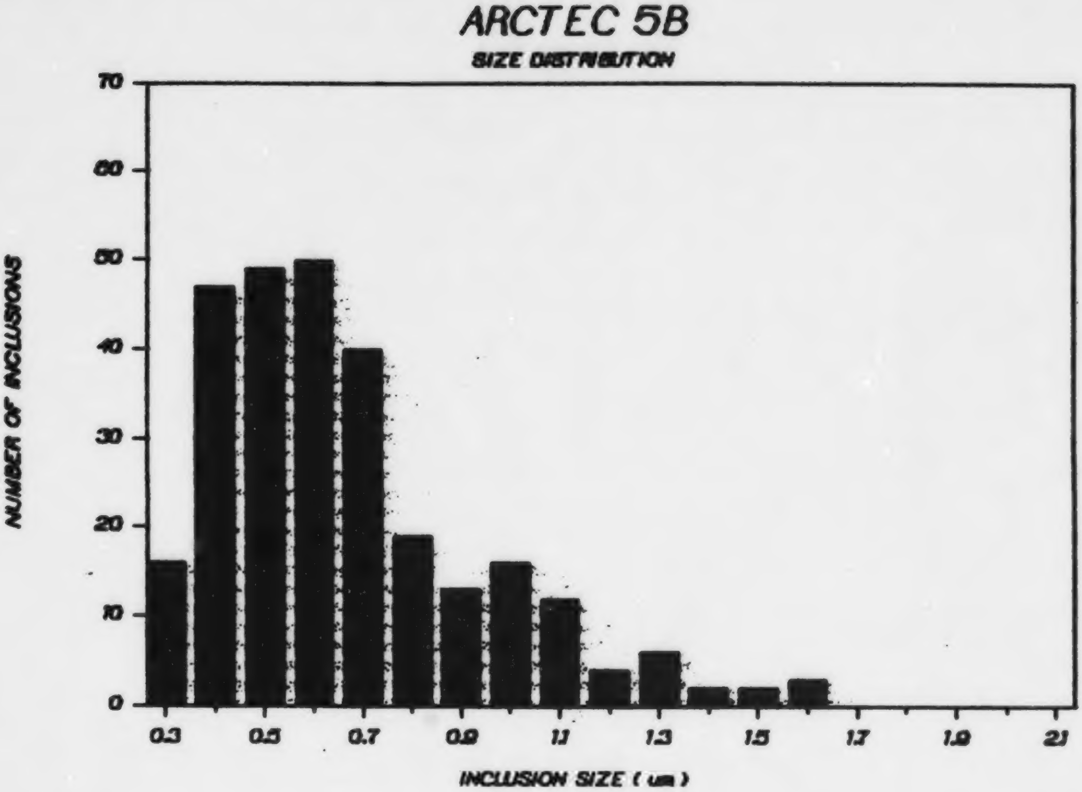
ARCTEC 5B
SIZE DISTRIBUTION
NUMBER OF INCLUSIONS
70
60
50
40
30
20
10
0
0.3
0.5
0.7
0.9
1.1
1.3
1.5
1.7
1.9
2.1
INCLUSION SIZE (um)

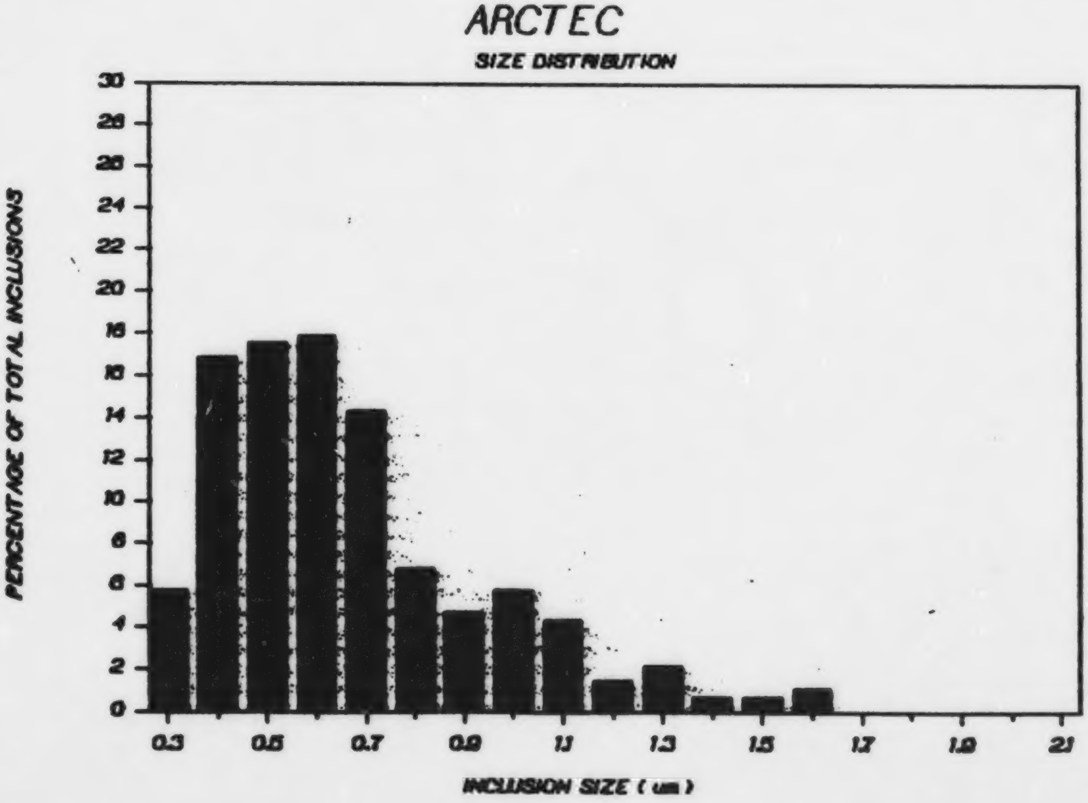
ARCTEC
SIZE DISTRIBUTION
PERCENTAGE OF TOTAL INCLUSIONS
30
28
26
24
22
20
18
16
14
12
10
8
6
4
2
0
0.3
0.5
0.7
0.9
1.1
1.3
1.5
1.7
1.9
2.1
INCLUSION SIZE (um)

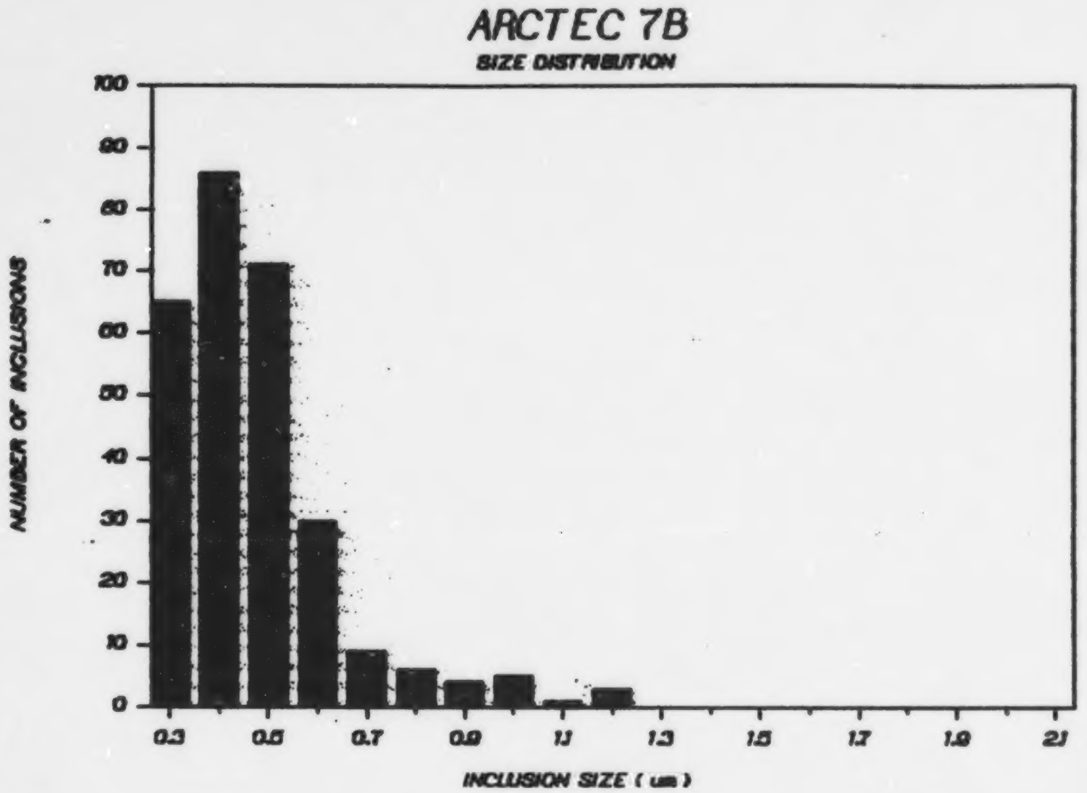
ARCTEC 7B
SIZE DISTRIBUTION
NUMBER OF INCLUSIONS
100
90
80
70
60
50
40
30
20
10
0
0.3
0.5
0.7
0.9
1.1
1.3
1.5
1.7
1.9
2.1
INCLUSION SIZE (um)

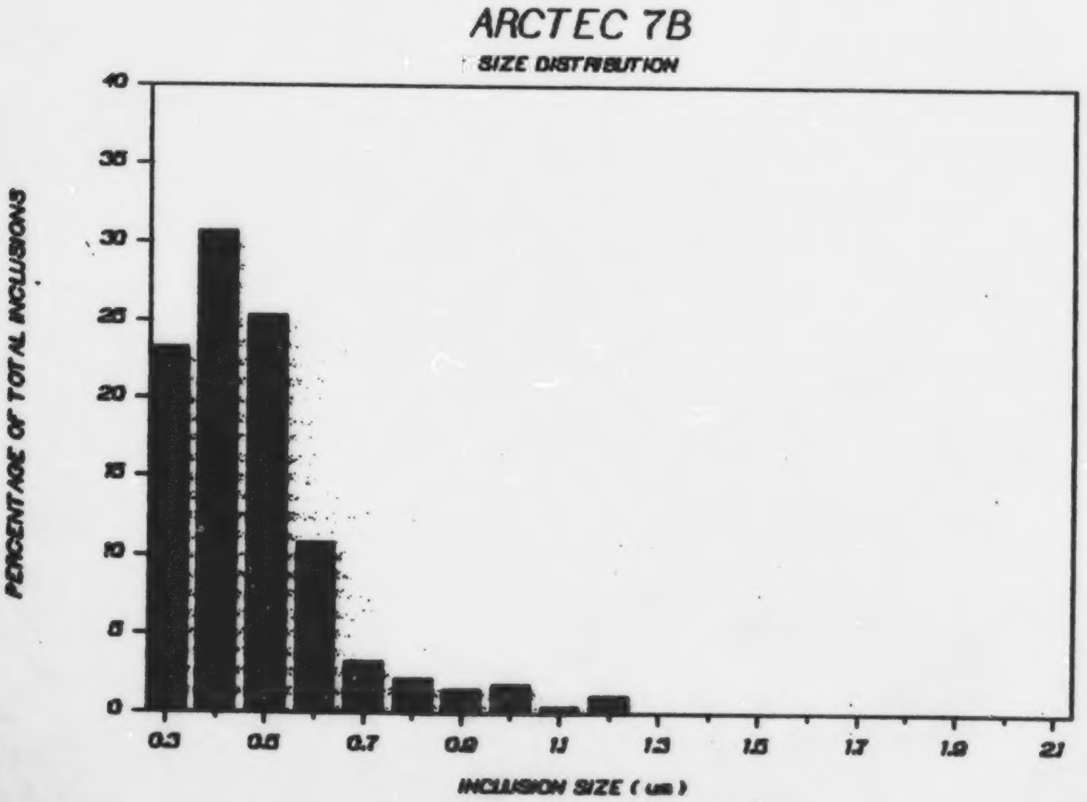
ARCTEC 7B
SIZE DISTRIBUTION
PERCENTAGE OF TOTAL INCLUSIONS
40
35
30
25
20
15
10
5
0
0.3
0.5
0.7
0.9
1.1
1.3
1.5
1.7
1.9
2.1
INCLUSION SIZE (um)

APPENDIX B

TYPE DISTRIBUTIONS FOR THE MAJOR CHEMICAL TYPES

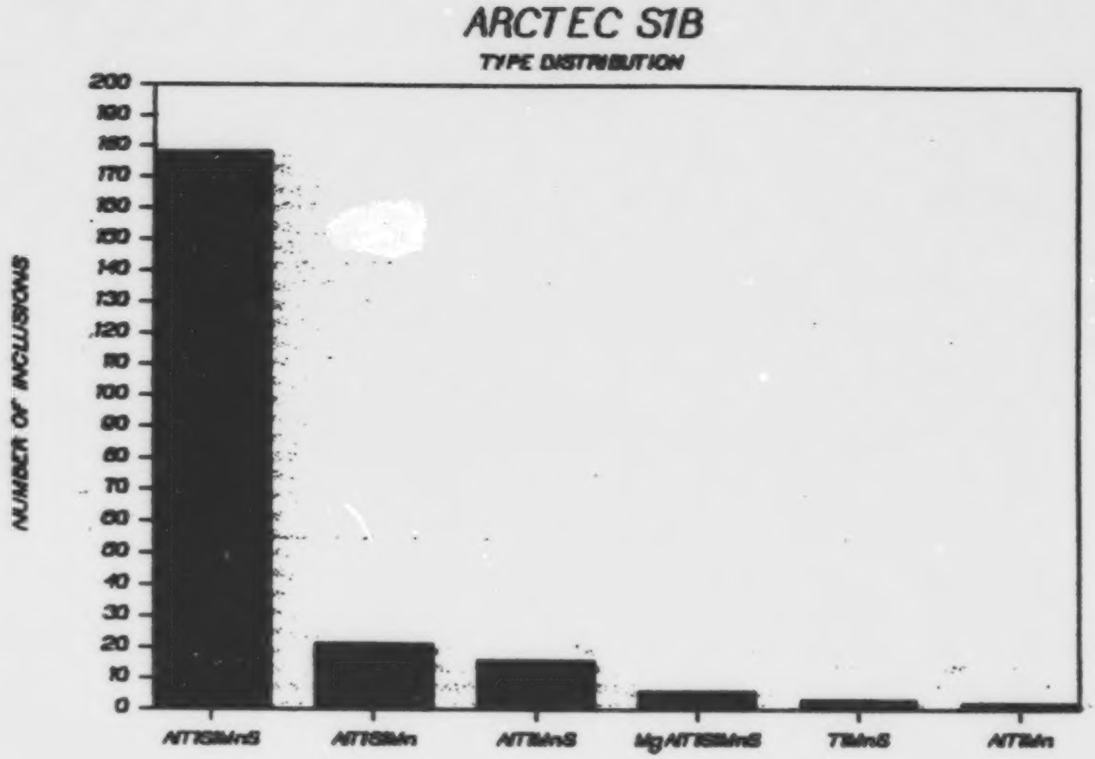
ARCTEC S1B
TYPE DISTRIBUTION
NUMBER OF INCLUSIONS
200
190
180
170
160
150
140
130
120
110
100
90
80
70
60
50
40
30
20
10
0
AlTiSiMnS
AlTiSiMn
AlTiMnS
MgAlTiSiMnS
TiMnS
AlTiMn

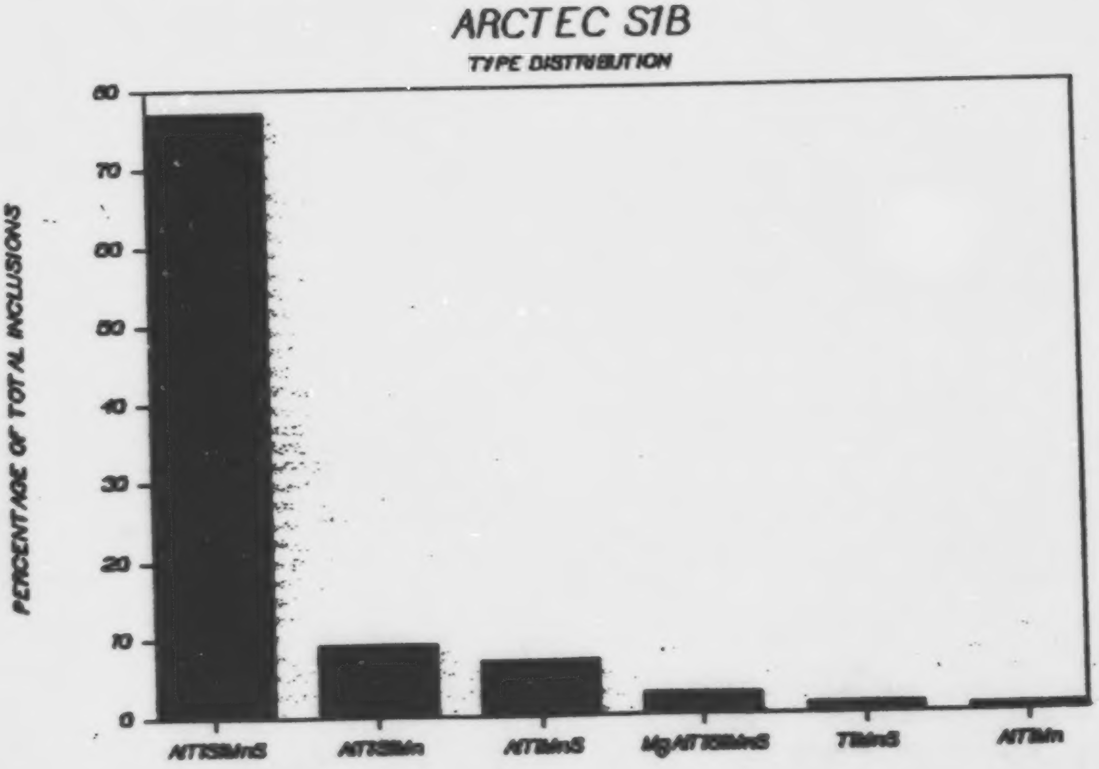
ARCTEC S1B
TYPE DISTRIBUTION
PERCENTAGE OF TOTAL INCLUSIONS
80
70
60
50
40
30
20
10
0
AlTiSiMnS
AlTiSiMn
AlTiMnS
MgAlTiSiMnS
TiMnS
AlTiMn

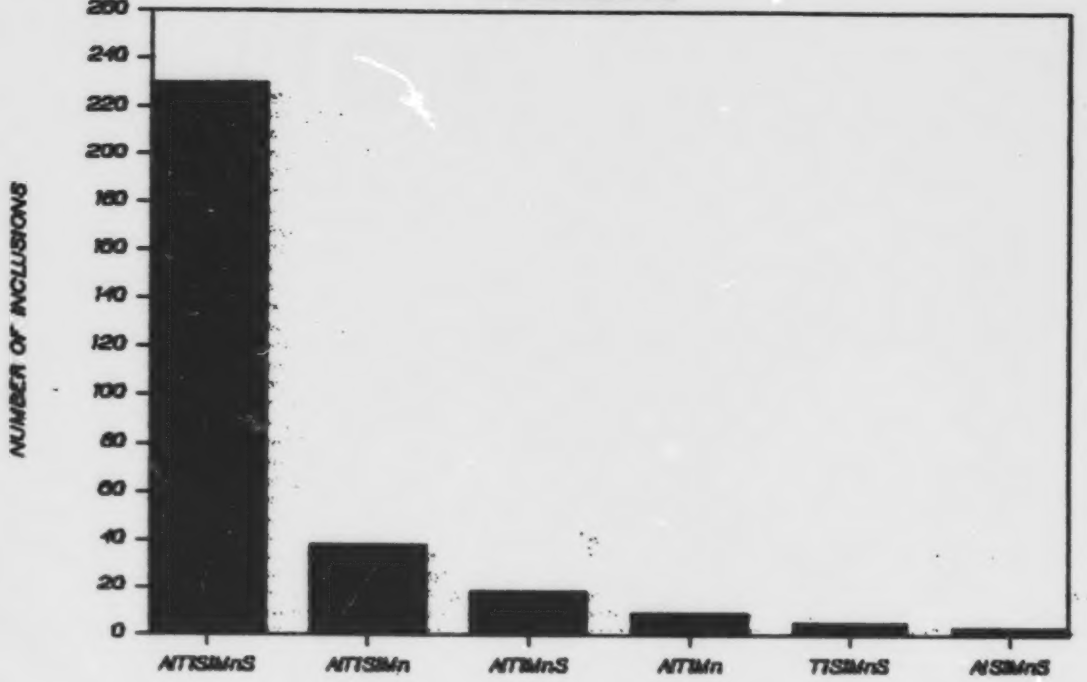
ARCTEC 3B

TYPE DISTRIBUTION

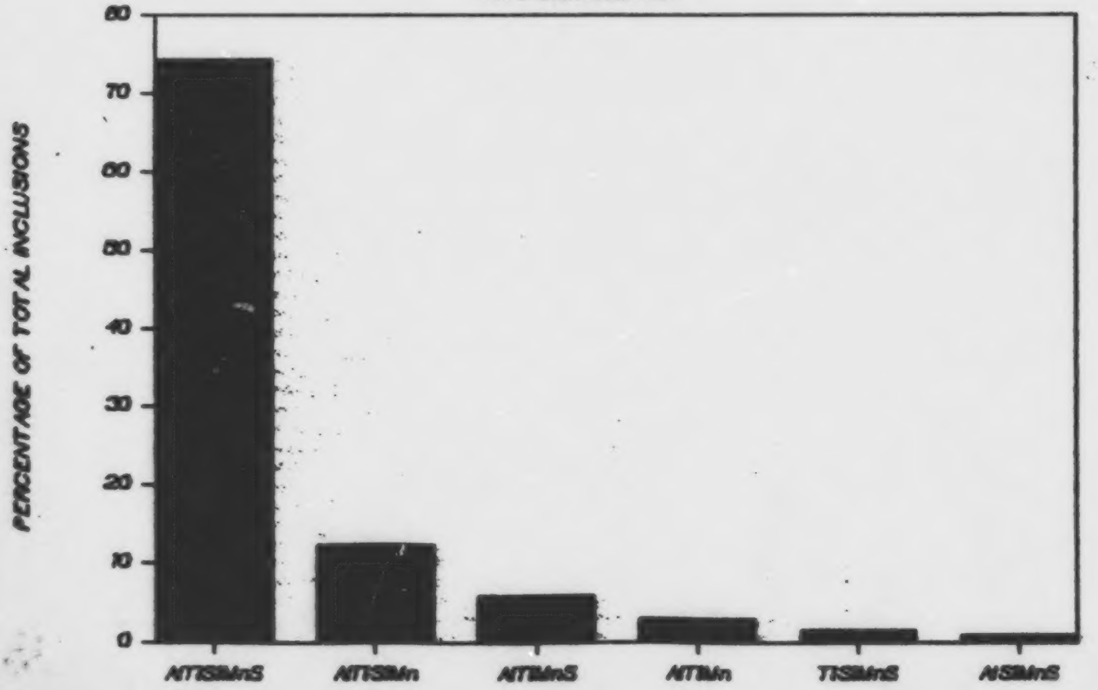
ARCTEC 3B

TYPE DISTRIBUTION

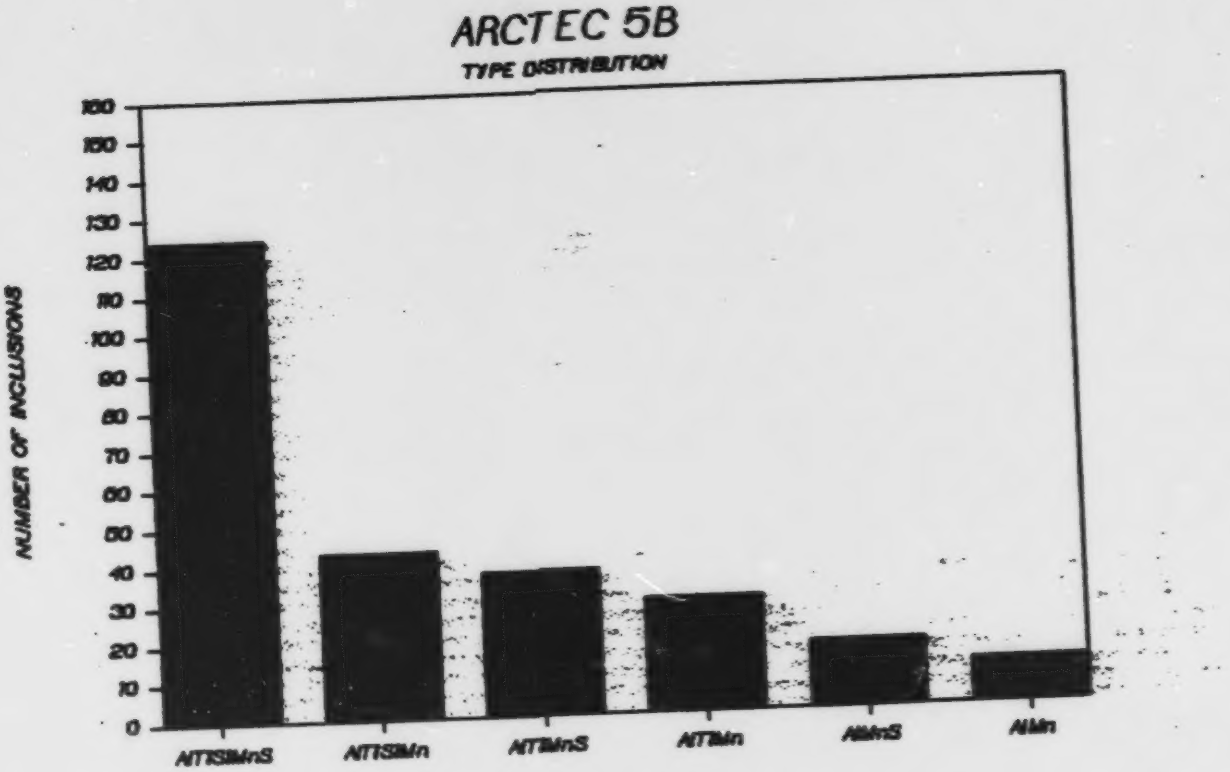
ARCTEC 5B
TYPE DISTRIBUTION
NUMBER OF INCLUSIONS
160
150
140
130
120
110
100
90
80
70
60
50
40
30
20
10
0
AlTiSiMnS
AlTiSiMn
AlTiMnS
AlTiMn
AlMnS
AlMn

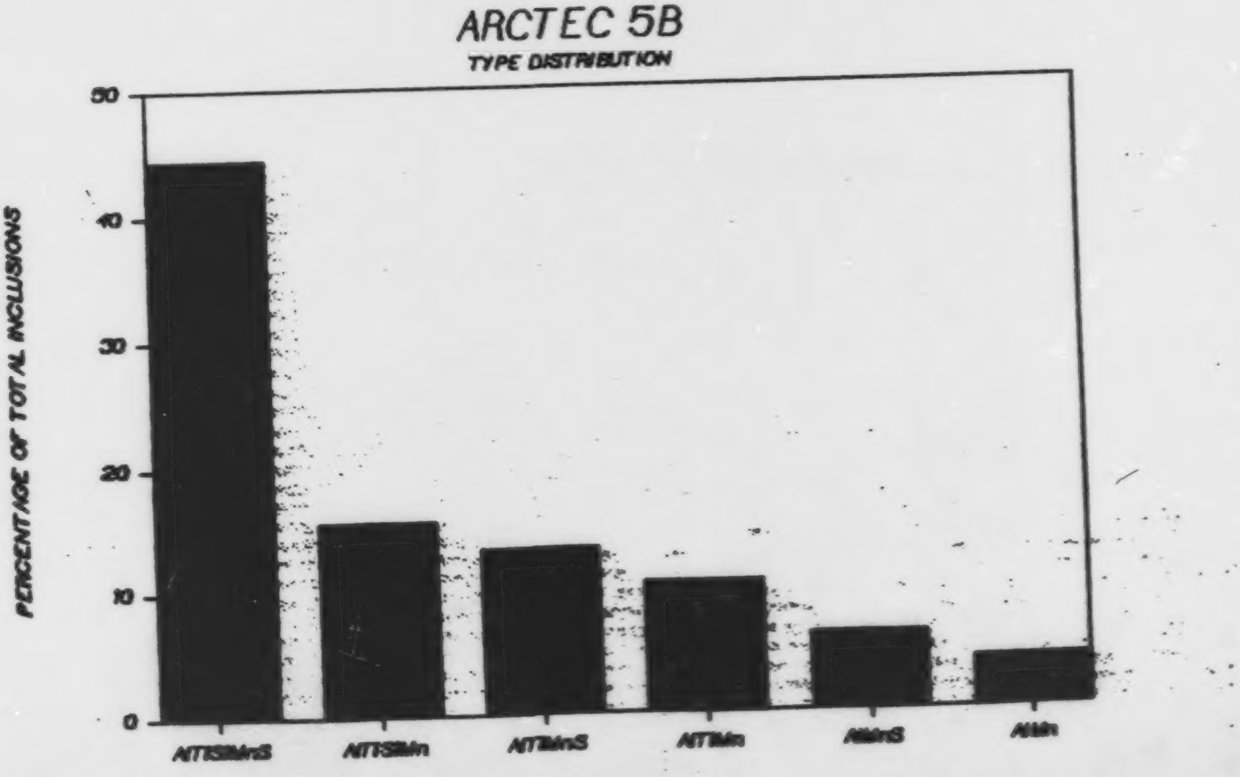
ARCTEC 5B
TYPE DISTRIBUTION
PERCENTAGE OF TOTAL INCLUSIONS
50
40
30
20
10
0
AlTiSiMnS
AlTiSiMn
AlTiMnS
AlTiMn
AlMnS
AlMn

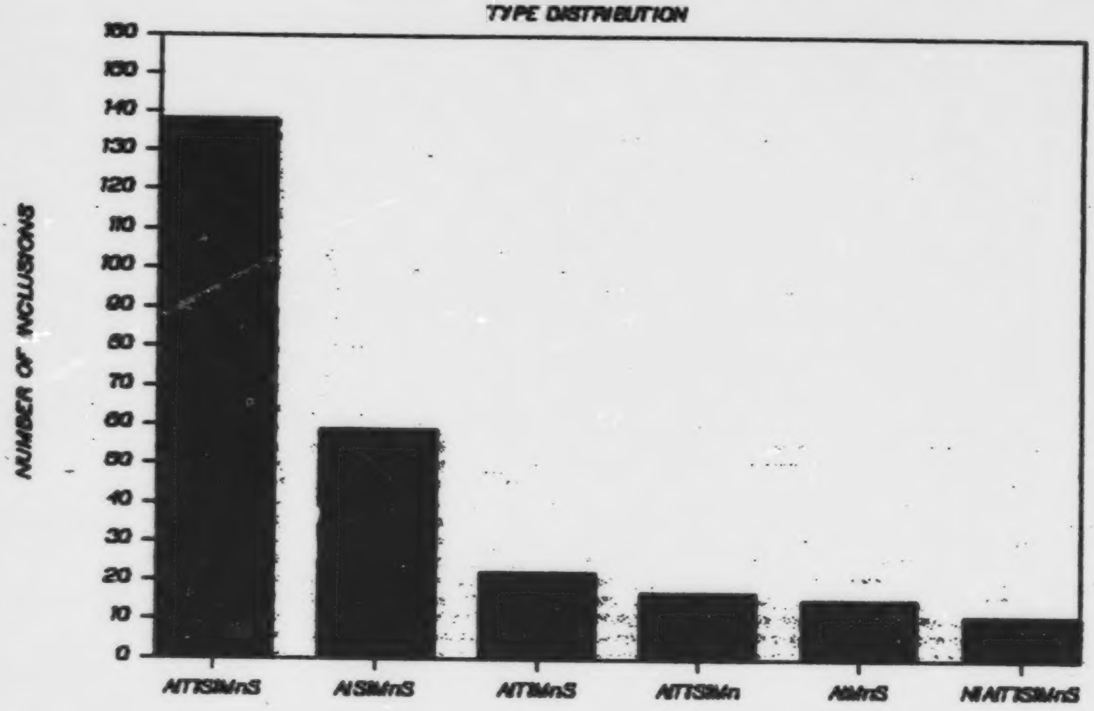

ARCTEC 7B

TYPE DISTRIBUTION

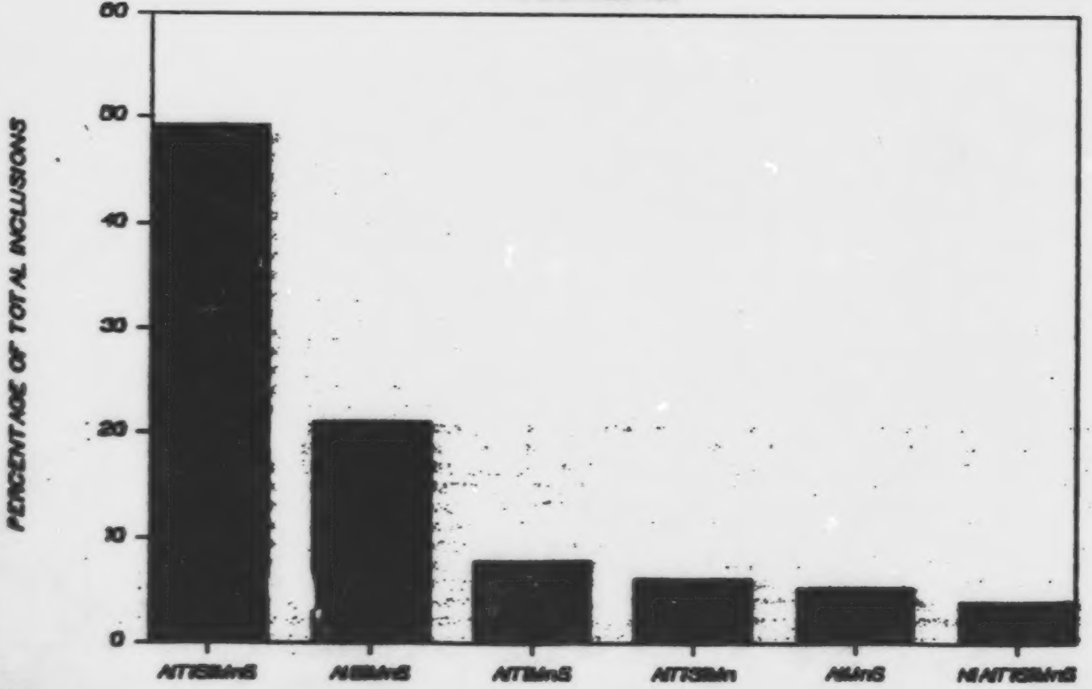

ARCTEC 7B

TYPE DISTRIBUTION

APPENDIX C

SIZE DISTRIBUTIONS FOR THE MAJOR CHEMICAL TYPES

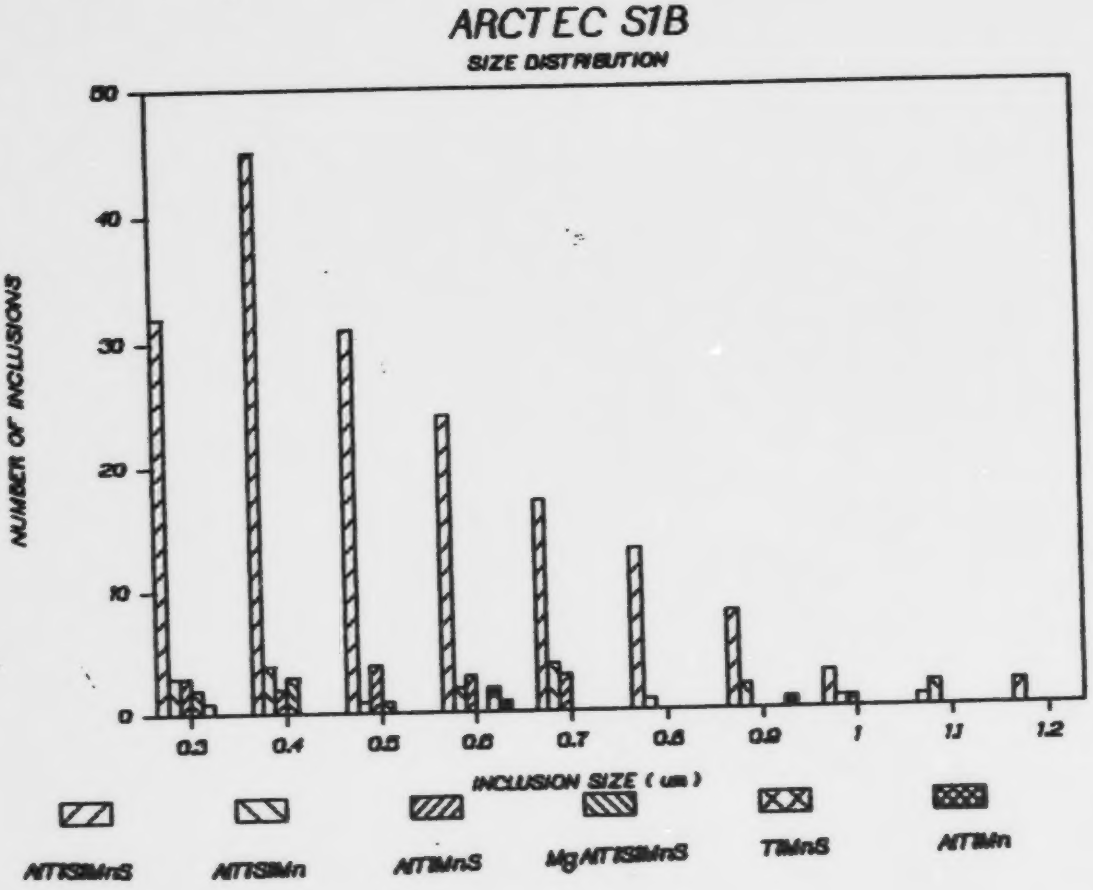
ARCTEC S1B
SIZE DISTRIBUTION
NUMBER OF INCLUSIONS
50
40
30
20
10
0
0.3
0.4
0.5
0.6
0.7
0.8
0.9
1
1.1
1.2
INCLUSION SIZE (um)
AlTiSiMnS
AlTiSiMn
AlTiMnS
MgAlTiSiMnS
TiMnS
AlTiMn

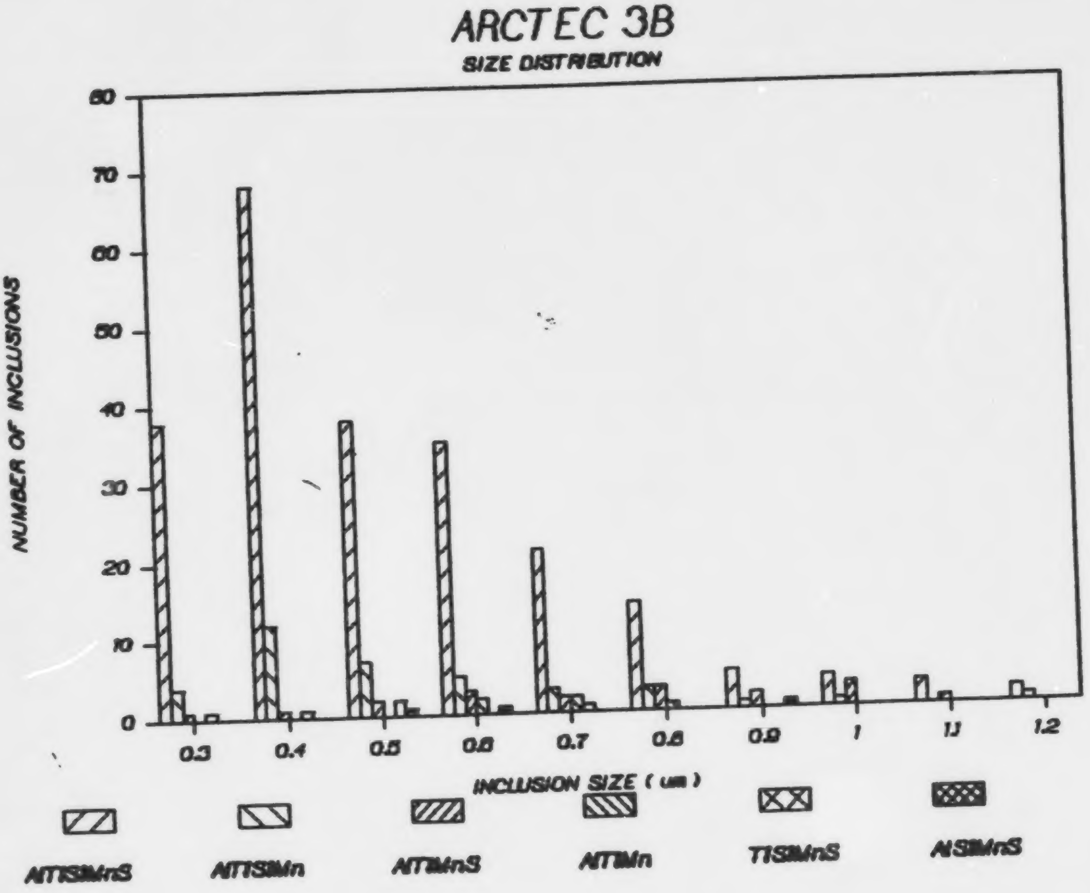
ARCTEC 3B
SIZE DISTRIBUTION
NUMBER OF INCLUSIONS
0
10
20
30
40
50
60
70
80
0.3
0.4
0.5
0.6
0.7
0.8
0.9
1
1.1
1.2
INCLUSION SIZE (um)
AlTiSiMnS
AlTiSiMn
AlTiMnS
AlTiMn
TiSiMnS
AlSiMnS

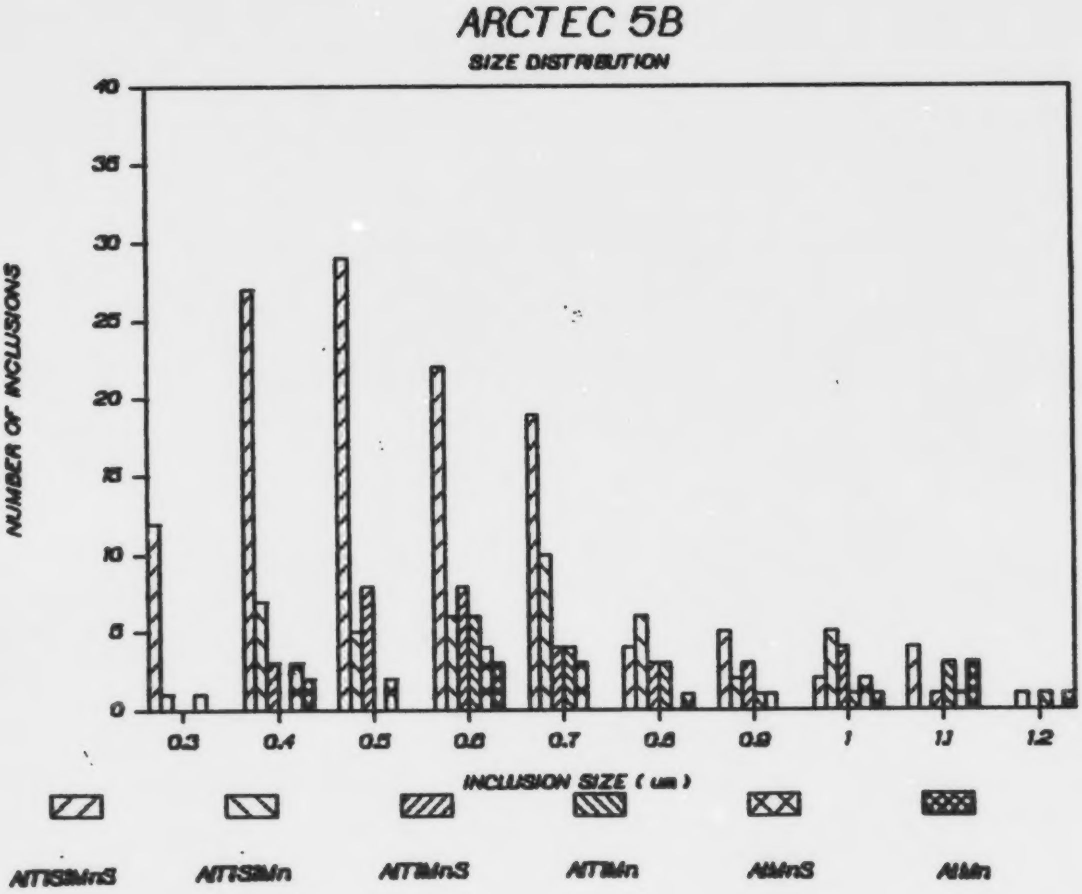
ARCTEC 5B
SIZE DISTRIBUTION
NUMBER OF INCLUSIONS
0
5
10
15
20
25
30
35
40
0.3
0.4
0.5
0.6
0.7
0.8
0.9
1
1.1
1.2
INCLUSION SIZE (um)
AlTiSiMnS
AlTiSiMn
AlTiMnS
AlTiMn
AlMnS
AlMn

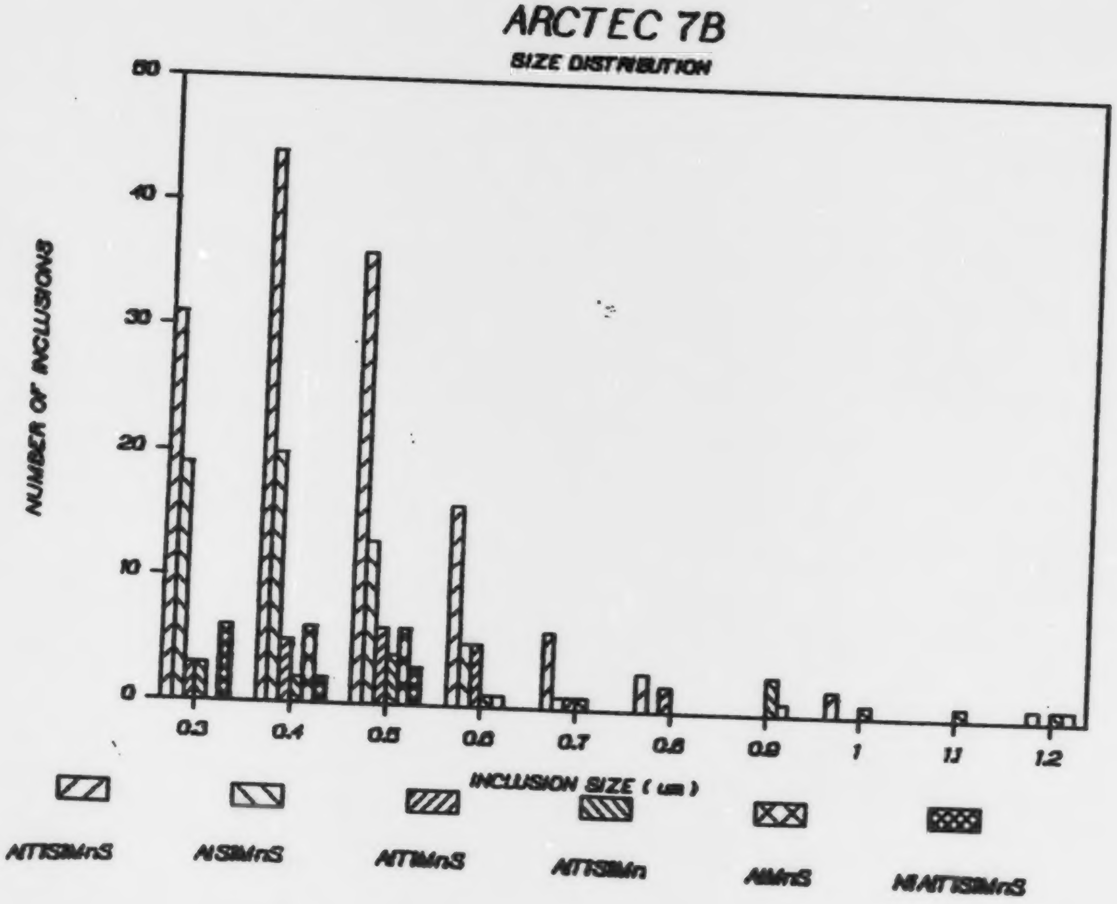
ARCTEC 7B
SIZE DISTRIBUTION
NUMBER OF INCLUSIONS
50
40
30
20
10
0
0.3
0.4
0.5
0.6
0.7
0.8
0.9
1
1.1
1.2
INCLUSION SIZE (um)
AlTiSiMnS
AlSiMnS
AlTiMnS
AlTiSiMn
AlMnS
NiAlTiSiMnS

APPENDIX B

Drop Weight Test Results

Table B1

Summary of Drop Weight Tests for Submerged Arc Welds
Consumable A, 5.0 kJ/mm

Test Temperature (°C)	As Welded*	Stress Relieved**
-40	---	No Break
-50	No Break	---
-55	No Break No Break	---
-60	Break	No Break
-70	Break	No Break No Break
-75	---	Break

*Impact energy of 400J is used.
**Impact energy of 540J is used.

Table B2

Summary of Drop Weight Tests for Submerged Arc Welds Consumable A, 3.5 kJ/mm

Test Temperature (°C)	As Welded*	Stress Relieved**
-40	---	No Break
-50	No Break	---
-60	No Break	No Break
		No Break
		Break
-65	---	Break
-70	No Break	Break
	No Break	
-75	Break	---

*Impact energy of 400J is used.
**Impact energy of 540J is used.

Table B3

Summary of Drop Weight Tests for Submerged Arc Welds Consumable B, 5.0 kJ/mm

Test Temperature (°C)	As Welded*	Stress Relieved**
-35	No Break	No Break
-40	---	No Break Break Break
-45	---	Break
-50	No Break No Break	Break
-60	No Break No Break	Break
-65	Break	---

*Impact energy of 400J is used.
**Impact energy of 540J is used.

Table B4

Summary of Drop Weight Tests for Submerged Arc Welds Consumable B, 3.5 kJ/mm

Test Temperature (°C)	As Welded*	Stress Relieved**
-40	No Break	---
-45	---	No Break
		Break
-50	No Break	Break
		Break
-55	No Break	---
	Break	
-60	Break	Break

*Impact energy of 400J is used.
**Impact energy of 540J is used.

Table B5

Summary of Drop Weight Tests for Submerged Arc Welds
Consumable A, 3.5 kJ/mm
Interpass Temperature of 232°C (S9B)

Temperature (°C)	Break/No Break Condition
-60	No Break
	No Break
-65	Break
	Break
-70	Break

Impact energy of 400J is used.

Table B6

Summary of Drop Weight Tests for Submerged Arc Welds
Consumable A, 3.5 kJ/mm
High Lateral Restraint and High Angular Restraint (S10B)

Temperature (°C)	Break/No Break Condition
-40	No Break
-50	No Break
-55	No Break
	No Break
-60	Break
	Break

Impact energy of 540J is used.

APPENDIX C

CVN Test Results

Table C1

CVN Impact Test Data for Consumable A
5.0 kJ/mm in As Welded Condition (Plate S1B)

Temperature °C	Subsurface				Root			
	Impact Energy (J)	Lateral Expansion (mm)	% Shear	Average Impact Energy (J)	Impact Energy (J)	Lateral Expansion (mm)	% Shear	Average Impact Energy (J)
0	163 141	2.2 2.1	N.B. N.B.	152	150 163	2.4 2.4	N.B. N.B.	157
-20	140 153	1.8 1.8	70 70	147	148 146	2.3 2.3	N.B. N.B.	147
-40	125 136	1.8 1.6	50 50	131	163 150	2.4 2.2	N.B. N.B.	157
-60	114 95	1.6 1.4	50 50	105	153 118	2.2 1.6	N.B. 60	136
-70	61 73 --	0.8 1.1 --	30 30 --	67	108 75 16*	1.4 1.0 0.36	60 20 10	66 (92)*
-75	-- --	--	-- --	-- --	30 22	0.46 0.38	10 10	26
-80	43 52	0.78 0.76	20 20	48	14 12	0.23 0.23	10 10	13
-90	27 20	0.36 0.28	10 10	24	-- --	--	-- --	-- --
-100	12 11	0.36 0.46	10 10	12	-- --	-- --	-- --	-- --

*Average of two data points only.

Table C2

CDVN Impact Test Data for Consumable A
5.0 kJ/mm in Stress Relieved Condition (S2A)

Temperature °C	Subsurface				Root			
	Impact Energy (J)	Lateral Expansion (mm)	% Shear	Average Impact Energy (J)	Impact Energy (J)	Lateral Expansion (mm)	% Shear	Average Impact Energy (J)
0	147	2.6	N.B.	146	151	2.5	N.B.	149
	145	2.4	N.B.		146	2.4	N.B.	
-20	153	2.3	N.B.	152	153	2.1	80	150
	151	1.8	70		146	2.5	N.B.	
-40	145	2.1	70	131	142	2.1	80	139
	116	1.8	50		136	2.2	80	
-60	111	1.8	50	102	81	1.4	50	79
	93	1.5	50		77	1.2	50	
-70	66	1.0	30	64	65	1.1	40	53
	61	1.0	30		41	0.71	20	
-80	29	0.56	10					
	27	0.53	20	20	61	1.1	40	37
	16	0.61	20					
	8	0.28	10		12	0.25	5	
-85	--	--	--	--	11	0.28	10	11
					11	0.25	10	
-90	41	0.79	10	32	12	0.25	5	12
	23	0.48	10		11	0.36	5	

N.B. = No Break

Table C3

CVN Test Data for Consumable A
3.5 kJ/mm in As Welded Condition (S3A)

Temperature °C	Subsurface				Root			
	Impact Energy (J)	Lateral Expansion (mm)	% Shear	Average Impact Energy (J)	Impact Energy (J)	Lateral Expansion (mm)	% Shear	Average Impact Energy (J)
0	155 155	2.5 2.5	N.B. N.B.	155	161 157	2.4 2.5	N.B. N.B.	159
-20	146 144	2.4 2.5	N.B. N.B.	145	151 151	2.3 2.3	N.B. N.B.	151
-40	155 152	2.1 2.0	N.B. 80	154	149 144	1.7 1.8	60 60	147
-60	144 129	1.9 1.8	70 50	137	114 109	1.3 1.5	60 60	112
-70	106 96	1.6 1.5	50 50	101	118 107	1.8 1.4	70 40	113
-75	--	--	--	--	56 46	0.76 0.66	30 20	51
-80	49 46	0.79 0.76	30 30	48	26 12	0.38 0.18	10 10	19
-85	30 15	0.56 0.36	15 15	23	--	--	--	--
-90	14 12	0.36 0.28	10 10	13	--	--	--	--

Table C4

CVN Impact Test Data for Consumable A
3.5 kJ/mm in Stress Relieved Condition (S4A)

Temperature °C	Subsurface				Root			
	Impact Energy (J)	Lateral Expansion (mm)	% Shear	Average Impact Energy (J)	Impact Energy (J)	Lateral Expansion (mm)	% Shear	Average Impact Energy (J)
0	155 151	2.2 2.0	N.B. 70	153	158 157	2.5 2.6	N.B. N.B.	158
-20	152 145	2.1 2.0	N.B. 70	149	147 140	2.0 2.5	N.B. 80	147
-40	145 101	2.1 1.6	60 60	123	132 120	2.0 1.8	70 70	126
-60	143 125	2.0 1.7	60 60	134	107 107	1.7 1.7	50 50	107
-70	69 58	1.1 0.91	50 40	64	64	1.1	30	64
-80	92 74 57 21	1.2 1.2 0.94 0.48	40 40 20 20	61	56 51	0.99 0.81	20 20	54
-90	--	--	--	--	19 15 11	0.43 0.48 0.31	10 10 10	15
-100	14 9	0.31 0.28	10 10	12	--	--	--	--

N.B. = No Break

Table C5

CVN Impact Test Data for Consumable B
5.0 kJ/mm in As Welded Condition (Plate S5B)

Temperature °C	Subsurface				Root			
	Impact Energy (J)	Lateral Expansion (mm)	% Shear	Average Impact Energy (J)	Impact Energy (J)	Lateral Expansion (mm)	% Shear	Average Impact Energy (J)
0	(71)	(1.0)	(50)	(66)*	136	1.6	60	134
	(61)	(0.86)	(40)		132	1.7	50	
	115	1.8	70					
	89	1.4	60	102				
-20	(35)	(0.53)	(25)	(35)	91	1.1	40	73
	(34)	(0.33)	(30)		55	0.81	20	
	72	1.1	70					
	50	0.91	60	61				
-30	(38)	(0.61)	(20)	(37)	--	--	--	--
	(35)	(0.58)	(20)		--	--	--	
-40	(20)	(0.36)	(10)	(18)	76	1.0	40	76
	(15)	(0.20)	(10)		76	1.0	40	
	49	0.86	50	45				
	41	0.81	30					
-50	(14)	(0.25)	(0)	(13)	61	0.86	10	52
	(12)	(0.20)	(0)		42	0.58	10	
	49	0.89	40					
	31	0.66	20	40				
-60	(--)	(--)	(--)	(--)	29	0.46	10	26
					22	0.23	10	
	51	0.97	30					
	38	0.69	30	45				
-70	27	0.51	10	--	--	--	--	--
	26	0.51	10	27				
-80	(--)	(--)	(--)	(--)	23	0.36	0	19
					14	0.20	0	
	16	0.41						
	16	0.36		16				
-90	(--)	(--)	(--)	(--)	14	0.18	0	13
					12	0.16	0	

*Bracketed figure is from samples which have 90:10 ratio of unrefined:refined regions

Table C6

CVN Test Data for Consumable B
5.0 kJ/mm in Stress Relieved Condition (S6A)

Temperature °C	Subsurface				Root			
	Impact Energy (J)	Lateral Expansion (mm)	% Shear	Average Impact Energy (J)	Impact Energy (J)	Lateral Expansion (mm)	% Shear	Average Impact Energy (J)
25	--	--	--	--	110	1.4	50	110
0	118	1.80	70	116	111	1.7	60	80
	114	1.70	70		88	1.2	40	
					42	0.69	30	
-10	107	1.7	70	107	--	--	--	--
-20	103	1.4	60	91	98	0.66	30	97
	78	1.1	50		96	1.4	50	
-30	32	0.84	40	32	72	1.0	50	69
					65	0.99	50	
-40	82	1.4	40	78	60	1.1	30	54
	74	1.2	50		48	0.74	10	
-50	44	0.91	50	30	68	0.89	30	54
	15	0.41	20		40	0.69	10	
-60	45	0.84	50	42	30	0.56	15	23
	39	0.79	40		16	0.31	5	
-70	30	0.51	20	26	--	--	--	--
	22	0.48	20					
-80	16	0.46	20	16	16	0.31	5	15
	15	0.31	10		13	0.25	5	

Table C7

CVN Test Data for Consumable B
3.5 kJ/mm in As Welded Condition (S7A)

Temperature °C	Subsurface Impact Energy (J)	Subsurface Lateral Expansion (mm)	Subsurface % Shear	Subsurface Average Impact Energy (J)	Root Impact Energy (J)	Root Lateral Expansion (mm)	Root % Shear	Root Average Impact Energy (J)
25	118 92	1.4 1.7	90	105	--	--	--	--
0	110 107	1.5 1.4	60 60	109	146 144	1.9 1.9	70 80	145
-10	--	--	--	--	125	1.7	90	125
-20	96 87	1.5 1.5	40 40	92	100 91	1.5 1.3	40 40	96
-30	--	--	--	--	119			119
-40	63 60	0.94 0.84	30	62	72 72	1.1 1.0	40 30	72
-50	35 32	0.66 0.56	20 20	34	57 37	0.89 0.61	30 25	47
-60	38 35	0.64 0.66	30 20	37	31 27	0.56 0.41	20 20	29
-70	17 17	0.36 0.36	20 20	17	--	--	--	--
-80	15 13	0.33 0.25	10 5	14	33 20	0.53 0.41	10 10	27
-85	--	--	--	--	20 15	0.43 0.33	10 10	18

Table C8

CVN Test Data for Consumable B
3.5 kJ/mm in Stress Relieved Condition (S8A)

Temperature °C	Subsurface				Root			
	Impact Energy (J)	Lateral Expansion (mm)	% Shear	Average Impact Energy (J)	Impact Energy (J)	Lateral Expansion (mm)	% Shear	Average Impact Energy (J)
0	156 111	2.1 1.7	80 70	134	155 144	1.9 2.2	80 N.B.	150
-20	122 101	1.7 1.5	60 40	112	145 139	1.8 1.9	80 80	142
-40	64 58	0.81 0.99	40 40	61	114 68 58	1.6 1.1 0.99	80 30 40	80
-50	93 45	1.2 0.81	30 30	69	--	--	--	--
-60	103 76 35	1.4 1.2 0.66	40 30 30	71	118 63 49	1.8 0.99 0.81	40 40 10	77
-70	14 9	0.38 0.28	20 10	12	42 28	0.69 0.56	10 10	35
-80	37 34	0.64 0.51	10 10	36	22 15	0.41 0.38	10 10	19
-90	6	0.23	10	6	12 11	0.36 0.28	10 10	12

N.B. = No Break

Table C9

CVN Test Data for Consumable A
3.5 kJ/mm in As Welded "High Restraint" Condition (S9A)

Temperature °C	Subsurface				Root			
	Impact Energy (J)	Lateral Expansion (mm)	% Shear	Average Impact Energy (J)	Impact Energy (J)	Lateral Expansion (mm)	% Shear	Average Impact Energy (J)
0	154	2.7	N.B.	153	153	2.4	N.B.	153
	151	2.6	N.B.		153	2.3	N.B.	
-20	155	2.7	N.B.	155	159	1.9	80	158
	155	2.5	N.B.		157	1.9	80	
-40	152	1.9	80	148	152	2.1	N.B.	148
	144	2.6	N.B.		144	1.9	50	
-50	--	--	--	--	144	1.9	70	131
					118	1.7	60	
-60	150	2.0	80	147	96	1.4	50	94
	143	2.0	80		92	1.4	50	
-70	57	1.1	20	50	65	1.0	40	41
	43	0.76	20		16	0.34	10	
-75	--	--	--	--	37	0.58	10	25
					12	0.20	10	
-80	51	0.91	20	46	11	0.20	5	11
	40	0.84	20		11	0.20	5	
-90	19	0.41	10	17	--	--	--	--
	14	0.43	10					
-100	9	0.33	10	8	--	--	--	--
	7	0.23	10					

Table C10

CVN Test Data for Consumable A
3.5 kJ/mm in As Welded Condition (S10A)

Temperature °C	Subsurface				Root			
	Impact Energy (J)	Lateral Expansion (mm)	% Shear	Average Impact Energy (J)	Impact Energy (J)	Lateral Expansion (mm)	% Shear	Average Impact Energy (J)
0	158	2.6	N.B.*	156	148	2.5	N.B.	147
	154	2.4	N.B.		146	2.5	N.B.	
-20	145	2.3	N.B.	145	160	2.3	N.B.	158
	144	2.3	N.B.		156	2.4	N.B.	
-40	158	2.3	60	158	160	2.0	80	160
	157	1.9	N.B.		159	2.0	80	
-60	145	1.8	50	139	152	1.8	70	129
	137	1.9	50		130	1.7	70	
	134	1.7	50		106	1.5	60	
-70	133	1.8	40	111	64	1.0	40	43
	125	1.9	50		43	0.79	20	
	109	1.6	30		32	0.61	30	
	76	1.2	30		32	0.69	20	
-80	74	1.1	20	41	37	0.64	10	20
	31	0.46	10		12	0.20	10	
	19	0.33	10		11	0.31	10	

*N.B. = No Break

Table C11

CVN Test Data for Consumable A
3.5 kJ/mm in As Welded Condition (S11A)

	Subsurface				Root			
Temperature °C	Impact Energy (J)	Lateral Expansion (mm)	% Shear	Average Impact Energy (J)	Impact Energy (J)	Lateral Expansion (mm)	% Shear	Average Impact Energy (J)
0	154 152	2.4 2.4	N.B.* N.B.	153	158 151	2.2 2.3	N.B. N.B.	155
-20	158 151	2.1 2.3	N.B. N.B.	155	160 158	2.2 2.0	N.B. N.B.	159
-40	147 145	1.9 1.7	70 70	146	157 141	1.7 1.7	80 60	149
-60	114 92	1.7 1.3	40 40	103	125 104	1.7 1.4	50 50	115
-65	--	--	--	--	68	1.0	30	43
-70	30	0.38	20	30	19 15	0.28 0.18	10 10	17
-75	--	--	--	--	14 9	0.15 0.08	10 10	13
-80	90 84 20 74	1.2 1.1 0.33 1.0	40 40 10 40	67	41 14	0.61 0.36	20 10	28
-90	10	0.15	10	10	--	--	--	--
-100	14 10	0.15 0.05	10 10	12	--	--	--	--

*No Break

Table C12

CVN Test Data for Consumable A
3.5 kJ/mm in As Welded Condition (S11B)

	Subsurface				Root			
Temperature °C	Impact Energy (J)	Lateral Expansion (mm)	% Shear	Average Impact Energy (J)	Impact Energy (J)	Lateral Expansion (mm)	% Shear	Average Impact Energy (J)
0	154 147	2.3 2.2	N.B. N.B.	151	154 137	2.3 2.4	N.B. N.B.	146
-20	160 153	2.3 1.7	N.B. N.B.	157	160 157	2.2 2.3	N.B. N.B.	159
-40	156 133	2.4 1.7	N.B. 50	146	150 149	1.9 1.7	60 70	150
-60	128 87	1.7 1.3	50 40	108	130 125 98	1.6 1.6 1.4	50 60 40	118
-65	112 93	1.6 1.3	40 40	103	-- --	-- --	-- --	-- --
-70	81	1.2	30	81	110 64	1.5 0.99	40 30	87
-75	92 37 16	1.4 0.46	30 10	49	114 104	1.6 1.4	40 40	109
-80	16 12	0.23 0.20	10 10	14	35 27 21	0.43 0.38 0.20	10 10 10	28

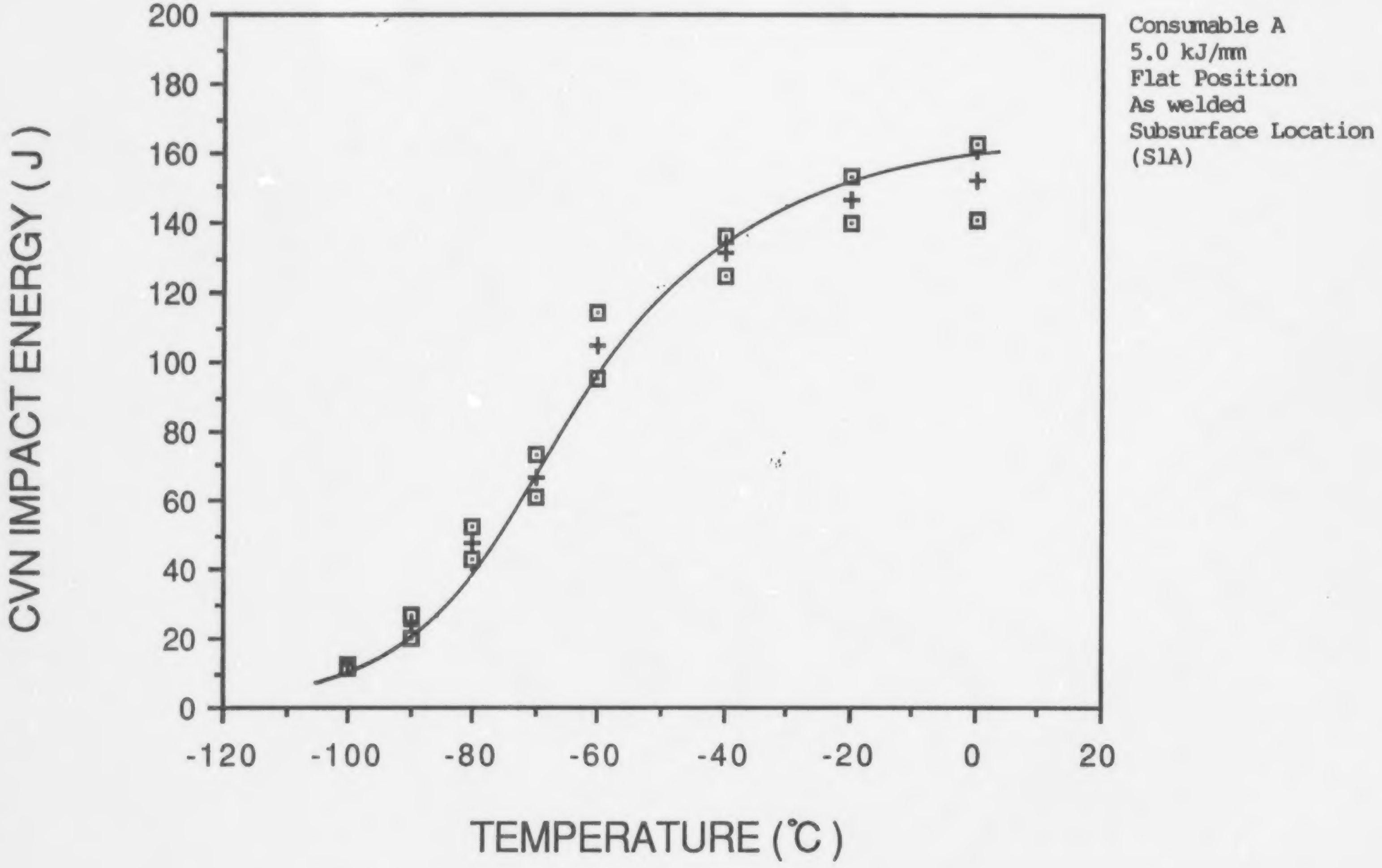

Figure C1 CVN transition curve for subsurface location of S1A

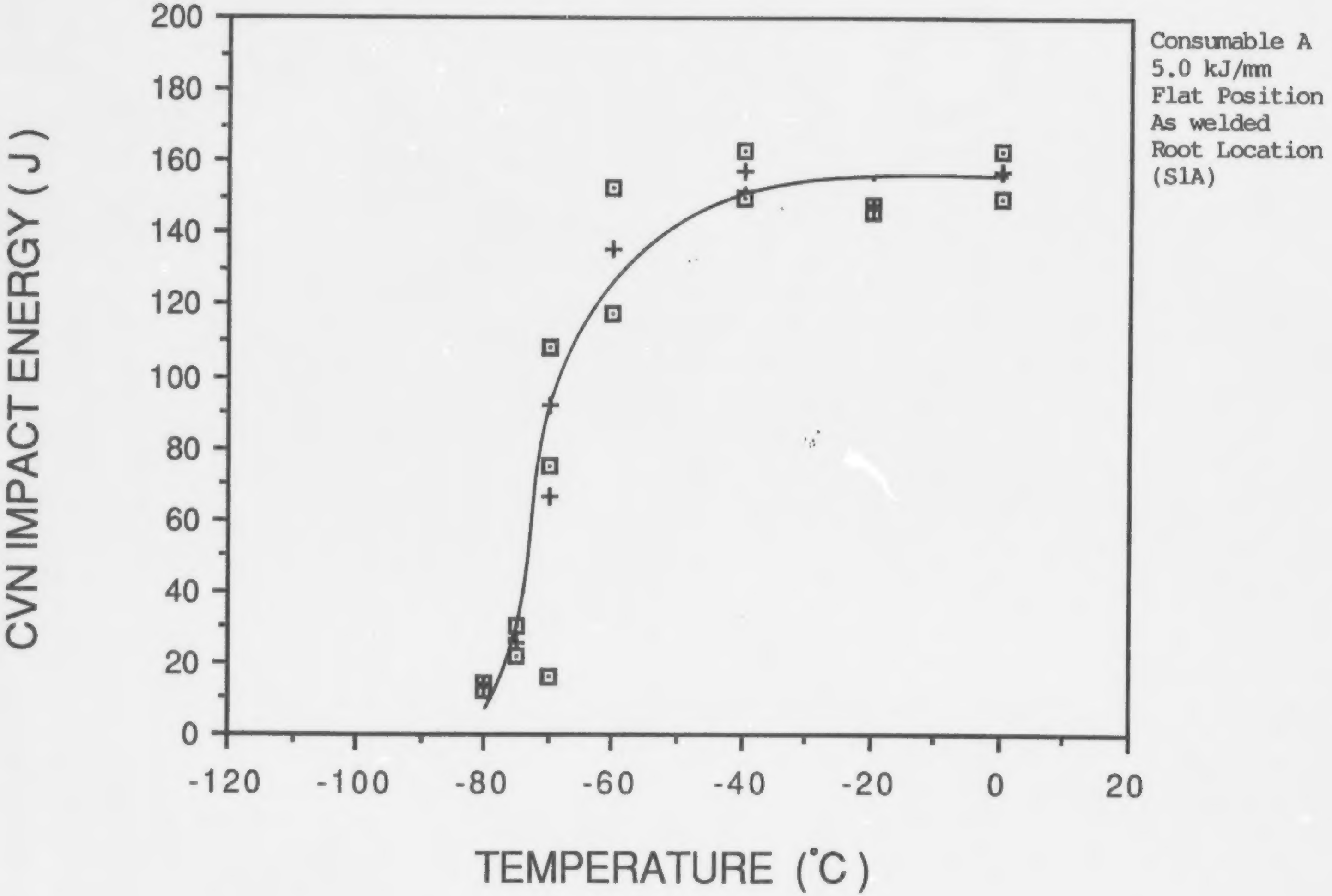

Figure C2 CVN transition curve for root location of S1A

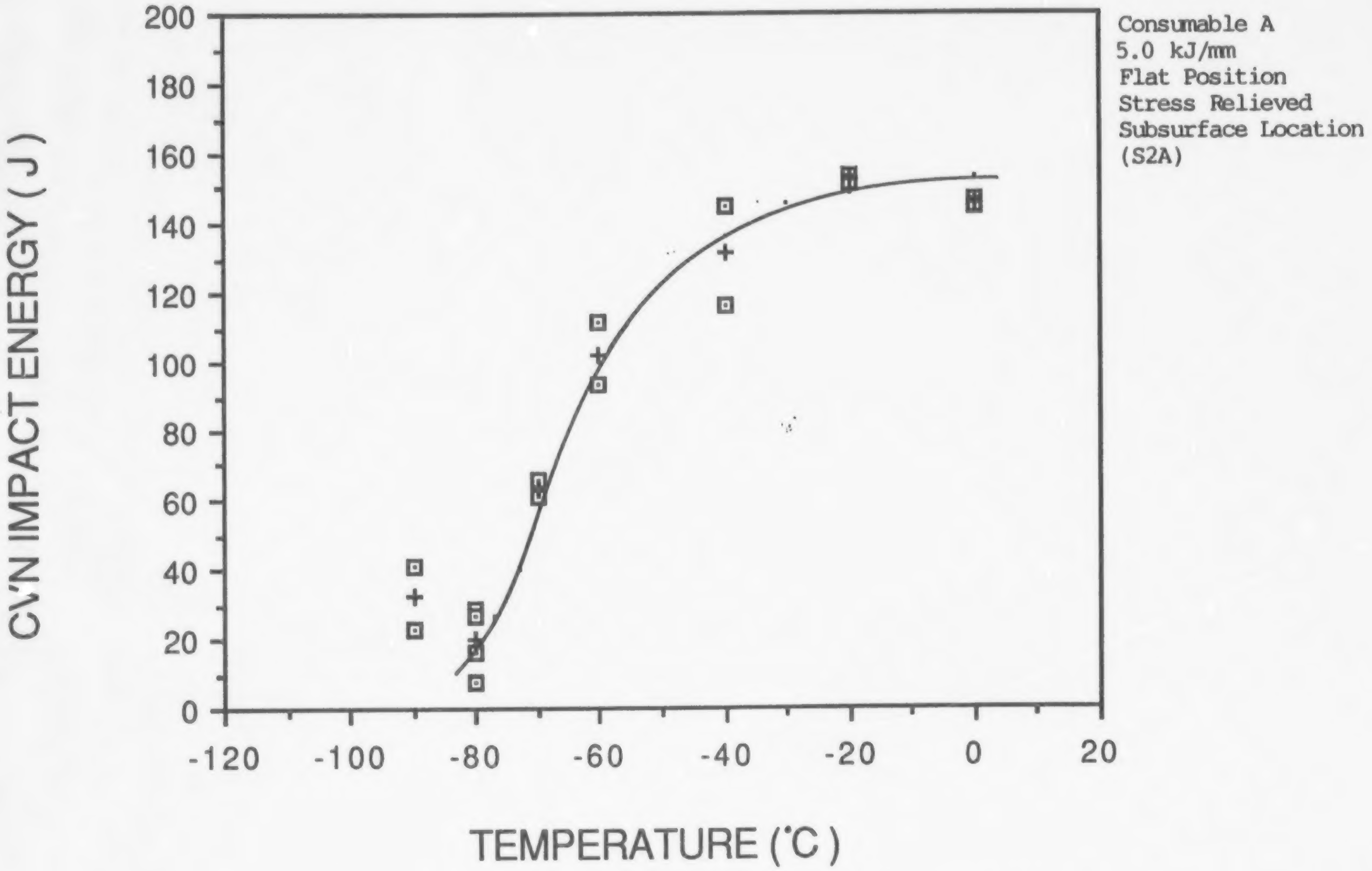

Figure C3 CVN transition curve for subsurface location of S2A

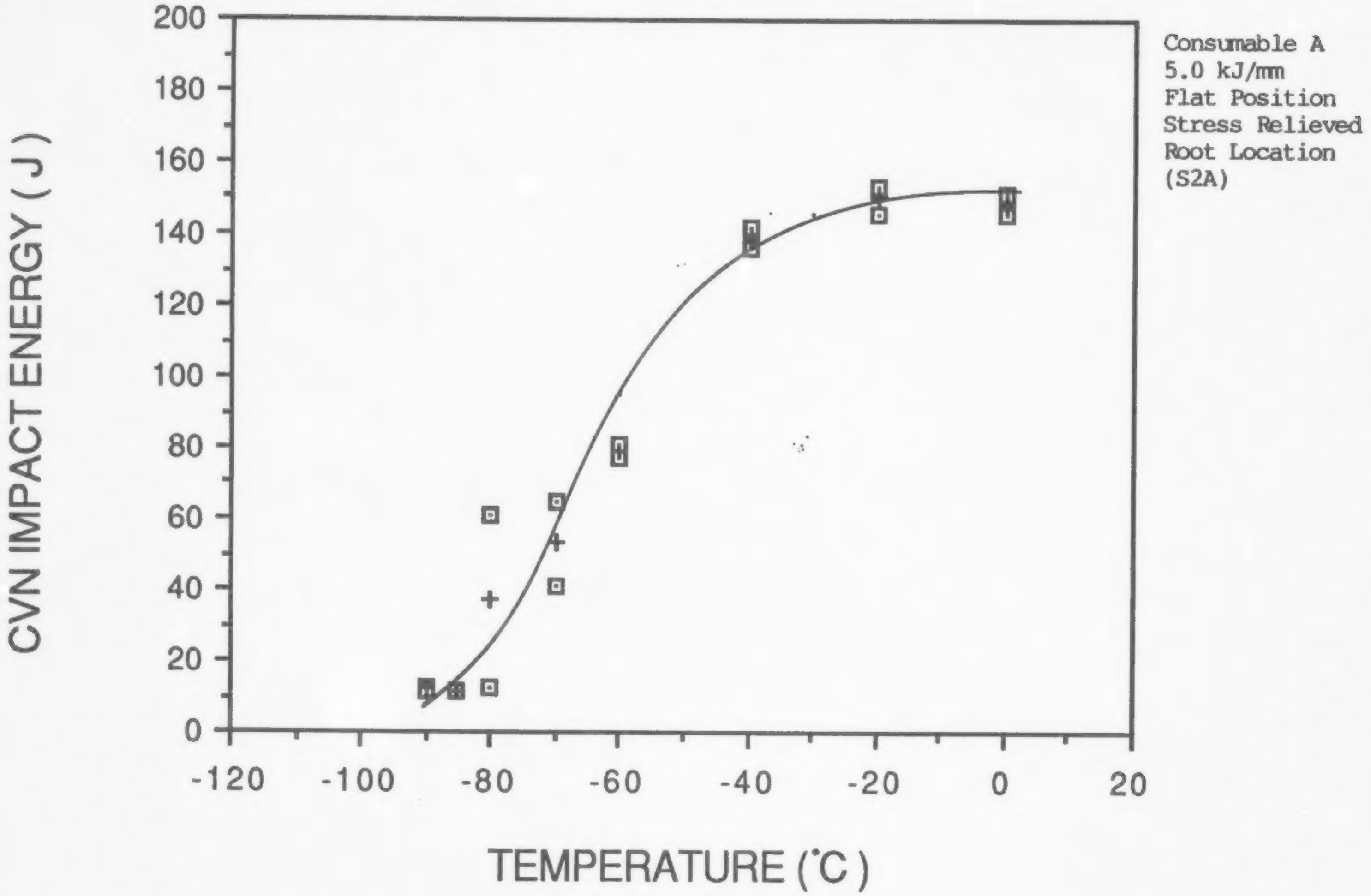

Figure C4 CVN transition curve for root location of S2A

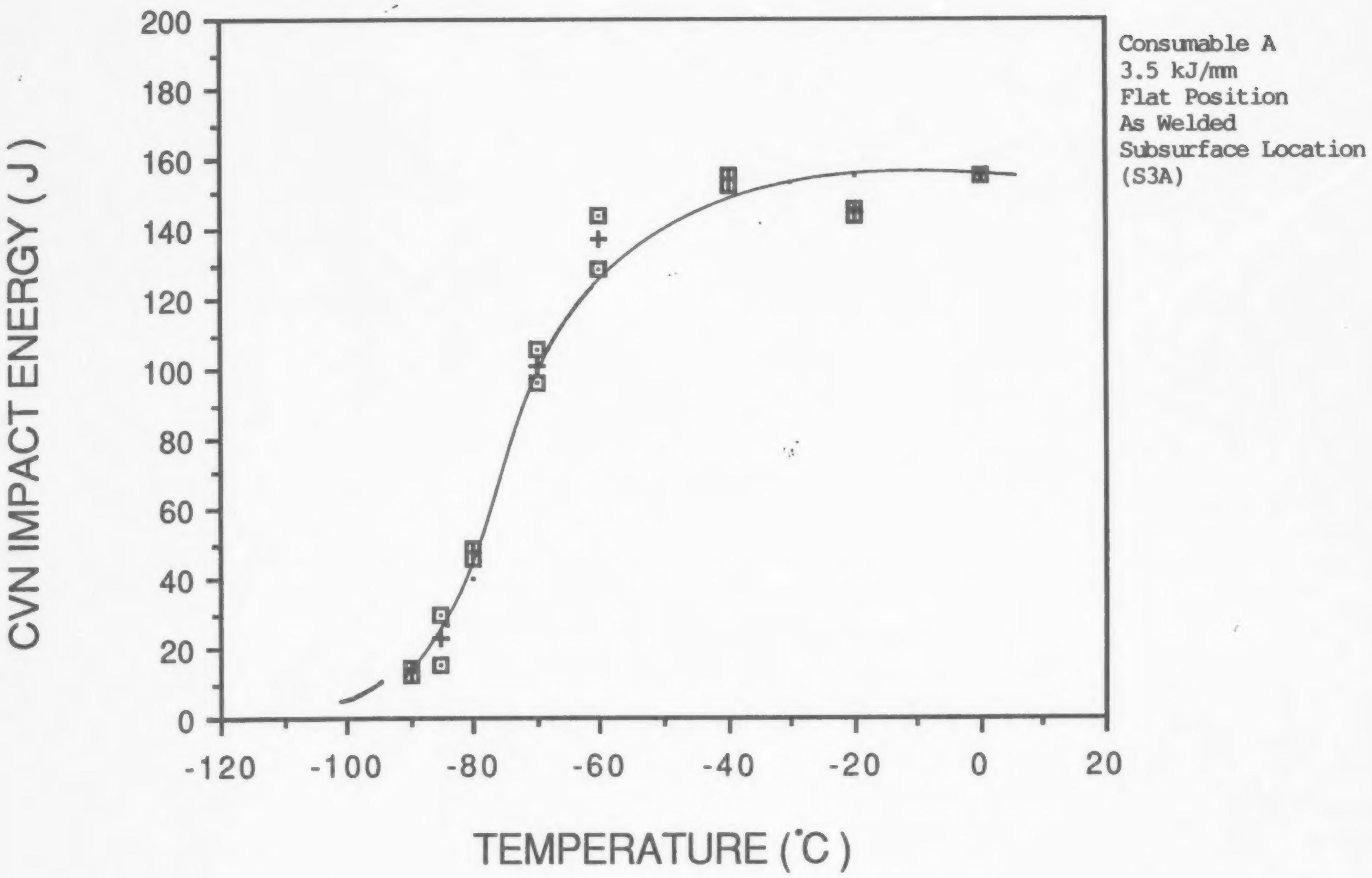

Figure C5 CVN transition curve for subsurface location of S3A

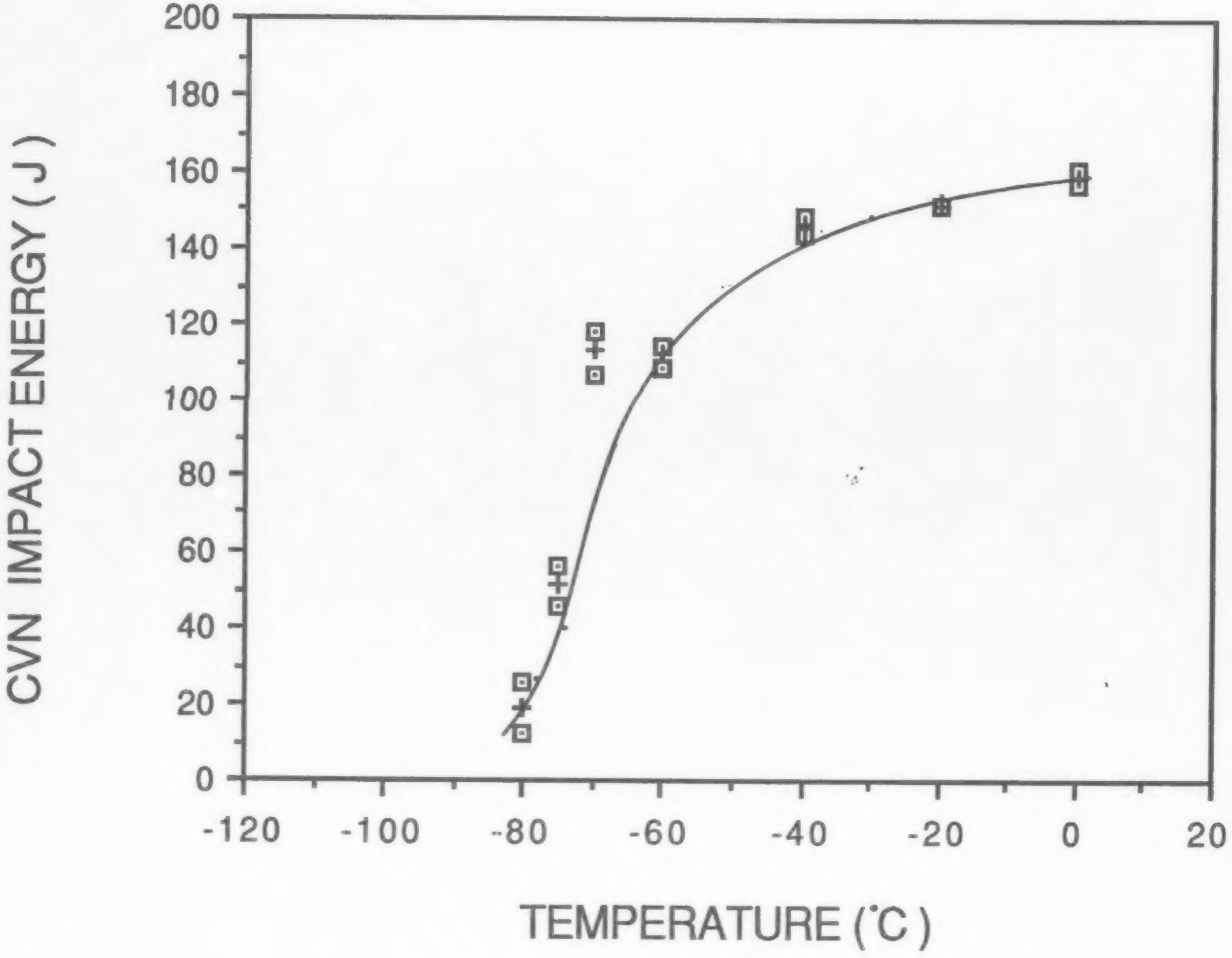

Consumable A
3.5 kJ/mm
Flat Position
As Welded
Root Location
(S3A)

Figure C6 CVN transition curve for root location of S3A

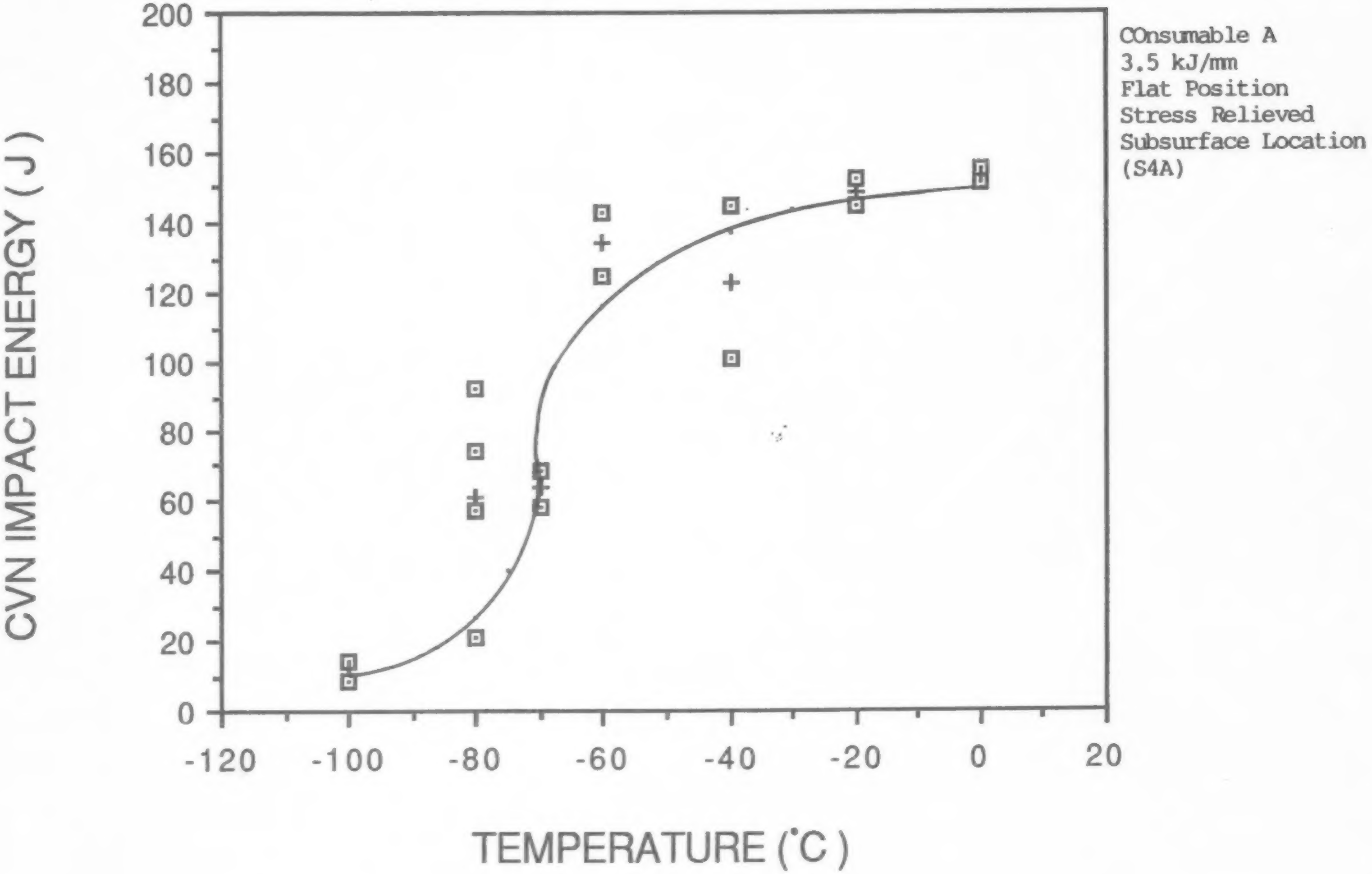

Figure C7 CVN transition curve for subsurface location of S4A

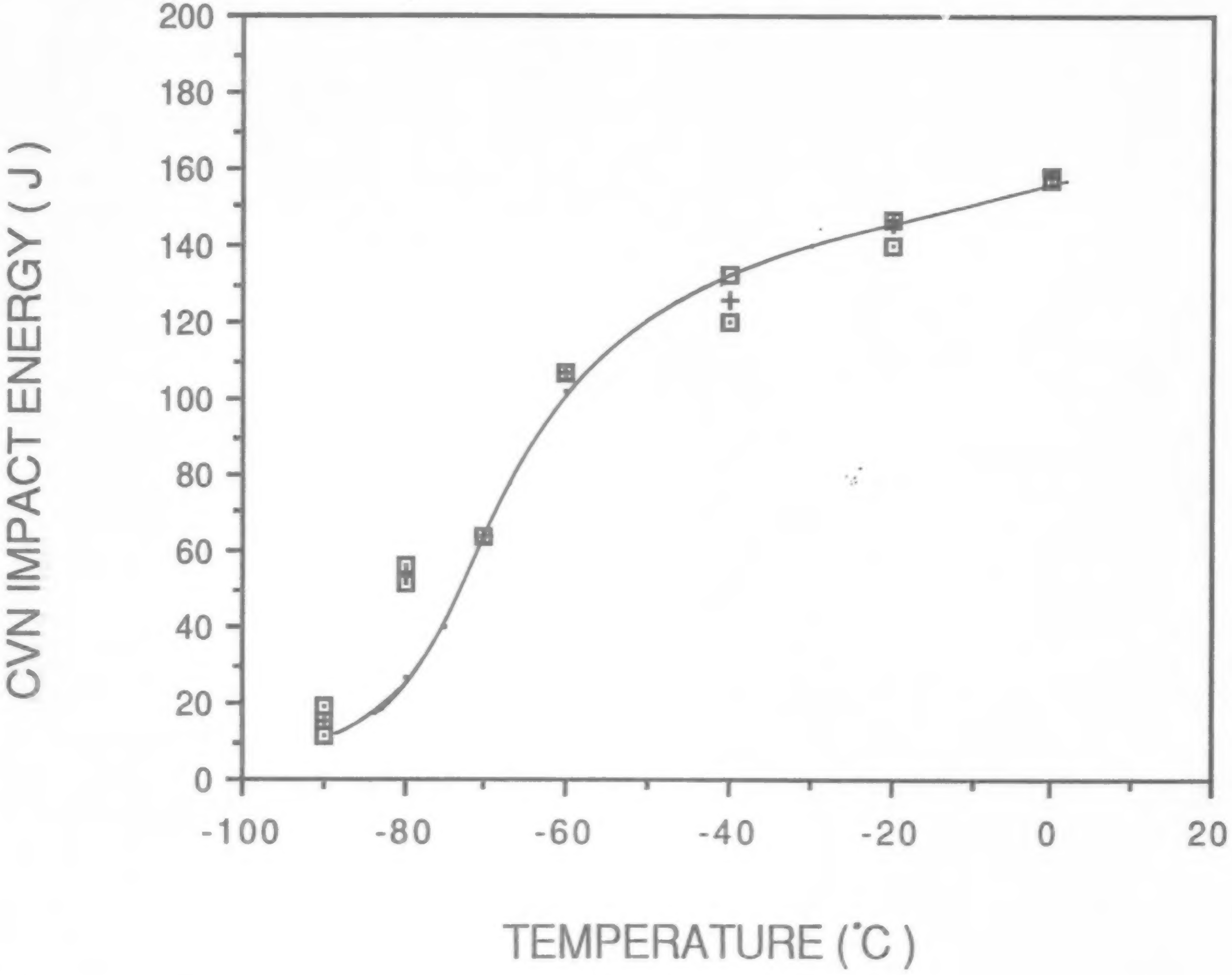

Consumable A
3.5 kJ/mm
Flat Position
Stress Relieved
Root Location
(S4A)

Figure C8 CVN transition curve for root location of S4A

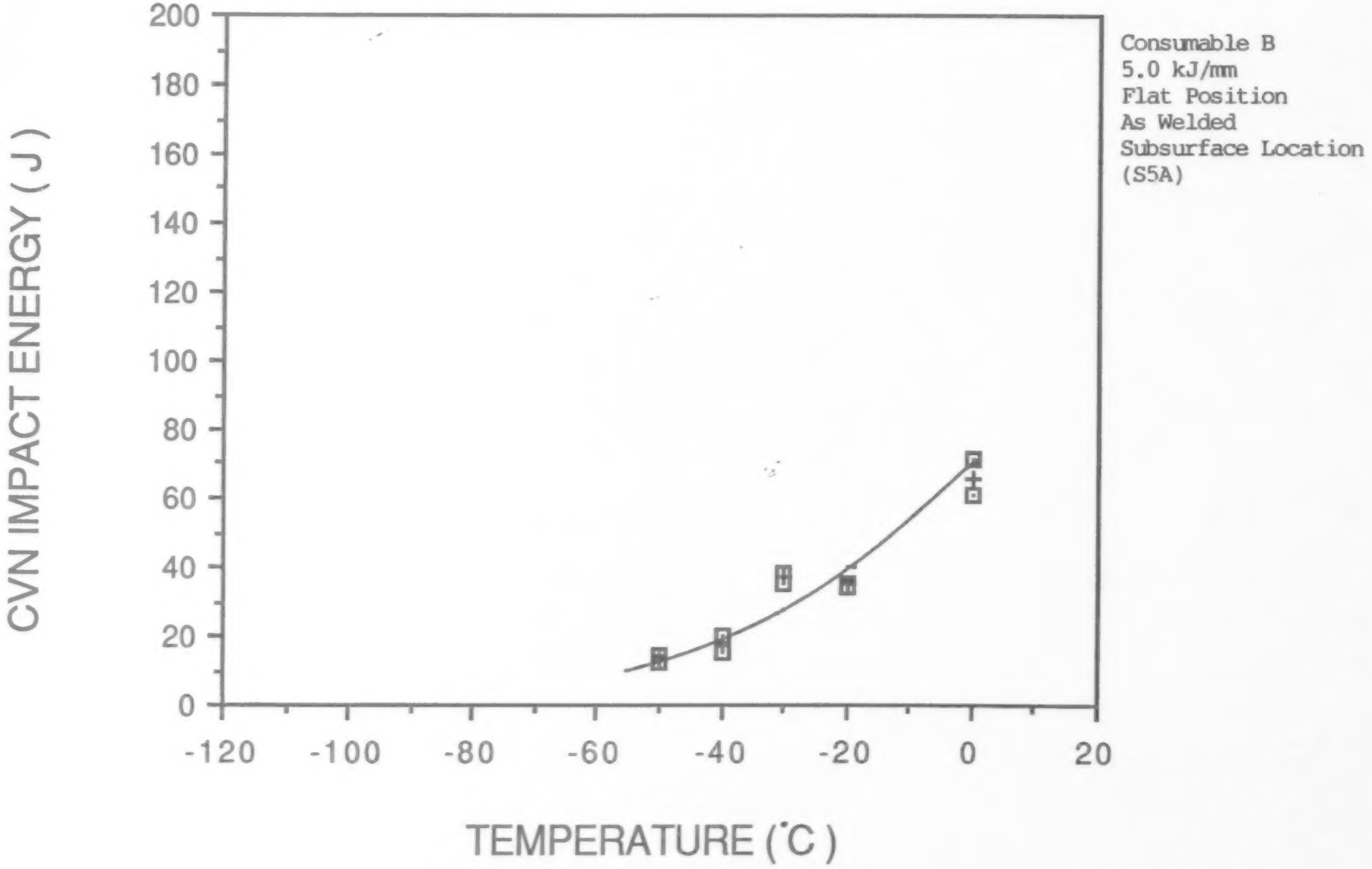

Figure C9 CVN transition curve for subsurface location (90% columnar region) of S5A

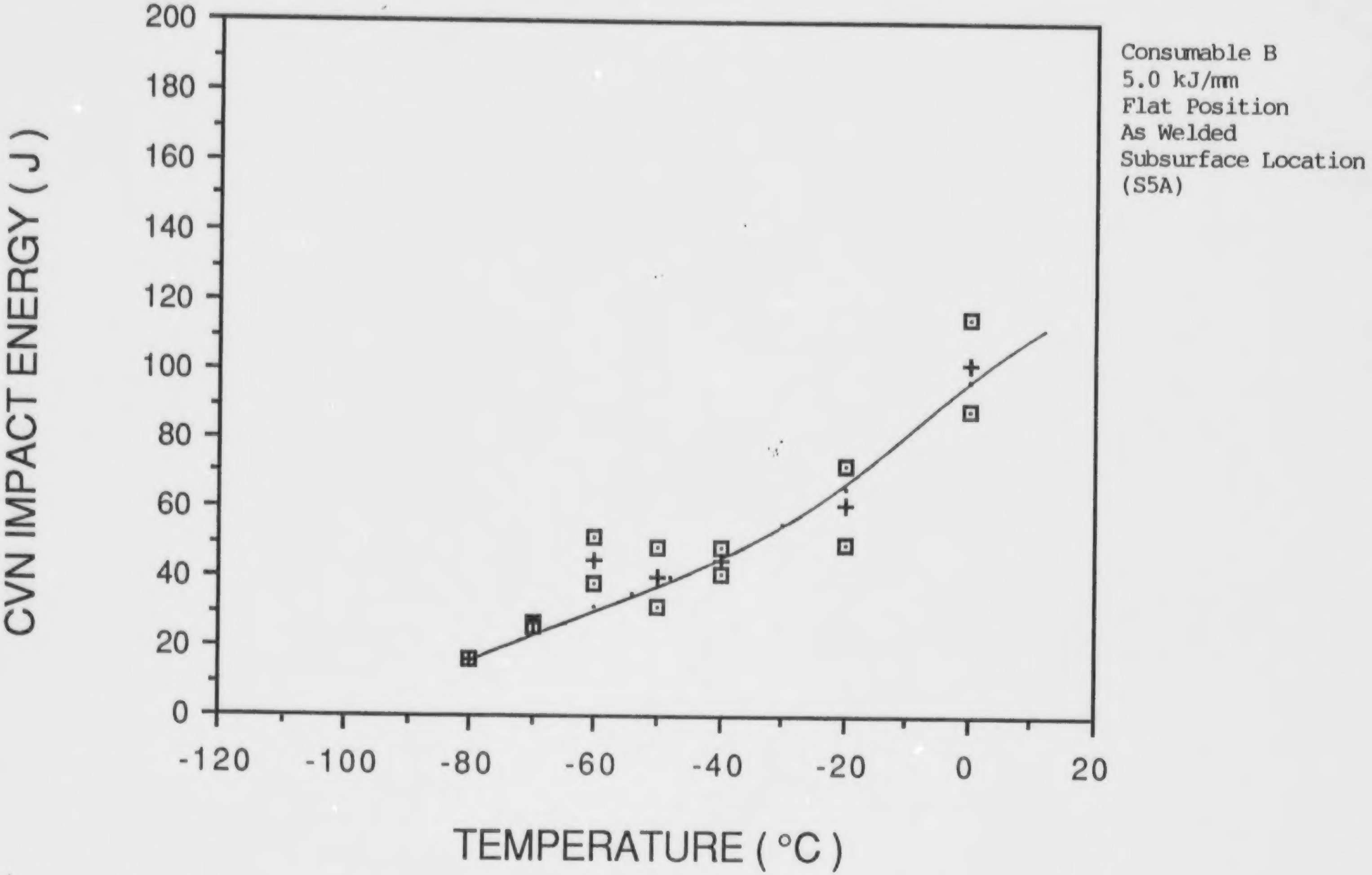

Figure C10 CVN transition curve for subsurface location (50% columnar region) of S5A

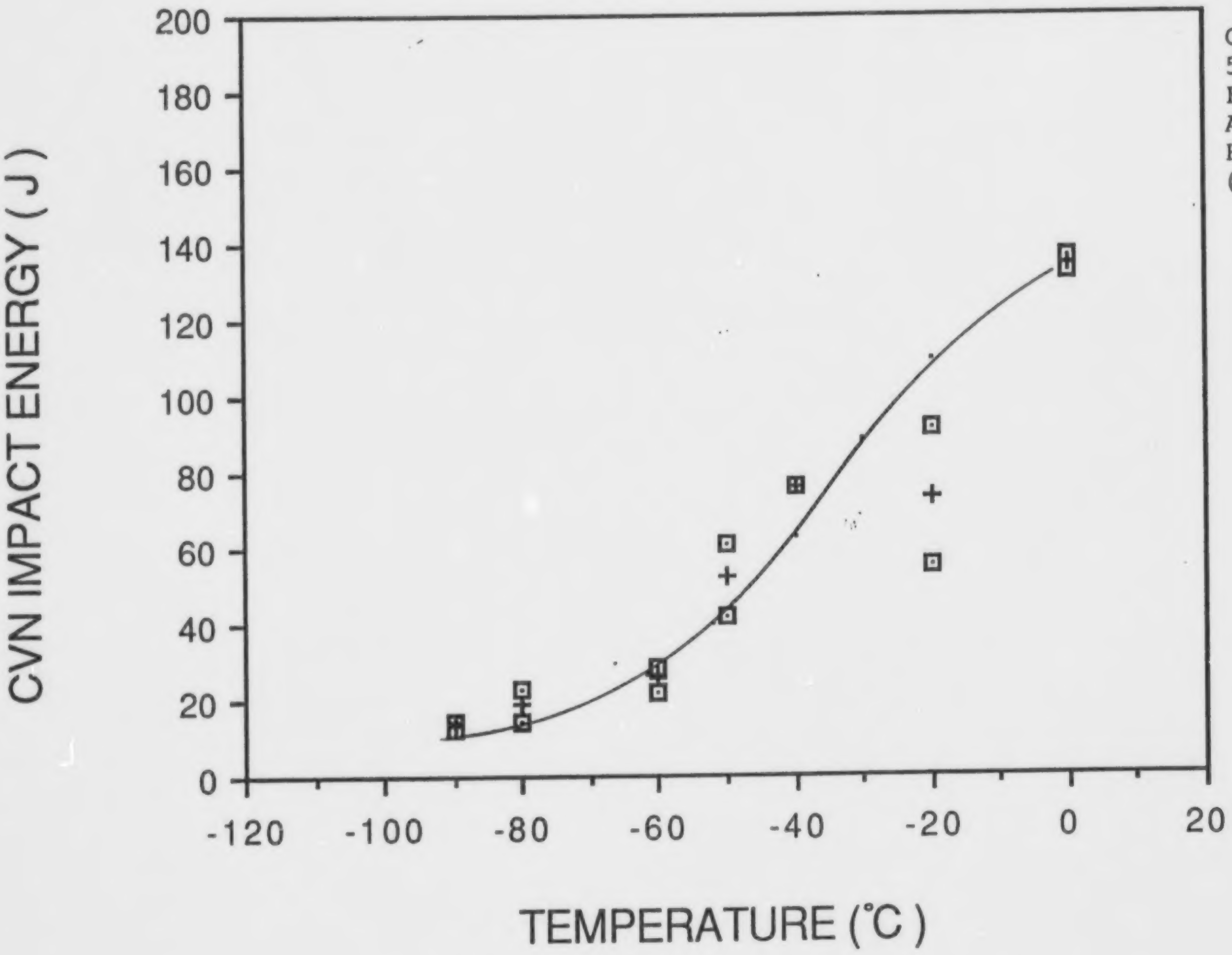

Consumable B
5.0 kJ/mm
Flat Position
As Welded
Root Location
(S5A)

Figure C11 CVN transition curve for root location of S5A

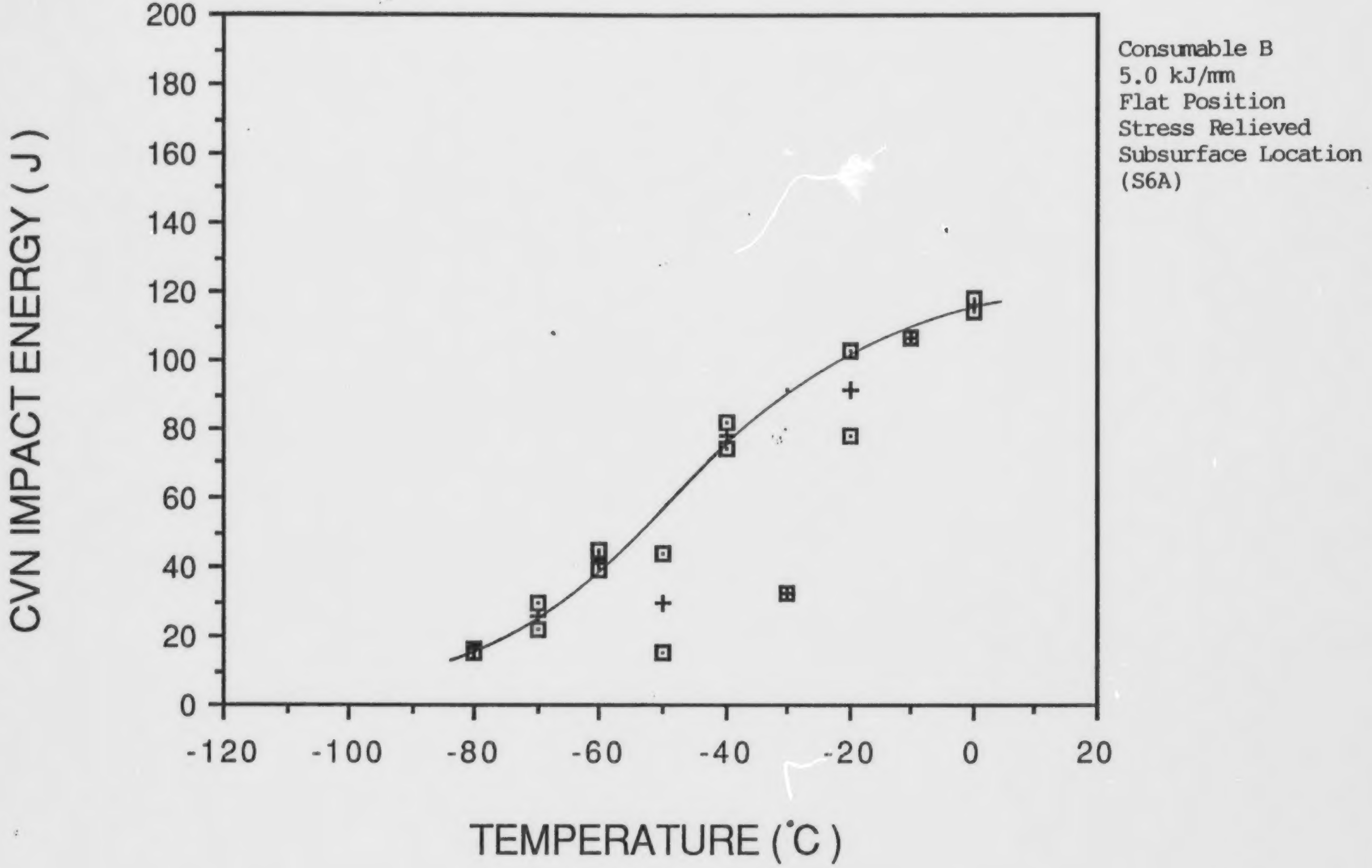

Figure C12 CVN transition curve for subsurface location of S6A

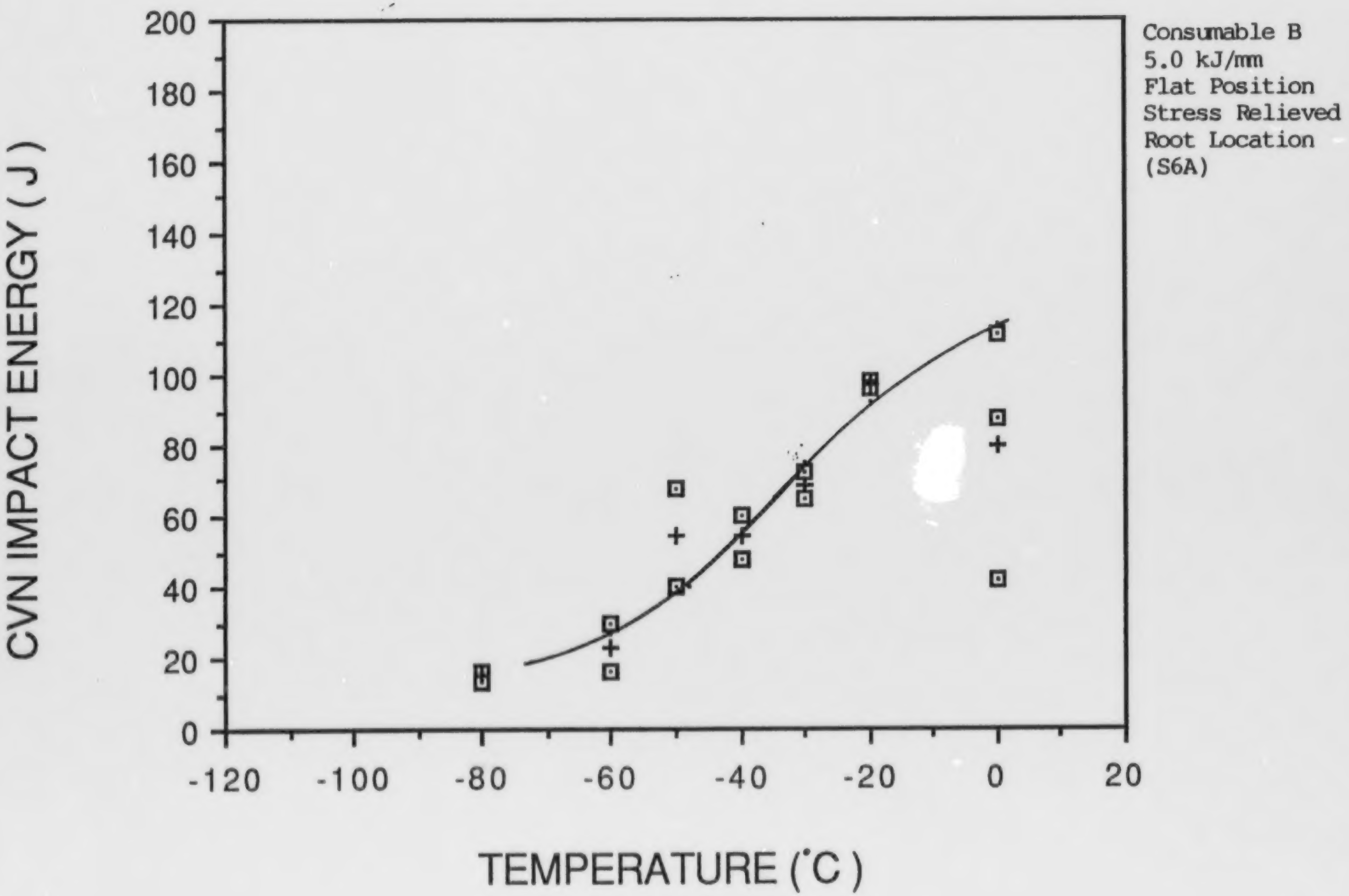

Figure C13 CVN transition curve for root location of S6A

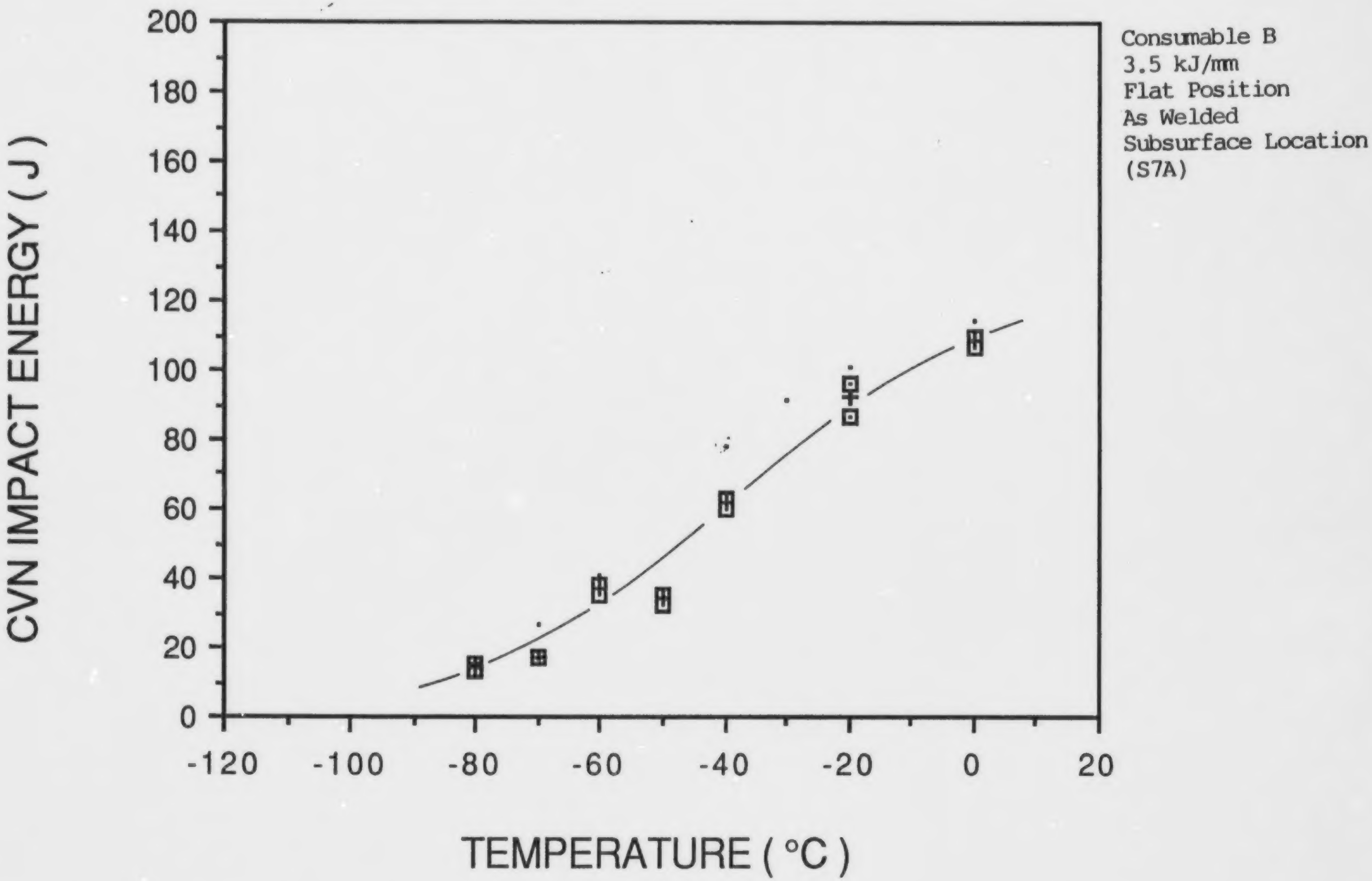

Figure C14 CVN transition curve for subsurface location of S7A

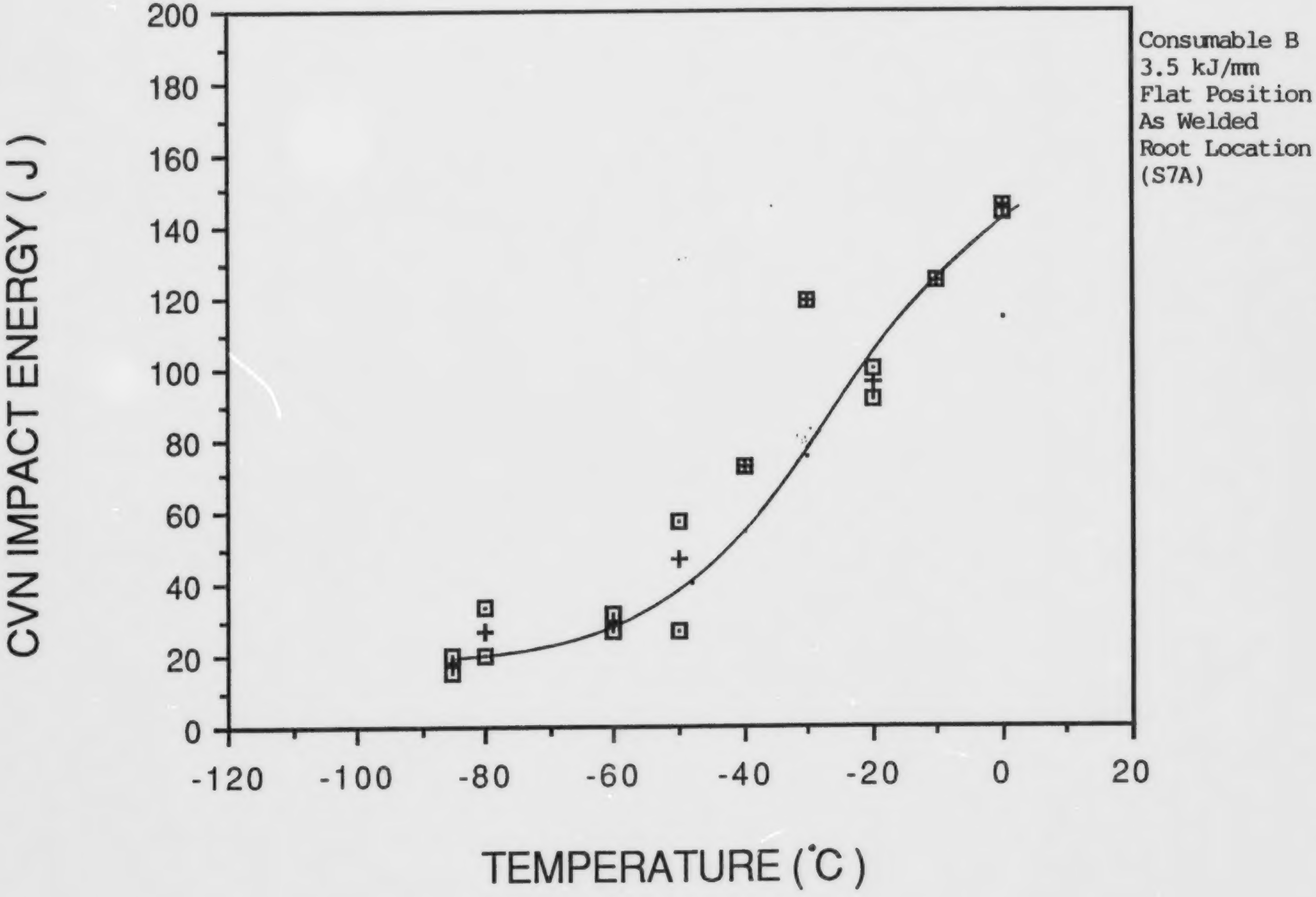

Figure C15 CVN transition curve for root location of S7A

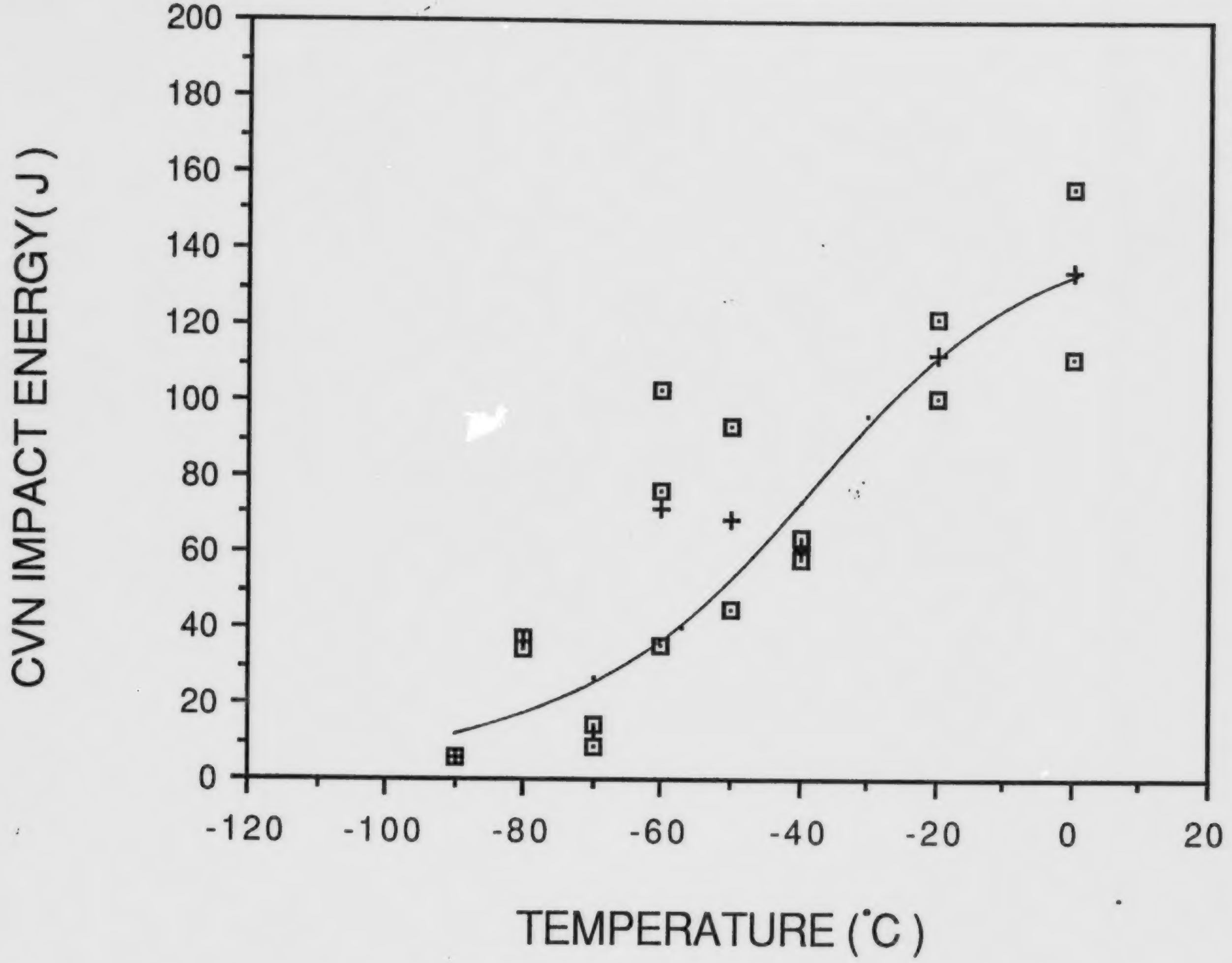

Consumable B
3.5 kJ/mm
Flat Position
Stress Relieved
Subsurface Location
(S8A)

Figure C16 CVN transition curve for subsurface location of S8A

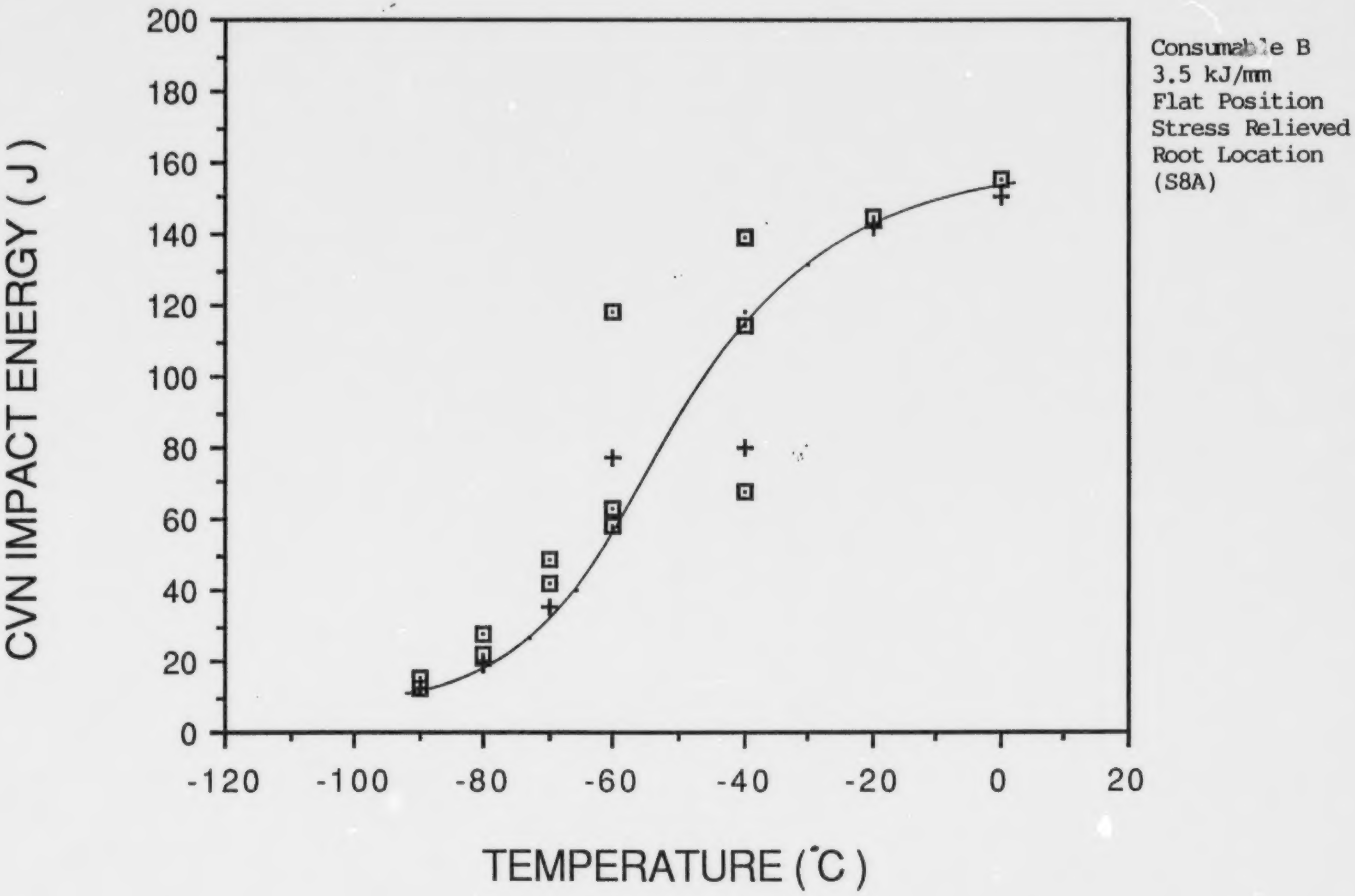

Figure C17 CVN transition curve for root location of S8A

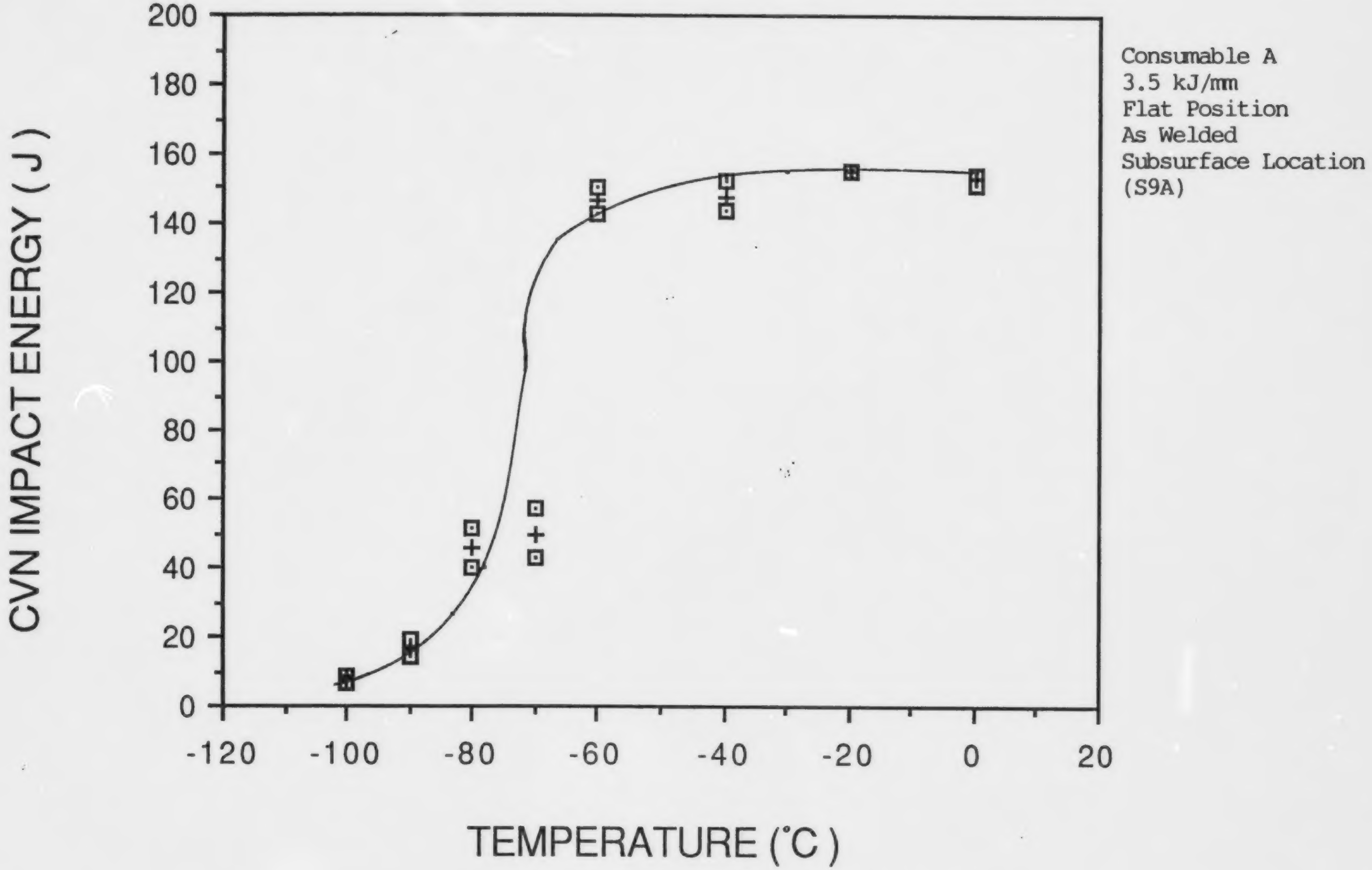

Figure C18 CVN transition curve for subsurface location of S9A

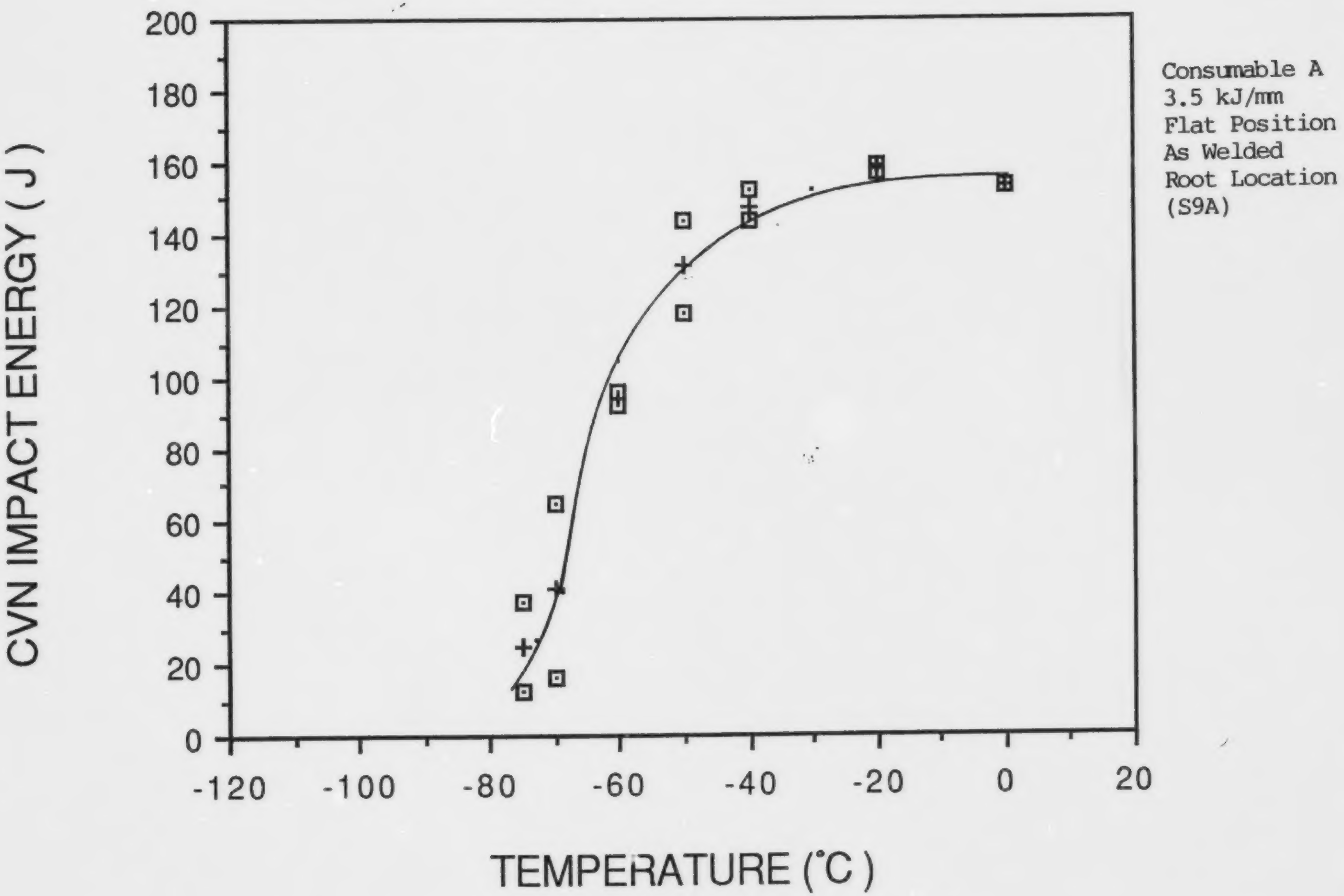

Figure C19 CVN transition curve for root location of S9A

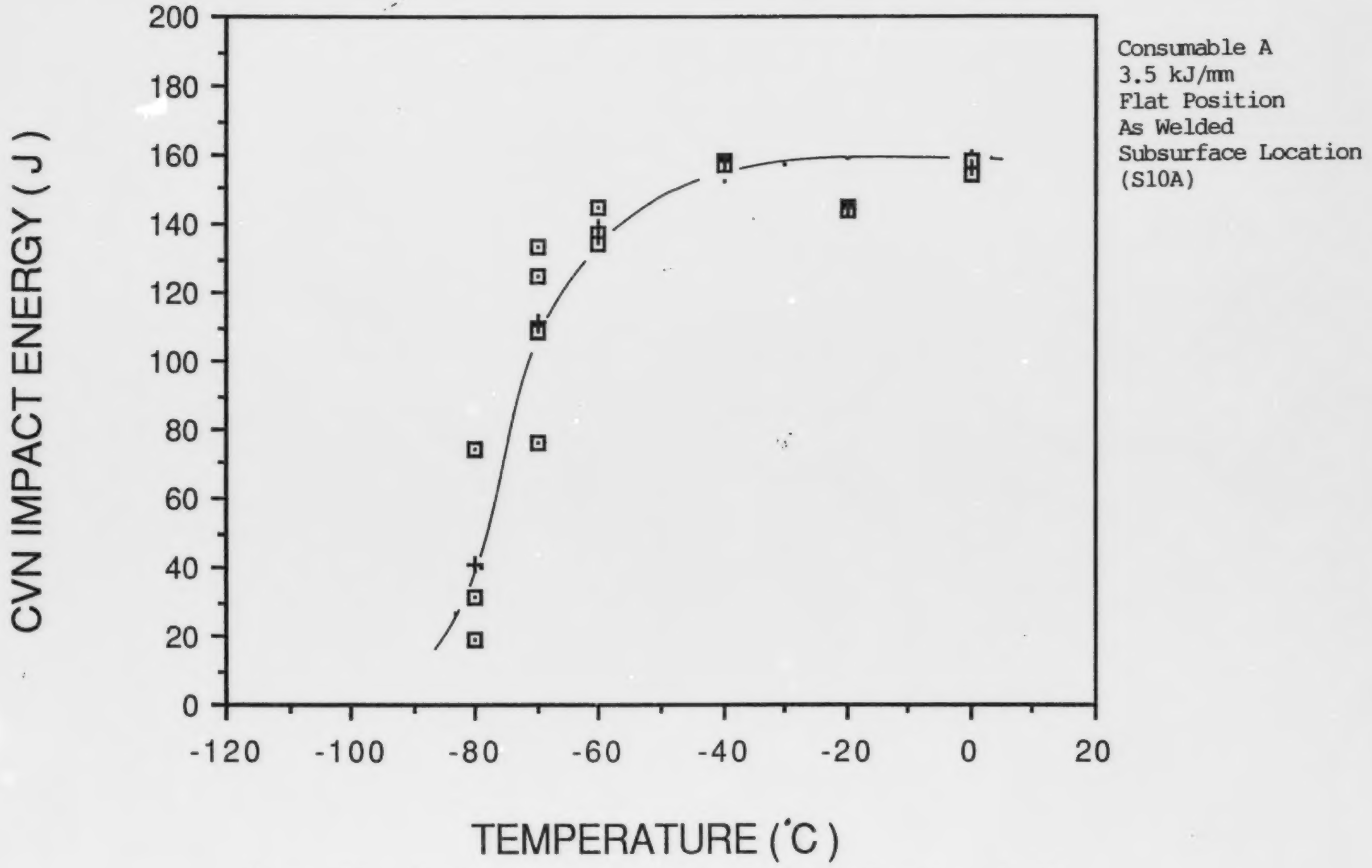

Figure C20 CVN transition curve for subsurface location of S10A

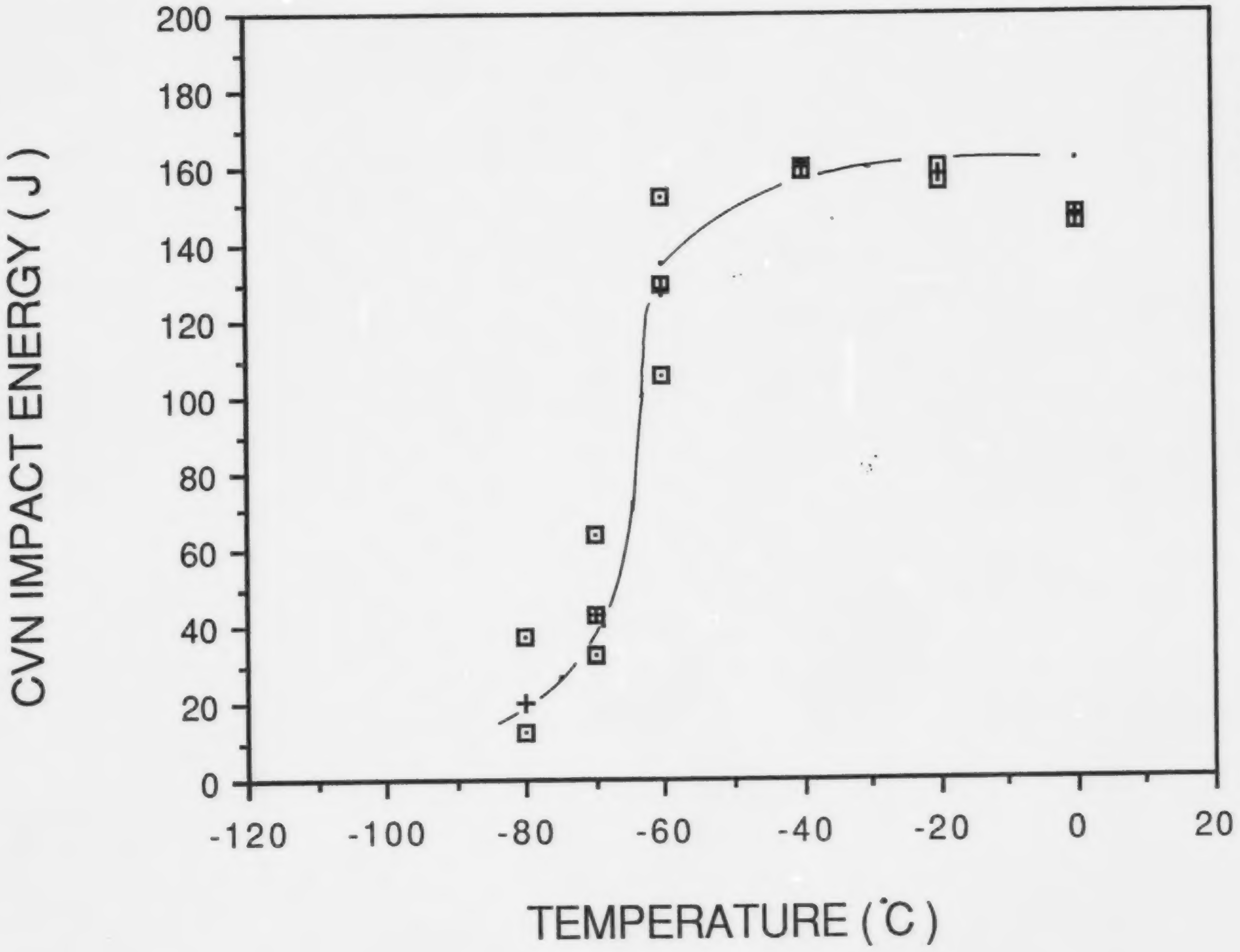

Consumable A
3.5 kJ/mm
Flat Position
As Welded
Root Location
(S10A)

Figure C21 CVN transition curve for root location of S10A

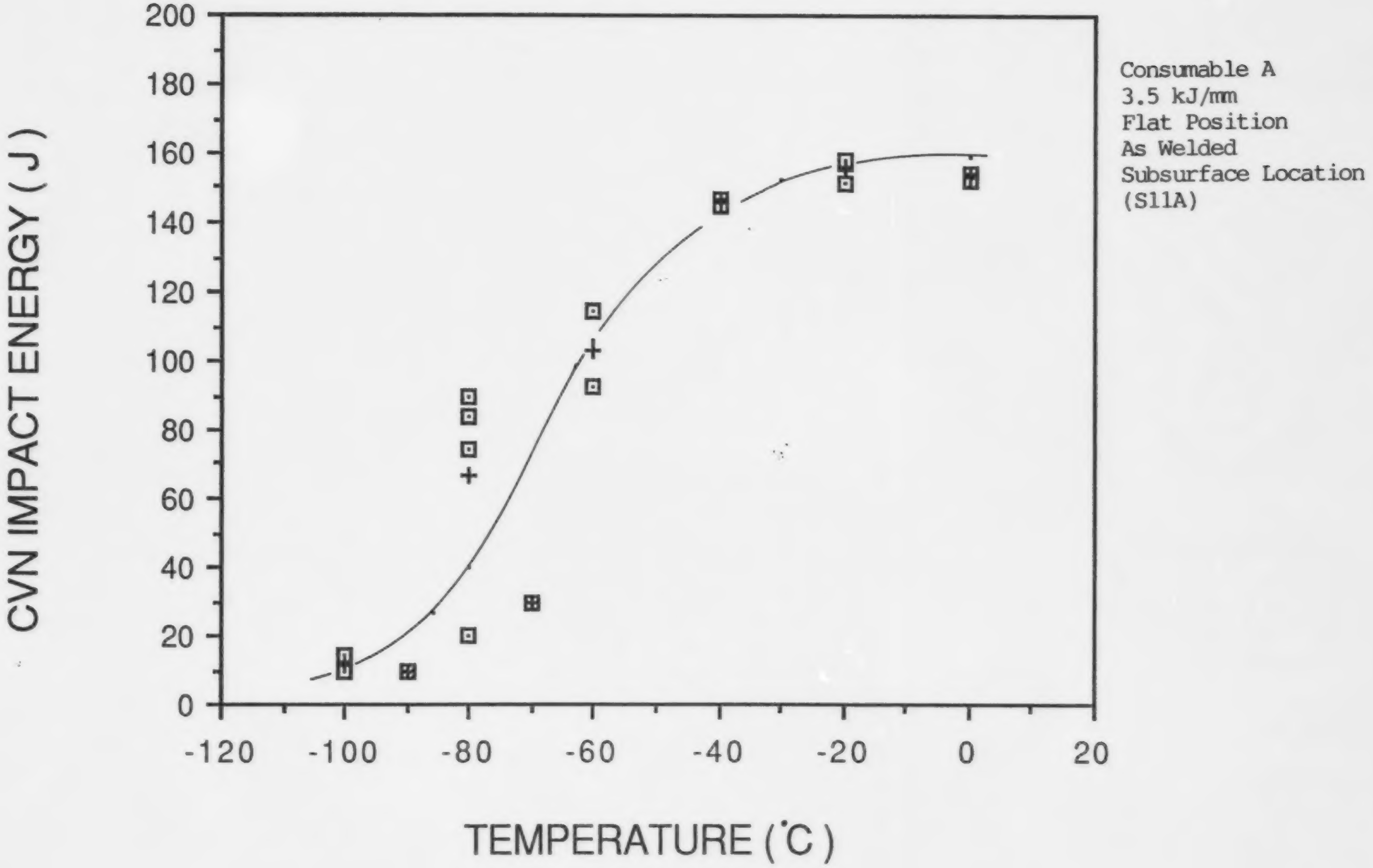

Figure C22 CVN transition curve for subsurface location of S11A

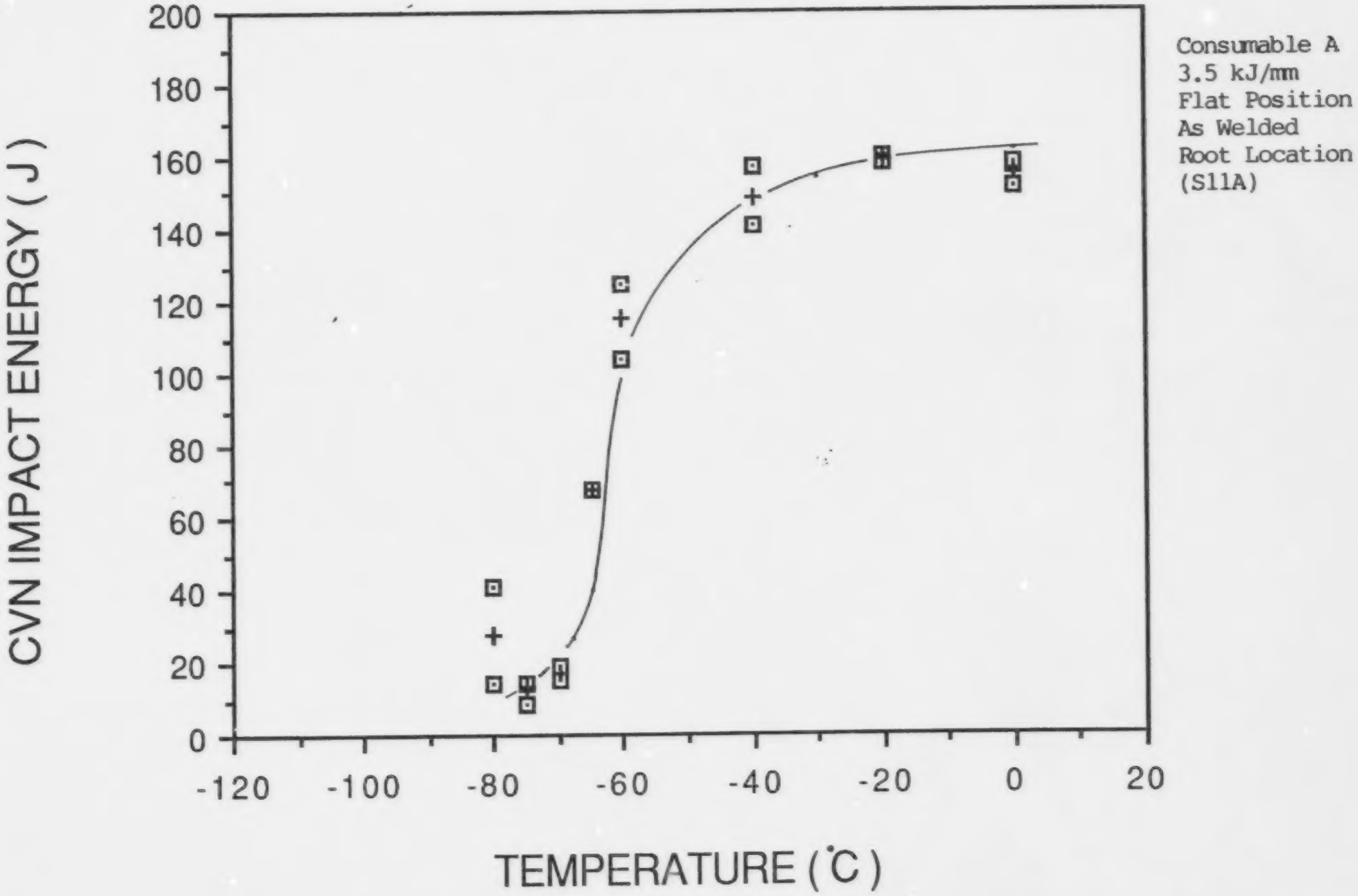

Figure C23 CVN transition curve for root location of S11A

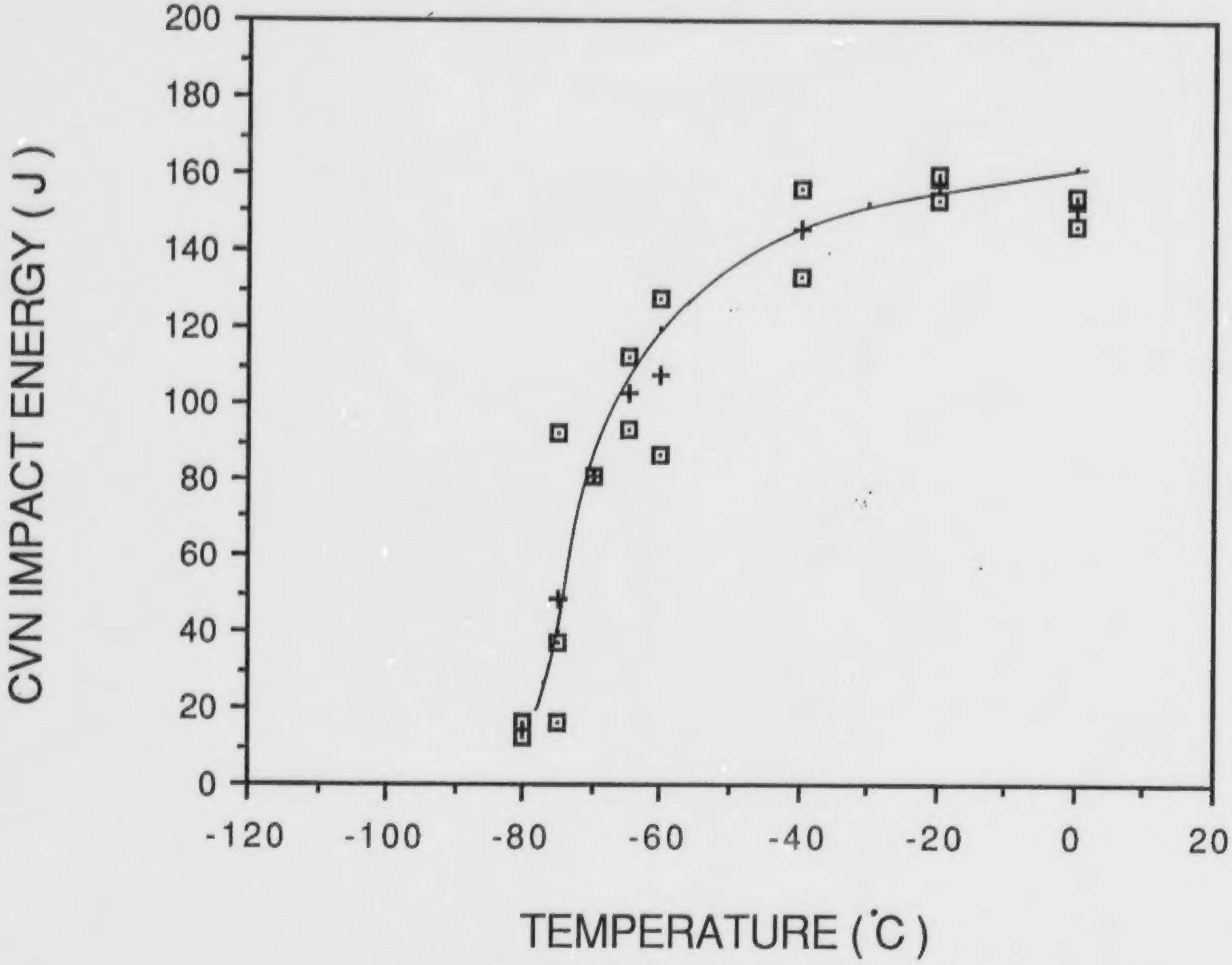

Consumable A
3.5 kJ/mm
Flat Position
As Welded
Subsurface Location
(S11B)

Figure C24 CVN transition curve for subsurface location of S11B

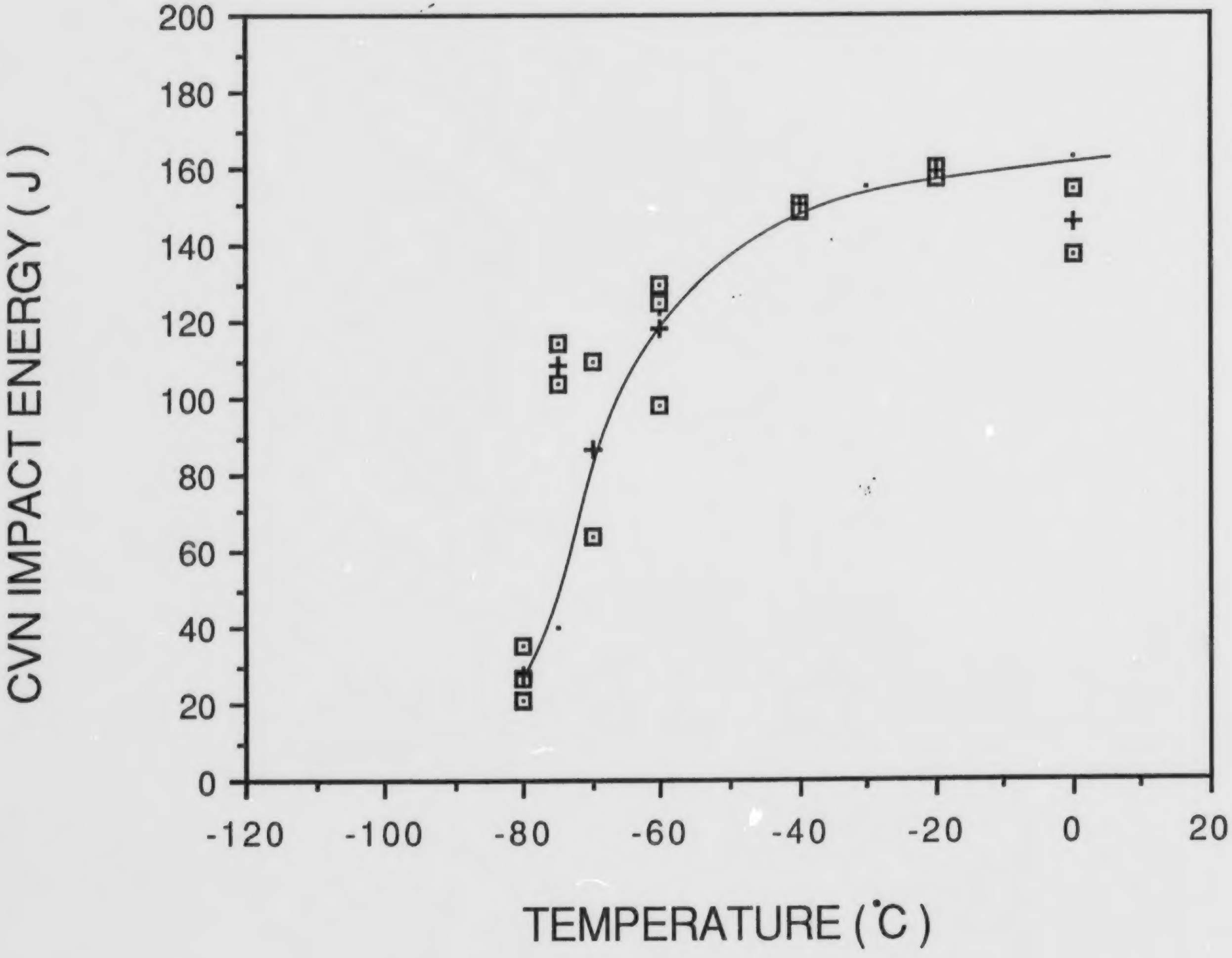

Consumable A
3.5 kJ/mm
Flat Position
As Welded
Root Location
(S11B)

Figure C25 CVN transition curve for root location of S11B

APPENDIX D

CTOD Test Results

Specimen ID	Temperature (°C)	A2 (25%) (IN)	A3 (50%) (IN)	A4 (75%) (IN)	A ave. (IN)	B (IN)	W (IN)	Aave/W	Y	YIELD (KSI)	Vp (IN)	Pmax (LB)	ELASTIC (mm)	PLASTIC (mm)	CTOD (mm)
S3A-1	-30	1.945	1.998	1.886	1.943	1.891	3.794	0.512	11.03	66.10	0.3125	50625	0.1312	2.0964	2.228
S3A-2	-30	1.840	1.931	1.930	1.900	1.895	3.793	0.501	10.65	66.10	0.3800	51750	0.1273	2.6310	2.758
S3A-3	-30	1.877	1.956	1.917	1.917	1.893	3.788	0.506	10.82	66.10	0.3350	49500	0.1206	2.2868	2.407
S3B-1	-50	1.924	1.979	1.949	1.951	1.893	3.781	0.516	11.18	66.10	0.3638	50625	0.1349	2.4138	2.549
S3B-2	-50	1.947	1.998	1.895	1.947	1.892	3.780	0.515	10.65	66.10	0.0938	45750	0.1001	0.6240	0.724
S3B-3	-50	1.945	2.000	1.901	1.949	1.892	3.787	0.515	11.14	66.10	0.3688	50250	0.1319	2.4566	2.589
S4A-1	-30	1.867	1.883	1.907	1.886	1.891	3.785	0.498	10.54	66.10	0.5000	51000	0.1218	3.4890	3.611
S4A-2	-30	1.907	1.925	1.896	1.909	1.896	3.779	0.505	10.78	66.10	0.5000	52125	0.1326	3.4200	3.553
S4A-3	-30	1.874	1.895	1.903	1.891	1.893	3.775	0.501	10.65	66.10	0.5000	49500	0.1172	3.4627	3.580
S4B-1	-50	1.872	1.902	1.869	1.881	1.894	3.780	0.498	10.54	66.10	0.4838	54000	0.1363	3.3813	3.518
S4B-2	-50	1.899	1.882	1.881	1.887	1.891	3.778	0.500	10.61	66.10	0.1650	45750	0.0995	1.1469	1.246
S4B-3	-50	1.872	1.872	1.872	1.872	1.889	3.790	0.494	10.41	66.10	0.5013	53250	0.1297	3.5404	3.670
S1A-1	-30	1.922	2.004	1.972	1.966	1.889	3.785	0.519	11.29	63.80	0.3963	51750	0.1494	2.6031	2.753
S1A-2	-30	1.920	1.962	1.901	1.928	1.891	3.781	0.510	10.98	63.80	0.3825	53250	0.1495	2.5824	2.732
S1A-3	-30	1.865	1.949	1.912	1.909	1.887	3.780	0.505	10.78	63.80	0.3838	53625	0.1468	2.6275	2.774
S1B-1	-50	1.934	1.967	1.873	1.925	1.892	3.778	0.509	10.93	63.80	0.0438	46125	0.1111	0.2960	0.407
S1B-2	-50	1.887	1.956	1.934	1.926	1.893	3.780	0.509	10.93	63.80	0.0175	42750	0.0953	0.1183	0.214
S1B-3	-50	1.870	2.052	1.996	1.973	1.891	3.783	0.521	11.37	63.80	0.0650	43875	0.1088	0.4244	0.533
S2A-1	-30	1.919	1.914	1.868	1.900	1.892	3.780	0.503	10.71	63.80	0.1540	46408	0.1079	1.0609	1.169
S2A-2	-30	1.861	1.901	1.901	1.888	1.891	3.780	0.499	10.58	63.80	0.4190	51750	0.1311	2.9139	3.045
S2A-3	-30	1.919	1.897	1.857	1.891	1.892	3.780	0.500	10.54	63.80	0.2290	51750	0.1300	1.5886	1.719
S2B-1	-50	1.930	1.914	1.931	1.925	1.890	3.779	0.509	10.93	63.80	0.1725	45375	0.1077	1.1661	1.274
S2B-2	-50	1.871	1.903	1.897	1.890	1.889	3.791	0.499	10.58	63.80	0.2325	48750	0.1163	1.6205	1.737
S2B-3	-50	1.923	1.903	1.847	1.891	1.892	3.793	0.499	10.58	63.80	0.4025	52500	0.1344	2.8061	2.940
S9A-1	-30	1.939	1.993	1.901	1.944	1.889	3.791	0.513	11.07	66.10	0.4150	48750	0.1229	2.7778	2.901
S9A-2	-30	2.022	2.113	1.994	2.043	1.891	3.779	0.541	12.16	66.10	0.3750	44625	0.1244	2.3147	2.439
S9A-3	-30	1.898	1.973	1.933	1.935	1.891	3.779	0.512	11.03	66.10	0.3400	48375	0.1202	2.2816	2.402
S9B-1	-50	1.928	2.028	1.906	1.954	1.892	3.787	0.516	11.18	66.10	0.1580	45000	0.1066	1.0482	1.155
S9B-2	-50	1.887	1.947	1.923	1.919	1.891	3.782	0.507	10.85	66.10	0.2040	50250	0.1254	1.3869	1.512
S9B-3	-50	1.976	2.075	1.947	1.999	1.898	3.775	0.530	11.71	66.10	0.4300	44625	0.1146	2.7416	2.856
S10A-1	-30	1.934	1.934	1.934	1.934	1.887	3.776	0.512	11.03	66.90	0.3169	51750	0.1366	2.1250	2.262
S10A-2	-30	1.900	1.985	1.948	1.944	1.883	3.778	0.515	11.14	66.90	0.3800	50250	0.1319	2.5296	2.661
S10A-3	-30	1.934	1.995	1.884	1.938	1.890	3.775	0.513	11.07	66.90	0.3594	50625	0.1313	2.4022	2.534
S10A-4	-50	1.976	2.037	1.926	1.980	1.891	3.776	0.524	11.48	66.90	0.3422	44625	0.1096	2.2157	2.325
S10A-5	-50	1.891	1.995	1.948	1.945	1.887	3.779	0.515	11.14	66.90	0.3444	51000	0.1352	2.2936	2.429
S10A-6	-50	1.956	1.992	1.877	1.942	1.892	3.776	0.514	11.11	66.90	0.3538	50625	0.1319	2.3588	2.491
S11A-1	-30	1.899	2.010	1.914	1.941	1.889	3.776	0.514	11.11	66.90	0.3144	49528	0.1267	2.0968	2.224
S11A-2	-30	1.918	2.009	1.947	1.958	1.895	3.786	0.517	11.22	66.90	0.3559	49706	0.1290	2.3537	2.483
S11A-3	-30	1.929	1.979	1.880	1.929	1.889	3.785	0.510	10.96	66.90	0.3696	51098	0.1310	2.4962	2.627
S11A-4	-50	1.924	2.049	1.985	1.986	1.889	3.784	0.525	11.52	66.90	0.1191	44835	0.1115	0.7705	0.882
S11A-5	-50	1.935	1.981	1.871	1.929	1.888	3.788	0.509	10.93	66.90	0.4359	50569	0.1276	2.9482	3.076
S11A-6	-50	1.924	1.983	1..879	1.953	1.886	3.778	0.517	11.22	66.90	0.3658	49304	0.1284	2.4186	2.547
S11B-1	-30	1.910	1.999	1.942	1.950	1.890	3.789	0.515	11.14	66.90	0.3938	50366	0.1312	2.6219	2.753
S11B-2	-30	1.937	2.006	1.872	1.938	1.895	3.772	0.514	11.11	66.90	0.4200	50962	0.1335	2.8029	2.936
S11B-3	-30	1.922	1.989	1.907	1.939	1.890	3.779	0.513	11.07	66.90	0.3713	50512	0.1306	2.4834	2.614
S11B-4	-50	1.947	2.049	2.003	2.000	1.888	3.785	0.528	11.64	66.90	0.1309	44615	0.1127	0.8377	0.950
S11B-5	-50	1.960	2.034	1.921	1.972	1.890	3.781	0.521	11.37	66.90	0.0726	44725	0.1080	0.4742	0.582
S11B-6	-50	1.949	1.999	1.895	1.948	1.898	3.781	0.515	11.14	66.90	0.1063	46080	0.1091	0.7065	0.816

Table D1

Summary of CTOD Values for Submerged Arc Welds of Consumable A

Specimen ID	Temperature (°C)	A2 (25%) (IN)	A3 (50%) (IN)	A4 (75%) (IN)	A ave. (IN)	B (IN)	W (IN)	Aave/W	Y	YIELD (KSI)	Vp (IN)	Pmax (LB)	ELASTIC (mm)	PLASTIC (mm)	CTOD (mm)
S7B-1	-10	2.044	2.156	2.044	2.081	1.891	3.787	0.550	12.55	85.00	0.0225	43688	0.0985	0.1352	0.234
S7B-2	-10	1.938	1.988	1.930	1.952	1.893	3.777	0.517	11.22	85.00	0.0188	45938	0.0871	0.1241	0.211
S7B-3	-10	1.934	2.016	1.964	1.971	1.887	3.789	0.520	11.33	85.00	0.0575	44250	0.0827	0.3768	0.459
S7A-1	-30	1.912	1.986	1.929	1.942	1.894	3.783	0.513	11.07	85.00	0.0063	36375	0.0530	0.0418	0.005
S7A-2	-30	1.879	1.935	1.902	1.905	1.890	3.780	0.504	10.75	85.00	0.0125	39000	0.0578	0.0858	0.144
S7A-3	-30	1.923	1.978	1.888	1.930	1.891	3.790	0.509	10.93	85.00	0.0138	44625	0.0779	0.0930	0.171
S8B-1	-10	1.949	1.932	1.922	1.934	1.890	3.783	0.511	11.00	85.00	0.1025	46500	0.0859	0.6891	0.775
S8B-2	-10	1.821	1.817	1.817	1.818	1.894	3.783	0.481	9.99	85.00	0.0513	48375	0.0764	0.3759	0.452
S8B-3	-10	1.882	1.865	1.830	1.859	1.893	3.782	0.492	10.34	85.00	0.1900	53250	0.0993	1.3508	1.450
S8A-1	-30	1.890	1.851	1.851	1.864	1.890	3.783	0.493	10.38	85.00	0.0188	43875	0.0681	0.1329	0.201
S8A-2	-30	1.836	1.873	1.882	1.864	1.892	3.782	0.493	10.38	85.00	0.0325	45375	0.0727	0.2303	0.303
S8A-3	-30	1.854	1.866	1.885	1.868	1.891	3.782	0.494	10.41	85.00	0.0463	45750	0.0744	0.3265	0.401
S5B-1	-10	2.110	2.188	2.108	2.135	1.892	3.787	0.564	13.19	83.10	0.0100	37125	0.0803	0.0575	0.138
S5B-2	-10	1.960	2.049	1.963	1.991	1.890	3.787	0.526	11.56	83.10	0.0075	38625	0.0669	0.0484	0.115
S5B-3	-10	1.937	1.980	1.905	1.941	1.894	3.784	0.513	11.07	83.10	0.0025	35625	0.0520	0.0167	0.069
S5A-1	-30	1.900	1.982	1.937	1.940	1.892	3.787	0.512	11.03	83.10	0.0125	39375	0.0632	0.0838	0.147
S5A-2	-30	1.946	2.057	1.953	1.985	1.890	3.787	0.524	11.48	83.10	0.0038	32438	0.0465	0.0243	0.071
S5A-3	-30	1.934	1.987	1.919	1.947	1.894	3.784	0.514	11.11	83.10	0.0075	40500	0.0677	0.0500	0.118
S6B-1	-10	1.860	1.845	1.765	1.823	1.892	3.781	0.482	10.03	83.10	0.0313	42750	0.0617	0.2283	0.290
S6B-2	-10	1.828	1.871	1.919	1.873	1.893	3.784	0.495	10.44	83.10	0.0881	51750	0.0977	0.6205	0.718
S6B-3	-10	1.809	1.864	1.892	1.855	1.896	3.782	0.490	10.28	83.10	0.0450	50250	0.0891	0.3209	0.410
S6A-1	-30	1.916	1.898	1.864	1.893	1.898	3.780	0.501	10.65	83.10	0.0000	30750	0.0358	0.0000	0.036
S6A-2	-30	1.891	1.878	1.841	1.870	1.890	3.779	0.495	10.44	83.10	0.0625	44250	0.0718	0.4402	0.512
S6A-3	-30	1.958	1.920	1.872	1.917	1.890	3.782	0.507	10.85	83.10	0.0525	49125	0.0955	0.3575	0.453

Table D2

Summary of CTOD Values for Submerged Arc Welds of Consumable B

Volume

2

FLEET TECHNOLOGY LIMITED
A FLEET AEROSPACE COMPANY

FLEET TECHNOLOGY LIMITED

E62522C

FINAL REPORT

EVALUATION OF HEAT AFFECTED ZONE AND WELD METAL TOUGHNESS IN SELECTED STEELS
(PHASE II)

VOLUME II: GAS METAL ARC WELDING PROGRAM

By

C. Chiu
L. Malik

Work on this project was jointly funded by AMCA International Limited, and by Metals Technology Laboratories (CANMET, EMR) under the auspices of the Program for Energy R&D (PERD).

CANMET Scientific Authority: Dr. J.E.M. Braid
DSS File No. 06SQ.23440-4-9056-1
DSS Contract Serial No. 0SQ85-00137

Prepared by:

MATERIALS TECHNOLOGY CENTRE
A Division of Fleet Technology Limited
311 Legget Drive
Kanata, Ontario, K2K 1Z8

115pp

MICROMEDIA

March 1989

ABSTRACT

Four gas metal arc welds have been prepared using Argon-5% carbon dioxide shielding gas and three consumable wires giving weld deposits alloyed with Mn-Mo, Mn-Si, and Ti-B respectively. All welds were made at 3.0 kJ/mm heat input, and the one with Ti-B weld metal was examined in the stress relieved condition also. The CVN and CTOD toughness of the weld deposits, in comparison to that at 1.7 kJ/mm in another study, has been qualitatively explained in terms of their composition, strength, microstructure and inclusion distributions.

The Ti-B weld deposits had the best toughness on account of their low nitrogen content, and the ability to retain relatively high amount of acicular ferrite at the high input used in the program.

The Mn-Mo deposit also retained its excellent microstructure with large proportion of acicular ferrite; however, its higher hardness and nitrogen content are believed to have led to its mediocre toughness. It is anticipated that a stress relief heat treatment would considerably enhance the deposit toughness.

The Mn-Si deposit suffered considerable reduction in toughness due primarily to its low hardenability leading to considerable reduction in acicular ferrite content and coarsening of the microstructure.

RÉSUMÉ

On a réalisé quatre soudures à l'arc sous protection gazeuse avec électrode fusible en utilisant comme gaz de protection de l'argon contenant 5% de dioxyde de carbone et trois fils fusibles. On a obtenu des dépôts alliés avec du Mn-Mo, du Mn-Si et du Ti-B respectivement. Toutes les soudures ont été réalisées avec un apport calorifique de 3,0 kJ/mm, et celle qui été alliée avec du Ti-B a aussi été examinée en condition de relaxation des contraintes. La résilience des dépôts déterminée par essai Charpy et par essai de déplacement d'ouverture de la pointe de fissure, par comparaison avec celle déterminée à 1,7 kJ/mm dans une autre étude, a été expliquée qualitativement en fonction de la composition, de la résistance, de la microstructure et de la distribution des inclusions.

Les dépôts au Ti-B avaient la meilleure résilience en raison de leur faible teneur en azote et de leur capacité de retenir une quantité relativement élevée de ferrite aciculaire à l'apport élevé utilisé dans le programme.

Le dépôt au Mn-Mo a aussi conservé son excellente microstructure avec une fraction importante de ferrite aciculaire; toutefois, on estime que sa plus grande dureté et sa plus forte teneur en azote sont responsables de sa résilience médiocre. On prévoit qu'un traitement thermique de relaxation des contraintes améliorerait considérablement la résilience du dépôt.

Le dépôt au Mn-Si avait une résilience considérablement réduite, en raison principalement de sa faible trempabilité, ce qui a entrainé une baisse considérable de la teneur en ferrite aciculaire et un grossissement de la microstructure.

TABLE OF CONTENTS

VOLUME II: GAS METAL ARC WELDING PROGRAM

Page

Abstract (i)

1.0 INTRODUCTION 1

2.0 EXPERIMENTAL DESCRIPTIONS AND METHODOLOGY 2

- 2.1 Materials and Consumables 2
  - 2.1.2 Gas Metal Arc Welding Consumables 2
- 2.2 Welding Procedure and Joint Preparation 2
  - 2.2.1 Groove Preparation 2
  - 2.2.2 Welding Fixture 3
  - 2.2.3 Preheat and Interpass Temperature 3
  - 2.2.4 Welding Procedure and Parameters 3
  - 2.2.5 Post Weld Heat Treatment 3
- 2.3 Specimen Preparation 3
- 2.4 Chemical Analysis 4
- 2.5 Inclusion Analysis 4
- 2.6 Quantitative Metallography 4
  - 2.6.1 Macrostructure Along the Centreline 4
  - 2.6.2 Microstructure in the Last Bead 5
- 2.7 Mechanical Testing 5
  - 2.7.1 Hardness Testing 5
  - 2.7.2 CVN Testing 5
  - 2.7.3 Tensile Testing 5
  - 2.7.4 Drop Weight Testing 5
  - 2.7.5 CTOD Testing 5
- 2.8 Gapped Bead On Plate (GBOP) Testing 6
- 2.9 Hydrogen Testing 6

3.0 RESULTS AND DISCUSSION 7

- 3.1 Weld Metal Composition 7
- 3.2 Inclusion Analysis 7
- 3.3 Quantitative Metallography 9
  - 3.3.1 Macrostructure 9
  - 3.3.2 Microstructural Characterization 9
- 3.4 Tensile Properties 10
- 3.5 Drop Weight Testings 10
- 3.6 CVN Notch Toughness 11
- 3.7 CTOD Toughness 12
- 3.8 SEM Fractography on Selected CTOD Specimens 13
- 3.9 Weld Metal Diffusible Hydrogen Content 13
- 3.10 Gapped Bead On Plate Testing 13

4.0 CONCLUDING SUMMARY 14

5.0 REFERENCES 15

TABLE OF CONTENTS (Cont'd)

TABLES

FIGURES

APPENDIX A - Inclusion Analysis

APPENDIX B - Drop Weight Test Results

APPENDIX C - CVN Test Results

APPENDIX D - CTOD Test Results

1.0 INTRODUCTION

In a previous study on weld metal toughness of GMAW deposits[1], attempts were made to correlate deposit composition to its toughness. For the deposits prepared from six commercial wires, the CVN and CTOD toughness were rationalized on the basis of hardenability, microstructure and inclusion distributions. The relevant conclusions regarding three of the six wires to be employed in the present program are summarized as follows:

(i) **Mn-Si deposit** - Although the microstructure in this weld had substantial amounts of grain boundary ferrite (softening effect) and ferrite with aligned second phase (embrittling effect), this weld had the best combination of CVN and CTOD toughness. The observed optimum toughness was attributed to its low hardenability and cleanliness in terms of oxygen and nitrogen contents. However, it was surmised that at a larger heat input (slower cooling rate), this type of deposit will suffer the most significant reduction in weld metal toughness because of its low hardenability and microstructure coarsening, i.e. increase in the proportion of coarse grain boundary and polygonal ferrite.

(ii) **Ti-B deposit** - Next to the Mn-Si weld, this type of weld metal had the best toughness. The good toughness properties were due to the balanced additions of Ti and B that provide a high acicular ferrite content without incurring excessive hardenability. Hence, it was surmised that at higher heat inputs, the toughness may reduce moderately because although the Ti-B addition is capable of retaining relatively high proportions of acicular ferrite, the microstructural coarsening may lower toughness.

(iii) **C-Mn-Mo deposits** - The Mo addition had led to high acicular ferrite contents and high hardness as well. However, the CVN toughness shown by the deposit ranked fourth among the six deposits. It was inferred that the deleterious effect of excessive hardening had offset the improved toughness by high acicular ferrite content, resulting in relatively lower CVN toughness. Nevertheless, it is expected that at higher heat inputs, the Mo addition would help retain the desirable microstructure of acicular ferrite, and the slower cooling rate would reduce the hardness by softening. Thus, the C-Mn-Mo weld metal would retain its toughness by a combination of high acicular ferrite content and microstructural softening.

In summary, the objective of the present program is to validate the hypothesis regarding the effect of heat input on toughness for each of the selected consumables.

2.0 EXPERIMENTAL DESCRIPTIONS AND METHODOLOGY

2.1 Materials and Consumables

2.1.2 Base Plate

The base plate employed for all welds was a 50mm thick C-Mn microalloyed normalized steel plate conforming to CSA G40.21 Grade 350WT. The chemical compositions and mechanical properties, as per mill test report, are included in Table 2.1.

2.1.2 Gas Metal Arc Welding Consumables

Three consumable wires (subsequently designated as A, B and C) were selected for the experiments, with the objective to study the low temperature fracture toughness of weld metal in three families represented by these consumables, viz. C-Mn-Mo (consumable A); Mn-Si (consumable B); and Ti-B (consumable C). The selection of these consumables was made on the basis of their CVN and CTOD toughness extracted from a previous project[1].

According to the respective manufacturers, these wires are designed for gas shielded welding of 350 MPa (50 ksi) steels for low temperature service. The preferred shielding gas is Argon based with 5-25% CO_2. For consumable A, the 1.1mm (0.045") diameter wire is a Mn-Si-Mo alloyed and copper coated, conforming to the designation AWS A5.28 ER80S-D2. For consumable B, the 1.2mm (0.047") diameter wire is a Mn-Si alloyed and copper coated, meeting the classification AWS 5.28 ER70S-G. For consumable C, the 1.2mm (0.047") diameter wire is Ti-B alloyed and copper coated, conforming to AWS 5.28 ER70S-G. The wire compositions are included with weld metal chemistries in Table 3.1.

2.2 Welding Procedure and Joint Preparation

2.2.1 Groove Preparation

Only one joint geometry was used throughout the entire gas metal arc welding program. The welded assembly was nominally 915mm (36") X 610mm (24") with a double V geometry of 2/3 (50° included angle) and 1/3 (60° included angle) (Figure 2.1). The welding direction was transverse to the rolling direction of the base plate.

In order to ensure consistency between welds, the groove surfaces were machine finished to desired dimensions and angles. Prior to the gas metal arc welding of the root pass on the first side, a single low heat input pass of gas metal arc weld using the same respective consumable was deposited on the root of the second side to prevent burnthrough.

Consumable	Trade Name	Manufacturer	AWS 5.28
A	HI-84	Linde	ER80S-D2
B	YM-28E	Nippon	ER70S-G
C	YM-36E	Nippon	ER70S-G

This page can be removed at the discretion of the Scientific Authority.

2.2.2 Welding Fixture

The same welding fixture was used throughout the entire gas metal arc welding program. It is designed to minimize both the angular distortion and lateral shrinkage transverse to welding direction. A schematic representation of the welding fixture is included in Figure 2.2.

2.2.3 Preheat and Interpass Temperature

For the entire program, the preheat and interpass temperature was 150° which satisfies the CSA W59 requirements for 65°C minimum for 50mm thick 350WT steel. The preheat was applied by an oxy-fuel rosebud heating torch. Appropriate Tempilstiks were used to monitor the preheat and interpass temperatures during the course of welding.

2.2.4 Welding Procedure and Parameters

A total of 4 welds of 1.8m (6′) length were made. The experimental matrix for these welds is included in Table 2.2. Back-gouging was undertaken at the root pass of side one to remove the low heat input pass and subsequently widened by grinding to provide a wider groove (Figure 2.3).

In order to maintain consistency and meaningful comparisons among different welds, the sequence and positioning of bead depositions were the same for all welds. Relative to side one, the welding direction was reversed on side two.

2.2.5 Post Weld Heat Treatment

For consumable C, one welded assembly was tested in the as-welded condition and another in the stress relieved condition. The thermal cycle for stress relieving was as per CSA W59 (1984), Clause 5.1.2. The welded plates were placed in an electric furnace at room temperature; heated at a rate of 50°C/hour; soaked at 600°C for 2 hours; and furnace cooled at 50°C/hour to room temperature.

2.3 Specimen Preparation

For all four welds, Charpy (CVN), tensile, drop weight and crack tip opening displacement (CTOD) specimens were machined as per ASTM E23, ASTM A370, ASTM E208 (1984a), and BS 5762, respectively.

The standard size (10mm X 10mm) CVN specimens were taken from two locations, viz. subsurface and root. Prior to extraction, the cross section of the full thickness weldment was surface ground and etched with 10% Nital to reveal the macrostructure. The subsurface Charpies were taken 2mm below the plate surface on side 2, whereas the root Charpies were extracted from side 1, but located at 2mm from the root pass of side 2 (Figure 2.4). For both subsurface and root locations, the notch coincided with the weld centreline which is determined by the mid-point of the narrowest portion of the root.

The P-2 type drop weight specimens were taken from 2mm below the plate surface of side 2 (Figure 2.5). The crack starter bead was deposited transverse to the welding direction with hardfacing electrode at 180-200A and slow traveling speed of 150-170mm/min. The two-bead technique was used with start position at each end and stop positions overlapping at the center.

The all weld metal 6.25mm dia. round tensile specimens with 25mm gauge length were taken longitudinally with the tensile axis location at 8mm from the plate surface of side 1 (Figure 2.6).

Although the plate thickness was 50mm, the thickness in Bx2B CTOD specimens was reduced to 48mm to avoid any lack of reinforcement in the capping layer. The notch root coincided with the weld centreline (Figure 2.7).

2.4 Chemical Analysis

Welds in the as-welded condition were selected for chemical analysis. For each selected weld, all-weld-metal samples were machined from corresponding subsurface and root CVN notch locations, and were sent to Ortech International for chemical analysis for the following elements, viz. C, Mn, Si, S, P, Mo, Ni, Cr, Cu, Nb, V, O, N, Ti, B, Zr, and Al. C and S were analysed by Leco methods; O and N by vacuum fusion; and the balance by DC plasma spectrometry.

2.5 Inclusion Analysis

Since the inclusions are high temperature transformation products, the post weld heat treatment should not affect the inclusion distribution. Hence, the inclusion analysis was undertaken for the welds in the as-welded conditions only. The exact description of methodology is included in Appendix A. Briefly, an area of 2mm (parallel to weld centreline) X 0.5mm at the T/2 location is selected for analysis. Each inclusion is identified by shape, composition and size. The presence of an element in an inclusion is defined by either having a K_α peak of at least 5% relative intensity. For each weld, the inclusions are classified according to size and composition.

2.6 Quantitative Metallography

Welds in as welded condition were selected for metallographic characterization. The transverse sections were polished to a 1 micron diamond finish and subsequently etched with 2% Nital for metallographic examination.

2.6.1 Macrostructure Along the Centreline

For each weld, the macrostructure along the weld centreline was characterized as columnar unrefined region, coarse grain reheated zones, and fine grain reheated zones. The percentage distribution of each structure was calculated by the linear intercept method.

2.6.2 Microstructure in the Last Bead

For each weld in the as-welded condition, the as-deposited microstructure in the final bead on side 2 was characterized by point counting as per IIW designations[2]. The point counting was carried out in 100X10 grids at a magnification of 500X, except for the Mn-Si weld for which the magnification was 250X because of its coarse microstructure. The x and y intervals for the grid were 0.05mm and 0.2mm respectively.

2.7 Mechanical Testing

2.7.1 Hardness Testing

For each weld, Vickers (10kg load) hardness profiles were taken along the centreline and at mid-thickness of both CVN locations. Readings were taken at 5mm intervals along the centreline from cap to cap and every 3mm along the mid thickness at each CVN location.

2.7.2 CVN Testing

For each weld, 16 CVN specimens were extracted from each of the root and subsurface locations. The notch profiles were checked frequently for adherence to ASTM E23. The test temperature ranged from 20°C to -120°C.

2.7.3 Tensile Testing

For each weld, tensile specimens were tested at temperatures ranging from 20°C to -50°C. The lower temperature was maintained by passing liquid nitrogen through an enclosed copper tube cooling chamber. The temperature was monitored by a thermocouple attached directly onto the specimen. The tests were carried out at a strain rate of 0.02/min. An extensometer was used for the room temperature tests only.

2.7.4 Drop Weight Testing

For each weld, up to 8 drop weight P-2 specimens were tested at temperatures ranging from -20 to -70°C. With an impact energy of 400J for all tests, a break or no break condition was prescribed for each specimen by whether the crack had reached at least one side of the specimen or not. A nil ductility transition (NDT) temperature is determined as the highest temperature at and below which all tests yield a break condition.

2.7.5 CTOD Testing

The specimen geometry for the machined specimens is included in Figure 2.7.

In order to ensure a smooth fatigue crack front, local compression was carried out for all specimens in the as-welded condition as per the procedure outlined by Towers and Robinson[3]. The ligament below the notch is locally compressed from both sides by circular indentors of 25mm diameter. The indented area extended from 5mm overlapping the notch root to at least 5mm from the side to avoid bulging. Local compression is not required for stress relieved welds.

The fatigue precracking was carried out in two stages, i.e. a higher fatigue load range was used for accelerated crack initiation and propagation initially; then it was reduced to satisfy the stress intensity specified in BS 5762. The maximum load range for each stage is:

$$P_f = \text{Peak load during cracking} = \frac{\beta \sigma_y B^{3/2} W^{1/2}}{Y}$$

where β = 0.6 for the first 1mm of precracking
β = 0.4 for the next 3mm of precracking
σ_y = yield strength

The test temperature was monitored by a thermocouple attached to the specimen and maintained within 2°C of the specified temperature. At each temperature, three CTOD specimens prepared from each weld were tested as per BS 5762. After the tests, the specimens were broken to measure the effective crack sizes.

2.8 Gapped Bead On Plate (GBOP) Testing

In order to assess the cold cracking susceptibility of the weld metal deposited by the respective wires, the GBOP tests were carried out with the test blocks machined from the same 350WT steel used in this program. The dimension of the test blocks for the GBOP tests are included in Figure 2.8. The test assembly consists of two blocks of the same dimensions except one has a machined recess of 0.75mm. At a predetermined preheat, the assembly is pneumatically clamped together with 10 MPa pressure. A weld bead is deposited across the machined recess using the respective consumables under investigation. The welded blocks are left under pressure for 24 hours, then left for another 24 hours without pressure. The welded blocks are then heated to dull red heat in the vicinity of the gap and allowed to cool to room temperature. The weld bead is snapped open and the extent of cold cracking is determined by the presence/absence of the blue colour oxide layer.

The weld beads were deposited at 175A, 22V and 100mm/min. The preheat temperatures were room temperature, 75°C, and 150°C.

2.9 Hydrogen Testing

For each consumable, the diffusible hydrogen in weld metal was measured by a single pass weld deposited on degassed A36 steel blocks held together in a copper jig. The welding parameters of 27V, 225A, and 3.6mm/sec were used. Once the weld bead was deposited, it was released from the copper jig and quenched in liquid nitrogen. The diffusible hydrogen content in weld metal was determined over mercury using the ISO 3690 method.

3.0 RESULTS AND DISCUSSION

3.1 Weld Metal Composition

The compositions for weld metals in the as-welded condition for both subsurface and root locations are tabulated in Table 3.1. Weld metal compositions for the previous 1.7 kJ/mm weld deposits are also included in Table 3.1(b) for reference. In addition, the calculated carbon equivalents (IIW) and Pcm values are also tabulated in Table 3.2.

In all three welds, there is no significant variation in compositions among the subsurface and root locations. Considering the Nb and V contents in the base plate, the trace amounts of these two elements in all welds suggest a low dilution condition.

Although the manufacturer of consumable A claims the wire is a C-Mn-Mo consumable with Ti additions, the wire and weld metal analysis suggest that the Ti addition is marginal, in both 3.0 and 1.7 kJ/mm welds.

In comparison with the lower heat input welds, the O and N contents for the C-Mn-Mo and Mn-Si welds increase significantly with heat input whereas the Ti-B weld shows little change. Given the small unbalance factors in these two former welds (Table 3.2), the C-Mn-Mo and Mn-Si welds would be more susceptible to strain aging effects. In addition to O and N contents, the Mn recoveries are higher, especially in the case of Ti-B deposit, resulting in larger Mn contents in the bulk weld metal of the present program. The Si recovery is, however, somewhat lower in the larger heat input welds. Although a different power source is used in the present program, it is unlikely that the composition change is a result of this factor. Furthermore, although the composition for the single Vee 1.7 kJ/mm weld depositions are obtained from the undiluted region, the low dilution conditions from the present programs discount the role of joint geometry and dilution as possible causes for change in composition. Rather, it is likely due to the effect of heat input.

In the submerged arc welding program, it was reported that in higher heat input weld, the Mo content at the subsurface location is higher than at the root location. In the present GMAW program, the same trend can be observed. Kohno et al[4] have reported experimental results showing that the Mo content decreases with the increasing number of weld passes in the Mo-Ti-B SAW deposits, i.e. the subsurface Mo content is smaller than the root location. The apparent contradictions cannot be presently rationalized.

3.2 Inclusion Analysis

The inclusion analysis is summarized in Tables 3.3-3.7. The full documentation of the inclusion analysis is attached in Appendix A.

For the C-Mn-Mo weld of consumable A, the overall inclusion area fraction and number density increase consistent with higher oxygen content at 3.0 kJ/mm (240ppm vs. 170ppm). The inclusions are characterized by Mn, Si and S with varying trace amounts of Ti and Al. At higher heat input, relative contents of Mn found in the inclusions decreases with a concomitant increase in relative Si contents. Shape factors also undergo a drastic reduction with higher heat input, implying that inclusions are becoming less equiaxed. Despite the relatively unchanging inclusion sizes, both in overall average or individual inclusion types, the inclusion size distribution and number densities are shifting towards larger sizes at the higher heat input, leading to higher number densities of larger inclusions.

For Mn-Si welds of consumable B, the inclusions are characterized by Mn, Si and Al with trace amounts of S and Ti. At higher heat input, the diversity of inclusion types reduces such that the largest group of dominant inclusion types occupies 46% of all inclusions versus 18% in the 1.7 kJ/mm weld. In terms of inclusion composition, the relative content of Mn found in inclusions decreases, whereas there is a moderate increase in Si and Al contents. Although the overall average inclusion diameter and area fraction do not change appreciably with heat input, there is a definite trend of inclusions shifting to larger sizes as indicated by the inclusion proportions and densities.

For Ti-B weld of consumable C, the inclusions are characterized as by Ti-rich, and containing Mn, Si and Al with a trace amount of S. Regardless of inclusion types, this weld has the largest average inclusion size among the three welds in the present program. Despite the small difference in oxygen and O+S contents with heat input, 170 vs. 181ppm for 1.7 and 3.0 kJ/mm respectively, the difference in inclusion distribution is significant (Tables 3.3 and 3.6). Both the area fraction and average inclusion size are larger because most inclusions participate in a general shift to larger sizes as indicated by the increase in proportions and number density of each size grouping. A general trend can be observed that the inclusion number density in the size greater than 0.5μm increases at the expense of smaller inclusions such that with higher heat input, the most significant increase occurs in the intermediate size grouping of diameter in the range 0.5-1.0μm. For instance, at 1.7 kJ/mm, 70-90% of all dominant inclusions have diameters smaller than 0.5μm, whereas at 3.0 kJ/mm, there are at least 50% of all dominant inclusions with diameters in the range of 0.5-1.0μm. In terms of inclusion composition, the relative alloy contents of dominant inclusions have not changed with higher heat input although the diversity of dominant inclusion types reduces such that the largest group of dominant inclusions occupies >50% of all inclusions versus 13% in 1.7 kJ/mm.

By reproducing the plot of length/width aspect ratio developed from the submerged arc welding program, (Figure 3.1), the shape factors in the present program, ranging from 0.73 to 0.87 correspond to a length/width aspect ratio of ~2. Hence, the assumption of equivalence among area fraction and volume fraction no longer appears to be valid since there is a significant deviation from Widgery's approximation[5] (Figure 3.2):

$$\text{Volume fraction } (V_f) = 5.5\ (O+S)$$

The volume fraction of inclusion for the present study can also be estimated as follows:

$$\text{Volume fraction } (\%) = \left(\frac{100\pi}{6}\right) N_s[D^2_{avg} + D^2_{std}]$$

where N_s = number of inclusions per micron^2

D_{avg} = average inclusion diameter in micron

D_{std} = standard deviation in diameter

When the estimated volume fraction is plotted against O+S, along with Widgery's prediction (Figure 3.2), it is shown that despite moderate scatter for the Ti-B deposits, there is reasonable agreement among the estimated inclusion volume fractions with O+S contents, i.e. higher O+S contents lead to a larger inclusion volume fraction.

3.3 Quantitative Metallography

3.3.1 Macrostructure

The macrostructural distributions along the weld centreline in the through thickness dimension are tabulated in Table 3.8. The representative macrographs are included in Figures 3.3-3.6 for reference.

For all three welds, the macrostructures are characterized by a high proportion of the columnar region. The large as-deposited macrostructure is due to the majority of layers being comprised of a single pass. In comparison, the single V lower heat input welds had a relatively smaller proportion of as-deposited columnar structure, because of the welding procedure which employed two to three passes per layer. Examination of macrographs indicates the characteristic "finger" pattern of bead morphology commonly found in Ar rich-CO_2 gas shielded welding.

3.3.2 Microstructural Characterization

The microstructural characterizations on the last deposited bead are tabulated in Table 3.9. The representative micrographs are included in Figures 3.7-3.9.

For the C-Mn-Mo weld of consumable A, the microstructure is characterized by fine intragranular acicular ferrite interspersed with ferrite with aligned second phase of large length/width aspect ratio. The absence of coarse grain boundary ferrite is in accordance with the effect of Mo on the hardenability of steels and weld metals. It is of interest to note that the C-Mn-Mo weld has the finest microstructure among the three welds in the present program. In general, the heat input has a negligible influence on the microstructural distribution, and the presence of Mo appears to be responsible for retaining the high acicular ferrite content at the higher heat input.

For the Mn-Si weld of consumable B, the microstructure is coarse enough to be resolved even at 100X magnification, and therefore the microstructural characterization was undertaken at 250X instead of the 500X normally used. The microstructure is dominated by ferrite with aligned second phase along with substantial amounts of coarse grain boundary ferrite, polygonal ferrite, and ferrite with non-aligned second phase. In comparison to the lower heat input welds, there is a drastic decrease in acicular ferrite. Because of the lack of alloying elements, the large reduction in acicular ferrite content with larger heat input is in accordance with the expectation for this weld. Although the inclusion size distribution shifts to the intermediate size range at the higher heat input, the absence of Ti may reduce their efficacy to act as nucleation sites for acicular ferrite.

For the Ti-B weld of consumable C, the microstructure is characterized by moderate amounts of acicular ferrite. Higher heat input has led to a moderate reduction in acicular ferrite contents with a concomitant increase in polygonal ferrite.

3.4 Tensile Properties

The tensile properties and Vickers hardness (10kg load) measurements are summarized in Tables 3.10 and 3.11.

In comparing the three welds in the as-welded condition, the C-Mn-Mo weld of consumable A has the highest strength/hardness because of its highest carbon equivalent, and therefore higher hardenability. Although Mn-Si and Ti-B welds have similar carbon equivalents, the higher hardness/strength in Ti-B welds is due to the finer microstructure resulting from the microalloying elements. Stress relief heat treatment in the Ti-B weld of consumable C has led to a slight reduction in strength and hardness.

All three welds prepared with a heat input of 3.0 kJ/mm show higher hardness at the root location than the subsurface location.

3.5 Drop Weight Testings

The full documentation of drop weight test results is given in Appendix B. The nil ductility temperatures are summarized in Table 3.12.

Comparison among the three welds indicates that the Ti-B weld of consumable C in the as-welded condition or stress relieved condition, and C-Mn-Mo weld metal of consumable C have similar nil ductility transition temperatures (-60° to -65°C). The Mn-Si weld has a higher NDT temperature (-40°C). The CVN toughness in the subsurface locations for both C-Mn-Mo and Mn-Si deposits are similar (the 40J transition temperature is only 4°C higher in Mn-Si weld, Section 3.6), yet the observed NDT temperature of consumable B is 20°C higher. Considering that the same drop weight impact energy is used for all tests, the higher NDT temperature of Mn-Si deposit could partly be due to its lower strength, in addition to the adverse affect of its coarse microstructure.

3.6 CVN Notch Toughness

The full documentation of CVN data and individual transition curves is included in Appendix C. The transition temperatures and comparative transition curves are included in Table 3.13 and Figures 3.10 and 3.11 respectively.

As a general observation, it is seen that subsurface CVN toughness is better than that at the root location, the one exception being the Mn-Si weld metal, consumable B. By superimposing the CVN notch location on the weld cross-section macrograph (Figures 3.10 and 3.11), it is found that for this deposit, the percent of reheated region sampled by the notch at the root location is ≈80%, whereas for the subsurface location, the notch sampled only 40% reheated region. This particular factor is believed to be responsible for the superior CVN toughness at the root location for the weld deposit B.

In comparison, in weld C, the root notch location sampled only 30% reheated region vs. 60% for the subsurface location, thus explaining the ≈30° increase in transition temperature for the root location. In weld A, both the root and subsurface notch locations sampled approximately 50% reheated region, and therefore a part of the ≈32 to 34°C increase in transition temperature for the root location could be due to its higher nitrogen content (very low unbalance factor), leading to strain aging damage at the root region. For the Ti-B deposit, the total nitrogen content is low, and the unbalance factor sufficiently high so that little free nitrogen is expected to be available to cause strain aging.

The stress relief treatment of the Ti-B deposit also leads to an increase in the transition temperature - by about 20°C for the subsurface location and 2 to 7°C at the root location. Conceivably, this could be caused by the decomposition of the aligned and non-aligned phase into carbides which in turn would have some embrittling effect.

Comparing the CVN toughness of the 3.0 kJ/mm welds at the subsurface location with that of the 1.7 kJ/mm welds at T/2 location[1], for C-Mn-Mo weld metal (A), there is only a minor difference consistent with virtually no change in the proportion of various microconstituents at the two heat inputs. In the case of the Ti-B weld metal (C), the higher heat input increases the proportion of polygonal ferrite and ferrite with second phase, yet there is a further decrease in transition temperature. In light of the similar compositions in the two welds, the effect is probably related to differences in the amounts of reheated regions of the macrostructure sampled by the notches.

The Mn-Si weld deposits made with consumable B, on the other hand, seem to suffer a significant increase in the transition temperature - from -100°C at 1.7 kJ/mm to -58°C at 3.0 kJ/mm. This is attributed to microstructural coarsening and the drastic reduction in the acicular ferrite proportion. Further, the large proportions of ferrite with aligned second phase offers a lower resistance to brittle fracture.

3.7 CTOD Toughness

The full documentation of the individual CTOD test data is included in Appendix D. The average and range of CTOD values obtained are summarized in Table 3.14 In terms of CTOD toughness, these welds can be ranked as:

C-Mn-Mo < Mn-Si < as-welded Ti-B < stress-relieved Ti-B

In the as-welded condition, the deposits from all three consumables have similar CTOD toughness at -30°C (Figure 3.12). When the average CTOD values at -10°C are included, the CTOD values for both Mn-Si and C-Mn-Mo welds are insensitive to the test temperatures, whereas CTOD values of Ti-B weld increase at the higher temperature. Hence, it is surmised that the 0.1mm transition temperature for C-Mn-Mo and Mn-Si welds is close to -10°C, whereas for the Ti-B weld metal in as-welded condition, it is between -20 and -30°C. Despite a slight adverse effect of stress relief shown on CVN toughness, CTOD values for the Ti-B weld metal improve with stress relief heat treatment such that the 0.1mm transition temperature shifts to below -30°C. While the low CTOD toughness of Mn-Si deposit is obviously related to its poor microstructure, that for C-Mn-Mo deposit must be related to its high strength and strain aging damage at the root.

In comparing the CTOD values for the high heat input welds (3.0 kJ/mm) with those at the lower heat input (1.7 kJ/mm), it must be kept in mind that the larger plate thickness in the present program (32 vs. 50mm) would introduce a larger constraint in the CTOD specimens, leading to reduced CTOD toughness. Further, in double V joints, the root location coincides with the higher constrained area, i.e. middle 1/3 of the through thickness CTOD specimens whereas the root location in a single V joint is located at the least constrained area near the specimen surface. Since higher constraint leads to lower apparent fracture toughness, the double V joints of a thicker plate would have a lower CTOD toughness than a single V joint of a thinner plate. It should also be noted (Table 3.4) that higher heat input leads to an increase in the proportion of the inclusions greater than 1μm diameter for all three weld deposits and that in turn would lead to a greater likelihood of cleavage initiation and hence lower CTOD toughness.

3.8 SEM Fractography on Selected CTOD Specimens

Among the six CTOD specimens selected for SEM fractographic examination, attempts to locate the cleavage initiation sites were successful for three specimens only. The SEM micrographs and the EDX spectrums for the initiation sites are included in Figures 3.13-3.20.

In each case, the EDX spectrum of the cleavage initiation site is different from the surrounding matrix. Furthermore, the relative compositions of cleavage initiation sites are in agreement with the dominant inclusions for the respective welds. For instance, the relative composition of the cleavage initiation site found in the stress relieved Ti-B weld are similar to that of Ti-Al-Mn-S inclusions found in the weld metal (Figure 3.14, Table 3.6). Hence, it is surmised that the inclusions act as cleavage initiation sites.

Relative to the through thickness dimension, the cleavage initiation site is preferentially located in the reheated region of first and second passes of side 1, i.e. immediately below the root pass of side 2. This observation is in accordance with the earlier discussion regarding low toughness in double V joint caused by the root location situated at the more constrained area.

3.9 Weld Metal Diffusible Hydrogen Content

The diffusible hydrogen contents in the weld metals were 3.16ml/100g, 2.49ml/100g and 2.46ml/100g for consumables A, B and C respectively. These wires can be classified as very low hydrogen consumables.

3.10 Gapped Bead On Plate Testing

Based on the amount of cracking observed at various preheat temperatures (Table 3.15) the 10% cracking preheat temperature can be estimated to be:

Consumable A: >150°C
Consumable B: ≥ 75°C
Consumable C: ≈150°C

The highest cold cracking susceptibility of weld deposit A, and lowest for weld deposit B represented by the above numbers seems to be a direct reflection of the weld metal hardness. All the same, these numbers reflect a fairly high susceptibility to weld metal cold cracking despite the low weld metal hydrogen content. A probable cause for this is believed to be the shape of the GMA weld bead whereby "finger penetration" of the bead is subjected to a rather high cooling rate, higher than that estimated on the basis of heat input only.

4.0 CONCLUDING SUMMARY

The CVN and CTOD toughness of GMA weld deposits made by three consumable wires at 3 kJ/mm heat input have been determined and compared with those of welds made at 1.7 kJ/mm. The results have been qualitatively rationalized in terms of microstructure, macrostructure, nitrogen content, deposit strength and inclusion size distribution. The investigation points to caution in comparing CVN and CTOD results from different studies on account of the effect of macrostructure sampled by the CVN notch, and of the groove design and CTOD specimen size on the respective toughness values measured. Nevertheless, the main observations can be summarized as:

(i) At 3.0 kJ/mm, the consumables can be ranked in the order of increasing toughness as:

CVN: Mn-Si (AW) $\leq$ C-Mn-Mo (AW) $\leq$ Ti-B (SR) < Ti-B (AW)

CTOD: C-Mn-Mo (AW) < Mn-Si (AW) < Ti-B (AW) < Ti-B (SR)

where AW and SR stand for as-welded and stress-relieved conditions respectively.

(ii) In comparison with the welds at 1.7 kJ/mm in another study,

- the Mn-Si deposit suffers considerable reduction in toughness, as anticipated, on account of coarsening of the microstructure, and considerable reduction in acicular ferrite proportion.
- the C-Mn-Mo deposit retains its excellent microstructure, and the CVN toughness at the subsurface location. However, its high nitrogen content could be a factor in strain aging damage in the root region. Because of its high strength, it is anticipated that a stress relief treatment could considerably enhance the toughness of these deposits.
- the Ti-B deposit was quite successful in retaining its CVN toughness at the higher heat input, however, part of the reduction in CTOD values is most likely due to an increase in the volume fraction of inclusions >1μm in diameter. The stress relief treatment is effective in improving the CTOD values to some extent. Overall, the relatively low nitrogen content of the deposit, and the presence of Ti and B seem effective in providing good toughness values over a wider heat input range, and in both as-welded and stress relieved conditions.

5.0 REFERENCES

[1] Chiu, C. and Malik, L., "Toughness Evaluation of GMA Welding Consumables for Offshore and Petrochemical Applications - Interim Report". FTL/Arctec Canada Report 2517C (1987).

[2] Pargeter, R.J. and Dolby, R.E., "Identification and Quantitative Description for Ferritic Steel Weld Metal Microstructure". IIW Doc. IX-1323-84 (1984).

[3] Towers, O.L. and Robinson, P., "Procedures for Fatigue Cracking Fracture Toughness Test Pieces, With Particular Reference to Weldments". WI Research Bulletin, 23, 112-120 (1982).

[4] Kohno, R., Takami, T., Mori, N. and Nagano, K., "New Fluxes of Improved Weld Metal Toughness for HSLA Steels". Welding Journal 12, p. 373s-380s (1982).

[5] Widgery, D.J., "Deoxidation Practice for Mild Steel Weld Metal". Welding Journal, 55, p. 57s-68s (1976).

TABLES

Table 2.1

Characterizations of the Base Plate

C	Mn	S	P	Si	Cr	Ni	Al	Nb	V	Cu
0.14	1.27	0.01	.017	0.29	0.03	0.17	0.04	0.032	0.043	0.2

Yield Strength (MPa)	Ultimate Tensile Strength (MPa)	% Elongation	CVN Impact Energy @ -60°C (J)	
			Transverse	Longitudinal
364	510	29	66	129

Table 2.2

Experimental Matrix for Gas Metal Arc Program

Consumable	Heat Input (kJ/mm)	Post Weld Condition	Weld I.D.
C-Mn-Mo (A)	3.0	As Welded	G1A G1B
Mn-Si (B)	3.0	As Welded	G2A G2B
Ti-B (C)	3.0	As Welded	G3A G3B
	3.0	Stress Relieved	G4A G4B

Table 2.3

Welding Parameters for Gas Metal Arc Welds

	Gas	Flow Rate (litre/min)	Voltage	Current	Travelling Speed (mm/sec)	Electrode Stick Out (mm)	Polarity	Heat Input (kJ/mm)
First Root Pass on both sides 1 and 2	95% Ar - 5% CO_2	22	28	320	3.0	19	DC-RP	3.0
Fill up for both sides 1 and 2	95% Ar - 5% CO_2	22	30	300	3.0	19	DC-RP	3.0
Backing pass	95% Ar - 5% CO_2	22	28	300	4.0	19	DC-RP	2.1

Table 3.1(a)

Summary of Weld Metal Compositions of Gas Metal Arc Welds in As Welded Condition (3.0 kJ/mm)

Consumable	Location	C	Mn	Si	S	P*	Ti	Mo	Al	Zr	O	N	Cr	Ni	Cu	V	Nb	B
C-Mn-Mo (A)	Sub-surface	0.08	*1.48	0.60	0.016	0.012	0.008	0.54	0.013	0.003	0.0240	0.0109	0.03	0.09	0.170	0.009	0.002	<0.001
	Root	0.08	1.57	0.36	0.019	0.012	0.005	0.39	0.011	0.002	0.0217	0.0090	0.03	0.09	0.16	0.010	0.004	<0.001
	Wire Analysis	0.11	1.75	0.67	0.015	0.010	<0.01	0.56	<0.01	<0.005	0.0056	0.0100	0.03	0.08	0.10	<0.01	--	N/A
Mn-Si (B)	Sub-surface	0.06	1.44	0.45	0.004	0.007	<0.001	<.01	0.007	0.002	0.0287	0.0042	0.003	0.04	0.25	0.007	0.004	<0.001
	Root	0.06	1.42	0.48	0.004	0.008	<0.001	<.01	0.008	0.003	0.0224	0.0055	0.03	0.06	0.257	0.011	0.006	<0.001
	Wire Analysis	0.04	1.38	0.61	0.004	0.010	0.001	0.01	0.006	<0.005	0.0070	0.0046	0.02	0.02	0.23	0.003	--	<0.0006
Ti-B (C)	Sub-surface	0.05	1.59	0.245	0.003	0.009	0.035	<.01	0.005	0.002	0.0181	0.0063	0.02	0.06	0.24	0.007	0.004	0.003
	Root	0.06	1.54	0.265	0.003	0.008	0.030	<.01	0.006	0.002	0.0172	0.0043	0.02	0.08	0.24	0.010	0.005	0.001
	Wire Analysis	0.05	1.65	0.46	0.002	0.011	0.06	0.01	0.007	<0.005	0.0057	0.0024	0.02	0.05	0.24	0.003	--	0.005

-- All compositions are in weight percent.
-- Wire analysis by atomic absorption.
-- Weld metal analysis by DC Plasma.
*Rechecked value by atomic absorption.

Table 3.1(b)
Chemical Compositions for the Weld Metal Prepared With 1.7 kJ/mm[1]

	Consumable A	Consumable B	Consumable C
C (w/o)	0.10 (0.09)	0.09 (0.08)	0.06 (0.05)
Mn (w/o)	1.56 (1.84)	1.21 (1.43)	1.29 (1.72)
Si (w/o)	0.50 (0.57)	0.52 (0.60)	0.34 (0.40)
Cr (w/o)	0.06 (0.03)	0.06 (0.02)	0.05 (0.02)
Ni (w/o)	0.07 (0.05)	0.05 (0.02)	0.06 (0.05)
Mo (w/o)	0.50 (0.52)	<0.01 (<0.01)	<0.01 (<0.01)
Cu (w/o)	0.18 (0.23)	0.24 (0.25)	0.23 (0.24)
V (w/o)	<0.01 (<0.01)	<0.01 (<0.01)	<0.01 (<0.01)
Ti (w/o)	<0.01 (<0.01)	<0.01 (<0.01)	0.035 (0.05)
Al (w/o)	<0.01 (<0.01)	<0.01 (<0.01)	<0.01 (<0.01)
Zr (w/o)	0.003 (<0.005)	<0.002 (<0.005)	<0.002 (<0.005)
P (w/o)	0.016 (0.012)	0.012 (0.013)	0.012 (0.012)
S (w/o)	0.008 (0.009)	0.009 (0.009)	0.004 (0.010)
B (w/o)	<0.0001 (0.001)	0.0001 (0.001)	0.0027 (0.002)
O (w/o)	0.017 (0.0065)	0.015 (0.0071)	0.017 (0.0060)
N (w/o)	0.008 (0.0078)	0.003 (0.0019)	0.004 (0.0029)

*The bracketed value is the composition of the wire.

Table 3.2

Consumable	Location	CE	P_{cm}	Al/O^2	Ti/Al	Ti/B	Unbalance Factor	B/N	O + S
C-Mn-Mo (A)	Subsurface	0.457	0.227	22.57	--	--	0.0009	--	0.0390
	Root	0.444	0.213	23.36	--	--	0.0012	--	0.0367
Mn-Si (B)	Subsurface	0.327	0.163	8.50	--	--	0.0022	--	0.0317
	Root	0.326	0.163	15.94	--	--	0.0029	--	0.0254
Ti-B (C)	Subsurface	0.341	0.167	15.26	7.0	11.67	0.0090	0.476	0.0201
	Root	0.344	0.166	20.28	5.0	30.00	0.0109	0.233	0.0202

$$P_{cm} = C + (Mn + Cr + Cu)/20 + Si/30 + Mo/15 + V/10 + Ni/60 + 5B$$

$$CE = C + Mn/6 + (Cu + Ni)/15 + (Cr + Mo + V)/5$$

$$\text{Unbalance Factor} = 14 \left[\frac{Ti}{48} + \frac{Al}{27} + \frac{V}{51} + \frac{Nb}{93}\right] - N$$

Table 3.3

Summary of Inclusion Distributions for Gas Metal Arc Welding Program

Consumable	Heat Input	O + S (wt %)*	Area Fraction (%)	Inclusion Density $(\times 10^5/cm^2)$	Average Diameter (μm)	Average Shape Factor	Estimated Volume Fraction (%)
C-Mn-Mo (A)	1.7**	0.0250	0.12	7.3	0.43	0.87	0.079
	3.0	0.0367	0.72	16.0	0.45	0.73	0.198
Mn-Si (B)	1.7**	0.0240	0.21	5.8	0.52	0.83	0.142
	3.0	0.0254	0.44	9.0	0.49	0.85	0.128
Ti-B (C)	1.7**	0.0210	0.08	6.6	0.36	0.82	0.052
	3.0	0.0202	0.39	6.0	0.65	0.80	0.195

*The O + S values are T/2 location and root locations for 1.7 kJ/mm and 3.0 kJ/mm deposits respectively.

**These inclusion analyses are extracted from 32mm plate with heat input of 1.7 kJ/mm.

Table 3.4

Summary of Inclusion Size Distribution

Consumable	Heat Input (kJ/mm)	$0.2 \leq$ diameter < 0.5 (micron)		$0.5 \leq$ diameter < 1.0 (micron)		$1.0 \leq$ diameter ≤ 2.0 (micron)		O + S (wt %)
		% of all inclusions	density ($10^5/cm^2$)	% of all inclusions	density ($10^5/cm^2$)	% of all inclusions	density ($10^5/cm^2$)	
C-Mn-Mo (A)	1.7	74.4	5.4	25.3	1.8	0.3	0.03	0.025
	3.0	67.8	10.8	30.0	4.0	2.1	0.03	0.0367
C-Mn-Si (B)	1.7	62.9	3.7	35.6	2.1	1.5	0.9	0.024
	3.0	52.9	4.8	44.8	4.0	2.3	0.2	0.0254
Ti-B (C)	1.7	85.0	5.6	15.0	1.0	---	---	0.021
	3.0	39.7	2.4	50.9	3.1	9.4	0.6	0.0202

Table 3.5
Summary of Dominant Inclusions Distributions
(G1B)

3.0 kJ/mm	Avg. Dia. micron	Percent Distribution (%)	Shape Factor	Proportion (%)			Density ($X10^5/cm^2$)			Relative Contents (%)				
				$0.2 \le d < 0.5$	$0.5 \le d < 1.0$	$d \ge 1.0$	$0.2 \le d < 0.5$	$0.5 \le d < 1.0$	$d \ge 1.0$	Si	Mn	Al	S	Ti
Al-Ti-Si-Mn-S	0.45	55.7	0.81	67.2	31.1	1.7	6.0	2.8	0.2	30	31	10	17	8
Si-Mn-S	0.45	10.9	0.58	65.2	34.8	---	1.1	0.6	---	28	38	0	32	0
Ti-Si-Mn-S	0.43	10.9	0.66	76.1	21.7	2.2	1.3	0.4	0.04	22	33	1	29	13
Al-Si-Mn-S	0.44	9.2	0.67	71.8	28.2	---	1.1	0.4	---	31	31	13	23	0
Overall	0.45	100.0	0.73	67.8	30.0	2.1	10.8	4.8	0.3	--	--	--	--	--

1.7 kJ/mm	Avg. Dia. micron	Percent Distribution (%)	Shape Factor	Proportion (%)			Density ($X10^5/cm^2$)			Relative Contents (%)				
				$0.2 \le d < 0.5$	$0.5 \le d < 1.0$	$d \ge 1.0$	$0.2 \le d < 0.5$	$0.5 \le d < 1.0$	$d \ge 1.0$	Si	Mn	Al	S	Ti
Ti-Si-Mn-S	0.43	38.1	0.89	70.0	30.0	--	1.9	0.8	--	19	48	1	17	12
Cu*-Ti-Si-Mn-S	0.44	13.1	0.89	71.1	29.0	--	0.7	0.3	--	21	45	1	15	11
Si-Mn-S	0.41	10.0	0.89	82.8	17.2	--	0.6	0.1	--	17	55	1	24	0
Al-Ti-Si-Mn-S	0.49	9.3	0.88	81.5	14.8	3.7	0.6	0.1	0.03	23	44	6	12	12
Overall	0.43	100.0	0.87	74.4	25.3	0.3	5.4	1.8	0.03	--	--	--	--	--

*The relative content of Cu is 4

Table 3.6
Summary of Dominant Inclusions Distributions (G3B)

3.0 kJ/mm	Avg. Dia. micron	Percent Distribution (%)	Shape Factor	Proportion (%)			Density ($X10^5/cm^2$)			Relative Contents (%)				
				$0.2 \le d < 0.5$	$0.5 \le d < 1.0$	$d \ge 1.0$	$0.2 \le d < 0.5$	$0.5 \le d < 1.0$	$d \ge 1.0$	Si	Mn	Al	S	Ti
Al-Ti-Si-Mn-S	0.56	50.6	0.80	41.3	52.1	4.8	1.3	1.6	0.1	9	10	11	6	61
Al-Ti-Si-Mn	0.55	22.4	0.81	44.6	54.1	1.4	0.6	0.7	0.02	10	10	13	0	65
Al-Ti-Mn-S	0.66	7.0	0.86	21.7	65.2	13.0	0.09	0.3	0.05	1	8	15	5	69
Overall	0.65	100.0	0.80	39.7	50.9	9.4	2.4	3.1	0.6	--	--	--	--	--

1.7 kJ/mm	Avg. Dia. micron	Percent Distribution (%)	Shape Factor	Proportion (%)			Density ($X10^5/cm^2$)			Relative Contents (%)				
				$0.2 \le d < 0.5$	$0.5 \le d < 1.0$	$d \ge 1.0$	$0.2 \le d < 0.5$	$0.5 \le d < 1.0$	$d \ge 1.0$	Si	Mn	Al	S	Ti
Al-Ti-Mn	0.46	12.8	0.85	69.2	30.8	--	0.6	0.3	--	1	10	7	0	78
Al-Ti-Mn-S	0.40	11.5	0.85	77.1	22.9	--	0.6	0.2	--	1	13	6	6	71
Ti-Mn	0.42	8.9	0.87	74.1	25.9	--	0.4	0.2	--	1	16	1	0	79
Ti-Si-Mn-S	0.32	8.5	0.74	88.5	11.5	--	0.5	0.06	--	8	15	1	7	66
Ti-Si-Mn	0.34	7.9	0.83	91.7	8.3	--	0.5	0.04	--	7	15	2	0	73
Ti-Mn-S	0.38	7.5	0.83	82.6	17.4	--	0.4	0.09	--	2	13	2	6	74
Al-Ti-Si-Mn-S	0.35	6.2	0.84	89.5	10.5	--	0.4	0.04	--	8	16	6	7	59
Al-Ti-Si-Mn	0.30	5.9	0.78	100.0	--	--	0.4	---	--	7	14	8	1	69
Overall	0.36	100.0	0.82	84.9	15.1	--	5.6	0.1	--	--	--	--	--	--

Table 3.7
Summary of Dominant Inclusions Distributions
(G2B)

3.0 kJ/mm	Avg. Dia. (micron	Percent Distribution (%)	Shape Factor	Proportion (%)			Density ($X10^5/cm^2$)			Relative Contents (%)				
				$0.2 \le d < 0.5$	$0.5 \le d < 1.0$	$d \ge 1.0$	$0.2 \le d < 0.5$	$0.5 \le d < 1.0$	$d \ge 1.0$	Si	Mn	Al	S	Ti
Al-Si-Mn-S	0.49	46.3	0.86	51.4	46.4	2.2	2.1	1.9	0.09	49	29	13	6	0
Al-Ti-Si-Mn-S	0.47	26.8	0.86	56.6	42.5	1.0	1.4	1.0	0.02	47	28	12	6	4
Al-Si-Mn	0.50	13.4	0.85	52.8	45.3	0.5	0.6	0.5	0.02	53	30	15	0	0
Overall	0.49	100.0	0.85	52.9	44.8	2.2	4.8	4.0	0.2	--	--	--	--	--

1.7 kJ/mm	Avg. Dia. (micron	Percent Distribution (%)	Shape Factor	Proportion (%)			Density ($X10^5/cm^2$)			Relative Contents (%)				
				$0.2 \le d < 0.5$	$0.5 \le d < 1.0$	$d \ge 1.0$	$0.2 \le d < 0.5$	$0.5 \le d < 1.0$	$d \ge 1.0$	Si	Mn	Al	S	Ti
Al-Si-Mn-S	0.51	17.6	0.84	47.2	52.8	--	0.5	0.5	--	39	45	8	5	0
Al-Si-Mn	0.49	17.1	0.90	51.4	48.6	--	0.5	0.5	--	42	48	5	1	1
Si-Mn-S	0.49	6.8	0.86	57.1	35.7	7.1	0.2	0.1	0.03	40	49	1	5	0
Al-Ti-Si-Mn-S	0.44	6.8	0.83	64.3	35.7	--	0.3	0.1	--	39	44	5	4	5
Al-Si-Mn	0.56	5.9	0.90	33.3	66.7	--	0.1	0.2	--	41	46	5	1	1
Si-Mn	0.50	5.4	0.86	90.9	0	9.1	0.3	--	0.03	40	55	1	1	0
Overall	0.52	100.0	0.83	62.9	35.6	1.5	3.7	2.1	0.09	--	--	--	--	--

Table 3.8

Summary of Macrostructure Characterizations

Consumable	Post Weld Condition	Columnar Region (%)	Coarse Grain (%)	Fine Grain (%)
C-Mn-Mo (A)	As Welded	77.1	14.1	8.87
Mn-Si (B)	As Welded	61.8	13.0	25.2
Ti-B (C)	As Welded	58.9	9.3	31.8
	Stress Relieved	65.5	8.8	25.7

Table 3.9

Summary of Microstructure Characterization
Gas Metal Arc Welds

	Heat Input (kJ/mm)	Grain Boundary Ferrite (%)	Polygonal Ferrite	Ferrite With Aligned Second Phase (%)	Ferrite With Non-Aligned Second Phase (%)	Acicular Ferrite (%)
C-Mn-Mo (A)	1.7*	7.8	0.8	7.8	2.3	81.3
	3.0	4.7	2.1	6.6	3.9	82.7
Mn-Si (B)	1.7*	15.2	5.1	16.9	5.3	57.5
	2.2*	4.5	8.9	25.2	5.5	55.2
	3.0**	10.6	11.3	48.1	17.0	13.0
Ti-B (C)	1.7*	12.6	2.6	2.3	0.2	82.1
	3.0	11.4	12.1	5.4	5.5	65.6

*This data are extracted from previous projects on 32mm plate with single V geometry.

**The characterization is carried out with 250X magnification due to coarse structure; all others are carried out at 500X.

Table 3.10

Summary of Tensile Data of Gas Metal Arc Welds

CONSUMABLE	POST WELD HEAT TREATMENT	TEMPERATURE (°C)	YIELD STRENGTH (MPa)	ULTIMATE TENSILE STRENGTH (MPa)	% ELONGATION	REDUCTION IN AREA (%)
C-Mn-Mo (A)	As welded (G1)	20	642	712	22.8	29.5
		-10	621	728		
		-30	648	747	19.6	29.0
Mn-Si (B)	As welded (G2)	20	430	516	32.2	54.5
		-10	434	534		
		-30	455	559	29.1	54.3
Ti-B (C)	As welded (G3)	20	495	576	32.1	57.2
		-10	493	582		
		-30	514	607	29.0	56.1
	Stress Relieved (G4)	20	472	570	31.7	55.1
		-30	454	532	32.2	49.0
		-50	477	602		

-- All stress calculations are of engineering stress.

-- All tests are carried out with strain rates of 0.02/min.

Table 3.11

Summary of Hardness Measurements

Consumable	Post Weld Condition	Average Vickers (10Kg) Hardness		
		Centreline	Root	Subsurface
C-Mn-Mo (A)	As Welded	261 (243-294)*	266 (264-268)	257 (247-266)
Mn-Si (B)	As Welded	198 (182-219)	208 (192-218)	183 (180-185)
Ti-B (C)	As Welded	221 (193-274)	224 (191-247)	210 (203-215)
	Stress Relieved	209 (179-254)	218 (181-230)	197 (181-227)

*The bracketed figure is the range of hardness measurements.

Table 3.12

Summary of Nil Ductility Transition (NDT) Temperatures
Gas Metal Arc Welds

Consumable	Post Weld Condition	
	As Welded	Stress Relieved
C-Mn-Mo (A)	-60	---
Mn-Si (B)	-40	---
Ti-B (C)	-65	-60

Table 3.13

Summary of CVN Impact Properties for Gas Metal Arc Welds

(a) 3.0 kJ/mm

Consumable	PWHT Condition	Location	Transition Temperature (°C)			CVN Impact Energy (J)					
			40J	35J	27J	0°C	-20°C	-30°C	-40°C	-60°C	-80°C
C-Mn-Mo (A)	As welded	Subsurface	-62	-66	-73	110	91	80	68	42	20
		Root	-28	-33	-41	69	50	38	28	15	-
Mn-Si (B)	As welded	Subsurface	-58	-61	-65	157	148	139	121	36	10
		Root	-68	-69	-72	157	151	146	139	104	14
Ti-B (C)	As welded	Subsurface	-114	-115	-116	155	156	156	155	151	147
		Root	-84	-85	-87	156	154	154	151	138	71
	Stress Relieved	Subsurface	-94	-95	-97	158	158	158	158	155	146
		Root	-77	-80	-85	155	153	149	142	83	35

(b) 1.7 kJ/mm[1]

Consumable	PWHT Condition	Location	Transition Temperature		CVN Impact Energy (J)				
			40J	27J	0°C	-20°C	-30°C	-40°C	-60°C
C-Mn-Mo (A)	As welded	T/2	-68	-76	134	123	112	98	56
Mn-Si (B)	As welded	T/2	-100	-103	129	129	128	127	124
Ti-B (C)	As welded	T/2	-96	-98	134	134	134	133	131

Table 3.14

Summary of CTOD Values
Gas Metal Arc Welds

Consumable	Heat Input (kJ/mm)	Temperature (°C)	Average CTOD Values (mm)	
			As Welded	Stress Relieved
C-Mn-Mo (A)	1.7	N/T	N/T	N/T
	3.0	-10	0.095 (0.087-0.106)	
		-30	0.086 (0.084-0.089)	
Mn-Si (B)	1.7	-10	1.67 (1.55-1.75)	
		-30	0.81 (0.64-1.16)	
		-50	0.56 (0.18-0.086)	
	2.2	-10	1.47 (1.40-1.59)	
		-30	0.38 (0.19-0.64)	
		-50	0.24 (0.21-0.28)	
	3.0	-10	0.15 (0.99-0.17)	
		-30	0.14 (0.07-0.20)	
Ti-B (C)	1.7	-10	1.60 (1.53-1.70)	
		-30	0.65 (0.12-1.71)	
		-50	0.33 (0.06-0.65)	
	3.0	-10	0.38 (0.23-0.50)	
		-30	0.13 (0.08-0.16)	0.34 (0.27-0.44)
		-50	N/T	0.13 (0.03-0.32)

N/T = Not Tested

Table 3.15

Summary of G-BOP Tests

Consumable	Percent Cracking		
	20°C	75°C	150°C
A	70-80	70-80	50-60
B	50-60	10-15	5-10
C	30-40	20-25	10-15

FIGURES

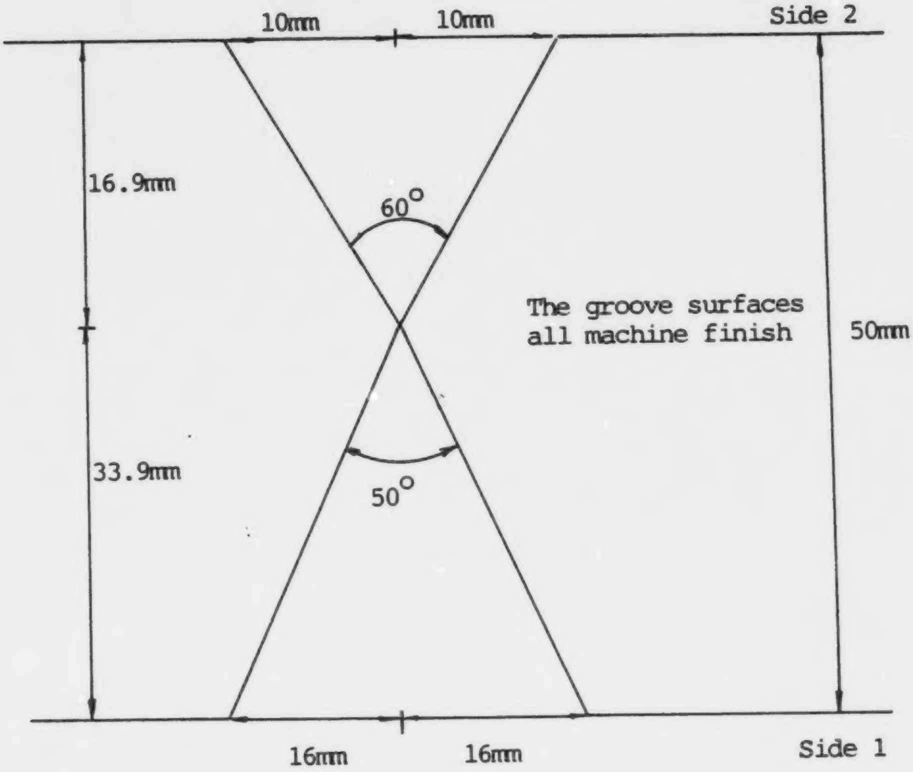
10mm
10mm
Side 2
16.9mm
60°
The groove surfaces all machine finish
50mm
33.9mm
50°
16mm
16mm
Side 1

Figure 2.1: Schematic representation of double V joint geometry

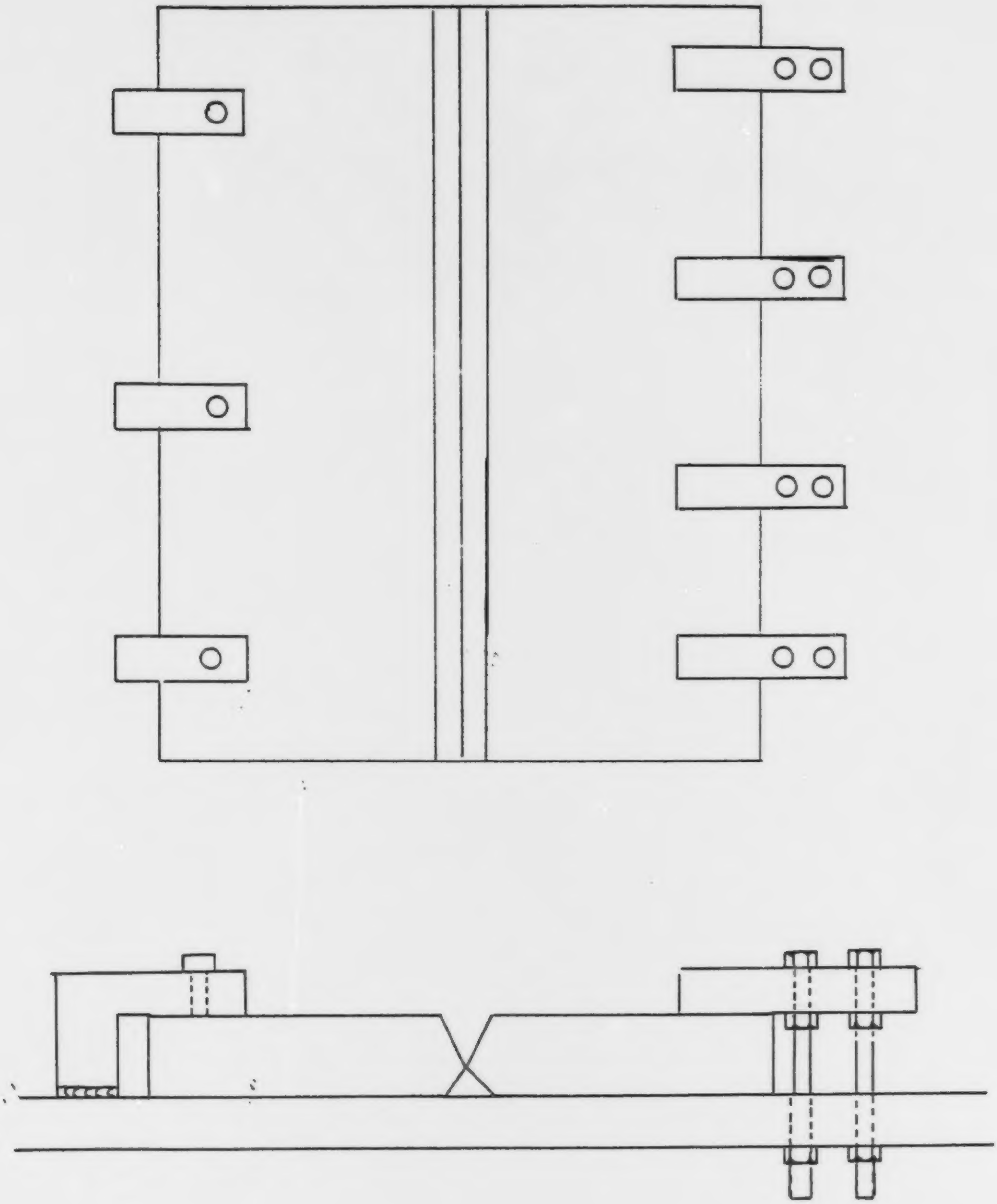

Figure 2.2 Schematic illustration of restraint set up for all welds

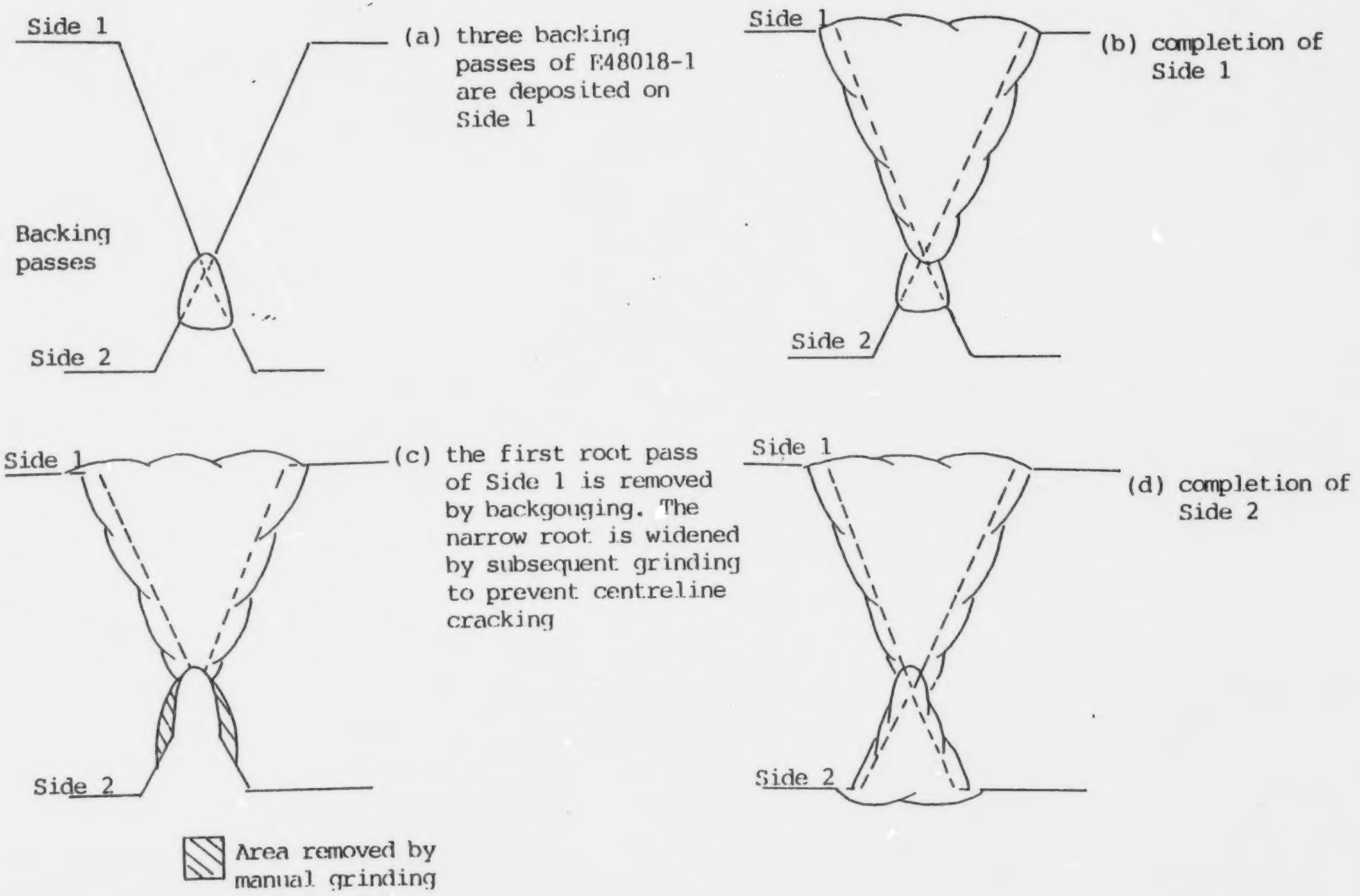
Side 1
Side 2
Backing passes
Side 1
Side 2
Side 1
Side 2
Side 1
Side 2
▨ Area removed by manual grinding

(a) three backing passes of E48018-1 are deposited on Side 1

(b) completion of Side 1

(c) the first root pass of Side 1 is removed by backgouging. The narrow root is widened by subsequent grinding to prevent centreline cracking

(d) completion of Side 2

Figure 2.3: Schematic representation of welding sequence

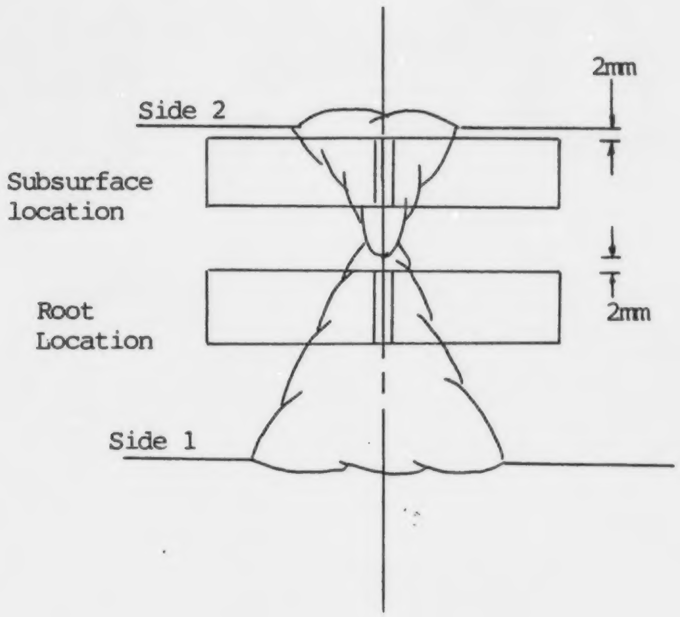
2mm
Side 2
Subsurface location
Root Location
2mm
Side 1

Figure 2.4: Schematic representation of CVN toughness

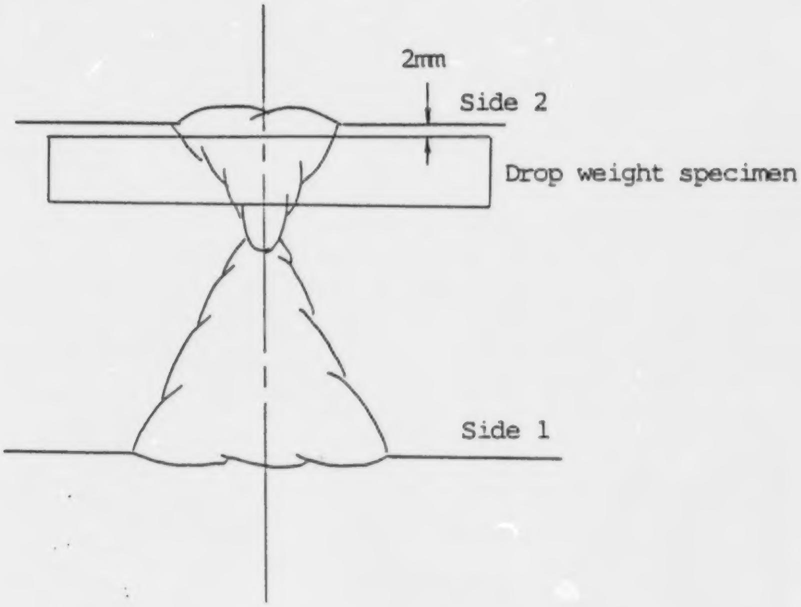
2mm
Side 2
Drop weight specimen
Side 1

Figure 2.5: Location of extraction of drop weight P-2 specimens

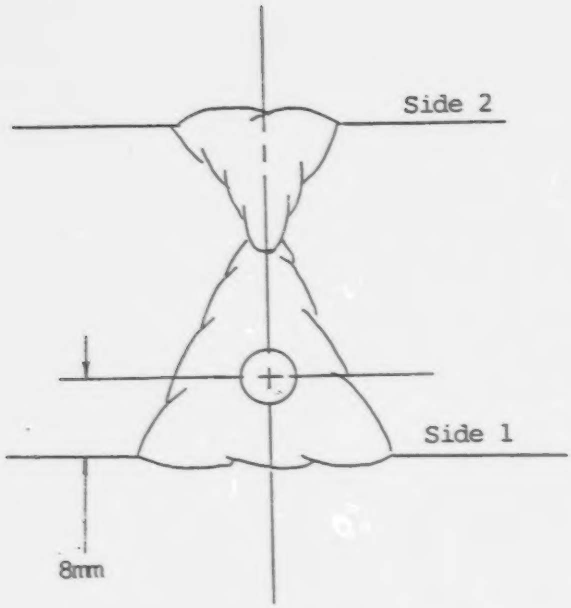
Side 2
Side 1
8mm

Figure 2.6: All weld metal round tensile specimens

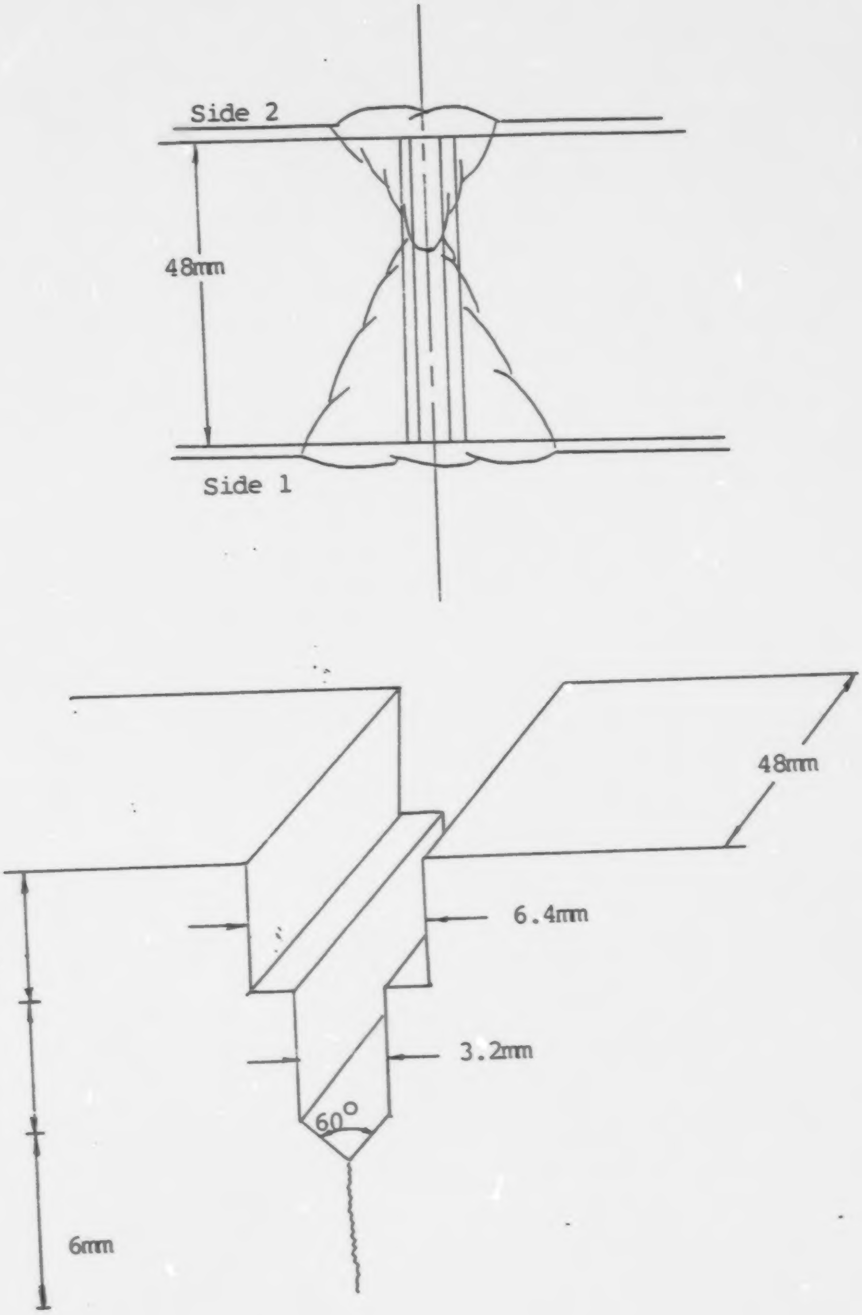
Side 2
48mm
Side 1
48mm
6.4mm
3.2mm
60°
6mm

Figure 2.7: CTOD specimens

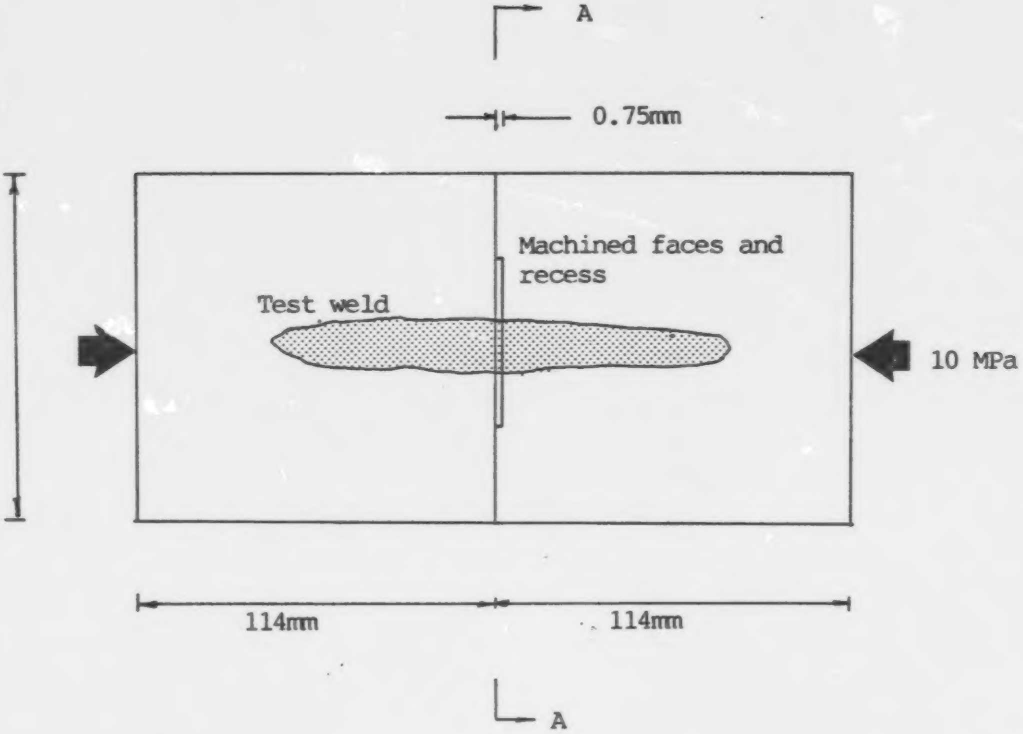
A
0.75mm
Machined faces and recess
Test weld
114mm
10 MPa
114mm
114mm
A

(a) Top view

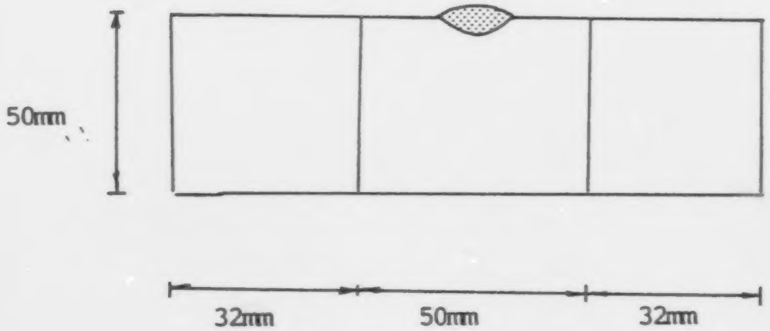
50mm
32mm
50mm
32mm

(b) Section A-A

Figure 2.8 G-BOP Test specimens

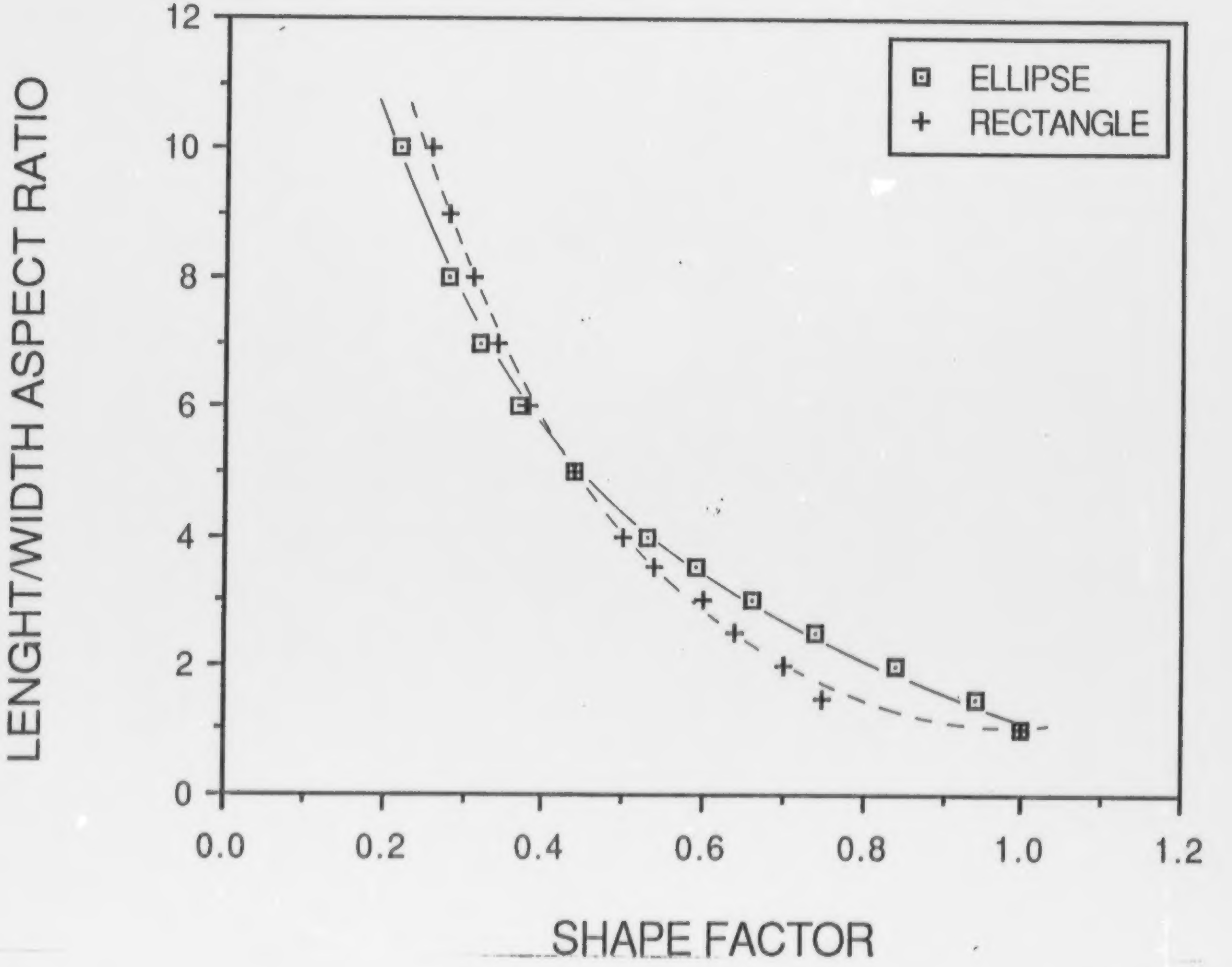

Figure 3.1: The plot of length/width ratio vs. shape factor reproduced from submerged arc welding program.

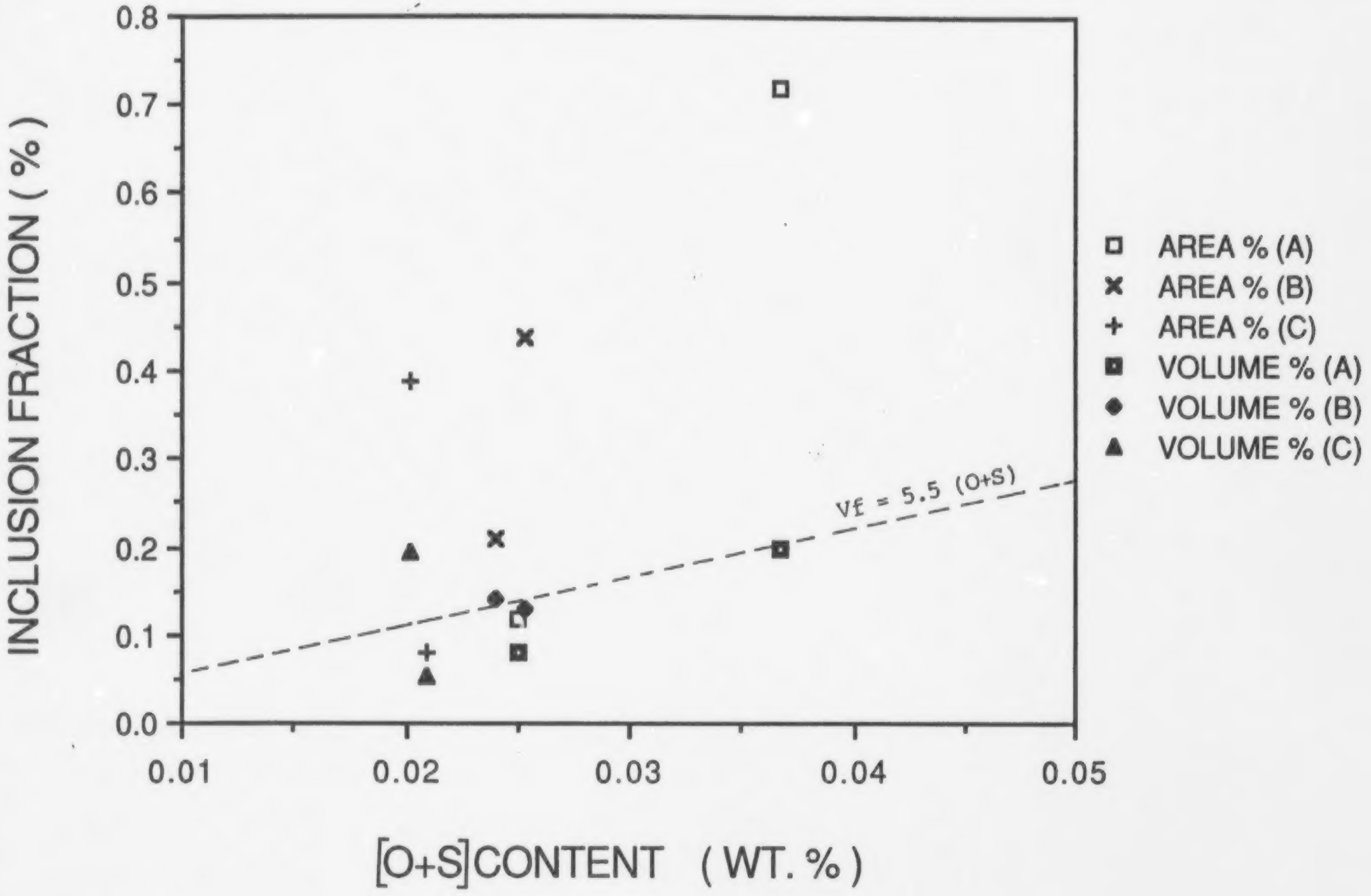

Figure 3.2: The effect of O+S contents on the inclusion volume fractions and area fractions

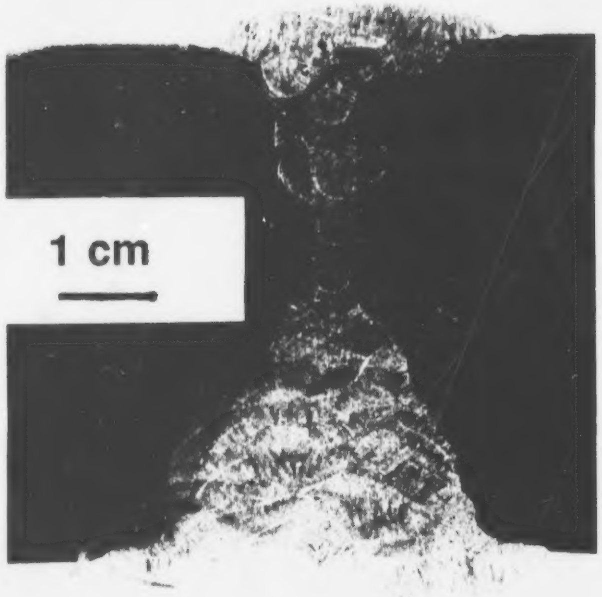

Figure 3.3: Through thickness macrograph of weld prepared with Consumable A in as-welded condition (G1B) (1.4X, Neg. 11214)

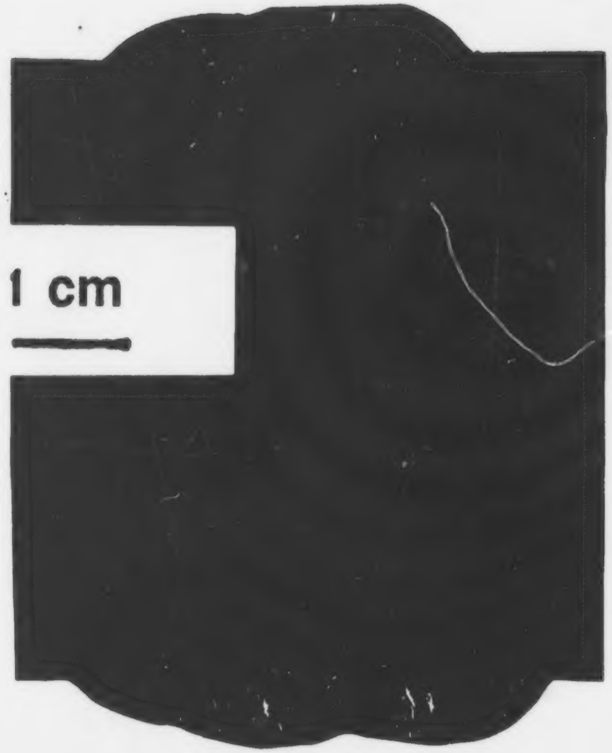

Figure 3.4 Through thickness macrograph of weld prepared with Consumable B in as-welded condition (G2B) (1.7X, Neg. 11217)

Figure 3.5: Through thickness macrograph of weld prepared with Consumable C in as-welded condition (G3B) (1.4X, Neg. 11214)

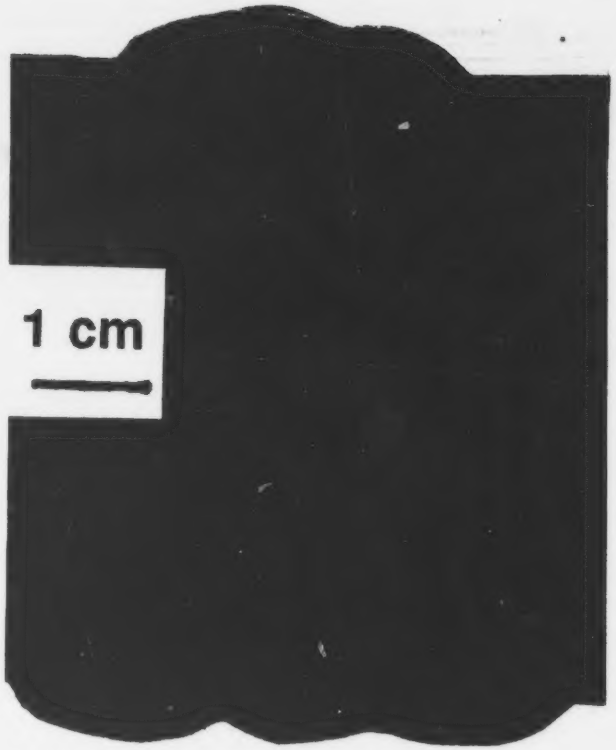

Figure 3.6 Through thickness macrograph of weld prepared with Consumable C in stress relieved condition (G4B 1.7X, Neg. 11218)

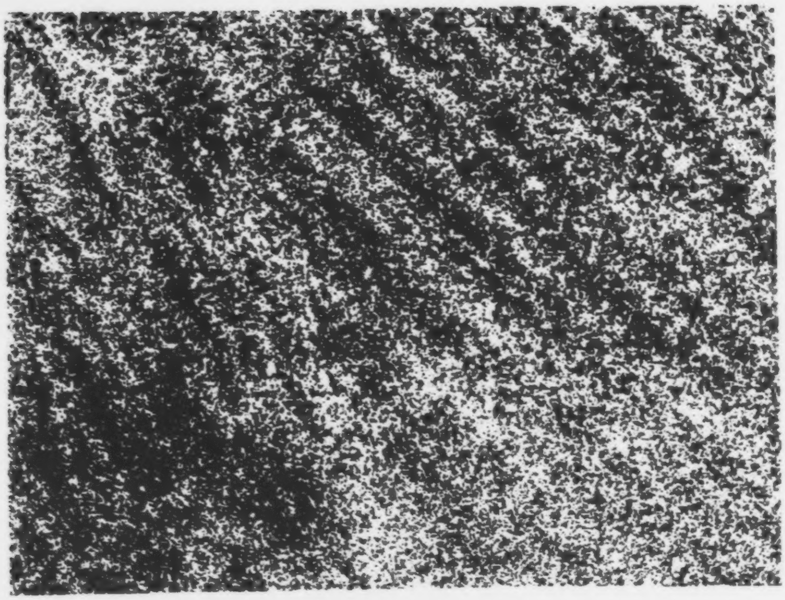

(a) (100X, Neg. 11212)

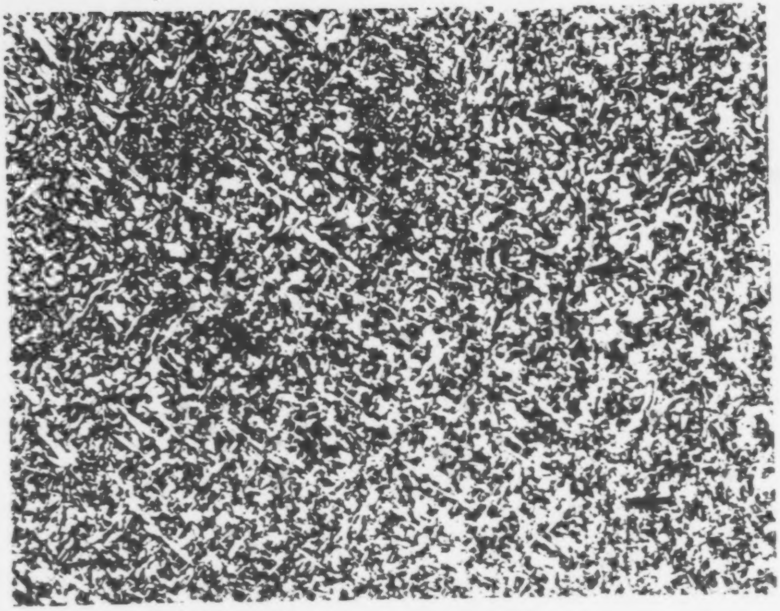

(b) (500X, Neg. 11213)

Figure 3.7 Representative microstructure of C-Mn-Mo weld prepared with Consumable A. Note the fine intragranular ferrite size and the grain boundary ferrite denoted by arrows (G1B)

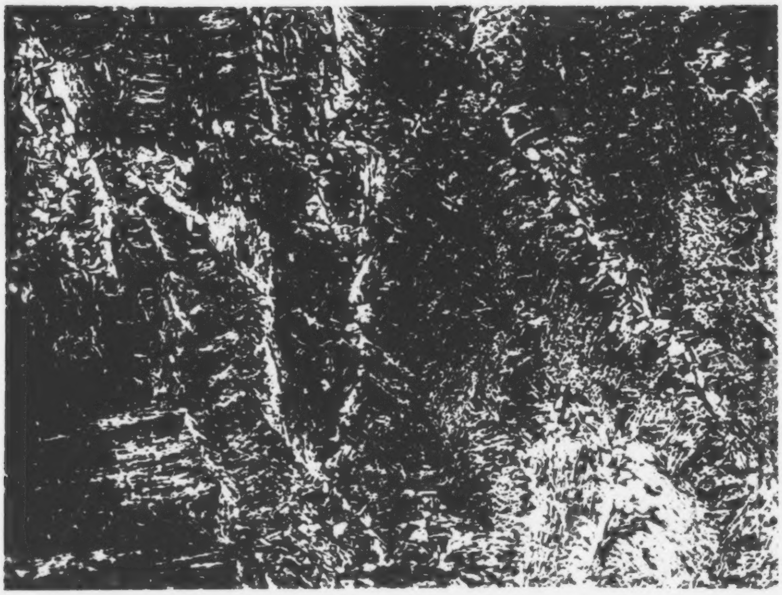

(a) (100X, Neg. 11215)

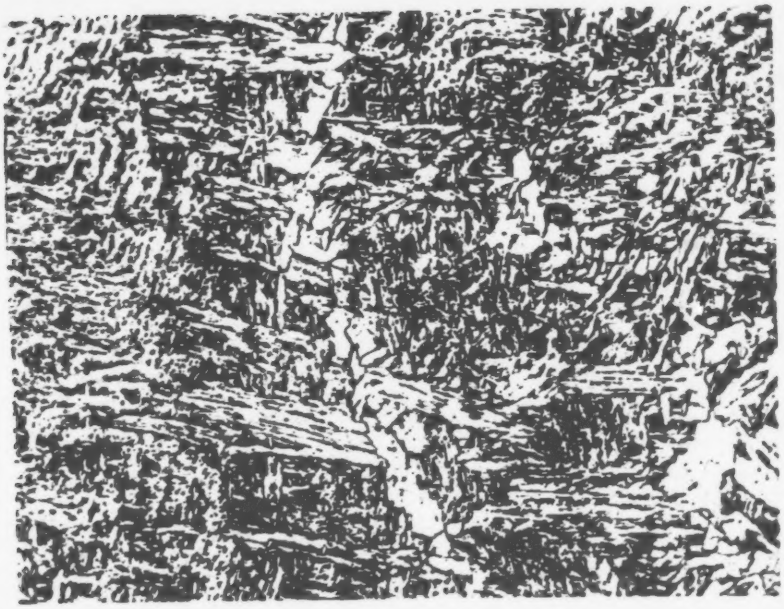

(b) (250X, Neg. 11216)

Figure 3.8 Representative microstructure of Mn-Si weld prepared with Consumable B. Note the coarse structure and the predominantly bainitic structure (G2B)

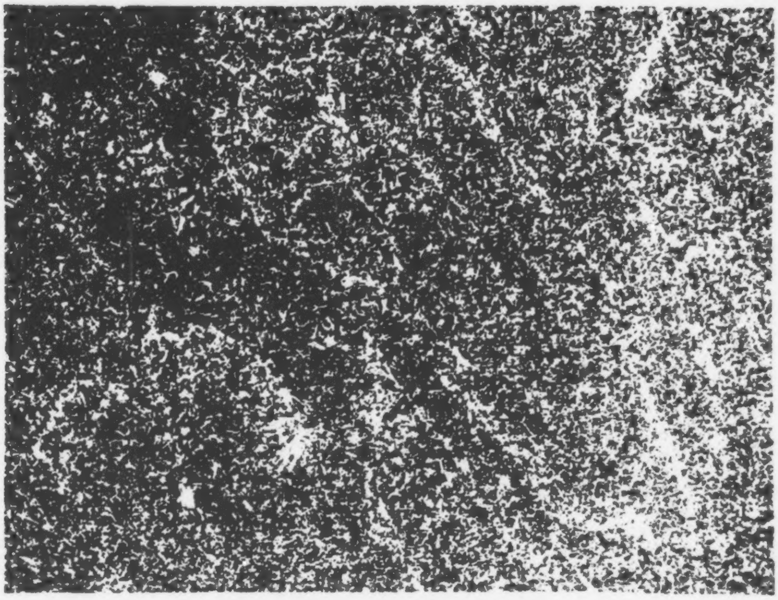

(a) (100X, Neg. 11208)

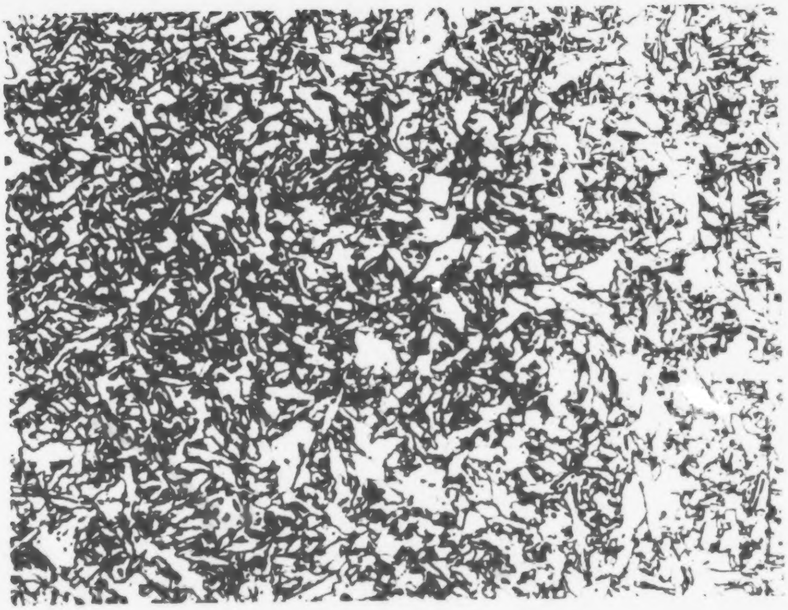

(b) (500X, Neg. 11209)

Figure 3.9: Representative microstructure of Ti-B weld prepared with Consumable C. Note the common occurrence of coarse ferrite phases both in grain boundary ferrites and polygonal ferrites.

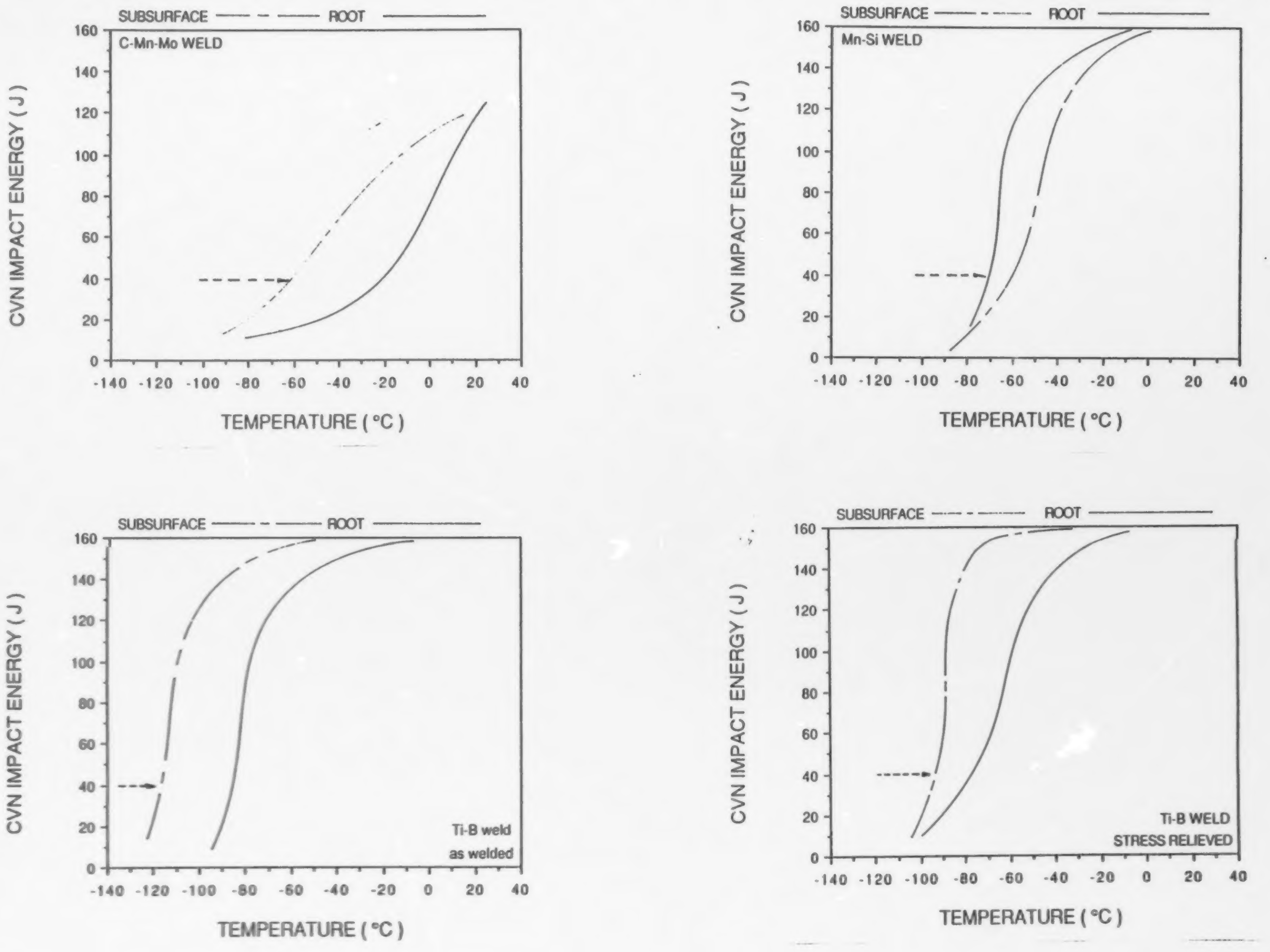

Figure 3.10: Comparative CVN transition curves to illustrate the effect of through thickness variation on CVN toughness.

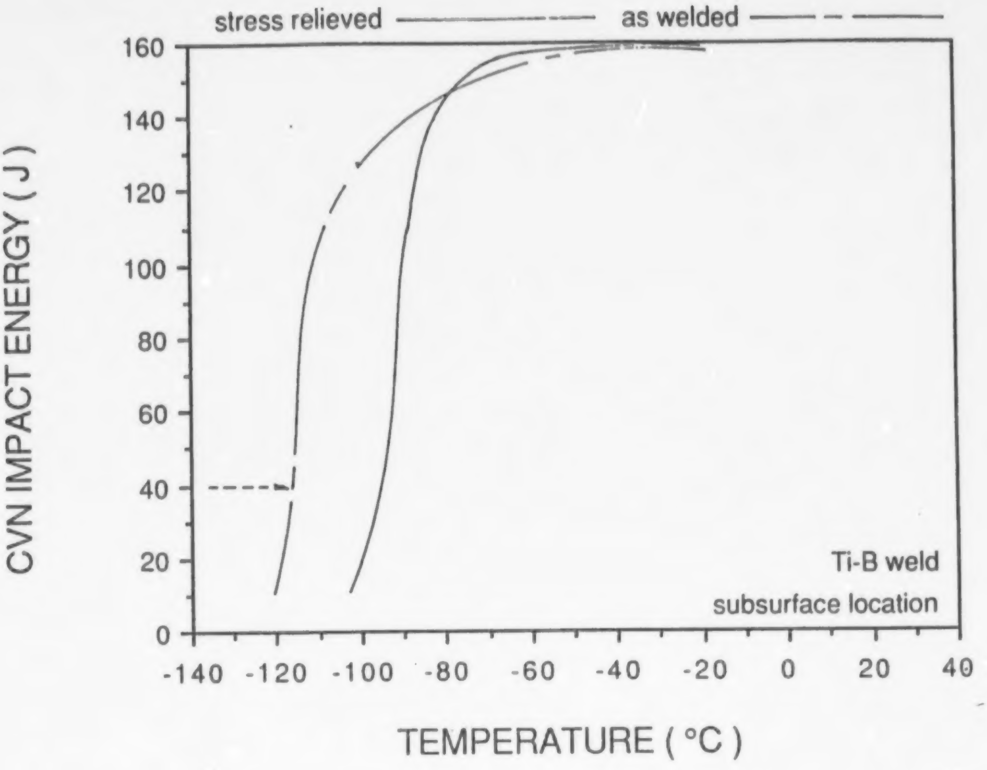

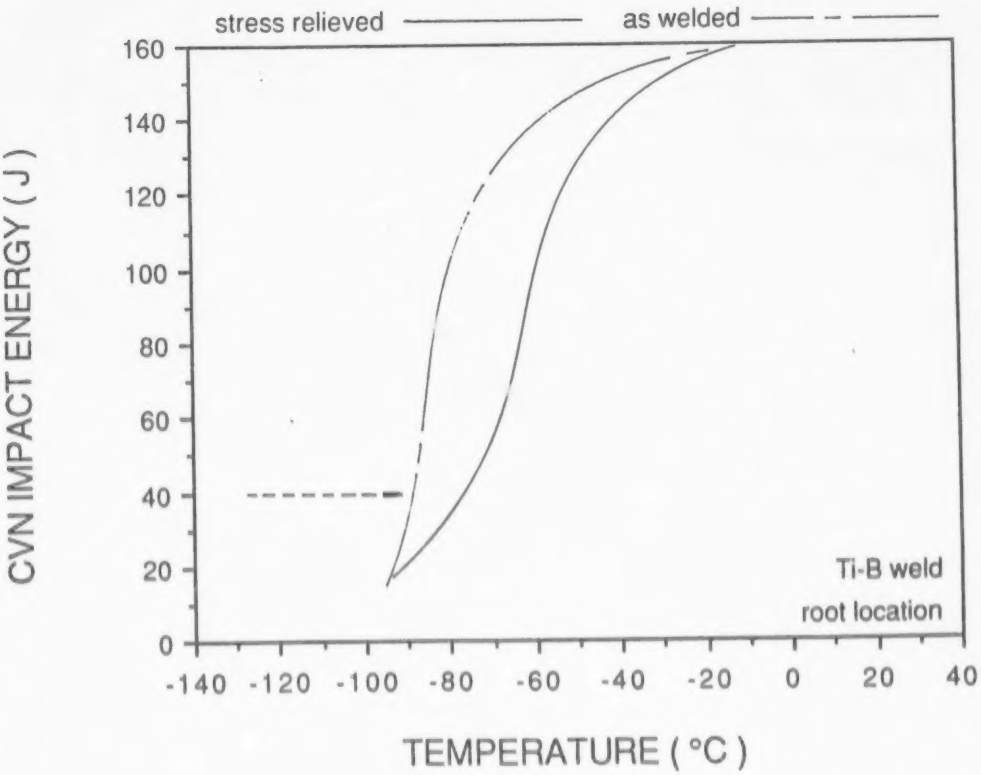

Figure 3.11: Comparative CVN transition curves illustrates the effect of stress relief heat treatment on CVN toughness

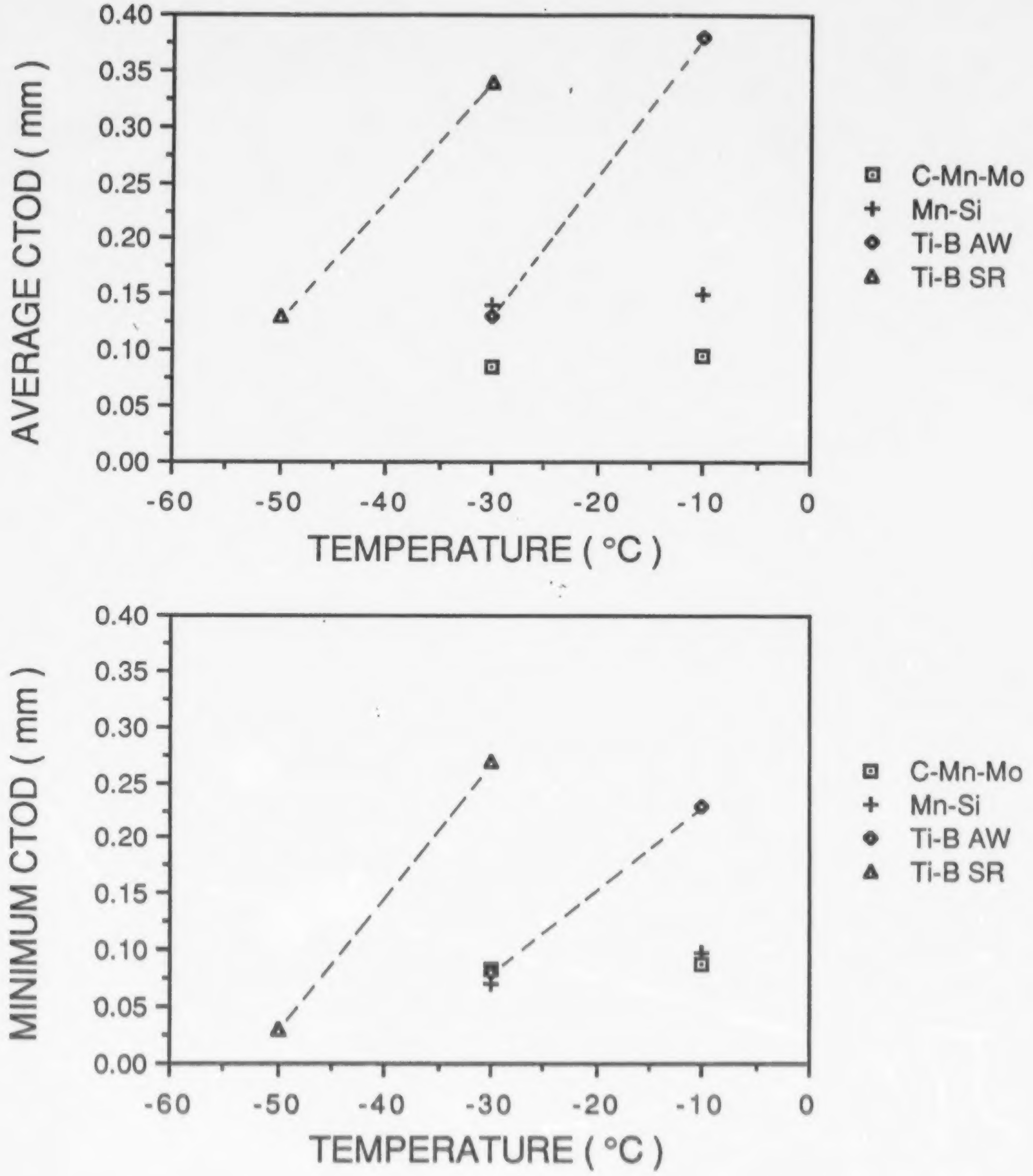

Figure 3.12: Variations of CTOD values with test temperature are illustrated.

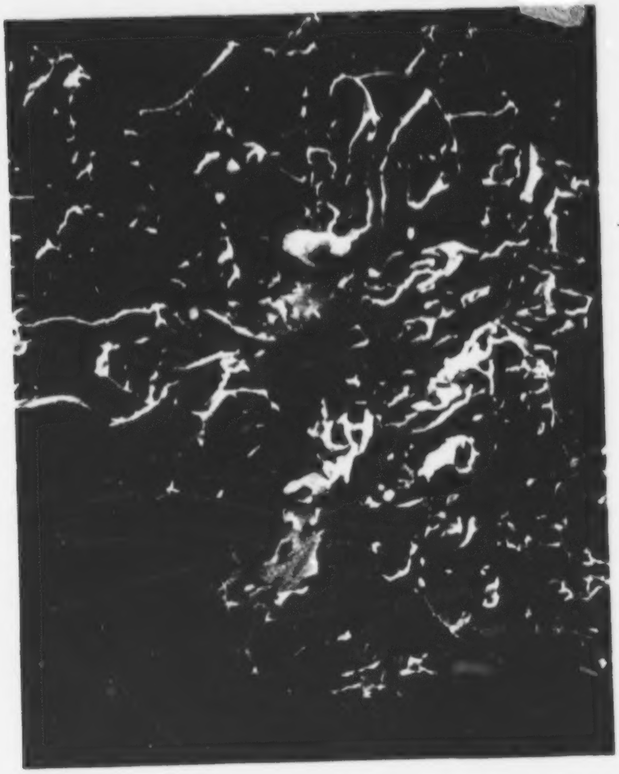

Figure 3.13: Cleavage initiation site in the stress relieved Ti-B weld (4G2, -30°C, CTOD = 0.26mm) (1000X, Neg. 786)

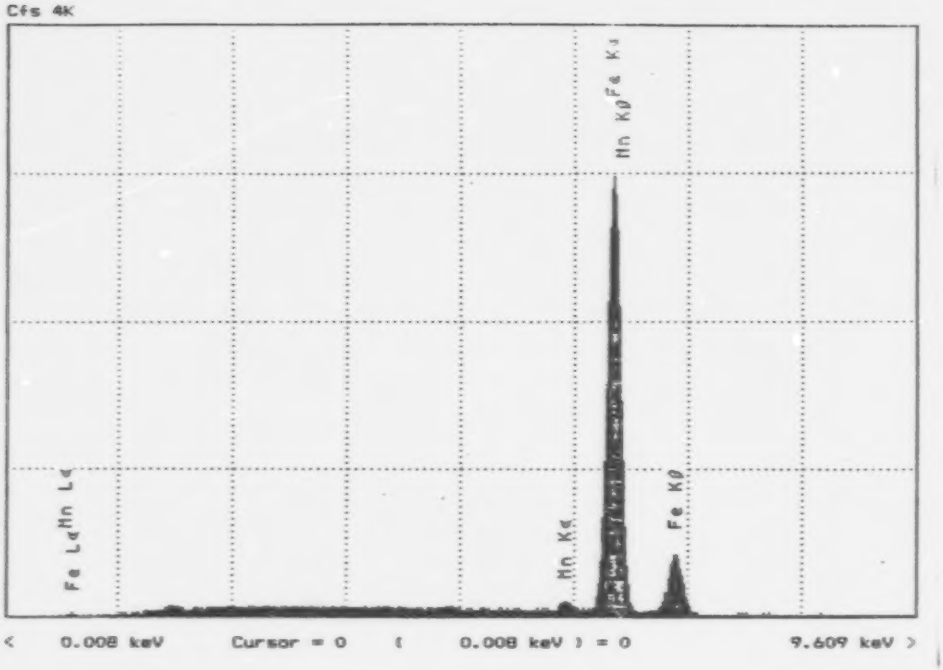

(a) Surrounding Matrix

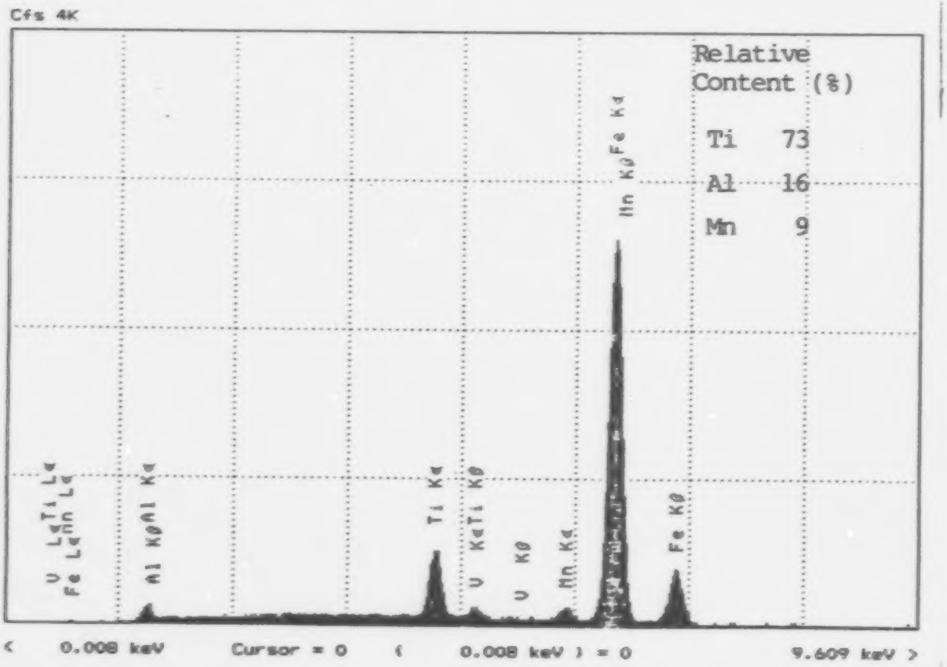

(b) Cleavage initiation site

Figure 3.14: The significant difference in EDX spectrum confirms the role of inclusion acting as cleavage initiation site (4G2)

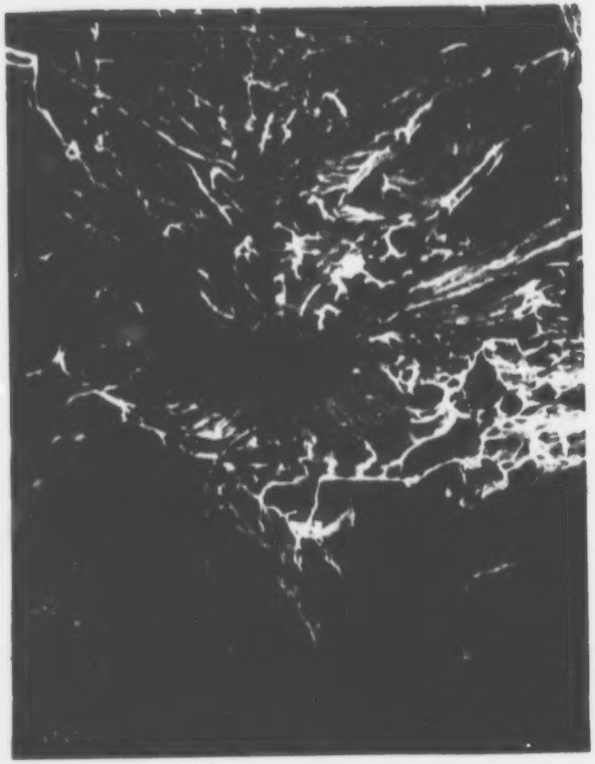

Figure 3.15 Cleavage initiation site found in as-welded Mn-Si weld (2G3, $-30^{0}C$, CTOD = 0.07mm) (1000X, Neg. 806)

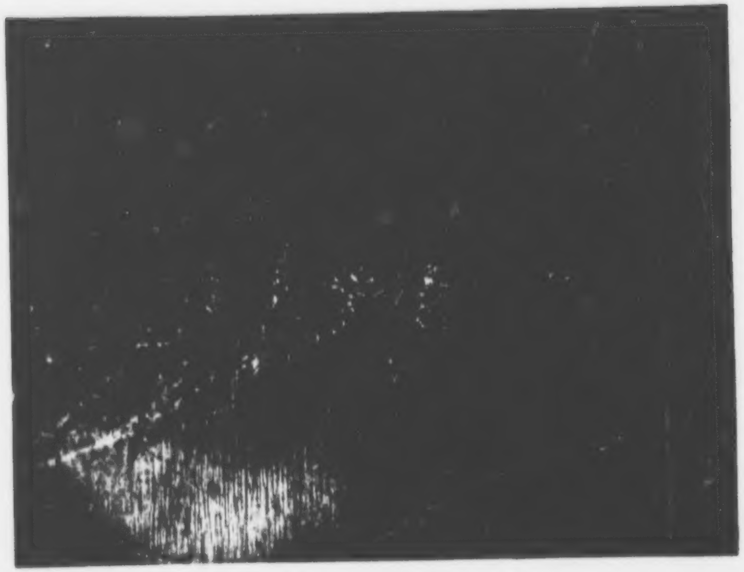

Figure 3.16 The cleavage initiation site is located at the reheated zone of first root pass of side 2 (5X, Neg. 11218)

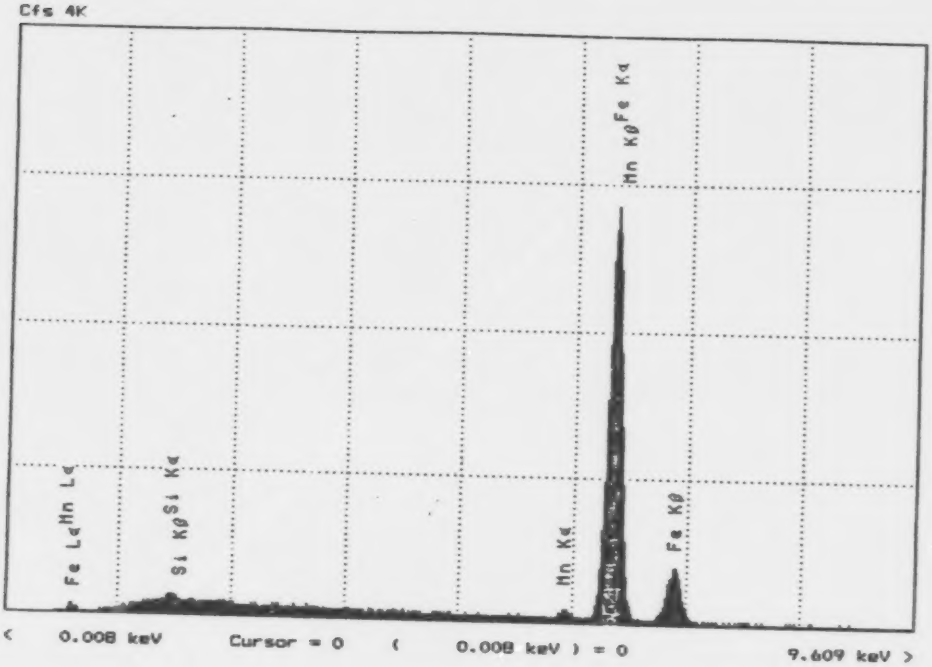

(a) Surrounding Matrix

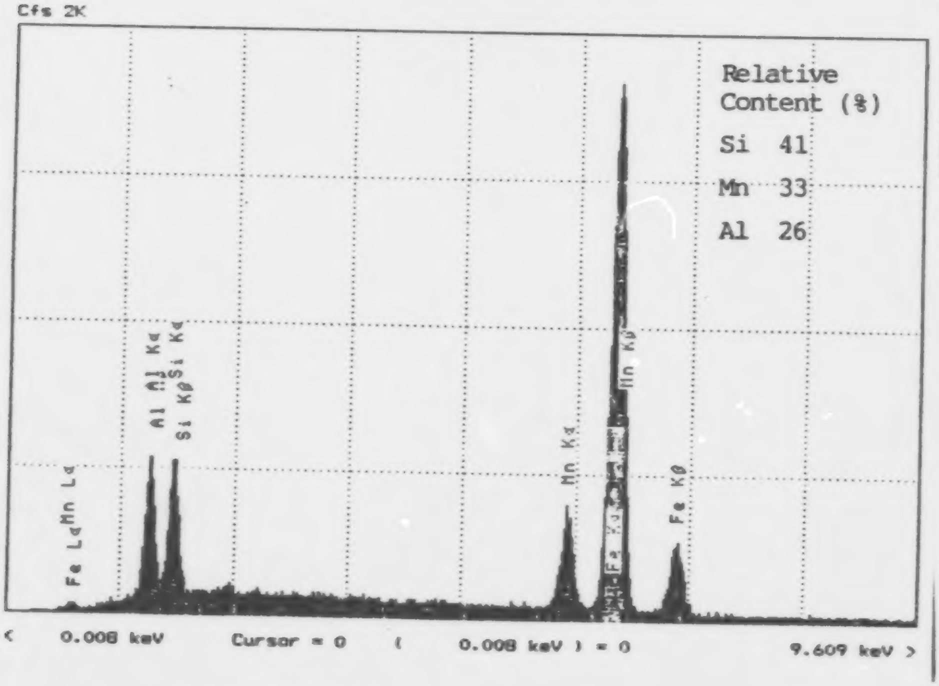

(b) Cleavage initiation site

Figure 3.17: The different EDX spectrums confirm the role of inclusion acting as cleavage initiation site (2G3)

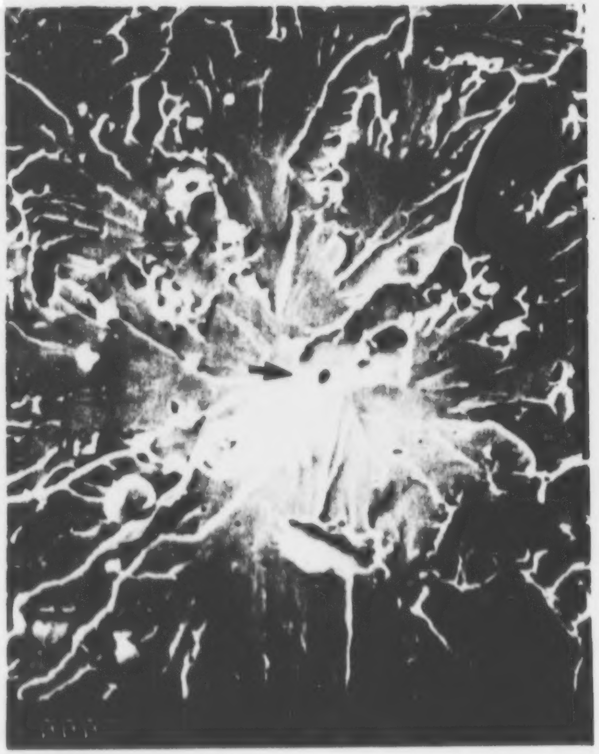

Figure 3.18 Cleavage initiation site in as-welded Mn-Si weld (265, $-10^{o}C$, CTOD = 0.16mm) (1000X, Neg. 789)

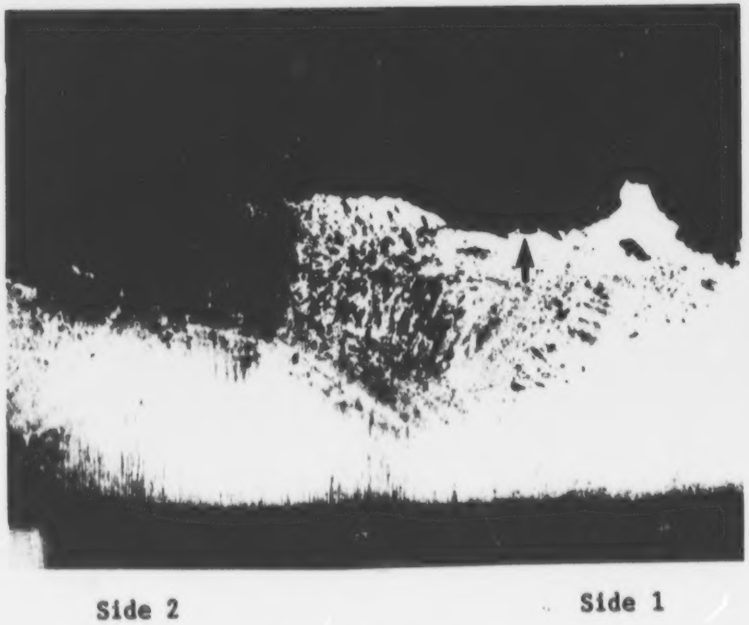

Figure 3.19: The location of the cleavage initiation site of Fig. 3.18 is located on the second pass of side 1 (5X, Neg. 11219)

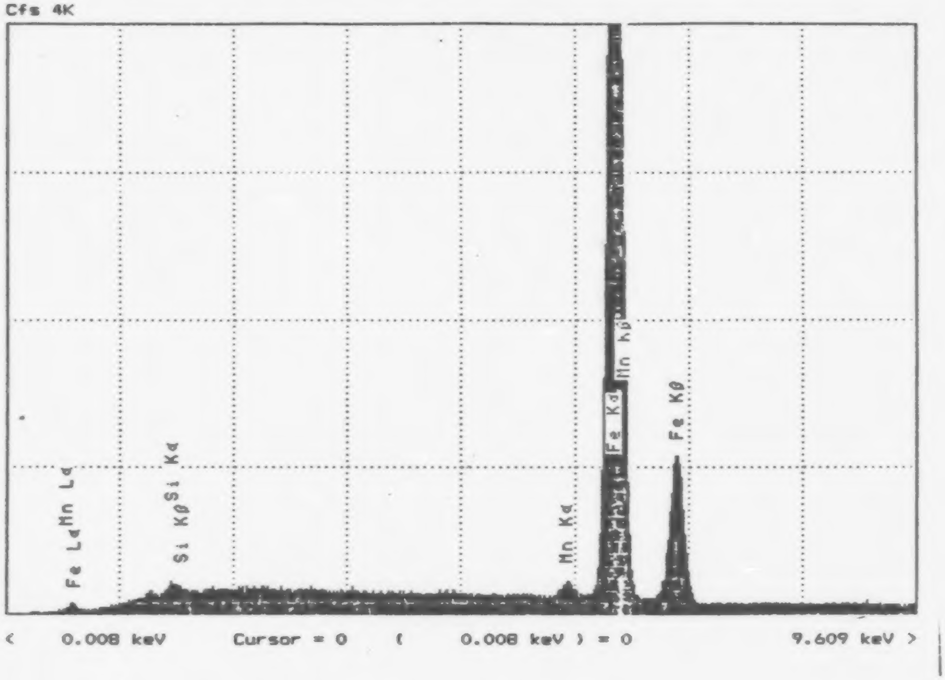

(a) Surrounding Matrix

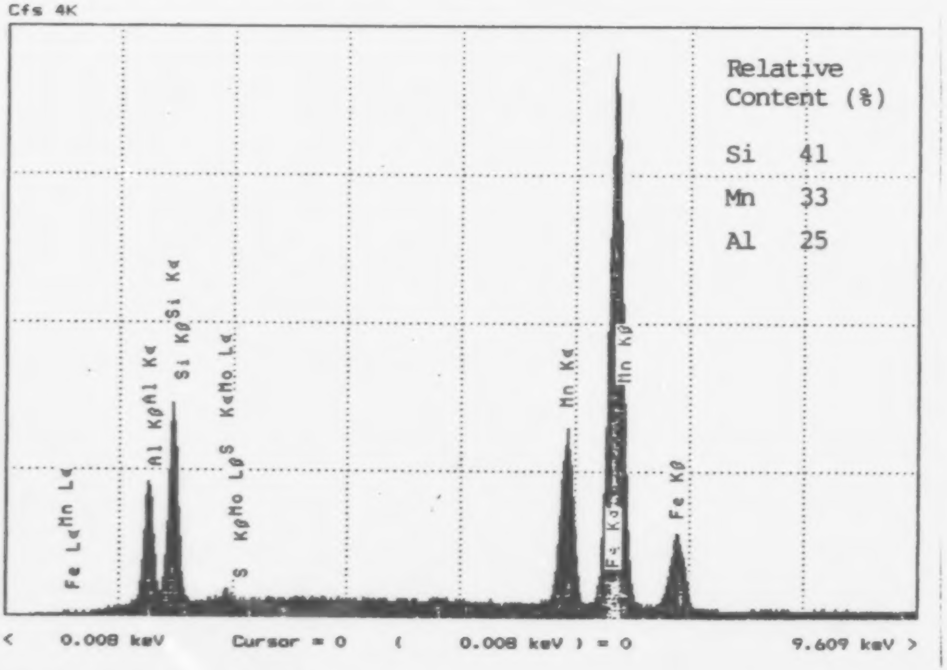

(b) Cleavage initiation site

Figure 3.20: The different EDX spectrums confirm the role of inclusion acting as cleavage initiation site

APPENDIX A

Inclusion Analysis

CDT
Centre de Développement Technologique
École Polytechnique de Montréal

— REPORT —

QUANTITATIVE ANALYSIS BY COMPUTER CONTROLLED SCANNING ELECTRON MICROSCOPY OF INCLUSIONS IN WELD SAMPLES

prepared for:

MATERIALS TECHNOLOGY CENTRE
ARCTEC
311 Legget Drive
Kanata, Ontario
K2K 1Z8

March 1988 CDT PROJECT P919

CDT
Centre de Développement Technologique
École Polytechnique de Montréal

CDT PROJECT P919

— REPORT —

QUANTITATIVE ANALYSIS BY COMPUTER CONTROLLED SCANNING ELECTRTON MICROSCOPY OF INCLUSIONS IN WELD SAMPLES

prepared for:

MATERIALS TECHNOLOGY CENTRE
ARCTEC
311, Legget Drive
Kanata, Ontario
K2K 1Z8

by

Lawrence R. Cutler, Ph.D.
Gilles L'Espérance, Ph.D.
Department of Metallurgical Engineering

submitted by:

LE CENTRE DE DÉVELOPPEMENT TECHNOLOGIQUE
DE L'ÉCOLE POLYTECHNIQUE DE MONTRÉAL
Campus de l'Université de Montréal
Case postale 6079, Succursale A
Montréal (Québec) H3C 3A7

March 1988

Lawrence R. Cutler

Lawrence R. Cutler, Ph.D

Gilles L'Espérance, Ph.d

Report on Quantitative Analysis by Computer Controlled Scanning Electron Microscopy of Inclusion in Weld Samples

by

Lawrence R. Cutler Ph.D. and Gilles L'Espérance Ph.D.
Département de Génie Métallurgique
Ecole Polytechnique

A: INTRODUCTION

Mr. Chris Chiu of ARCTEC asked the Center for Microscopy and Characterization of Materials $(CM)^2$ of the Metallurgical Engineering Department of Ecole Polytechnique to characterize the inclusions in three steel specimens. A characterization of the chemical composition and size distribution of the inclusions was requested.

This was accomplished with the aid of the Particle Recognition and Characterization (PRC) which runs on the Tracor-Northern Model TN-2000 Energy Dispersive X-ray analyser equipped with a digital scan generator. This system combines three powerful tools, namely:

- Scanning Electron Microscope (SEM) with high resolution and multiple image display modes

- Energy Dispersive X-ray spectroscopy with the ability to detect elements with atomic numbers greater than 10.
- Digital Scan Generator which allows computer control of the electron beam in the SEM and digitization of the resultant video signal or the acquisition of X-ray data from specific locations.

This combination forms the basis of a Scanning Electron Microscope based automatic image analysis system (SEM-AIA). This setup gives great flexibility since the type of data collected can be easily modified just by changing the data acquisition or data reduction programs. In the case of PRC, the program controls the electron beam in the (SEM) and digitizes the resultant video signal thereby allowing the acquisition of information based on the local variations in contrast. In the present study, inclusions were detected by variations in the signal level of the backscattered electron image (BEI) which is related to the average atomic weight, Z. Areas with larger values of Z appear brighter in the BEI.

The particle recognition and characterization program (PRC) was developed to characterize the size, shape and chemical composition of particles. The data can be classed according to the average diameter and/or the chemical composition of the individual particles. Specific inclusion types can be further classed by the relative abundance or ratios of the elements present.

This report presents the results of a characterization by the PRC programs of the inclusions in the samples supplied by Mr. Chiu. Classification of the inclusions according to size, chemical composition and shape factor was achieved. The significance and the limitations of the data and techniques are also discussed.

B: METHODOLOGY

1- Specimen Preparation and Observation

Three steel specimens were received from ARCTEC in the polished state. In order to identify the zones in the weld sample, these samples were lightly etched to reveal the weld metal zone. Hardness impressions were made at the mid thickness and the centerline of the weld. The specimens were then repolished ished using only diamond polishing compound which will not introduce Al into the sample surface and hence the analysis of Al in the inclusions is possible. Analysis of the inclusion size and chemical type was done at the mid-thickness locations as was requested. Observations and measurements were done using the JEOL 820 SEM in the BEI inverse and normal observation modes.

2- Operation of the PRC Program

The inclusions can be differentiated from the matrix due to variations in the BEI signal levels. Since the inclusions are lighter than the matrix ($Z<Fe$), the inverse BEI was used so that the inclusions will have a higher video signal level than the matrix.

For the PRC program, a window of analysis was then selected so that the lower threshold was just above the BEI signal level of the matrix. This adjustment was critical since the small inclusions could be lost due to the small difference in contrast between them and the matrix. The upper threshold was left at its maximum value.

The PRC program sweeps the electron beam across the specimen until the resultant video signal level exceeds the lower threshold. The center of the particle is then located. The size, area and shape factor of the inclusion is measured by tracing a series of eight diameters through the center. At this point, a X-ray spectrum is obtained from the center of the inclusion and the intensities of selected peaks are recorded along with the size information of the particle. This process is repeated for the entire field of view. Multiple fields can also be measured during the analysis of a specimen.

Data recorded include the shape factor which is the surface area of the inclusion times 4 pi divided by the perimeter squared . The shape factor for a sphere is 1, for a square 0.78 and a particle with a length to width ratio of five to one 0.43. This measure of the shape factor is quite accurate for convex particles but can be in error for highly elongated irregular inclusions.

3- Setup of PRC

Considerable care was exercised in the setup of the elemental classifications in the PRC program. Initially, the specimens were scanned using the BEI mode to determine the size and type of inclusion present. Representative X-ray spectra were taken from various regions to determine the range of elements present in the inclusions. The elemental types then formed to reflect these observations. Trial analysis were done using these elements in order to be sure that no other elements were present in the inclusions.

In this series of specimens, Si,S,Ti,Mn,and Al were present although the relative amounts of each varied greatly. Since all the inclusions had an average diameter under 3 μm, the inclusions were grouped into 0.1 μm bins in the histograms.

In order to have a good resolution of the smaller inclusions as well as to include as many inclusions as possible into each field a magnification of 4000 was used. An accelerating voltage of 12 kV was used to reduce the size of the X-ray generation zone in order to increase the relative intensities of the light element Kα peaks as compared to the Fe peak which is emitted from the matrix. This is especially important for analysis of the smaller inclusions.

All analysis were done using exactly the same experimental conditions, (i.e. accelerating voltage, working distance, beam current) in order to be able to compare the data from sample to sample. If this is not done, the relative peak height can vary which does not reflect changes in the specimen composition.

The data for the relative intensities of the elements, size, shape factor, maximum and minimum diameter, average diameter and perimeter were saved to disk for each of the inclusions. This data was transferred over to the IBM personal computer. A database manager was used to find the type classification for each of the inclusions. If an element was present in more than 2 percent relative weight, that element appears in the the type classification for that inclusion. For example, a type TiMnSi contains at least 2 percent relative weight of Ti, Mn and Si. After classification, the inclusions were counted according to their size and type classification.

The area fraction of occupation , the average size and the nearest neighbour distance was calculated for each of the samples. The nearest neighbour distance is calculated from 0.5/square root of the number of inclusions per unit area. The average diameter and average relative intensities of each of the major inclusion types were calculated.

4 - Limitations of PRC

PRC was designed to characterize the size, shape and chemical composition of individual particles of regular convex shape. It cannot deal very well with multi-phase or irregularly shaped inclusions such as highly elongated stringers. Possible difficulties include:

- the chemical composition measured will be the average value near the center of the inclusion which will not reflect the variations in composition in complex inclusions.
- irregularly shaped inclusions may be treated as multiple inclusions
- the low contrast of the small inclusions may mean that they may not be found

The relative abundance of the elements measured can in no way be considered a measure of the chemical composition of the inclusions. A large proportion of the X-ray signal comes from the iron matrix but if the solubilities of the elements in the inclusions are low in Fe as is usually is the case the spectre recorded reflect changes in the relative composition of the inclusions. Absorption effects can reduce the intensities of the various elements which can change the relative intensities of the peaks somewhat. No matrix corrections (ZAF) were performed and not all of the possible elements present such as oxygen can be measured by the X-ray detector. Still, these measures give valuable data concerning the elements present and the relative abundance of each. These data are indispensable for the understanding of the relationship of processing history and composition to the inclusion characteristics. At this time, there is no other way to obtain such detailed information.

C: RESULTS

1- Size Classification

The size distributions for the three steel specimens are presented in Appendix A. For all the specimens most of the inclusions are under 2,0 μm in diameter. The most numerous size classification is the 0.5 or 0.6 micron range.

2- Chemical Composition Classification

The major chemical classification type contains significant quantities of Mn and Si in 1GB2 and 2GB3 whereas the inclusions in 63B2 are rich in Ti. S is also a significant element in the inclusions in 1GB2 whereas Al is present in moderate quantities in most of the inclusions for all three sample. These results are summarized in Table 1 which is a summary of the relative average intensities of the major inclusion types along with the average diameter of the inclusions. Histograms of the major inclusion types are presented in Appendix B.

3- Combined Chemical Composition and Size Classification

The results for the size classifications for each chemical type are presented in Appendix C. The data can be broken down even further. Histograms of size groupings for an individual inclusion types can be tabulated and plotted. This is done for the most numerous inclusion types for the three specimens as can be seen Appendix D . Although generally there is not a great difference in the size of the most numerous class for each of the inclusion types for all three specimens , the inclusions that are extremly rich in Ti in 63B2 tend to have a somewhat higher average diameter of 0.5 to 0.6 as compared to 0.4 to 0.5 in the other two welds.

4 Area Fraction and Nearest Neighbour Distances

The results of the volume fraction, average diameter, inclusion density and nearest neighbour distance is presented in Table 2 Weld 1GB2 has the smallest average diameter of all of the welds but has the highest density per unit area which results in the highest volume fraction of inclusions. By constrast 63B2 has the largest average diameter at 0.65 but has the lowest density which results in the lowest volume fraction of inclusions. 2GB3 is in between these limits.

D:CONCLUSIONS

1- The major inclusion types and composition of these inclusions varied greatly from sample to sample.

2- The most numerous size range is either in the 0.4 to 0.5 or the 0.5 to the 0.6 micron range.

3- Ti additions to the inclusions tend to increase the average diameter of the inclusions.

TABLE 1

AVERAGE RELATIVE PEAK INTENSITIES OF THE MAJOR INCLUSION TYPES

		AVERAGE RELATIVE PEAK INTENSITIES percent						
SPECIMEN	INCLUSION TYPE	Si	S	Ti	Mn	Al	Average Diameter (um)	Percentage of Total
26B3	AlSiMnS	49	6	0	29	13	0.49	46.3
	AlTiSiMnS	47	6	4	28	12	0.47	26.8
	AlSiMn	53	0	0	30	15	0.50	13.4
	All						0.49	
16B2	AlTiSiMnS	30	17	8	31	10	0.45	55.7
	SiMnS	28	32	0	38	0	0.45	10.9
	TiSiMnS	22	29	13	33	1	0.43	10.9
	AlSiMnS	31	23	0	31	13	0.44	9.2
	All						0.45	
63B2	AlTiSiMnS	9	6	61	10	11	0.56	50.6
	AlTiSiMn	10	0	65	10	13	0.55	22.4
	AlTiMnS	1	5	69	8	15	0.66	7.0
	All						0.65	

TABLE 2

SUMMARY OF THE AREA FRACTION AND NEAREST NEIGHBOUR DISTANCE

Sample Name	Number of Inclusions	Number of Fields	Total Area cm^2	Number of Inclusions per cm^2	Area Fraction Percent	Nearest-Neighbour Distance microns	Average Diameter microns	Dominant Inclusion Type
16B2	422	12	2.64E-04	1.6E+06	0.72	4.0	0.45	AlTiSiMnS
26B3	395	20	4.40E-04	9.0E+05	0.44	5.3	0.49	AlSiMnS
63B2	330	25	5.50E-04	6.0E+05	0.39	6.5	0.65	AlTiSiMnS

APPENDIX A

SIZE DISTRIBUTIONS

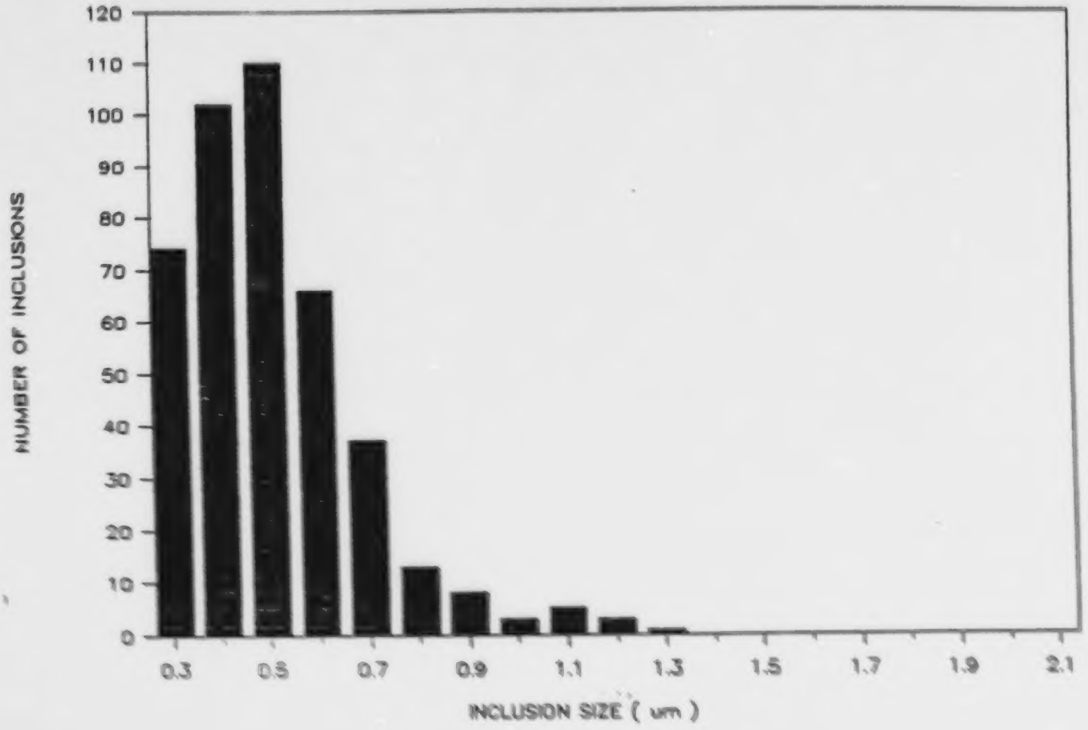
ARCTEC 1GB2

SIZE DISTRIBUTION

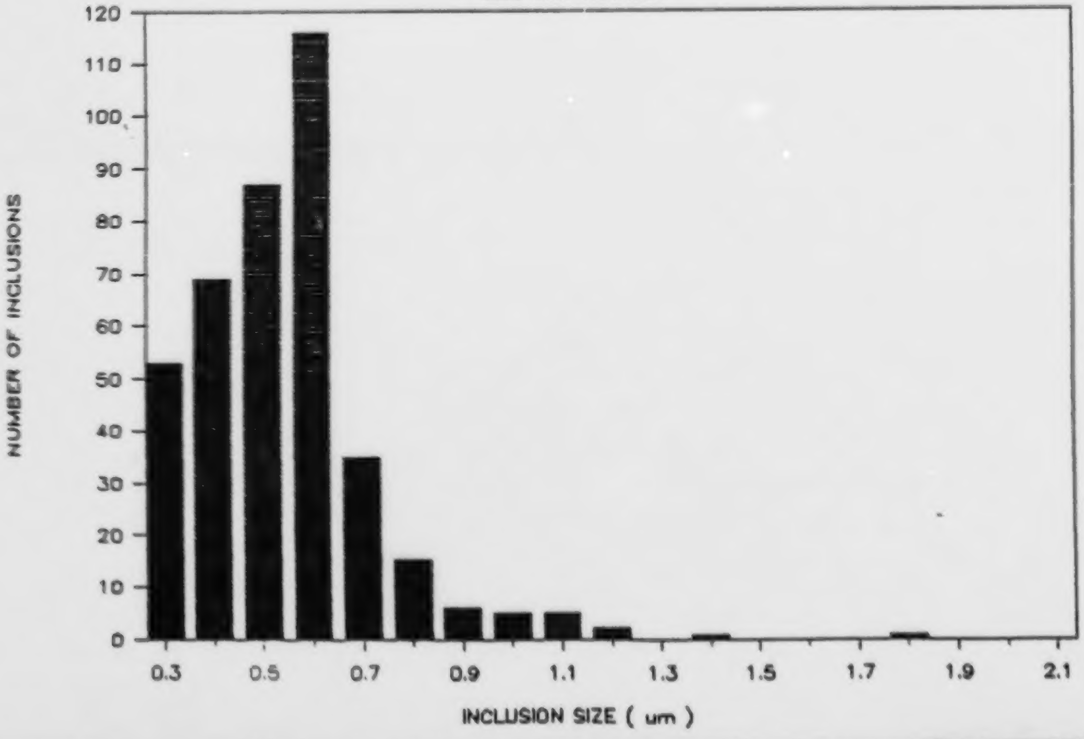
ARCTEC 2GB3

SIZE DISTRIBUTION

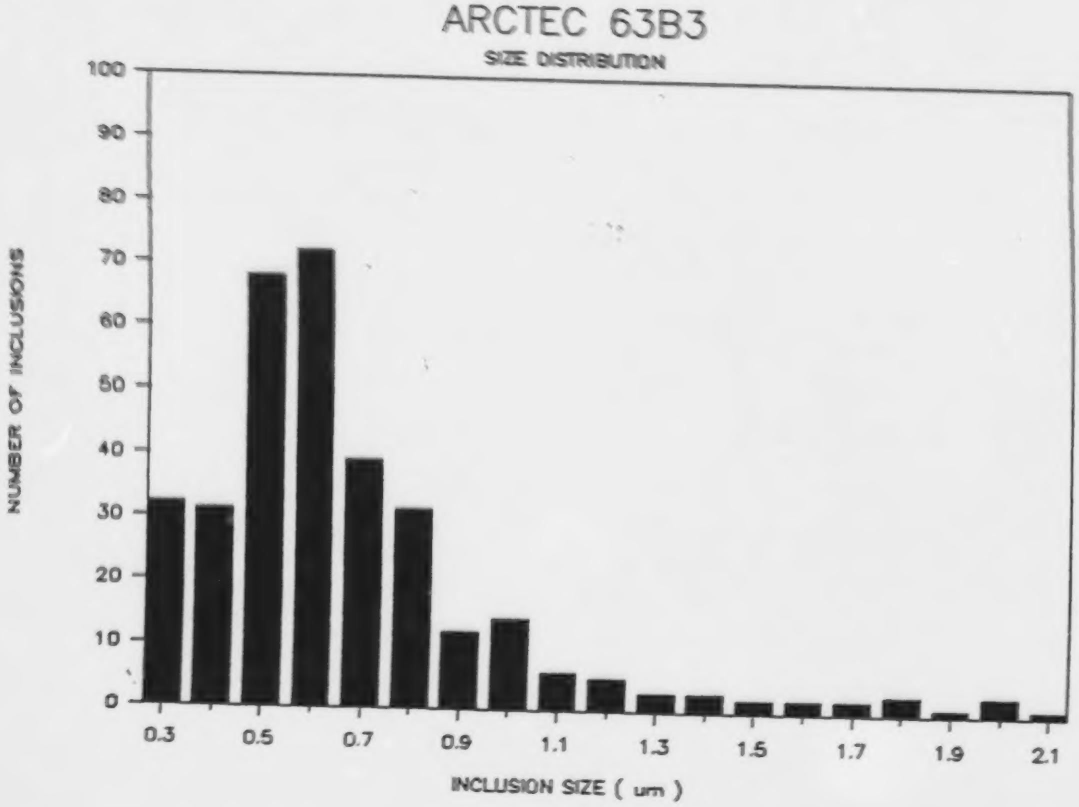ARCTEC 63B3
SIZE DISTRIBUTION
NUMBER OF INCLUSIONS
100
90
80
70
60
50
40
30
20
10
0
0.3
0.5
0.7
0.9
1.1
1.3
1.5
1.7
1.9
2.1
INCLUSION SIZE (um)

ARCTEC 1GB2

SIZE DISTRIBUTION

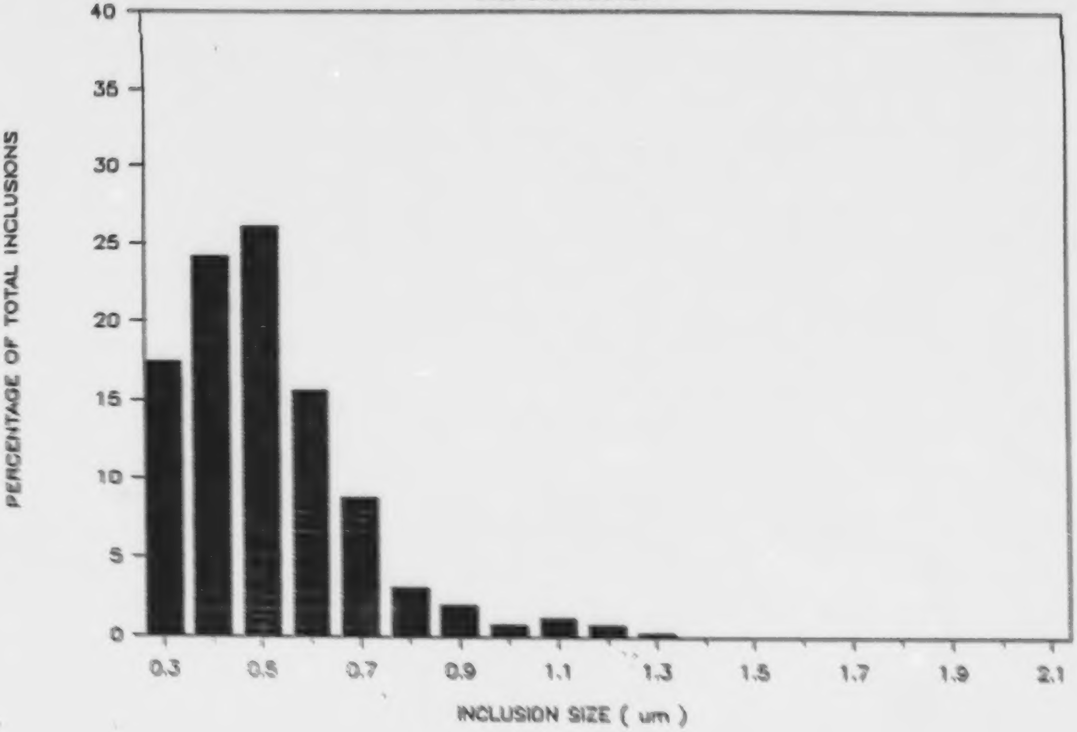

ARCTEC 2GB3

SIZE DISTRIBUTION

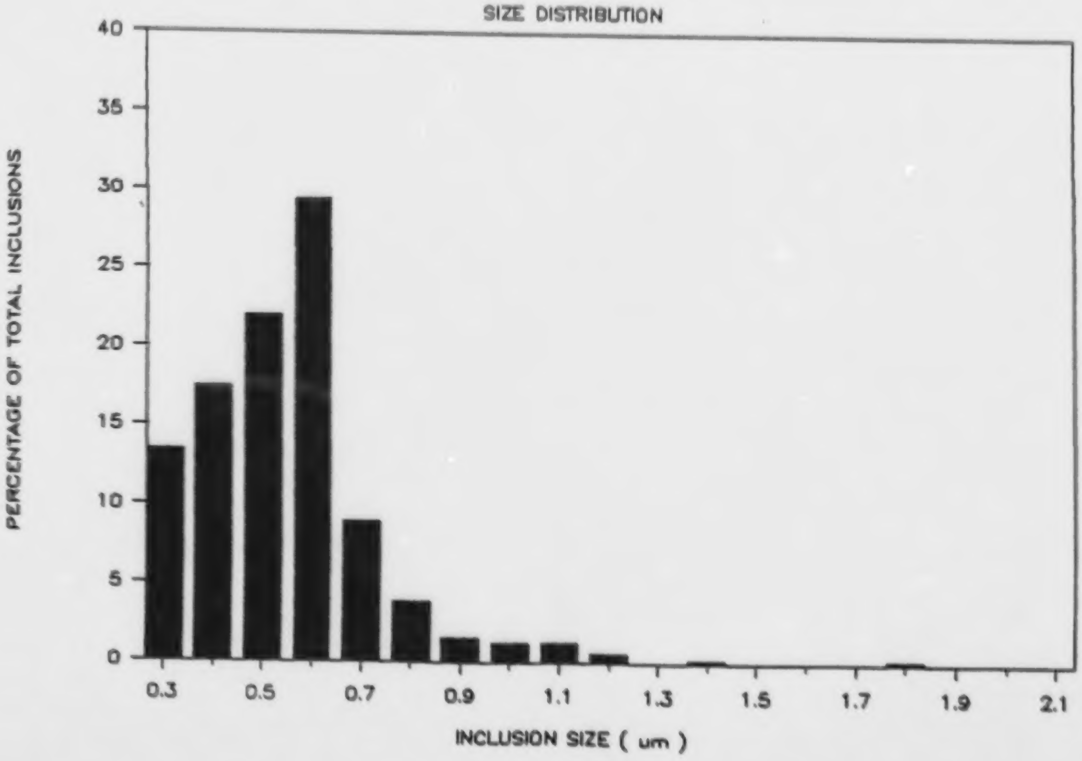

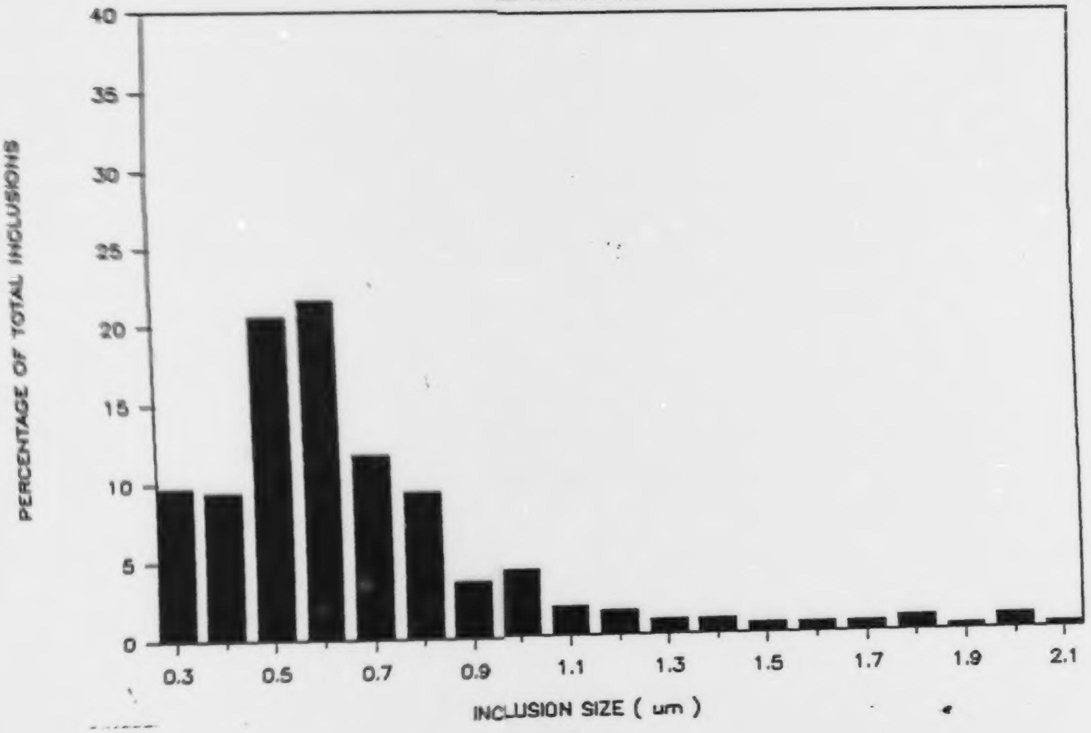

ARCTEC 63B3

SIZE DISTRIBUTION

APPENDIX B

TYPE DISTRIBUTIONS FOR THE MAJOR CHEMICAL TYPES.

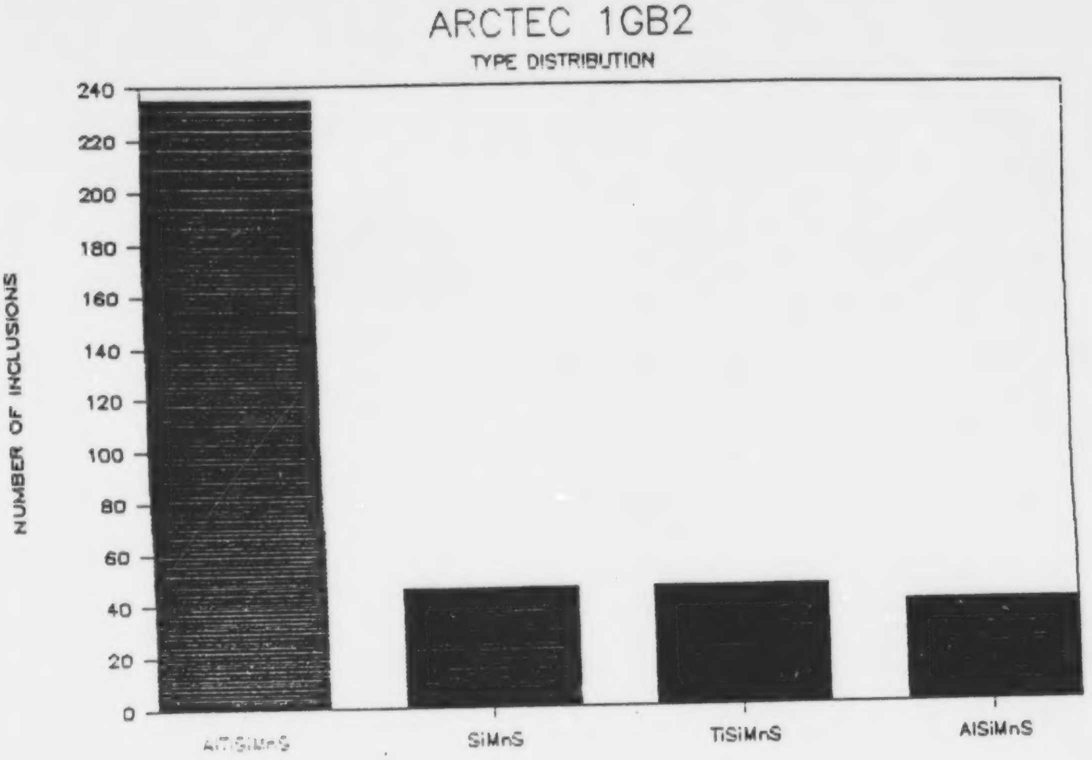
ARCTEC 1GB2
TYPE DISTRIBUTION
NUMBER OF INCLUSIONS
0
20
40
60
80
100
120
140
160
180
200
220
240
AlTiSiMnS
SiMnS
TiSiMnS
AlSiMnS

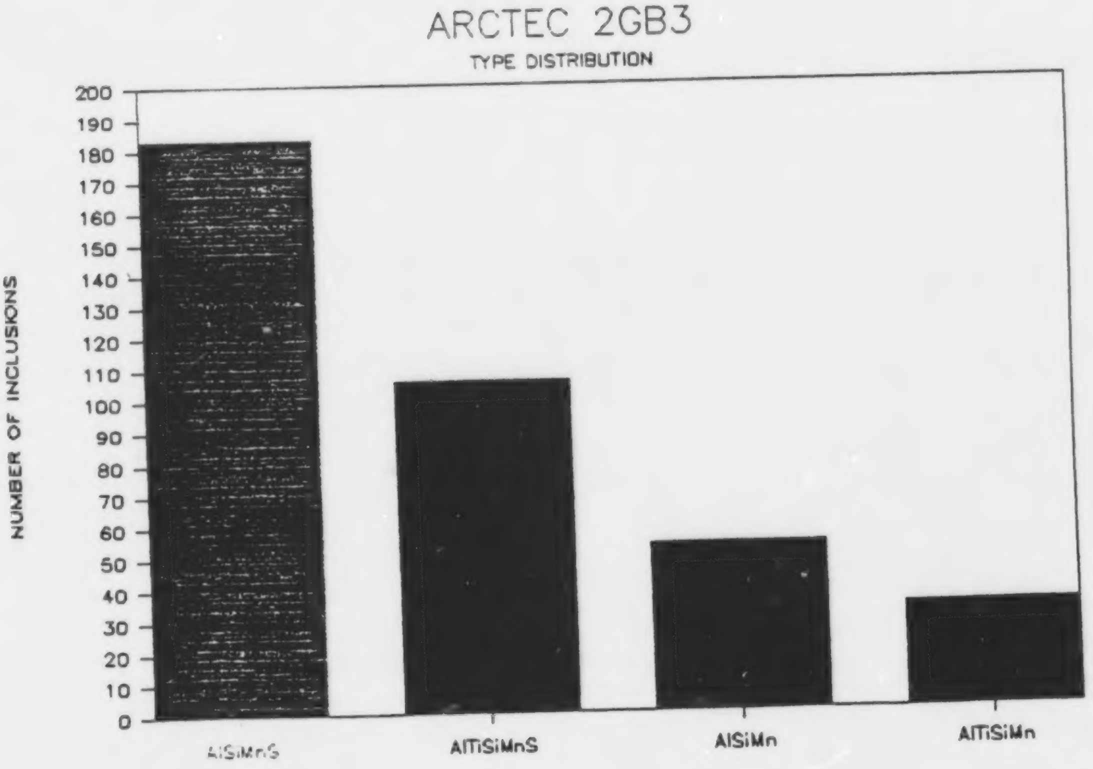
ARCTEC 2GB3
TYPE DISTRIBUTION
NUMBER OF INCLUSIONS
0
10
20
30
40
50
60
70
80
90
100
110
120
130
140
150
160
170
180
190
200
AlSiMnS
AlTiSiMnS
AlSiMn
AlTiSiMn

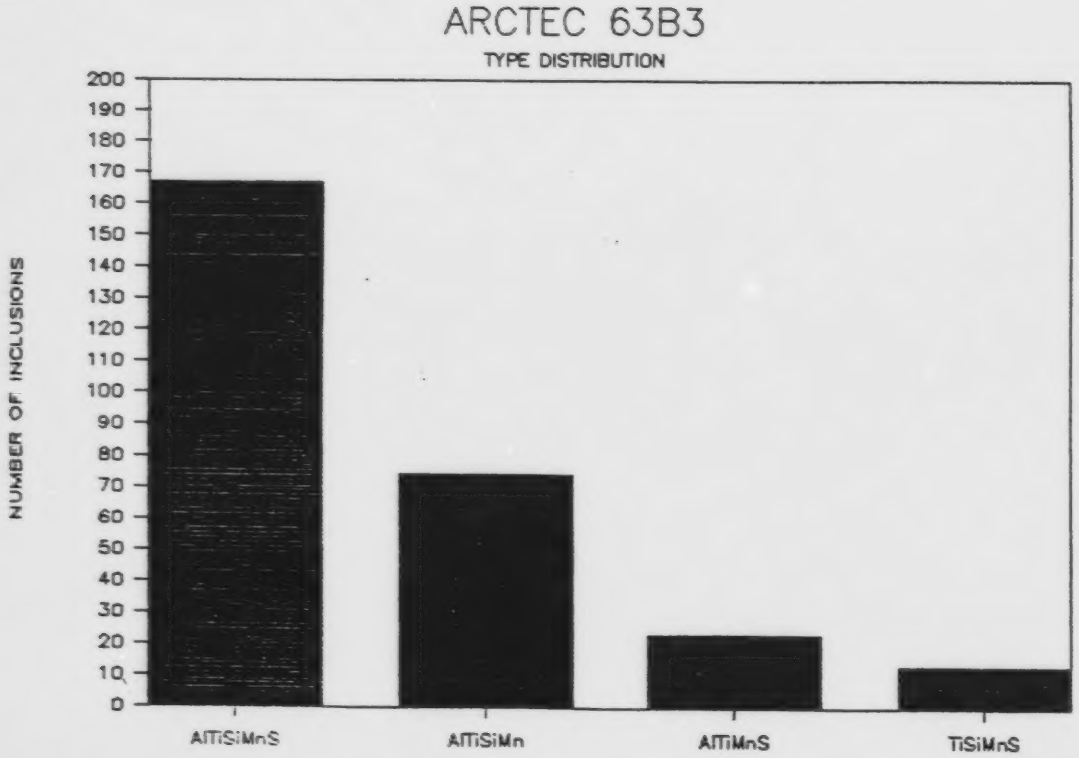
ARCTEC 63B3
TYPE DISTRIBUTION
NUMBER OF INCLUSIONS
0
10
20
30
40
50
60
70
80
90
100
110
120
130
140
150
160
170
180
190
200
AlTiSiMnS
AlTiSiMn
AlTiMnS
TiSiMnS

ARCTEC 1GB2

TYPE DISTRIBUTION

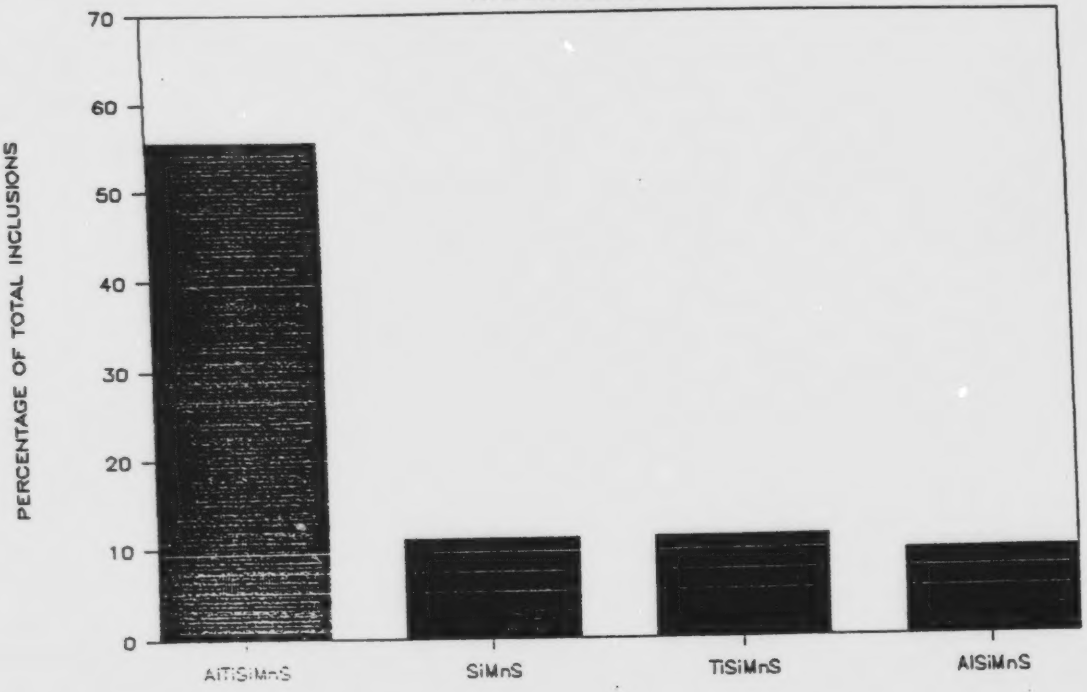

ARCTEC 2GB3

TYPE DISTRIBUTION

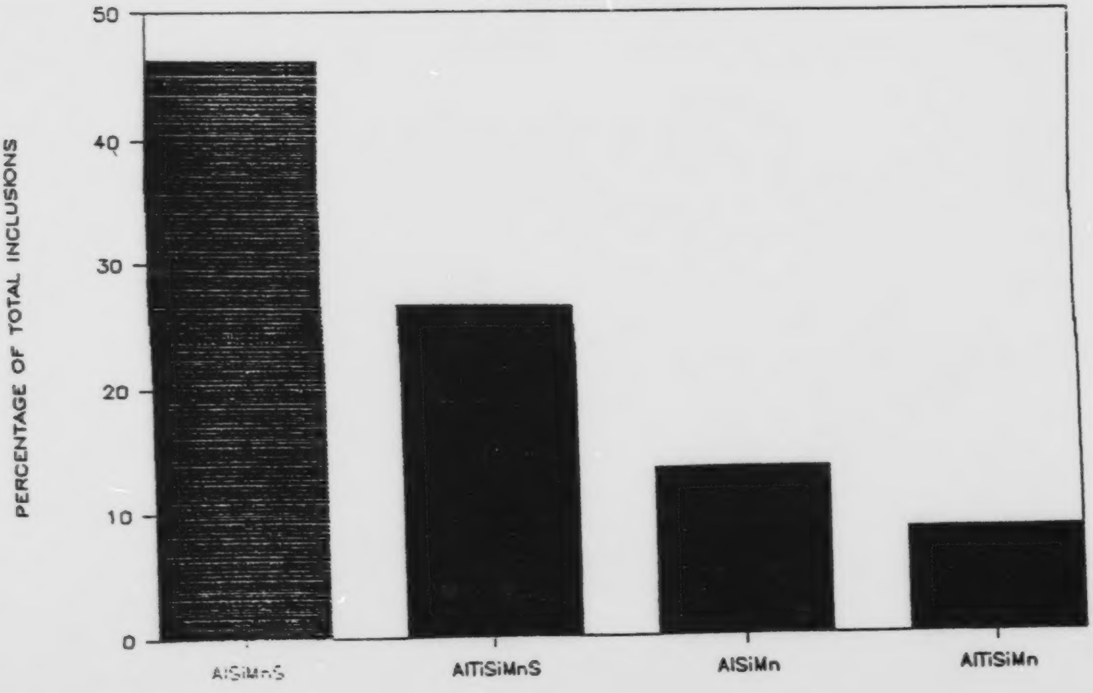

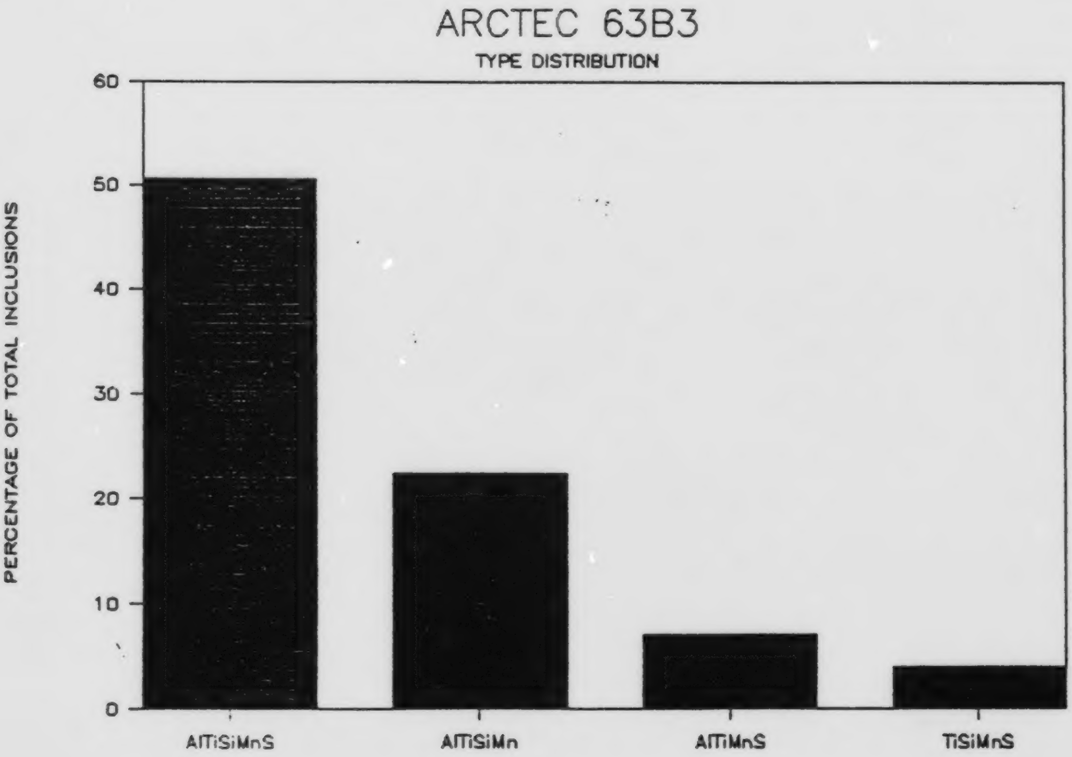
ARCTEC 63B3
TYPE DISTRIBUTION
PERCENTAGE OF TOTAL INCLUSIONS
60
50
40
30
20
10
0
AlTiSiMnS
AlTiSiMn
AlTiMnS
TiSiMnS

APPENDIX C

TABULATIONS OF THE TYPE AND SIZE CLASSIFICATIONS

SPECIMEN NAME: 1GB2
NUMBER OF
INCLUSIONS: 422

CHEMICAL TYPE SIZE RANGE OF INCLUSIONS

From	0.2	0.3	0.4	0.5	0.6	0.7	0.8	0.9	1	1.1	1.2	1.3	1.4	1.5	1.6	1.7	1.8	1.9	2	TOTAL	PERCENTAGE
To	0.3	0.4	0.5	0.6	0.7	0.8	0.9	1	1.1	1.2	1.3	1.4	1.5	1.6	1.7	1.8	1.9	2	2.1	NUMBER	
AlTiSiMnS	38	52	68	36	27	5	4	1	2	2	0	0	0	0	0	0	0	0	0	235	55.7
SiMnS	9	12	9	8	5	1	2	0	0	0	0	0	0	0	0	0	0	0	0	46	10.9
TiSiMnS	8	17	10	7	1	1	0	1	1	0	0	0	0	0	0	0	0	0	0	46	10.9
AlSiMnS	8	11	9	4	3	2	1	1	0	0	0	0	0	0	0	0	0	0	0	39	9.2
AlSiMn	2	4	5	1	0	0	0	0	0	0	0	0	0	0	0	0	0	0	0	12	2.8
SiMn	2	1	2	3	1	1	0	0	0	0	0	0	0	0	0	0	0	0	0	10	2.4
AlTiSiMn	3	2	1	3	0	0	0	0	0	0	0	0	0	0	0	0	0	0	0	9	2.1
TiMnS	0	0	2	0	0	0	1	0	1	1	0	0	0	0	0	0	0	0	0	5	1.2
MnS	1	0	1	1	0	1	0	0	0	0	1	0	0	0	0	0	0	0	0	5	1.2
AlSiS	2	1	1	0	0	0	0	0	0	0	0	0	0	0	0	0	0	0	0	4	0.9
TiSiMn	1	1	1	0	0	0	0	0	0	0	0	0	0	0	0	0	0	0	0	3	0.7
TiSiS	0	0	1	1	0	0	0	0	0	0	0	0	0	0	0	0	0	0	0	2	0.5
AlMn	0	0	0	1	0	1	0	0	0	0	0	0	0	0	0	0	0	0	0	2	0.5
Si	0	0	0	0	0	0	0	0	1	0	0	0	0	0	0	0	0	0	0	1	0.2
AlTiSiS	0	1	0	0	0	0	0	0	0	0	0	0	0	0	0	0	0	0	0	1	0.2
SiS	0	0	0	0	0	1	0	0	0	0	0	0	0	0	0	0	0	0	0	1	0.2
TiMn	0	0	0	1	0	0	0	0	0	0	0	0	0	0	0	0	0	0	0	1	0.2
																				0	0.0
TOTAL NUMBER	74	102	110	66	37	13	8	3	5	3	1	0	0	0	0	0	0	0	0		
PERCENTAGE	17.5	24.2	26.1	15.6	8.8	3.1	1.9	0.7	1.2	0.7	0.2	0.0	0.0	0.0	0.0	0.0	0.0	0.0	0.0		

```
SPECIMEN NAME:   2GB3
NUMBER OF
INCLUSIONS:  395

CHEMICAL TYPE                    SIZE RANGE OF INCLUSIONS

         From  0.2  0.3  0.4  0.5  0.6  0.7  0.8  0.9    1  1.1  1.2  1.3  1.4  1.5  1.6  1.7  1.8  1.9    2 TOTAL    PERCENTAGE
           To  0.3  0.4  0.5  0.6  0.7  0.8  0.9    1  1.1  1.2  1.3  1.4  1.5  1.6  1.7  1.8  1.9    2  2.1 NUMBER
===================================================================================================================
AlSiMnS         25   35   34   54   17    9    1    4    1    1    0    1.   0    0    0    1    0    0    0    183  46.3
AlTiSiMnS        8   20   32   31   10    4    0    0    0    1    0    0    0    0    0    0    0    0    0    106  26.8
AlSiMn           7    7   14   15    4    1    4    0    1    0    0    0    0    0    0    0    0    0    0     53  13.4
AlTiSiMn         4    3    6   14    3    1    1    1    0    0    0    0    0    0    0    0    0    0    0     33   8.4
TiSiMnS          4    0    0    1    0    0    0    0    0    0    0    0    0    0    0    0    0    0    0      5   1.3
TiSiMn           1    2    0    0    0    0    0    0    0    0    0    0    0    0    0    0    0    0    0      3   0.8
SiMn             0    0    1    0    0    0    0    0    1    0    0    0    0    0    0    0    0    0    0      2   0.5
TiSi             2    0    0    0    0    0    0    0    0    0    0    0    0    0    0    0    0    0    0      2   0.5
AlTiSi           0    1    0    0    1    0    0    0    0    0    0    0    0    0    0    0    0    0    0      2   0.5
Si               0    0    0    0    0    0    0    0    2    0    0    0    0    0    0    0    0    0    0      2   0.5
SiMnS            0    1    0    0    0    0    0    0    0    0    0    0    0    0    0    0    0    0    0      1   0.3
SiS              1    0    0    0    0    0    0    0    0    0    0    0    0    0    0    0    0    0    0      1   0.3
AlSiS            0    0    0    1    0    0    0    0    0    0    0    0    0    0    0    0    0    0    0      1   0.3
TiSiS            1    0    0    0    0    0    0    0    0    0    0    0    0    0    0    0    0    0    0      1   0.3

---------------- ---- ----|---- ---- ---- ---- ---- ---- ---- ---- ---- ---- ---- ---- ---- ---- ---- ---- --------------
TOTAL NUMBER    53   69   87  116   35   15    6    5    5    2    0    1    0    0    0    1    0    0    0
PERCENTAGE    13.4 17.5 22.0 29.4  8.9  3.8  1.5  1.3  1.3  0.5  0.0  0.3  0.0  0.0  0.0  0.3  0.0  0.0  0.0
```

```
SPECIMEN NAME:   6383
NUMBER OF
INCLUSIONS:  330

CHEMICAL TYPE                  SIZE RANGE OF INCLUSIONS

        From  0.2  0.3  0.4  0.5  0.6  0.7  0.8  0.9    1  1.1  1.2  1.3  1.4  1.5  1.6  1.7  1.8  1.9    2 TOTAL   PERCENTAGE
          To  0.3  0.4  0.5  0.6  0.7  0.8  0.9    1  1.1  1.2  1.3  1.4  1.5  1.6  1.7  1.8  1.9    2  2.1 NUMBER
=================================================================================================================================
AlTiSiMnS      17   16   36   42   22   17    3    6    3    3    1    0    0    0    1    0    0    0    0      167  50.6
AlTiSiMn        5    7   21   17    6    9    5    3    1    0    0    0    0    0    0    0    0    0    0       74  22.4
AlTiMnS         0    2    3    6    4    2    1    2    2    1    0    0    0    0    0    0    0    0    0       23   7.0
TiSiMnS         4    1    1    5    1    0    0    1    0    0    0    0    0    0    0    0    0    0    0       13   3.9
Si              0    0    0    0    0    0    0    0    0    0    0    2    2    1    0    2    1    3    1       12   3.6
AlTiMn          0    0    0    0    3    1    1    1    0    0    2    0    0    0    0    0    0    0    0        8   2.4
AlSiMnS         1    1    2    0    0    0    0    1    0    1    0    0    0    0    1    0    0    0    0        7   2.1
SiMnS           3    1    0    0    0    0    0    0    0    0    0    0    0    1    0    0    0    0    0        5   1.5
AlTiSiS         0    0    2    0    3    0    0    0    0    0    0    0    0    0    0    0    0    0    0        5   1.5
TiSiMn          1    1    0    1    0    0    1    0    0    0    0    0    0    0    0    0    0    0    0        4   1.2
SiMn            0    1    1    0    0    0    1    0    0    0    0    0    0    0    0    0    0    0    0        3   0.9
AlTiSi          0    0    1    0    0    1    0    0    0    0    0    0    0    0    0    0    0    0    0        2   0.6
AlSiMn          1    0    0    0    0    1    0    0    0    0    0    0    0    0    0    0    0    0    0        2   0.6
AlSi            0    0    0    1    0    0    0    0    0    0    0    0    0    0    0    0    0    0    0        1   0.3
Ti              0    1    0    0    0    0    0    0    0    0    0    0    0    0    0    0    0    0    0        1   0.3
TiSi            0    0    1    0    0    0    0    0    0    0    0    0    0    0    0    0    0    0    0        1   0.3
AlTiS           0    0    0    0    0    0    0    0    0    0    0    0    0    0    0    1    0    0    0        1   0.3
AlTi            0    0    0    0    0    0    0    0    0    0    0    1    0    0    0    0    0    0    0        1   0.3

--------------- ---- ---- ---- ---- ---- ---- ---- ---- ---- ---- ---- ---- ---- ---- ---- ---- ---- ---- ---- -------------
TOTAL NUMBER   32   31   68   72   39   31   12   14    6    5    3    3    2    2    2    3    1    3    1
PERCENTAGE    9.7  9.4 20.6 21.8 11.8  9.4  3.6  4.2  1.8  1.5  0.9  0.9  0.6  0.6  0.6  0.9  0.3  0.9  0.3
```

APPENDIX D

SIZE DISTRIBUTIONS FOR THE MAJOR CHEMICAL TYPES

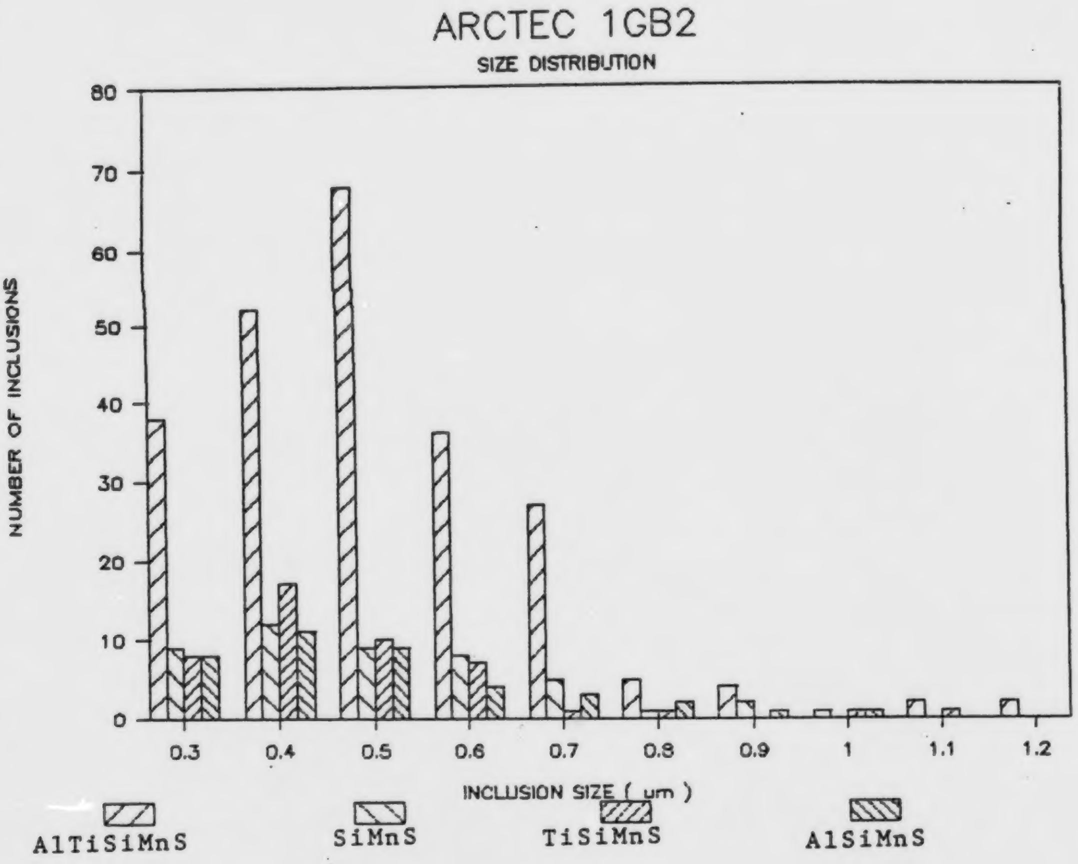
ARCTEC 1GB2
SIZE DISTRIBUTION
NUMBER OF INCLUSIONS
0
10
20
30
40
50
60
70
80
0.3
0.4
0.5
0.6
0.7
0.8
0.9
1
1.1
1.2
INCLUSION SIZE (um)
AlTiSiMnS
SiMnS
TiSiMnS
AlSiMnS

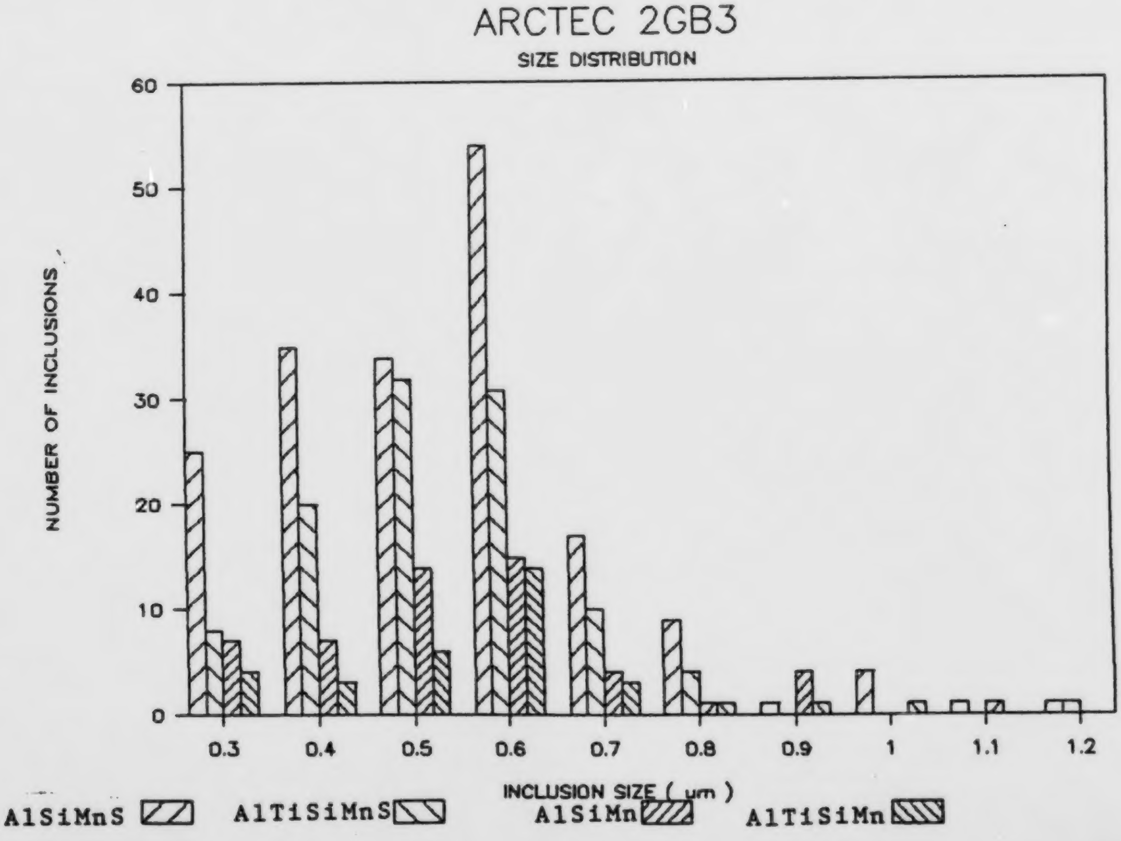
ARCTEC 2GB3
SIZE DISTRIBUTION
NUMBER OF INCLUSIONS
0
10
20
30
40
50
60
0.3
0.4
0.5
0.6
0.7
0.8
0.9
1
1.1
1.2
INCLUSION SIZE (um)
AlSiMnS
AlTiSiMnS
AlSiMn
AlTiSiMn

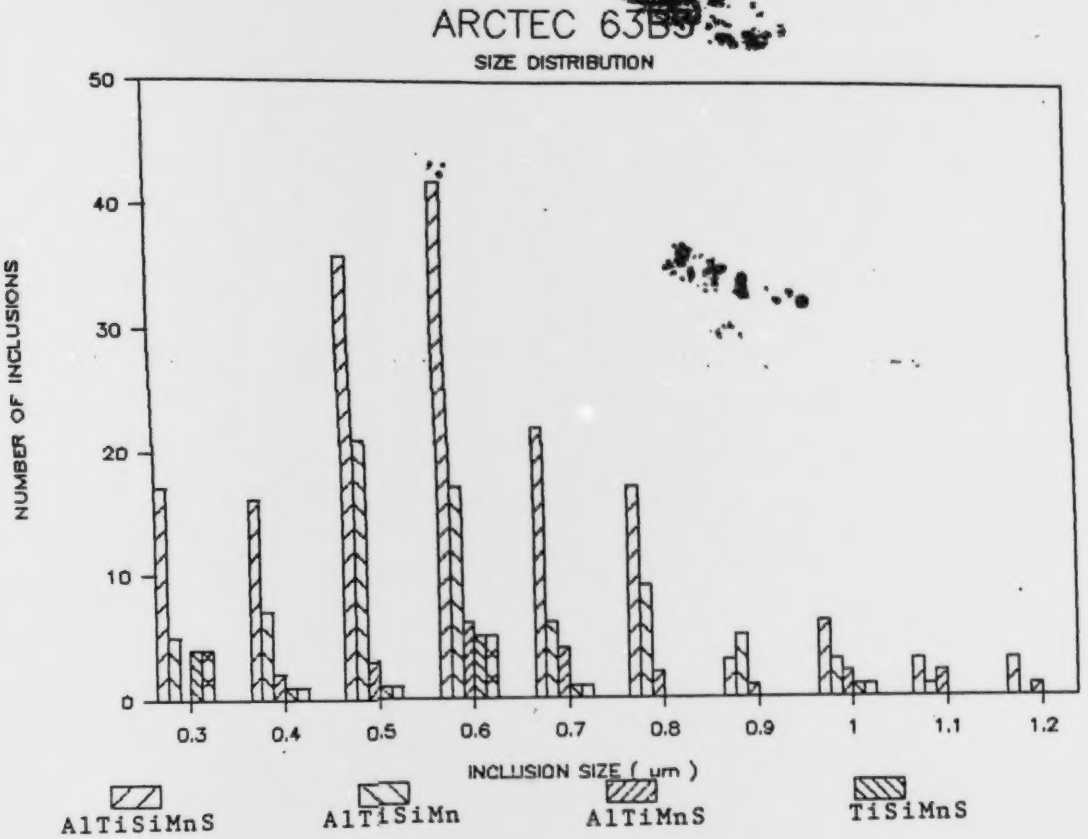
ARCTEC 63B5
SIZE DISTRIBUTION
NUMBER OF INCLUSIONS
0
10
20
30
40
50
0.3
0.4
0.5
0.6
0.7
0.8
0.9
1
1.1
1.2
INCLUSION SIZE (um)
AlTiSiMnS
AlTiSiMn
AlTiMnS
TiSiMnS

APPENDIX B

Drop Weight Test Results

Table B1

Summary of Drop Weight Test Results for Gas Metal Arc Welds (3.0 kJ/mm)

Test Temperature (°C)	C-Mn-Mo Weld	Mn-Si Weld	Ti-B Weld	
	As Welded	As Welded	As Welded	Stress Relieved
-20	No Break	---	---	---
-30	---	No Break	---	---
-35	---	No Break No Break	---	---
-40	---	Break Break	---	---
-55	No Break No Break	---	No Break	No Break No Break
-60	Break Break	---	No Break No Break	Break Break
-65	---	---	Break Break	---
-75	---	---	Break	Break

APPENDIX C

CVN Test Results

Table C1

CVN Test Data for Consumable A
3.0 kJ/mm in As Welded Condition (G1A)

Temperature °C	Subsurface				Root			
	Impact Energy (J)	Lateral Expansion (mm)	% Shear	Average Impact Energy (J)	Impact Energy (J)	Lateral Expansion (mm)	% Shear	Average Impact Energy (J)
25	--	--	--	--	126	1.6	70	126
0	113 108	1.5 1.2	70 60	111	76 62	1.1 1.0	50 40	69
-10	--	--	--	--	47	0.91	50	47
-20	92 85	1.8 2.3	60 N.B.	89	53 50	0.84 0.81	30 30	52
-30	--	--	--	--	50 30	0.84 0.61	40 30	40
-40	78 66 48	0.99 0.89 0.71	50 40 40	64	25 23	0.43 0.48	20 20	24
-50	64 47	0.89 0.81	40 40	56	20 18	0.43 0.46	10 10	19
-60	47 44 38	0.71 0.81 0.56	20 30 20	43	18 12	0.36 0.23	20 10	15
-70	51 33	0.71 0.46	20 20	42	--	--	--	
-80	21 17	0.36 0.23	10 10	19	11 9	0.15 0.13	10 10	10

Table C2

CVN Test Data for Consumable A
3.0 kJ/mm in As Welded Condition (G2A)

Temperature °C	Subsurface				Root			
	Impact Energy (J)	Lateral Expansion (mm)	% Shear	Average Impact Energy (J)	Impact Energy (J)	Lateral Expansion (mm)	% Shear	Average Impact Energy (J)
0	159 150	2.4 2.4	N.B.* N.B.	155	158 158	2.5 2.2	N.B. 70	158
-20	153 147	2.4 2.3	N.B. N.B.	150	152 135	2.6 1.9	N.B. 80	144
-40	127 113 28	1.7 1.7 0.28	70 80 20	89	158 133	2.6 2.0	N.B. 70	146
-50	74 47	1.2 0.91	10 10	61	--	--	--	--
-60	54 46 37	0.89 0.76 0.56	10 10 10	46	148 143 15	2.5 2.0 0.31	N.B. 70 10	102
-70	23 16	0.41 0.31	0 0	20	116 9 4	1.9 0.18 0.15	30 10 0	43
-80	12 8	0.15 0.08	0 0	10	107 7	1.7 0.23	30 0	57

*N.B. = No Break

Table C3

CVN Test Data for Consumable A
3.0 kJ/mm in Stress Relieved Condition (G3A)

	Subsurface				Root			
Temperature °C	Impact Energy (J)	Lateral Expansion (mm)	% Shear	Average Impact Energy (J)	Impact Energy (J)	Lateral Expansion (mm)	% Shear	Average Impact Energy (J)
0	156 147	2.2 2.2	N.B.* N.B.	152	157 155	2.4 2.5	N.B. N.B.	156
-20	156 147	2.2 2.2	N.B. N.B.	152	156 152	2.4 2.5	N.B. N.B.	154
-40	159 154	2.2 2.1	N.B. N.B.	157	152 149	2.5 2.6	N.B. N.B.	151
-60	153 148	2.2 2.1	N.B. N.B.	151	147 126	1.7 1.7	70 60	137
-70	--	--	--	--	126 123	1.8 1.6	20 20	125
-80	159 153	2.2 2.1	N.B. N.B.	156	128 45 41	2.2 0.69 0.58	60 10 10	71
-90	131 27	1.7 0.41	20 10	131** (79)	28 19 10	0.31 0.31 0.25	10 10 10	19
-100	137 111	1.7 1.5	N.B. 10	124	--	--	--	--
-120	19 4	0.20 0	0 0	12	--	--	--	--

*N.B. = No Break

**The 27J data is ignored

Table C4

CVN Test Data for Consumable A
3.0 kJ/mm in Stress Relieved Condition (G4A)

Temperature °C	Subsurface				Root			
	Impact Energy (J)	Lateral Expansion (mm)	% Shear	Average Impact Energy (J)	Impact Energy (J)	Lateral Expansion (mm)	% Shear	Average Impact Energy (J)
0	157 151	2.2 2.3	N.B.* N.B.	154	155 154	2.1 2.5	80 N.B.	155
-20	151 144	2.2 2.2	N.B. N.B.	148	151 30	2.0 0.64	70 20	151***
-40	159 157	2.3 2.3	N.B. N.B.	158	152 133	2.2 1.9	N.B. 70	143
-60	158 156	2.3 2.2	N.B. N.B.	157	84 80	1.4 1.2	50 40	82
-70	--	--	--	--	87 8	1.4 0.10	30 0	48
-80	157 156 7	2.1 2.1 0.10	N.B. N.B. 10	157** (107)	47 41 18	0.76 0.71 0.43	10 20 10	35
-90	148 79 42	1.9 1.2 0.64	N.B. 10 10	90	--	--	--	--
-100	15 14	0.43 0.25	0 0	15	8 5	0.15 0.20	0 0	7

*N.B. = No Break

**The average of 2 data points when the 7J data is ignored.

***The 30J data is ignored.

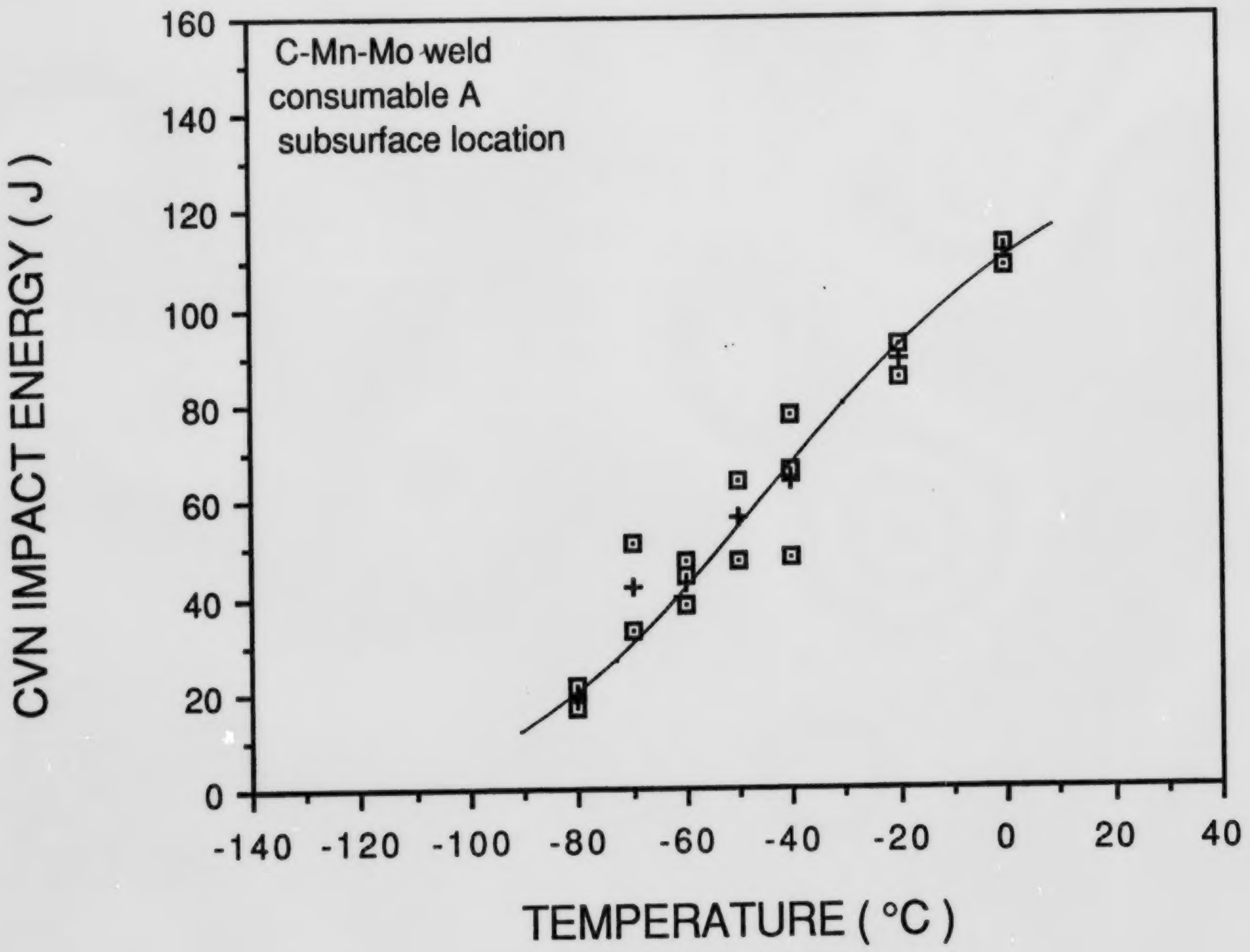

Figure C1: CVN transition curve for the subsurface location from C-Mn-Mo weld prepared with Consumable A (G1A)

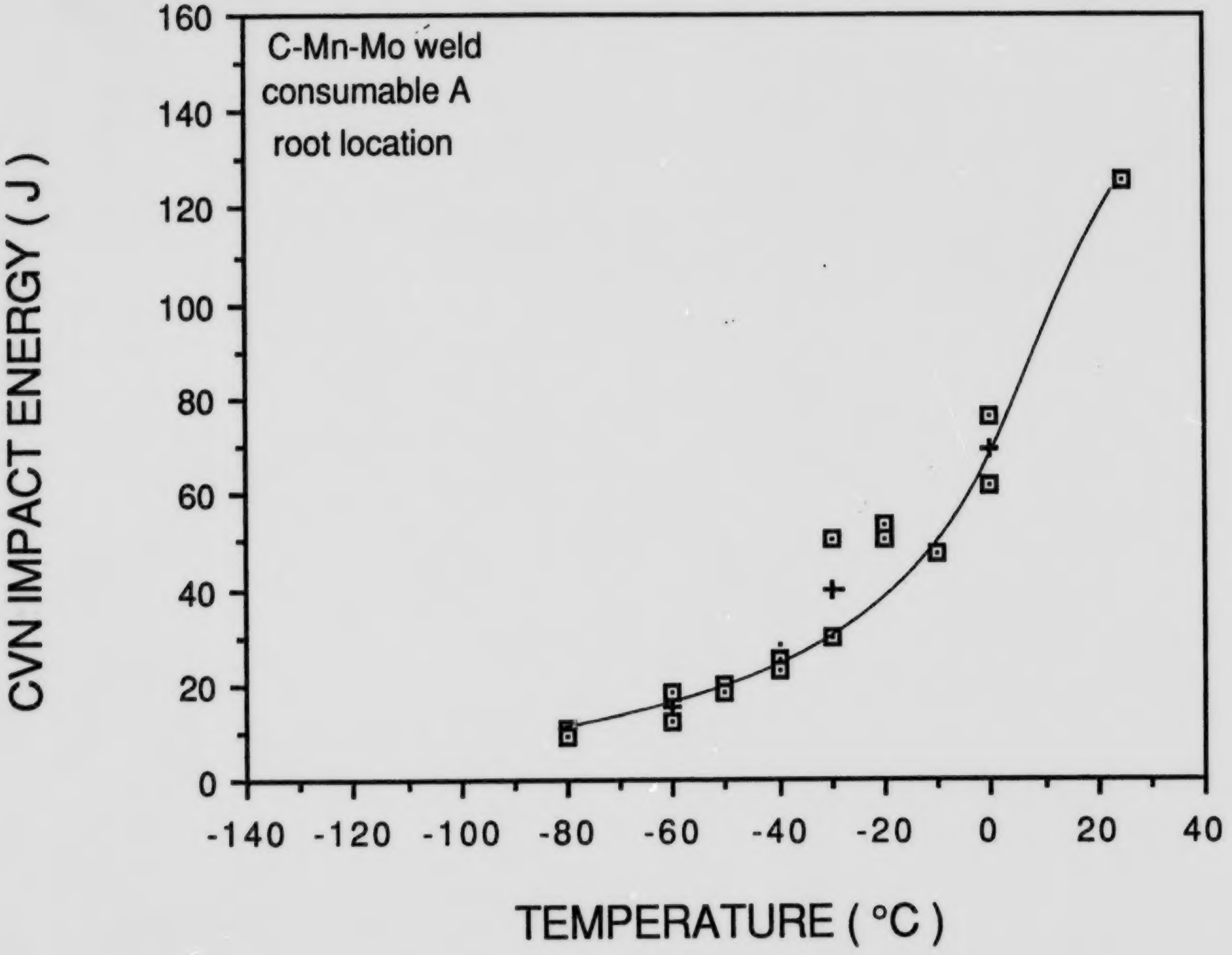

Figure C2: CVN transition curve for the root location from C-Mn-Mo weld prepared with Consumable A (G1A)

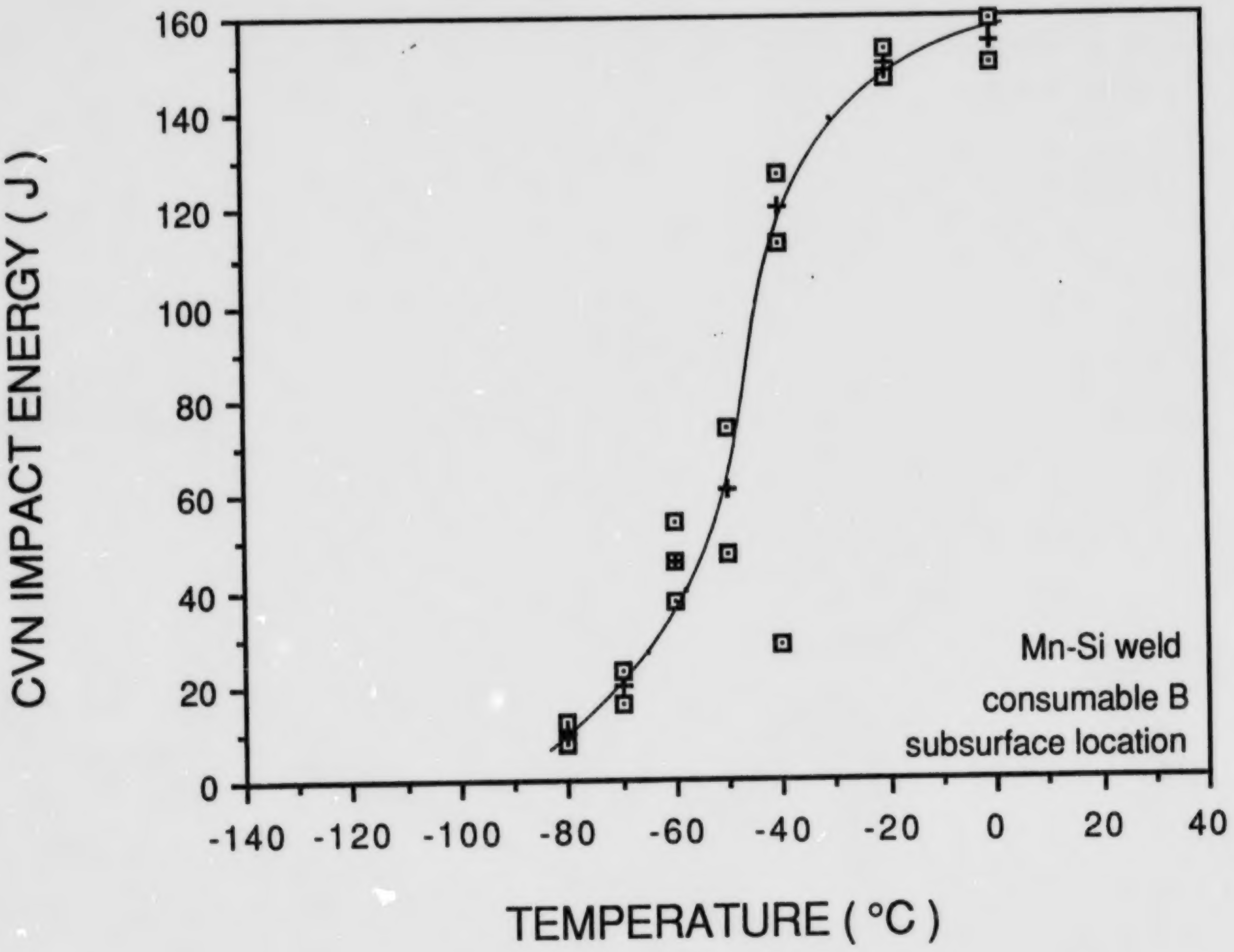

Figure C3: CVN transition curve for the subsurface location from Mn-Si weld prepared with Consumable B (G2A)

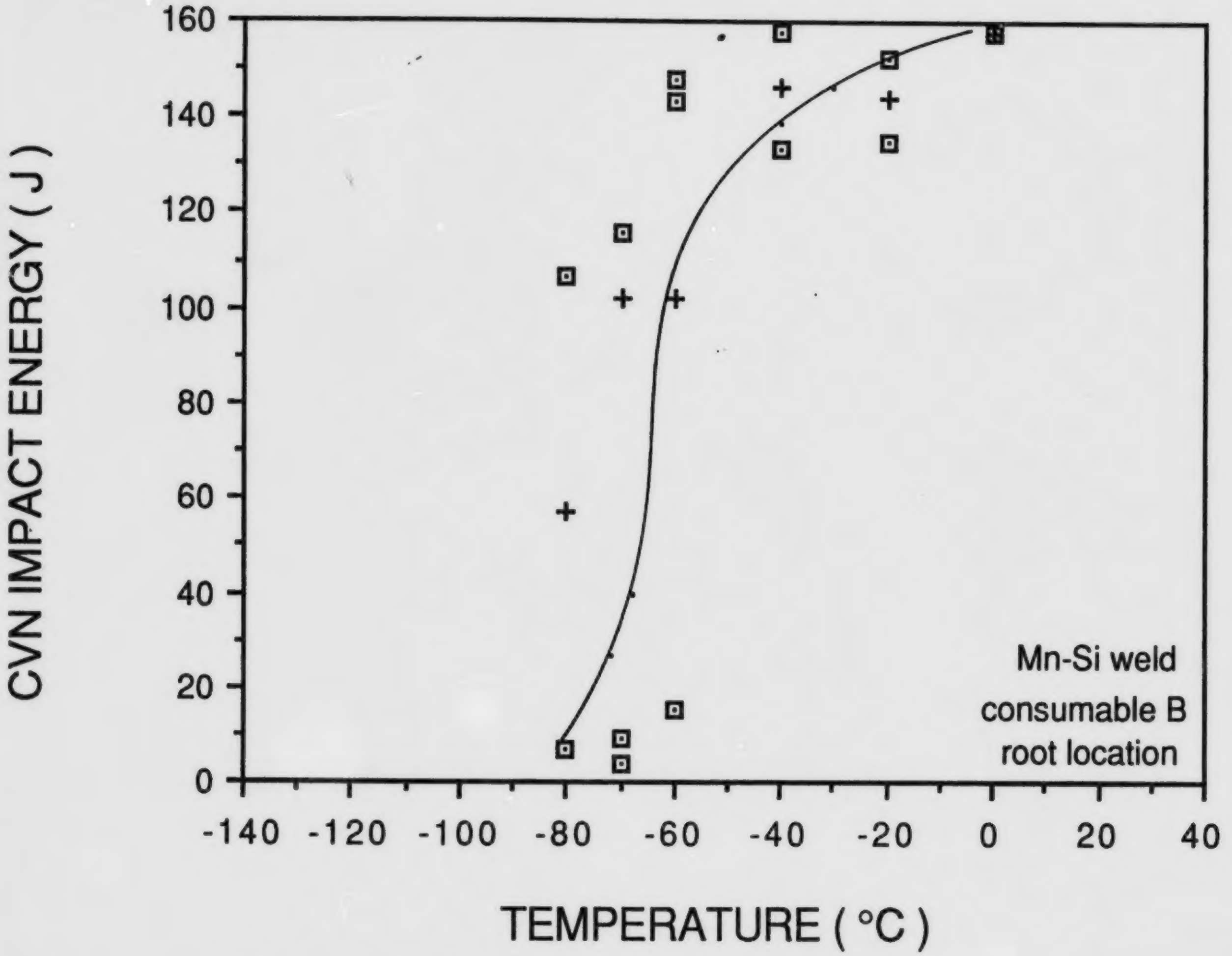

Figure C4: CVN transition curve for the root location from Mn-Si weld prepared with Consumable B (G2A)

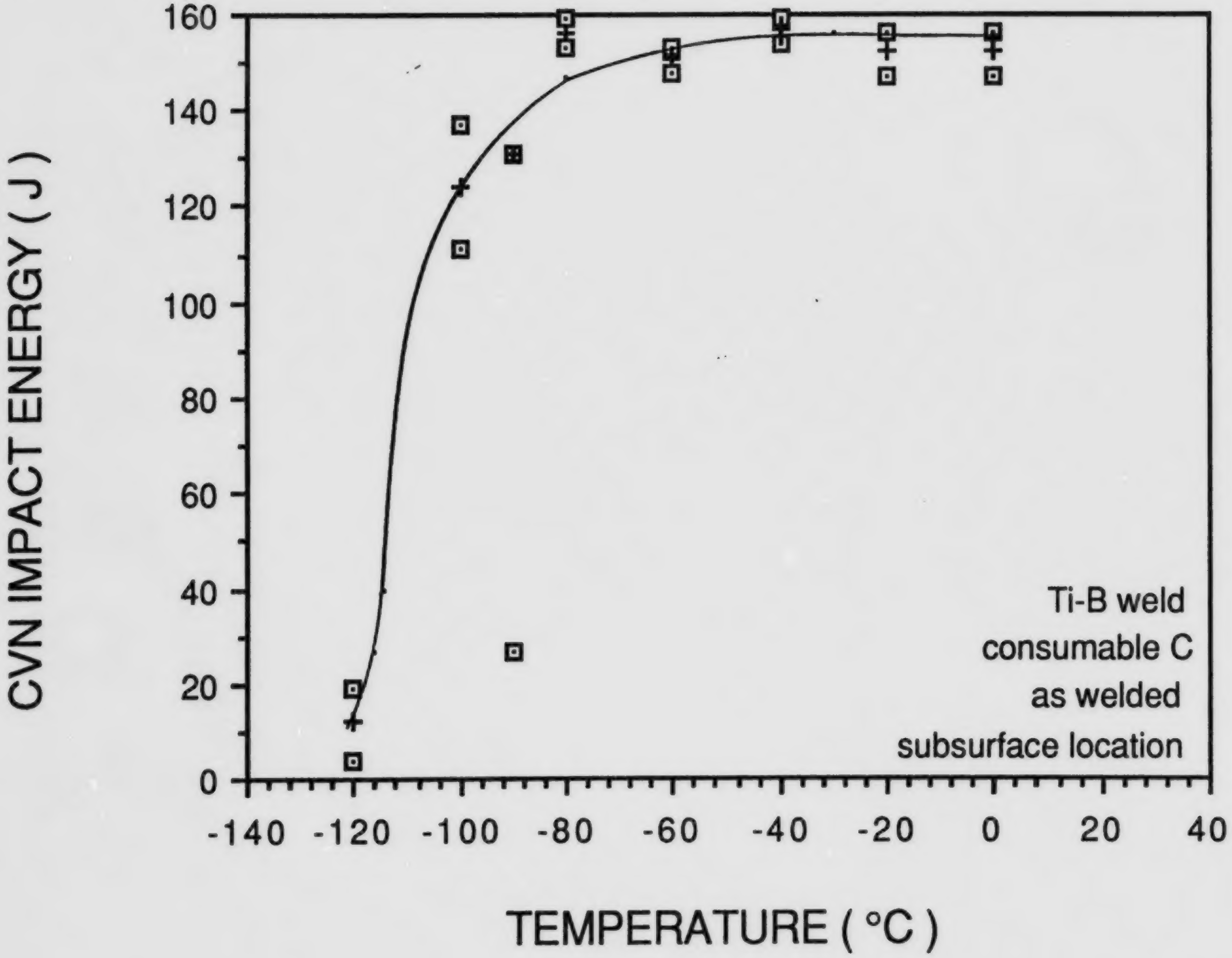

Figure C5: CVN transition curve of subsurface location from the as welded Ti-B weld prepared with Consumable C (G3A)

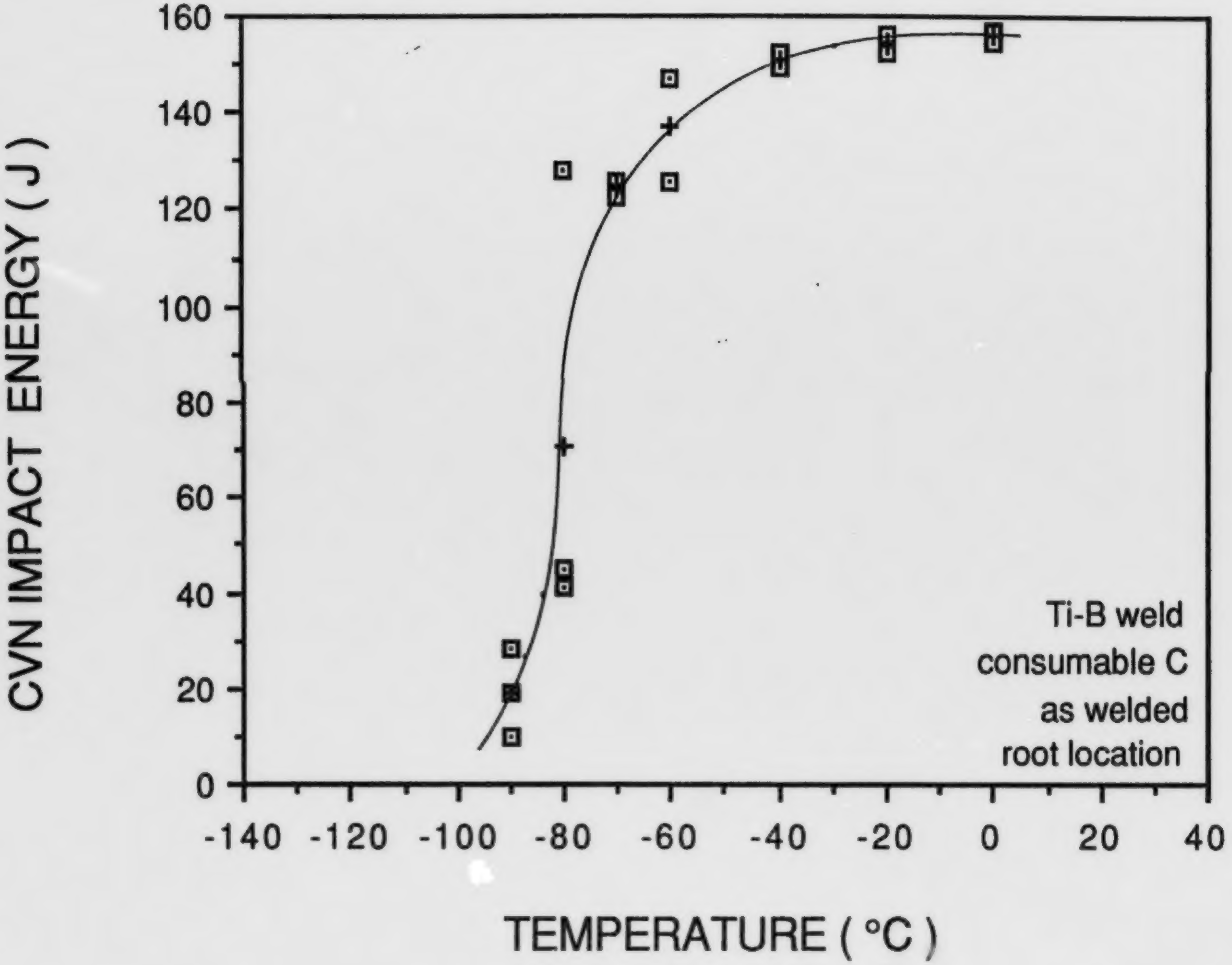

Figure C6: CVN transition curve of root location from as welded Ti-B weld prepared with Consumable C (G3A)

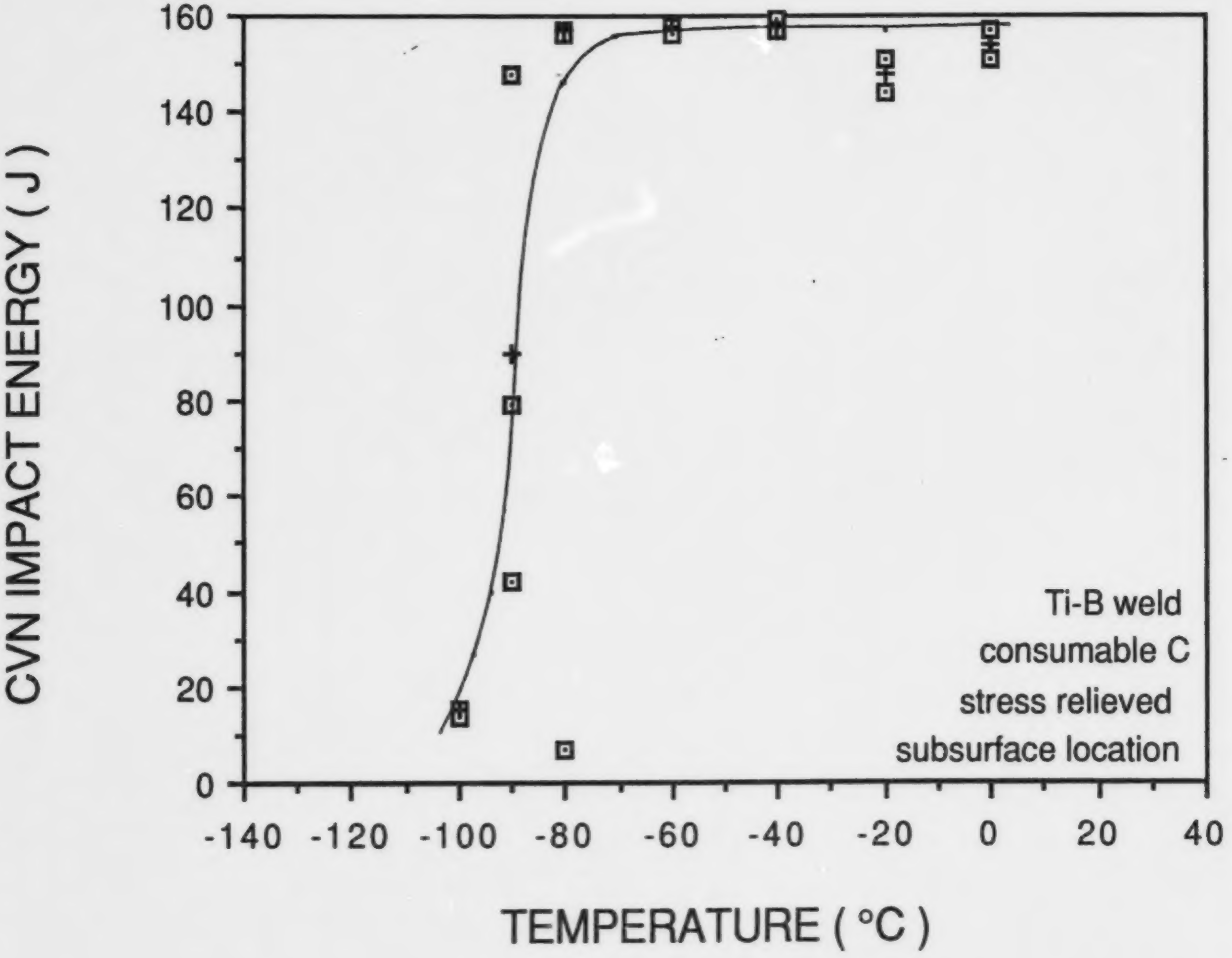

Figure C7: CVN transition curve of subsurface location from stress relieved Ti-B weld prepared with Consumable C (G4A)

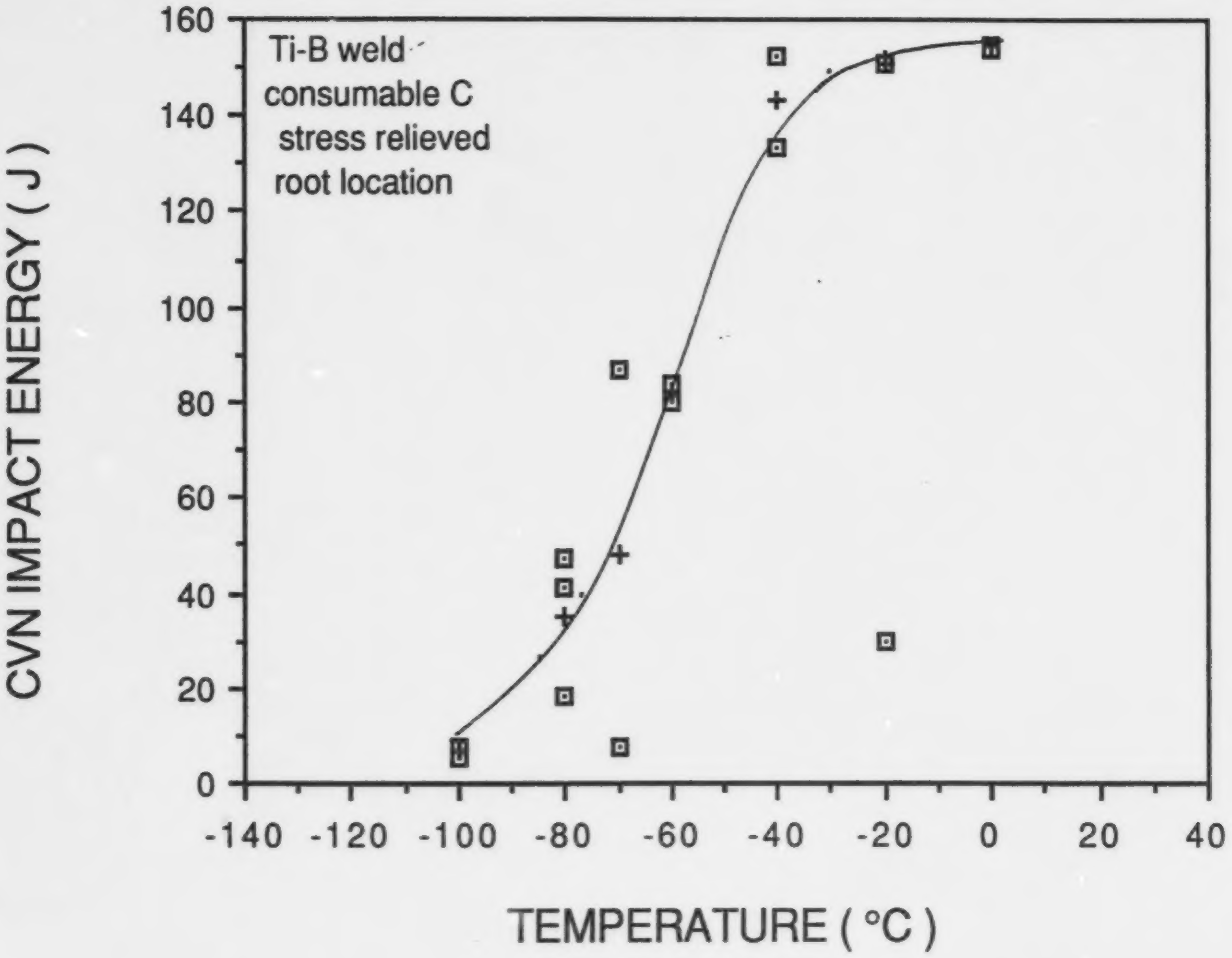

Figure C8: CVN transition curve of root location from stress relieved Ti-B weld prepared with Consumable C (G4A)

APPENDIX D

CTOD Test Results

Specimen ID	Temperature (C)	A2 (25%) (IN)	A3 (50%) (IN)	A4 (75%) (IN)	A ave. (IN)	B (IN)	W (IN)	Aave/W	Y	YIELD (KSI)	Vp (IN)	Pmax (LB)	ELASTIC (mm)	PLASTIC (mm)	CTOD (mm)
1G4	-10	1.8752	1.9327	1.9024	1.9034	1.8807	3.7803	0.5035	10.75	90.0	0.00531	37313	0.0504	0.0365	0.0870
1G5	-10	1.8957	1.9437	1.8465	1.8953	1.8756	3.7799	0.5014	10.65	90.0	0.00625	37313	0.0498	0.0432	0.0930
1G6	-10	1.9193	1.9193	1.8772	1.9052	1.8665	3.7823	0.5037	10.75	90.0	0.00875	35250	0.0457	0.0601	0.1058
1G1	-30				ram up too fast invalid test					94.0					
1G2	-30	1.9107	1.9520	1.8623	1.9358	1.8748	3.7780	0.5124	11.03	94.0	0.00719	33188	0.0405	0.0482	0.0887
1G3	-30	1.8858	1.9622	1.9886	1.9240	1.8724	3.7780	0.5093	10.93	94.0	0.00513	36750	0.0489	0.0347	0.0836
2G4	-10	1.9299	1.9756	1.9201	1.9419	1.8803	3.7780	0.5140	11.11	83.0	0.01500	36560	0.0740	0.1001	0.1740
2G5	-10	1.9071	1.9535	1.8984	1.9197	1.8760	3.7768	0.5083	10.89	83.0	0.01331	37260	0.0742	0.0903	0.1644
2G6	-10	1.9075	2.0095	1.9190	1.9453	1.8805	3.4960	0.5564	12.82	83.0	0.00688	27106	0.0585	0.0403	0.0988
2G1	-30	1.9461	2.0043	1.9031	1.9537	1.8894	3.7819	0.5166	11.22	86.0	0.01063	36000	0.0691	0.0704	0.1395
2G2	-30	1.9181	2.0343	1.9528	1.9935	1.8819	3.7673	0.5292	11.67	86.0	0.01844	37875	0.0837	0.1177	0.2014
2G3	-30	1.9386	1.9969	1.9035	1.9502	1.8697	3.7748	0.5166	11.22	86.0	0.00344	29250	0.0467	0.0228	0.0694
3G4	-10	1.9374	2.0154	1.9161	1.9563	1.8886	3.7846	0.5169	11.22	71.5	0.04875	40313	0.0800	0.3225	0.4025
3G5	-10	1.9181	2.0098	1.9094	1.9458	1.8665	3.7780	0.5150	11.14	71.5	0.02438	38250	0.0728	0.1622	0.2349
3G6	-10	1.9713	2.0343	1.9240	1.9765	1.8665	3.7772	0.5233	11.44	71.5	0.06625	37680	0.0745	0.4303	0.5048
3G1	-30	1.9169	2.0343	1.9815	1.9776	1.8976	3.7795	0.5232	11.44	74.5	0.00563	29625	0.0427	0.0366	0.0793
3G2	-30	1.9071	1.9803	1.8965	1.9280	1.8886	3.7752	0.5107	11.37	74.5	0.01156	37219	0.0673	0.0779	0.1452
3G3	-30	1.9260	1.9740	1.8953	1.9318	1.8870	3.7780	0.5113	11.37	74.5	0.01281	38906	0.0737	0.0861	0.1598
4G1	-30	1.9484	1.8504	1.8287	1.8759	1.8937	3.7791	0.4964	10.54	65.8	0.05130	40219	0.0760	0.3598	0.4358
4G2	-30	1.9429	1.8839	1.8626	1.8965	1.8921	3.7756	0.5023	10.68	65.8	0.03130	32625	0.0515	0.2159	0.2674
4G3	-30	1.9000	1.9327	1.9846	1.9391	1.8886	3.7677	0.5147	11.14	65.8			0.0000	0.0000	0.0000
4G4	-30	1.9772	1.9461	1.9209	1.9480	1.8846	3.7772	0.5157	11.18	69.2	0.03750	38563	0.0679	0.2489	0.3168
4G5	-50	1.8591	1.9055	1.9476	1.9041	1.8937	3.7776	0.5040	10.75	69.2	0.00031	24000	0.0268	0.0021	0.0289
4G6	-50	1.9492	1.9291	1.8748	1.9177	1.8862	3.7760	0.5079	10.89	69.2	0.00000	24806	0.0298	0.0000	0.0298

Table D1 Summary of CTOD results

Volume

3

FLEET TECHNOLOGY LIMITED
A FLEET AEROSPACE COMPANY

FLEET TECHNOLOGY LIMITED E62522C

FINAL REPORT

EVALUATION OF HEAT AFFECTED ZONE AND WELD METAL TOUGHNESS IN SELECTED STEELS
(PHASE II)

VOLUME III: FLUX CORED ARC WELDING PROGRAM

by

C. Chiu
L. Malik

Work on this project was jointly funded by AMCA International Ltd., and by Metals Technology Laboratories (CANMET, EMR) under the auspices of the Program for Energy R&D (PERD).

CANMET Scientific Authority: Dr. J.E.M. Braid
DSS File NO. 06SQ.23440-4-9056-1
DSS Contract Serial No. 0SQ85-00137

Prepared by

MICROMEDIA

Materials Technology Centre
A Division of Fleet Technology Limited
311 Legget Drive
Kanata, Ontario
K2K 1Z8

238pp

ABSTRACT

A series of fourteen welded assemblies have been prepared using the gas shielded flux cored arc welding process with the objective of examining the effect of welding procedural variables on weld metal toughness. All the welds were made using one of three different commercially available consumables and the Ar-25% CO_2 gas shielding. Procedural variables studied included heat input, post weld heat treatment, welding position, lateral joint restraint, and their influence was assessed by microstructure characterization, deposit composition, CVN and CTOD toughness.

The results indicate that better toughness is achieved at lower heat input, and that both higher heat input and stress relief heat treatment lead to deterioration in toughness. One exception to this general observation was the CTOD toughness of stress relieved welds made in 3G position. These had better toughness CTOD than the corresponding as-welded joints. The adverse effect of the stress relief heat treatment was more pronounced at the lower heat input. Welds in the vertical up position had better toughness than similar welds in the flat position. These observations are qualitatively related to changes in weld metal composition and microstructure.

Contrary to expectation, single vee welds made with high lateral joint restraint had better CVN toughness, and better root region CTOD toughness as assessed by surface notched specimens.

In this study, the single vee welds had better CVN and CTOD toughness, however the precise reasons for this were not clear.

Résumé

On a realisé une série de quatorze assemblages de soudures à l'arc en fil-flux sous protection gazeuse. L'objectif était d'examiner l'effet des variables introduites dans le procedé sur la résilience de l'alliage. Les soudures ont été faites en utilisant un des trois fusibles existants sur le marché, et sous la protection gazeuse Ar-25% CO2. Les variables introduites dans le procedé de soudure étudié a inclus; l'apport calorifique, le traitement thermique après soudure, la position du soudage et le bridage latèral du joint, et leur influence a été evaluée par la caractérisation microstructure, la composition des dépôts et la résilience par essai Charpy, et l'essai de déplacement d'ouverture de la pointe de fissure.

Les résultats ont indiqué qu'une meilleure résilience peut être obtenue avec un apport calorifique inférieur. Il a été remarqué aussi, qu'un apport calorifique supérieur avec un traitement thermique de relaxation des contraintes ont conduit à la détérioration de la résilience. Une exception à cette observation générale était la résilience obtenue par essai de déplacement d'ouverture de la pointe de fissure faite en position 3G sur le dépôt lors de la relaxation des contraintes. Ces soudures avaient une meilleure résilience par essai de déplacement d'ouverture de la pointe de fissure par rapport aux soudures des joints correspondants. Les effets défavorables du traitement thermique de relaxation des contraintes étaient plus prononcés avec des apports calorifiques inférieurs. Les soudures effectuées en position vericale avaient une meilleure résilience que celles effectuées en position horizontale. Ces observations sont reliées qualitativement à la composition et la microstructure de l'alliage.

Contrairement à ce que l'on prévoyait, les soudures uniques d'une forme "V" faites avec un bridage latèral élevé du joint ont donné une meilleure résilience par essai Charpy. Il a aussi été remarqué, que la résilience par essai de déplacement d'ouverture de la pointe de fissure de la région racine était meilleure, lorsque celle-ci était évaluée par des éprouvettes entaillées à la surface.

Durant cette étude, la résilience, par essai Charpy et par essai de déplacement d'ouverture de la pointe de fissure, des soudures uniques d'une forme "V" ont montré de meilleurs résultats. Néanmoins, la raison précise de ces résultats n'a pas été claire.

TABLE OF CONTENTS

VOLUME III: FLUX CORED ARC WELDING PROGRAM

Page

Abstract (i)

1.0 INTRODUCTION 1

2.0 EXPERIMENTAL DESCRIPTIONS AND METHODOLOGY 5

- 2.1 Materials and Consumables 5
- 2.2 Welding Procedure and Joint Preparation 6
- 2.3 Lateral Shrinkage Measurements 7
- 2.4 Specimen Preparation 8
- 2.5 Chemical Analysis 9
- 2.6 Inclusion Analysis 9
- 2.7 Quantitative Metallography 9
- 2.8 Mechanical Testing 10
- 2.9 Gapped Bead On Plate (GBOP) Testing 12
- 2.10 Hydrogen Testing 12

3.0 RESULTS AND DISCUSSION 13

- 3.1 Weld Metal Composition 13
- 3.2 Inclusion Analyses 14
- 3.3 Quantitative Metallography 17
  - 3.3.1 Macrostructure 17
  - 3.3.2 Microstructural Characterization 17
- 3.4 Lateral Shrinkage Measurements 19
- 3.5 Tensile Properties and Hardness Results 20
- 3.6 Drop Weight Testing 21
- 3.7 CVN Notch Toughness 21
- 3.8 CTOD Toughness 24
- 3.9 SEM Fractography on Selected CTOD Specimens 25
- 3.10 Weld Metal Diffusible Hydrogen Content 26
- 3.11 Gapped Bead On Plate (GBOP) Testing 26

4.0 CONCLUDING SUMMARY 27

5.0 REFERENCES 29

TABLES

FIGURES

APPENDIX A - Inclusion Analysis Report

APPENDIX B - Data on Transverse Shrinkage

APPENDIX C - Data on Drop Weight Testing

APPENDIX D - Data and Transition Curves From CVN Testing

APPENDIX E - Data on CTOD Testing

APPENDIX F - Fractographs on Selected CTOD Specimens

1.0 INTRODUCTION

In an earlier investigation[1.1], the weld metal toughness of deposits obtained from several gas shielded flux cored wires was evaluated. All these welds were made semi-automatically in the vertical up position (3G) at a nominal heat input of 2.2 kJ/mm, and evaluation was carried out for the 'as-welded' deposits only. The relevant conclusions were summarized as follows:

(i) Among the sixteen commercial consumables, the deposit from consumable designated as A in the present program had the best combination of CVN and CTOD toughness, which was related to its microstructure, inclusion distribution and composition.

(ii) In terms of microstructural control to maximize CTOD toughness, a high proportion of acicular ferrite (which offers greater resistance to cleavage initiation) as well as lowering the grain boundary ferrite (which offers lower resistance to cleavage initiation) are equally important.

(iii) Inclusions act as cleavage initiation site to lower toughness; this effect is enhanced if the inclusion is located in the grain boundary ferrite.

(iv) The size, distribution and type of inclusions are important in regard to their roles in initiating cleavage fracture and assisting in the nucleation of acicular ferrite.

In production welding situations, however, one would like to be able to use the same consumable for different plate thicknesses and joint geometries for as-welded, as well as stress relieved welds, for welding in all positions, etc. It was therefore, the objective of the investigation to choose two consumables with better toughness from the previous comparative study, and then to study the effect of the following welding procedural variables:

- heat input;
- stress relief;
- welding position; and,
- joint restraint.

Heat Input - As far as the effect of heat input is concerned, it is well known that within the commonly used range of heat input in welding applications (1.5 to 3 kJ/mm for small diameter flux cored wires), higher heat inputs lead to deterioration in toughness. However, with optimum alloying, including Ti-B in rutile cored wires, attempts have been made to reduce this sensitivity to heat input.

Stress Relief - The stress relief treatment in plain C-Mn weld deposits usually tends to enhance the deposit toughness. This is related to the softening of the microstructure, and partial removal of the strain aging damage in the as-welded deposits. However, with the presence of micro-alloying elements, stress relieving treatment also leads to carbonitride precipitation which does not permit any significant softening of the deposit. The flux cored deposits of rutile cored wires, as a result, suffer from substantial reduction in toughness as a result of the post-weld heat treatment.

The manufacturer of consumable A has developed a modified version of the wire (Consumable B in the program), which has the same classification as consumable A, gives a deposit with virtually the same composition but is recommended for welds to be stress relieved, thereby implying that deposits of consumable B do not suffer as much degradation on stress relieving as would consumable A deposit, and that in the stress relieved condition, consumable B deposit would have better toughness than consumable A deposit.

Welding Position - In the early work done during the 70's and early 80's, it was found that the welds made in the vertical up position had poor toughness than those made in the flat position. The main factors responsible for the reduction in toughness were believed to be higher nitrogen content of the semi-automatically made welds in the 3G position, and their larger heat input on account of weaving [1.2-1.4].

However, the larger heat input argument needs to be used with caution. If the current and voltage are on the low side, and the weave is wide (in effect an oscillation), then the weld pool has discrete lateral travel, and the heat input based on vertical travel speed only will be a gross overestimate. On the other hand, if the weave is small so that in effect a single wider pool is moving upwards, then the conventional heat input calculation may be a reasonable representation of the effective heat input.

Evans[1.5] has concluded that at the same heat input, vertical up position does not necessarily lead to a lower toughness deposit, the other key factors being nitrogen and oxygen contents. While the amount of nitrogen depends on the arc length, Evans indicated that welds made in the 3G position have higher oxygen content due to the turbulence in, and the location of the slag layer relative to the weld pool.

In a vertical position, the slag layer cascades downward with the gravity pull. Hence, when the slag flows away from the weld pool, the weld pool becomes more exposed to the arc atmosphere leading to possible oxygen ingress and subsequently higher oxygen content. Furthermore, the larger ascending inclusions may be entrapped in the weld metal rather than in the slag phase (Figure 1.1). In contrast, for welds in the flat position, the more vigorous turbulence in weld pool and the stationary slag layer would ensure a more efficient deoxidation process and subsequent removal of inclusions in slag phase.

With small diameter flux cored wires, it is usually not necessary to weave in the 3G position. Therefore, for examining the effect of welding position, all the welds were made in the automatic mode using stringer beads in both the flat and vertical positions. The comparison was carried out at the 2.0 kJ/mm heat input only.

Restraint - Restraint influences the weld metal toughness, primarily by its effect on the amount of free shrinkage accommodated by the plastic strain in the weld zone, and its subsequent aging.

In the literature, low restraint situations are defined as those which permit large angular distortion, leading to strain concentration and aging in the root beads. Thus, root beads can be expected to have poorer toughness than the subsurface regions[1.6-1.7].

Imposing a high restraint to prevent angular distortion is supposed to lead to better weld toughness[1.8]. However, it is believed that the effect of higher restraint is to further increase the plastic strain in the weld metal, though this would be more uniformly distributed along the weld thickness so that the difference between toughness at subsurface and root locations would be minimized. In comparison to the 'angular distortion' situation, the root location ought to have higher toughness, and the subsurface location should have lower toughness.

For this program, an attempt was made to examine the effect of lateral restraint only, while keeping angular restraint high. Thus, the weld with high lateral restraint would be expected to give lower toughness values than that made at the lower lateral restraint.

*** CONFIDENTIAL ***

CONSUMABLE	TRADE NAME	MANUFACTURER	AWS CLASSIFICATION
A	DW-55L (for as-welded application)	Kobe	A5.29 E80T1-K2
B	DWA-55L (for stress relief application)	Kobe	A5.29 E80T1-K2
C	OK Tubrod 15.17	ESAB	5.20 E81T1-Nil

This page can be removed at the discretion of the Scientific Authority.

2.0 EXPERIMENTAL DESCRIPTIONS AND METHODOLOGY

2.1 Materials and Consumables

Base Plate: The base plate used for all the welds was 50 mm thick normalized C-Mn microalloyed steel conforming to CSA G40.21 Grade 350 WT. The chemical composition and mechanical properties, as per mill test report, are included in Table 2.1.

Flux Cored Arc Welding Consumables: Three consumables (subsequently designated as A, B and C) were selected for the experiments. The selection of these consumables was made on the basis of CVN and CTOD data available from a previous CANMET funded study on toughness of FCAW deposits[2.1], and on commercial technical literature on the recent generation of flux cored consumables. The toughness data provided by the respective manufacturers for the three consumables are included in Table 2.2. In summary, the three selected consumables are primarily C-Mn-(1-1.5%)Ni wire with all position welding capabilities. These consumables are designed for multi-pass welding of Al-killed steel plates for low temperature applications.

The consumable designated as A is a 1.2 mm diameter flux cored wire with a rutile core and gives a C-Mn-1.5% Ni deposit meeting the requirements of AWS A5.29 E80T1-K2. It is designed for 100% CO_2 gas shielding. In the previous FCAW study[2.1], the same consumable yielded the best weld metal toughness among the sixteen consumables evaluated in conjunction with Ar-25% CO_2 gas shielding.

Consumable C is also a 1.2 mm diameter wire with rutile core and is an improved version of one of the better wires evaluated in the previous FCAW study. The wire is classified to AWS A5.29 E81T1-Ni1, giving a C-Mn-1% Ni deposit.

Consumable B is a modified version of consumable A. The manufacturer claims that the modified version is more capable of retaining deposit toughness in the stress relieved condition.

2.2 Welding Procedure and Joint Preparation

Groove Preparation: Two joint geometries (double vee and single vee) have been used in the flux cored arc welding program. The welded assemblies were nominally 915 mm (36") x 610 mm (24"). The double vee geometry was 2/3 - 1/3 with 60° and 50° included angles respectively, and a 3 mm (1/8") gap at the root. The single vee geometry had an included angle of 50° and a root gap of 6 mm (0.24") (Figures 2.1 and 2.2) and was employed for welds wherein the effect of joint restraint was evaluated. The backing bars for single vee welds were prepared from the same base plate material. The welding direction was transverse to the rolling direction of the base plate.

In order to ensure consistency between welds, the groove surfaces were machine finished to the desired dimensions.

Welding Fixture: The same welding fixture was used for all double vee welds. It is designed to control both the angular distortion and lateral shrinkage transverse to welding direction. A schematic representation of the welding fixture is included in Figure 2.3. For the welds made in the 3G position the same table was turned 90° after clamping the base material plates, thereby enabling one to maintain the same restraint for 1G and 3G welds.

Different modifications to welding jigs were made for the two remaining welds intended for restraint studies. These were:

(i) High angular restraint and high lateral restraint: additional restraint was provided by fillet welding a series of 25 mm (1") thick stiffeners, located 150 mm (6") apart along the weld length and 25 mm (1") thick side plates. The design is a modified version of the restraint set up reported in a Welding Institute (UK) study [2.2]. The subsequent shrinkage measurements confirmed the success of the restraint set up. The set up is illustrated in the Figures 2.4 and 2.5.

(ii) High angular restraint and low lateral restraint: Spacer blocks with larger surface area were inserted between the clamping bolt and the plates, with the objective of lowering normal stress and enabling relatively free lateral movement without compromising the angular restraint. Friction was minimized by covering all contacting surfaces with Mo disulphide grease that can provide low friction and tolerance to high temperature. The resultant angular and lateral measurements indicated that the relatively free lateral shrinkage was allowed with minor angular distortion only. The set up is schematically illustrated in Figure 2.6.

Preheat and Interpass Temperature: Throughout the entire flux cored arc welding program, the preheat and interpass temperatures were 50° and 150°C respectively. The preheat was applied by an oxy-fuel rose bud heating torch. Appropriate Tempilsticks were used to monitor the preheat and interpass temperatures during the course of welding.

Welding Procedure and Parameters: A total of 14 welds were made with different combinations of consumables, post-weld heat treatment conditions, heat input, joint geometry and restraint condition. Eight of these welds comprised two lengths of 0.9 m (3′) each. The remaining 6 welds were single lengths of 0.9 m (3′) each. For these latter 6 welds, the mechanical testing was limited to CVN and CTOD tests only. The experimental matrix for the program and welding parameters are included in Tables 2.3 and 2.4. For double vee welds, back-gouging was undertaken at the root pass of side one and subsequently widened by grinding to provide a wider groove for the root pass of second side (Figure 2.7). Back-gouging was not needed for single vee welds.

In order to maintain consistency and meaningful comparisons among different welds, the sequence and positioning of the beads were the same for all welds. Relative to side 1, the welding direction was reversed on side 2. Run on and run off tabs (75 mm length) were attached to each assembly.

Post Weld Heat Treatment: For the selected welded assemblies shown in Table 2.3, the thermal cycles for stress relieving were carried out as per CSA W59 (1984) Clause 5.1.2. The welded plates were inserted into an electric furnace at room temperature; heated at a rate of 50°C/hour; soaked at 600°C for 2 hours; and furnace cooled at 50°C/hour to room temperature.

2.3 Lateral Shrinkage Measurements

For the single vee welds selected for restraint study, lateral shrinkage was measured at seven locations along the weld length on the plate surface. For the first half of the weld, transverse shrinkage was measured every 75 mm (3") along the weld length and the last location for measurement was located at 1/4 length from the end of the weld. At each location, a series of shallow holes were drilled and tapped (about 75 mm apart across the weld), into which short screws were inserted. The purpose of the screws is to provide rigid reference points for shrinkage measurements. The set up is schematically illustrated in Figure 2.8.

Prior to deposition of first root pass but after clamping, spacings between all the pairs of screws across the weld locations, viz. L1, L2, and L3, were measured at room temperature. After the first root pass was deposited, the weld was allowed to cool to room temperature, and spacing of screws was measured again. The same procedure was repeated after completion of the following stages:

- completion of the second pass;
- completion of the third pass (approximately T/4);
- completion of the 12th pass (approximately T/2);
- completion of the 22nd pass (approximately 3T/4); and,
- completion of the entire weld.

The measurements after the completion of each stage were taken with the plate remaining under restraint and at room temperature. The additional cooling time of 2-4 hours after each stage could, in principle, influence the toughness results. However, the relatively short cooling time is less than the overnight interruption during production, and therefore the additional cooling required for the transverse shrinkage measurements can be considered as typical of production welding practice.

2.4 Specimen Preparation

The Charpy (CVN), tensile, drop weight and crack tip opening displacement (CTOD) specimens were machined as per ASTM E23, ASTM A370, ASTM E208 (1984a) and BS 5762 Standards respectively.

In the case of double vee joints, standard (10 mm x 10 mm) CVN specimens were taken from two locations, viz. 5 mm subsurface on side 2 and the root. The specimens for the latter location were extracted from side 1 and at ≈2 mm from the root pass of side 2 (Figure 2.9). For the root location, the notch coincided with the weld centerline which was determined by the mid-point of the narrowest weld width at the root. Prior to extraction of subsurface CVN specimens, the cross section of full thickness weldment was surface ground and etched with 10% Nital to reveal the macrostructure. The notch location was shifted from the weld centerline as needed, such that 50% each of as deposited and reheated macrostructures were sampled by the notch. The objective was to compare the toughnesses without the interference of variations in macrostructural distribution at the CVN notch.

In the case of single vee joints, three CVN locations were selected, viz. subsurface, T/2 and root locations. The subsurface and root locations are located at 2 mm from the surfaces of the plate. The notch locations for both of T/2 and subsurface CVN specimens are shifted from the weld centerline to yield an approximate 50/50 ratio of unrefined and refined regions.

The P-2 type drop weight specimens were taken from 2 mm below the plate surface on side 2 (Figure 2.10). The crack starter bead was deposited transverse to the test weld with a hardfacing consumable at 180-200A and travel speed of 150 - 170 mm/min. The two bead technique was used with start position at both ends and stop positions overlapping at the center.

For the selected double vee joints, all weld metal 6.25 mm diameter round tensile specimens with 25 mm gauge length were taken longitudinally with the tensile axis located at 8mm from the plate surface of side 1 (Figure 2.11). For single vee joints, one round tensile specimen was extracted from each of subsurface, T/2 and root locations.

Although the plate thickness was 50 mm, the thickness 'B' of B x 2B CTOD specimens was reduced to 48 mm to avoid any lack of reinforcement in the capping layer. The notch root coincided with the weld centerline (Figure 2.12).

2.5 Chemical Analysis

Welds representing the as welded condition only were selected for chemical analysis. All weld metal samples were machined from corresponding subsurface and root CVN notch locations, and sent to ORTECH International for chemical analysis of the following elements: C, Mn, Si, S, P, Mo, Ni, Cr, Cu, Nb, V, O, N, Ti, B, Zr and Al. C and S were analyzed by Leco methods, O and N by vacuum fusion and the remaining by D.C. Plasma spectrometry.

2.6 Inclusion Analysis

Since the inclusions are high temperature transformation products, the post weld heat treatment would not affect the inclusion distribution. Hence, the inclusion analysis was undertaken for the welds in as-welded condition only. The exact description of methodology is included in Appendix A. Briefly, an area of 2 mm (parallel to weld centerline) x 0.5 mm at T/2 location is selected for analysis. Each inclusion is identified by shape, composition and size. The presence of an element in an inclusion is defined by either having a K_α peak of at least 5% relative intensity or 2w/o. For each weld, the inclusions are classified according to size and composition.

2.7 Quantitative Metallography

Welds in as-welded condition were selected for metallographic characterization. The transverse sections were polished to 1 micron diamond finish and subsequently etched with 2% Nital for metallographic examination. Attempts were also made to use other etchants to help characterize the amount and nature of the second phase constituents (martensite-austenite-carbide); however, these were not successful.

Macrostructure along the centerline: For each weld, the macrostructure along the weld centerline was characterized as columnar unrefined, coarse grain reheated and fine grain reheated regions. The percentage distribution of each structure was calculated by the linear intercept method.

Microstructure in the last bead: For each weld in the as-welded condition, the as-deposited microstructure in the final bead on side 2 was characterized by point counting as per IIW designations [2.3]. The point counting was carried out in 100 x 10 grids at a magnification of 500x. The X intervals and Y intervals for the grid were 0.05 mm and 0.2 mm respectively. Quantitative microstructural analysis was also attempted for the stress relieved welds. The point counting was carried out using a 50 x 10 grid at a magnification of 400x.

2.8 Mechanical Testing

Hardness Testing: For each weld, Vickers (10 Kg) hardness profiles were obtained along the weld centerline and along a line corresponding to the mid-thickness of each CVN specimen location. Readings were taken every 5 mm intervals along the centerline from cap to cap and every 3 mm along the mid thickness at each CVN locations.

CVN Testing: For each double vee weld, 16 CVN specimens were extracted from each of the root and subsurface locations. The notch profiles were checked frequently for adherence to ASTM E23. The test temperature ranged from 20°C to -100°C, the objective being to obtain the CVN transition curves, and transition temperatures.

For the single vee welds, 30 - 32 CVN specimens were extracted and tested for each location (subsurface, T/2 and root locations).

Tensile Testing: Tensile specimens were tested at temperatures ranging from 20°C to -50°C. The lower temperature was maintained by passing liquid nitrogen through an enclosed copper tube cooling chamber. The temperature was monitored by a thermocouple attached directly onto the specimen. The tests were carried out at a strain rate of 0.02/min. Extensometer was used for the room temperature test.

Drop Weight Testing: For each weld, up to 8 drop weight P-2 specimens were tested at temperatures ranging from -20 to -80°C. With impact energy of 400J for all tests, a break or no break condition was prescribed for each specimen corresponding to whether or not the crack reached at least one side of the specimen. A nil ductility transition (NDT) temperature was determined as the highest temperature at and below which all tests will yield a break condition.

CTOD Testing: The BX2B specimen geometry for the machined specimens is included in Figure 2.12.

In order to ensure a relatively straight fatigue crack front, the notch tips were locally compressed for all specimens in the 'as-welded' condition as per the procedure outlined by Towers and Robinson [2.4]. The ligament below the notch was locally compressed from both sides by circular indentors of 25 mm diameter. The indented area extended from 5 mm overlapping the notch root to at least 5 mm from the opposite side to avoid bulging. Local compression was not required for CTOD specimens from stress relieved welds.

The fatigue precracking was carried out in two stages; i.e. a higher fatigue load range was used initially to facilitate crack initiation, and then reduced to satisfy and meet the stress intensity specified in BS 5762. The maximum load range for each stage was estimated from:

$$P_f = \text{Peak load during precracking} = \frac{\beta \sigma_y B^{3/2} W^{1/2}}{Y}$$

where β = 0.6 for the first 1 mm of precracking

β = 0.4 for the next 3 mm of precracking

Y = value of compliance function given in BS5762

σ_y = yield strength

The test temperature was monitored by a thermocouple attached to the specimen and maintained within 2°C of the specified temperature. Usually, three specimens were tested, as per BS5762, at the chosen temperature since some scatter in CTOD toughness is always expected, and triplicate tests would give a better indication of CTOD toughness for further comparisons in the investigation. After the tests, the specimens were broken to measure the effective crack sizes.

For the single vee welds, additional BXB surface notched CTOD specimens were also prepared. The specimen geometry is included in Figure 2.13. The objective was to evaluate the CTOD toughness at the root location by aiming the fatigue crack to sample the columnar region of the third pass. The selection of the fatigue crack location is based on the last single pass layer in the root at which the transverse shrinkage measurements are available to assess the local restraint condition as well as it would provide a sufficient depth of the fatigue crack to give an a/W value close to the minimum allowed in the BS5762. However, the resultant a/W values fell within the range of 0.1 - 0.14 which is lower than the minimum value of 0.15 allowed in BS5762. Nevertheless, the Y values used in these BXB specimens were estimated by curve fitting the Y versus a/W data given in BS5762.

2.9 Gapped-Bead on Plate (GBOP) Testing

In order to assess the cold cracking susceptibility of the weld metal, the GBOP tests were carried out for the three consumables with the test blocks machined from the same 350WT steel used in this program. The dimensions of the test blocks for the GBOP tests are included in Figure 2.13. The test assembly consists of two blocks of the same dimensions except that one has a machined recess of 0.75 mm. At a predetermined preheat, the assembly is pneumatically clamped together with 10 MPa pressure. A weld bead is deposited across the machined recess using the respective consumables under investigation. The welded blocks are left under pressure for 24 hours, then left another 24 hours without pressure. Then the welded blocks are heated to a dull read heat in the vicinity of the gap and allowed to cool to room temperature. The weld bead is snapped open and the extent of cold cracking is determined by the presence/absence of the blue- colour oxide layer.

The welding parameters for depositing the weld beads were: 180A, 24V and 2.5 mm/min. The preheat temperatures for the blocks were: room temperature, 50°C and 75°C.

2.10 Hydrogen Testing

For each consumable, the diffusible hydrogen content in the weld metal was determined using the ISO 3690 method. The welding parameters of 24V, 180A, and 2.5 mm/sec were used.

3.0 RESULTS AND DISCUSSION

3.1 Weld Metal Composition

The compositions for both subsurface and root locations from selected welds are tabulated in Table 3.1. In addition, the calculated carbon equivalents (IIW) and Pcm values are also included in Table 3.2. In summary, all welds have shown high oxygen contents (520-720 ppm) in relation to those obtained in the previous submerged arc (relatively basic flux) and gas metal arc (low oxygen potential shielding gas) programs. The reason for these high oxygen contents is obviously the rutile core of the wires. However, it should be noted that these oxygen levels are lower than those reported in the previous FCAW [3.1] study using the same wire for welds made in the 3G position (semi-automatic). The moderate nitrogen content (40-80ppm) is due to control on arc length by fully automatic application of the process. The calculated unbalance factors are also included in Table 3.2. Virtually all values are greater than 100ppm indicating the small magnitude of free nitrogen. For consumable A, the C, Ti, B and Ni contents were also higher in the previous study[3.1], their respective values being .055, .07, 1.74 and .0024 wt %.

Effect of Heat Input in Flat Position: The weld deposits for all three wires are C-Mn-Ni-Ti type, with Nb and V being present as residuals. Deposits from consumable C have somewhat higher carbon content, and lower Mn, Si, Ni, Ti and boron contents. Higher heat input leads to some reduction in Mn and Si contents which is consistent with the observations by Lathabai & Stout[3.2]. Also, increase in heat input as well as changing the welding position from flat (1G) to vertical up (3G) seem to lead to an increase in the deposit oxygen content (Figure 3.1). Even higher oxygen content in the previous study [3.1] may have been due to a slightly longer electrode stick out and the semi-automatic application of the process. Welding in 3G position also leads to higher carbon. These observations are in accordance with the results reported by Evans [3.3]. Titanium contents are also larger in the 3G welds of consumable B. The higher alloy recovery may be due to shorter arc length used in out of position welds (Table 2.4).

Comparing consumables A and B, the weld deposit compositions are similar with the exception of oxygen which is slightly higher in consumable B deposits; thus the subsequent discussion on the effect of stress relief on weld metal toughness treats the two deposits as from one consumable but in different post weld heat treatment condition.

The weld metal compositions in the subsurface and root locations are quite similar and there is no consistent trend regarding the difference in compositions between the two locations.

3.2 Inclusion Analyses

The inclusion analyses are summarized in Tables 3.3 to 3.6. The full documentation of results is included in Appendix A. The inclusion characteristics are discussed in terms of overall distribution and individual size groupings; viz,

- $0.1\ \mu m \leq$ inclusion diameter $< 0.5\ \mu m$;
- $0.5\ \mu m \leq$ inclusion diameter $< 1.0\ \mu m$; and,
- inclusion diameter $\geq 1.0\ \mu m$.

It is important to note the inclusion analysis in the flux cored arc welding program is undertaken with a different image analysis equipment than the one used in submerged arc welding and gas metal arc welding programs. The main difference among the two equipments lies in the lower bound detection limit on inclusion size. The lower detection limit for the image analysis equipment employed in the present program is 0.1 μm versus 0.2 μm for the previous programs. Assuming everything is constant, then the image analysis equipment used in the present program would yield a slightly larger area fraction and a higher inclusion number density.

Since the inclusions are primarily desulphurization or deoxidation products, the area fractions may correlate with the total contents of oxygen and sulphur (subsequently abbreviated as (O + S)) (Figure 3.2). Most of the inclusion area fractions are larger than the values predicted by Widgery [3.4]. The large scatter is probably due to the aspect ratio being less than 1, i.e. non-spherical inclusions such that the assumption of equivalence among the volume fraction and area fraction is no longer valid. Hence, volume fractions are estimated from the inclusion diameters and densities as follows:

$$\text{Volume fraction (\%)} = \frac{100\ \pi N_s\ (D_{ave} + D_{std})}{6}$$

where N_s = number density of inclusions in microns per sq cm

D_{ave} = average inclusion diameter in microns

D_{std} = standard deviation in average diameter in microns

In general, the estimated volume fractions are smaller than the area fractions (Table 3.3). Although the volume fraction provides a better correlation with (O + S) (Figure 3.2), significant deviation from the predicted values remains in the smaller heat input welds of consumables A and B. Nevertheless, the estimated volume fractions follow the general trend of increasing inclusion volume fraction with larger (O + S) content; at least for the deposits of consumables A and C.

Comparison Among the Three Consumables: The majority of inclusions in all three consumables are basically Ti-Mn-S with varying amounts of Si and Ca. It is of interest to note that the presence of Si in dominant inclusions generally increases the inclusion size and its aspect ratio. A similar though more moderate effect of Si on inclusion size was also observed in the shielded metal arc weld program[3.5] and in the Ti-B welds of submerged arc weld program. The presence of Ca has minor effects on inclusions. Furthermore, Al is absent from any of the dominant inclusion types. In each of the welds, the proportions of Al bearing inclusions range from 0 - 3% only.

Compared with the previous FCAW study[3.1] involving consumable A, Al (relative content of 5 - 15%) was detected in ≈ 20% of inclusions. Furthermore, the most dominant inclusions in the previous FCAW program was Ti-Mn-S-Si with relative contents of 51%, 34%, 5% and 8% for Ti, Mn, S and Si respectively.

Since the weld metal compositions are broadly similar in the deposits of the three consumables, it is of interest to compare the inclusion distribution under similar conditions. In the 2.0 kJ/mm deposits of consumables A and C in 1G position, there are no significant differences (in terms of type, overall proportion, and average diameter) among the dominant inclusion types despite a difference of 77 ppm in (O + S) content between the two deposits. The main difference lies in the number density of larger inclusions (> 1 μm) which increases with the higher (O + S) content found in the 1G deposit of consumable C (Figure 3.3).

In the 2.0 kJ/mm deposits of consumables B and C in 3G position, there are significant differences among the inclusions e.g. the proportion of each dominant inclusion is different, even though the sizes are similar. The most dramatic difference lies in the number density of larger inclusions (> 1 μm) which for consumable B is much lower, despite a larger (O + S) content.

Effect of Heat Input - Recalling the results of weld metal composition, the main effect in larger heat input is the increase in oxygen and subsequently (O + S) content. Hence, it is anticipated that the inclusion content would increase with heat input. The inclusions analysis of consumable A weld deposits at the two heat inputs shows that all inclusion characteristics (average diameters, number density and area/volume fractions) assumes higher values for the higher heat input deposits as a result of the larger (O + S) content.

In terms of relative composition of inclusions in consumable A, larger heat input leads to moderate reduction of Ti content with a concomitant increase in Mn content found in each dominant inclusion type. Comparison among the inclusion sizes of Ti-Mn-S with Ti-Mn-S-Si types demonstrates that the effect of Si on inclusions size, i.e. the Si bearing inclusions have larger inclusion size. It appears that the Si effect on inclusion size is more prominent at higher (O + S) content and higher heat input. For instance, when the heat input increases from 2.0 to 3.0 kJ/mm, the proportions of Si bearing inclusions increases from 6% to 38 - 48% of all inclusions. Furthermore, the proportion of Si bearing inclusions in the large inclusion (>1 μm) group increases from 23% to over 90% at higher heat input.

Effect of Welding Position at 2.0 kJ/mm: The possible effect of welding position 1G versus 3G on inclusion distribution was investigated only for the deposits of consumable C. The inclusions are characterized as basically Ti-Mn-S with varying amounts of Ca and Si (Table 3.6). In terms of composition, the relative content of Ti in the inclusions decreases with a concomitant increase in relative Mn content when the welding position changes from flat to vertical position. Similar effect of Si on inclusion sizes is observed.

Given the higher oxygen or (O + S) contents in 3G welds, it is expected to have more inclusions in 3G deposits. However, the overall inclusion characteristics (average size, number density or volume fraction) do not change significantly with the welding position or the (O + S) content (Table 3.6). Furthermore, although the higher (O + S) contents in 3G welds do not lead to different dominant inclusions, it does affect the proportion of each dominant type. For instance, the Ti-Mn-S-Si inclusions occupy only 6% of all inclusions for the 1G weld versus 46% of all inclusions in 3G position. The predominance of larger inclusion species of Si bearing inclusions is in accordance with the argument presented in Section 1. Because of the cascading slag which tends to flow away from the weld pool, the ascending inclusions are trapped in the weld metal rather than in the slag phase. Because of its low affinity for sulphur, the increased recovery of Si in inclusion is likely due to the larger oxygen contents in 3G welds i.e. increase from 630 ppm to 721 ppm. Furthermore, the aspect ratio for all dominant inclusions decreases at higher (O + S) content, i.e. higher (O + S) contents lead to less equiaxed inclusions.

3.3 Quantitative Metallography

3.3.1 Macrostructure

The macrostructural distributions along the weld centerline in the through thickness dimension are tabulated in Table 3.7. The representative macrographs are included in Figures 3.4 to 3.17 for reference. In summary, all double vee joints have more than 60% reheated regions at the weld centerline. Larger heat input further enhances the proportion of the reheated region. In comparison, the flat position welds of consumable C have more reheated regions along the weld centerline than both consumables A and B, whereas the 3G welds have similar macrostructure proportions made with consumables B and C. The macrostructure for the 1G deposits of consumables A and B are virtually identical at each heat input, thus confirming the similarity among the two consumables.

Relative to the welds made in the flat position, it seems that the proportion of reheated regions increases moderately for out of position welds. The shorter stick-out and 20° push angle used in out of position welding may increase the penetration resulting in a larger reheated region associated with each bead.

3.3.2 Microstructural Characterization

The microstructural characteristics of the last deposited bead are tabulated in Table 3.8, and the representative micrographs are included in Figures 3.18 to 3.31 for reference. The second phase associated with ferrite (aligned or nonaligned) is a generic term and includes, individually or in combination, the martensite, the retained austenite, and carbide constituents. While the special etchants did not work for these deposits to reveal the characteristics of the M-A-C phase, previous studies on C-Mn-Ni SMAW deposits[3.7,3.8,3.9] have indicated that M-A phase is present in both as-deposited and reheated regions. The amount of M-A phase was constant up to about 2% Ni and increased thereafter until about 3.5%[3.9]. Secondly, M-A constituent also seems to be present in the second phase that is trapped between the basket weave acicular ferrite laths[3.8]. Despite the abundance of Ti bearing inclusions in all deposits, their acicular ferrite proportion is relatively low, ranging from 23-54%. The microstructures instead have substantial amounts of ferrite with second phase. This phase is usually associated with the grain boundary in deposit C and therefore may be termed as Widmanstatten ferrite. In deposit A, in comparison, the ferrite with aligned second phase is found in grain interiors and therefore likely to be upper bainite. These effects in turn may be qualitatively related to deposit compositions, i.e. higher oxygen contents (528-766 ppm) reduce hardenability by promoting the formation of Widmanstatten ferrite; however, in deposit A, this influence is more than compensated by its richer chemistry (higher carbon equivalent, Table 3.2).

For consumable A, the 3G deposit in the earlier study[3.1] had much higher acicular ferrite proportion (>80%) and this could be related not only to latter's higher Ti and B content, but also higher carbon content (.06-.08%) since, as pointed out by Bahdeshia[3.6], C content in the range .03 to .07% can have a tremendous influence on the transformation behaviour.

For deposits of both consumables A and C in 1G position, larger heat input leads to larger proportions of acicular ferrite and ferrite with non-aligned second phase at the expense of ferrite with aligned second phase. It is of interest to note that the proportions of ferrite with second phases (both aligned and non-aligned) are similar in deposits of both the consumables at the same heat inputs. In comparison, deposits of consumable C have a higher acicular ferrite content than consumable A. Furthermore, the amount of acicular ferrite also in deposits welded in 3G position, possibly due to higher C contents therein.

With regard to the effect of the stress relief heat treatment, the weld metal deposited in 3G position with consumable B shows significant precipitation taking place at grain boundaries which was absent in the as-welded deposit (Figure 3.32). Similar extensive precipitation occurred in the welds made in the flat position. Visual examination of these photomicrographs (Figures 3.33 and 3.34) suggest the prevalence of grain boundary precipitation is not effected by the changes in welding position or heat input. However, a more definitive quantification on the exact sizes and density of these precipitates would require a detailed image analysis. In addition, examination at higher magnification is required to ascertain the presence/absence of microprecipitates.

Regardless of welding position and heat input, similar extensive grain boundary precipitations are also observed in the deposits of consumable C (Figures 3.35-3.37).

Due to the prevalence of grain boundary precipitation after stress relief heat treatment, an attempt to quantify the extent of precipitation was made by microstructure characterization with point counting. Since there is no established practice/guidelines regarding the designation of microstructural phase in stress relief state, the following designations were used:

- coarse ferrite - this is the equivalent of grain boundary ferrite and polygonal ferrite in the as-welded state.
- acicular ferrite - this is the ferrite that retain its acicular appearance but has no grain boundary precipitation.
- ferrite with precipitated second phase - wherein the grain boundaries are delineated with precipitates.

The point counting was undertaken on the last deposited bead on the second side of stress relieved welds at a magnification of 400X with 500 points. The results are tabulated in Table 3.9. These crude estimates concur with the optical examination that there is extensive precipitation taking place as a result of stress relief heat treatment. Based on previous studies[3.7,3.8,3.10], the precipitates visible in the optical microscope are presumably cementite, and they are the decomposition product of the M-A phase.

3.4 Lateral Shrinkage Measurements

The transverse lateral shrinkage measurements are summarized in Table 3.10. The full documentation of shrinkage measurements is included in Appendix B.

Since the magnitude of restraint can be assessed, at least qualitatively, by the extent of transverse shrinkage across the weld, the data of shrinkage measurements is discussed in terms of angular and lateral restraint conditions for each weld. Given the much smaller transverse shrinkage in the high restraint weld, it is suffice to say that the rigid restraint set up was effective to limit transverse shrinkage and minimize angular distortion.

In the high restraint weld (F11A), the fillet welded side plates and stiffeners offer such high rigidity that the plate movement is limited, therefore the transverse (free) shrinkage is accommodated primarily by weld zone deformation and elastic extension (stress) in the parent plate. The observed increases in L1 and L3 spacings, i.e. tension in the base plate away from the welded region is therefore as anticipated (Appendix B, Table B.2). In contrast, since the low restraint set up (F10A) allows relatively free movement in response to weld contraction, the (free) transverse shrinkage is accommodated by relatively smaller amount of weld zone deformation and some physical plate movement. Because of the relative ease in the plate movement, the resultant tension in the base plate is low, thus the recorded changes in L1 and L3 spacings are small in the low restraint weld (Appendix B, Table B.1).

However, before proceeding further with the analysis of the shrinkage data numbers, it should be noted that in discussing the restraint welds in the submerged arc welding program, it was speculated that the spacing measurements on the plate surface may underestimate the actual transverse shrinkage at the root pass. In fact, the joint geometry (included angle and gap opening) may have been changing. In order to address this experimental uncertainty, cross sections were taken at the completion of each pass for the first three root passes and the joint openings measured at T/4, T/2, and 3T/4 locations (macogrpahs are included in Appendix B, Figures B.1 to B.6). These measurements, however, show no significant changes in the through thickness dimensions for each of the three root passes (Table 3.11). It is therefore surmised that the measurement technique is adequate for assessing the shrinkage measurements due to the root passes.

Another possible source of error in the shrinkage measurement is the occurrence of angular distortion which may lead to overestimation of the transverse shrinkage, i.e. the actual spacings would have been larger than the measured spacing such that the apparent measured shrinkage is larger than the true value. Based on simple geometric considerations as schematically illustrated in Figure 3.38, the estimated error from the angular distortion is:

$$\partial = 2L\,[1 - \sin(90 - \beta)]$$

where β is the measured angular distortion.

Since L2 spacing is about 76 mm, the error associated with the largest angular distortion of 1.0° corresponds to a maximum error of 0.02 mm which is similar to the typical scatter in any set of measurements. The transverse shrinkage measurements are, therefore, deemed valid, even for the low restraint weld.

In examining the progressive increase in shrinkage, it is noted that for both the 'restraint' welds, there is a trend of decreasing incremental shrinkage with further weld passes as each preceding layer contributes further restraint for the succeeding deposits (Figure 3.39). This implies that relative to the total shrinkage at the completion of the weld, the shrinkage accompanying the root passes are disproportionately large. In the low restraint weld, the total shrinkage from the first three root passes contributes almost 50% of the total transverse shrinkage whereas it is about 30% for the high restraint weld. Since lower measured shrinkage implies greater plastic strain in the weld zone for the same welding procedure, the 'high restraint' weld metal should be more susceptible to strain age embrittlement. The difference at root locations, however, may be somewhat smaller on account of the possible effect of local bending and angular distortion on the magnitude of plastic strain at the root in the low restraint weld.

3.5 Tensile Properties and Hardness Results

The tensile properties and Vickers hardness (10 Kg load) measurements are summarized in Tables 3.12 to 3.15.

In summary, all deposits show decreasing tensile strengths and hardness with higher heat input and stress relief heat treatment. For a given heat treatment and heat input, the deposits of consumable C have lower hardness and strength than for consumables A and B. In the 'restraint welds', it is of interest to observe the through thickness variation in average hardness with the anticipated plastic deformation in each restraint condition. Recalling that in the higher restraint case, plastic deformation would be higher and more uniform in the through thickness dimension. It is expected that the hardness would follow a similar trend. In the root and T/2 locations, the average hardness in the high restraint welds is higher than the low restraint weld (Table 3.12). The negligible difference in hardness at the subsurface locations between the two welds suggests that the influence exerted by external restraint becomes secondary when the weld is ≈ 90% filled.

3.6 Drop Weight Testing

The full documentation of drop weight test results is tabulated in Appendix C. The nil ductility temperature data are summarized in Table 3.16. Even though the data base is rather small, it seems that larger heat input leads to higher NDT temperature. The reduction in toughness is more severe in the 'stress relieved' deposits of consumable B than in the 'as-welded' deposits of consumable A. If it is assumed that consumables A and B are essentially similar then it would seem that the stress relief treatment at the lower heat input can lead to some further lowering of the NDT temperature, whereas at the higher heat input, there is potential for an increase in the NDT temperature.

3.7 CVN Notch Toughness

The full documentation of CVN data and individual transition curves is included in Appendix D. The transition temperatures and comparative transition curves are included in Tables 3.17 to 3.20 and Figures 3.40 to 3.52 respectively.

Prior to further discussion on the observed CVN toughness, it is important to reiterate the assumption being made viz. the deposits of consumables A and B are similar in light of their identical AWS classification, consumable B as a modified version of A, and weld deposit analyses.

Effect of Heat Input: Heat input was a variable for the welds made in the flat position only.

For the as-welded deposits of consumable A, the upper shelf energy for higher heat input deposit is larger than that for the lower heat input deposit (Figure 3.40). This occurs in spite of the higher (O+S) content of the high heat input deposit, presumably because of its significantly lower yield and ultimate strength. Considering the 40J transition temperature, it is unaffected by the increase in heat input for the subsurface location. However, at the root location, the 3.0 kJ/mm deposit had a lower transition temperature by 12°C (Table 3.17). Since the experimental uncertainty in determination of 40J transition temperature is estimated to be approximately 5°C, the improvement in the 40J transition temperature at the root location is considered to be a valid observation. The improved notch toughness at low temperature is attributed partially to the higher acicular ferrite at the larger heat input (Table 3.8).

For consumable B deposits in stress relieved condition, both the subsurface and root locations show reductions in CVN toughness at the higher heat input (Figure 3.40). The increase in 40J transition temperature being 19°C and 24°C for the subsurface and root locations respectively (Table 3.18). In terms of the upper shelf toughness the effect of heat input is very marginal for consumable B deposits.

For the as-welded deposits of consumable C, higher heat input shifts the entire transition curve to higher temperature (Figure 3.41) resulting in increases of 14°C (root) and 22°C (sub- surface) in the 40J transition temperatures (Table 3.19). In the stress relieved condition, the same adverse effect of heat input on CVN toughness presist such that the 40J transition temperatures increase by 14°C (subsurface) and 45°C (root) for the higher heat input deposit.

In summary, higher heat input generally leads to reduced notch toughness regardless of specimen locations or the post weld heat treatment condition. The only exception seems to have been the root location for the consumable A deposit where the 40J transition temperature decreased by 12°C. Overall, consumable A deposit in the as-welded condition seemed more resistant to decline in toughness as a result of increased heat input. However, consumable C had better toughness to begin with at the lower heat input, so that at the higher heat input, the toughness of deposits from consumable A and C are comparable. For some unexplained reason, the root region of the higher heat input -stress relieved weld with consumable C showed the largest observed increase in the transition temperature (45°C).

The different responses of deposits A and C can be rationalized in terms of microstructural changes accompanying the increase in heat input. In deposit A, the acicular ferrite content increases, whereas the ferrite with aligned second phase decreases, thus explaining the absence of any deterioration in CVN toughness. In contrast, although similar changes in microstructure occur in deposits of consumable C, the amount of grain boundary ferrite, that is coarser as well, increases and the ferrite with aligned second phase is more frequently located adjacent to the grain boundary ferrite, thus leading to lower CVN toughness.

Effect of Stress Relief Heat Treatment: Regardless of CVN specimen locations, welding positions, and heat inputs, the stress relief heat treatment consistently shows an adverse effect on CVN toughness by shifting the transition curves to higher temperatures (Figures 3.42 and 3.43).

Treating consumables A and B to be surrogates for each other as mentioned before, the observed deterioration in the 40J transition temperature is no more than 24°C for the deposits made at 2.0 kJ/mm. At 3 kJ/mm, however, the increase in transition temperatures can be as high as 35 to 43°C (Figure 3.44).

The deleterious effect of stress relief on CVN toughness is rationalized by the presence of grain boundary precipitates after stress relief. Recalling the microstructural observations presented in Section 3.3.2, it was shown that stress relief had led to significant precipitation of second phase (carbides) at grain boundaries. The prevalence of grain boundary precipitates in the stress relieved deposits may lead to an embrittling effect by offering a fracture propagation path of lower crack resistance. In contrast, in the as-welded condition, the second phase is comprised of martensite and retained-austenite aggregates (MA) which are of small size and randomly distributed. The random distribution of MA does not significantly reduce the toughness except when it is in the form of ferrite with aligned second phase for which the crack propagation is facilitated along a path. Hence, it is surmised that the grain boundary precipitation is responsible for the reduced CVN toughness of stress relieved deposits.

Effect of Specimen Location:

The differences in the 40J transition temperatures with specimen location for various welds are summarized in Table 3.21. There is no obvious trend in regard to CVN toughness being consistently better for one location than the other. The difference in 40J transition temperature between the two locations is usually in the range ± 10°C, the lone exception being the stress relieved weld made at 3 kJ/mm with consumable C. Since the first pass on side 1 was only partially removed by backgouging, and CVN specimens typically sampled 50% unrefined-refined macrostructures at each location, these numbers suggest that the strain aging and/or dilution effects usually associated with toughness deterioration at root locations are not particularly dominant with the consumables investigated here, and that may be due to the relatively low nitrogen content of the deposits.

Effect of Welding Position

The effect of welding position on changes in the 40J CVN transition temperature is summarized in Table 3.22. Presuming the equivalence of consumables A and B, the 3G welds seem to have lower transition temperature than the 1G welds. With consumable C on the other hand the differences are marginal.

Overall, the majority of CVN results show that the toughness of the vertical up welds in this investigation is similar or better than that of welds made in the flat position. Although this observation seems to contradict the general perception that welds made in the 3G position have inferior toughness to those made in the 1G position [3.11], it should be noted that in this program, comparisons are being made without the interference due to simultaneous variation in heat input, weaving, macrostructure at the CVN notch, etc. Furthermore, the microstructural characterization shows that in the 3G position, the acicular ferrite content is higher than in the 1G position for both consumables B and C.

Effect of Joint Restraint: At each of the CVN specimen locations, the high restraint deposit consistently shows better CVN toughness than the low restraint weld (Figures 3.50 and 3.51), the difference in 40J transition temperature being ≈ 16°C. The variation in the 40J transition temperature from different specimen locations is rather small for each weld.

In the presence of high lateral restraint, more uniform toughness is expected along the weld thickness and that is as observed. It was also expected that high restraint welds will have lower toughness but the results contradict this. This discrepancy cannot be attributed to the minor difference in macrostructures sampled since all specimens had approximately 50% as-deposited region, or to the small angular distortion subsequent to the 2nd pass (0.4° for low restraint joint and 0.1° for the high restraint joint), because the reduction in toughness persists at the subsurface location also.

Effect of Joint Geometry - Double Vee Versus Single Vee: Although the single vee welds are made under different restraint conditions compared to the double vee welds, the observed CVN toughness from the two extreme lateral restraint conditions should represent the range of toughness achievable with restraint as a variable, and should straddle the toughness of the reference double vee weld. The observed 40J transition temperature is within the range of ≈ -90° to -61°C for the restraint single vee welds but the CVN toughness observed in the double vee deposits, regardless of procedural parameters, is usually much lower. For the same consumable A, the lowest 40J transition temperature is -47°C at 2 kJ/mm heat input for all the double vee welds. Since the macrostructure at the CVN notch is ≈ 50% refined and 50% unrefined in each case, the influence of joint geometry is not easily explained. The only difference between the single vee and double vee welds seems to be the former lower yield strength by ≈ 35 MPa at room temperature.

Comparison Between the Three Consumables: In comparing the results for welds made with different consumables but under nominally similar conditions, it is observed that the deposits of consumable C usually gave lower 40J transition temperatures than those from consumables A or B (ten out of twelve transition curves). Marginally higher acicular ferrite content as well as the lower strength of the consumable C weld deposits are both believed to be responsible for their better toughness, at least in the as-welded condition.

3.8 CTOD Toughness

The full documentation of the individual CTOD test data is included in Appendix E. The average CTOD values are summarized in Tables 3.23 and 3.24.

The direction of changes in CTOD values with heat input, stress relief treatment, welding position, restraints, etc. are best assessed by comparing the values at -30°C. The overall trends are similar to those for CVN toughness values. Thus, increasing the heat input from 2 to 3 kJ/mm leads to a substantial reduction in CTOD values for both consumable A and C deposits in the as-welded condition. In the stress relieved condition, heat input has only a marginal effect on the CTOD values.

The effect of stress relief treatment on welds made in the 1G position is also to reduce the CTOD toughness, though the effect is more pronounced at the lower heat input. At the higher input, the effect is once again very marginal, and as a matter of fact, consumable C deposit shows a slight increase in the CTOD values.

The welds made in the 3G position are somewhat unique in that the stress relief treatment leads to significant increase in CTOD values for both consumables A and C. This is observed in spite of the higher carbon content of the welds made in the 3G position so that compared to the 1G position, the volume fraction of carbides (cementite) can be expected to be higher in 1G welds thereby providing more numerous sites for initiation. Presumably, these are subcritical in size from the point of view of cleavage initiation.

Effect of Joint Restraint and Geometry: As far as the effect of joint restraint is concerned, the result in Table 3.24 indicate that the lower restraint weld has marginally better CTOD toughness, both at -30°C and -50°C. This is consistent with the hypothesis presented before that larger plastic deformation of the weld zone in high restraint welds should lead to lower toughness. It should be recalled that the CVN toughness results indicated an opposite trend.

It was speculated that the restraint would affect the toughness of the first few passes deposited to a greater extent. However, for single vee welds, these are nearer the weld surface, whereas initiation in CTOD specimens occurring in the middle third of the thickness. Therefore, surface notched CTOD specimens were tested with fatigue crack front located in the as deposited region of the third pass from the root. Contrary to expectation, but similar to CVN results, the results (Table 3.24) show significantly higher CTOD toughness for the high restraint weld at -30°C.

Finally, it should be noted that as was the case for CVN toughness, the CTOD values are higher for the single vee welds in comparison with those obtained from the double vee welds.

3.9 SEM Fractography on Selected CTOD Specimens

The micrographs and EDX analysis of successful SEM fractographic examinations are included in Appendix F. The results are discussed in the following paragraphs.

Twenty-four CTOD specimens from double vee weldments were selected for SEM fractographic analysis. Attempts to locate the cleavage initiation site were successful in only eight of these specimens. The methodology used was as follows. First, a low power stereoscope is used to identify probable fracture initiation site(s); next, SEM examination is carried out to locate the cleavage initiation site by following the cleavage river lines back to its origin (Figure 3.53). Detailed observation of its surrounding fractographic features are noted; EDX spectrums for both the cleavage initiation site and its surrounding matrix are taken and compared to verify its nature, then careful sectioning and polishing are carried out in an attempt to identify the microstructure associated with the cleavage initiation site. However, the success rate for the latter procedure is low. The criterion for successful observation on microstructure adjacent to the initiation site is that the polishing/observation plane be within 10 μm of the site itself, otherwise the separation is considered to be larger than the average microstructural features relevant to the cleavage initiation site.

The SEM observation on cleavage sites are summarized as follows:

(i) In terms of through thickness dimension, the initiation sites were consistently located in the first or second root pass of side 1.

(ii) In the majority of the successful attempts, the fracture initiation occured in the reheated regions (both fine grain and coarse grain).

(iii) The observed cleavage initiation sites were relatively large in size (> 0.5 μm - 2.0 μm). The EDX spectra from the cleavage initiation sites were in agreement with the dominant inclusion types as reported in the inclusion analysis (Section 3.2), viz. Ti-Mn-Si-(S). The presence of Si in most of the inclusions detected for the cleavage initiation is in accordance with the observation of effect of Si on inclusion size. A surprising observation is the detection of Al in cleavage initiating inclusions despite low proportion of such inclusions reported in the present inclusion analysis.

(iv) There was no evidence found in the eight successfully examined specimens, that would indicate the cleavage initiation at second phase precipitates although Abson [3.12] had reported one such observation. Furthermore, despite occasional slag and porosity present near the much smaller initiation sites (Figure F7, Appendix F), the cleavage river lines do not radiate from the slag or porosity. The slag/porosity observed in some specimens therefore is not expected to have affected the CTOD values significantly.

3.10 Weld Metal Diffusible Hydrogen Content

The diffusible hydrogen contents in the weld metals were found to be 2.52 ml/100 g, 1.95 ml/100 g and 3.45 ml/100 g of deposited or fused weld metal for consumables A, B and C respectively. These flux cored wires can be classified as low hydrogen consumables.

3.11 Gapped Bead on Plate (GBOP) Testing

With the exceptions of consumable C test at 20°C (Table 3.25) there was no weld metal cracking observed in any of the other tests. This is consistent with the relatively low weld metal diffusible hydrogen content and qualitatively points to good resistance to weld metal hydrogen cracking.

4.0 CONCLUDING SUMMARY

A total of fourteen flux cored arc welds have been prepared with three commercially available consumables, and incorporating changes in welding procedural variables such as heat input, post weld condition, welding position and lateral joint restraint. The observed changes in CVN and CTOD toughness have been qualitatively explained in terms of the deposit chemistry, macrostructure and microstructure, inclusion distribution, etc. The principal observations can be summarized as follows:

(i) Effect of Heat Input: With only one exception, viz. the CVN toughness of the 1G deposit with consumable A, higher heat input has led to reduced toughness. The exception shown by consumable A to this general trend has been rationalized by the observed changes in microstructure - higher acicular ferrite content and lower inter-granular ferrite with aligned second phase.

(ii) Effect of Stress Relief: Although stress relief heat treatment had led to reduced CVN and CTOD toughness for 1G deposits, the observations for the welds in the 3G position were conflicting in that stress relief was accompanied by lower CVN toughness but higher CTOD toughness.

The lower CTOD toughness of the 1G deposits on stress relieving is attributed to the presence of accompanying general precipitation, including that at grain boundaries.

(iii) Effect of CVN Specimen Location: There was no consistent trend of subsurface specimens yielding superior or inferior toughness than the root specimens. This, it is believed, is due to the relatively low nitrogen content of the weld metal so that there is limited strain aging damage, and the differences in toughness for the specimens extracted from the two locations are likely due to other reasons such as minor variations in local macro and microstructure.

(iv) Effect of Welding Position: Welds made in the 3G position (stringer beads, 2 kJ/mm) had higher toughness than the corresponding welds in the 1G position. Although this observation is in apparent contradiction to the general perception that 3G welds have inferior toughness in comparison with 1G welds, the findings are consistent with the observation of higher acicular ferrite in the 3G position, most likely caused by their higher carbon content than for the 1G welds.

(v) Effect of Lateral Joint Restraint (Single Vee Welds): Although lower toughness was anticipated for the higher restraint weld, the CVN results and surface notched CTOD specimens (root side notch) show the opposite. The through thickness CTOD specimens, however, did indicate marginally superior toughness for the lower restraint weld.

The relatively small total nitrogen content, as well as the low free nitrogen content of weld metal as implied by the near optimum value of unbalance factor, may be once again responsible for the absence of the anticipated effect of restraint in toughness.

(vi) Comparison Between the Consumables: Weld deposits made with consumable C have usually shown better CVN and CTOD toughness than those from consumable A (as-welded conditions) and consumable B (stress relieved condition). In the as-welded condition, this could be attributed to greater acicular ferrite content and lower strength of the consumable C deposit. However, higher heat input and stress relief treatment lead to greater deterioration in consumable C deposit toughness so that at higher heat input or in stress relieved condition, at least the CVN toughness values are comparable.

5.0 REFERENCES

- Section 1.0 - Introduction

[1.1] Bala, S. and Santyr, S., "Evaluation of Flux Cored Arc Welding Consumables for Offshore and Arctic Structures Fabrication". AMCA International Ltd. Report 7-185-096 (1984).

[1.2] Dawes, M.G., "Fracture Initiation in Weld Metal". Welding and Metal Fabrication, 40, p.95-103 (1972).

[1.3] Nicholson, S. and Rogers, P.F., "Controlling Weld Metal Toughness in Manual Metal Arc Welds". Welding in Offshore Construction, Welding Institute (1974).

[1.4] Still, J.R., George, M.J. and Terry, P., "Economic Welding Parameters for Demanding Applications". Metal Construction, 10, p.488-492, (1978).

[1.5] Evans, G.M., "Effect of Welding Position on the Microstructures and Properties of C-Mn All Weld Metal Deposits". Welding Research Abroad, 29, p.58-69, (1983).

[1.6] Cochrane, R.C., Terry, P., and Garland, J.G., "Root Run Toughness in Multipass Manual Metal". Welding and Metal Fabrication, 44, p.441-448, (1976).

[1.7] Robinson, J.L., "A Study of Factors Controlling Root Toughness in Multipass Manual Arc Welds in C-Mn Steels". Welding Institute Research Report 41/1977/M (1977).

[1.8] Leggett, R.H., "Studies on the Dependence of Weld Metal Toughness on the Level of Test Panel Restraint: Final Report". Welding Institute Research Report 255/1984 (1984).

- Section 2.0 - Experimental Descriptions and Methodology

[2.1] Bala, S.R. and Santyr, S., "Evaluation of Flux Cored Arc Welding Consumables for Offshore and Arctic Structures Fabrication". AMCA International Ltd. Report 7-185-096 (1984).

[2.2] Leggett, R.H., "Studies on the Dependence of Weld Metal Toughness on the Level of Test Panel Restraint: Final Report". Welding Institute Research Report 255/1984 (1984).

[2.3] Pargeter, R.J. and Dolby, R.E., "Identification and Quantitative Description for Ferritic Steel Weld metal Microstructure". IIW Doc. IX-1323-84 (1984).

[2.4] Towers, O.L. and Robinson, P., "Procedures for Fatigue Cracking Fracture Toughness Test Pieces, With Particular Reference to Weldments". Welding Institute Research Bulletin, 23, p.112-120 (1982).

- Section 3.0 - Results and Discussion

[3.1] Bala, S.R. and Santyr, S., "Evaluation of Flux Cored Arc Welding Consumables for Offshore and Arctic Structures Fabrication". AMCA International Ltd. Report 7-185-096 (1984).

[3.2] Lathabai, S. and Stout, R.D., "Shielding Gas and Heat Input Effects on Flux Cored Weld Metal Properties". Welding Journal, 64, p.303s-313s, (1985).

[3.3] Evans, G.M., "Effect of Welding Position on the Microstructure and Properties of C-Mn All Weld Metal Deposits". Welding Research Abroad, 29, p.58-69, (1983).

[3.4] Widgery, D.J., "Deoxidation Practice for Mild Steel Weld Metal". Welding Journal, 55, p.57s-68s, (1976).

[3.5] Bala, S., Chiu, C. and Morrison, K., "Evaluation of Heat Affected Zone and Weld Metal Toughness in Selected Steels - Phase II". AMCA International Ltd. Report 7-185-141-099 (1986).

[3.6] Bahdeshia, H.K.D.H., "Modelling of Fusion Zone Microstructure in Steel Welds". Keynote Lecture No. 8, Second ASM International Conference on Trends in Welding Research, Gatlinburg, TN (1989).

[3.7] Bala, S.R., Chiu, C., and Morrison, K., "Evaluation of Heat Affected Zone and Weld Metal Toughness in Selected Steel - Phase II". AMCA International Report 7-185-141-099/I (1986).

[3.8] Braid, J.E.M. and Gianetto, J.A., "The Effects of PWHT on the Toughness of Shielded Metal Arc Weld Metals for Use in Canadian Offshore Structure Fabrication". Welding for Challenging Environments, WIC, (1986).

[3.9] Taylor, D..S. and Evans, G.M., "Development of MMA Electrodes for Offshore Fabrication". Metal Construction, 15, p. 438-443, (1983).

[3.10] Evans, G.M., "The Effect of Stress Relieving on the Microstructure and Properties of C-Mn All Weld Metal Deposits". Welding Journal, 63, p. 326s-334s, (1984).

[3.11] Dawson, G.W. and Judson, P., "Procedural Guidelines for the Achievement of Tough Welded Joints in Structural Steels For Offshore Applications". Second International Conference on Offshore Welded Structures, The Welding Institute (1983).

[3.12] Abson, D.J., "Microstructure and Mechanical Properties of Vertical Up C-Mn-Ni Steel Semi-automatic Weld Metal". Welding Institute Research Report 344/1987 (1987).

TABLES

Table 2.1

Characterizations of the Base Plate

C	Mn	S	P	Si	Cr	Ni	Al	Nb	V	Cu
0.14	1.27	0.01	.017	0.29	0.03	0.17	0.04	0.032	0.043	0.2

Yield Strength (MPa)	Ultimate Tensile Strength (MPa)	% Elongation	CVN Impact Energy @ -60°C (J)	
			Transverse	Longitudinal
364	510	29	66	129

Table 2.2

Summary of Typical Chemistries and Toughness for the Three Consumables (Manufactuer's Information)

Consumable	Hydrogen Content ml/100g	Yield Strength (MPa)	Typical Weld Metal Composition (w/o)						Typical CTOD Toughness -10° C (mm)		Typical CVN Toughness @ 60°C (J)	
			C	Mn	Si	S	P	Ni	Vertical	Flat	Flat	Vertical
A	4.3	502	0.04	1.3	0.28	0.01	0.01	1.5	0.7 - 1.3 @ 1.9 kJ/mm	0.8 - 0.9 @ 1.9kJ/mm	46-56 @ 1.9 kJ/mm	42 @1.0 kJ/mm
B	3.8	502	0.05	1.3	0.28	0.01	0.01	1.4	1.0 - 1.2 @ 2.2 kJ/mm	0.7 - 0.9 @ 1.7kJ/mm	62-85 @ 1.7 kJ/mm	55-78 @2.2 kJ/mm
C	N/A[+]	540	0.05	1.2	0.35	N/A	N/A	1.0	Not Available		96J at -40°C	

*The CTOD toughness is evaluated at -10°C, multipass weldments, double V geometry, 40mm thick and as welded condition.

[+] N/A = Not Available

Table 2.3
Experimental Matrix For
Flux Cored Arc Welds

Consummable	Position	Joint Geometry	Heat Input (kJ/mm)	Post Weld Condition	Weld I.D.
A	Flat (1G)	Double V	2.0	AV*	F5A,F5B
			3.0	AV	F1A,F1B
		Single V	2.0(LR)*	AV	F10A,F10B
			2.0(HR)	AV	F11A,F11B
B	Flat (1G)	Double V	2.0	SR	F6A,F6B
			3.0	SR	F2A,F2B
	Vertical Up (3G)	Double V	2.0	AV	F7B
				SR	F7A
C	Flat (1G)	Double V	2.0	AV	F9B
				SR	F9A
			3.0	AV	F3A,F3B
				SR	F4A,F4B
	Vertical Up	Double V	2.0	AV	F8B
				SR	F8A

* AV = As Welded; SR = Stress Relieved
LR = Low Restraint; HR = High Restraint

Table 2.4

Summary of Welding Procedures
Flux Cored Arc Welds

Shielding Gas	Gas Flow Rate (l/min)	Joint Geometry	Welding Post'n	Heat Input (kJ/mm)	Volt. (V)	Current (Amp)	Travel Speed (mm/sec)	Electrode Stickout (mm)	Polarity
75% Ar 25% CO_2	20	Double V	1G	2.0	25	250	3.2	19	DC-RP
				3.0	32	300	3.2	19	DC-RP
			3G*	2.0	24	180	2.2	16	DC-RP
		Single V	1G	2.0	30	300	4.5	19	DC-RP

*20° push angle

CONSUMABLE	POSITION	HEAT INPUT (KJ/mm)	PWHT	PLATE ID	LOCATION	C	Mn	Si	S	P	Ti	Mo	Al	Nb	O	N	Cr	Ni	Cu	V	B
A	1G	2.0	AW	F3B	SUBSURFACE	0.033	1.51	0.34	0.010	0.013	0.036	0.007	0.003	0.014	0.0556	0.0080	0.041	1.290	0.031	0.008	0.0009
A	1G	2.0	AW	F3B	ROOT	0.031	1.48	0.62	0.010	0.014	0.016	0.004	0.002	0.010	0.0563	0.0046	0.040	1.320	0.020	0.014	0.0014
A	1G	3.0	AW	F1B	SUBSURFACE	0.042	1.42	0.45	0.011	0.008	0.021	0.005	0.003	0.016	0.0526	0.0030	0.041	1.270	0.044	0.022	0.0017
A	1G	3.0	AW	F1B	ROOT	0.032	1.40	0.47	0.011	0.013	0.046	0.006	0.002	0.016	0.0716	0.0071	0.037	1.350	0.030	0.021	0.0013
B	1G	2.0	SR	F4A	SUBSURFACE	0.035	1.30	0.33	0.013	0.015	0.029	0.007	0.002	0.014	0.0658	0.0042	0.041	1.310	0.021	0.010	0.0013
B	1G	2.0	SR	F4A	ROOT	0.036	1.34	0.33	0.013	0.015	0.035	0.007	0.003	0.017	0.0676	0.0043	0.041	1.300	0.004	0.012	0.0015
B	1G	3.0	SR	F3B	SUBSURFACE	0.043	1.34	0.27	0.014	0.012	0.028	0.007	0.003	0.013	0.0765	0.0041	0.041	1.350	0.052	0.024	0.0018
B	1G	3.0	SR	F3B	ROOT	0.046	1.30	0.30	0.013	0.010	0.050	0.006	0.003	0.016	0.0680	0.0040	0.041	1.340	0.041	0.022	0.0013
B	3G	2.0	AW	F7B	SUBSURFACE	0.062	1.18	0.55	0.012	0.011	0.044	0.007	0.006	0.015	0.0772	0.0032	0.042	1.340	0.045	0.022	0.0005
B	3G	2.0	AW	F7B	ROOT	0.057	1.32	0.23	0.013	0.015	0.046	0.007	0.006	0.017	0.0687	0.0040	0.041	1.340	0.053	0.024	0.0013
C	1G	2.0	AW	F5B	SUBSURFACE	0.053	1.18	0.37	0.010	0.013	0.029	0.001	0.007	0.022	0.0683	0.0052	0.029	0.030	0.041	0.031	0.0014
C	1G	2.0	AW	F6B	ROOT	0.048	1.15	0.35	0.011	0.015	0.025	0.001	0.006	0.018	0.0630	0.0037	0.028	0.087	0.030	0.029	0.0019
C	1G	3.0	AW	F2B	SUBSURFACE	0.062	1.15	0.33	0.012	0.007	0.018	0.001	0.000	0.012	0.0710	0.0049	0.028	0.085	0.041	0.029	0.0022
C	1G	3.0	AW	F2B	ROOT	0.057	0.94	0.30	0.011	0.008	0.028	0.001	0.006	0.015	0.0711	0.0053	0.026	0.080	0.034	0.026	0.0021
C	3G	2.0	AW	F6B	SUBSURFACE	0.062	0.96	0.26	0.010	0.011	0.029	0.001	0.010	0.017	0.0680	0.0041	0.027	0.083	0.048	0.030	0.0010
C	3G	2.0	AW	F6B	ROOT	0.070	1.01	0.26	0.011	0.012	0.026	0.001	0.005	0.016	0.0721	0.0046	0.027	0.087	0.047	0.029	0.0021

Table 3.1: Summary of weld metal composition

CONSUMABLE	POSITION	PLATE ID	HEAT INPUT (KJ/mm)	LOCATION	O+S (WT %)	Unbalance factor (WT %)	CE (IIW) (WT %)	Pcm (WT %)
A	1G	F5B	2.0	SUBSURFACE	0.0656	0.0108	0.3863	0.1566
A	1G	F5B	2.0	ROOT	0.0663	0.0065	0.3791	0.1583
A	1G	F1B	3.0	SUBSURFACE	0.0638	0.0131	0.3799	0.1596
A	1G	F1B	3.0	ROOT	0.0828	0.0158	0.3711	0.1510
B	1G	F6A	2.0	SUBSURFACE	0.0788	0.0126	0.3538	0.1429
B	1G	F6A	2.0	ROOT	0.0808	0.0161	0.3989	0.1572
B	1G	F2B	3.0	SUBSURFACE	0.0906	0.0142	0.3509	0.1490
B	1G	F2B	3.0	ROOT	0.0820	0.0206	0.3739	0.1553
B	3G	F7B	2.0	SUBSURFACE	0.0892	0.0210	0.3652	0.1690
B	3G	F7B	2.0	ROOT	0.0827	0.0217	0.4309	0.1780
C	1G	F9B	2.0	SUBSURFACE	0.0683	0.0177	0.3305	0.1589
C	1G	F9B	2.0	ROOT	0.0740	0.0174	0.3147	0.1412
C	1G	F3B	3.0	SUBSURFACE	0.0838	0.0143	0.3283	0.1601
C	1G	F3B	3.0	ROOT	0.0821	0.0174	0.2837	0.1419
C	3G	F8B	2.0	SUBSURFACE	0.0789	0.0203	0.3147	0.1625
C	3G	F8B	2.0	ROOT	0.0831	0.0162	0.3133	0.1586

Table 3.2: Summary of carbon equivalents

Table 3.3

Summary of Overall Inclusion Distribution

Consumable	Welding Position	Heat Input (kJ/mm)	O+S at Root Location (w/o)	Area Fraction (%)	Average Diameter (micron)	Inclusion Density $(X10^5/cm^2)$	Average Aspect Ratio	Estimated Volume Fraction (%)
A	1G	2.0	0.0663	0.33	0.60	7.52	0.67	0.24
		3.0	0.0828	0.77 (0.39)	0.67 (0.56)	16.6 (10.4)	0.75 (0.73)	0.52 (0.26)
	3G*	2.0	0.1021	0.61	0.53	--	--	--
B	3G	2.0	0.0808	0.44	0.55	12.2	0.73	0.29
C	1G	2.0	0.0740	0.69	0.65	15.9	0.77	0.46
	3G	2.0	0.0831	0.95	0.67	14.2	0.73	0.48

*The results are extracted from previous FCAW work.

Table 3.4
Distributions of Dominant Inclusions
Consumable A, 1G Position As Welded Condition

(a) 2.0 kJ/mm (F5B)

Inclusion Types	Avg. Dia. micron	% Dist. (%)	Aspect Ratio	Proportion (%)			Density (X10^5/cm^2)			Avg.Relative Contents (%)				
				$0.1 \le d < 0.5$	$0.5 \le d < 1.0$	$d \ge 1.0$	$0.1 \le d < 0.5$	$0.5 \le d < 1.0$	$d \ge 1.0$	Si	Mn	Ca	S	Ti
Ti-Mn-S	0.56	78.2	0.68	49.7	39.7	10.6	2.92	2.33	0.62	--	23	--	12	65
Ti-Mn-S-Ca	0.58	9.5	0.67	60.0	22.5	7.5	0.43	0.16	0.12	--	23	3	12	62
Ti-Mn-S-Si	1.32	5.0	0.79	14.3	38.1	47.6	0.05	0.14	0.18	2	24	--	12	63
Overall	0.60	100.0	----	49.3	36.3	14.5	3.71	2.73	1.08	--	--	--	--	--

(b) 3.0 kJ/mm (F1B)

Inclusion Types	Avg. Dia. micron	% Dist. (%)	Aspect Ratio	Proportion (%)			Density (X10^5/cm^2)			Avg.Relative Contents (%)				
				$0.2 \le d < 0.5$	$0.5 \le d < 1.0$	$d \ge 1.0$	$0.2 \le d < 0.5$	$0.5 \le d < 1.0$	$d \ge 1.0$	Si	Mn	Ca	S	Ti
Ti-Mn-S	0.50 (0.38)	46.8 (41.1)	0.74 (0.70)	52.3 (75.0)	46.2 (23.3)	1.5 (1.7)	4.04 (3.21)	3.56 (1.00)	0.12 (0.07)	- (-)	37 (35)	- (-)	14 (14)	49 (52)
Ti-Mn-Si-S	0.96 (0.73)	33.8 (41.4)	0.77 (0.77)	13.8 (26.6)	50.0 (54.8)	36.2 (18.6)	0.77 (1.14)	2.79 (2.36)	2.02 (0.73)	6 (5)	33 (32)	- (-)	10 (10)	51 (53)
Ti-Mn-S-Ca	0.47 (0.39)	8.6 (10.72)	0.71 (0.72)	50.0 (86.2)	50.0 (13.8)	(--) (--)	0.71 (0.61)	0.71 (0.10)	(-) (-)	- (-)	34 (35)	5 (4)	12 (12)	49 (50)
Ti-Mn -S-Si-Ca	(0.60)	4.0 (5.1)	(0.77)	9.1 (40.9)	72.7 (45.4)	18.2 (13.6)	0.06 (0.22)	0.48 (0.24)	1.12 (0.07)	6 (8)	34 (33)	3 (3)	13 (12)	44 (44)
Overall	0.67 (0.43)	100.0 (100.0)		37.1	47.5	15.4	6.18	7.90	2.55					

Table 3.5

Distributions of Dominant Inclusions
Consumable B, 2.0 kJ/mm, As Welded, 3G Position (F7B)

Inclusion Types	Avg. Dia. micron	% Dist. (%)	Aspect Ratio	Proportion (%)			Density ($X10^5/cm^2$)			Avg. Relative Contents (%)				
				$0.1 \le d < 0.5$	$0.5 \le d < 1.0$	$d \ge 1.0$	$0.1 \le d < 0.5$	$0.5 \le d < 1.0$	$d \ge 1.0$	Si	Mn	Ca	S	Ti
Mn-Ti-S-Si	0.67	43.8	0.76	27.9	58.1	14.0	1.49	3.09	0.74	10	44	--	12	34
Mn-Ti-S	0.36	29.8	0.69	82.8	17.2	-	3.00	0.62	-	-	50	--	18	32
Mn-Ti -S-Si-Ca	0.65	11.5	0.76	40.4	46.8	12.8	0.56	0.65	0.18	9	42	4	12	34
Mn-Ti-S-Ca	0.39	6.8	0.45	85.7	14.3	-	0.71	0.19	-	-	45	6	20	29
Overall	0.44	100.0	--	38.4	8.1	6.50	4.60	0.98	-	-	-	--	--	--

Table 3.6

Distribution of Dominant Inclusions
Consumable C, 2.0 kJ/mm As Welded

(a) 1G Position (F9B)

Inclusion Types	Avg. Dia. micron	% Dist. (%)	Aspect Ratio	Proportion (%)			Density $(X10^5/cm^2)$			Avg. Relative Contents (%)				
				$0.1 \le d < 0.5$	$0.5 \le d < 1.0$	$d \ge 1.0$	$0.1 \le d < 0.5$	$0.5 \le d < 1.0$	$d \ge 1.0$	Si	Mn	Ca	S	Ti
Ti-Mn-S	0.58	70.3	0.77	38.3	58.0	3.7	4.27	6.79	0.41	-	34	-	17	49
Ti-Mn-S-Ca	0.58	13.9	0.77	38.6	57.1	4.3	0.85	1.26	0.09	-	31	6	15	48
Ti-Mn-S-Si	1.3	6.3	0.81	-	21.9	78.1	-	0.22	0.79	5	32	-	11	53
Overall	0.65	100.0		36.0	53.5	10.5	5.72	8.49	1.67	-	-	-	-	-

(b) 3G Position (F8B)

Inclusion Types	Avg. Dia. micron	% Dist. (%)	Aspect Ratio	Proportion (%)			Density $(X10^5/cm^2)$			Avg. Relative Contents (%)				
				$0.1 \le d < 0.5$	$0.5 \le d < 1.0$	$d \ge 1.0$	$0.1 \le d < 0.5$	$0.5 \le d < 1.0$	$d \ge 1.0$	Si	Mn	Ca	S	Ti
Ti-Mn-S-Si	0.82	45.6	0.76	12.3	66.1	21.6	0.78	4.17	1.55	10	43	-	12	35
Ti-Mn-S	0.42	35.1	0.69	74.9	24.6	0.5	3.74	1.23	0.03	-	47	-	19	34
Ti-Mn-S-Ca	0.38	6.4	0.66	70.6	29.4	-	0.64	0.27	-	-	41	7	18	35
Overall	0.67	100.0		41.1	44.1	14.6	5.85	6.28	2.08	-	-	-	-	-

Table 3.7

Summary of Macrostructural Distributions Along Weld Centreline
Flux Cored Arc Welds

Consumable	Welding Position	Heat Input (kJ/mm)	Post Weld Condition	Columnar Grains (%)	Coarse Grain Reheated Region (%)	Fine Grain Reheated Region (%)
A	1G	2.0	As Welded	42.8	27.5	29.7
		3.0	As Welded	34.1	14.8	51.2
B	1G	2.0	Stress Relieved	44.4	26.9	28.7
		3.0	Stress Relieved	34.4	14.2	51.5
	3G	2.0	As Welded	37.7	19.2	43.2
			Stress Relieved	36.4	31.1	32.5
C	1G	2.0	As Welded	31.7	15.8	52.5
			Stress Relieved	24.5	13.8	61.8
		3.0	As Welded	25.8	15.4	58.8
			Stress Relieved	24.4	12.4	63.3
	3G	2.0	As Welded	34.1	14.8	51.2
			Stress Relieved	41.1	17.6	41.3

Table 3.8

Summary of Microstructure Characterization on As Welded Weldments
Flux Cored Arc Welds

Consumable	Welding Position	Heat Input (kJ/mm)	Grain Boundary Ferrite (%)	Polygonal Ferrite (%)	Ferrite With Non-aligned Second Phase (%)	Ferrite With Aligned Second Phase (%)	Acicular Ferrite (%)
A	1G	2.0 (F5A)	6.3	15.4	19.4	35.6	23.3
		3.0 (F1B)	4.5	13.4	25.5	19.8	36.8
B	3G	2.0 (F7B)	11.2	8.7	16.1	18.6	45.4
C	1G	2.0 (F9B)	3.7	10.4	18.9	34.5	32.2
		3.0 (F3A)	9.8	10.0	24.2	15.8	40.2
	3G	2.0 (F8B)	9.5	14.1	6.4	16.2	53.8

Table 3.9

Summary of Microstructure Characterization* on Stress Relieved Weldments
Flux Cored Arc Welds

Consumable	Welding Position	Heat Input (kJ/mm)	Plate I.D.	Acicular Ferrite (%)	Coarse Ferrite (%)	Ferrite With Precipitated Second Phase (%)
B	1G	2.0	F6A	34.0	17.2	48.8
		3.0	F2B	24.4	24.8	50.8
	3G	2.0	F7A	18.4	11.8	69.8
C	1G	2.0	F9A	27.2	17.8	55.0
		3.0	F4A	28.0	19.8	52.2
	3G	2.0	F8A	14.8	14.0	71.2

*500 counts at 400X magnification.

Table 3.10

Summary of Shrinkage Measurements from the Restraint Welds
Flux Cored Arc Welds

Stage	Average Transverse Shrinkage (mm)		Average Angular Distortion (°)
	Accumulative*	Between Successive Stage	Accumulative
Completion of First Pass	0.90 (0.18)	---	0.2 (0)
Completion of 2nd Pass	1.34 (0.30)	0.45 (0.12)	0.3 (0)
Completion of 3rd Pass (T/4)	1.80 (0.38)	0.46 (0.08)	0.4 (0)
Completion of 12th Pass (T/2)	3.04 (0.69)	1.24 (0.31)	0.5 (0.1)
Completion of 22nd Pass (3T/4)	3.43 (0.86)	0.39 (0.17)	0.6 (0.1)
Full completion	3.87 (1.12)	0.44 (0.26)	0.7 (0.1)

*Accumulative: The shrinkage is calculated on the difference of L_2 spacing relative to the initial measurements.

Successive: The shrinkage is calculated as the difference of L_2 spacings relative to the completion of previous stage.

The bracketed figure is the value obtained from high restraint welds.

Table 3.11

Summary of Joint Opening From the Restraint Welds

Restraint Condition	Stage	Joint Opening at Location (mm)		
		T/4	T/2	3T/4
High	First Pass	16.2	28.5	40.0
	Second Pass	16.2	28.5	40.0
	Third Pass	16.2	28.5	40.0
Low	First Pass	15.8	27.3	38.5
	Second Pass	16.2	27.7	39.0
	Third Pass	16.2	28.1	39.5

Table 3.12

Summary of Vickers Hardness Measurements
Flux Cored Arc Welds

Consumable	Welding Position	Heat Input (kJ/mm)	Post Weld Condition	Centreline	Subsurface	Root
A	1G	2.0	As Welded	242 (207-276)*	250 (235-256)	247 (233-256)
		3.0	As Welded	212 (185-240)	199 (160-227)	232 (215-243)
B	1G	2.0	Stress Relieved	221 (197-240)	211 (203-225)	235 (224-248)
		3.0	Stress Relieved	213 (191-238)	208 (202-213)	224 (218-233)
	3G	2.0	As Welded	229 (213-249)	231 (227-238)	234 (228-240)
		2.0	Stress Relieved	217 (187-240)	224 (213-233)	221 (209-230)
C	1G	2.0	As Welded	222 (189-253)	235 (212-251)	216 (209-222)
			Stress Relieved	204 (180-227)	217 (207-230)	223 (209-235)
		3.0	As Welded	199 (179-222)	201 (191-212)	207 (205-210)
			Stress Relieved	203 (176-238)	212 (205-221)	209 (198-221)
	3G	2.0	As Welded	212 (193-247)	223 (213-227)	210 (209-213)
			Stress Relieved	212 (188-230)	223 (213-235)	200 (193-206)

All welds are double V geometry.

*The range of hardness measurements is included in parentheses.

Table 3.13

Summary of Average Vickers Hardness for Restrained Flux Cored Arc Welds

Restraint Condition	Centreline	Root	T/2	Subsurface
Low Restraint	227 (202-245)	234 (2[illegible]40)	236 (224-249)	228 (203-254)
High Restraint	236 (210-258)	249 (236-264)	243 (224-256)	222 (206-247)

Table 3.14

Summary of Tensile Properties for Flux Cored Arc Welds

Consumable	Post Weld Condition	Heat Input (kJ/mm)	Temp. (°C)	Yield Strength (MPa)	Ultimate Tensile Strength (MPa)	% Elongation	Reduction in Area (%)
A	As Welded	2.0	20	626	669	25	70
			-10	638	667	26	68
			-30	665	658	29	69
		3.0	20	532	579	28	77
			-10	564	613	36	76
			-30	560	628	31	74
B	Stress Relieved	2.0	20	555	579	25	73
			-10	579	642	25	61
			-30	584	658	20	55
		3.0	20	480	553	32	76
			-10	511	596	29	73
			-30	522	598	28	74
C	As Welded	3.0	20	500	552	26	76
			-10	521	593	27	75
			-30	549	599	27	75
	Stress Relieved	3.0	20	469	541	32	77
			-10	512	582	31	76
			-30	526	592	37	75

Table 3.15

Summary of Tensile Properties
Restraint Flux Cored Arc Welds

Condition	Temperature (°C)	Yield Strength (MPa)	Ultimate Tensile Strength (MPa)	Percent Elongation	Reduction in Area (%)
Low Restraint	20	588	645	24	71
	-30	648	703	26	70
	-50	681	745	19	65
High Restraint	20	594	636	17	69
	-30	649	678	27	69
	-50	676	726	25	65

Table 3.16

Summary of NDT Temperatures (°C)

Consumable	Heat Input (kJ/mm)	As Welded	Stress Relieved
A	2.0	-70	N/A
	3.0	-65	
B	2.0	N/A	-80
	3.0	N/A	-55
C	3.0	-60	-60

All welds are prepared in flat position.

Table 3.17

Summary of CVN Impact Properties - Consumable A As Welded

(a) 1G deposition of the present program

Heat Input kJ/mm	Location	Transition Temperature (°C)			CVN Impact Energy (J)				
		27J	35J	40J	0°C	-20°C	-30°C	-40°C	-60°C
2.0	Subsurface	-61	-52	-47	74	64	56	47	28
	Root	-56	-48	-44	88	73	59	44	24
3.0	Subsurface	-55	-50	-47	118	95	78	55	21
	Root	-62	-58	-56	137	118	104	85	30

(b) 3G deposits from previous FCAW study[3.1]

Heat Input kJ/mm	Location	Transition Temperature (°C)		CVN Impact Energy (J)			
		27J	40J	25°C	-10°C	-30°C	-50°C
2.2	T/2	-67	-58	99	88	73	52

Table 3.18

Summary of CVN Impact Properties
Consumable B

Weld Position	Heat Input kJ/mm	Post Weld Condition	Location	Transition Temperature (°C)			CVN Impact Energy (J)				
				27J	35J	40J	0°C	-20°C	-30°C	-40°C	-60°C
1G	2.0	Stress Relieved	Subsurface	-43	-35	-30	78	53	40	30	16
			Root	-50	-44	-40	87	69	55	40	18
	3.0	Stress Relieved	Subsurface	-18	-14	-11	70	25	18	12	--
			Root	-24	-19	-16	79	33	20	12	--
3G	2.0	As Welded	Subsurface	-70	-66	-63	104	94	86	76	46
			Root	-68	-62	-58	125	108	94	74	37
		Stress Relieved	Subsurface	-52	-44	-39	102	75	56	41	20
			Root	-52	-46	-43	108	80	62	45	20

Table 3.19

Summary of CVN Impact Properties
Consumable C

Weld Position	Heat Input kJ/mm	Post Weld Condition	Location	Transition Temperature (°C)			CVN Impact Energy (J)				
				27J	35J	40J	0°C	-20°C	-30°C	-40°C	-60°C
1G	2.0	As Welded	Subsurface	-76	-71	-68	124	109	100	89	57
			Root	-68	-62	-59	151	138	128	114	39
		Stress Relieved	Subsurface	-58	-53	-50	87	80	73	60	25
			Root	-54	-50	-47	131	104	85	58	18
	3.0	As Welded	Subsurface	-53	-49	-46	130	100	80	57	18
			Root	-51	-47	-45	122	99	83	57	17
		Stress Relieved	Subsurface	-41	-38	-36	104	82	58	30	8
			Root	-11	-5	-2	43	21	15	12	--
3G	2.0	As Welded	Subsurface	-74	-68	-65	128	118	108	94	50
			Root	-72	-68	-66	146	131	119	102	54
		Stress Relieved	Subsurface	-57	-52	-49	114	100	87	63	24
			Root	-52	-48	-46	129	114	98	65	19

Table 3.20

Summary of CVN Impact Properties
Single V, Restraint Welds, Consumable A,
2.0 kJ/mm, 1G Position

Restraint Condition	Location	Transition Temp. (°C)			CVN Impact Energy @ (J)				
		40J	35J	27J	0°C	-20°C	-30°C	-40°C	-60°C
High Restraint	Subsurface	-78	-80	-83	128	125	121	115	92
	T/2	<-90	<-90	<-90	136	133	127	117	69
	Root	-79	-82	-86	126	116	108	99	74
Low Restraint	Subsurface	-64	-67	-74	146	131	121	108	50
	T/2	-66	-69	-75	141	138	133	126	70
	Root	-61	-65	-72	115	102	92	79	43

Table 3.21

Change in Transition Temperature (°C) Between the Subsurface and Root Locations (40J Transition Temperature at Subsurface - 40J Transition Temperature at Root)

Weld Deposit	As-Welded 2 kJ/mm	As-Welded 3 kJ/mm	Stress Relieved 2 kJ/mm	Stress Relieved 3 kJ/mm
A(1G)	- 3	+ 9		
B(1G)			+ 10	+ 5
(3G)	- 5		+ 4	
C(1G)	- 9	- 1	- 3	- 34
(3G)	+ 1		- 3	

Table 3.22

Change in Transition Temperature (°C) With Welding Position (40J Transition Temperature 1G - 40J Transition Temperature 3G)

Consumable	As-Welded Subsurface	As-Welded Root	Stress Relieved Subsurface	Stress Relieved Root
A/B	+16	+14	+ 9	+ 2
C	- 3	+ 7	- 1	- 1

Table 3.23

Summary of CTOD Values
Flux Cored Arc Welds

Consumable	Welding Position	Heat Input (kJ/mm)	Temp. (°C)	Post Weld Condition	
				As Welded	Stress Relieved
A	1G	2.0	-30	0.18 (0.058-0.369)	N/A
			-50	0.06 (0.044-0.073)	
		3.0	-10	0.16 (0.029-0.321)	
			-30	0.08 (0.071-0.078)	
B	1G	2.0	-10	N/A	0.08 (0.027-0.158)
			-30	N/A	0.04 (0.053-0.020)
		3.0	-10	N/A	0.10 (0.102-0.109)
			-30	N/A	0.07 (0.041-0.106)
	3G	2.0	-10	0.30 (0.122-0.494)	0.43 (0.119-0.895)
			-30	0.10 (0.050-0.166)	0.31 (0.150-0.495)
C	1G	2.0	-10	---	0.51 (0.125-1.09)
			-30	0.32 (0.109-0.666)	0.04 (0.040-0.042)
			-50	0.05 (0.035-0.068)	---
		3.0	-10	0.14 (0.027-0.181)	0.20 (0.064-0.408)
			-30	0.05 (0.034-0.071)	0.07 (0.039-0.131)
	3G	2.0	-30	0.49 (0.294-0.782)	0.63 (0.058-0.988)
			-50	0.21 (0.120-0.277)	0.08 (0.03-0.110)

Table 3.24

Summary of CTOD Values for Restrained Flux Cored Arc Welds

Restraint Condition	Temperature (°C)	Average CTOD Values (mm)	
		B X 2B Through Thickness	B X B Surface Notched
Low Restraint (F10A)	-30	0.38 (0.133-0.652)*	0.54 (0.380-0.752)
	-50	0.11 (0.091-0.134)	N/A
High Restraint (F11A)	-30	0.33 (0.086-0.498)	1.37 (1.13-1.62)
	-50	0.06 (0.038-0.072)	N/A

*Bracketed value denotes the range of CTOD values.

Table 3.25

Summary of Observed Cracking in G-BOP Tests

Consumable	Room Temp.	50°C	75°C
A	0 - 5%	0 - 5%	0 - 5%
B	0 - 5%	0 - 5%	0 - 5%
C	10 - 15%	0 - 5%	0 - 5%

Table 4.1

Summary of Estimated Cooling Rates*

Joint Geometry	Welding Position	Heat Input (kJ/mm)	$t_{800-500^{\circ}C}$ (sec)
Double V	1G	2.0	9.4
		3.0	14.4
	3G	2.0	9.4
Single V	1G	2.0	9.6

*Estimated from Bibby's model[1]

---

[1] Bibby, M., "Weld Quality Software for the HP71B Hand Held Computer". Dept. of Mechanical and Aeronautical Engineering, Carleton University Report, January 1987.

FIGURES

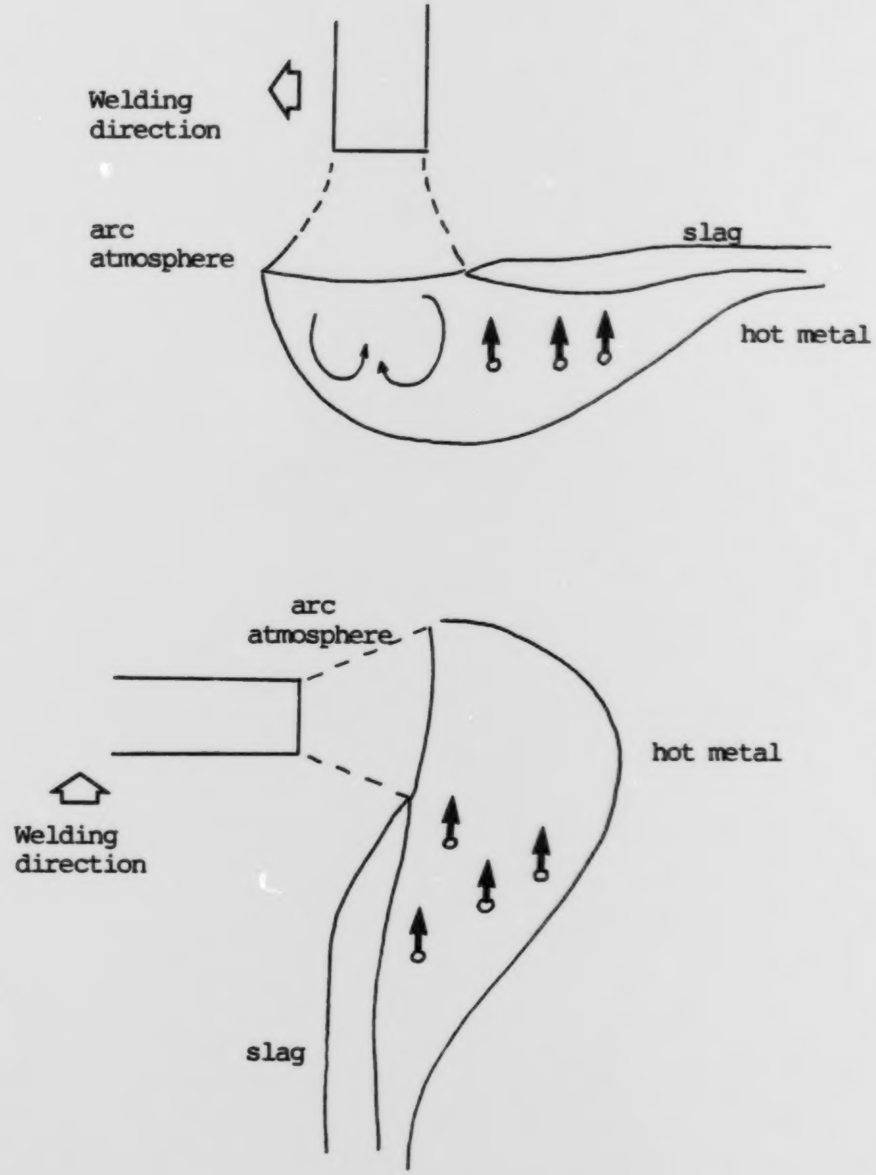
Welding direction
arc atmosphere
slag
hot metal
arc atmosphere
hot metal
Welding direction
slag

Figure 1.1: The influence of welding position on inclusion flotation

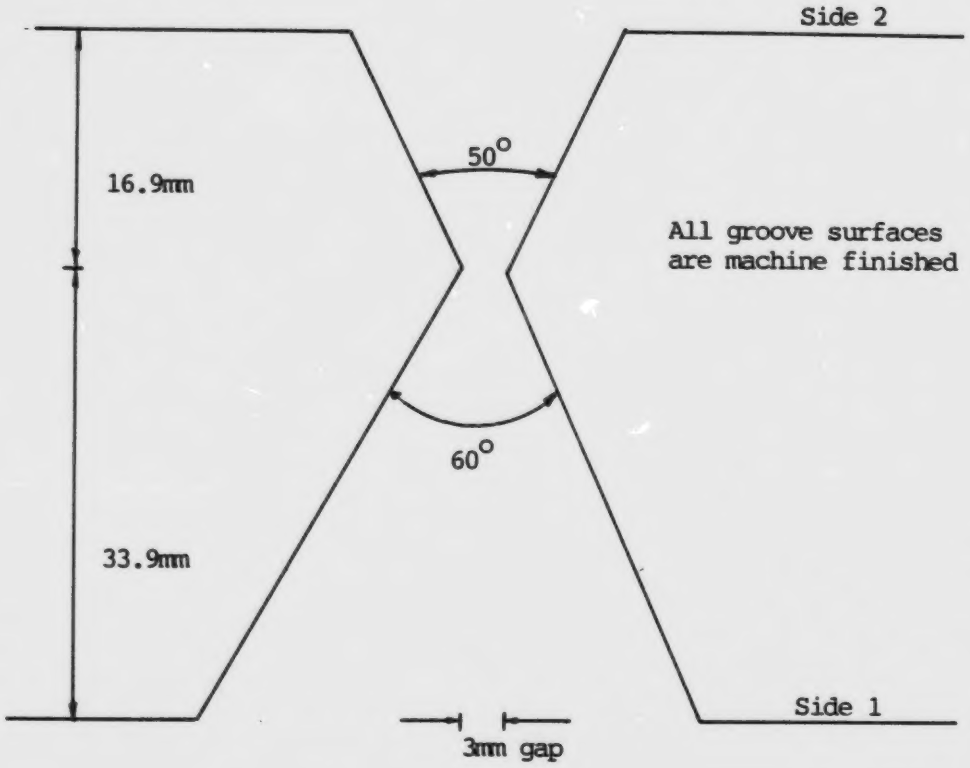

Side 2
50°
16.9mm
All groove surfaces
are machine finished
60°
33.9mm
Side 1
3mm gap

Figure 2.1: Schematic representation of double V joints

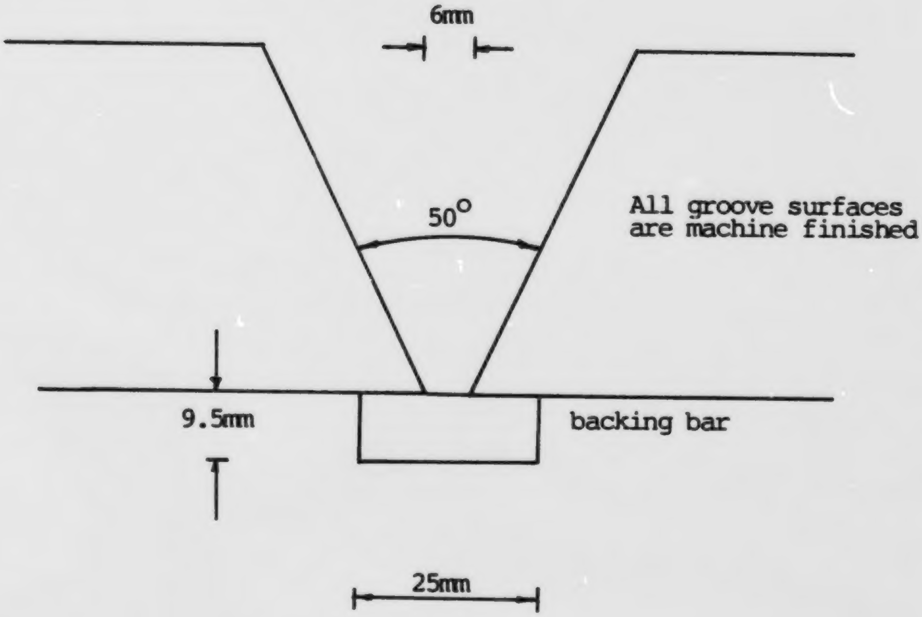
6mm
50°
All groove surfaces
are machine finished
9.5mm
backing bar
25mm

Figure 2.2: Schematic representation of joint geometry for single V welds

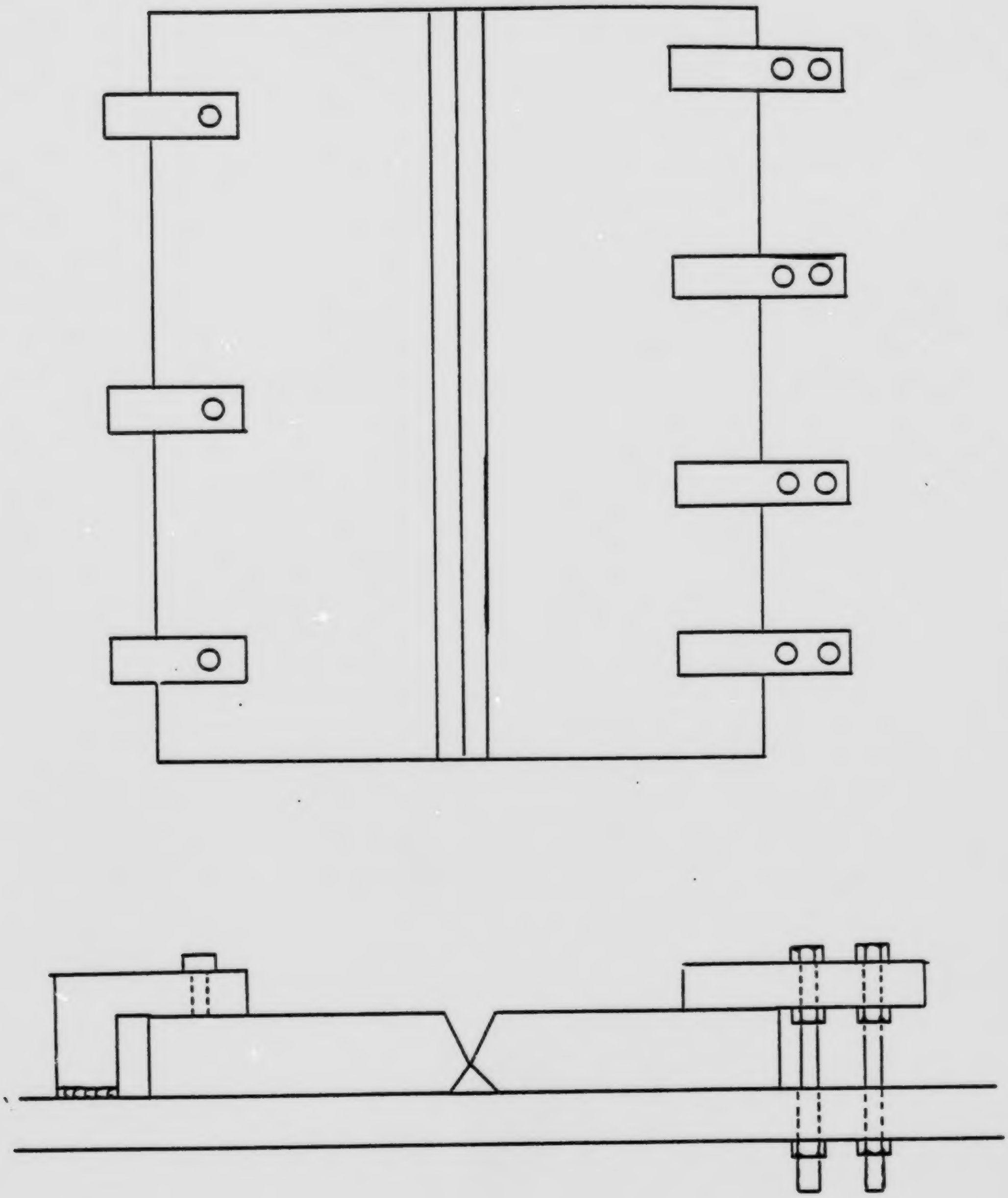

Figure 2.3: Schematic representation of welding jig used for F1-F9

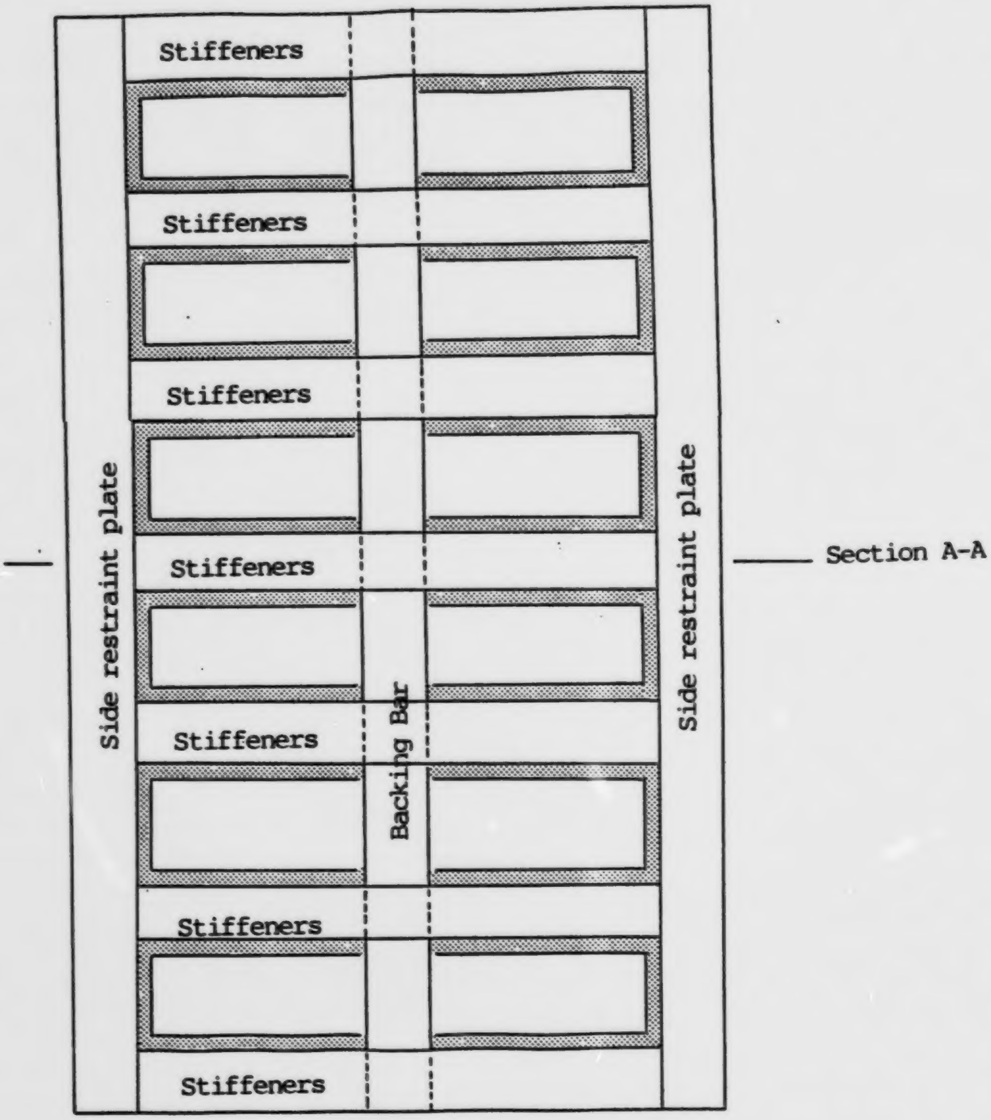
Stiffeners
Stiffeners
Stiffeners
Side restraint plate
Stiffeners
Side restraint plate
Section A-A
Stiffeners
Backing Bar
Stiffeners
Stiffeners

▨ 10mm (3/8") fillet weld with yield strength of 700 MPa

(a) Bottom view

Figure 2.4: Bottom view of high restraint single V weld (F11)

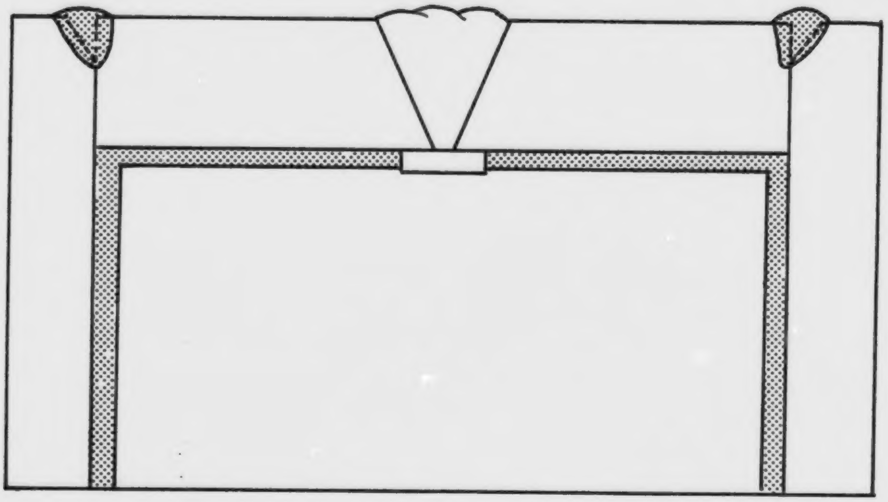

▨ 10mm leg fillet weld with yield strength of 700 MPa

(b) Section A-A

Figure 2.5: Cross section of high restraint single V weld (F11)

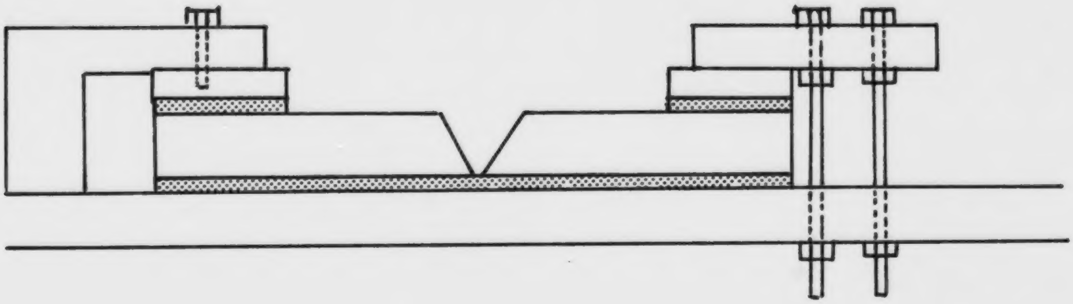

▨ High temperature MoS_2 grease

Figure 2.6: Schematic representation for low restraint set-up

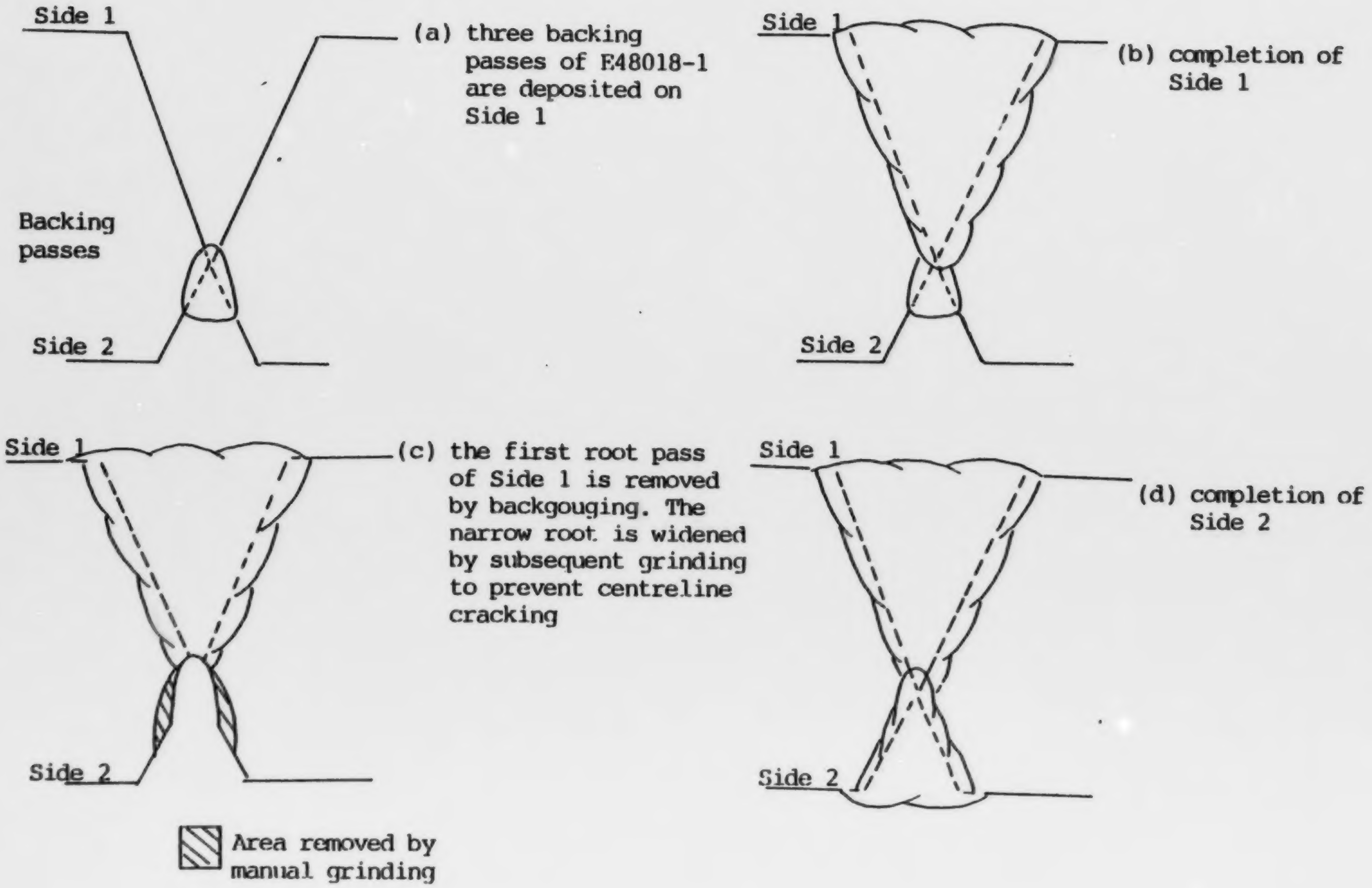
Side 1
Backing passes
Side 2
Side 1
Side 2
Side 1
Side 2
Side 1
Side 2
Area removed by manual grinding

(a) three backing passes of E48018-1 are deposited on Side 1

(b) completion of Side 1

(c) the first root pass of Side 1 is removed by backgouging. The narrow root is widened by subsequent grinding to prevent centreline cracking

(d) completion of Side 2

Figure 2.7: Schematic representation of welding sequence for double Vee joints F1-F9

Figure 2.8: Schematic illustration of locations for shrinkage measurements (F10A, F11A)

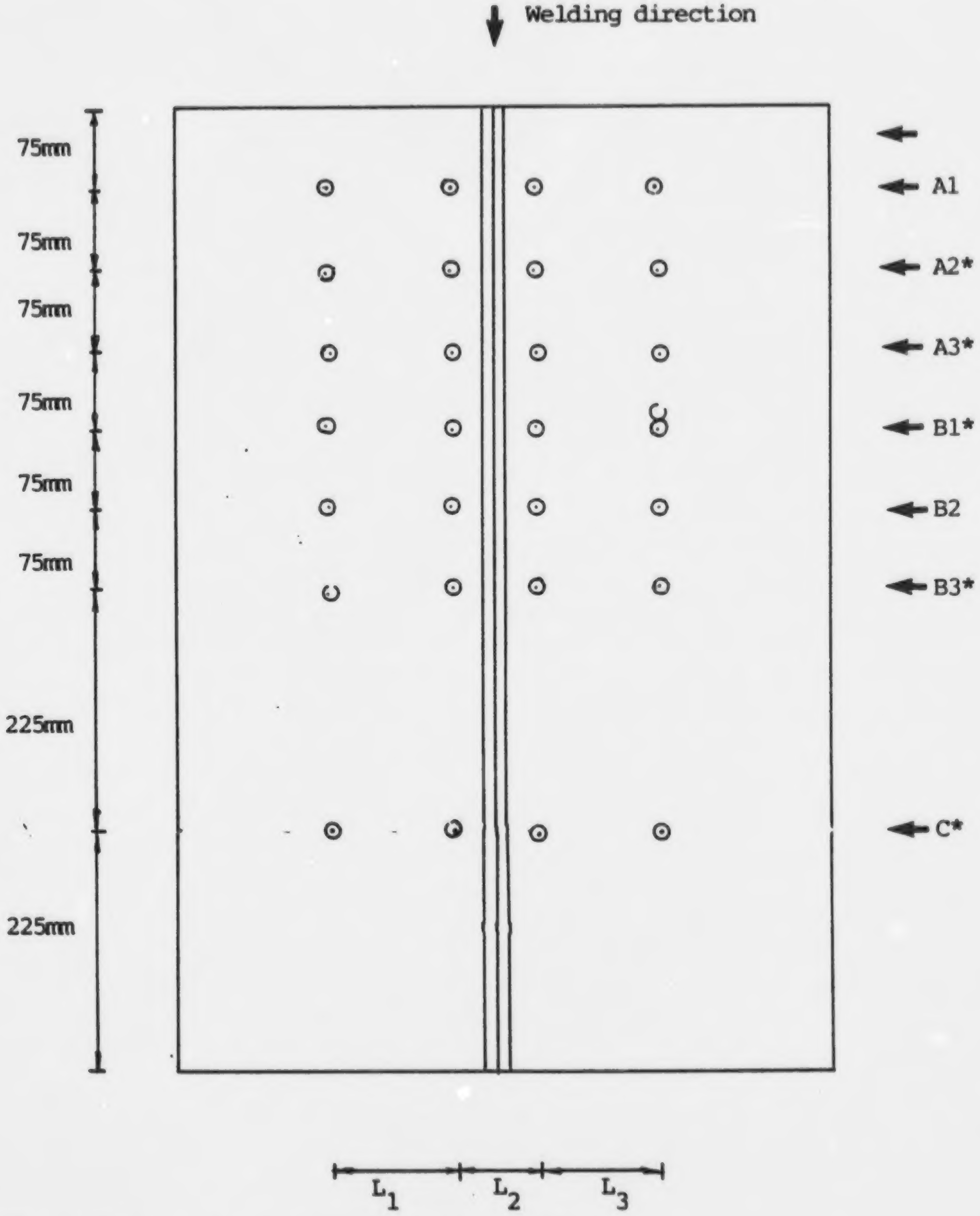
Welding direction
75mm
75mm
75mm
75mm
75mm
75mm
225mm
225mm
A1
A2*
A3*
B1*
B2
B3*
C*
L1
L2
L3

*The stiffeners located on the bottom surface

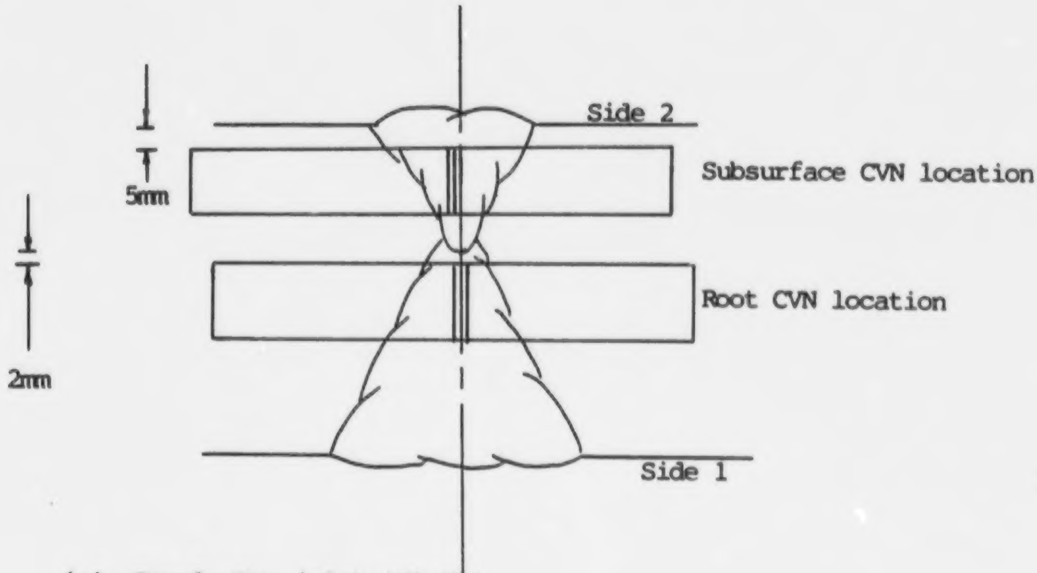
Side 2
5mm
Subsurface CVN location
2mm
Root CVN location
Side 1

(a) Douvle Vee joint (F1-F9)

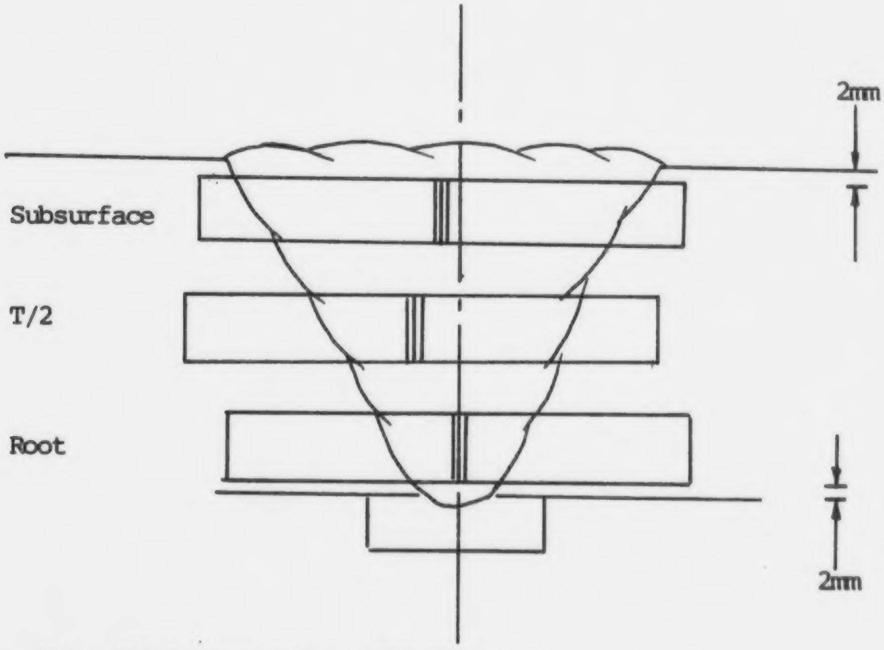
2mm
Subsurface
T/2
Root
2mm

(b) Single Vee joint (F10-F11)

Figure 2.9: Locations for extractions of CVN specimens

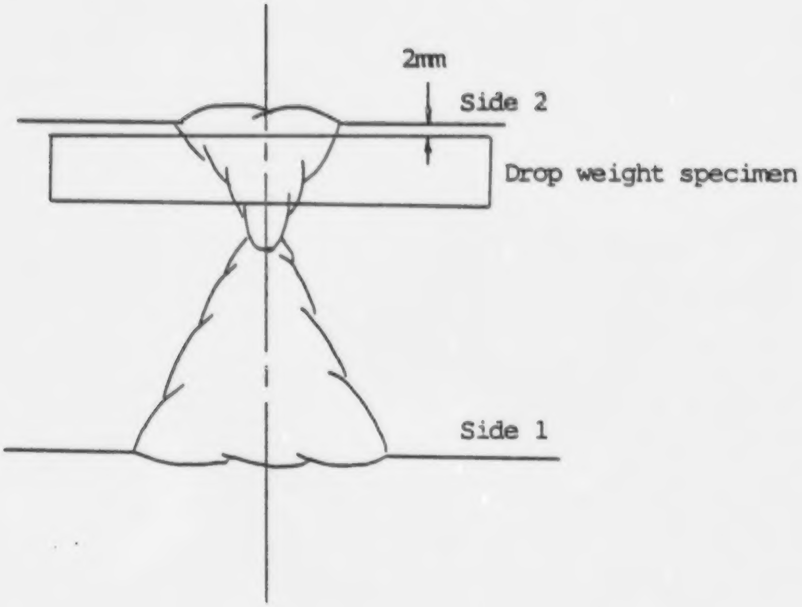
2mm
Side 2
Drop weight specimen
Side 1

Figure 2.10 Location of extraction of drop weight P-2 specimens (F1-F6)

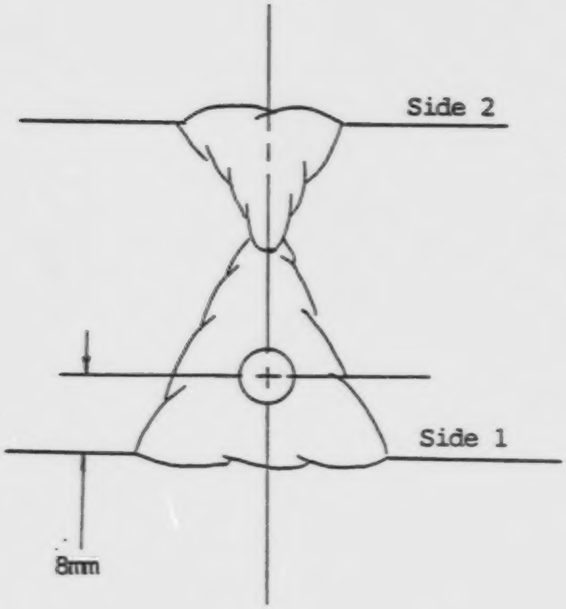
Side 2
Side 1
8mm

(a) Double Vee joint (F1-F6)

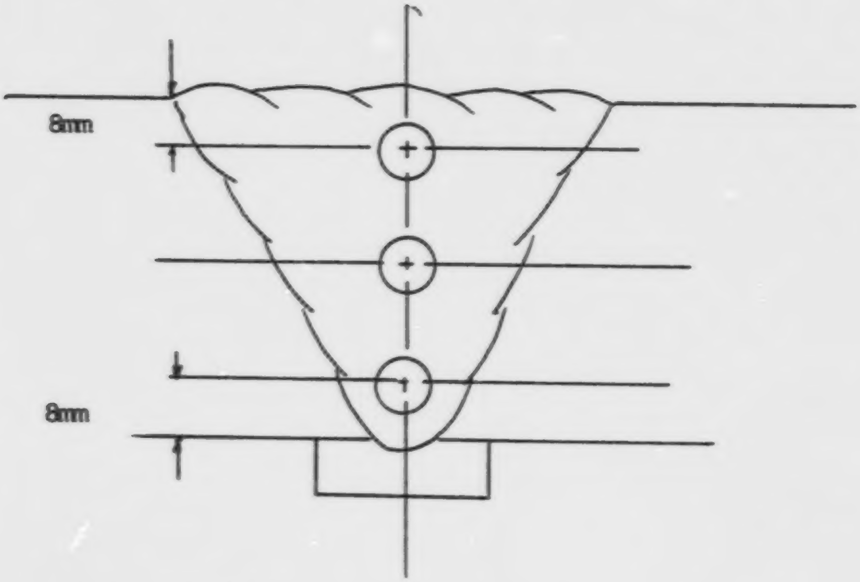

(b) Single Vee joint (F10-F11)

Figure 2.11: Location of extractions of tensile specimens

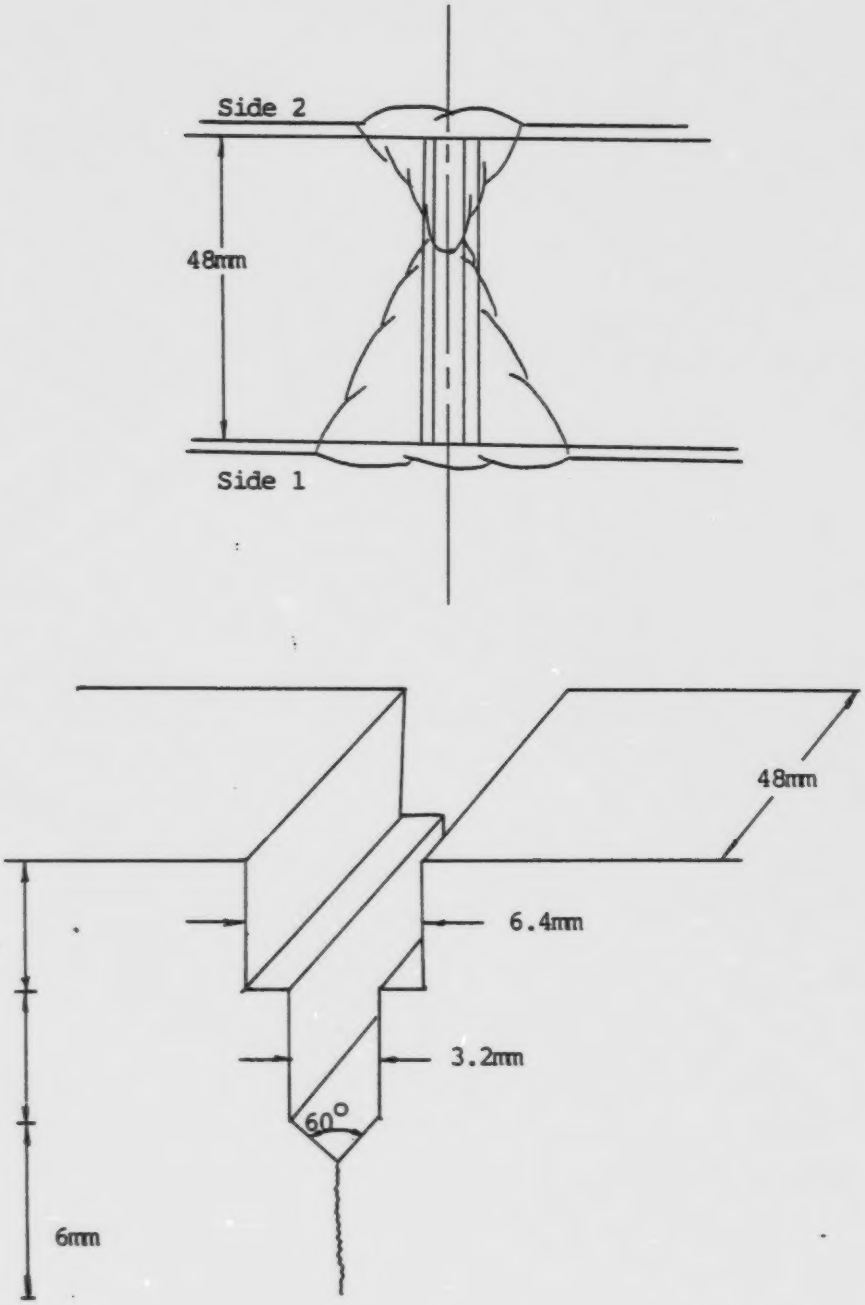
Side 2
48mm
Side 1
48mm
6.4mm
3.2mm
60°
6mm

Figure 2.12: Schematic illustration of B X 2B through thickness CTOD specimens (F1-F9)

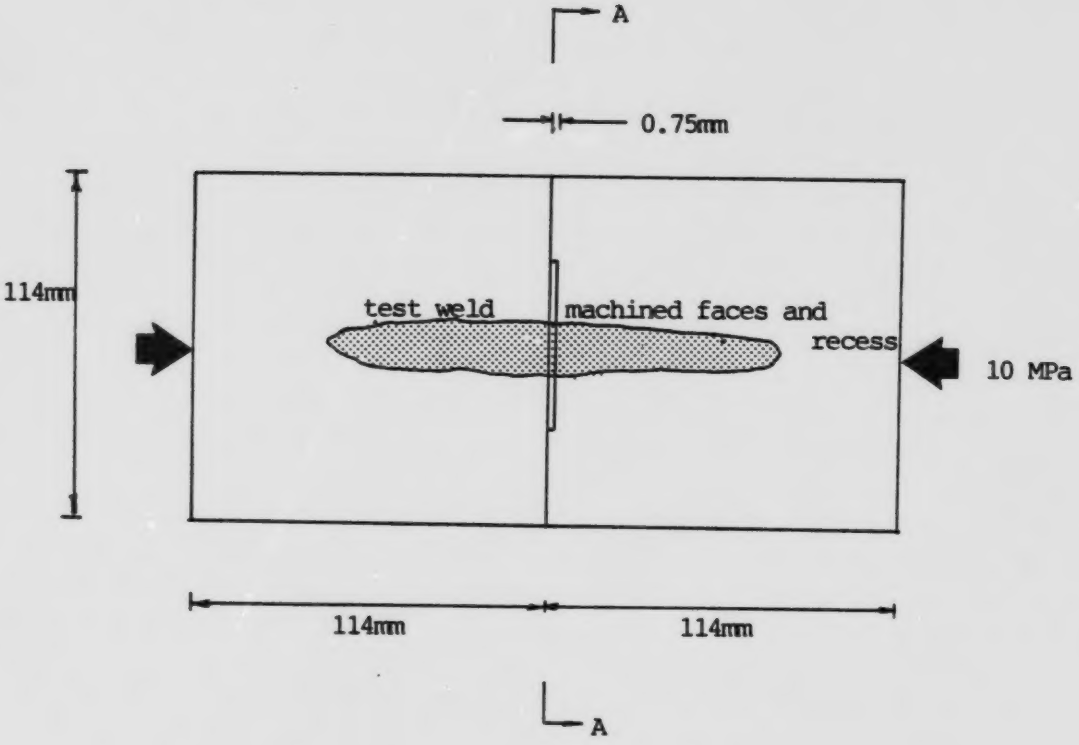
A
0.75mm
114mm
test weld
machined faces and
recess
10 MPa
114mm
114mm
A

(a) Top view

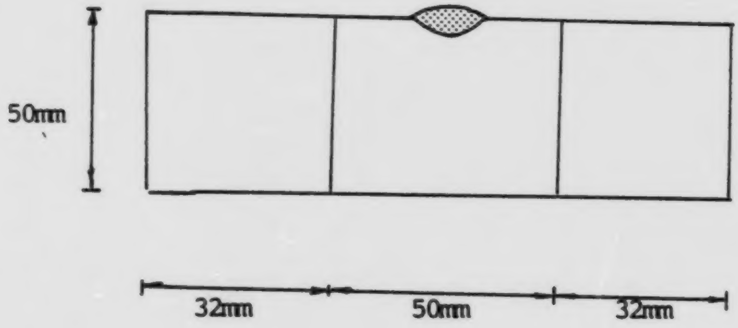
50mm
32mm
50mm
32mm

(b) Section A-A

Figure 2.13: G-BOP test specimens

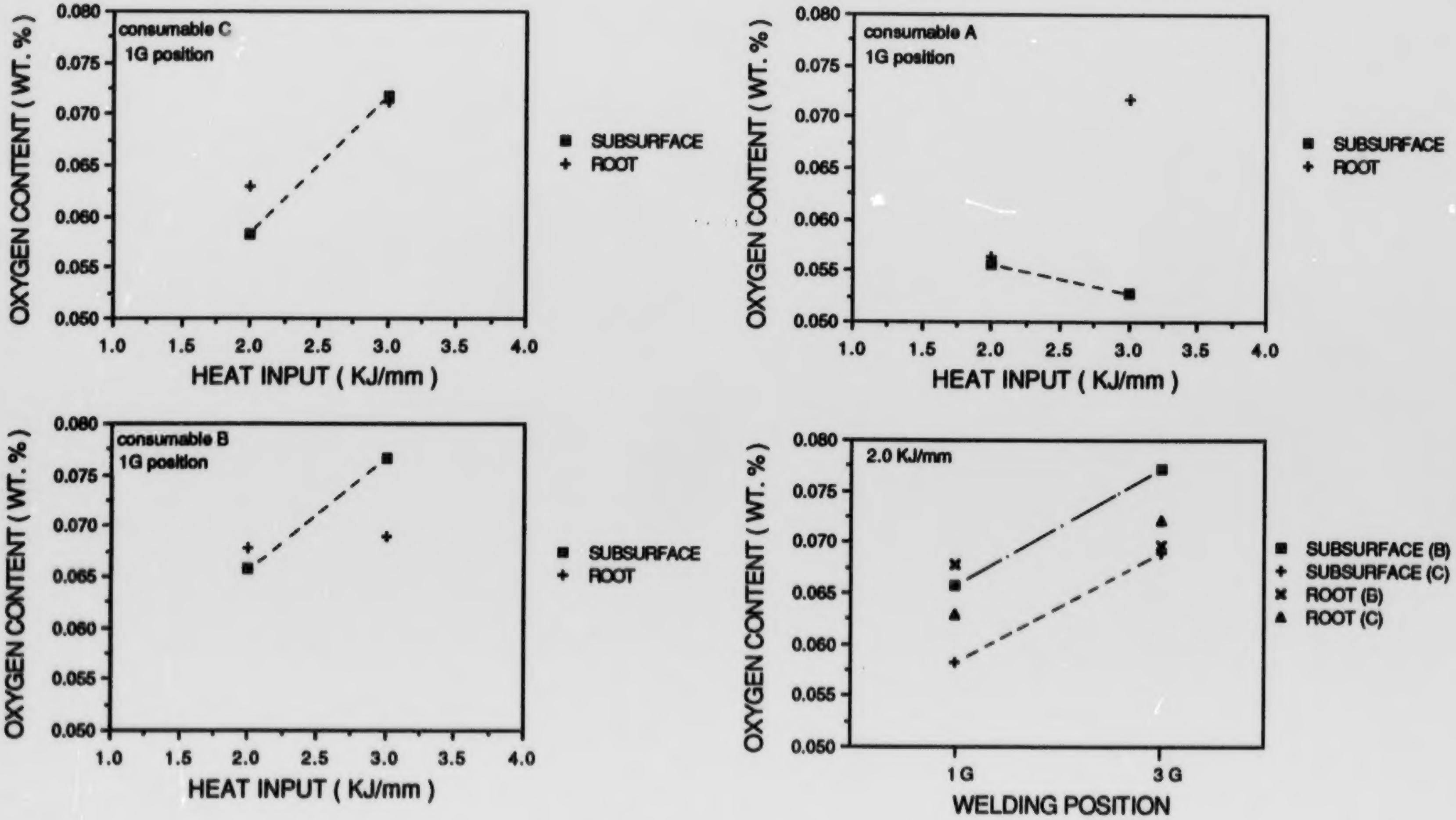

Figure 3.1: Effect of heat input and welding position on oxygen content

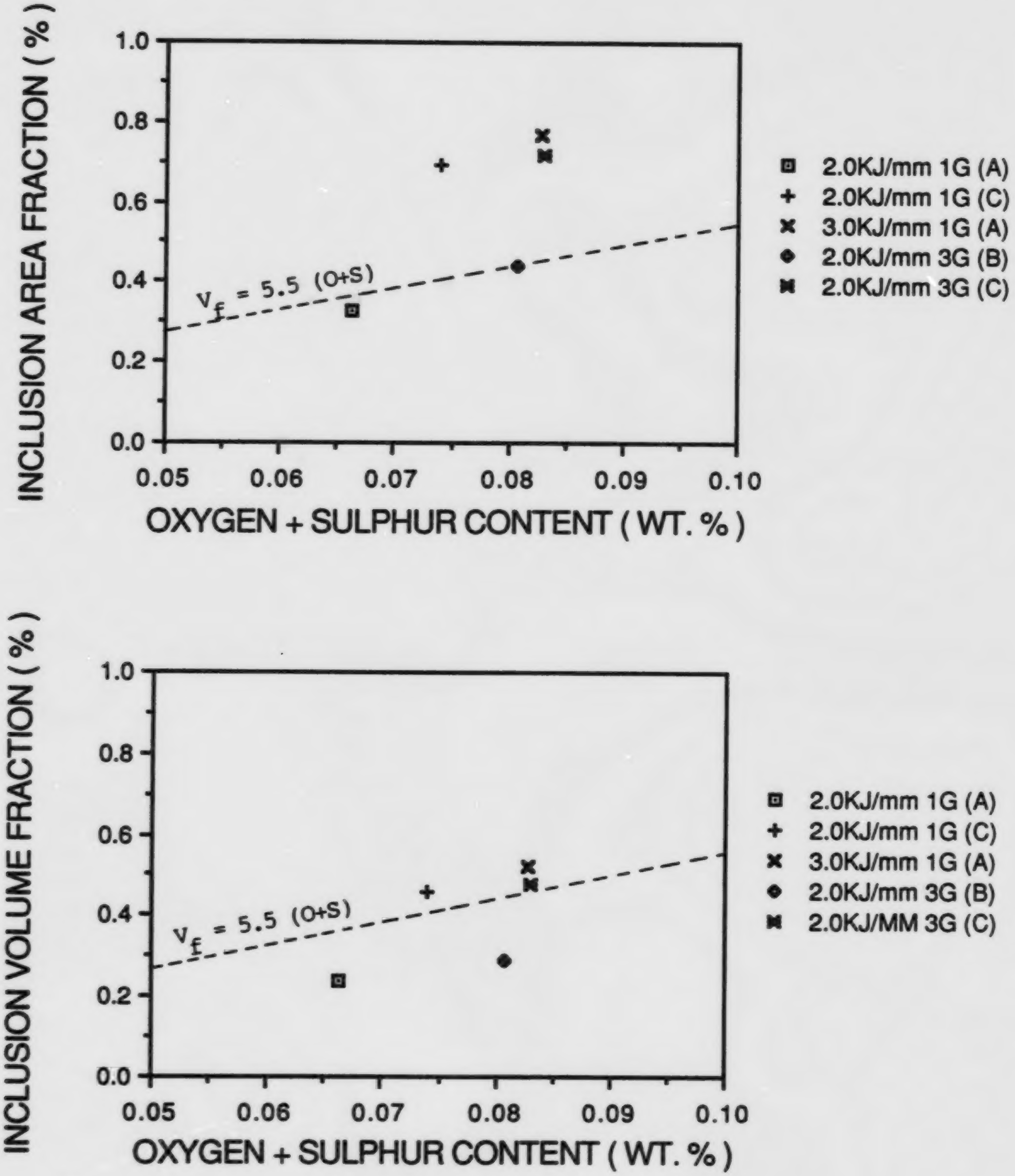

Figure 3.2: Effect of O+S content inclusion area fractions and inclusion volume fraction. The dotted line denotes the predicted values proposed by Widgery(3.4)

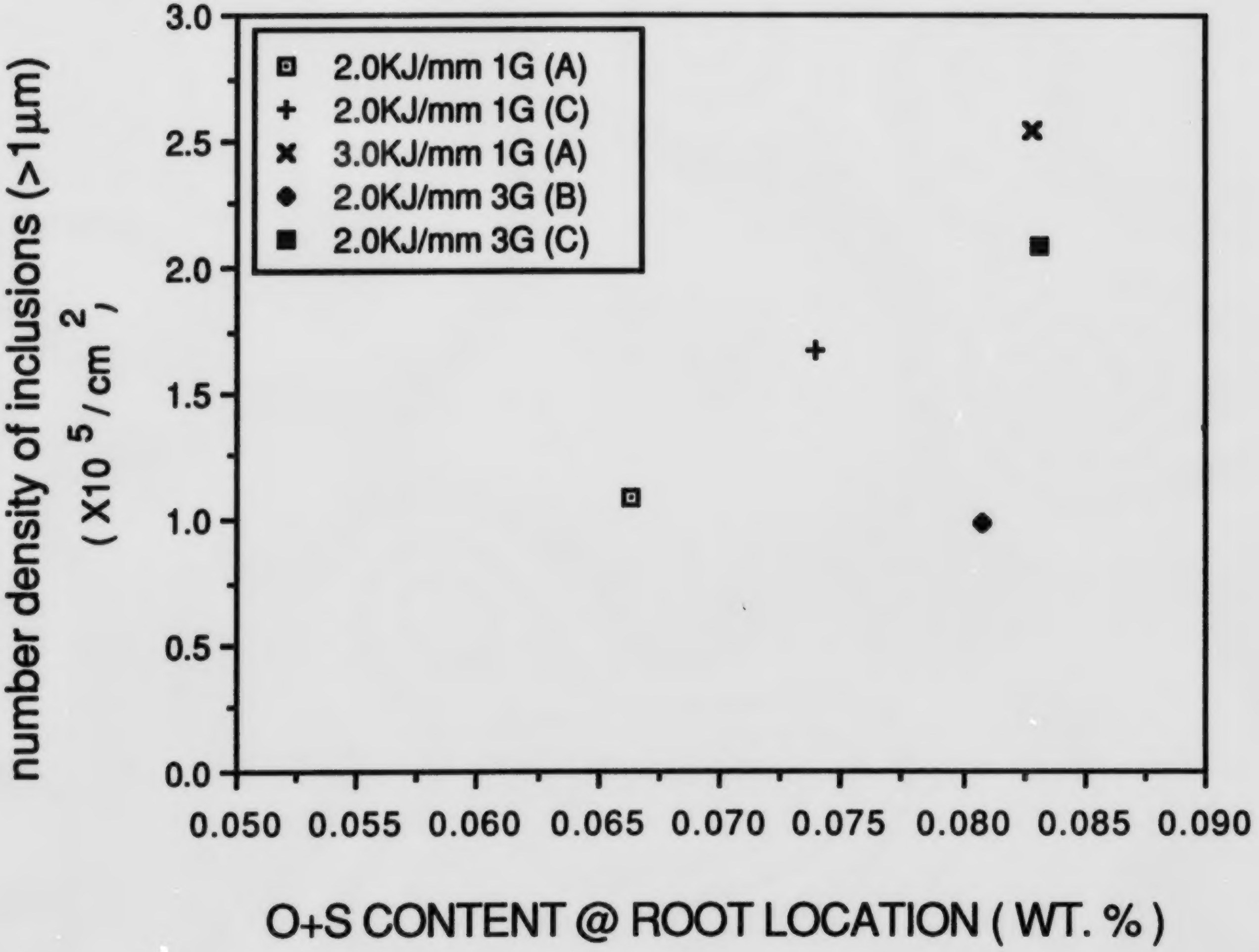

Figure 3.3: Effect of O+S on the number density of large inclusions

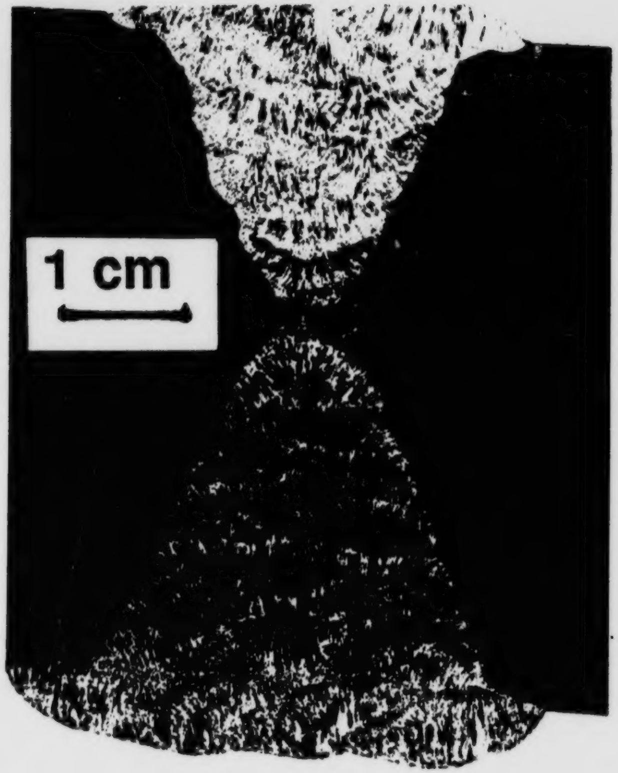

Figure 3.4 Macrograph of as-welded 2.0 kJ/mm weld deposited with Consumable A in 1G position (F5A) (2X, Neg. 11411)

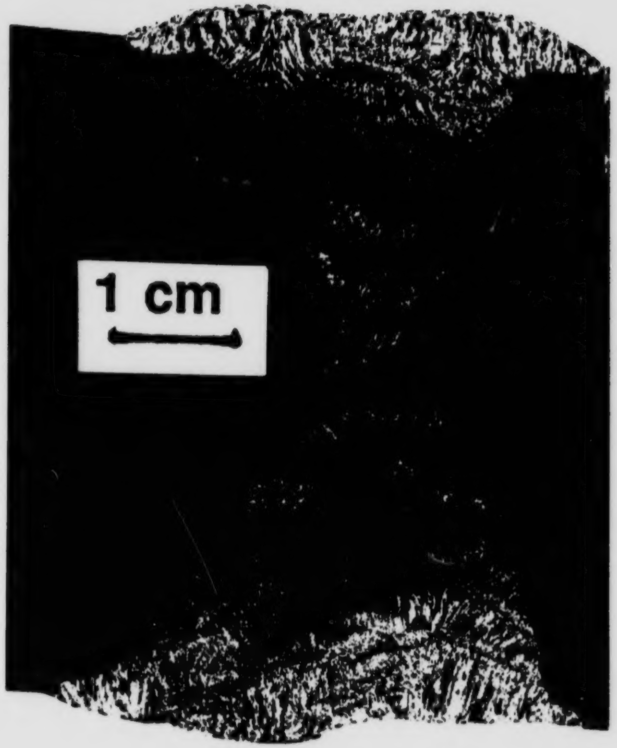

Figure 3.5 Macrograph of as-welded 3.0 kJ/mm weld deposited with Consumable A in 1G position (F1B) (2X, Neg. 11413)

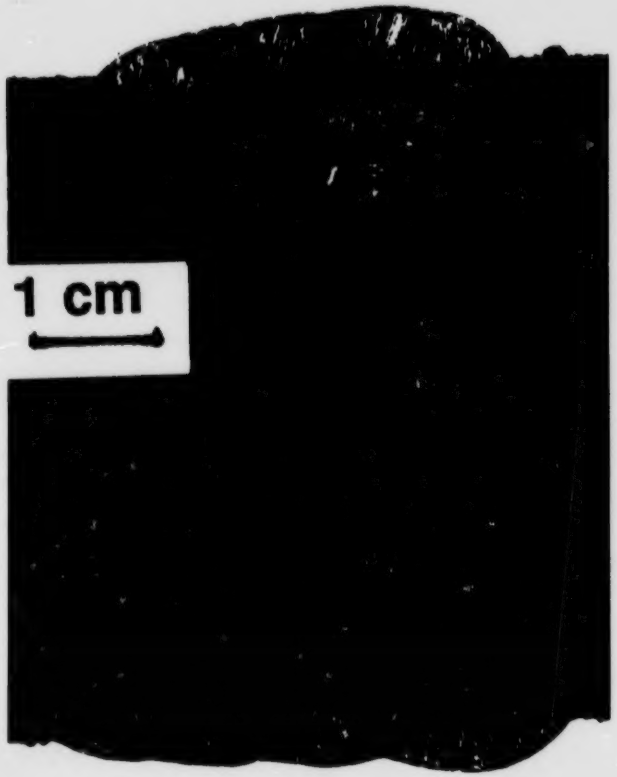

Figure 3.6 Macrograph of stress relieved 2.0 kJ/mm prepared with Consumable B in 1G position (F6A) (2X, Neg. 11409)

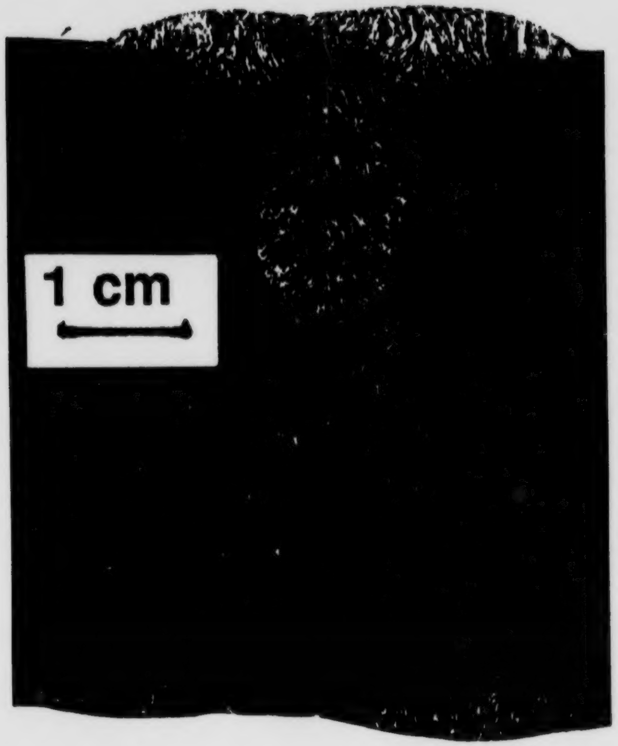

Figure 3.7 Macrograph of stress relieved 3.0 kJ/mm weld prepared with Consumable B in 1G position (F2B) (2X, Neg. 11412)

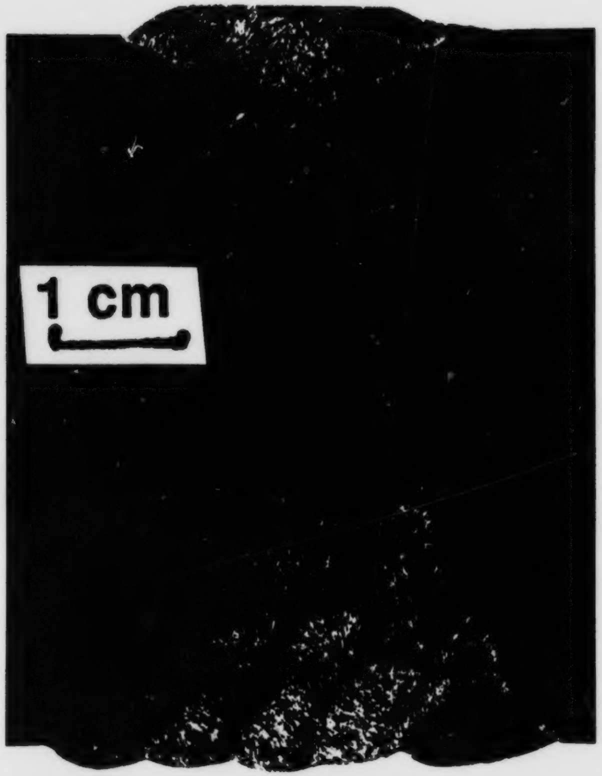

Figure 3.8 Macrograph of as-welded 2.0 kJ/mm weld deposited with Consumable B in 3G position (F7B) (2X, Neg. 11434)

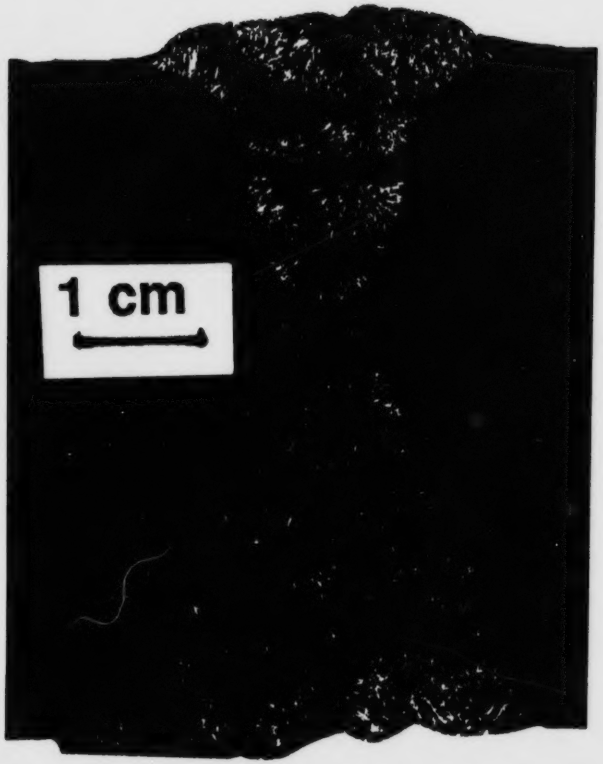

Figure 3.9 Macrograph of stress relieved 2.0 kJ/mm weld prepared with Consumable B in 3G position (F7A) (2X, Neg. 11408)

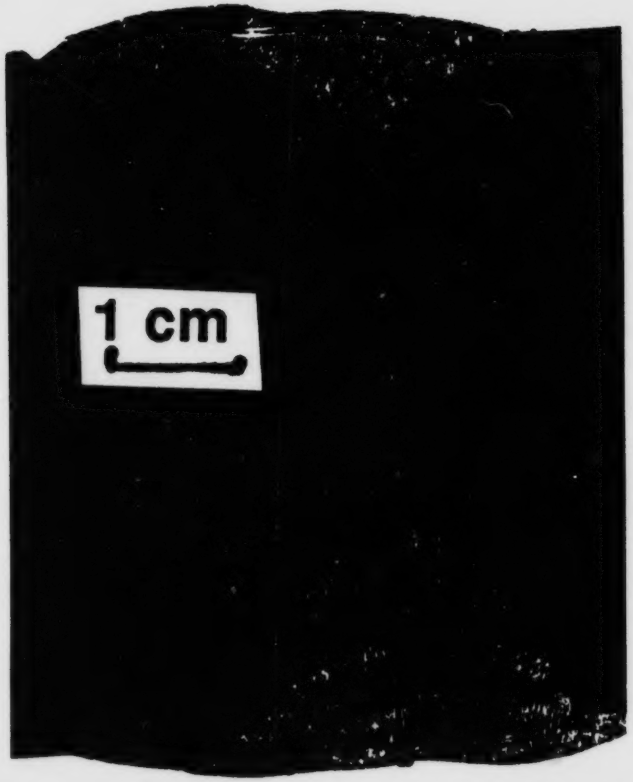

Figure 3.10 Macrograph of as-welded 2.0 kJ/mm weld deposited with Consumable C in 1G position (F9B) (2X, Neg. 11435)

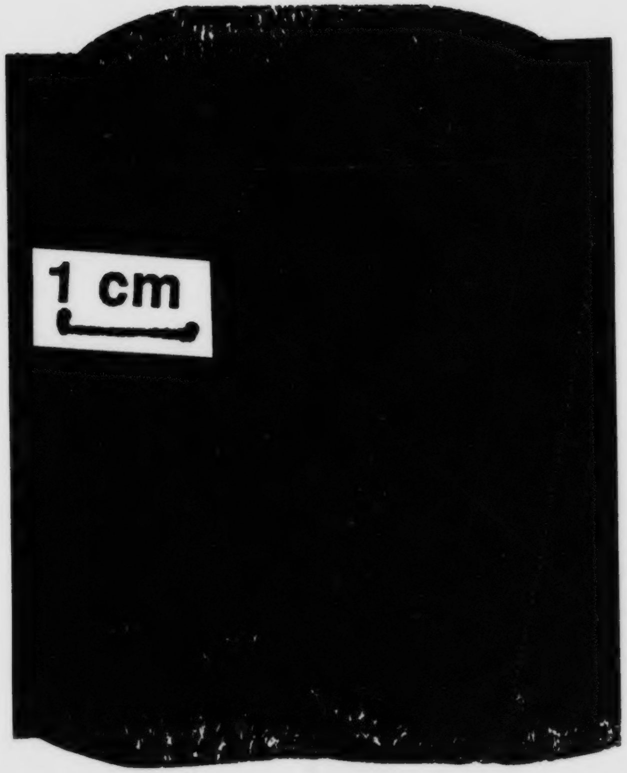

Figure 3.11 Macrograph of as-welded 3.0 kJ/mm weld prepared with Consumable C in 1G position (F3B) (2X, Neg. 11433)

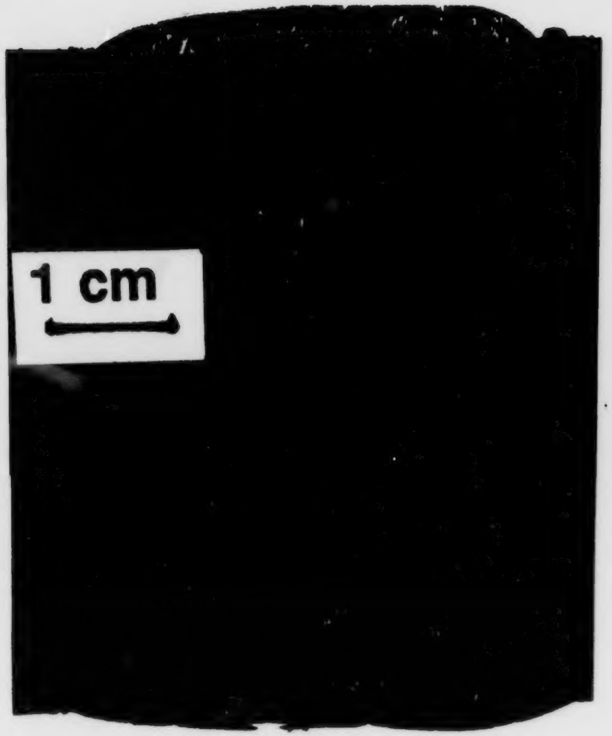

Figure 3.12 Macrograph of stress relieved 2.0 kJ/mm weld deposited with Consumable C in 1G position (F9A) (2X, Neg. 11406)

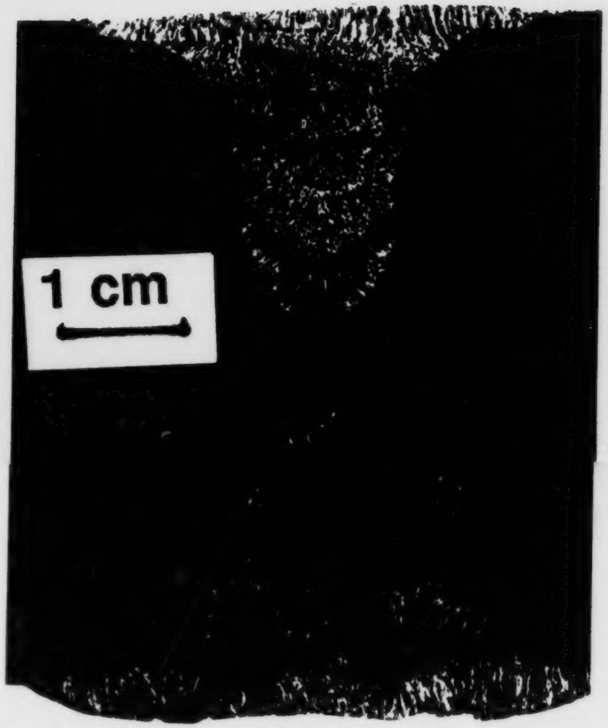

Figure 3.13 Macrograph of stress relieved 3.0 kJ/mm weld deposited with Consumable C in 1G position (F4B) (2X, Neg. 11410)

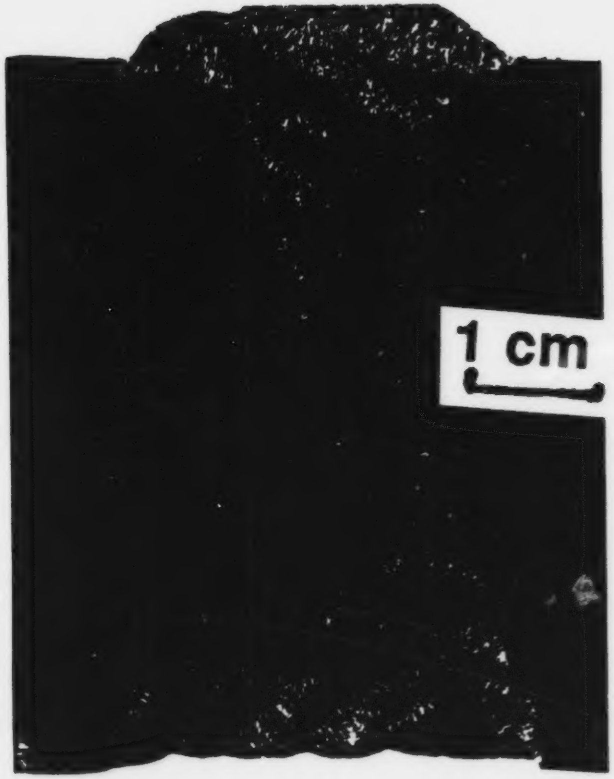

Figure 3.14 Macrograph of as-welded 2.0 kJ/mm weld deposited with Consumable C in 3G position (F8B) (2X, Neg. 11436)

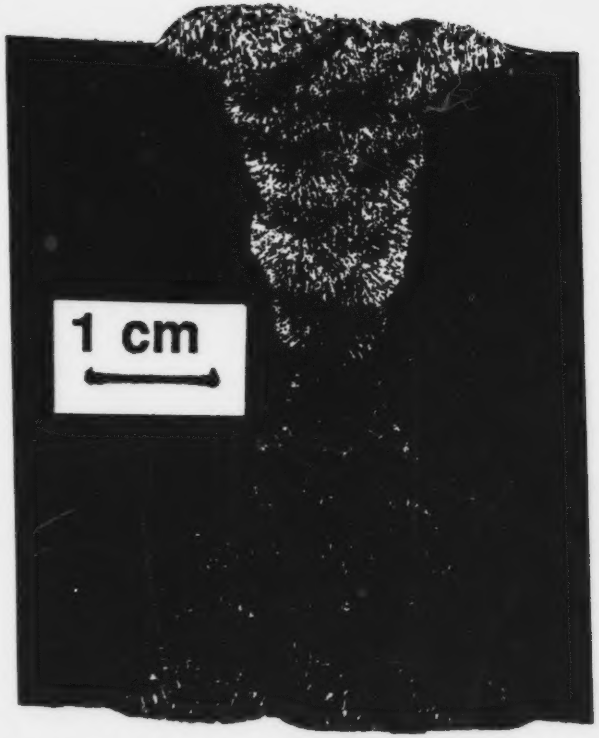

Figure 3.15 Macrograph of stress relieved 2.0 kJ/mm weld prepared with Consumable C in 3G position (F8A) (2X, Neg. 11407)

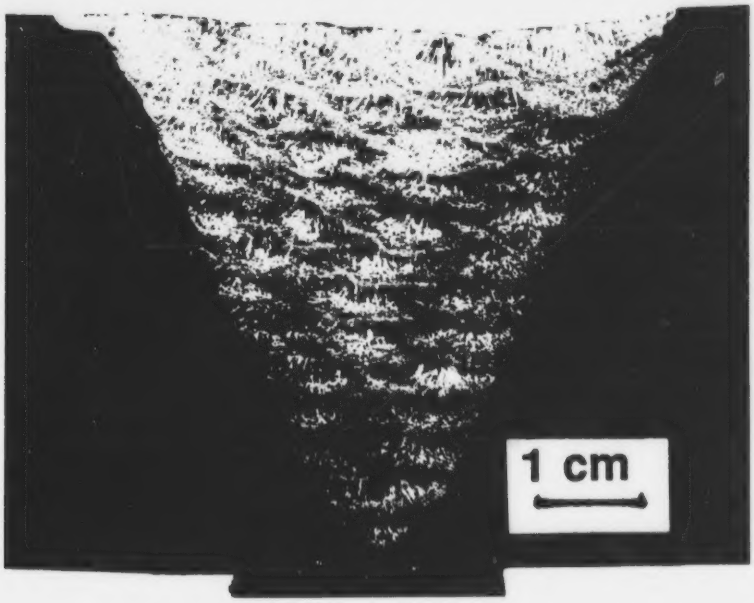

Figure 3.16: Macrograph of as-welded 2.0 kJ/mm weldments prepared with Consumable B in high angular and low lateral restraint conditions (F10A) (1.6X, Neg. 11392)

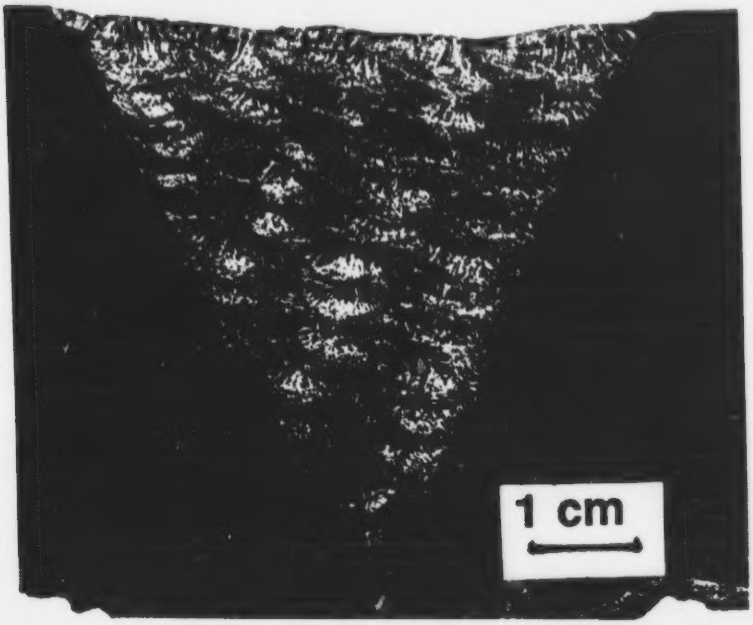

Figure 3.17: Macrograph of as-welded 2.0 kJ/mm weldment deposited with Consumable B in high angular and high lateral restraint conditions (F11A) (1.6X, Neg. 11391)

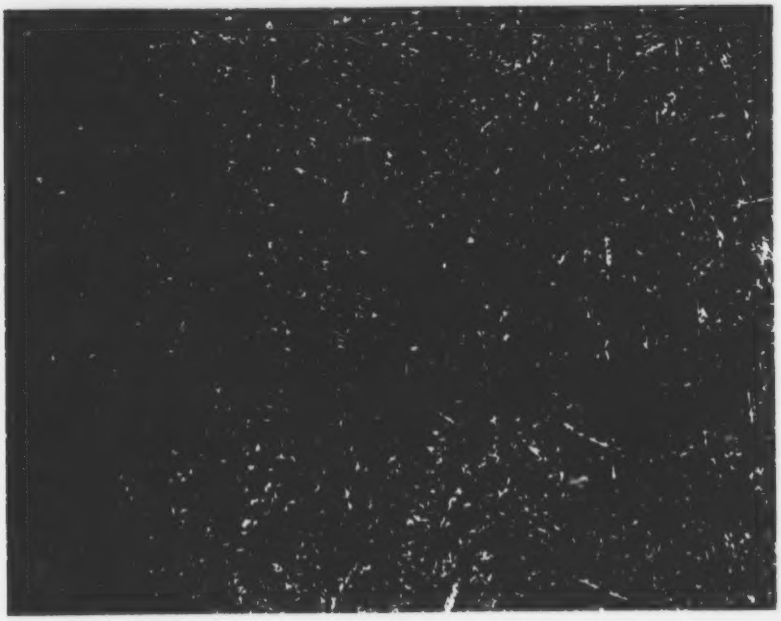

(a) (100X, Neg. 11396)

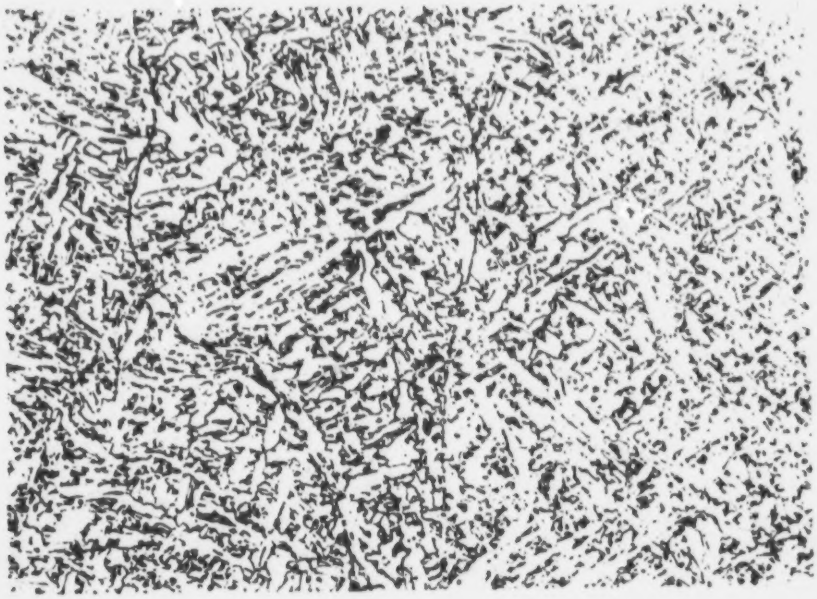

(b) (500X, Neg. 11405)

Figure 3.18: Representative microstructure of as-welded 2.0 kJ/mm veldment deposited in 1G position with Consumable A (F5A)

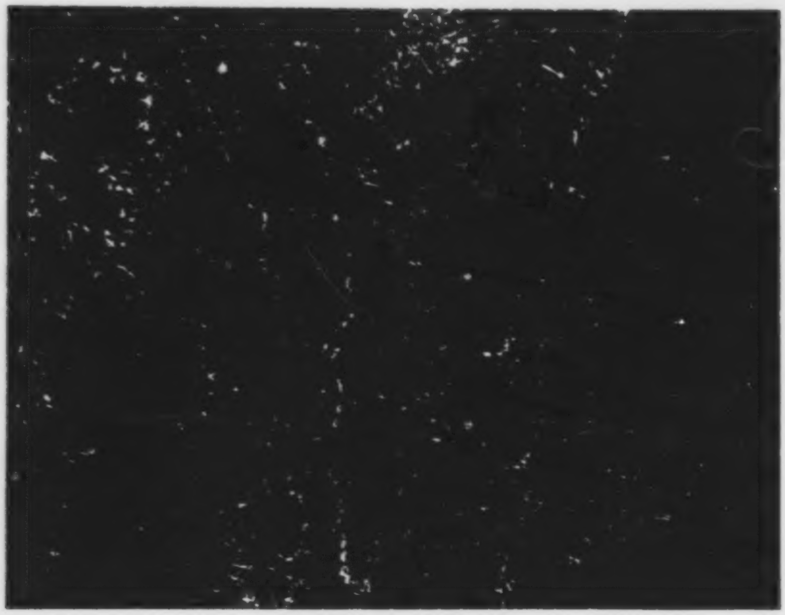

(a) (100X, Neg. 11398)

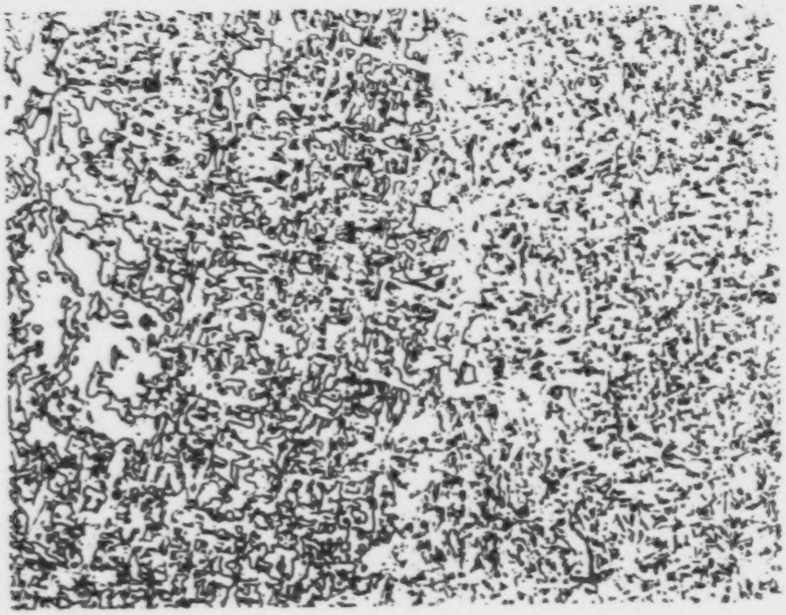

(b) (500X, Neg. 11404)

Figure 3.19: Representative microstructure of as-welded 3.0 kJ/mm weldment deposited in 1G position with Consumable A (F1B)

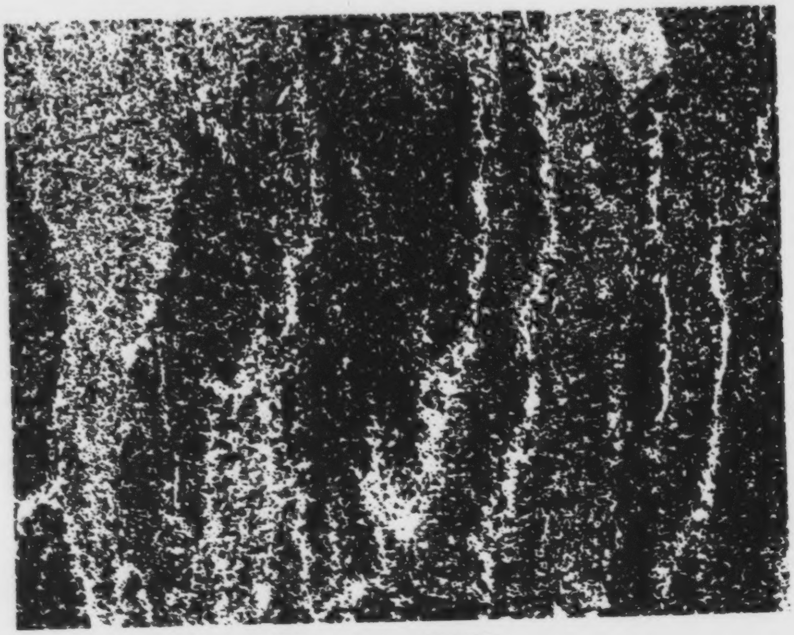

(a) (100X, Neg. 11375)

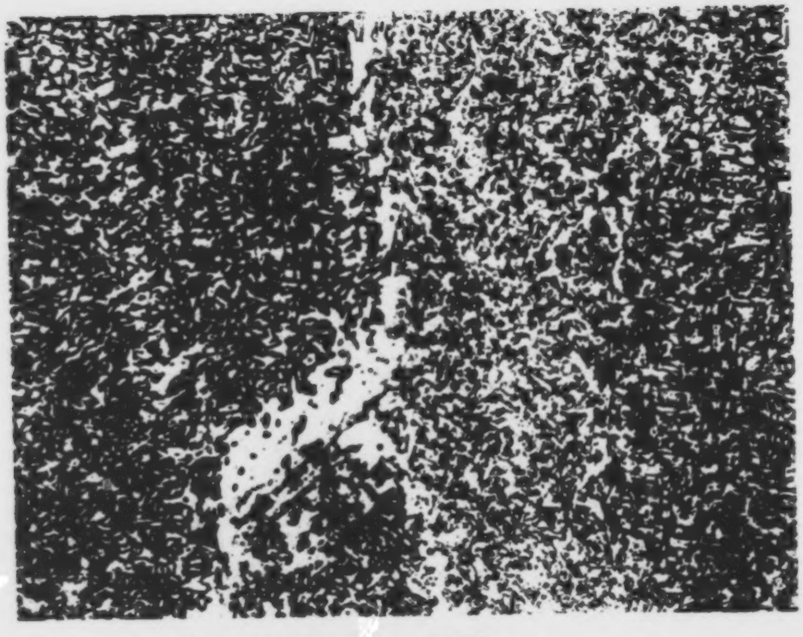

(b) (400X, Neg. 11376)

Figure 3.20: Representative microstructure of stress relieved 2.0 kJ/mm veldment deposited in 1G position with Consumable B (F6A)

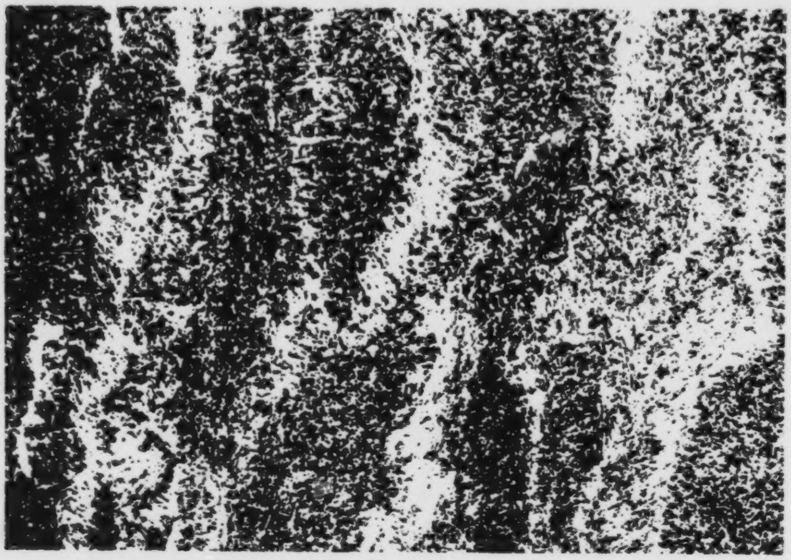

(a) (100X, Neg. 11373)

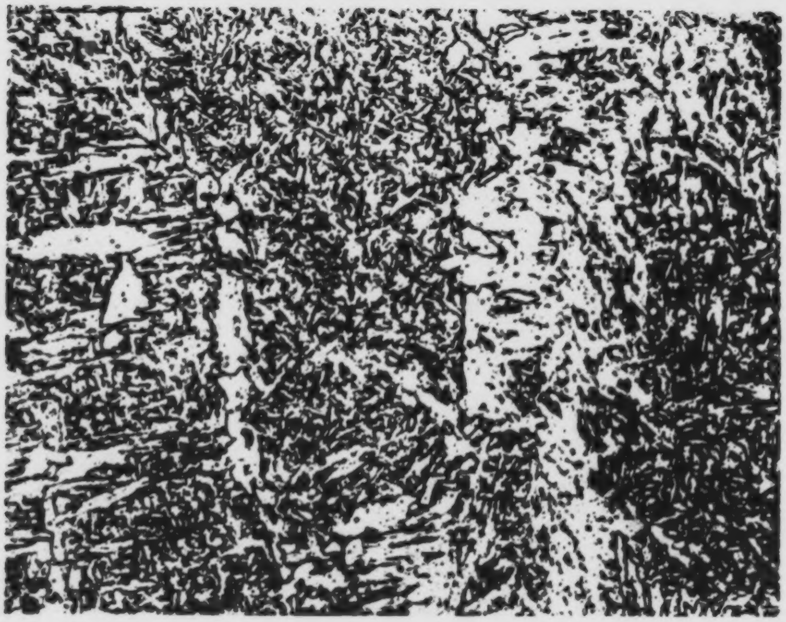

(b) (400X, Neg. 11374)

Figure 3.21: Representative microstructure of stress relieved 3.0 kJ/mm weldment deposited in 1G position with Consumable B (F2B)

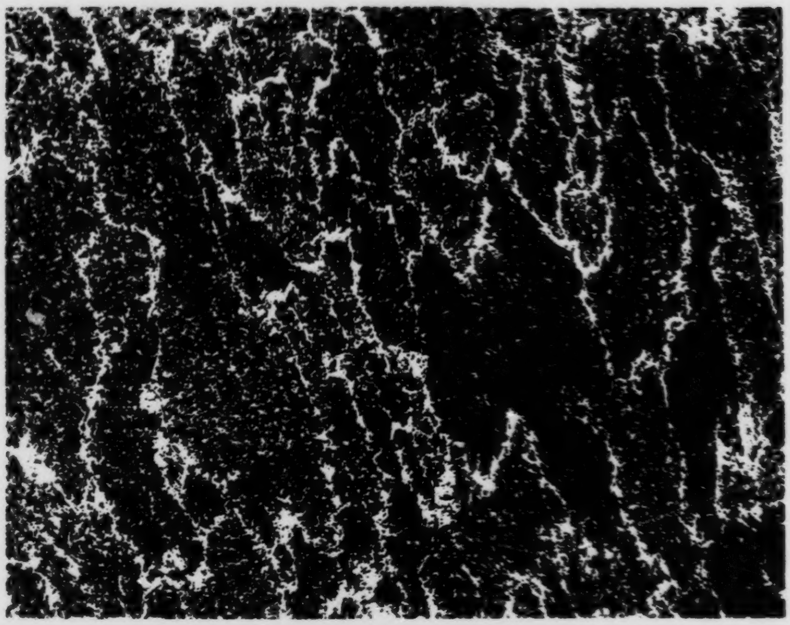

(a) (100X, Neg. 11383)

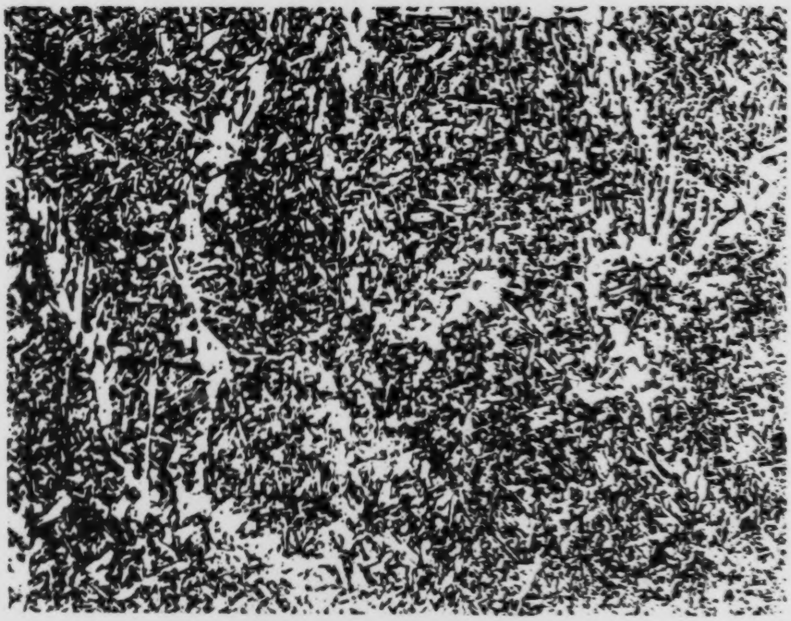

(b) (500X, Neg. 11385)

Figure 3.22: Representative microstructure of as-welded 2.0 kJ/mm weldment deposited in 3G position with Consumable B (F7B)

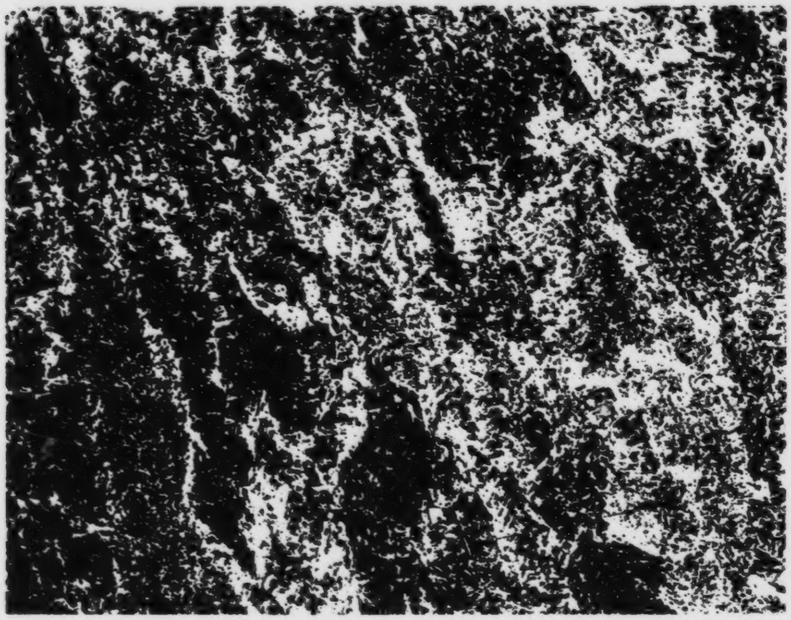

(a) (100X, Neg. 11377)

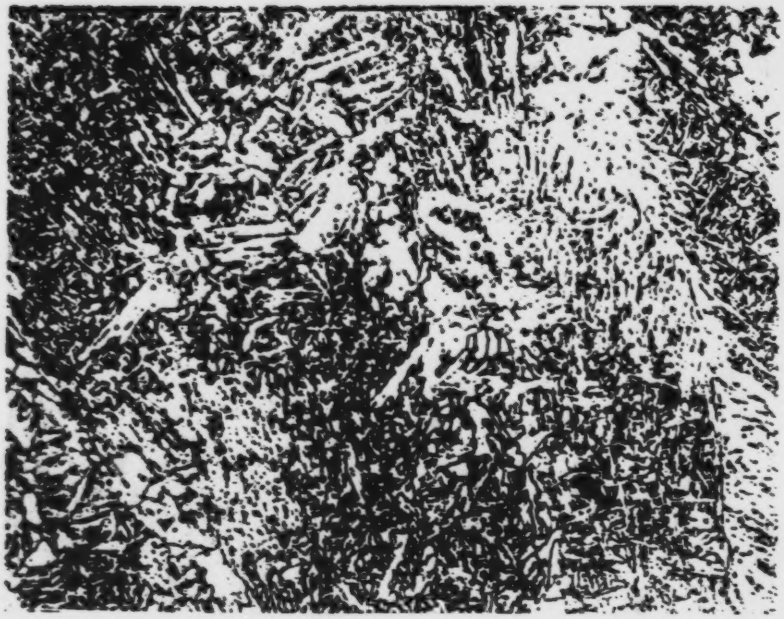

(b) (400X, Neg. 11378)

Figure 3.23: Representative microstructure of stress relieved 2.0 kJ/mm weldment deposited in 3G position with Consumable B (F7A)

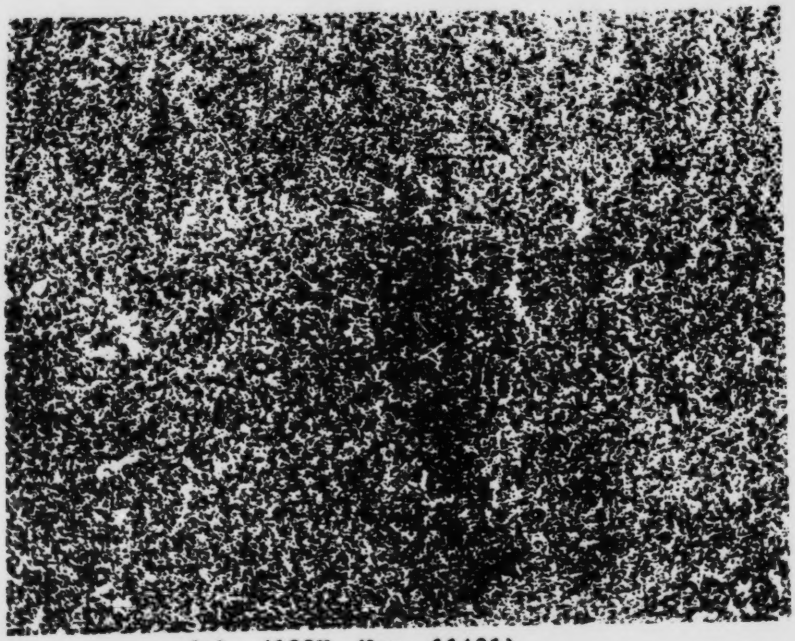

(a) (100X, Neg. 11431)

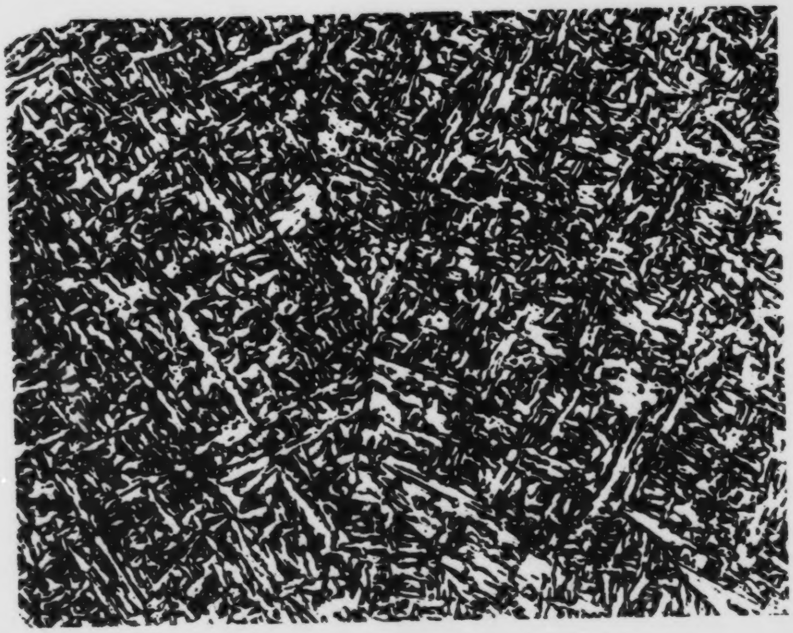

(b) (500X, Neg. 11432)

Figure 3.24: Representative microstructure of as-welded 2.0 kJ/mm weldment deposited in 1G position with Consumable C (F9B)

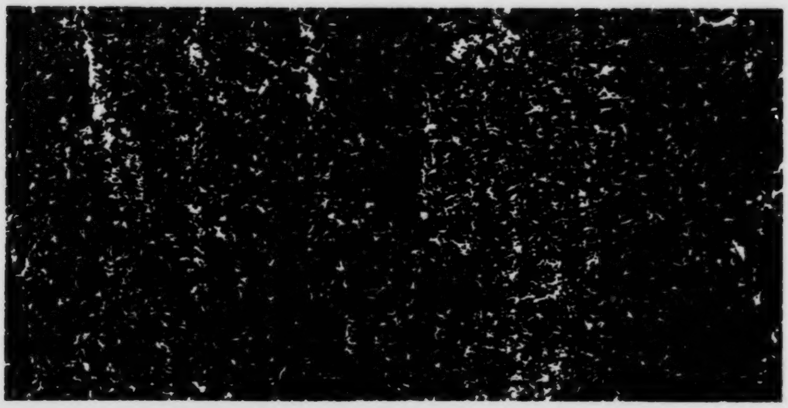

(a) (100X, Neg. 11400)

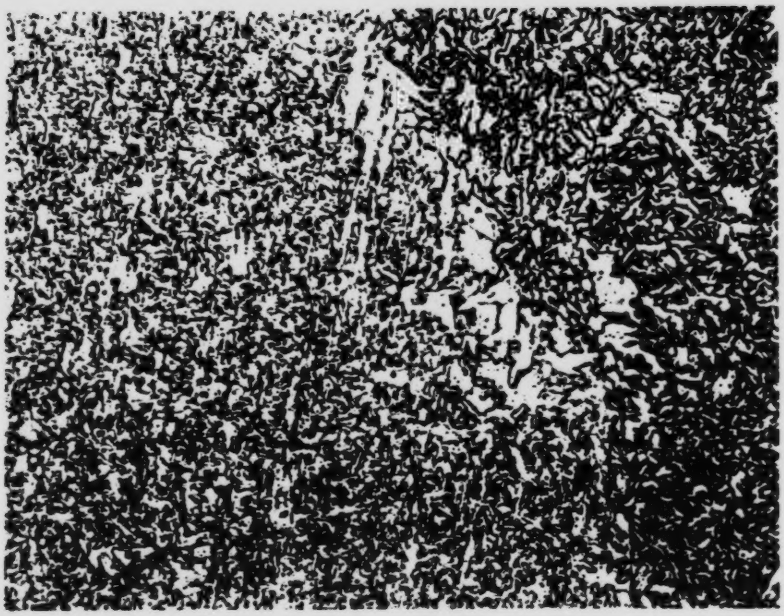

(b) (400X, Neg. 11402)

Figure 3.25: Representative microstructure of stress relieved 2.0 kJ/mm weldment deposited in 1G position with Consumable C (F9A)

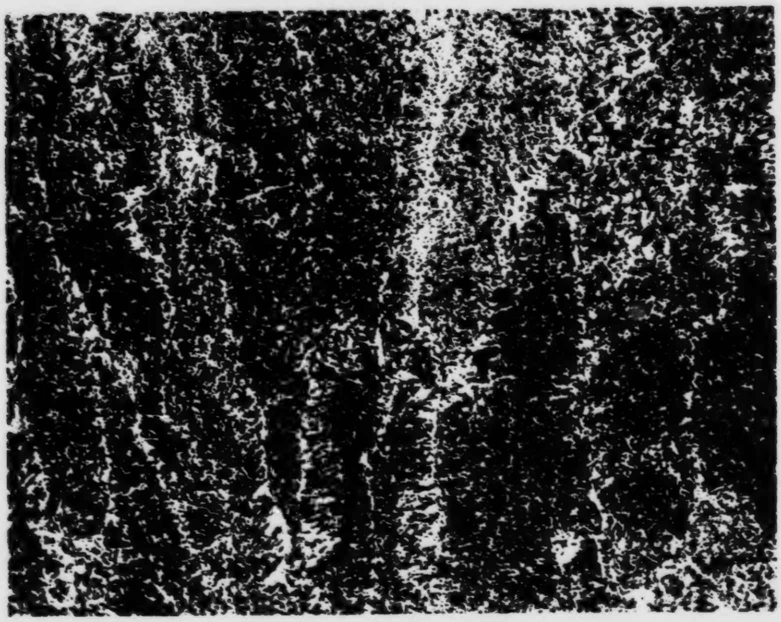

(a) (100X, Neg. 11372)

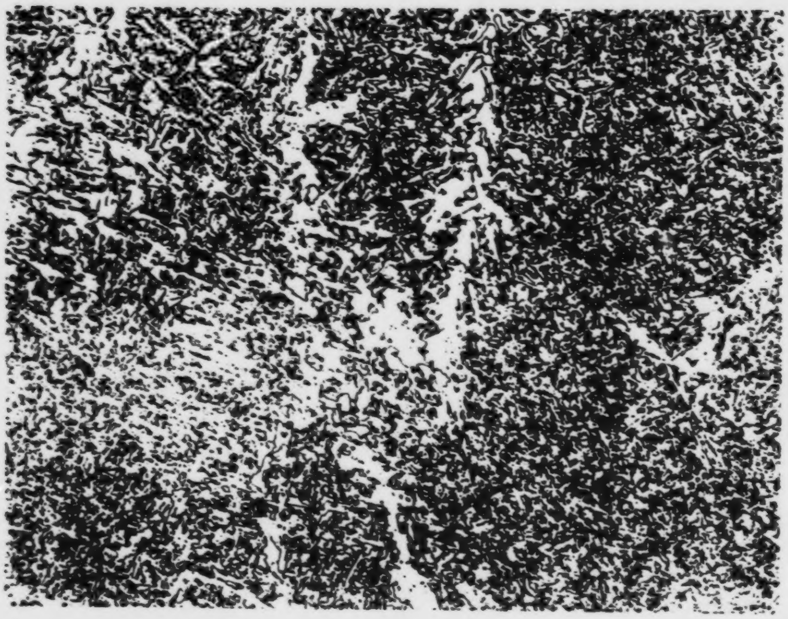

(b) (500X, Neg. 11443)

Figure 3.26: Representative microstructure of as-welded 3.0 kJ/mm weldment deposited in 1G position with Consumable C (F3B)

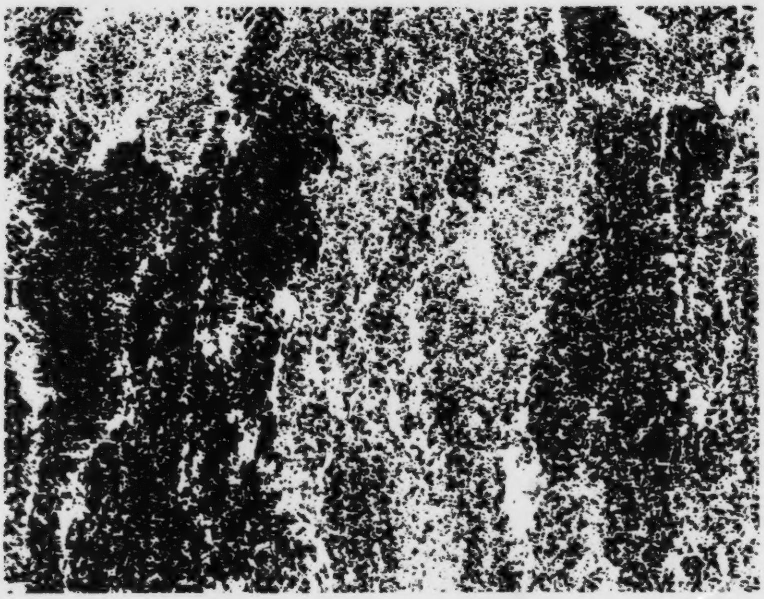

(a) (100X, Neg. 11389)

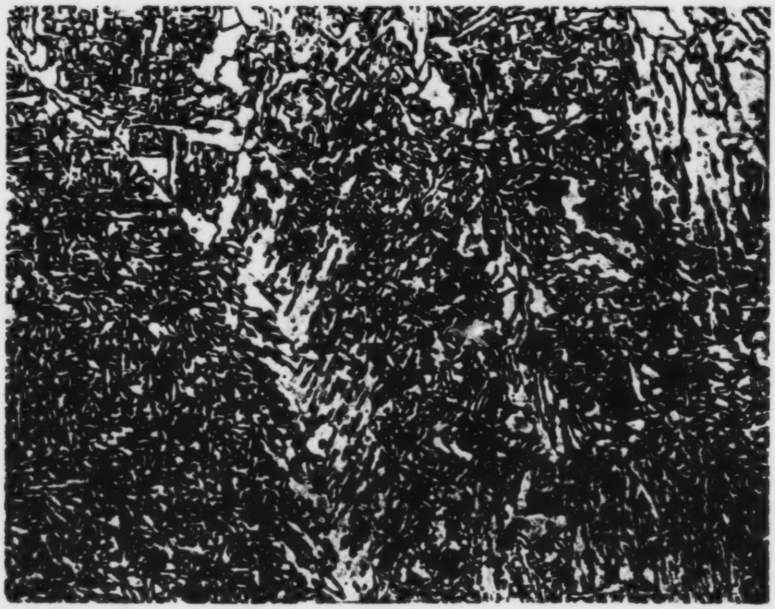

(b) (400X, Neg. 11403)

Figure 3.27: Representative microstructure of stress relieved 3.0 kJ/mm weldment deposited in 1G position with Consumable C (F4B)

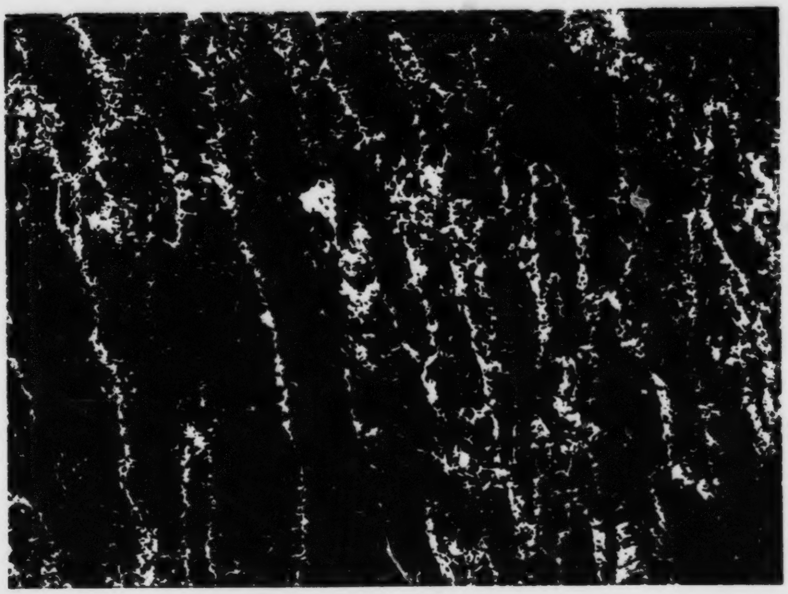

(a) (100X, Neg. 11393)

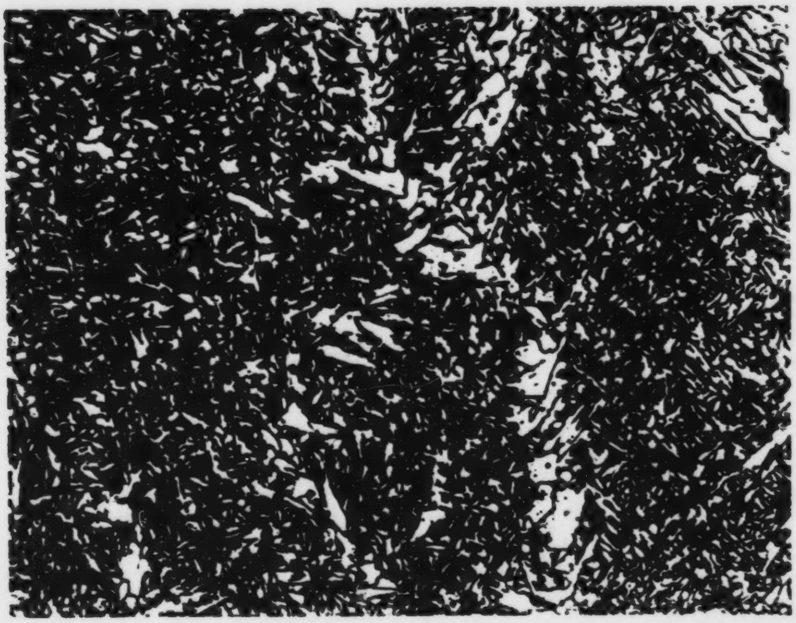

(b) (500X, Neg. 11395)

Figure 3.28: Representative microstructure of as-welded 2.0 kJ/mm weldment deposited in 3G position with Consumable C (F8B)

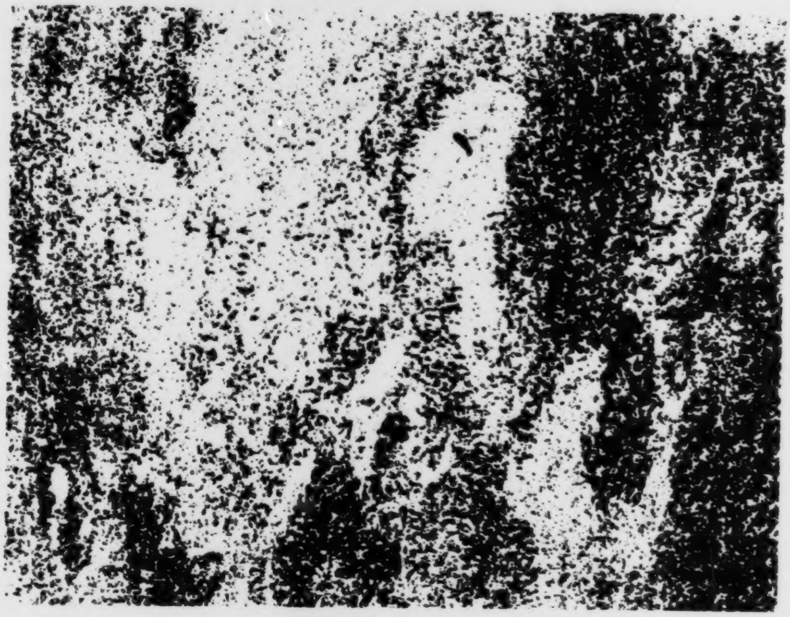

(a) (100X, Neg. 11379)

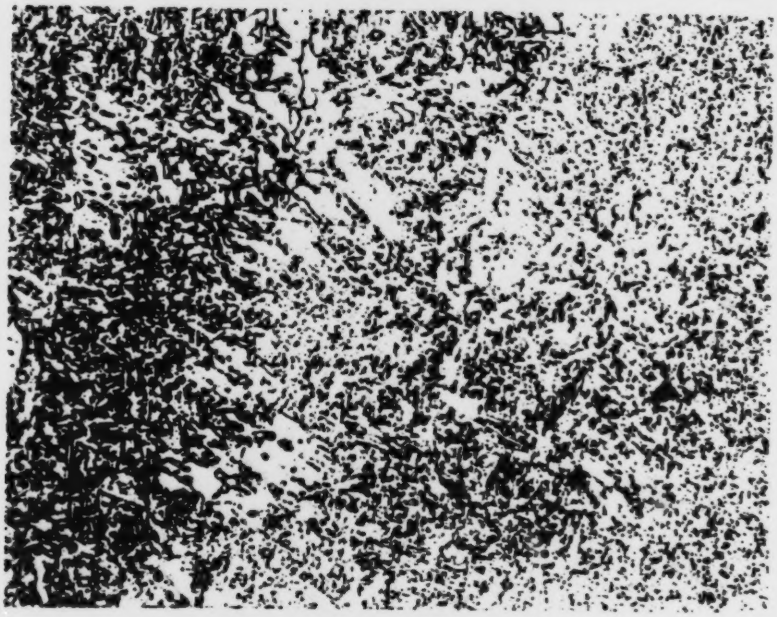

(b) (400X, Neg. 11381)

Figure 3.29: Representative microstructure of stress relieved 2.0 kJ/mm weldment deposited in 3G position with Consumable C (F8A)

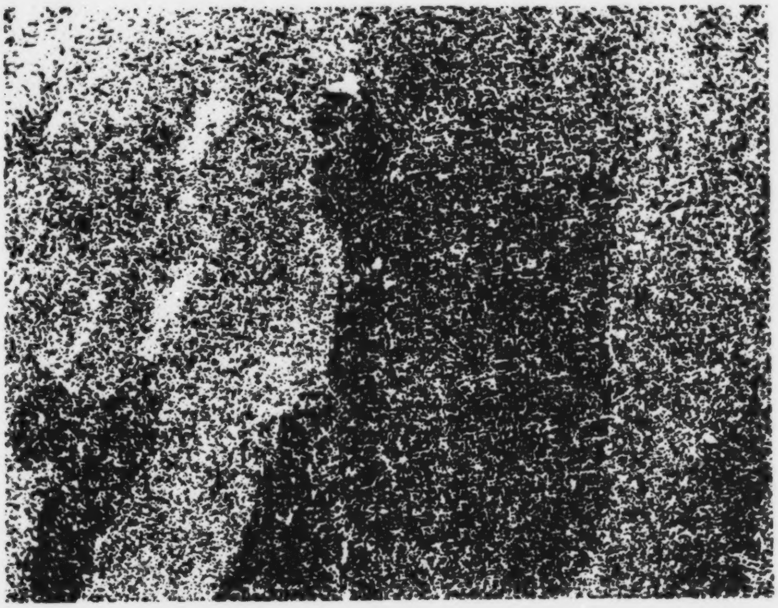

(a) (100X, Neg. 11464)

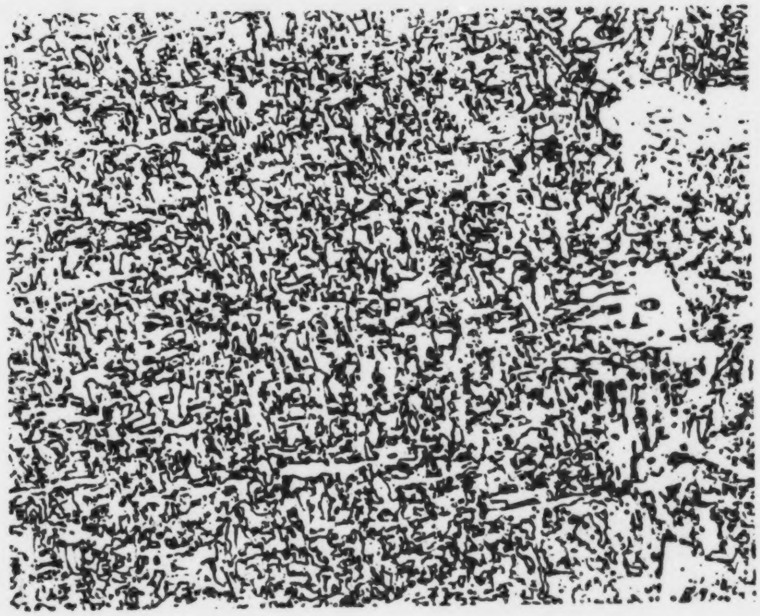

(b) (500X, Neg. 11465)

Figure 3.30: Representative microstructure of as-welded 2.0 kJ/mm weldment deposited in 1G position with Consumable B unmder "low restraint" condition (F10A)

(a) (100X, Neg. 11462)

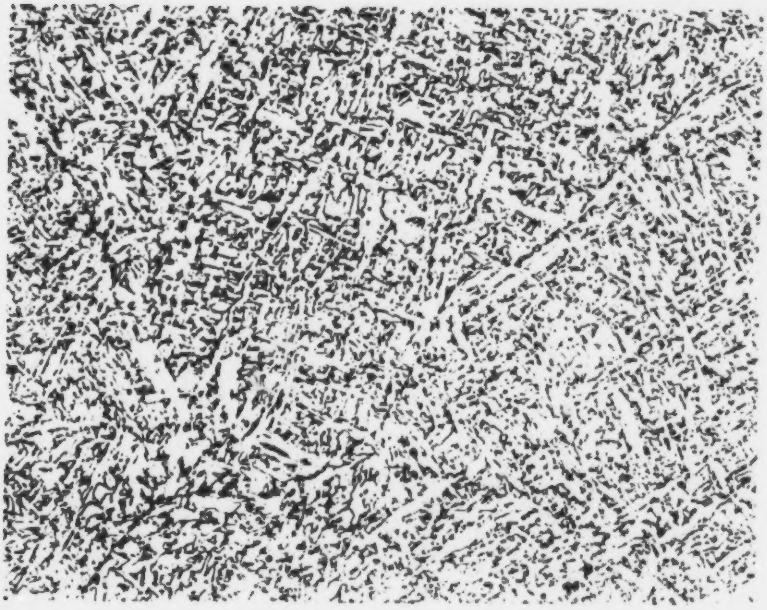

(b) (500X, Neg. 11463)

Figure 3.31: Representative microstructure of as-welded 2.0 kJ/mm weldment deposited in 1G position with Consumable B under "high restraint" condition (F11A)

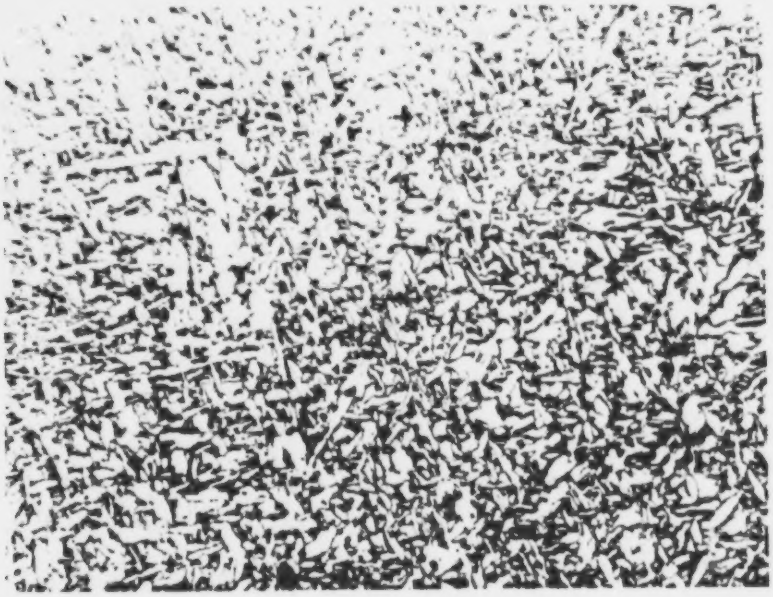

(a) As-welded condition (F7B) (1000X, Neg. 11384)

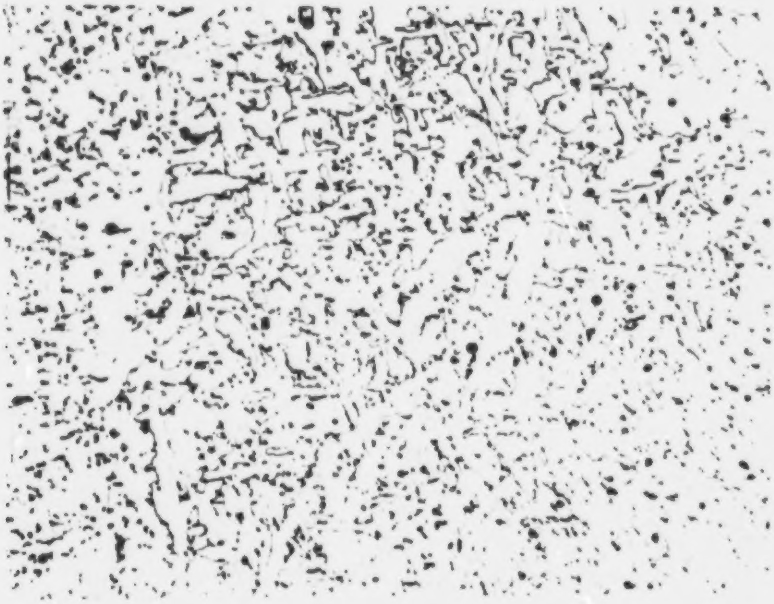

(b) Stress relieved condition (F7A) (1000X, Neg. 11380)

Figure 3.32: Higher magnification shows the occurrence of grain boundary precipitation after stress relief heat treatment on 2.0 kJ/mm weldment deposited in 3G position with Consumable B.

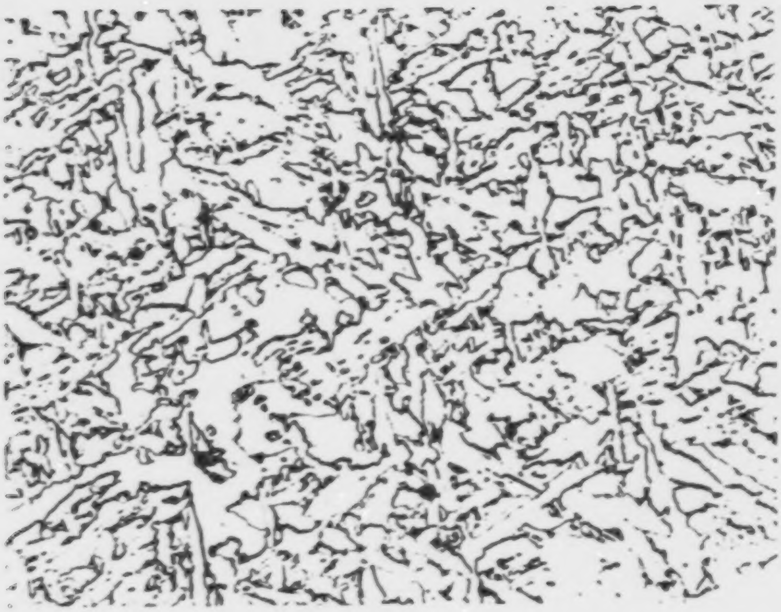

(a) 2.0 kJ/mm deposit, as-welded, Consumable A (F5A) (1000X, Neg. 11397)

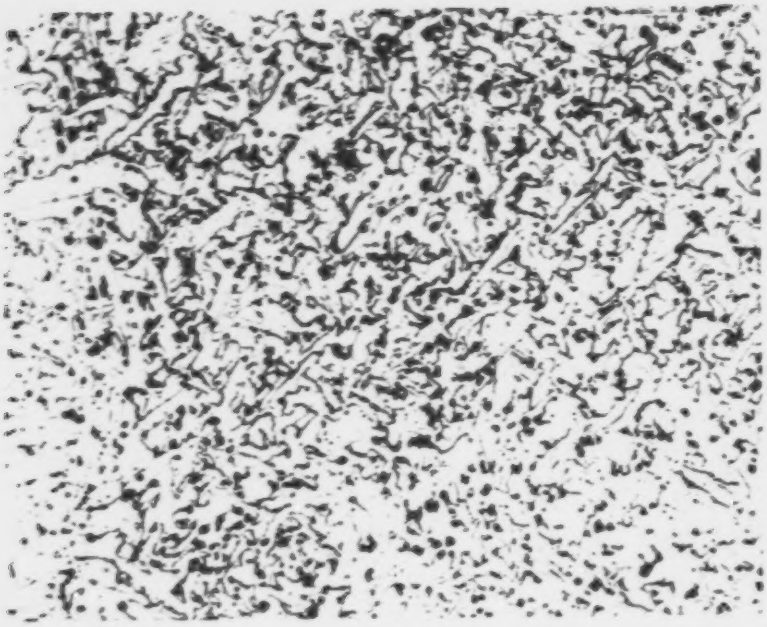

(b) 2.0 kJ/mm deposit, stress relieved, Consumable B (F6A) (1000X, Neg. 11386)

Figure 3.33: Higher magnification shows the occurrence of grain boundary precipitation after stress relief heat treatment in 1G deposits.

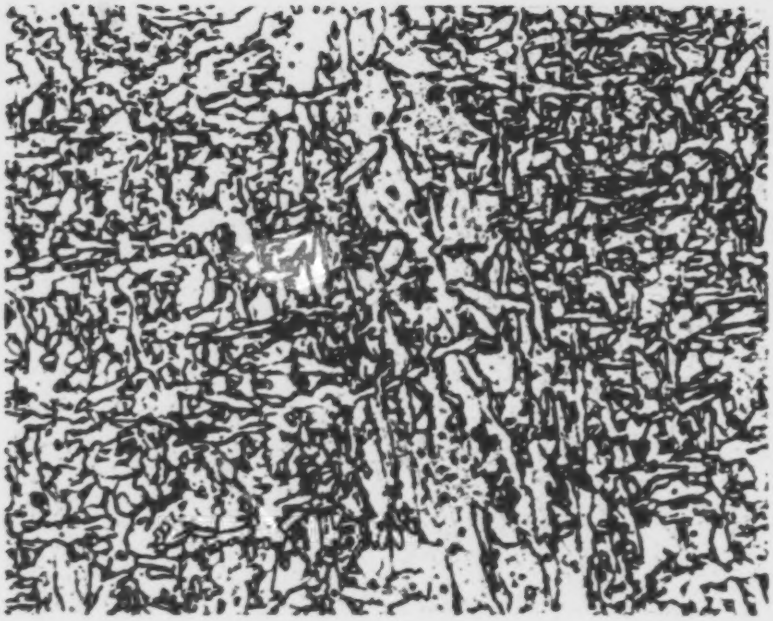

(a) 3.0 kJ/mm deposit, as-welded, Consumable A (F1B)
(1000X, Neg. 11399)

(b) 3.0 kJ/mm deposit, stress relieved, Consumable B (F2B)
(1000X, Neg. 11387)

Figure 3.34: Higher magnification shows the occurrence of grain boundary precipitation after stress relief heat treatment in 1G deposits

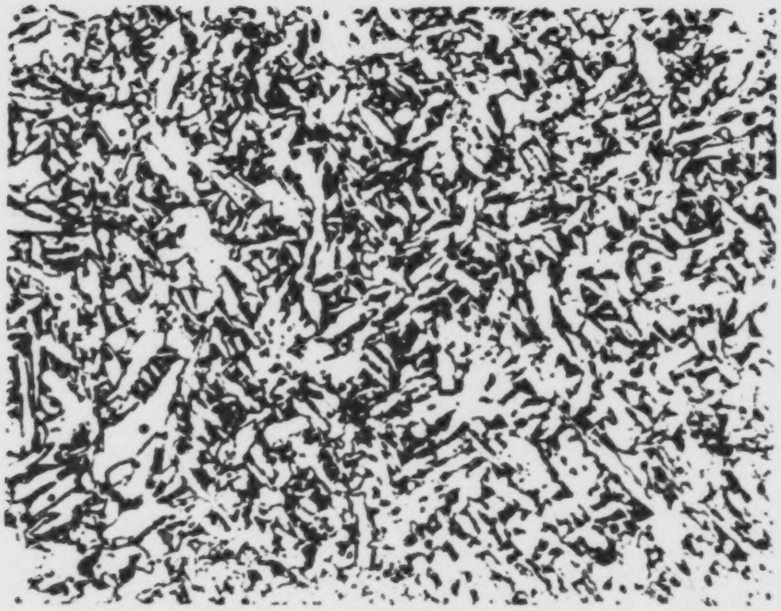

(a) As-welded condition (F9B) 1000X, Neg. 11390)

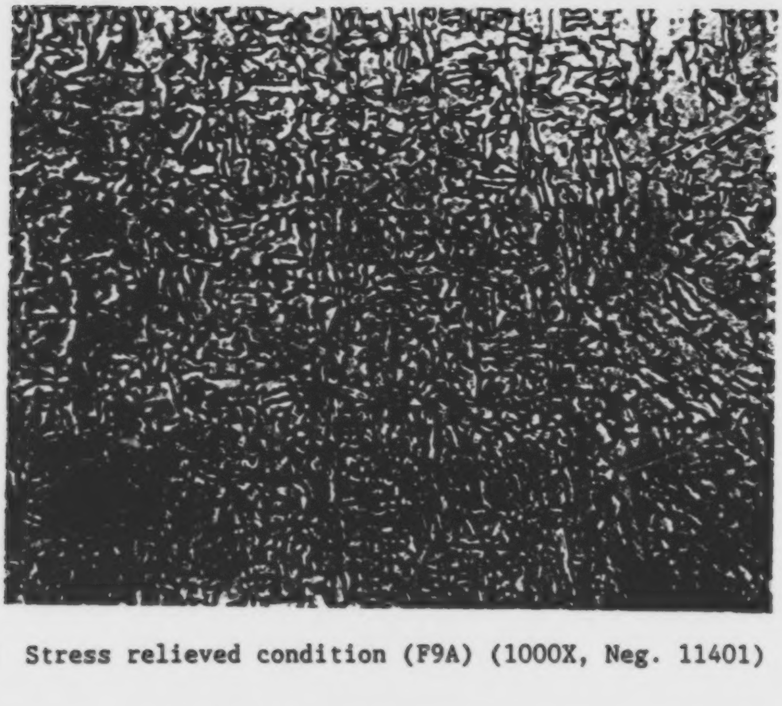

(b) Stress relieved condition (F9A) (1000X, Neg. 11401)

Figure 3.35: Higher magnification shows the occurrence of grain boundary precipitation after stress relief heat treatment on 2.0 kJ/mm weldment deposited in 1G position with Consumable C

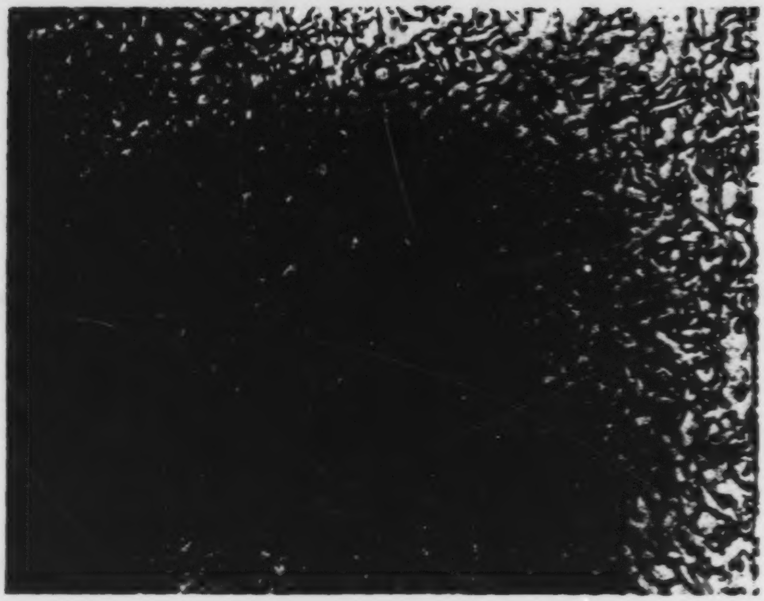

(a) As-welded condition (F3B) (1000X, Neg. 11388)

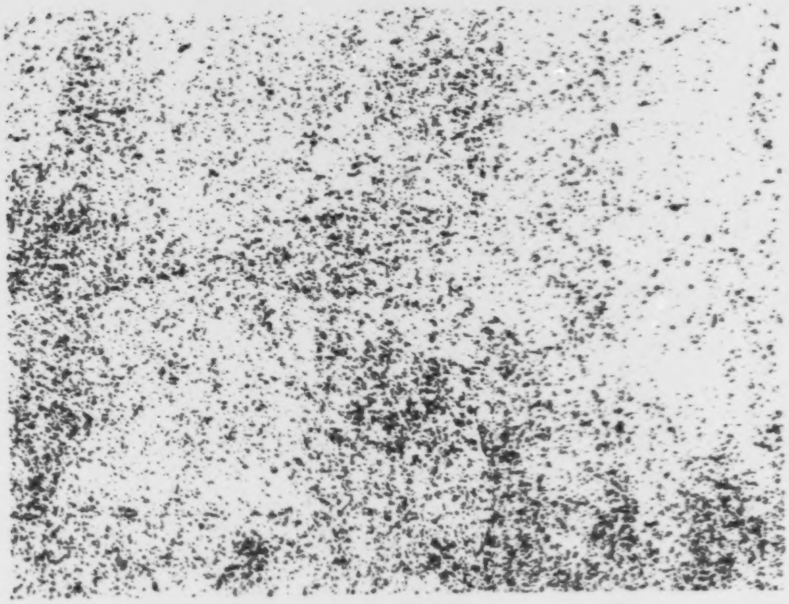

(b) Stress relieved condition (F4B) (1000X, Neg. 11564)

Figure 3.36: Higher magnification shows the occurrence of grain boundary precipitation on 3.0 kJ/mm weldment deposited in 1G position with Consumable C

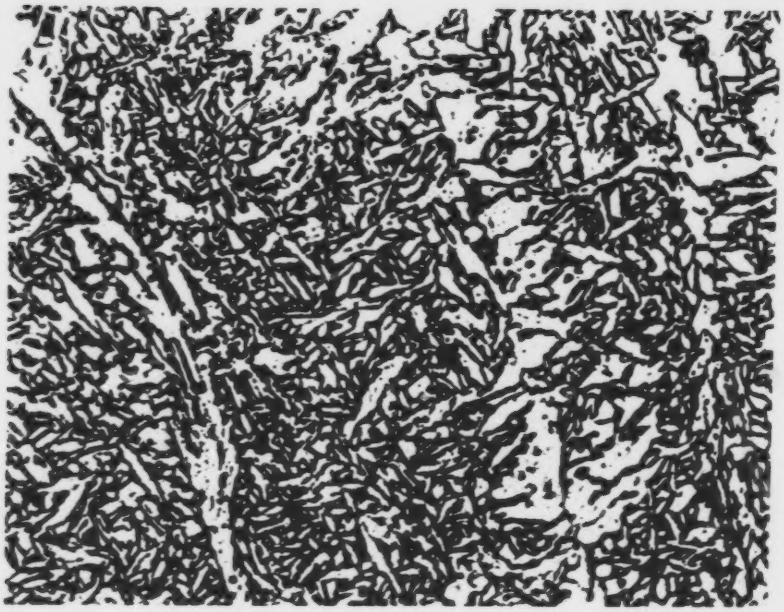

(a) As-welded condition (F8B) (1000X, Neg. 11394)

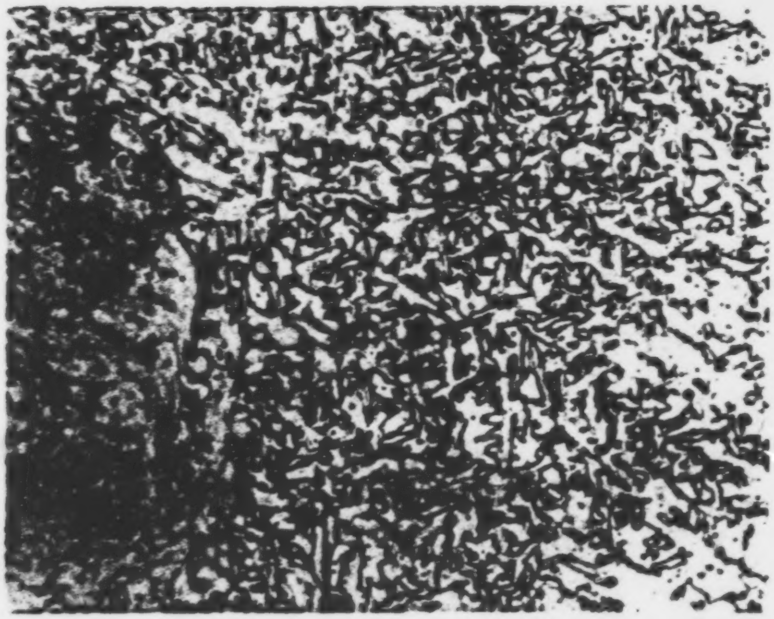

(b) Stress relieved condition (F8A) (1000X, Neg. 11382)

Figure 3.37: Higher magnification shows the occurrence of grain boundary precipitation after stress relief heat treatment on 2.0 kJ/mm weldment in 3G position with Consumable C.

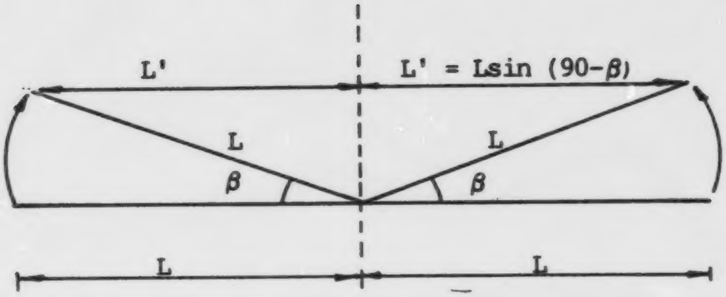

$2L = L_2$ spacings without the interference of angular distortion

$2L' = L_2$ spacings with angular distortion

$= 2L\sin(90-\beta)$

Therefore, error in $L_2 = 2L - 2L'$

$= 2L[1 - \sin(90-\beta)]$

Figure 3.38: Schematic illustration of the estimated error from angular distortion

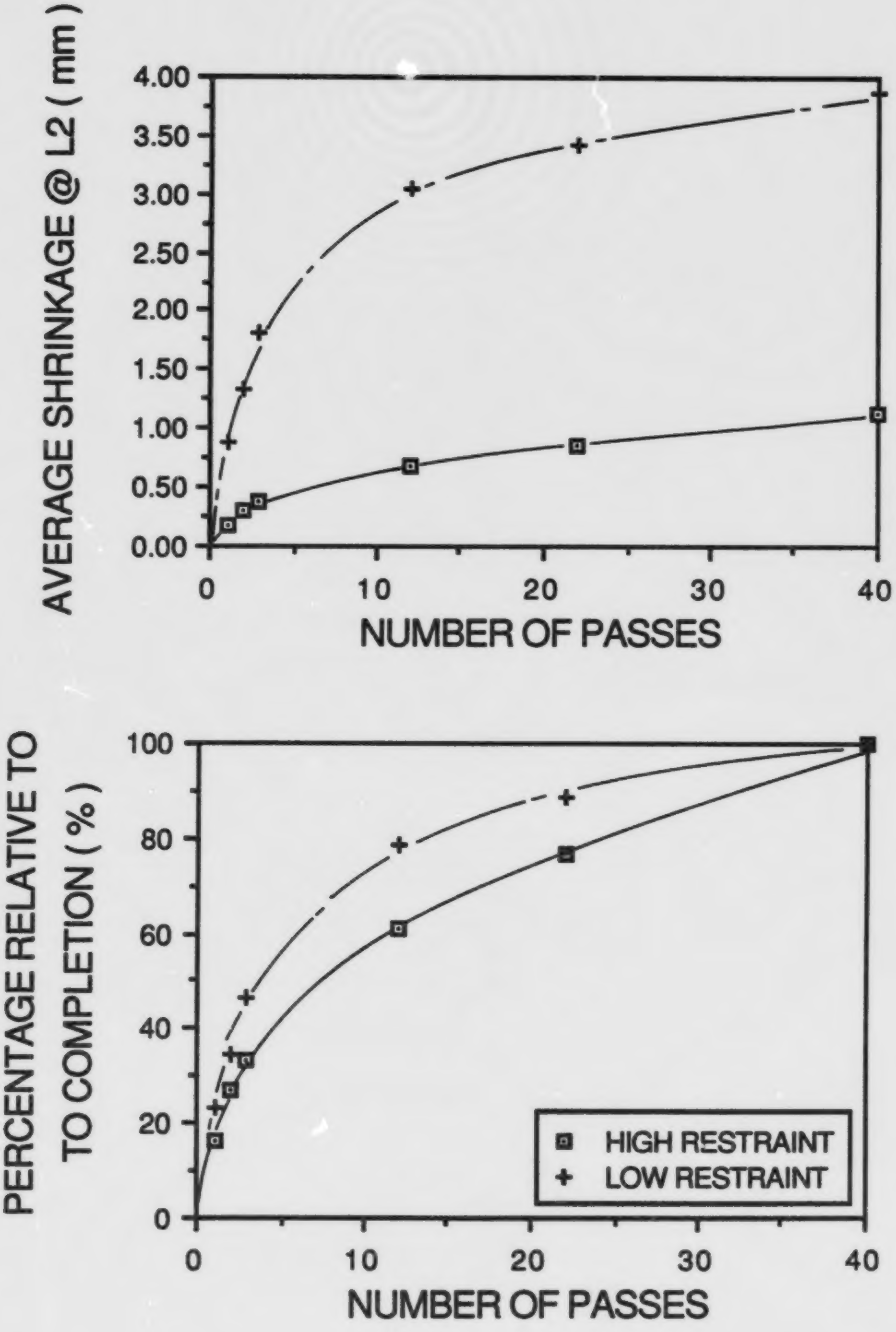

Figure 3.39: The decreasing trend of transverse shrinkage with additional weld passes is illustrated

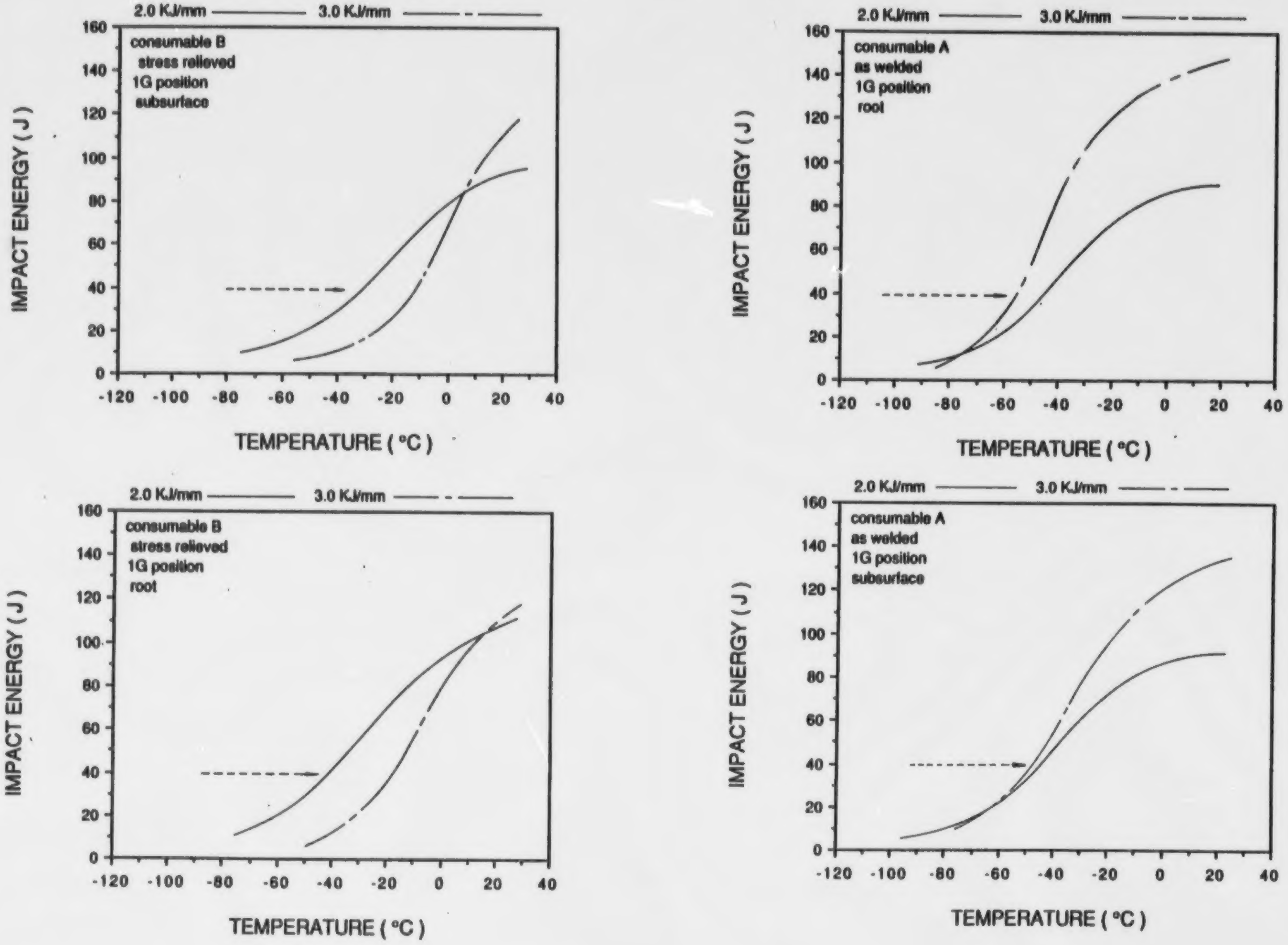

Figure 3.40: Effect of heat input on the CVN toughness of 1G deposits of Consumables A and B

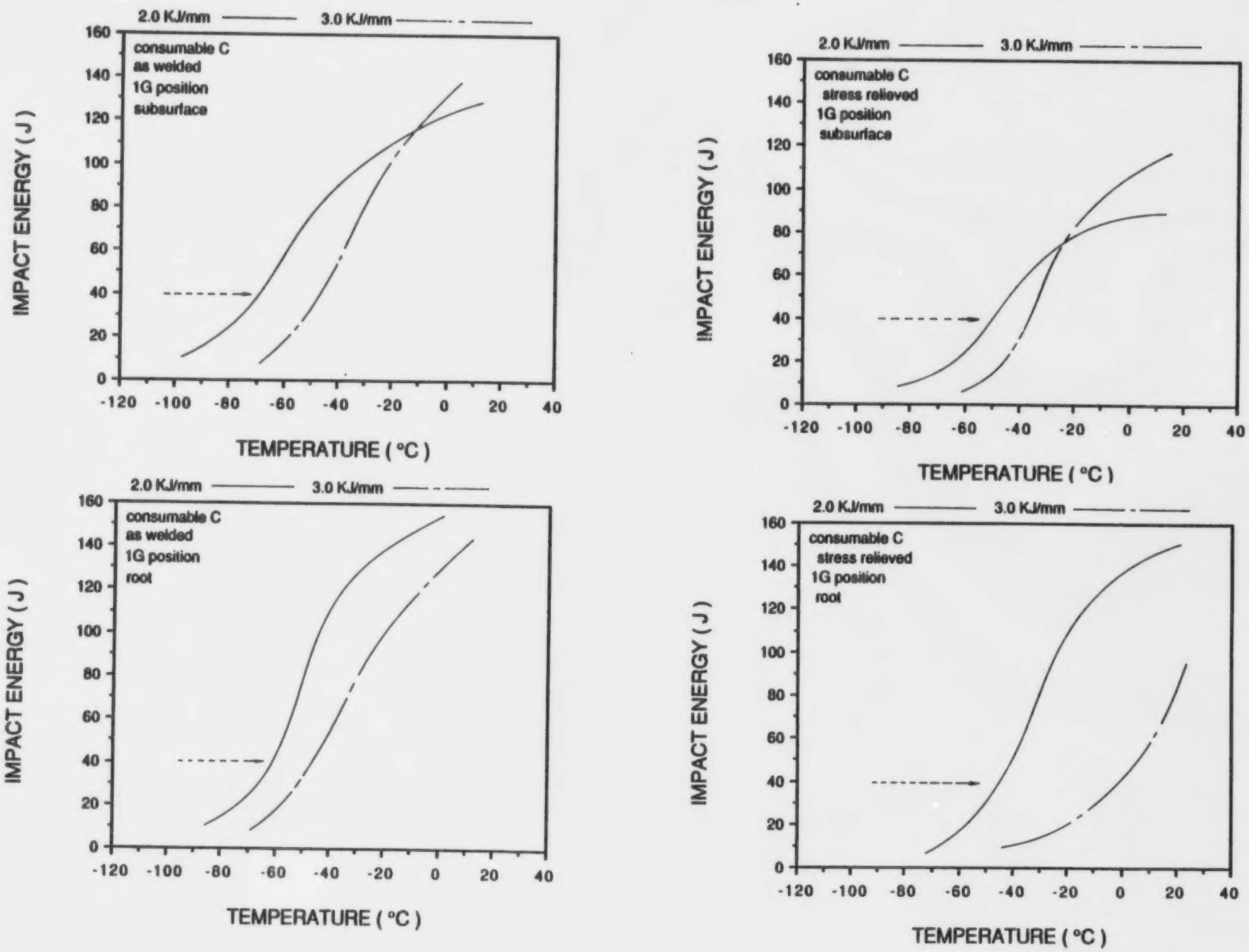

Figure 3.41: Effect of heat input on the CVN toughness of 1G deposits of Consumable C

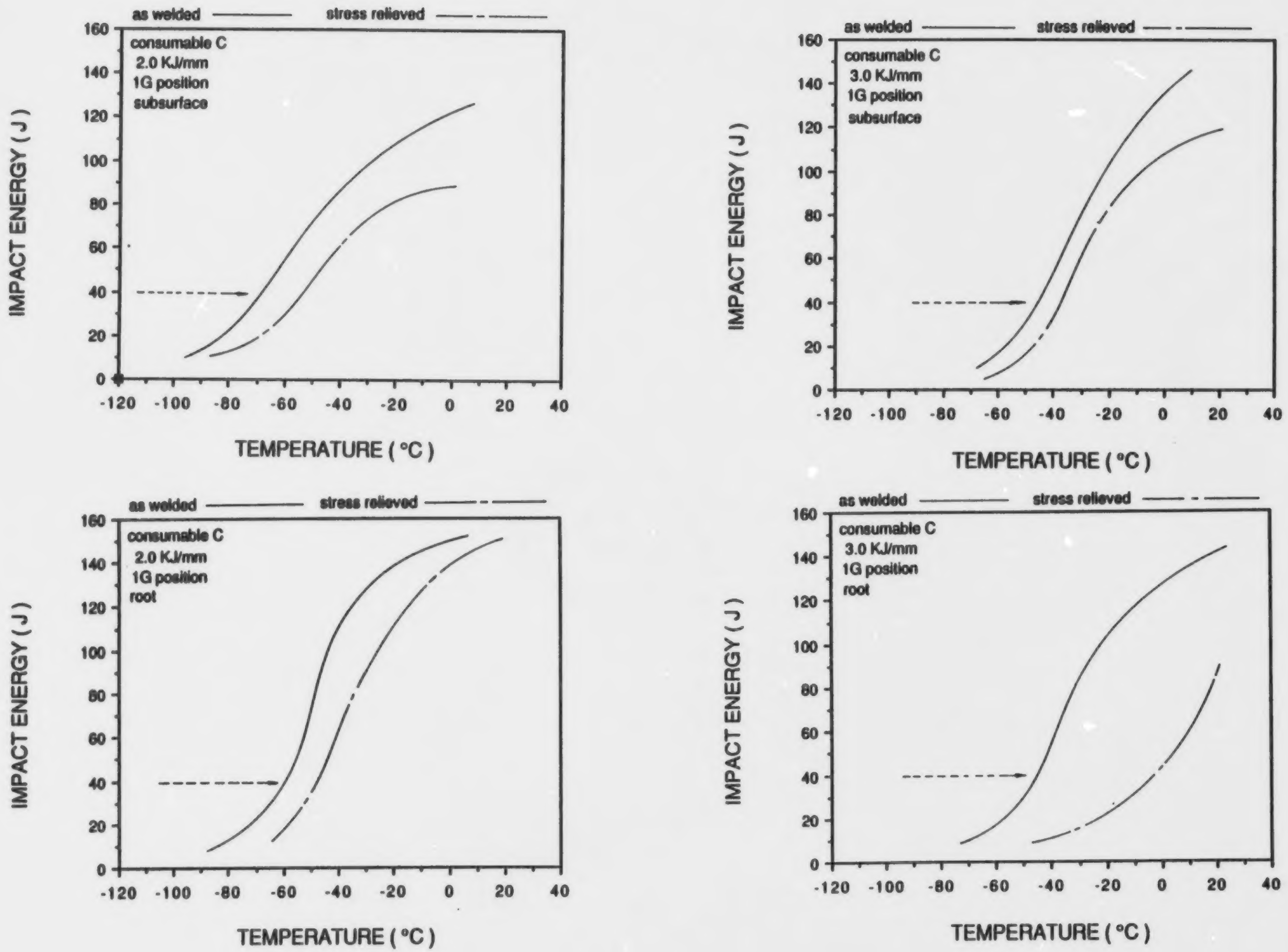

Figure 3.42: Effect of stress relief heat treatment on the CVN toughness of 1G deposits of Consumable C

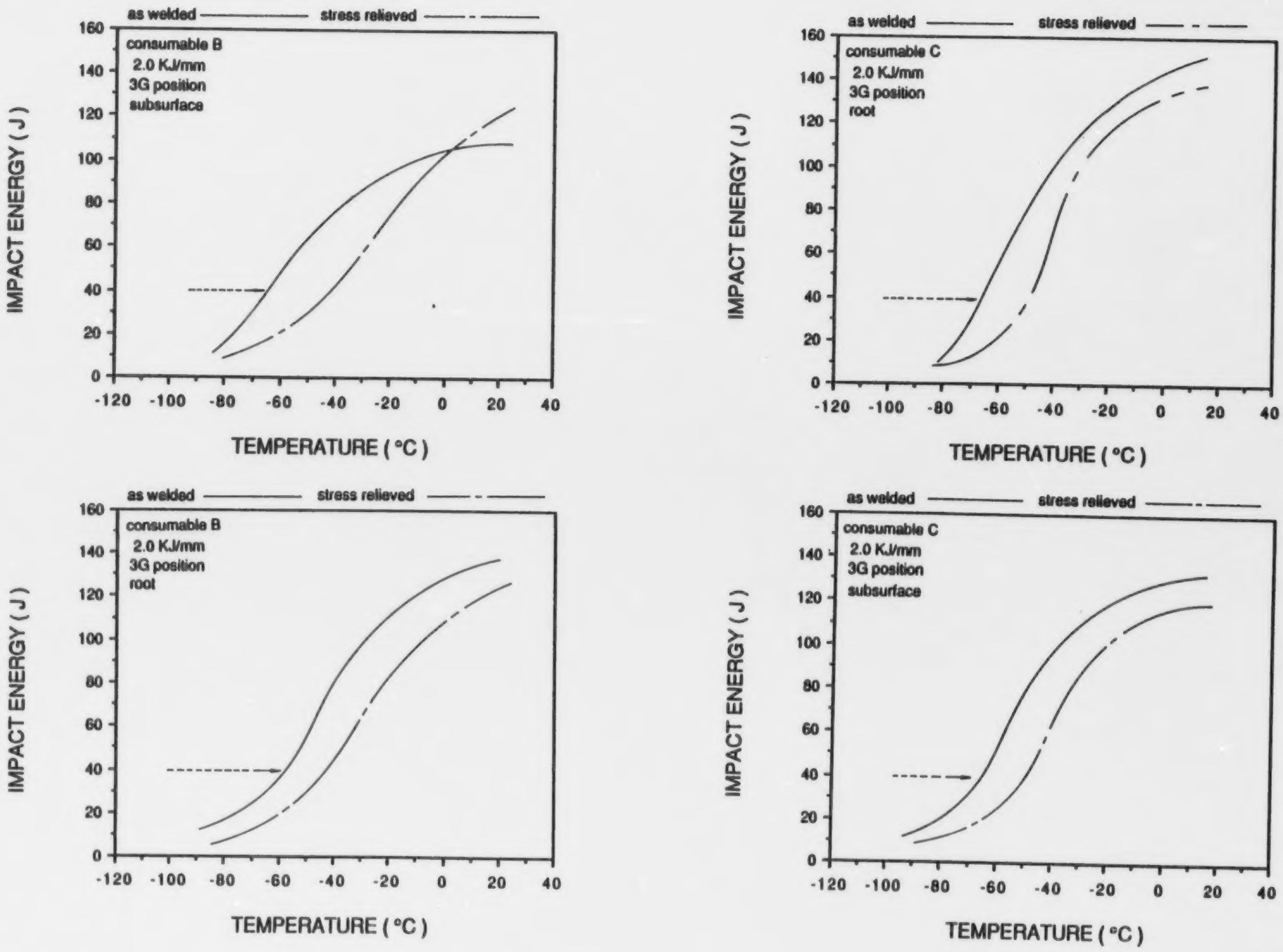

Figure 3.43: Effect of stress relief heat treatment on the CVN toughness of 3G deposits of Consumables B and C

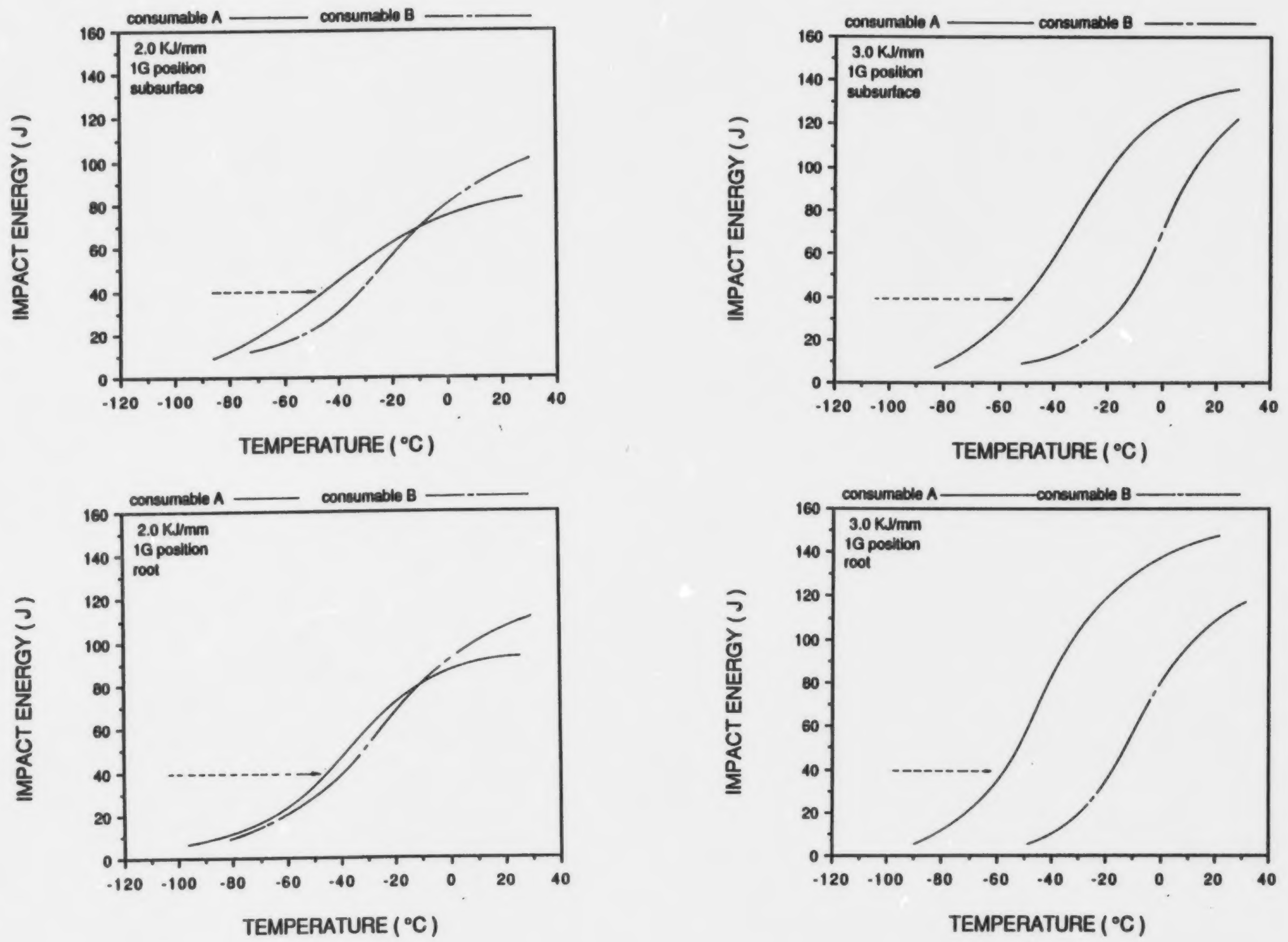

Figure 3.44: By considering the deposits of Consumable A as the equivalent of Consumable B in as-welded condition, the effect of stress relief heat treatment on CVN toughness can be approximated

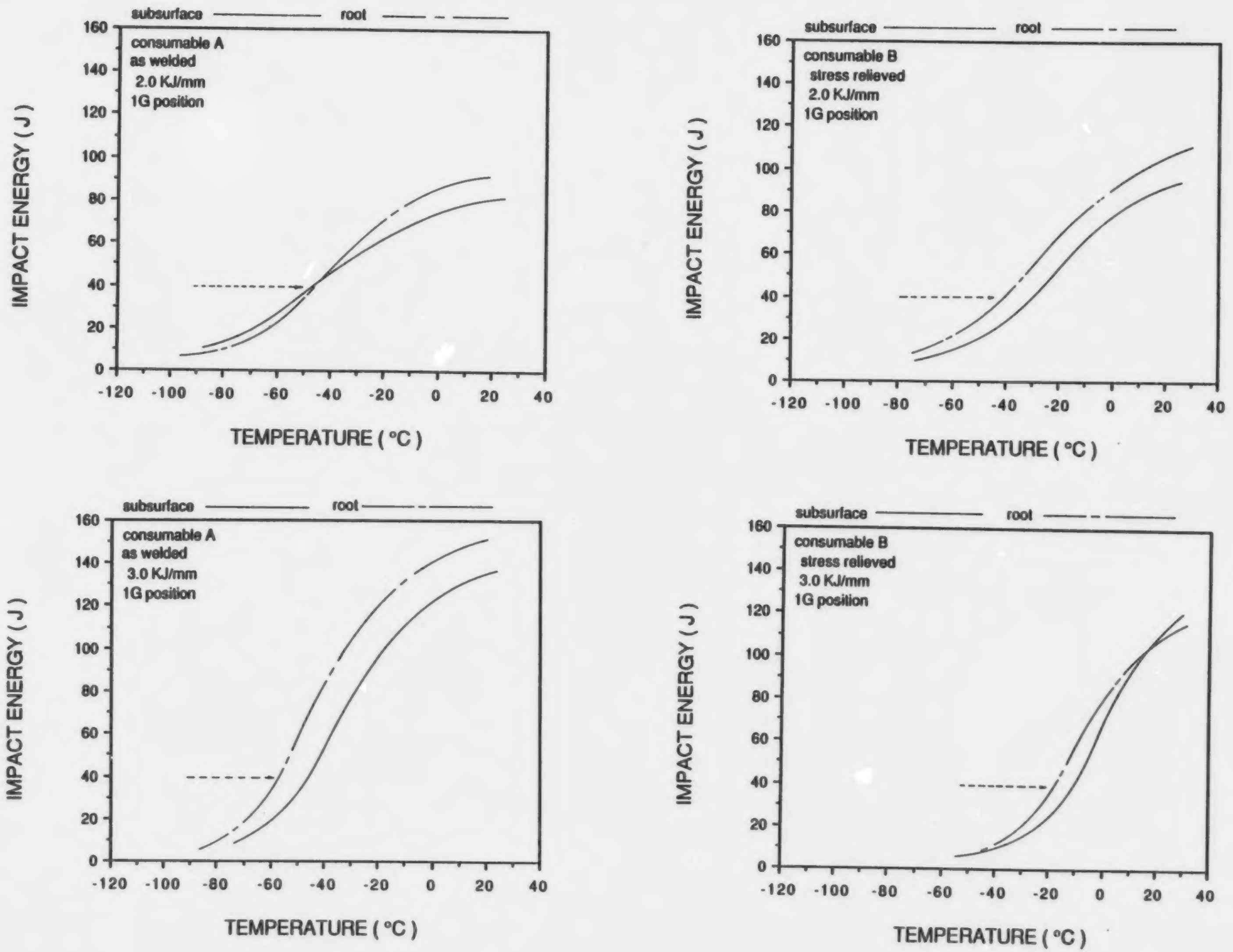

Figure 3.45: The through thickness variation in CVN toughness of 1G deposits of Consumables A and B

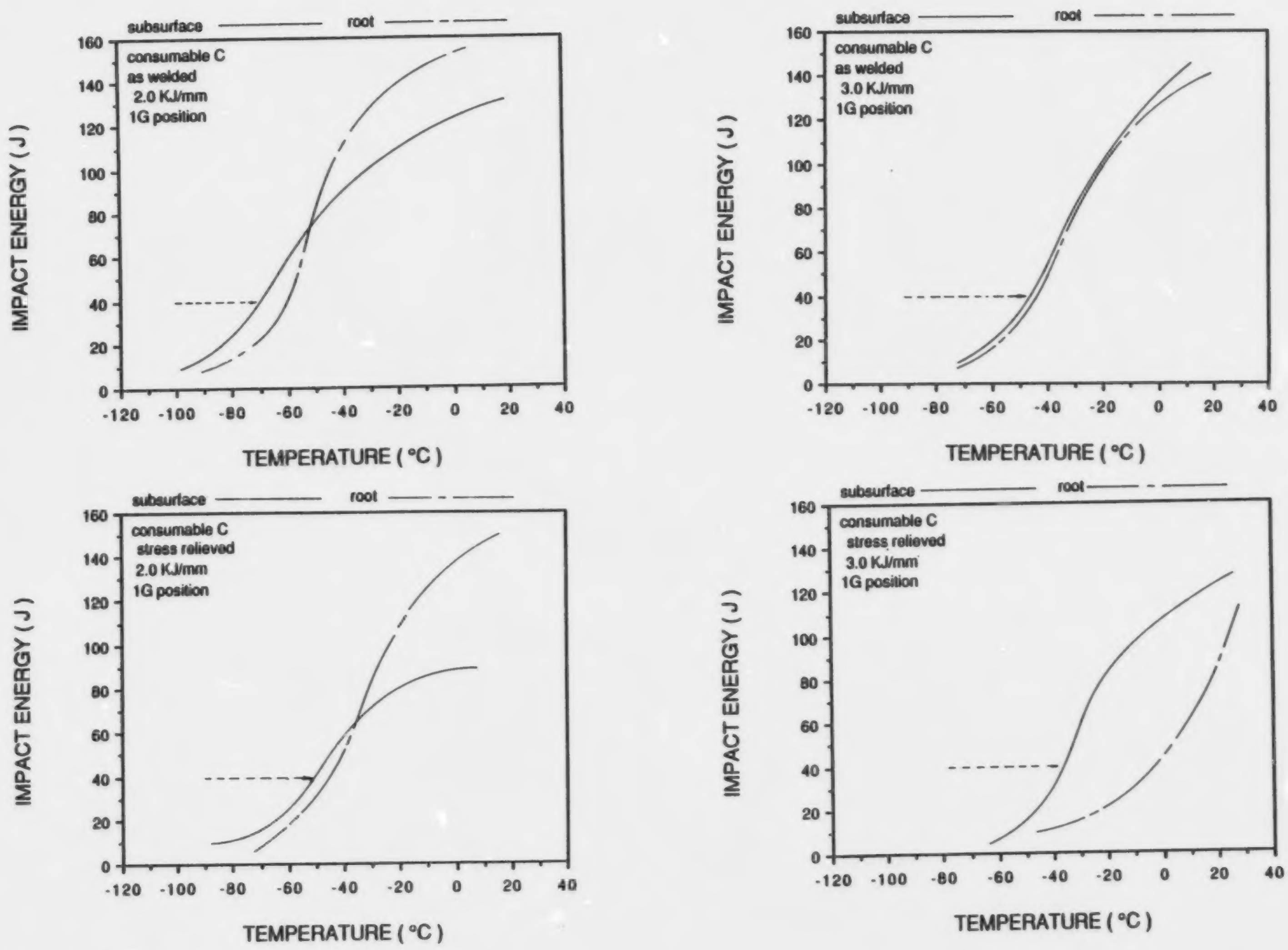

Figure 3.46: The through thickness variation of CVN toughness of 1G deposits of Consumable C

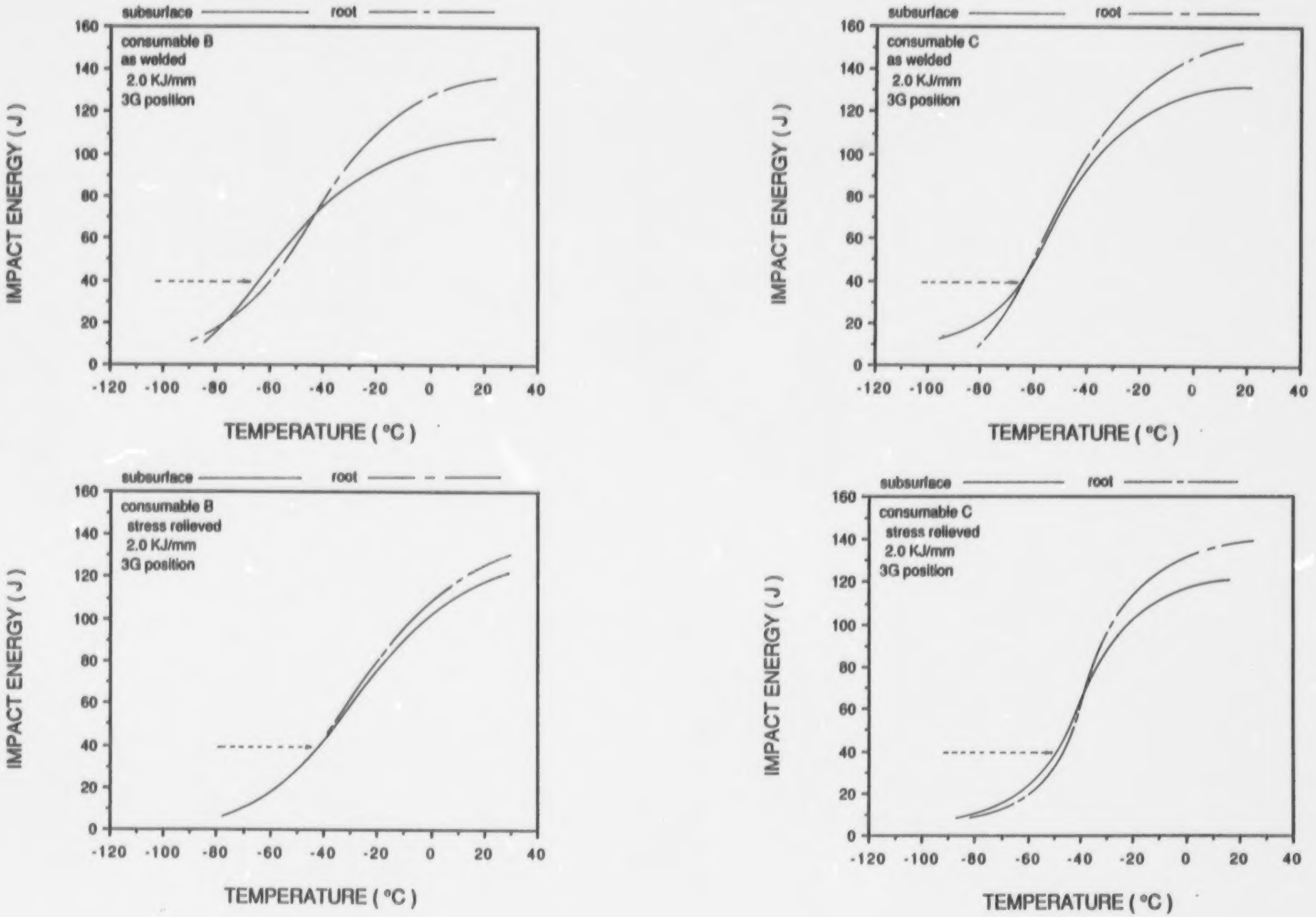

Figure 3.47: The through thickness variation in CVN toughness of 3G deposits of Consumable C

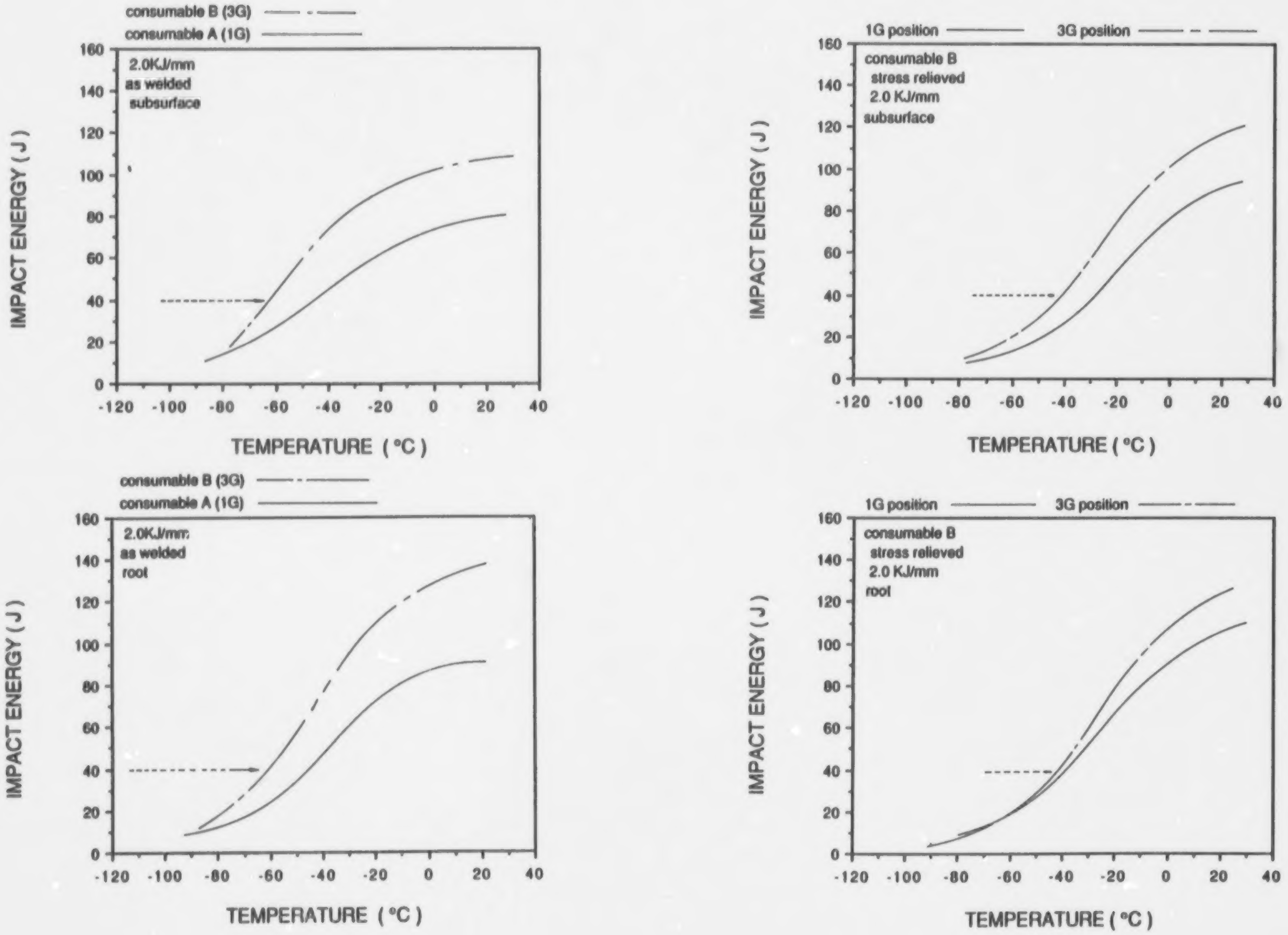

Figure 3.48: Effect of welding position on toughness of deposits of Consumables A and B

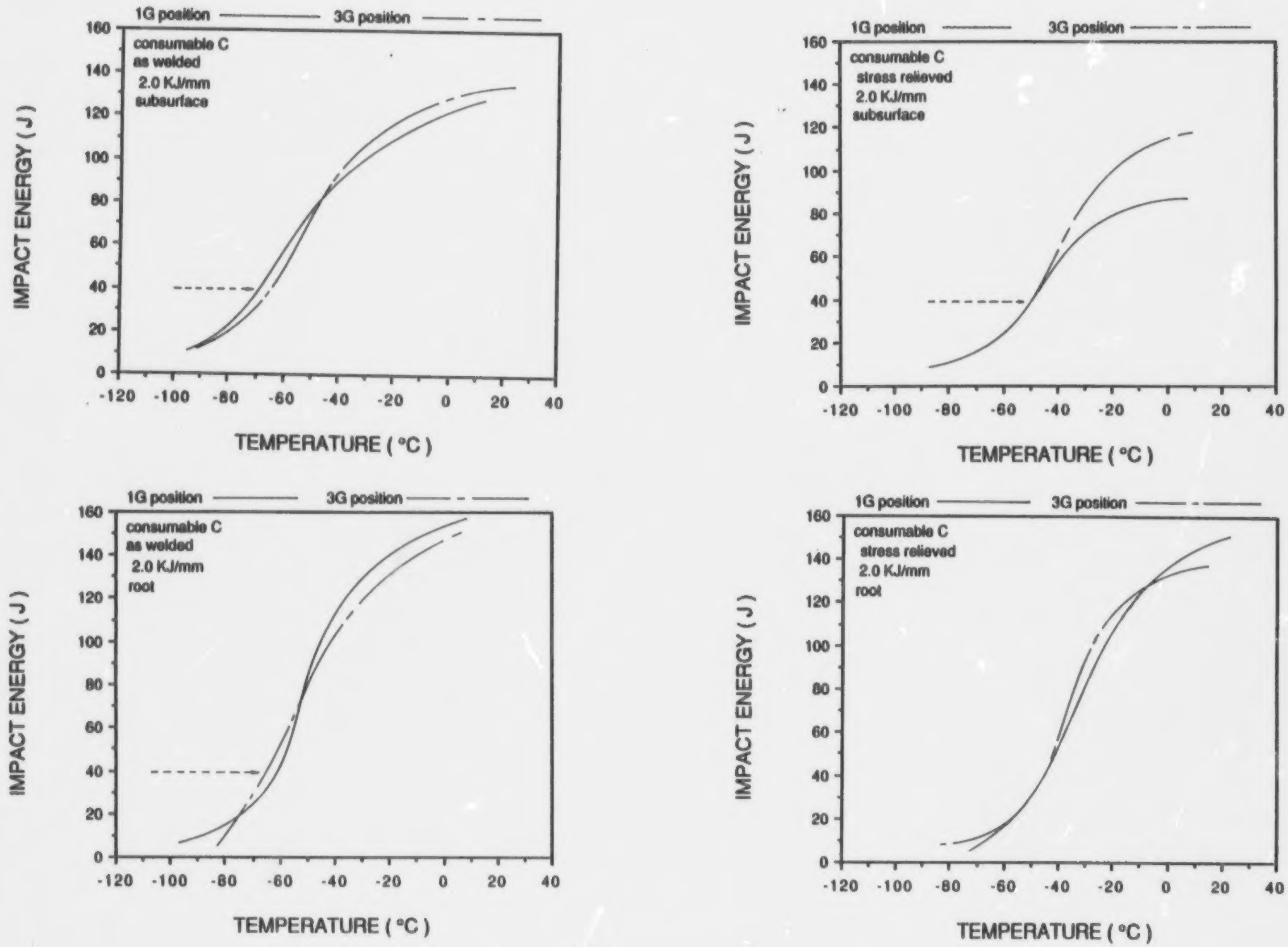

Figure 3.49: Effect of welding position on the CVN toughness of deposits of Consumable C

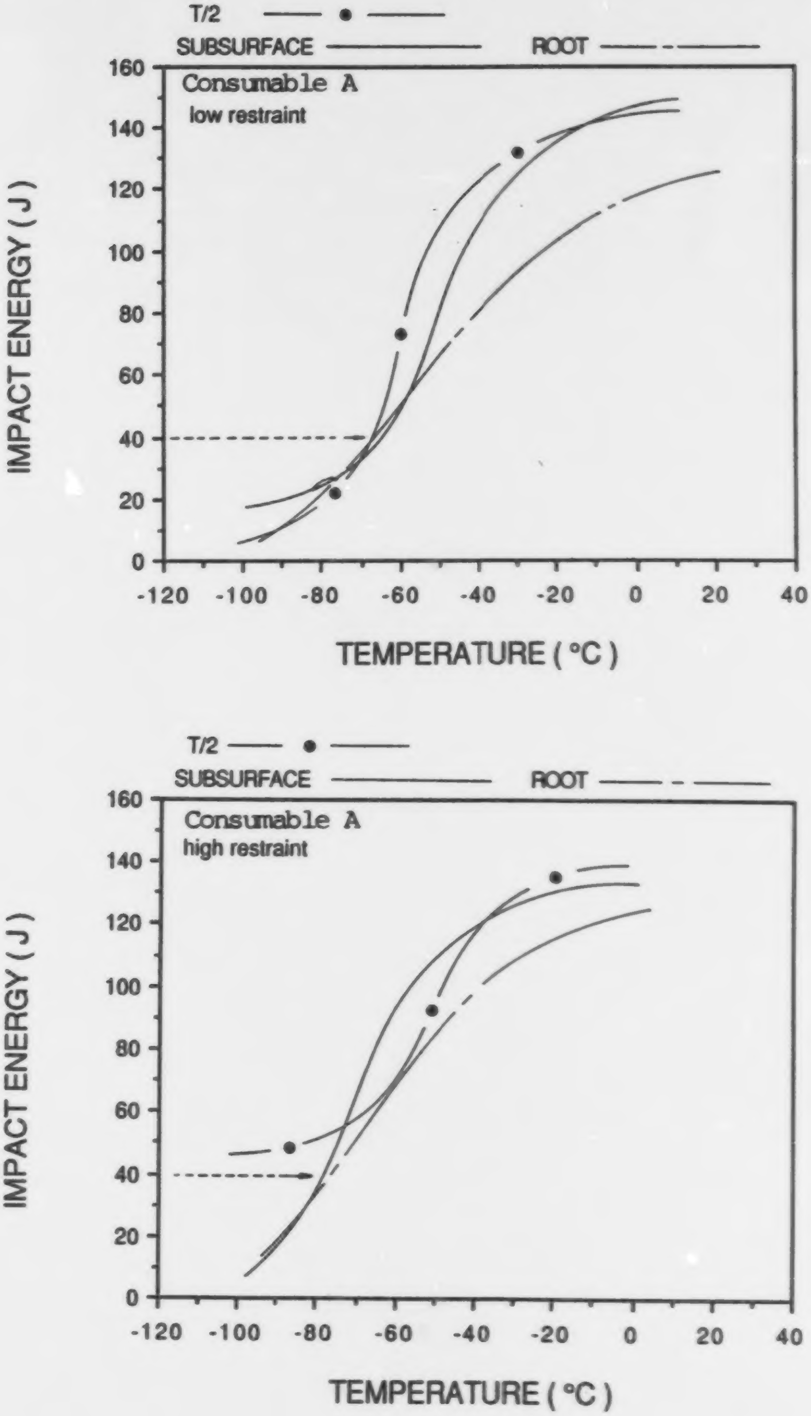

Figure 3.50: Effect of restraint condition on CVN toughness of as-welded 2.0 kJ/mm deposits of Consumable A with single V geometry

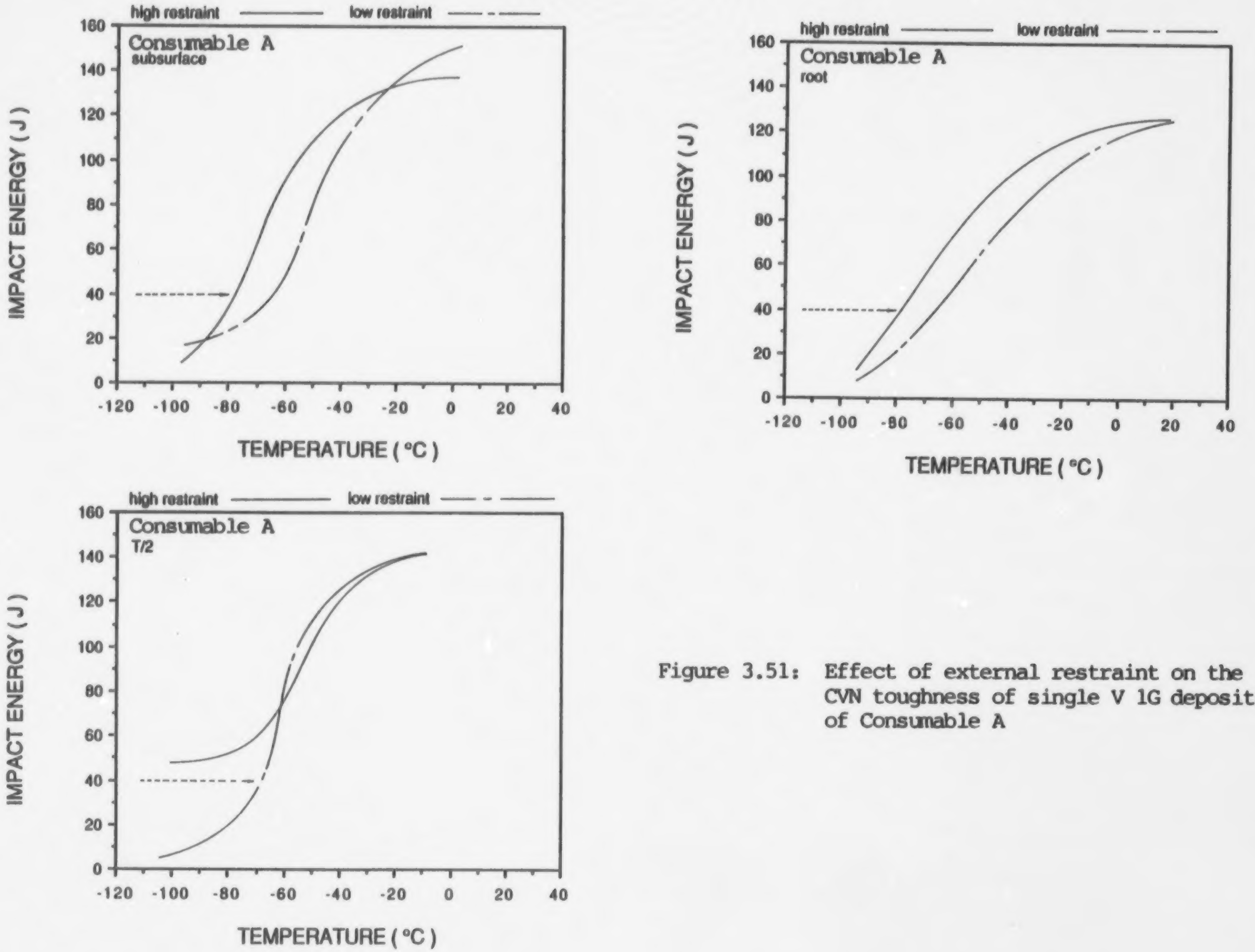

Figure 3.51: Effect of external restraint on the CVN toughness of single V 1G deposits of Consumable A

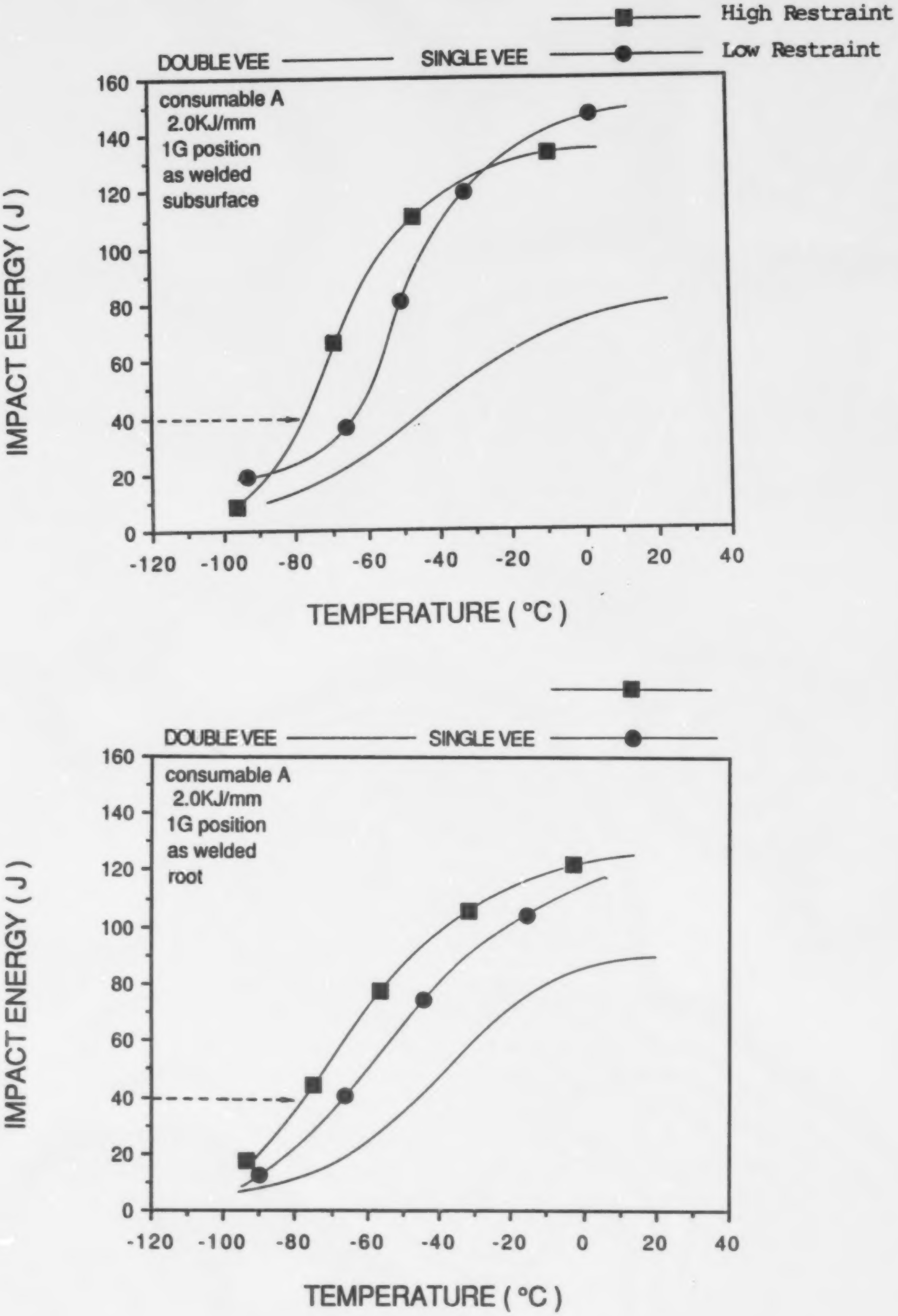

Figure 3.52: Effect of joint geometry on the CVN toughness of Consumable A

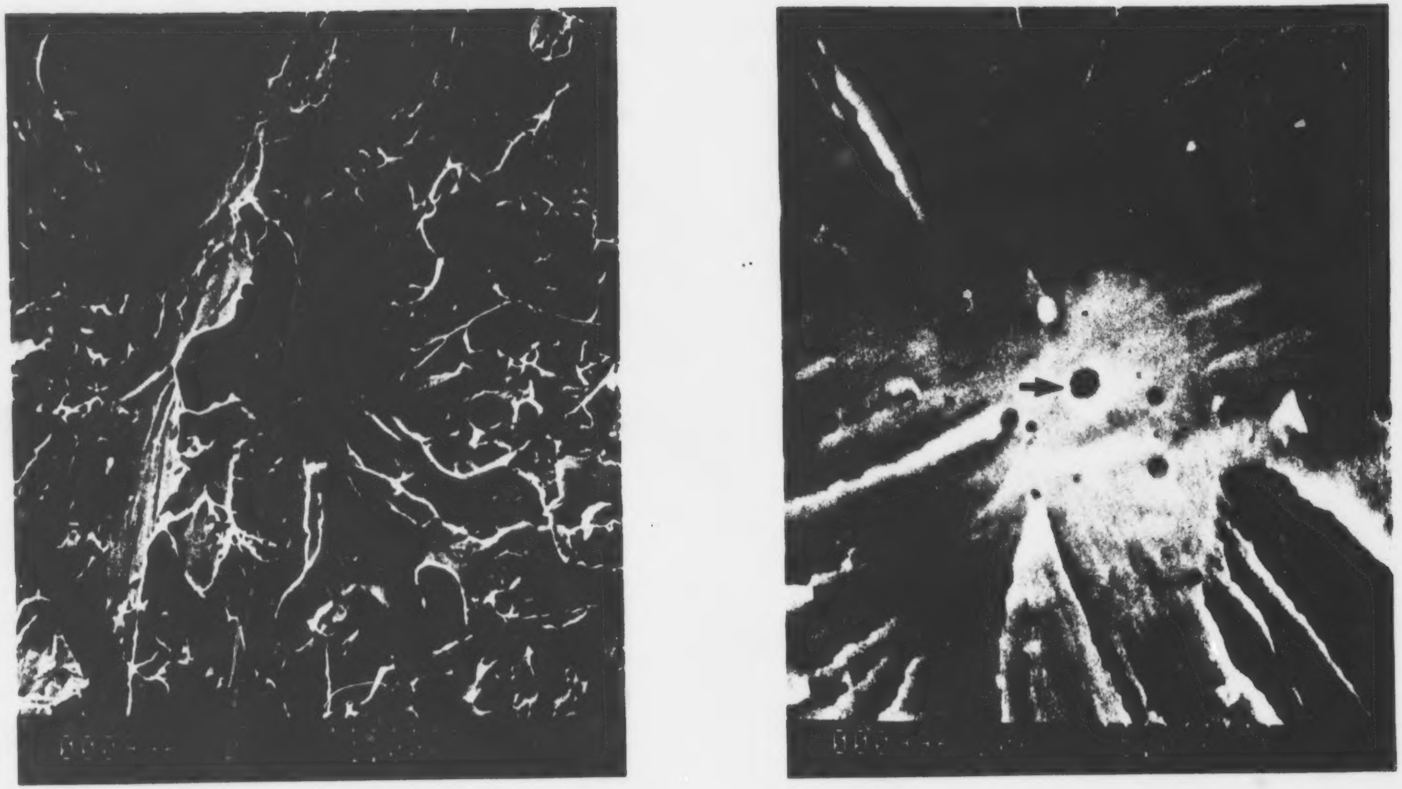

(a) (1000X, Neg. 996)

(b) (5000X, Neg. 996)

Figure 3.53: Representative SEM fractograph of cleavage initiation sites denoted by an arrow (1G, as-welded, 3.0 kJ/mm weld of Consumable A) (1F2)

APPENDIX A

Inclusion Analysis Report

-- **REPORT** --

CHARACTERIZATION OF THE SIZE AND CHEMISTRY OF INCLUSIONS AT THE MID-SECTION OF FIVE WELDS

prepared for:

Materials Technology Centre
ARCTEC
311, Legget Drive
Kanata (Ontario) K2K 1Z8

April 1989 C.D.T. Project P923

C.D.T. ÉCOLE POLYTECHNIQUE

C.D.T. Project P923

-- REPORT --

CHARACTERIZATION OF THE SIZE AND CHEMISTRY OF INCLUSIONS AT THE MID-SECTION OF FIVE WELDS

prepared for:

Materials Technology Centre
ARCTEC
Mr. C. Chin
311, Legget Drive
Kanata (Ontario) K2K 1Z8

by:

Lawrence R. Cutler, Ph.D.
Department of Metallurgical Engineering
ÉCOLE POLYTECHNIQUE

submitted by:

LE CENTRE DE DÉVELOPPEMENT TECHNOLOGIQUE
DE L'ÉCOLE POLYTECHNIQUE
Campus de l'Université de Montréal
Case postale 6079, Succursale A
Montréal (Québec) H3C 3A7

April 1989

Lawrence R. Cutler

Lawrence R. Cutler, Ph.D.

Gilles L'Espérance,
Project Director

Page

TABLE OF CONTENTS

1-INTRODUCTION 1

2-METHODOLOGY 3
    2.1-Specimen Preparation and Observation 3
    2.2-Operation of the Digiscan Program 4
    2.3-Setup of Digiscan 5

3-RESULTS 7

4-CONCLUSIONS 9

5-ANNEX A SUMMARY OF THE INCLUSION SIZE DISTRIBUTION AND TYPE 10

6-ANNEX B SIZE DISTRIBUTIONS FOR THE FOUR MAJOR INCLUSION TYPES 17

1- INTRODUCTION

Mr. Chris Chiu of Fleet Technologies Limited asked the Laboratory for Characterization and Microscopy of Materials, $(CM)^2$, of the Metallurgical Engineering Department of Ecole Polytechnique to characterize the inclusions in five weld specimens. A characterization of the chemical composition and size distribution of the inclusions was requested.

This was accomplished with the aid of the Digiscan program which runs on the Link AN10000 Energy Dispersive X-ray analyzer equipped with a digital scan generator and an ultra-thin window detector. This system combines three powerful tools, namely:

* Scanning Electron Microscope (SEM) with high resolution and multiple image display modes

* Energy Dispersive X-ray spectroscopy with the ability to detect elements with atomic numbers down to that of B

* Digital Scan Generator which allows computer control of the electron beam in the SEM and digitalization of the resultant video signal or the acquisition of X-ray data from specific locations.

This combination forms the basis of a Scanning Electron Microscope based automatic image analysis system (SEM-AIA). This setup gives great flexibility since the type of data collected can be easily modified just by changing the data acquisition or data reduction programs. In the case of Digiscan, the program controls the electron beam in the (SEM) and digitizes the resultant video signal thereby allowing the acquisition of information based on the local variations in contrast. In the present study, inclusions were detected by variations in the signal level of the backscattered electron image (BEI) which is related to the average atomic weight, Z. Areas with larger values of Z appear brighter in the BEI.

The Digiscan program was developed to characterize the size, shape and chemical composition of particles. The data can be classed according to the average diameter and/or the chemical composition of the individual particles. Specific inclusion types can be further classed by the relative abundance or ratios of the elements present.

This report presents the results of a characterization of the inclusions in the samples supplied by Mr. Chiu. Classification of the inclusions according to size and chemical composition was achieved. The significance and the limitations of the data and techniques are also discussed.

2- METHODOLOGY

2.1- Specimen Preparation and Observation

Five steel specimens were received from Fleet Technology in the as ground condition. After etching to find the centerline of the weld, Rockwell hardness impressions were made as reference points so the desired analysis area could be located after mounting and polishing the specimen. The specimens were then mounted and polished using only diamond polishing compound which will not introduce Al into the sample surface and hence affect the analysis of Al in the inclusions. Analysis of the inclusion size and chemical type was done at the mid-thickness locations as was requested. The 0.5 by 2.0 mm analysis region was scribed onto the specimen surface. The analysis locations were determined at random and are distributed uniformly throughout the analysis area. An example of the analysis region and the corresponding measuring fields are illustrated in Figure 1. The dark rectangles correspond to the measuring fields. These are visible since Carbon contamination due to the interaction of the electron beam with a surface Carbon layer results in the fixing of the Carbon on the surface and then reduces the secondary electron emission which results in a darker image. Observations and measurements were done using the JEOL 840 SEM in the BEI inverse and normal observation modes.

2.2- Operation of the Digiscan Program

The inclusions can be differentiated from the matrix due to variations in the BEI signal levels. Since the inclusions are lighter than the matrix (Z<Fe), the inverse BEI was used so that the inclusions will have a higher video signal level than the matrix. For the Digiscan program, a window of analysis was then selected so that the lower threshold was just above the BEI signal level of the matrix. This adjustment was critical since the small inclusions could be lost due to the small difference in contrast between them and the matrix. The upper threshold was left at its maximum value.

The Digiscan program sweeps the electron beam across the specimen in a 1024x1024 grid to locate the position of inclusions with a net area greater than a set minimum. The coordinates of these features are recorded and the program then determines the area as well as the maximum and minimum feret diameters by determining 60 feret diameters at angles of 6 degrees around the center of the individual inclusions. This is done at the maximum resolution of 4096 points per scan line on the SEM. At this point, a X-ray spectrum is obtained by scanning the entire inclusion surface once during the time that the x-ray spectrum is acquired. The intensities of selected peaks are recorded along with the size information of the particle. This process is repeated for the entire field of view. Multiple fields can also be measured during the analysis of a specimen.

2.3- Setup of Digiscan

Several trial analysis were performed to determine the elements that are present in the inclusions. Windows were set up for these elements. Background subtraction windows were set up in areas of the spectrum were no peaks are found. Through trial analysis on pure Fe samples, the ratios of the background noise for the elemental window to that of the background window closest to it were found, so that the background portion of the total elemental window could be subtracted out during the analysis of the inclusions. This permits the calculation of the net intensity of the elements present in the inclusion. An element was considered present if the net intensity of the element was 1.706 times the square root of the background peak intensity for this window which ensures that presence of the element is statistically significant and not just due to normal statistical variations. This is a far more objective criteria that has been employed in previous studies.

In this series of specimens, Al,Si,S,Ti,Mn, and Ca were present in the inclusions, although the relative amounts of each varied greatly. Since most of the inclusions had an diameter under 2 μm, the inclusions were grouped into 0.2 μm bins in the histograms.

In order to have a good resolution of the smaller inclusions as well as to include as many inclusions as possible into each field, a magnification of 4000 was used. An accelerating voltage of 13 kV was used to reduce the size of the X-ray generation zone in order to increase the relative intensities of the light element $K\alpha$ peaks as compared to the Fe peak which is emitted from the matrix. This is especially important for analysis of the smaller inclusions. The five analysis were done using exactly the same experimental conditions, (i.e.accelerating voltage, working distance, beam current) in order to be able to compare the data. If this is not done, the relative peak height can vary which does not reflect changes in the specimen composition.

The data for the total intensities of the elements, size, maximum, minimum and average feret diameter were saved to disk for each of the inclusions. This data was transferred over to the IBM personal computer. The FDCANAL program, developed in the $(CM)^2$, was used to find the type classification for each of the inclusions according to the statistical test described above. After classification, the inclusions were counted according to their size and type classification. The diameter is calculated from the total measured area by taking a circle of equivalent area. The area fraction of occupation , the average size and the number of inclusion per unit area were calculated for each of the samples. The average diameter and average relative intensities of each of the major inclusion types were calculated. The relative abundance of the elements measured can in no way be considered a measure of the chemical composition of the inclusions. A large proportion of the X-ray signal comes from the iron matrix but if the solubilities of the elements in the inclusions are low in Fe as is usually is the case, the spectra recorded reflect changes in the relative composition of the inclusions. Absorption effects can reduce the intensities of the various elements which can change the relative intensities of the peaks somewhat. No matrix corrections (ZAF) were performed and not all of the possible elements present such as oxygen were measured by the due to intensive peak overlap and the lack of information concerning the efficiency of absorption in the ultra-thin window. Still, these measures give valuable data concerning the elements present and the relative abundance of each. These data are indispensable for the understanding of the relationship of processing history and composition to the inclusion characteristics. At this time, there is no other way to obtain such detailed information.

In order to see the reproducibility of the results, the analysis was repeated for the 1B sample.

3- RESULTS

Summary tables of the size distribution and type for all the samples are found in Annex A. Size distribution histograms for the four most common inclusions in each weld are presented in Annex 2. The STiMn and the SiSTiMn inclusions are the dominate inclusion types. The peak in the frequency distribution for the STiMn is typically from 0.2 to 0.4μm whereas the maximum for the SiSTiMn is typically from 0.4 to 0.8μm. The addition of Si to the inclusions tends to increase the mean inclusion diameter.

Ca is present in only a small percentage of the inclusions. It is found in both of STiMn and SiSTiMn inclusion types.

There appears to be a difference in the size of the inclusions between the two analysis of the 1B weld, with the mean diameter being larger in the 1B as compared to the 1B-2 weld. The difference is mainly due to a difference in proportion of the smaller STiMn and the larger SiSTiMn and not to a large difference in the size range of the individual inclusion types. It appears from this result that these two type of inclusions are not arranged homogeneously in the analysis area, which is not surprising considering the possible significant segregation that could occur in the liquid metal pool prior to solidification. It should be noted that the type of inclusions and the general frequency of occurrence is similar in both 1B and 1B-2. This indicates that the analysis procedure is probably valid, the differences in the two results being due to the inherent variation in the weld metal.

In order to overcome this limitation of this inclusion characterization technique, it may be necessary to greatly increase the number of fields of measure in order to get a statistically accurate mean diameter if the sample demonstrates significant heterogeneity in inclusion size and/or inclusion type.

4- CONCLUSIONS

1- Two major types of inclusions were found in the welds, namely STiMn and SiSTiMn.

2- The STiMn inclusions tended to be somewhat smaller than the Si containing SiSTiMn.

3- The difference in the size distributions of the 1B weld for the two measurements made can be related to the difference in proportion of the STiMn and the SiSTiMn inclusion types.

5- ANNEX A

SUMMARY OF THE INCLUSION SIZE DISTRIBUTION AND TYPE

DATA SUMMARY 01-23-1989

Sample Name: 1B
Details: Fleet Technology
Number of Inclusions Analysed: 280
Number of Fields Analysed: 9
Total Field Area, μm^2: 16835
Inclusions per cm^2: 1663196
Area(Volume) Fraction, % : 0.772
Mean Diameter 0.66
Largest Inclusion Diameter Measured, μm : 2.78
Smallest Inclusion Diameter Measured, μm : 0.13

Class	From	Class Size, μm 0.0	0.2	0.4	0.6	0.8	1.0	1.2	1.4	1.6	1.8	2.0	2.2	2.4	2.6	2.8	Total Counts	Average Chemistries(%)						
Label	To	0.2	0.4	0.6	0.8	1.0	1.2	1.4	1.6	1.8	2.0	2.2	2.4	2.6	2.8	3.0		Mg	Al	Si	S	Ca	Ti	Mn
CaTiMn		1	2	0	1	0	0	0	0	0	0	0	0	0	0	0	4	0.0	0.0	0.0	0.0	5.6	61.9	32.5
SCaTiMn		2	8	7	7	0	0	0	0	0	0	0	0	0	0	0	24	0.0	0.0	0.0	12.3	4.9	48.5	34.3
STiMn		9	34	48	30	7	2	0	0	0	0	0	0	0	0	0	130	0.0	0.0	0.0	14.1	0.0	48.8	37.0
SiSCaTiMn		0	0	2	6	1	2	0	0	0	0	0	0	0	0	0	11	0.0	0.0	5.7	12.9	3.2	44.3	33.8
SiSTiMn		0	5	11	22	22	14	7	6	2	2	0	1	0	2	0	94	0.0	0.0	6.3	9.6	0.0	51.7	32.3
SiTiMn		0	0	0	0	1	1	0	0	0	0	0	0	0	0	0	2	0.0	0.0	8.9	0.0	0.0	56.7	34.4
TiMn		1	4	3	2	2	0	1	0	0	0	0	0	0	0	0	13	0.0	0.0	0.0	0.0	0.0	63.5	35.5
Totals		13	53	71	68	33	19	8	6	2	2	0	1	0	2	0		0.0	0.0	2.4	11.4	0.6	50.2	34.7
Fraction of Total Inclusion Area		.00	.03	.11	.21	.16	.14	.08	.08	.03	.04	.00	.03	.00	.09	.00								

DATA SUMMARY

01-23-1989

Sample Name: 1B-2
Details: Fleet Technology
Number of Inclusions Analysed: 428
Number of Fields Analysed: 22
Total Field Area, µm^2: 41152
Inclusions per cm^2: 1040037
Area(Volume) Fraction, % : 0.390
Mean Diameter 0.55
Largest Inclusion Diameter Measured, µm : 3.72
Smallest Inclusion Diameter Measured, µm : 0.12

Class	From	Class Size, µm															Total Counts	Average Chemistries(%)						
		0.0	0.2	0.4	0.6	0.8	1.0	1.2	1.4	1.6	1.8	2.0	2.2	2.4	2.6	2.8								
Label	To	0.2	0.4	0.6	0.8	1.0	1.2	1.4	1.6	1.8	2.0	2.2	2.4	2.6	2.8	3.0		Mg	Al	Si	S	Ca	Ti	Mn
CaTiMn		0	1	0	0	1	0	0	0	0	0	0	0	0	0	0	2	0.0	0.0	0.0	0.0	4.0	66.8	29.3
MgSiTiMn		0	0	0	0	0	0	0	0	0	0	0	0	1	0	0	1	1.5	0.0	9.0	0.0	0.0	67.8	21.7
SCaTiMn		4	13	11	1	0	0	0	0	0	0	0	0	0	0	0	29	0.0	0.0	0.0	11.5	3.7	50.1	34.6
STiMn		27	72	60	11	3	0	0	0	0	0	0	0	0	0	0	173	0.0	0.0	0.0	13.6	0.0	51.7	34.6
SiCaTiMn		1	0	0	1	0	0	0	0	0	0	0	0	0	0	0	2	0.0	0.0	3.4	0.0	3.6	60.6	32.4
SiSCaTiMn		1	5	7	3	3	1	2	0	0	0	0	0	0	0	0	22	0.0	0.0	7.8	11.9	2.7	44.4	33.1
SiSTiMn		7	18	38	53	28	14	11	2	0	1	0	1	0	0	0	173	0.0	0.0	5.2	9.6	0.0	53.3	31.9
SiTiMn		0	1	0	0	0	0	0	0	0	0	0	0	1	0	0	2	0.0	0.0	4.1	0.0	0.0	61.3	34.6
TiMn		3	10	4	1	1	0	0	0	0	0	0	0	0	0	0	19	0.0	0.0	0.0	0.0	0.0	65.3	34.7
Totals		43	120	120	70	36	15	13	2	0	1	0	1	2	0	0		0.0	0.0	2.6	10.8	0.4	52.1	33.0
Fraction of Total Inclusion Area		.01	.05	.15	.16	.14	.08	.10	.02	.00	.02	.00	.03	.06	.00	.00								

DATA SUMMARY 01-23-1989

Sample Name: 5B
Details: Fleet Technology
Number of Inclusions Analysed: 422
Number of Fields Analysed: 30
Total Field Area, µm^2: 56117
Inclusions per cm^2: 752002
Area(Volume) Fraction, % : 0.332
Mean Diameter 0.60
Largest Inclusion Diameter Measured, µm : 3.57
Smallest Inclusion Diameter Measured, µm : 0.12

		Class Size, µm																						
Class	From	0.0	0.2	0.4	0.6	0.8	1.0	1.2	1.4	1.6	1.8	2.0	2.2	2.4	2.6	2.8	Total Counts	Average Chemistries(%)						
Label	To	0.2	0.4	0.6	0.8	1.0	1.2	1.4	1.6	1.8	2.0	2.2	2.4	2.6	2.8	3.0		Mg	Al	Si	S	Ca	Ti	Mn
AlSiCaMn		0	0	0	0	1	0	0	0	0	0	0	0	0	0	0	1	0.0	5.2	57.0	0.0	29.3	0.0	8.6
CaMn		0	0	1	0	0	1	0	0	0	0	0	0	0	0	0	2	0.0	0.0	0.0	0.0	32.3	0.0	67.7
CaTiMn		2	0	0	0	0	1	0	0	0	1	0	0	0	0	0	4	0.0	0.0	0.0	0.0	24.5	36.4	39.1
Mn		0	0	0	0	1	0	1	0	0	0	0	0	0	0	0	2	0.0	0.0	0.0	0.0	0.0	0.0	100.0
SCa		1	0	0	0	0	0	0	0	0	0	0	0	0	0	0	1	0.0	0.0	0.0	47.2	52.8	0.0	0.0
SCaMn		1	0	0	0	0	0	0	0	0	0	0	0	0	0	0	1	0.0	0.0	0.0	34.0	20.8	0.0	45.2
SCaTiMn		7	13	4	8	1	1	3	3	0	0	0	0	0	0	0	40	0.0	0.0	0.0	11.8	3.3	62.0	22.9
STiMn		47	69	94	54	31	18	8	4	1	2	1	0	0	0	0	329	0.0	0.0	0.0	12.2	0.0	65.0	22.8
SiCaMn		0	1	0	0	0	0	0	0	0	0	0	0	0	0	0	1	0.0	0.0	35.5	0.0	16.2	0.0	48.3
SiMn		0	0	0	0	0	0	0	0	1	0	0	0	0	0	0	1	0.0	0.0	29.9	0.0	0.0	0.0	70.1
SiSCaMn		1	0	0	0	0	0	0	0	0	0	0	0	0	0	0	1	0.0	0.0	51.9	5.6	25.8	0.0	15.7
SiSCaTi		0	0	0	0	0	1	0	0	0	0	0	0	0	0	0	1	0.0	0.0	30.4	35.5	21.9	12.2	0.0
SiSCaTiMn		0	0	0	0	0	0	0	0	0	0	0	1	0	0	0	1	0.0	0.0	0.8	2.7	1.0	80.9	14.7
SiSMn		0	0	1	0	0	0	0	0	0	0	0	0	0	0	0	1	0.0	0.0	72.2	9.6	0.0	0.0	18.2
SiSTiMn		1	1	3	2	4	3	1	0	0	0	2	0	1	1	1	20	0.0	0.0	1.9	9.2	0.0	66.8	22.1
TiMn		6	3	1	2	0	1	0	0	0	0	0	0	0	0	0	13	0.0	0.0	0.0	0.0	0.0	75.1	24.9
Totals		66	87	104	68	38	28	13	7	2	3	3	1	1	1	1		0.0	0.0	0.7	11.4	1.1	62.6	23.5
Fraction of Total Inclusion Area		.01	.04	.11	.14	.13	.13	.09	.07	.02	.05	.06	.02	.03	.03	.04								

DATA SUMMARY 01-23-1989

Sample Name: 7B
Details: Fleet Technology
Number of Inclusions Analysed: 411
Number of Fields Analysed: 18
Total Field Area, µm^2: 33670
Inclusions per cm^2: 1220667
Area(Volume) Fraction, % : 0.439
Mean Diameter 0.55
Largest Inclusion Diameter Measured, µm : 5.74
Smallest Inclusion Diameter Measured, µm : 0.12

		Class Size, µm																Average Chemistries(%)						
Class	From	0.0	0.2	0.4	0.6	0.8	1.0	1.2	1.4	1.6	1.8	2.0	2.2	2.4	2.6	2.8	Total Counts							
Label	To	0.2	0.4	0.6	0.8	1.0	1.2	1.4	1.6	1.8	2.0	2.2	2.4	2.6	2.8	3.0		Mg	Al	Si	S	Ca	Ti	Mn
AlSiSTiMn		0	0	0	0	0	0	0	0	0	0	1	0	0	0	0	1	0.0	1.2	18.4	2.7	0.0	41.5	36.2
CaMn		0	1	0	0	0	0	0	0	0	0	0	0	0	0	0	1	0.0	0.0	0.0	0.0	27.4	0.0	72.5
CaTiMn		0	1	1	0	0	0	0	0	0	0	0	0	0	0	0	2	0.0	0.0	0.0	0.0	10.2	45.1	44.7
MgAlSiSTiMn		0	0	0	0	0	0	0	0	0	0	0	0	0	0	0	0	0.0	0.0	0.0	0.0	0.0	0.0	0.0
Mn		2	0	0	0	0	0	0	0	0	0	0	0	0	0	0	2	0.0	0.0	0.0	0.0	0.0	0.0	100.0
SCaMn		1	0	1	0	1	0	0	0	0	0	0	0	0	0	0	3	0.0	0.0	0.0	37.0	18.0	0.0	45.0
SCaTiMn		2	12	12	2	0	0	0	0	0	0	0	0	0	0	0	28	0.0	0.0	0.0	19.6	6.3	28.9	45.2
SMn		4	1	4	0	0	0	0	0	0	0	0	0	0	0	0	9	0.0	0.0	0.0	46.4	0.0	0.0	53.6
STiMn		22	54	38	6	2	0	0	0	0	0	0	0	0	0	0	122	0.0	0.0	0.0	18.3	0.0	31.7	50.0
SiCaMn		1	0	0	0	0	0	0	0	0	0	0	0	0	0	0	1	0.0	0.0	40.6	0.0	36.2	0.0	23.2
SiSCaTiMn		0	7	19	11	4	2	1	2	0	1	0	0	0	0	0	47	0.0	0.0	8.8	12.0	3.5	33.7	42.0
SiSTiMn		4	23	61	50	16	13	6	4	1	1	0	0	0	0	0	179	0.0	0.0	9.7	12.3	0.0	33.9	44.2
SiTiMn		0	0	1	1	0	0	0	0	0	0	0	0	0	0	0	2	0.0	0.0	6.9	0.0	0.0	42.4	50.7
TiMn		0	8	2	1	0	0	0	0	0	0	0	0	0	0	0	11	0.0	0.0	0.0	0.0	0.0	41.0	59.0
Totals		36	107	139	71	23	15	7	6	1	2	1	0	0	0	0		0.0	0.0	5.4	14.8	1.2	31.6	46.3
Fraction of Total																								
Inclusion Area		.00	.05	.18	.18	.10	.10	.06	.07	.02	.04	.02	.00	.00	.00	.00								

DATA SUMMARY

01-23-1989

Sample Name: 8B
Details: Fleet Techology
Number of Inclusions Analysed: 534
Number of Fields Analysed: 20
Total Field Area, µm^2: 37411
Inclusions per cm^2: 1427378
Area(Volume) Fraction, % : 0.953
Mean Diameter 0.68
Largest Inclusion Diameter Measured, µm : 10.53
Smallest Inclusion Diameter Measured, µm : 0.12

Class Size, µm

Class	From	0.0	0.2	0.4	0.6	0.8	1.0	1.2	1.4	1.6	1.8	2.0	2.2	2.4	2.6	2.8	Total Counts	Average Chemistries(%)						
Label	To	0.2	0.4	0.6	0.8	1.0	1.2	1.4	1.6	1.8	2.0	2.2	2.4	2.6	2.8	3.0		Mg	Al	Si	S	Ca	Ti	Mn
		3	0	0	0	0	0	0	1	0	0	0	0	0	0	0	4	0.0	0.0	0.0	0.0	0.0	0.0	0.0
AlS		1	0	0	0	0	0	0	0	0	0	0	0	0	0	0	1	0.0	42.7	0.0	57.3	0.0	0.0	0.0
AlSiSCaTiMn		0	0	0	0	0	0	0	0	0	0	1	0	0	0	0	1	0.0	1.5	13.3	3.2	1.6	50.5	30.0
AlSiSTiMn		0	0	0	0	0	0	0	2	2	2	2	0	3	0	0	11	0.0	2.2	17.9	5.1	0.0	39.8	35.1
CaTiMn		0	3	1	0	0	0	0	0	0	0	0	0	0	0	0	4	0.0	0.0	0.0	0.0	8.0	44.8	47.2
MgSiSTiMn		0	1	0	0	0	0	0	0	0	0	0	0	0	0	0	1	1.0	0.0	1.3	3.3	0.0	45.2	49.3
SCaTiMn		6	13	13	2	0	0	0	0	0	0	0	0	0	0	0	34	0.0	0.0	0.0	17.6	6.9	34.7	40.8
SMn		0	0	2	0	0	0	0	0	0	0	0	0	0	0	0	2	0.0	0.0	0.0	39.4	0.0	0.0	60.6
STiMn		23	69	62	23	9	0	0	0	0	0	0	0	0	1	0	187	0.0	0.0	0.0	18.9	0.0	34.4	46.7
SiMn		0	0	1	0	0	0	0	0	0	0	0	0	0	0	0	1	0.0	0.0	81.5	0.0	0.0	0.0	18.5
SiSCaTiMn		2	2	3	9	7	1	2	1	0	0	0	0	0	0	0	27	0.0	0.0	11.1	10.8	4.0	32.5	41.5
SiSMn		0	0	1	0	0	0	0	0	0	0	0	0	0	0	0	1	0.0	0.0	30.8	8.9	0.0	0.0	60.3
SiSTiMn		5	10	43	69	58	32	14	5	4	1	1	0	0	0	0	242	0.0	0.0	10.1	12.0	0.0	35.1	42.9
SiTiMn		1	0	2	1	0	0	0	0	0	0	0	0	0	0	0	4	0.0	0.0	11.2	0.0	0.0	33.3	55.4
TiMn		1	4	2	2	0	0	0	0	0	0	0	0	0	0	0	9	0.0	0.0	0.0	0.0	0.0	44.2	55.8
- Totals		42	102	130	106	74	33	16	9	6	3	4	0	3	1	0		0.0	0.1	5.8	14.1	0.7	34.1	43.5
Fraction of Total Inclusion Area		.00	.02	.07	.11	.13	.09	.06	.04	.04	.02	.04	.00	.04	.02	.00								

DATA SUMMARY

01-23-1989

Sample Name: 9B
Details: Fleet Technology
Number of Inclusions Analysed: 506
Number of Fields Analysed: 17
Total Field Area, μm^2: 31800
Inclusions per cm^2: 1591217
Area(Volume) Fraction, % : 0.686
Mean Diameter 0.64
Largest Inclusion Diameter Measured, μm : 2.78
Smallest Inclusion Diameter Measured, μm : 0.12

Class Size, μm

Class	From	0.0	0.2	0.4	0.6	0.8	1.0	1.2	1.4	1.6	1.8	2.0	2.2	2.4	2.6	2.8	Total Counts	Average Chemistries(%)						
Label	To	0.2	0.4	0.6	0.8	1.0	1.2	1.4	1.6	1.8	2.0	2.2	2.4	2.6	2.8	3.0		Mg	Al	Si	S	Ca	Ti	Mn
AlSiSCaTiMn		0	0	0	0	0	0	0	0	0	0	0	2	0	0	0	2	0.0	1.5	6.7	2.0	1.2	66.0	22.6
AlSiSTiMn		0	0	0	0	0	0	0	0	0	0	1	0	0	1	0	2	0.0	2.2	6.0	4.6	0.0	61.8	25.4
CaMn		1	0	0	0	0	0	0	0	0	0	0	0	0	0	0	1	0.0	0.0	0.0	0.0	29.1	0.0	70.9
CaTiMn		2	1	4	2	0	0	0	0	0	0	0	0	0	0	0	9	0.0	0.0	0.0	0.0	10.0	52.9	37.2
SCaTiMn		5	13	21	20	8	1	1	0	1	0	0	0	0	0	0	70	0.0	0.0	0.0	14.6	5.7	48.5	31.2
SMn		0	0	1	0	0	0	0	0	0	0	0	0	0	0	0	1	0.0	0.0	0.0	50.4	0.0	0.0	49.6
STiMn		22	72	99	99	50	11	2	0	0	0	0	0	0	0	0	355	0.0	0.0	0.0	17.0	0.0	48.9	34.0
SiSCaTiMn		0	0	0	0	1	3	0	1	0	0	0	0	0	0	0	5	0.0	0.0	3.4	13.4	2.8	50.1	30.4
SiSTiMn		0	0	2	3	2	7	6	4	3	1	3	1	0	0	0	32	0.0	0.0	4.4	8.9	0.0	56.6	30.1
SiTiMn		0	0	0	0	1	0	0	0	0	1	0	0	1	0	0	3	0.0	0.0	3.9	0.0	0.0	71.0	25.1
TiMn		3	2	11	5	2	1	0	0	0	0	0	0	0	0	0	24	0.0	0.0	0.0	0.0	0.0	61.7	38.3
Totals		33	88	138	129	64	23	9	5	4	2	4	3	1	1	0		0.0	0.0	0.4	14.8	1.1	49.9	33.5
Fraction of Total Inclusion Area		.00	.03	.13	.23	.18	.10	.05	.04	.04	.03	.06	.06	.02	.03	.00								

6- ANNEX B

SIZE DISTRIBUTIONS FOR THE FOUR MAJOR INCLUSION TYPES

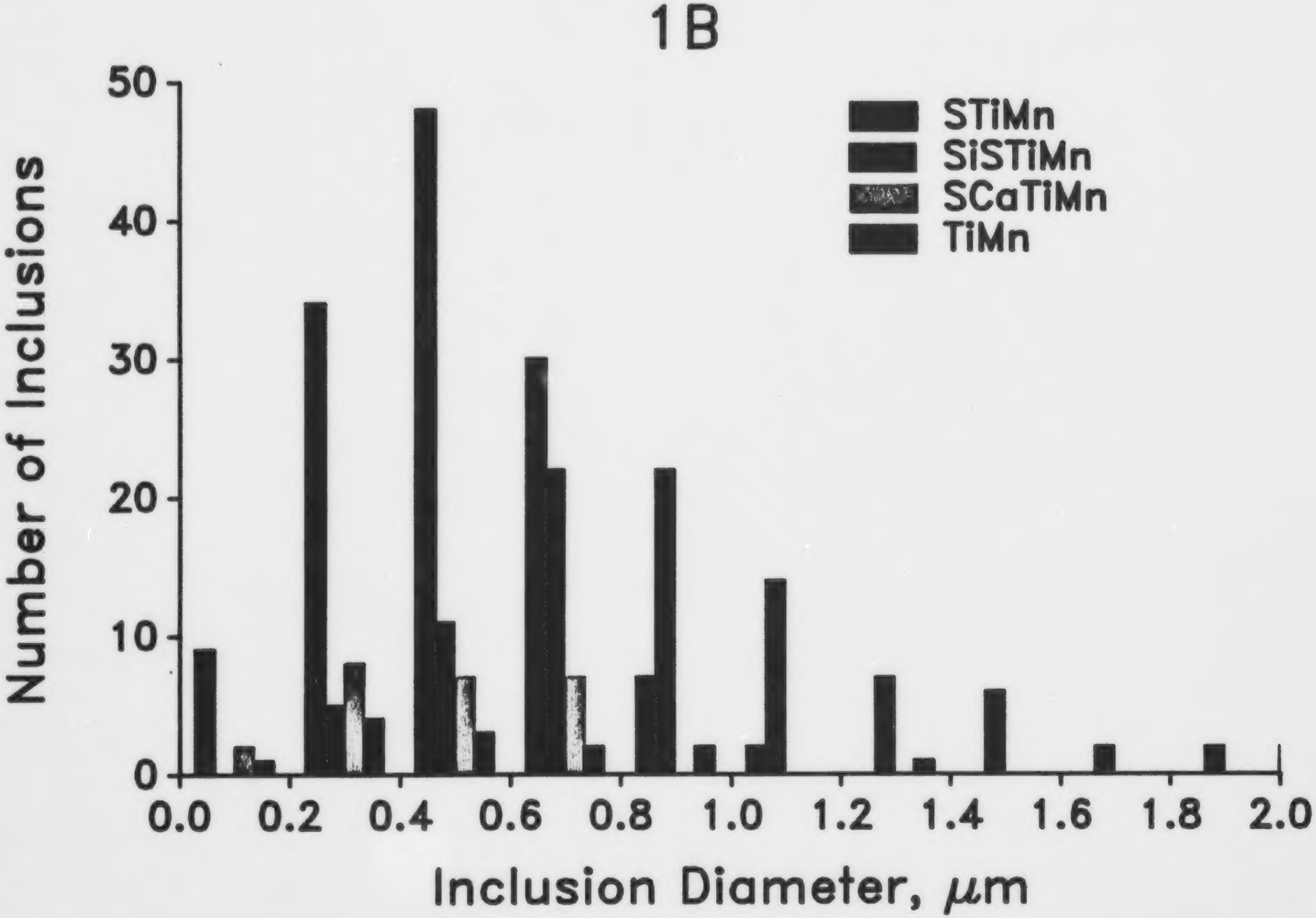
1B
Number of Inclusions
0
10
20
30
40
50
Inclusion Diameter, μm
0.0
0.2
0.4
0.6
0.8
1.0
1.2
1.4
1.6
1.8
2.0
STiMn
SiSTiMn
SCaTiMn
TiMn

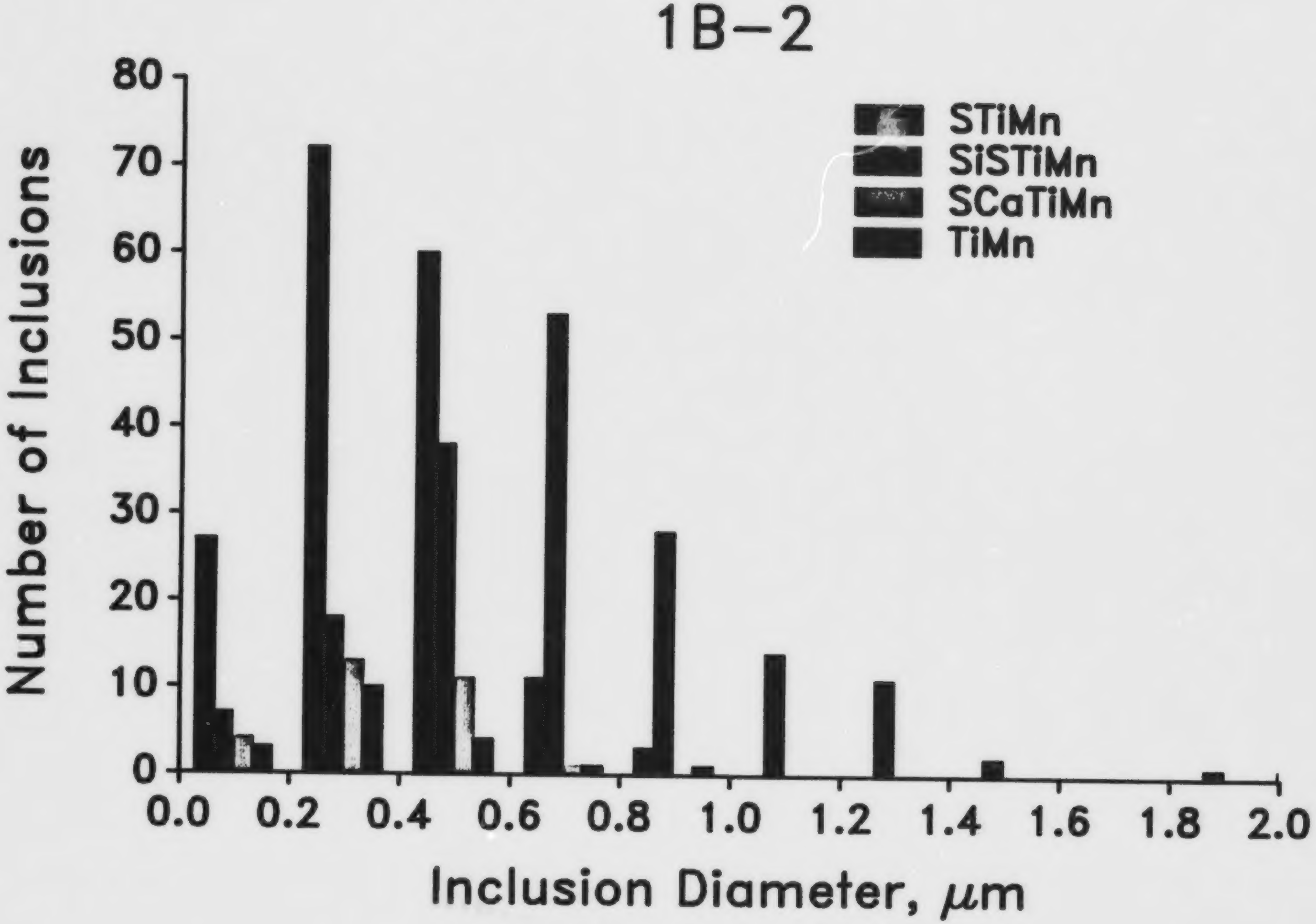
1B−2
STiMn
SiSTiMn
SCaTiMn
TiMn
Number of Inclusions
80
70
60
50
40
30
20
10
0
0.0
0.2
0.4
0.6
0.8
1.0
1.2
1.4
1.6
1.8
2.0
Inclusion Diameter, μm

5B

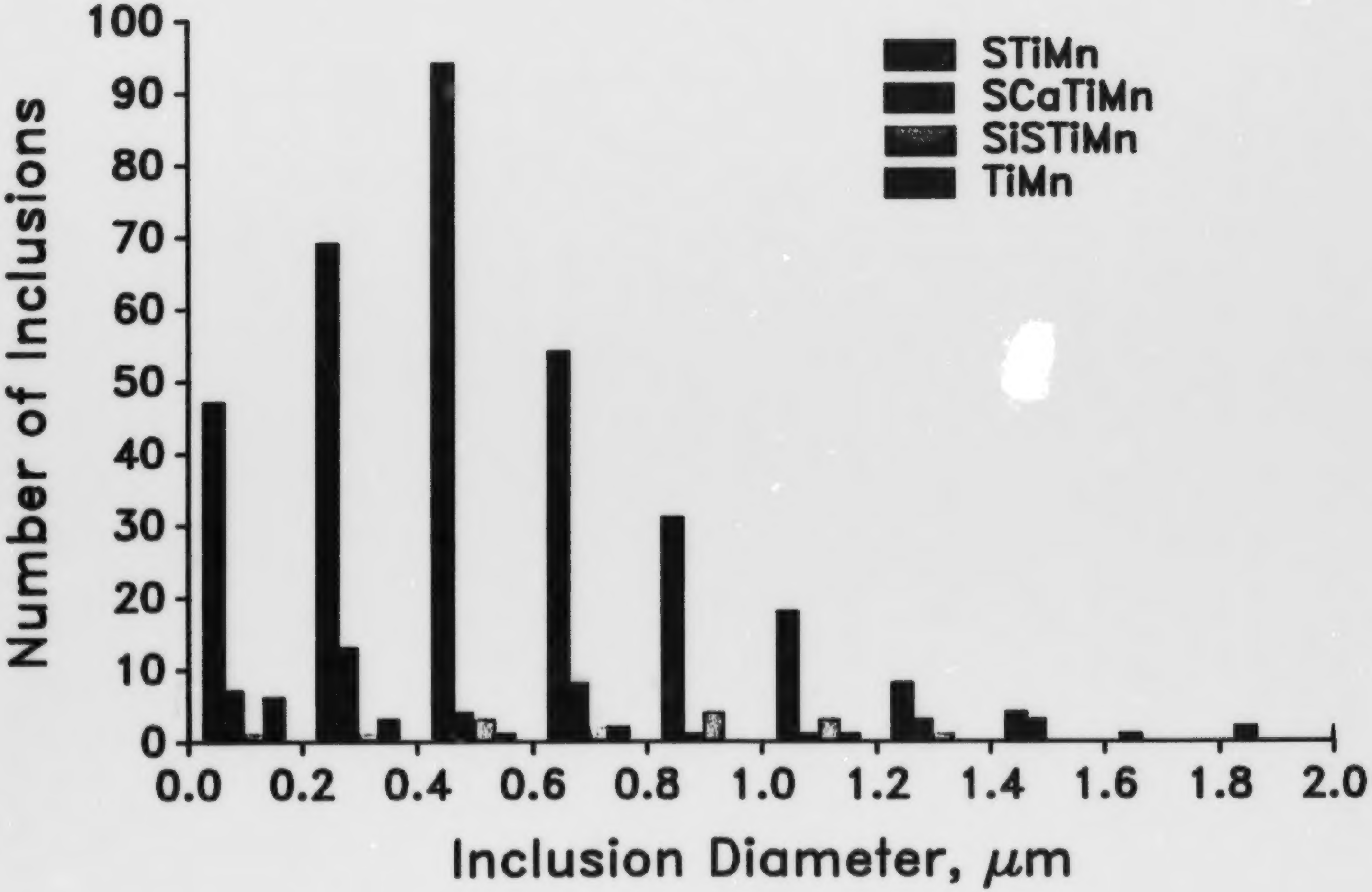
Number of Inclusions
100
90
80
70
60
50
40
30
20
10
0
0.0
0.2
0.4
0.6
0.8
1.0
1.2
1.4
1.6
1.8
2.0
Inclusion Diameter, μm
STiMn
SCaTiMn
SiSTiMn
TiMn

7B

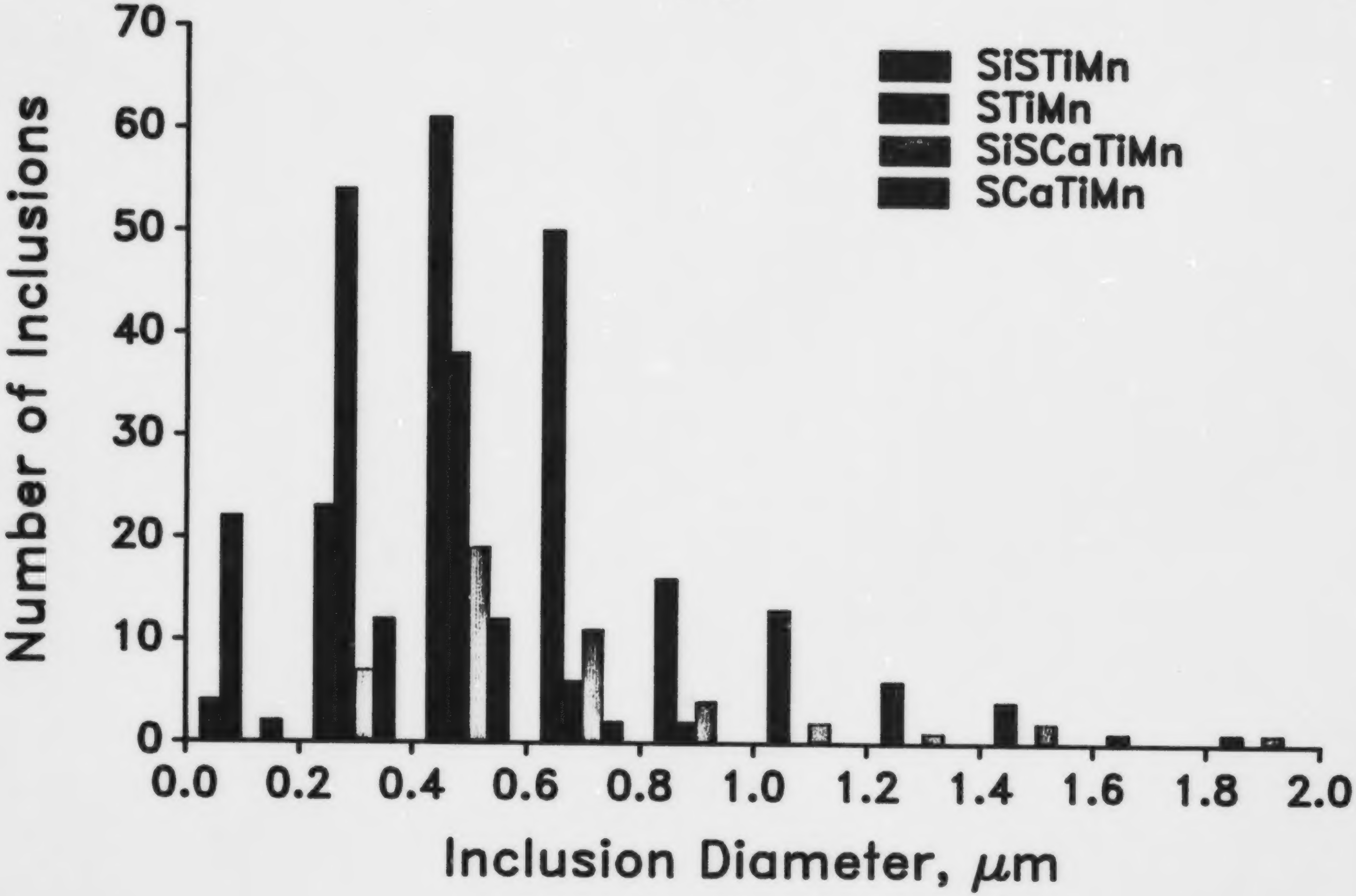
SiSTiMn
STiMn
SiSCaTiMn
SCaTiMn
Number of Inclusions
0
10
20
30
40
50
60
70
0.0
0.2
0.4
0.6
0.8
1.0
1.2
1.4
1.6
1.8
2.0
Inclusion Diameter, μm

8B

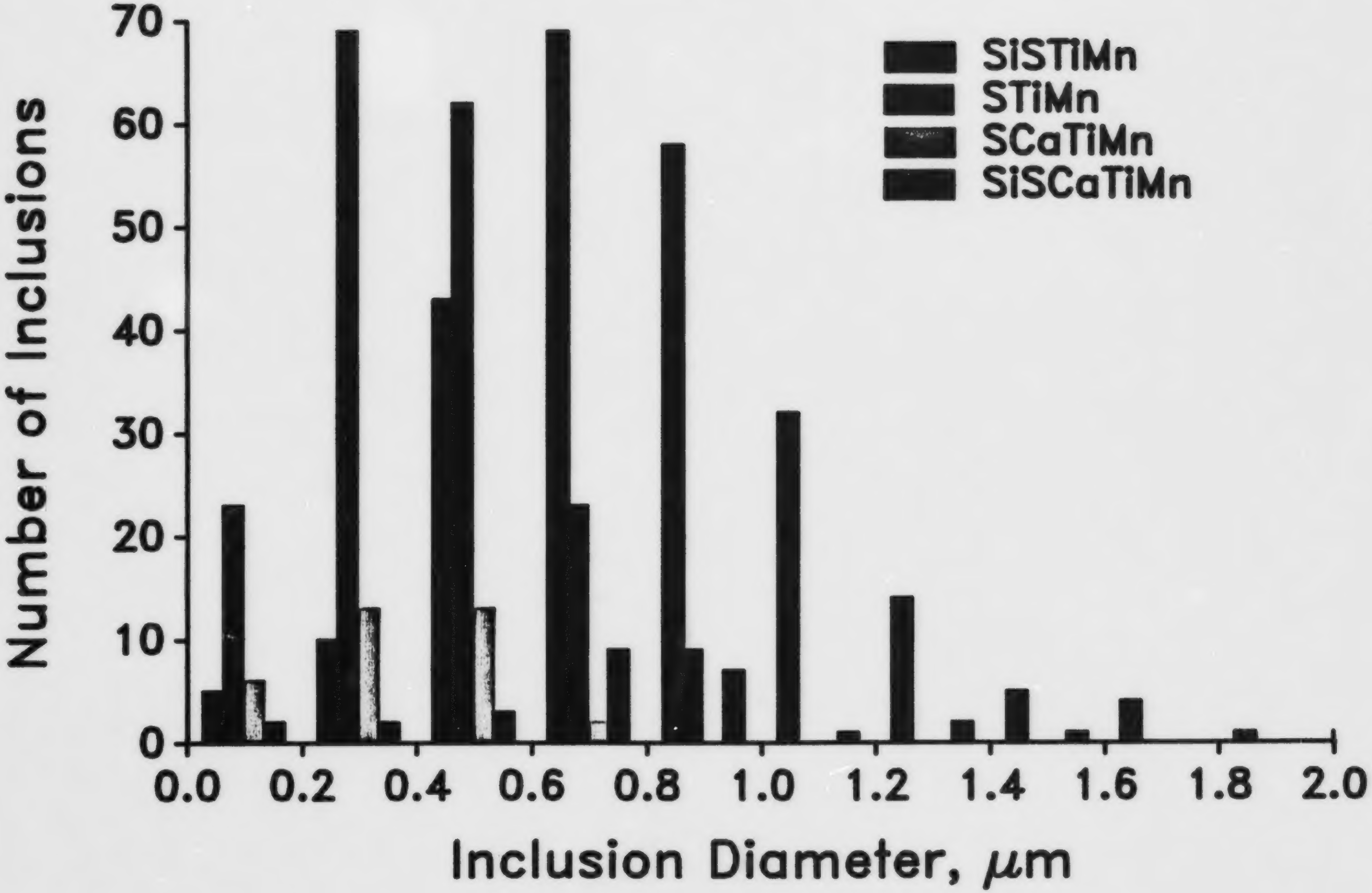
SiSTiMn
STiMn
SCaTiMn
SiSCaTiMn
Number of Inclusions
0
10
20
30
40
50
60
70
0.0
0.2
0.4
0.6
0.8
1.0
1.2
1.4
1.6
1.8
2.0
Inclusion Diameter, μm

9B

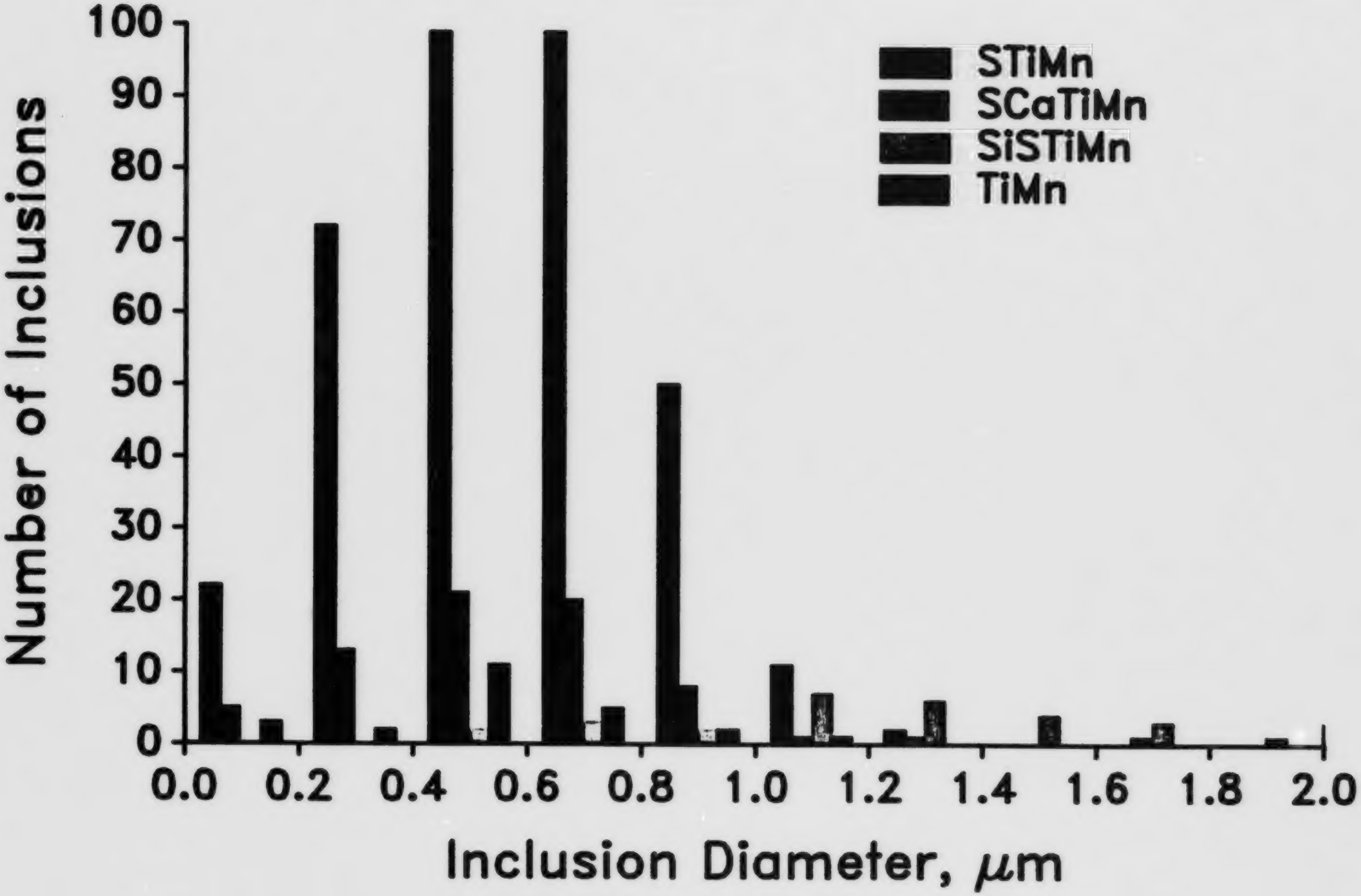
STiMn
SCaTiMn
SiSTiMn
TiMn
Number of Inclusions
0
10
20
30
40
50
60
70
80
90
100
0.0
0.2
0.4
0.6
0.8
1.0
1.2
1.4
1.6
1.8
2.0
Inclusion Diameter, μm

APPENDIX B

Data on Transverse Shrinkage

WELD ID F10A

DATE 1-Nov-90

ALL DIMENSIONS IN mm.

CLOCKWISE ROTATION DEFINED AS POSITIVE

CONDITION	LOCATION		L1		L1 AVE	SHRINKAGE		L2		L2 AVE.	SHRINKAGE		L3		L3 AVE.	SHRINKAGE	A3 RIGHT	A3 LEFT	B3 RIGHT	B3 LEFT	C RIGHT	C LEFT
ROOM TEMPERATURE ALL SET PRIOR TO PREHEAT UNDER RESTRAINT	A1	131.61	131.62	131.60	131.61		77.17	77.18	77.18	77.18		131.18	131.18	131.18	131.18		0.5	0.0	0.5	0.0	0.4	0.0
	A2	130.90	130.89	130.91	130.90		76.14	76.15	76.13	76.14		130.87	130.86	130.87	130.86							
	A3	131.09	131.08	131.10	131.09		77.60	77.58	77.58	77.59		131.78	131.77	131.78	131.78							
	B1	131.25	131.24	131.24	131.24		77.56	77.57	77.58	77.57		131.52	131.50	131.52	131.51							
	B2	131.35	131.30	131.48	131.38		77.79	77.79	77.79	77.79		131.62	131.61	131.60	131.61							
	B3	131.52	131.52	131.55	131.53		77.68	77.67	77.67	77.67		131.33	131.31	131.33	131.32							
	C	131.30	131.28	131.30	131.29		77.71	77.73	77.73	77.72		132.41	132.41	132.43	132.42							
ROOM TEMPERATURE AFTER FIRST PASS UNDER RESTRAINT	A1	131.61	131.61	131.60	131.61	0.00	76.38	76.36	76.37	76.37	-0.81	131.18	131.18	131.18	131.18	0.00	MEASURED	ANGLE				
	A2	130.90	130.90	130.90	130.90	0.00	77.29	77.27	77.29	77.30	-0.86	130.84	130.84	130.86	130.84	-0.02	0.3	0.3	0.4	0.3	0.4	0.4
	A3	131.09	131.09	131.09	131.09	0.00	76.71	76.78	76.72	76.71	-0.88	131.76	131.77	131.77	131.77	-0.02						
	B1	131.23	131.24	131.23	131.23	-0.01	76.67	76.67	76.67	76.67	-0.90	131.46	131.47	131.47	131.47	-0.05	ANGULAR	CHANGE				
	B2	131.30	131.34	131.34	131.33	-0.05	76.87	76.84	76.86	76.86	-0.93	131.57	131.58	131.56	131.56	-0.05	-0.2	0.3	-0.1	0.3	0.0	0.4
	B3	131.48	131.49	131.50	131.49	-0.03	76.70	76.78	76.71	76.70	-0.97	131.30	131.31	131.30	131.30	-0.02						
	C	131.28	131.27	131.27	131.27	-0.02	76.65	76.66	76.65	76.65	-0.87	132.38	132.38	132.40	132.39	-0.03						
ROOM TEMPERATURE AFTER SECOND PASS UNDER RESTRAINT	A1	131.61	131.60	131.60	131.60	-0.01	75.92	75.92	75.91	75.92	-1.26	131.20	131.20	131.20	131.20	0.02	MEASURED	ANGLE				
	A2	130.91	130.90	130.90	130.90	0.00	76.83	76.82	76.82	76.82	-1.32	130.89	130.88	130.87	130.88	0.01	0.0	0.2	0.3	0.3	0.3	0.3
	A3	131.08	131.08	131.08	131.08	-0.01	76.27	76.26	76.27	76.27	-1.33	131.79	131.78	131.80	131.79	0.01						
	B1	131.23	131.23	131.23	131.23	-0.01	76.53	76.53	76.52	76.53	-1.34	131.50	131.51	131.51	131.51	-0.01	ANGULAR	CHANGE				
	B2	131.36	131.36	131.36	131.36	-0.02	76.40	76.40	76.40	76.40	-1.39	131.59	131.60	131.60	131.60	-0.02	-0.5	0.2	-0.2	0.3	-0.1	0.3
	B3	131.50	131.50	131.52	131.50	-0.03	76.25	76.26	76.29	76.26	-1.42	131.32	131.32	131.32	131.32	0.00						
	C	131.27	131.27	131.30	131.27	-0.02	76.40	76.40	76.41	76.40	-1.32	132.42	132.40	132.41	132.42	0.00						
ROOM TEMPERATURE AFTER THIRD PASS UNDER RESTRAINT	A1	131.62	131.60	131.61	131.61	0.00	75.40	75.40	75.40	75.40	-1.78	131.19	131.19	131.18	131.19	0.01	MEASURED	ANGLE				
	A2	130.91	130.91	130.92	130.91	0.01	76.38	76.38	76.40	76.39	-1.75	130.86	130.87	130.86	130.86	0.00	0.0	0.4	0.2	0.3	0.0	0.4
	A3	131.04	131.07	131.09	131.07	-0.02	75.80	75.78	75.78	75.78	-1.81	131.77	131.77	131.77	131.77	-0.01						
	B1	131.20	131.22	131.21	131.21	-0.03	75.84	75.85	75.86	75.85	-1.92	131.48	131.48	131.48	131.48	-0.03	ANGULAR	CHANGE				
	B2	131.35	131.36	131.36	131.36	-0.03	75.93	75.95	75.94	75.94	-1.85	131.58	131.58	131.60	131.59	-0.02	-0.5	0.4	-0.3	0.3	-0.4	0.4
	B3	131.50	131.48	131.50	131.49	-0.03	75.79	75.78	75.70	75.75	-1.90	131.21	131.28	131.29	131.30	-0.02						
	C	131.28	131.29	131.29	131.29	-0.01	75.96	75.96	75.96	75.96	-1.76	132.38	132.38	132.38	132.38	-0.03						
ROOM TEMPERATURE AFTER 12TH PASS 1/8 LOCATION UNDER RESTRAINT	A1	131.67	131.69	131.69	131.68	0.07	74.10	74.17	74.18	74.15	-3.03	131.23	131.23	131.23	131.23	0.05	MEASURED	ANGLE				
	A2	130.88	130.88	130.90	130.89	0.00	75.08	75.08	75.10	75.09	-3.05	130.93	130.92	130.93	130.92	0.06	-0.2	0.7	0.0	0.7	-0.2	0.6
	A3	131.14	131.15	131.16	131.15	0.06	74.48	74.48	74.48	74.48	-3.11	131.84	131.84	131.83	131.84	0.06						
	B1	131.26	131.27	131.27	131.27	0.02	74.77	74.76	74.77	74.77	-3.10	131.56	131.55	131.54	131.55	0.04	ANGULAR	CHANGE				
	B2	131.42	131.44	131.44	131.43	0.05	74.67	74.68	74.69	74.68	-3.11	131.65	131.64	131.66	131.65	0.04	-0.7	0.7	-0.5	0.7	-0.6	0.6
	B3	131.57	131.58	131.55	131.56	0.03	74.57	74.58	74.58	74.58	-3.10	131.37	131.36	131.36	131.36	0.05						
	C	131.36	131.35	131.36	131.35	0.06	74.95	74.92	74.91	74.91	-2.81	132.45	132.46	132.45	132.46	0.04						
ROOM TEMPERATURE AFTER 22ND PASS 3/4 LOCATION UNDER RESTRAINT	A1	131.74	131.74	131.74	131.74	0.13	73.72	73.72	73.74	73.73	-3.45	131.32	131.31	131.33	131.32	0.14	MEASURED	ANGLE				
	A2	131.03	131.01	131.02	131.02	0.12	74.78	74.72	74.71	74.71	-3.43	131.00	131.00	130.99	131.00	0.13	-0.4	0.7	-0.2	0.0	-0.2	0.7
	A3	131.24	131.25	131.24	131.24	0.15	74.09	74.10	74.10	74.10	-3.50	131.92	131.92	131.94	131.92	0.14						
	B1	131.35	131.36	131.36	131.36	0.11	74.39	74.39	74.38	74.38	-3.40	131.66	131.66	131.67	131.66	0.15	ANGULAR	CHANGE				
	B2	131.48	131.49	131.51	131.49	0.11	74.27	74.27	74.26	74.27	-3.52	131.73	131.73	131.72	131.73	0.12	-0.8	0.7	-0.7	0.0	-0.6	0.7
	B3	131.62	131.62	131.63	131.62	0.10	74.22	74.21	74.28	74.22	-3.45	131.46	131.44	131.46	131.45	0.13						
	C	131.42	131.43	131.41	131.42	0.12	74.53	74.53	74.54	74.53	-3.19	132.54	132.54	132.54	132.54	0.12						
ROOM TEMPERATURE FILLED UP UNDER RESTRAINT	A1	131.81	131.82	131.80	131.81	0.20	73.28	73.28	73.27	73.28	-3.88	131.30	131.31	131.30	131.30	0.12	MEASURED	ANGLE				
	A2	131.05	131.07	131.06	131.06	0.16	74.16	74.16	74.17	74.17	-3.97	130.99	130.99	130.98	130.99	0.13	-0.50	0.60	-0.30	0.60	-0.30	0.60
	A3						73.67	73.66	73.66	73.66	-3.92	131.92	131.92	131.92	131.92	0.14						
	B1	131.38	131.38	131.38	131.38	0.14	73.56	73.56	73.57	73.56	-3.98	131.69	131.71	131.71	131.70	0.19	ANGULAR	CHANGE				
	B2	131.59	131.58	131.60	131.59	0.21	73.83	73.85	73.83	73.84	-3.95						-1.00	0.60	-0.80	0.60	-0.70	0.60
	B3	131.66	131.67	131.68	131.66	0.14	73.82	73.81	73.81	73.82	-3.85	131.53	131.54	131.52	131.53	0.21						
	C	131.37	131.36	131.37	131.37	0.08	74.09	74.10	74.10	74.09	-3.63	132.62	132.63	132.63	132.63	0.21						

Table B1

Summary of Shrinkage Measurements
For Low Restraint Weld (F10A)

WELD ID F11A

DATE 16-Nov-88

ALL DIMENSIONS IN mm.

* DENOTES STRONGBACK UNDERNEATH

CLOCKWISE ROTATION DEFINED AS POSITIVE

CONDITION	LOCATION	L1			L1 AVE	SHRINKAGE	L2			L2 AVE.	SHRINKAGE	L3			L3 AVE.	SHRINKAGE	A2 RIGHT	A2 LEFT	B2 RIGHT	B2 LEFT	C RIGHT	C LEFT
ROOM TEMPERATURE ALL SET PRIOR TO PREHEAT UNDER RESTRAINT	A1	131.12	131.12	131.13	131.12		75.40	75.40	75.40	75.40		131.68	131.68	131.67	131.68		0.2	0.2	0.2	0.2	0.2	0.2
	A2*	131.46	131.46	131.46	131.46		75.43	75.44	75.42	75.43		131.49	131.50	131.49	131.49							
	A3	131.50	131.51	131.50	131.50		76.08	76.10	76.10	76.09		131.12	131.11	131.11	131.11							
	B1*	131.48	131.47	131.47	131.47		76.46	76.47	76.45	76.46		131.20	131.21	131.20	131.20							
	B2	131.71	131.75	131.80	131.75		76.37	76.38	76.36	76.37		130.78	130.81	130.78	130.79							
	B3*	131.78	131.78	131.78	131.78		76.11	76.12	76.11	76.11		131.00	131.00	131.00	131.00							
	C*	131.27	131.29	131.28	131.28		76.41	76.40	76.39	76.40		130.16	130.16	130.17	130.16							
ROOM TEMPERATURE AFTER FIRST PASS UNDER RESTRAINT 16-Nov-88 5:30 PM	A1	131.11	131.12	131.12	131.12	-0.01	75.24	75.26	75.26	75.26	-0.14	131.67	131.67	131.68	131.68	0.00	MEASURED	ANGLE				
	A2*	131.47	131.46	131.47	131.47	0.01	75.25	75.26	75.24	75.25	-0.18	131.50	131.50	131.51	131.50	0.01	0.2	0.2	0.2	0.3	0.2	0.2
	A3	131.50	131.49	131.51	131.50	0.00	75.88	75.88	75.87	75.88	-0.21	131.13	131.13	131.12	131.13	0.01						
	B1*	131.48	131.47	131.46	131.47	0.00	76.30	76.29	76.31	76.30	-0.16	131.18	131.20	131.18	131.19	-0.01	ANGULAR	CHANGE				
	B2	131.75	131.75	131.80	131.75	0.00	76.17	76.17	76.17	76.17	-0.20	130.80	130.81	130.80	130.80	0.01	0.0	0.0	0.0	0.1	-0.1	0.0
	B3*	131.78	131.77	131.77	131.77	-0.01	75.90	75.88	75.91	75.90	-0.21	130.99	130.98	130.99	130.99	-0.01						
	C*	131.26	131.29	131.27	131.26	-0.02	76.21	76.22	76.22	76.22	-0.18	130.17	130.16	130.16	130.16	0.01						
ROOMP TEMPERATURE AFTER SECOND PASS UNDER RESTRAINT 17-Nov-88 8:30 AM	A1	131.12	131.13	131.12	131.12	0.00	75.15	75.13	75.13	75.14	-0.26	131.69	131.69	131.69	131.69	0.01	MEASURED	ANGLE				
	A2*	131.46	131.47	131.46	131.46	0.00	75.15	75.15	75.15	75.15	-0.28	131.49	131.49	131.49	131.49	0.00	0.1	0.2	0.2	0.2	0.1	0.2
	A3	131.52	131.52	131.51	131.52	0.01	75.74	75.73	75.75	75.74	-0.35	131.14	131.13	131.15	131.14	0.03						
	B1*	131.50	131.50	131.50	131.50	0.03	76.17	76.16	76.15	76.16	-0.30	131.18	131.20	131.18	131.18	-0.02	ANGULAR	CHANGE				
	B2	131.72	131.73	131.73	131.73	0.02	76.04	76.05	76.04	76.04	-0.33	130.82	130.83	130.83	130.83	0.03	-0.1	0.0	0.0	0.0	-0.2	0.0
	B3*	131.81	131.80	131.81	131.81	0.03	75.77	75.76	75.77	75.77	-0.34	131.02	131.01	131.01	131.01	0.01						
	C*	131.29	131.30	131.30	131.29	0.01	76.12	76.12	76.11	76.12	-0.28	130.20	130.20	130.22	130.21	0.05						
ROOM TEMPERATURE AFTER THIRD PASS UNDER RESTRAINT 17-Nov-88 1:00 PM	A1	131.14	131.15	131.14	131.14	0.02	75.10	75.10	75.10	75.10	-0.30	131.69	131.69	131.69	131.69	0.01	MEASURED	ANGLE				
	A2*	131.48	131.48	131.48	131.48	0.02	75.06	75.07	75.06	75.06	-0.37	131.50	131.50	131.51	131.50	0.01	0.2	0.3	0.2	0.2	0.1	0.3
	A3	131.51	131.50	131.52	131.51	0.01	75.67	75.68	75.66	75.66	-0.42	131.15	131.15	131.13	131.14	0.03						
	B1*	131.50	131.50	131.51	131.50	0.03	76.08	76.07	76.08	76.08	-0.38	131.21	131.21	131.18	131.20	0.00	ANGULAR	CHANGE				
	B2	131.78	131.78	131.74	131.78	0.03	75.97	75.97	75.95	75.96	-0.41	130.81	130.78	130.78	130.80	0.00	0.0	0.0	0.0	0.0	-0.2	0.1
	B3*	131.80	131.80	131.80	131.81	0.02	75.71	75.71	75.72	75.71	-0.40	131.00	130.99	130.99	130.99	-0.01						
	C*	131.29	131.29	131.31	131.30	0.02	76.04	76.04	76.05	76.04	-0.36	130.21	130.21	130.22	130.21	0.04						
ROOM TEMPERATURE AFTER 12TH PASS 1/2 LOCATION UNDER RESTRAINT 17-Nov-88 4:30-6:00 PM	A1	131.17	131.17	131.18	131.17	0.05	74.87	74.88	74.88	74.88	-0.51	131.72	131.72	131.71	131.72	0.04	MEASURED	ANGLE				
	A2*	131.48	131.47	131.48	131.48	0.02	74.78	74.79	74.78	74.79	-0.64	131.56	131.54	131.54	131.54	0.05	0.1	0.3	0.0	0.3	0.0	0.2
	A3	131.51	131.50	131.55	131.52	0.02	75.34	75.36	75.36	75.35	-0.73	131.16	131.16	131.17	131.16	0.05						
	B1*	131.53	131.52	131.52	131.52	0.05	75.77	75.76	75.76	75.76	-0.70	131.25	131.24	131.26	131.25	0.05	ANGULAR	CHANGE				
	B2	131.74	131.72	131.74	131.73	0.00	75.64	75.63	75.63	75.63	-0.74	130.85	130.84	130.85	130.85	0.06	-0.1	0.1	-0.2	0.1	-0.3	0.0
	B3*	131.81	131.80	131.80	131.81	0.03	75.38	75.38	75.38	75.38	-0.73	131.05	131.04	131.05	131.05	0.05						
	C*	131.34	131.34	131.35	131.34	0.06	75.72	75.74	75.72	75.73	-0.67	130.23	130.24	130.25	130.24	0.08						
ROOM TEMPERATURE AFTER 32ND PASS 3/4 LOCATION UNDER RESTRAINT 18-Nov-88 2:00-3:00 PM	A1	131.20	131.20	131.21	131.20	0.08	74.69	74.68	74.68	74.68	-0.72	131.79	131.81	131.80	131.80	0.12	MEASURED	ANGLE				
	A2*	131.52	131.53	131.52	131.52	0.06	74.58	74.58	74.58	74.58	-0.84	131.60	131.61	131.61	131.61	0.12	0.0	0.4	0.0	0.3	0.0	0.2
	A3	131.56	131.56	131.57	131.56	0.06	75.17	75.16	75.17	75.17	-0.93	131.23	131.24	131.23	131.23	0.12						
	B1*	131.56	131.56	131.57	131.56	0.09	75.58	75.57	75.58	75.58	-0.88	131.29	131.27	131.28	131.28	0.08	ANGULAR	CHANGE				
	B2	131.75	131.75	131.78	131.76	0.00	75.44	75.42	75.43	75.43	-0.94	130.90	130.92	130.91	130.91	0.11	-0.2	0.2	-0.2	0.1	-0.3	0.0
	B3*	131.84	131.85	131.85	131.85	0.07	75.25	75.24	75.25	75.25	-0.87	131.14	131.12	131.12	131.13	0.13						
	C*	131.38	131.39	131.38	131.38	0.11	75.60	75.58	75.60	75.59	-0.81	130.33	130.34	130.33	130.33	0.16						
ROOM TEMPERATURE FILLED UP UNDER RESTRAINT 21-Nov-88 11:30:00 AM - 3:30 PM	A1	131.25	131.25	131.24	131.25	0.13	74.38	74.40	74.41	74.40	-1.00	131.88	131.90	131.90	131.90	0.22	MEASURED	ANGLE				
	A2*	131.64	131.62	131.63	131.63	0.17	74.30	74.28	74.27	74.28	-1.15	131.68	131.67	131.67	131.68	0.18	0.10	0.30	0.00	0.30	0.10	0.30
	A3	131.73	131.73	131.75	131.74	0.23	74.97	74.96	74.94	74.95	-1.14	131.38	131.38	131.38	131.38	0.27						
	B1*	131.67	131.67	131.67	131.67	0.20	75.29	75.28	75.28	75.28	-1.17	131.47	131.47	131.45	131.46	0.26	ANGULAR	CHANGE				
	B2	131.83	131.80	131.88	131.83	0.08	75.22	75.22	75.22	75.22	-1.15	131.01	131.00	131.00	131.00	0.21	-0.10	0.10	-0.20	0.10	-0.20	0.10
	B3*	131.96	131.96	131.96	131.96	0.18	74.98	75.00	75.00	74.99	-1.12	131.20	131.18	131.18	131.18	0.18						
	C*	131.47	131.48	131.47	131.48	0.20	75.30	75.29	75.28	75.29	-1.11	130.43	130.44	130.43	130.43	0.26						

Table B2

Summary of Shrinkage Measurements
For High Restraint Weld (F11A)

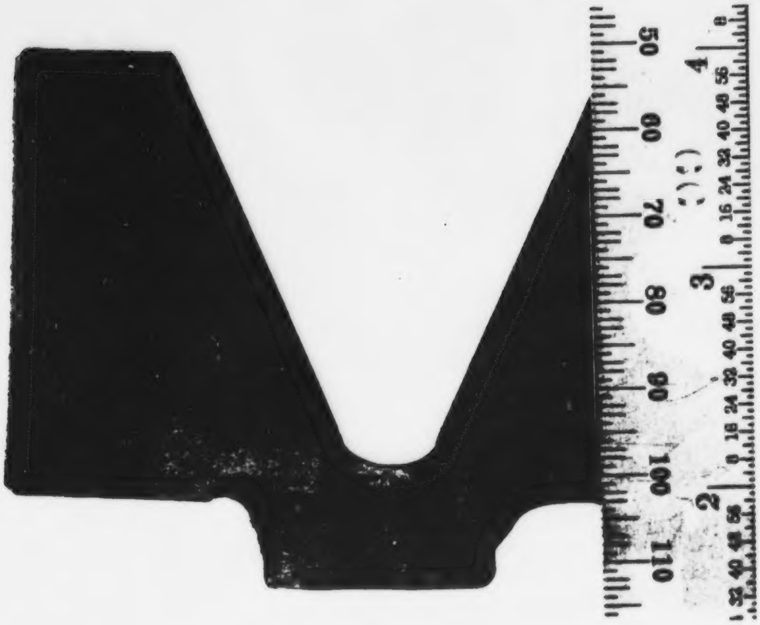
50
60
70
80
90
100
110
4
3
2

Figure B1: Joint Geometry After 1st Root Pass of Low Restraint Weld, I10A (1.3X, Neg. 11140)

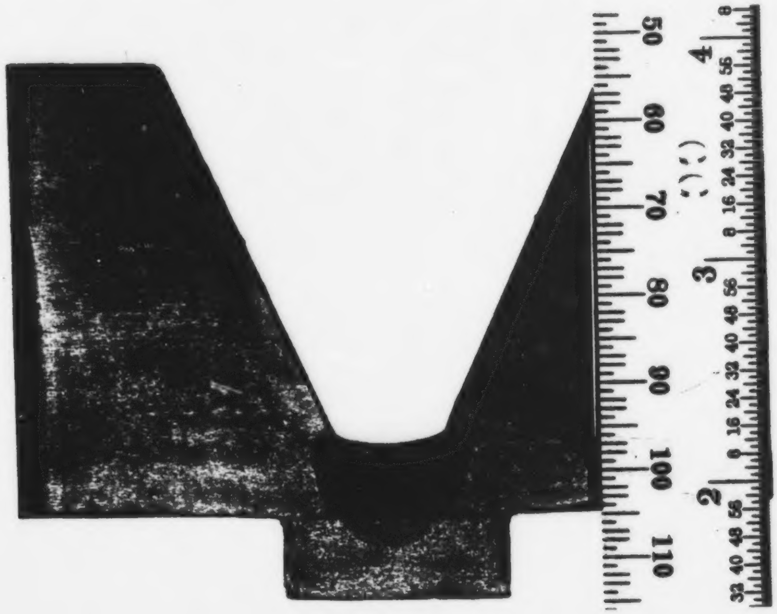
50
60
70
80
90
100
110
4
3
2

Figure B2: Joint Geometry After the Completion of 2nd Root Pass of Low Restraint Weld F10A (1.3X, Neg. 11141)

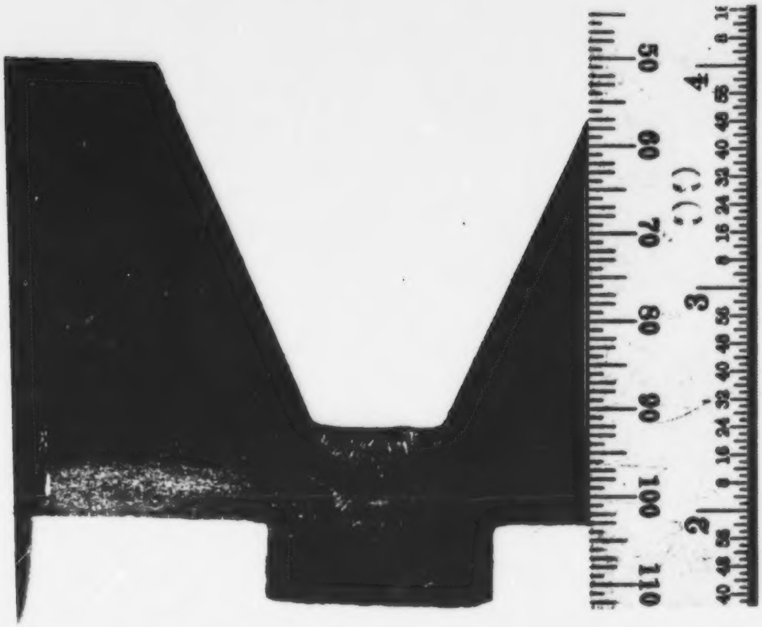
50
60
70
80
90
100
110
4
3
2

Figure B3: Joint Geometry After the Completion of 3rd Pass of Low Restraint Weld F10A (1.3X, Neg. 11142)

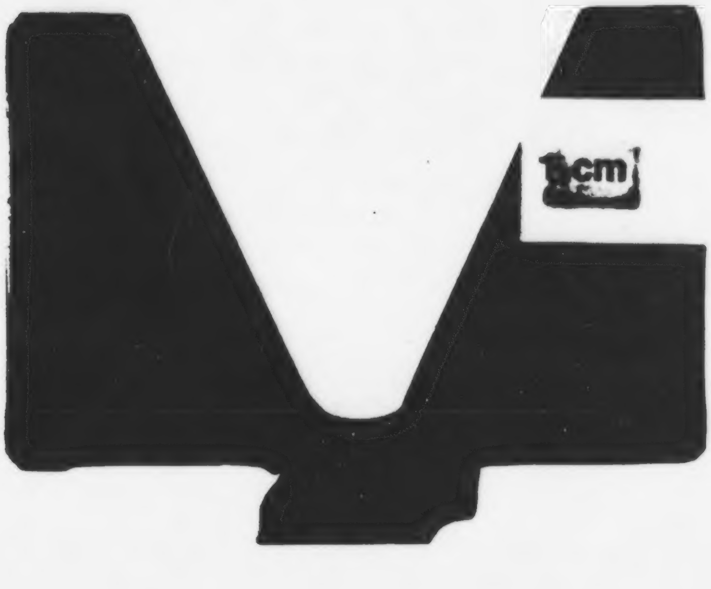

Figure B4: Joint Geometry After the Completion of 1st Root Pass of High Restraint Weld F11A (1.3X, Neg. 11137).

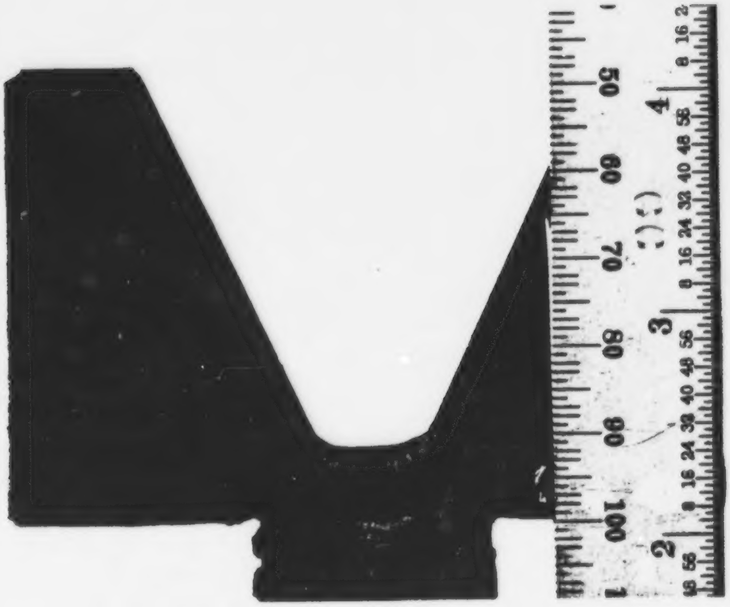

Figure B5: Joint Geometry After the Completion of 2nd Pass in High Restraint Weld F11A (1.3X, Neg. 11138)

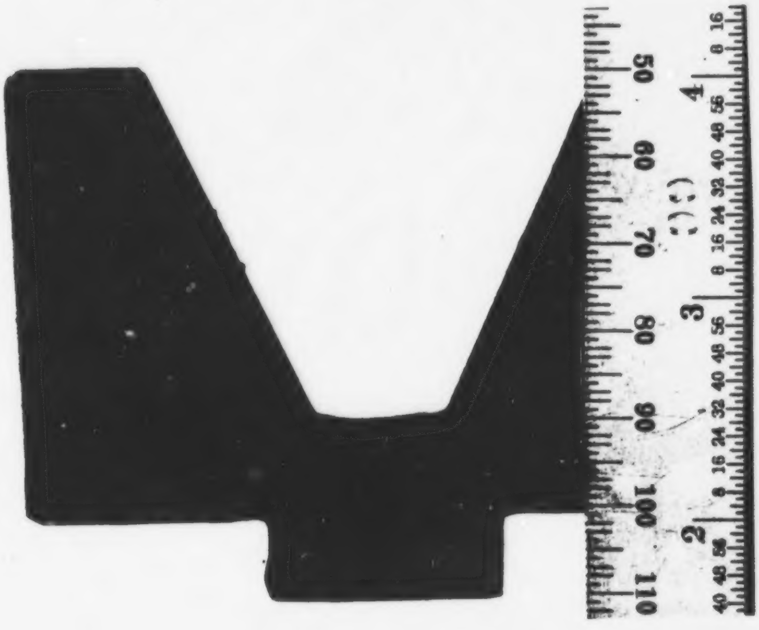

Figure B6: Joint Geometry After the Completion of 3rd Root Pass in High Restraint Weld F11A (1.3X, Neg. 11139)

APPENDIX C

Data on Drop Weight Testing

Table C1

Drop Weight Testing Results for Flux Cored Welds Consumable A, 1G Position, As Welded

Test Temperature (°C)	2.0 kJ/mm	3.0 kJ/mm
-20	---	No Break
-30	---	No Break
-40	No Break	No Break
-50	No Break	No Break
-60	No Break	No Break No Break
-65	No Break No Break	Break
-70	Break	---

Table C2

Drop Weight Test Results
Consumable B, 1G Position, Stress Relieved Condition

Test Temperature (°C)	2.0 kJ/mm	3.0 kJ/mm
-20	---	No Break
-30	---	No Break
-40	No Break	No Break
-50	No Break	No Break No Break
-55	---	Break
-60	No Break	Break
-70	No Break No Break	---
-75	No Break No Break	---
-80	Break	---

Table C3

Drop Weight Test Results
Consumable C, 1G Position, 3.0 kJ/mm

Test Temperature (°C)	As Welded	Stress Relieved
-20	No Break	No Break
-30	No Break	No Break
-40	No Break	No Break
-50	No Break	No Break
-55	No Break	No Break
	No Break	Break
-60	Break	Break

APPENDIX D

Data and Transition Curves From CVN Testing

Table D1

CVN Test Data for Consumable A
3.0 kJ/mm in As Welded Condition (F1A)

Temperature °C	Subsurface				Root			
	Impact Energy (J)	Lateral Expansion (mm)	% Shear	Average Impact Energy (J)	Impact Energy (J)	Lateral Expansion (mm)	% Shear	Average Impact Energy (J)
20	132	1.7	100		--	--	--	--
	134	2.0	100	133				
0	111	1.4	60		132	2.0	70	
	132	1.8	90	122	145	1.9	70	139
-20	92	1.3	50		114	1.7	70	
	96	1.3	50	92	123	1.6	60	119
-30	45	0.76	40		80	1.2	40	
	81	1.1	50	63	108	1.6	50	94
-40	39	0.64	30		38	0.71	30	
	65	0.97	40	52	93	1.2	50	65
-50	38	0.69	40		53	0.76	20	
	46	0.74	25	42	69	1.1	40	61
-60	18	0.38	20		28	0.51	20	
	27	0.43	20	23	45	0.76	20	37
-70	12	0.20	15		10	0.28	10	
	12	0.23	15	12	15	0.34	10	13
-80	--	--	--	--	5	0.18	10	
					15	0.33	10	10

Table D2

CVN Test Data for Consumable B
3.0 kJ/mm in Stress Relieved Condition (F2A)

Temperature °C	Subsurface				Root			
	Impact Energy (J)	Lateral Expansion (mm)	% Shear	Average Impact Energy (J)	Impact Energy (J)	Lateral Expansion (mm)	% Shear	Average Impact Energy (J)
20	97 115	1.5 1.7	60 70	106	108 110	1.6 1.8	60 60	109
0	64 74 83	0.91 1.1 1.2	30 40 40	74	45 56 70 84	0.89 1.0 1.2 1.3	40 40 50 50	64
-10	38 38 43	0.64 0.71 0.61	30 30 30	40	41 52 61 75	0.86 0.84 1.1 1.1	30 30 40 40	57
-20	23 39	0.43 0.66	20 20	31	28 41	0.74 0.76	30 30	35
-30	15 20	0.41 0.43	10 15	18	28 31	0.51 0.64	20 20	30
-40	12 18	0.23 0.33	10 15	15	11 11	0.36 0.38	10 10	11
-50	7 8	0.18 0.18	10 10	8	--	--	--	--

Table D3

CVN Test Data for Consumable C
3.0 kJ/mm in As Welded Condition (F3A)

Temperature °C	Subsurface				Root			
	Impact Energy (J)	Lateral Expansion (mm)	% Shear	Average Impact Energy (J)	Impact Energy (J)	Lateral Expansion (mm)	% Shear	Average Impact Energy (J)
20	--	--	--	--	139 141	2.1 2.0	100 90	140
0	126 135	1.7 1.7	70 70	131	120 122	1.9 1.9	80 70	121
-20	76 106	1.1 1.5	50 50	91	93 110	1.5 1.6	60 60	102
-30	69 95	1.1 1.2	40 40	82	--	--	--	--
-40	31 31	0.28 0.46	20 30	31	56 71	0.91 1.0	30 30	64
-45	41 110	0.69 1.5	25 50	76	--	--	--	--
-50	26 36	0.48 0.58	20 30	31	15 37 41	0.36 0.69 0.74	20 20 30	31
-60	12 15	0.20 0.25	15 10	14	20 22	0.43 0.41	20 10	21
-70	--	--	--	--	7 12	0.15 0.25	5 10	10

Table D4

CVN Test Data for Consumable C
3.0 kJ/mm in Stress Relieved Condition (F4A)

Temperature °C	Subsurface				Root			
	Impact Energy (J)	Lateral Expansion (mm)	% Shear	Average Impact Energy (J)	Impact Energy (J)	Lateral Expansion (mm)	% Shear	Average Impact Energy (J)
20	120	1.6	80	114	95	1.6	50	88
	107	1.4	70		87	1.3	50	
					83	1.3	40	
10	--	--	--	--	58	1.0	40	53
					48	0.66	20	
0	106	1.3	50	104	64	0.79	30	47
	102	1.4	50		41	0.76	25	
					35	0.61	20	
-10	--	--	--	--	31	0.53	20	26
					21	0.51	30	
-20	88	1.2	30	87	30	0.51	20	26
	85	1.1	40		22	0.48	20	
-30	63	0.94	20	61	20	0.41	20	18
	58	1.0	20		16	0.41	20	
-40	22	0.36	10	21	12	0.25	10	10
	19	0.33	10		8	0.33	10	
-50	24	0.48	10	20	--	--	--	--
	24	0.41	10					
	11	0.18	10					
-60	9	0.15	5	8	--	--	--	--
	7	0.13	5					

Table D5

CVN Test Data for Consumable A
2.0 kJ/mm in As Welded Condition (F5A)

Temperature °C	Subsurface				Root			
	Impact Energy (J)	Lateral Expansion (mm)	% Shear	Average Impact Energy (J)	Impact Energy (J)	Lateral Expansion (mm)	% Shear	Average Impact Energy (J)
20	82 82	1.4 1.3	60 50	82	88 81	1.2 1.4	90 90	85
0	76 70	1.2 1.0	60 50	73	104 85	1.6 1.4	80 100	95
-20	68 64	0.97 1.0	40 40	66	77 76	1.2 1.1	50 50	76
-30	--	--	--	--	56	0.91	30	56
-40	53 37	0.84 0.61	30 30	45	43 37	0.74 0.71	20 20	40
-50	45 37	0.74 0.51	25 30	41	--	--	--	--
-60	25 20	0.41 0.25	15 15	23	36 26	0.61 0.53	20 25	31
-70	26 18	0.48 0.38	25 20	22	--	--	--	--
-80	15 12	0.25 0.15	15 20	14	28 23 12	0.48 0.38 0.36	10 10 5	21
-90	--	--	--	--	8 7	0.18 0.15	10 5	8

Table D6

CVN Test Data for Consumable B
2.0 kJ/mm in Stress Relieved Condition (F6A)

Temperature °C	Subsurface				Root			
	Impact Energy (J)	Lateral Expansion (mm)	% Shear	Average Impact Energy (J)	Impact Energy (J)	Lateral Expansion (mm)	% Shear	Average Impact Energy (J)
20	92	1.4	80	92	129 83	2.0 1.4	90 100	106
0	85 80	1.3 1.1	50 50	83	121 85	1.8 1.4	80 80	103
-10	69 38	1.1 0.69	40 30	54	--	--	--	--
-20	44 30	0.66 0.51	30 20	37	47 34	0.91 0.77	40 40	41
-30	--	--	--	--	48 34	0.84 0.74	30 25	41
-40	39 30	0.66 0.51	30 20	35	100 64	1.6 0.94	40 40	82
-50	20 18	0.46 0.38	20 20	19	42 27	0.86 0.61	30 40	35
-60	22 14	0.38 0.25	20 20	18	28 16	0.51 0.25	10 15	22
-70	11 10	0.28 0.20	10 10	11	8 7	0.25 0.20	10 10	8

Table D7

CVN Test Data for Consumable B
2.0 kJ/mm in Stress Relieved Condition, 3G Position (F7A)

Temperature °C	Subsurface				Root			
	Impact Energy (J)	Lateral Expansion (mm)	% Shear	Average Impact Energy (J)	Impact Energy (J)	Lateral Expansion (mm)	% Shear	Average Impact Energy (J)
20	118 114	1.7 1.7	70 70	116	129 126	2.0 1.9	80 80	128
0	115 87	1.4 1.2	60 50	101	115 98	1.7 1.4	70 60	107
-20	80 70	1.1 0.99	50 30	75	76 60	1.3 0.97	40 30	68
-30	--	--	--	--	79 77	1.1 0.89	40 40	78
-40	38 37	0.61 0.58	20 15	38	46 41	0.91 1.0	30 40	44
-50	35 31	0.53 0.48	15 15	33	--	--	--	--
-55	24 20	0.43 0.38	10 10	22	--	--	--	--
-60	19 18	0.33 0.28	10 10	19	20 12	0.41 0.23	10 10	16
-70	12 11	0.25 0.28	10 10	12	19 11	0.41 0.28	10 10	15
-80	--	--	--	--	8 8	0.23 0.18	10 10	8

Table D8

CVN Test Data for Consumable B
2.0 kJ/mm in As Welded Condition, 3G Position (F7B)

Temperature °C	Subsurface				Root			
	Impact Energy (J)	Lateral Expansion (mm)	% Shear	Average Impact Energy (J)	Impact Energy (J)	Lateral Expansion (mm)	% Shear	Average Impact Energy (J)
20	107 103	1.5 1.7	100 60	105	--	--	--	--
0	114 84	1.6 1.3	60 50	99	132 119	1.9 1.8	90 70	126
-20	110 79	1.5 1.1	40 30	95	122 96	1.8 1.5	70 60	109
-40	50 45	0.79 0.69	30 30	48	81 46	1.3 0.79	40 30	64
-50	--	--	--	--	64 42	0.89 0.86	40 30	53
-60	57 41	0.86 0.66	30 20	49	50 35	0.84 0.61	20 20	43
-70	37 23	0.61 0.38	30 20	30	23 23	0.51 0.51	20 20	23
-80	27 14 11	0.48 0.25 0.23	20 10 10	17	16 14	0.36 0.28	10 10	15

Table D9

CVN Test Data for Consumable C
2.0 kJ/mm in Stress Relieved Condition, 3G Position (F8A)

Temperature °C	Subsurface				Root			
	Impact Energy (J)	Lateral Expansion (mm)	% Shear	Average Impact Energy (J)	Impact Energy (J)	Lateral Expansion (mm)	% Shear	Average Impact Energy (J)
20	--	--	--	--	138	2.4	100	138
0	120 107	1.7 1.7	70 60	114	130 126	1.7 1.9	80 80	128
-20	110 92	1.4 1.3	60 50	101	123 111	1.7 1.6	50 60	117
-40	58 53	0.91 0.76	30 30	56	76 58	1.3 1.0	40 30	67
-50	41 30	0.71 0.51	30 10	36	80 61 18	1.3 1.0 0.33	30 20 10	53
-55	46 27	0.76 0.48	20 20	--	--	--	--	--
-60	22 20	0.43 0.25	10 10	21	16 14	0.36 0.36	10 10	15
-70	18 12	0.33 0.25	10 10	15	16 9	0.38 0.23	10 10	13
-80	14 9	0.28 0.25	5 10	12	12 5	0.28 0.25	10 5	9

Table D10

CVN Test Data for Consumable B
2.0 kJ/mm in As Welded Condition, 3G Position (F8B)

Temperature °C	Subsurface				Root			
	Impact Energy (J)	Lateral Expansion (mm)	% Shear	Average Impact Energy (J)	Impact Energy (J)	Lateral Expansion (mm)	% Shear	Average Impact Energy (J)
20	130 125	1.9 1.6	100 100	128	--	--	--	--
0	130 125	1.8 1.7	70 70	128	147 146	2.0 2.2	100 100	147
-20	126 114	1.6 1.5	60 80	120	132 127	2.0 1.9	80 80	130
-30	--	--	--	--	119 114	1.6 1.6	60 60	117
-40	89 84	1.2 1.0	50 50	87	91 86	1.5 1.3	60 50	89
-50	--	--	--	--	87 66	1.4 1.1	40 40	77
-60	56 43	0.74 0.58	30 20	50	60 43	1.0 0.76	20 20	52
-70	36 26	0.51 0.43	15 20	31	42 32	0.76 0.58	20 20	37
-80	19 14	0.33 0.25	15 10	17	11 8	0.25 0.22	10 10	10
-90	18 13	0.25 0.46	10 15	16	--	--	--	--

Table D11

CVN Test Data for Consumable B
2.0 kJ/mm in Stress Relieved Condition, 1G Position (F9A)

Temperature °C	Subsurface				Root			
	Impact Energy (J)	Lateral Expansion (mm)	% Shear	Average Impact Energy (J)	Impact Energy (J)	Lateral Expansion (mm)	% Shear	Average Impact Energy (J)
0	91 81	1.3 1.1		86	145 130	1.9 1.8	80 80	138
-10	--	--	--	--	104 98	1.7 1.6	50 50	101
-20	102 50	1.4 0.86	40 30		106 104	1.6 1.4	50 50	105
-30	--	--	--	--	75 66	1.2 1.1	40 30	71
-40	62 47	0.91 0.84	25 25	55	92 57	1.4 0.97	40 30	75
-50	71 23	1.1 0.41	15	47	79 45	1.2 0.79	30 30	62
-60	14 12	0.23 0.23	10 10	13	19 14	0.38 0.36	10 15	13
-70	19 12	0.25 0.18	10 5	16	8 7	0.25 0.20	10 10	8
-80	23 7 5	0.71 0.23 0.15	5 5 5	12	--	--	--	--

Table D12

CVN Test Data for Consumable C
2.0 kJ/mm in As Welded Condition, 1G Position (F9B)

Temperature °C	Subsurface				Root			
	Impact Energy (J)	Lateral Expansion (mm)	% Shear	Average Impact Energy (J)	Impact Energy (J)	Lateral Expansion (mm)	% Shear	Average Impact Energy (J)
0	131 122	1.8 2.0	90 90	127	153 151	2.2 2.2	80 100	152
-20	126 59	1.8 1.0	80 50	93	141 126	2.0 2.0	80 90	134
-40	92 80	1.3 1.1	60 50	86	122 111	1.9 1.5	100 50	117
-50	--	--	--	--	87 85 43	1.3 1.3 0.79	50 40 30	71
-60	65 58	0.97 1.0	40 50	62	79 24 22	1.2 0.53 0.51	40 20 20	42
-70	42 33	0.84 0.53	30 20	38	38 23	0.64 0.51	20 15	31
-80	50 30	0.76 0.48	30 20	40	14 12	0.36 0.31	10 10	13
-90	14 8	0.23 0.23	10 10	11	--	--	--	--

Table D13

CVN Test Data for Consumable A, 2.0 kJ/mm, As Welded Condition, 1G Position, Single V Geometry, High Restraint (F10A)

Temperature °C	Subsurface				Root			
	Impact Energy (J)	Lateral Expansion (mm)	% Shear	Average Impact Energy (J)	Impact Energy (J)	Lateral Expansion (mm)	% Shear	Average Impact Energy (J)
0	149	2.3	100	147	125	1.8	70	118
	146	2.2	80		117	1.8	70	
	146	2.1	80		113	1.8	70	
-20	141	2.1	70	134	104	1.6	60	102
	138	2.2	90		102	1.5	70	
	122	1.8	70		100	1.8	70	
-30	122	1.8	70	115	108	1.7	60	92
	119	1.7	70		100	1.5	60	
	104	1.6	50		81	1.2	50	
					79	1.3	60	
-40	129	1.8	60	112	85	1.3	40	74
	127	1.9	70		81	1.3	40	
	80	1.2	30		74	1.1	50	
					57	1.0	30	
-50	116	1.6	40	87	104	1.5	60	65
	98	1.4	40		71	1.2	30	
	46	0.94	30		68	1.0	40	
					63	0.84	30	
					20	0.41	15	
-60	110	1.6	60	74	57	1.0	40	38
	80	1.2	50		43	0.79	30	
	75	1.1	40		35	0.71	20	
	60	1.0	30		31	0.53	20	
	46	0.89	30		26	0.58	30	
-70	50	0.79	25	26	44	0.76	15	31
	30	0.51	25		31	0.53	20	
	24	0.46	15		30	0.61	20	
	16	0.25	25		26	0.48	20	
	12	0.28	10		22	0.38	20	
-80	41	0.69	10	25	23	0.38	10	20
	31	0.64	10		20	0.41	10	
	16	0.25	10		18	0.38	10	
	10	0.33	15					
-90	33	0.66	10	21	--	--	--	--
	18	0.25	10					
	11	0.25	10					

Table D14

CVN Test Data for Consumable A, 2.0 kJ/mm in As Welded Condition, 1G Position, Single V Geometry, Low Restraint (F11B)

Temperature °C	Subsurface				Root			
	Impact Energy (J)	Lateral Expansion (mm)	% Shear	Average Impact Energy (J)	Impact Energy (J)	Lateral Expansion (mm)	% Shear	Average Impact Energy (J)
0	142	2.1	100	125	128	2.0	100	122
	126	1.9	90		128	1.9	90	
	106	1.8	100		111	1.7	100	
-20	142	2.1	90	124	130	1.8	100	119
	130	2.0	70		129	1.8	100	
	100	1.5	80		99	1.5	60	
-30	144	2.0	80	132	121	1.7	80	106
	134	1.9	70		102	1.5	70	
	119	1.7	60		96	1.5	70	
-40	130	2.0	80	117	96	1.4	50	92
	122	1.6	60		91	1.1	50	
	100	1.7	60		88	1.4	40	
-50	114	1.9	60	98	89	1.3	40	80
	96	1.4	50		84	1.2	50	
	84	1.3	40		66	1.1	40	
-60	114	1.6	50	98	88	1.2	40	77
	98	1.5	30		80	1.3	50	
	83	1.5	30		80	1.2	40	
					58	1.1	40	
-70	108	1.5	40	59	71	1.1	40	56
	80	1.1	50		63	0.94	40	
	54	0.91	20		58	1.1	40	
	41	0.69	20		58	0.94	30	
	12	0.41	20		30	0.53	20	
-80	64	0.94	20	46	60	0.94	30	47
	60	0.91	10		52	0.74	30	
	52	0.91	30		43	0.74	20	
	43	0.69	10		43	0.71	20	
	11	0.39	10		38	0.64	15	
-90	16	0.41	25	14	22	0.46	15	18
	15	0.38	5		17	0.25	10	
	11	0.36	10		15	0.34	15	

Table D15

CVN Test Data for Consumable A, 2.0 kJ/mm in As Welded Condition, 1G Position, Single V Geometry, T/2 Location

Temperature °C	High Restraint (F11A)				Low Restraint (F10A)			
	Impact Energy (J)	Lateral Expansion (mm)	% Shear	Average Impact Energy (J)	Impact Energy (J)	Lateral Expansion (mm)	% Shear	Average Impact Energy (J)
0	142 134 130	2.1 1.9 2.4	90 85 N.B.	135	139 136 114	2.2 2.0 2.1	100 100 100	130
-20	146 137 130	2.2 2.0 1.9	90 80 80	138	140 132 128	2.1 2.0 1.9	90 85 90	133
-30	141 134 127	2.0 1.9 1.9	80 80 80	134	134 130 130	1.8 2.0 1.8	80 100 60	131
-40	110 99 87	1.6 1.5 1.3	50 40 60	99	127 122 108	1.8 1.7 1.6	80 60 60	119
-50	145 136 34	1.9 1.7 0.79	70 60 30	105	102 100 88 43	1.5 1.4 1.5 0.91	40 50 60 20	83
-60	79 65 60	1.4 1.1 0.99	50 40 40	68	106 81 62	1.5 1.5 1.0	50 40 40	83
-70	127 37 23 20	1.7 0.66 0.51 0.38	50 25 20 10	52	69 54 46	1.0 0.86 0.71	30 20 20	56
-80	94 32 27 12	1.5 0.64 0.64 0.36	40 30 10 10	41	75 62 62 46 20	1.1 0.99 0.97 0.79 0.41	30 30 30 20 20	53
-90	18 15 12	0.46 0.41 0.25	20 10 10	15	81 73 41 36 16	1.2 1.1 0.74 0.76 0.36	30 30 30 25 20	49
-100	9 9 7	0.43 0.25 0.25	10 10 5	8	--	--	--	--

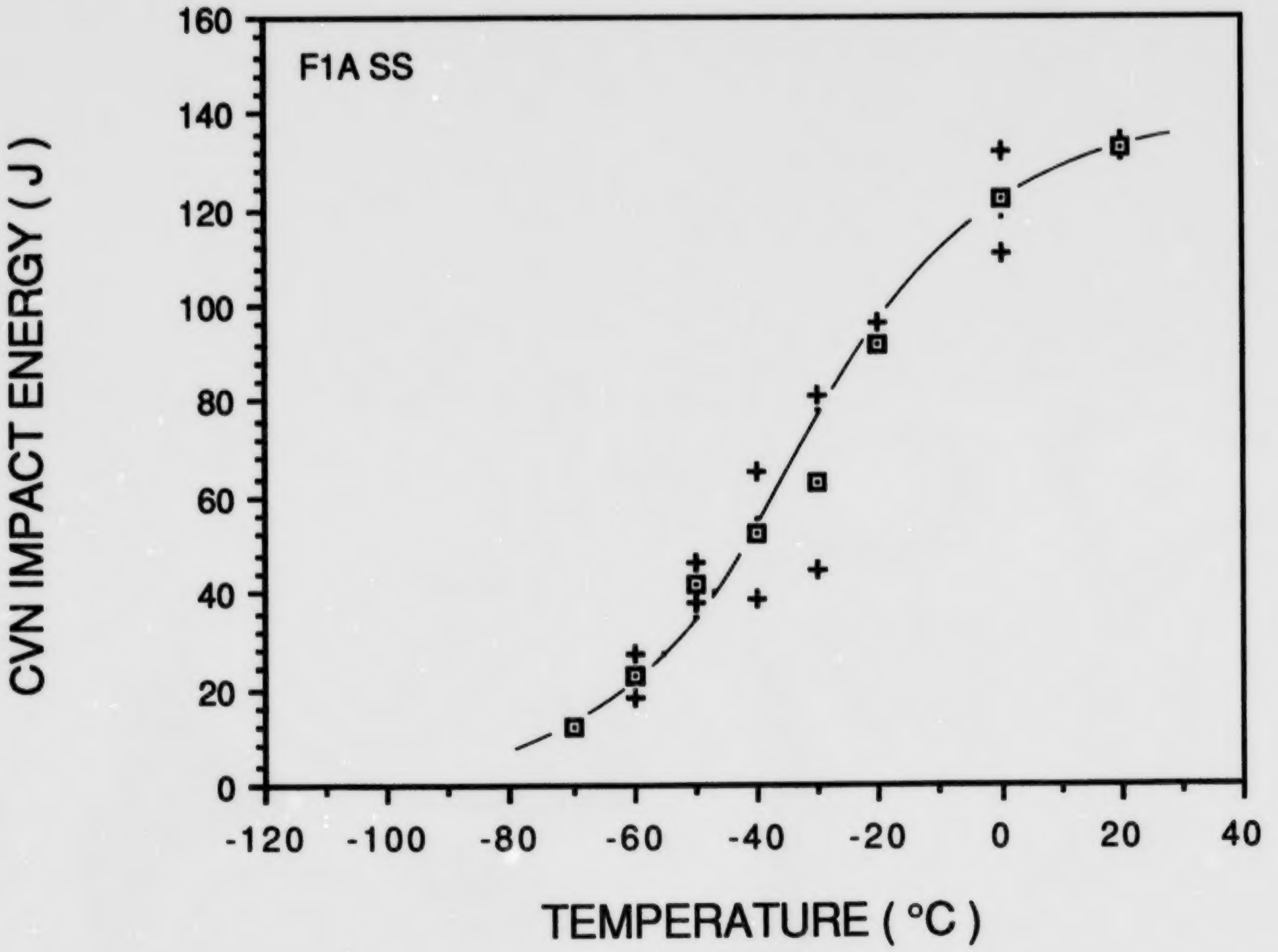

Figure D1: CVN transition for subsurface location of as welded 3.0 kJ/mm weld in 1G position of Consumable A

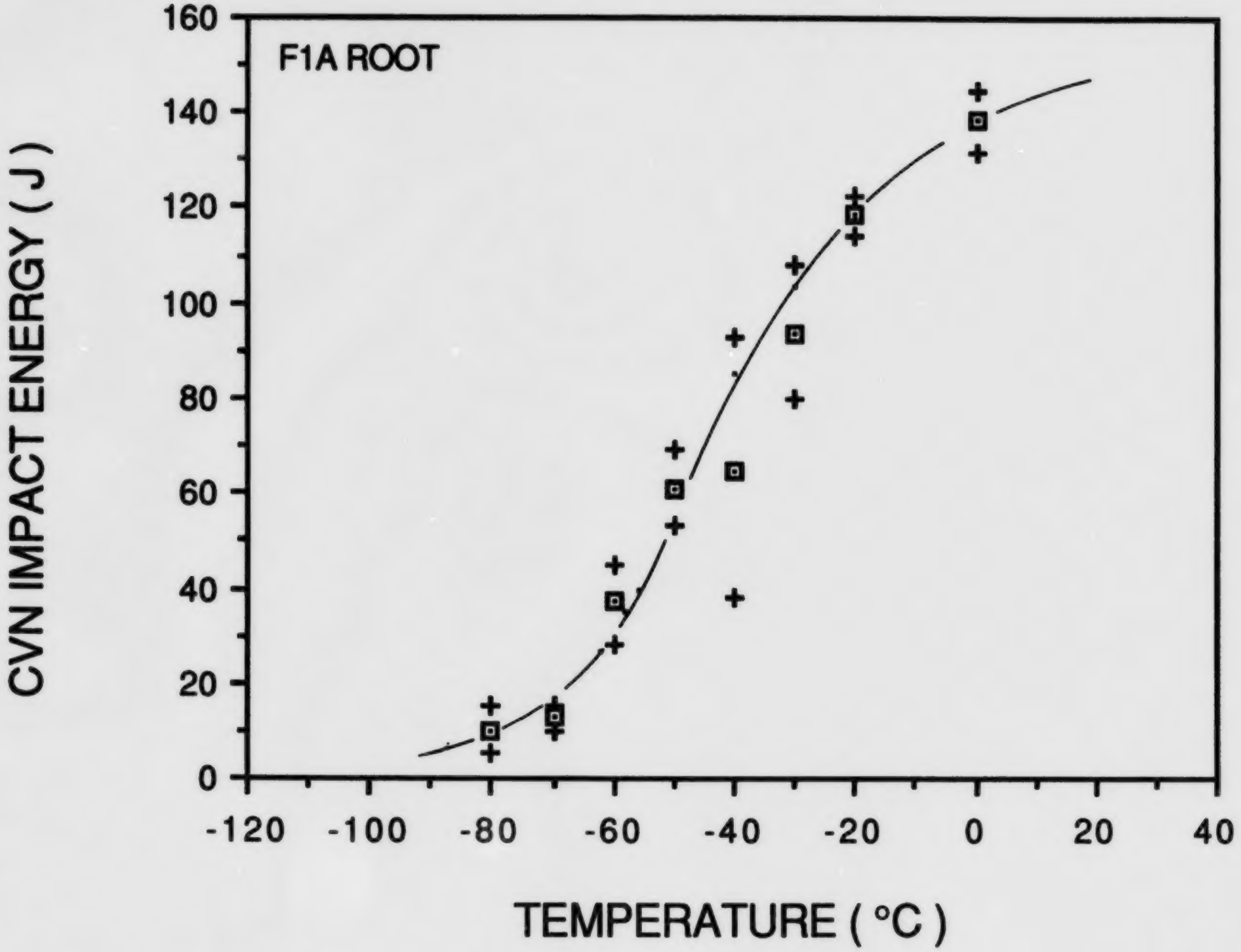

Figure D2: CVN transition curve for root location of as welded 3.0 kJ/mm weld in 1G position of Consumable A

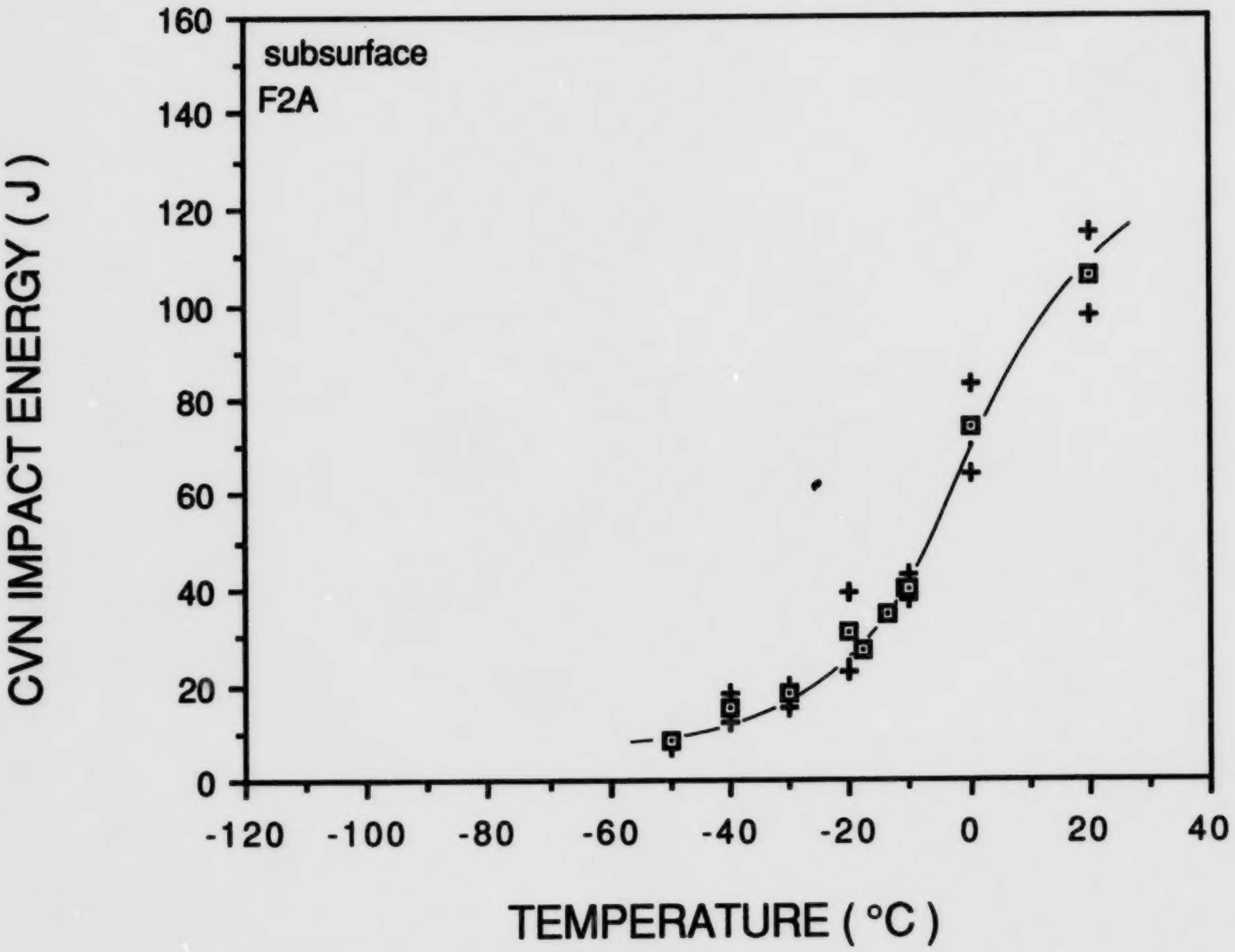

Figure D3: CVN transition curve for subsurface location of stress relieved 3.0 kJ/mm weld in 1G position of Consumable B

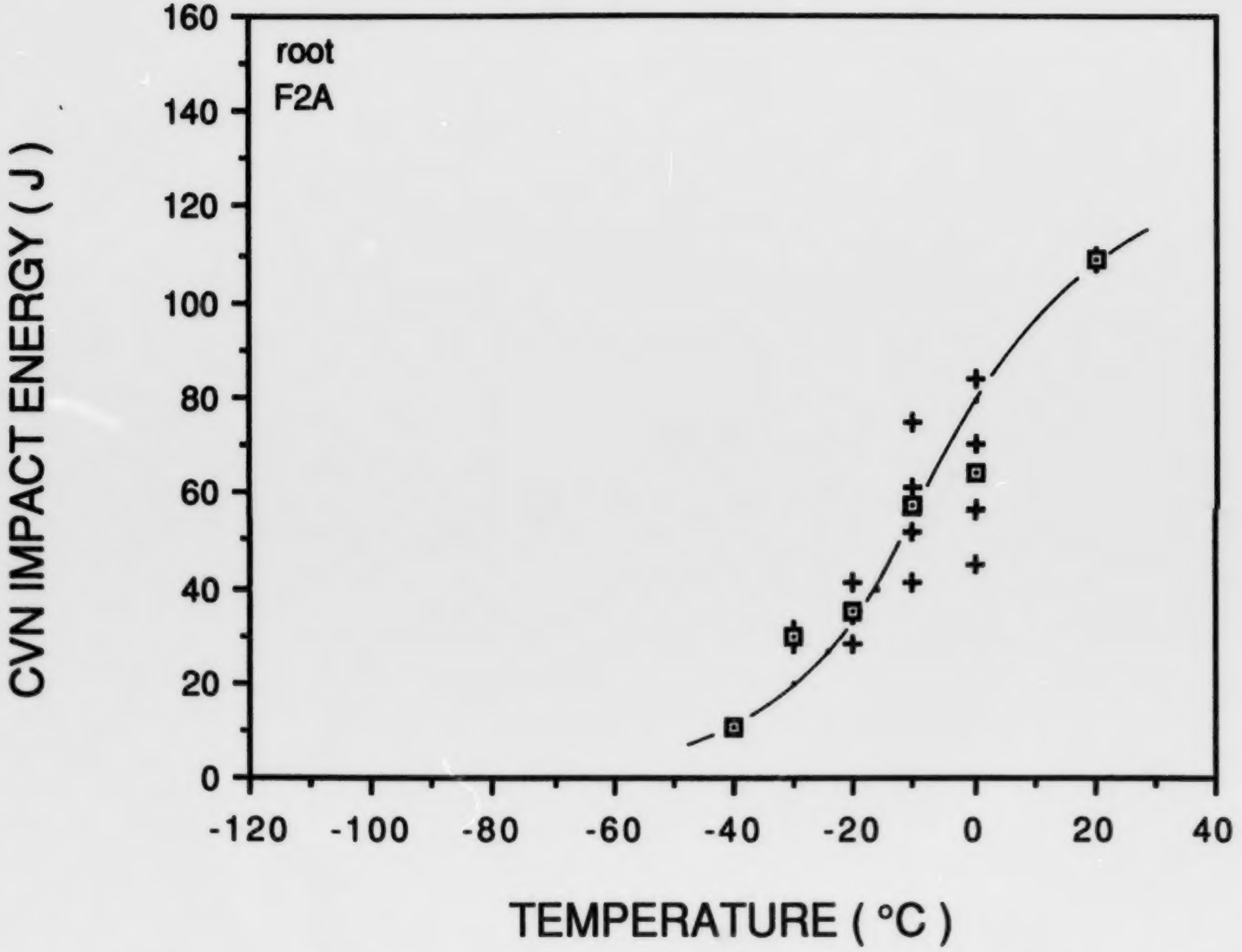

Figure D4: CVN transition curve for root location of stress relieved 3.0 kJ/mm weld in 1G position of Consumable B

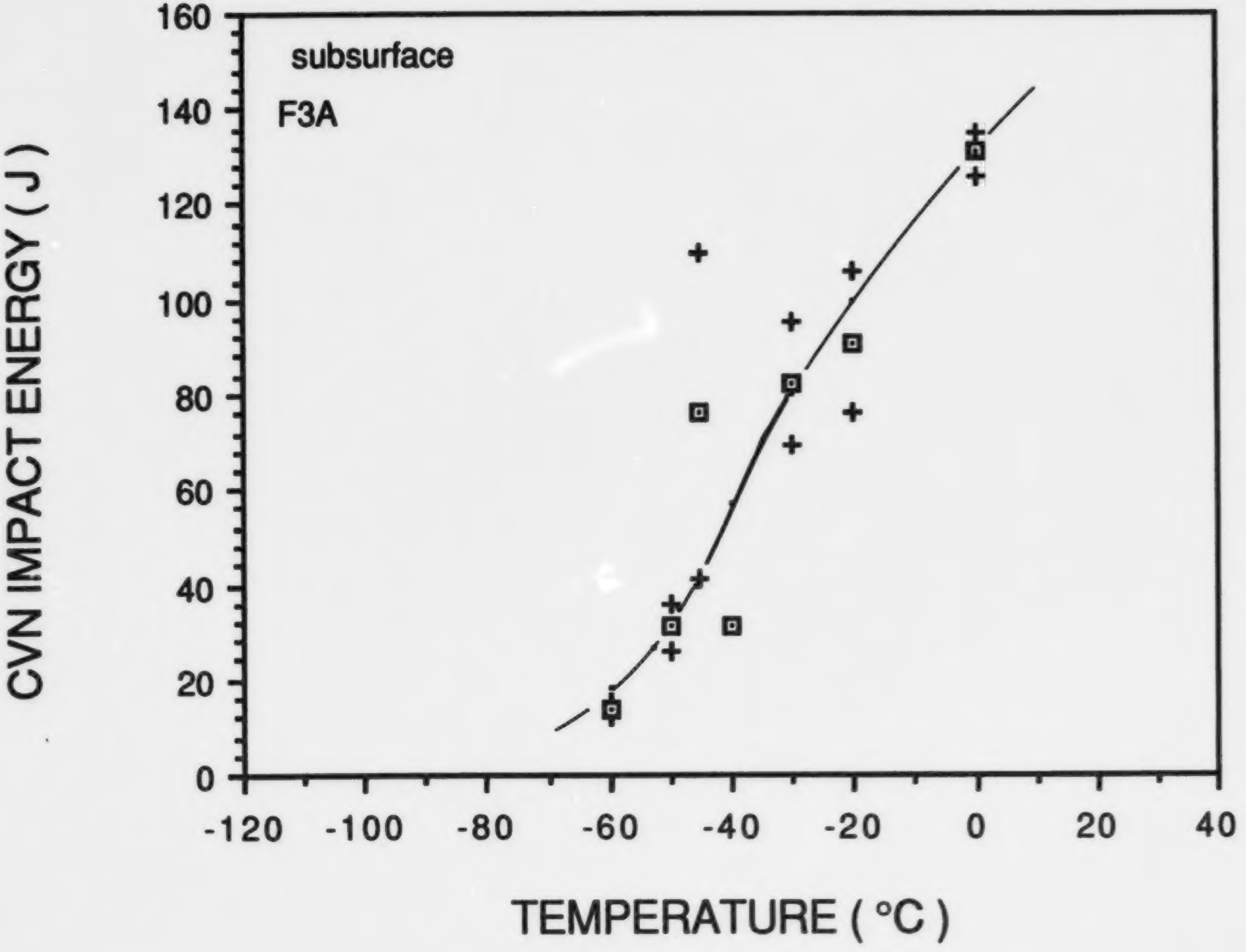

Figure D5: CVN transition curve for subsurface location of as welded 3.0 kJ/mm weld in 1G position of Consumable C

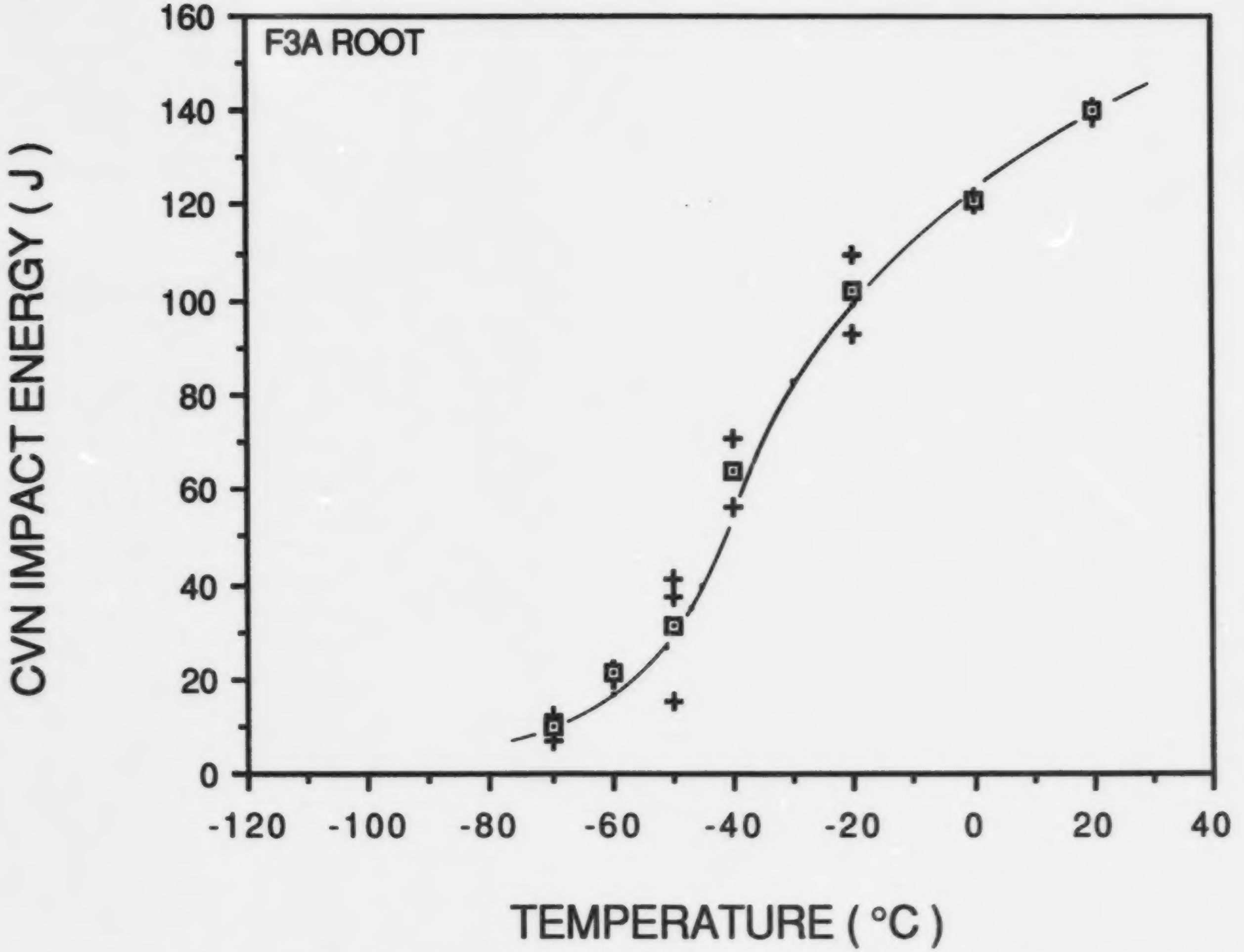

Figure D6: CVN transition curve for root location of as welded 3.0 kJ/mm weld in 1G position of Consumable C

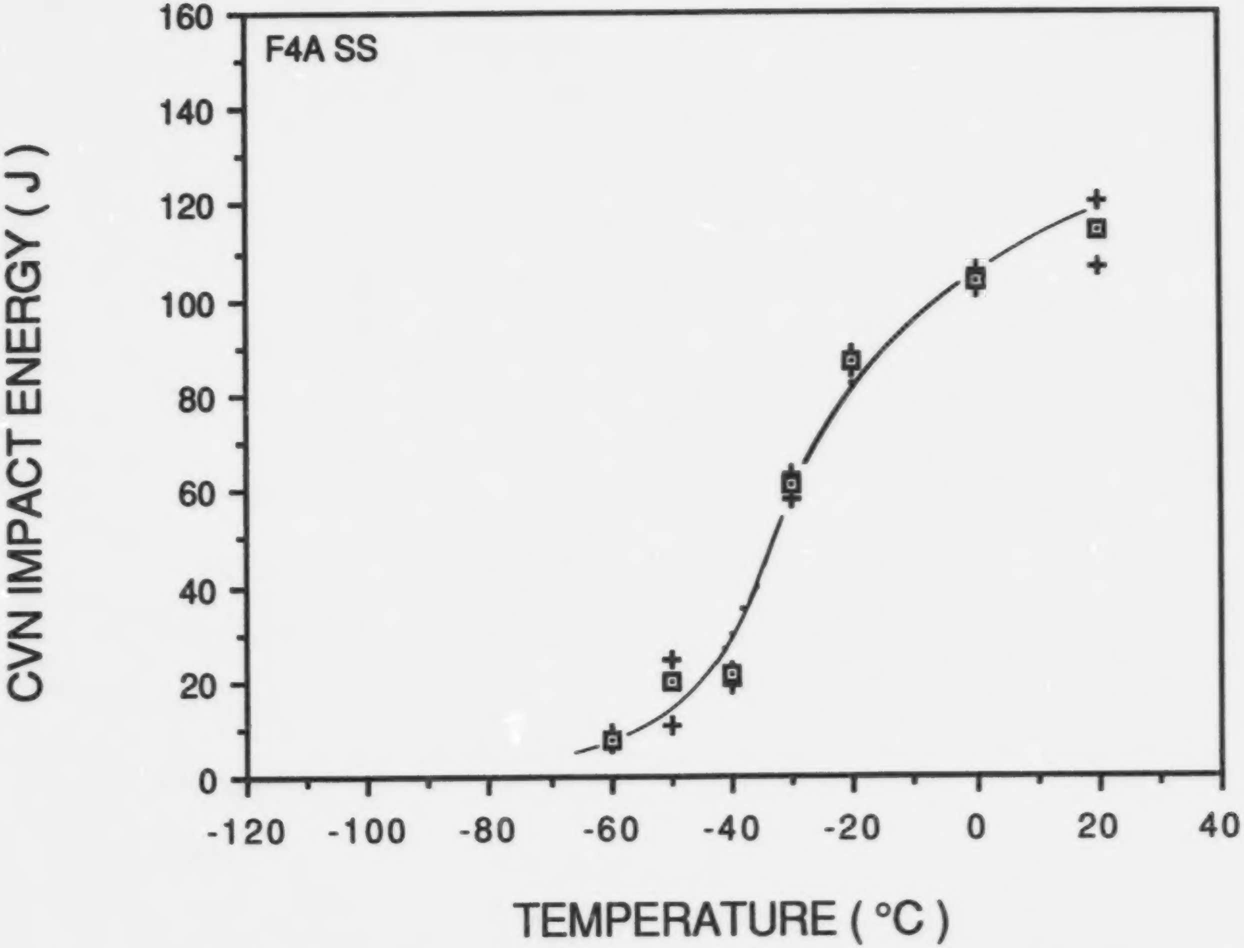

Figure D7: CVN transition curve for subsurface location of stress relieved 3.0 kJ/mm weld in 1G position of Consumable C

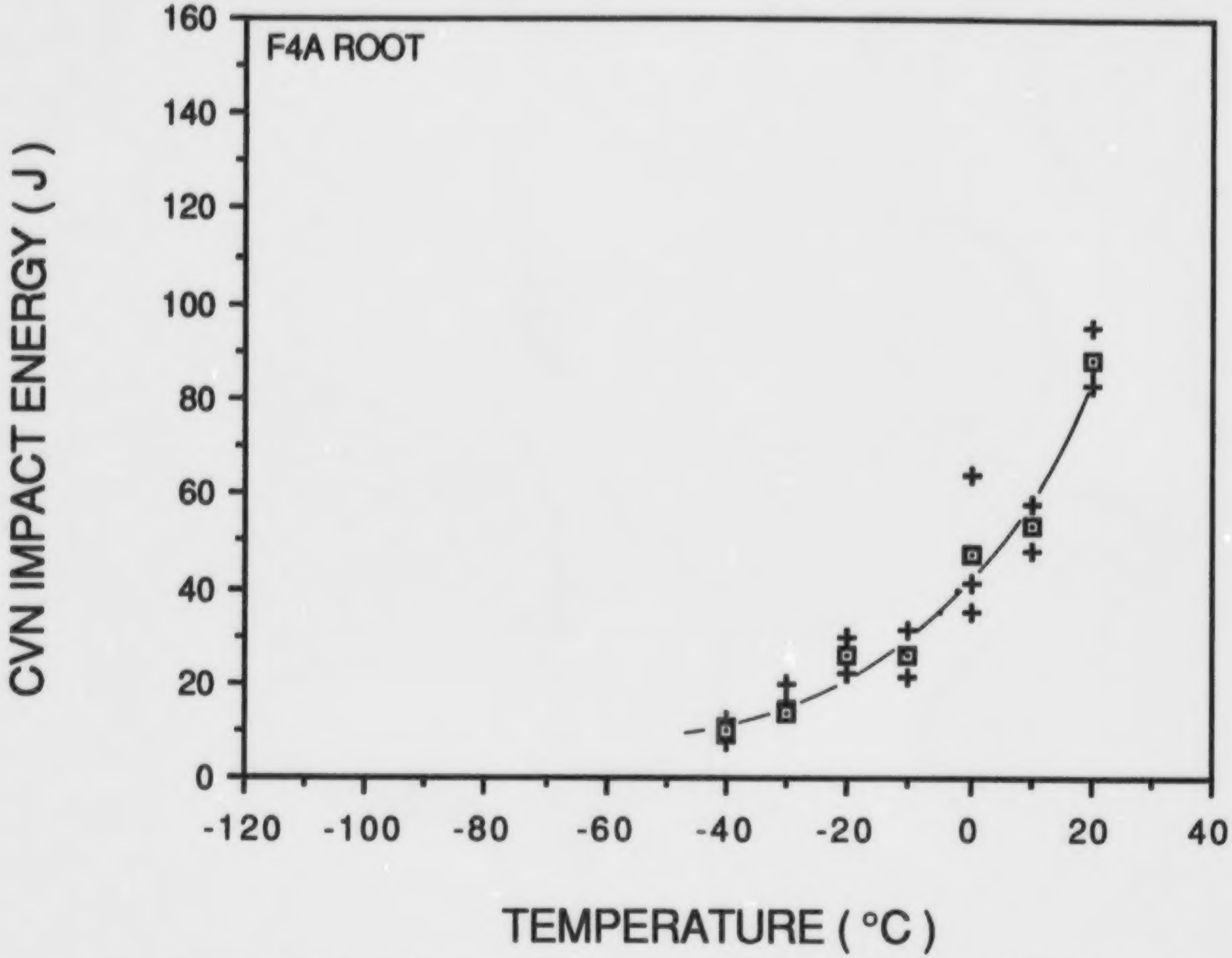

Figure D8: CVN transition curve for root location of stress relieved 3.0 kJ/mm weld in 1G position of Consumable C

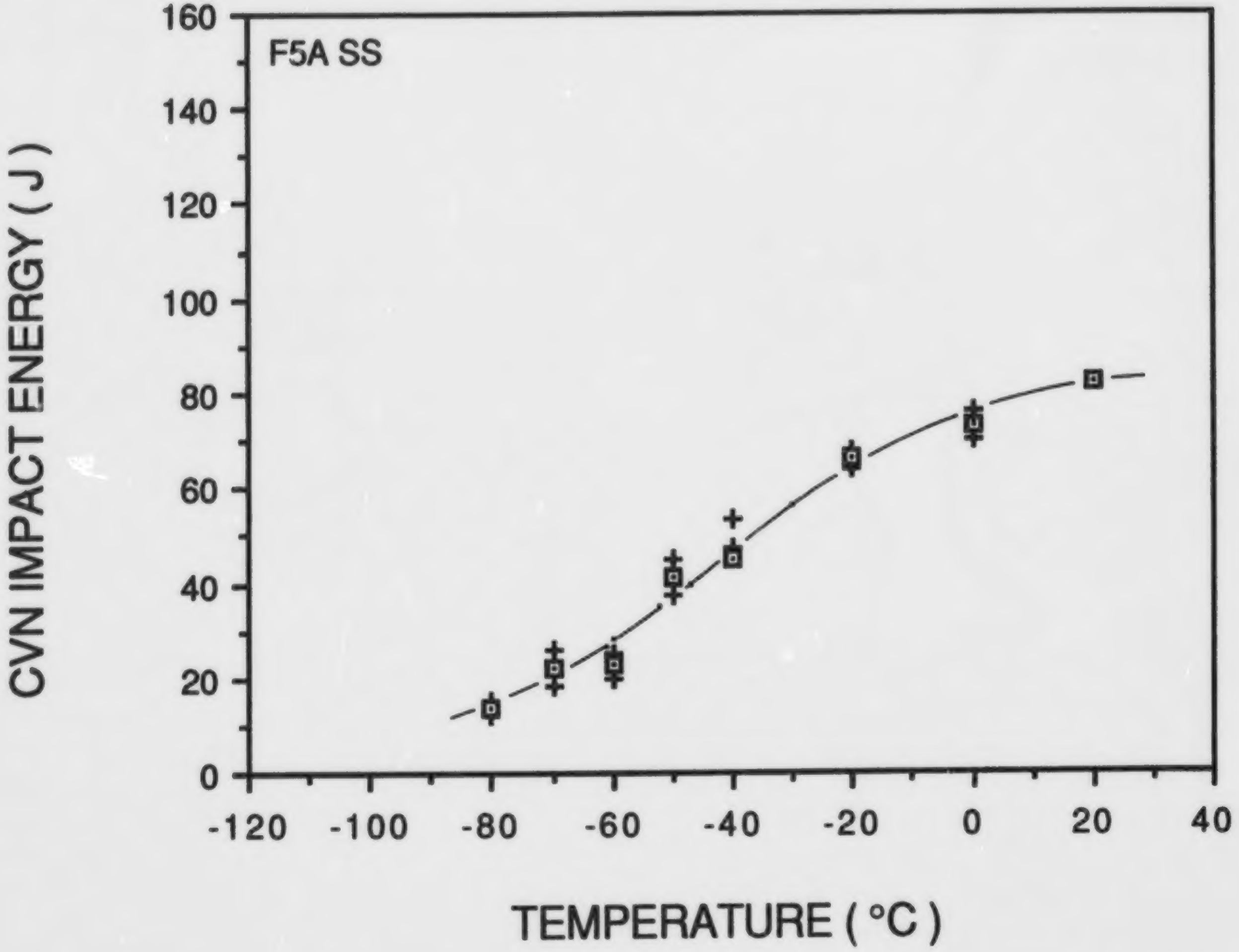

Figure D9: CVN transition curve for subsurface location of as welded 2.0 kJ/mm weld in 1G position of Consumable A

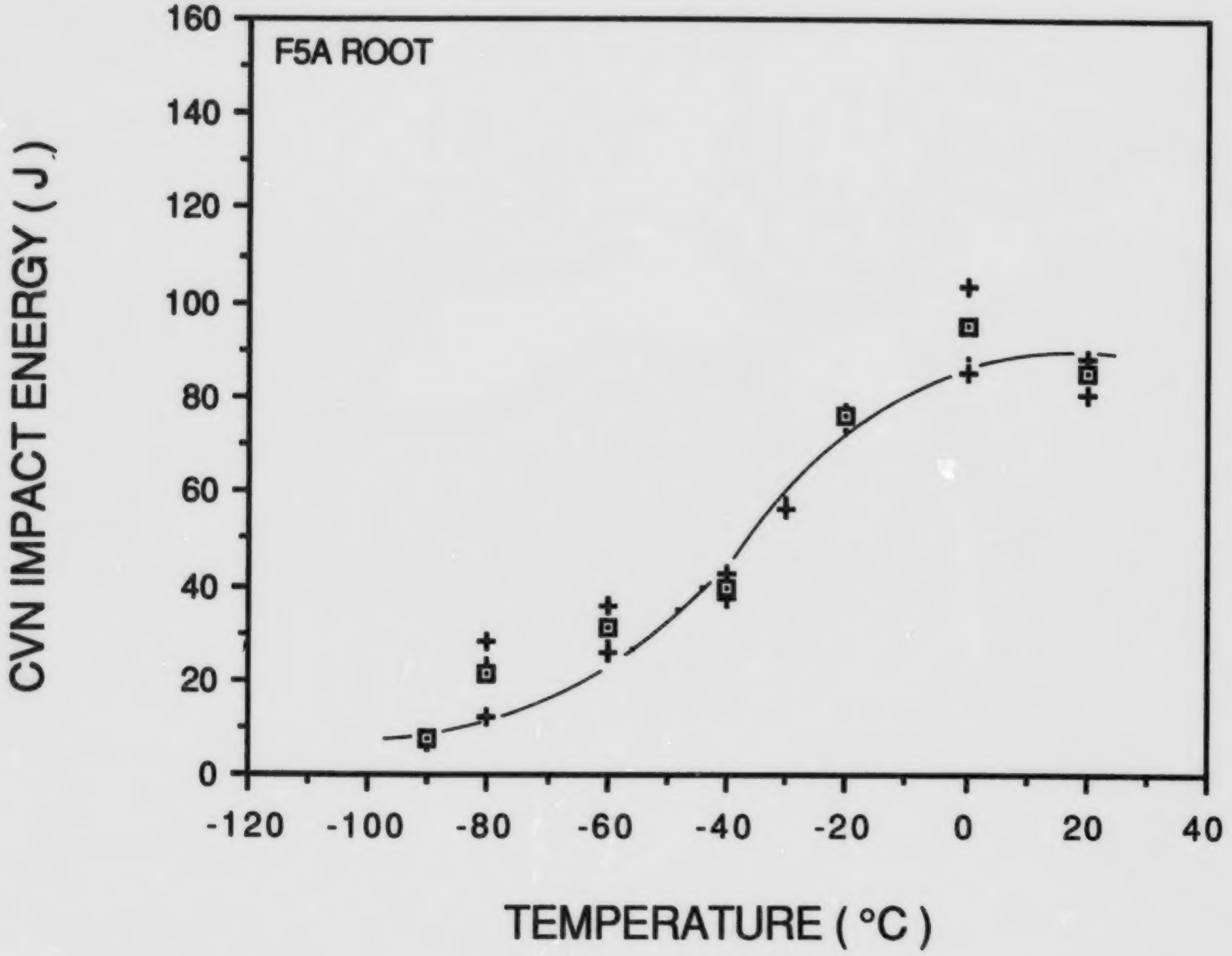

Figure D10: CVN transition curve for root location of as welded 2.0 kJ/mm weld in 1G position of Consumable A

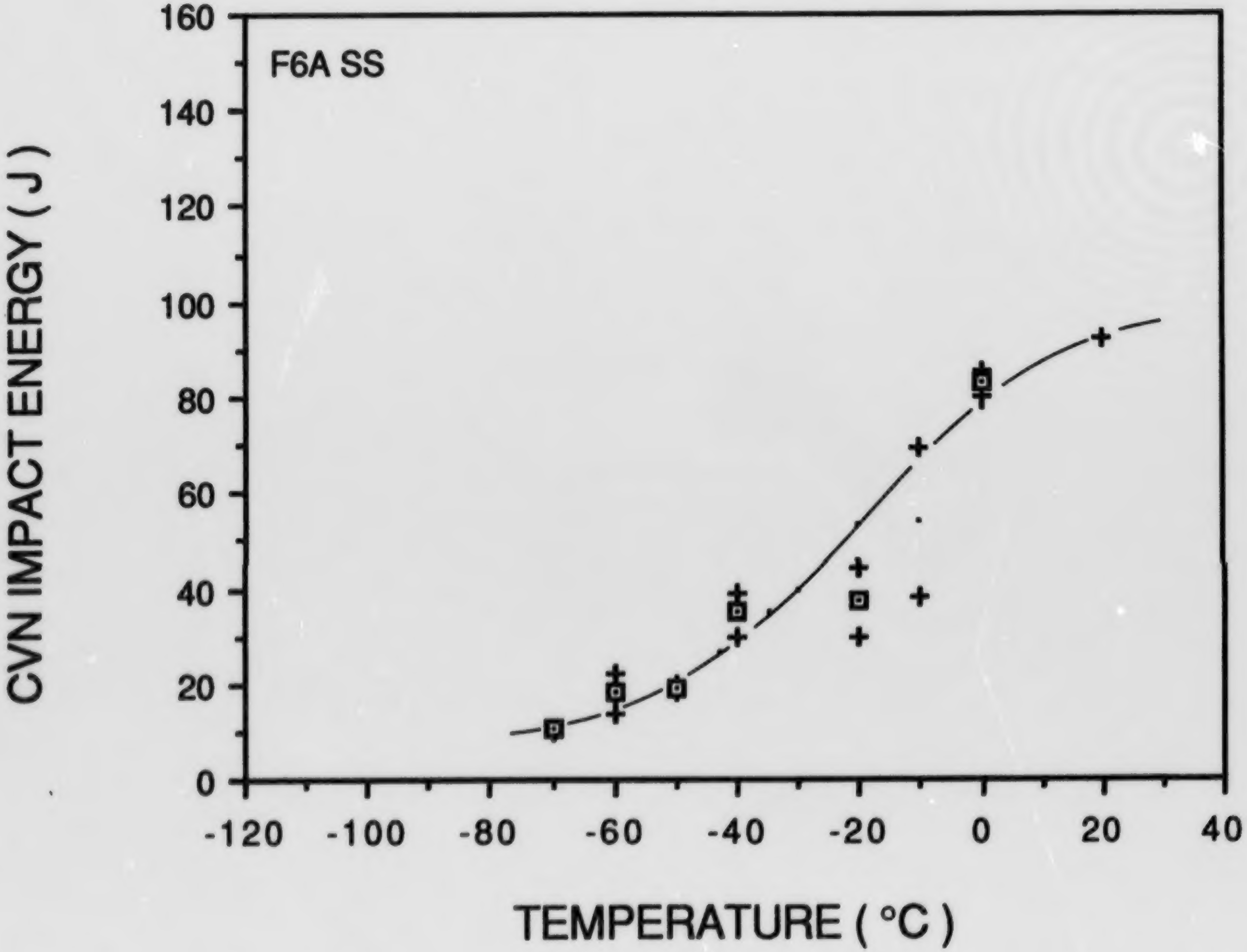

Figure D11: CVN transition curve for subsurface location of stress relieved 2.0 kJ/mm weld in 1G position of Consumable B

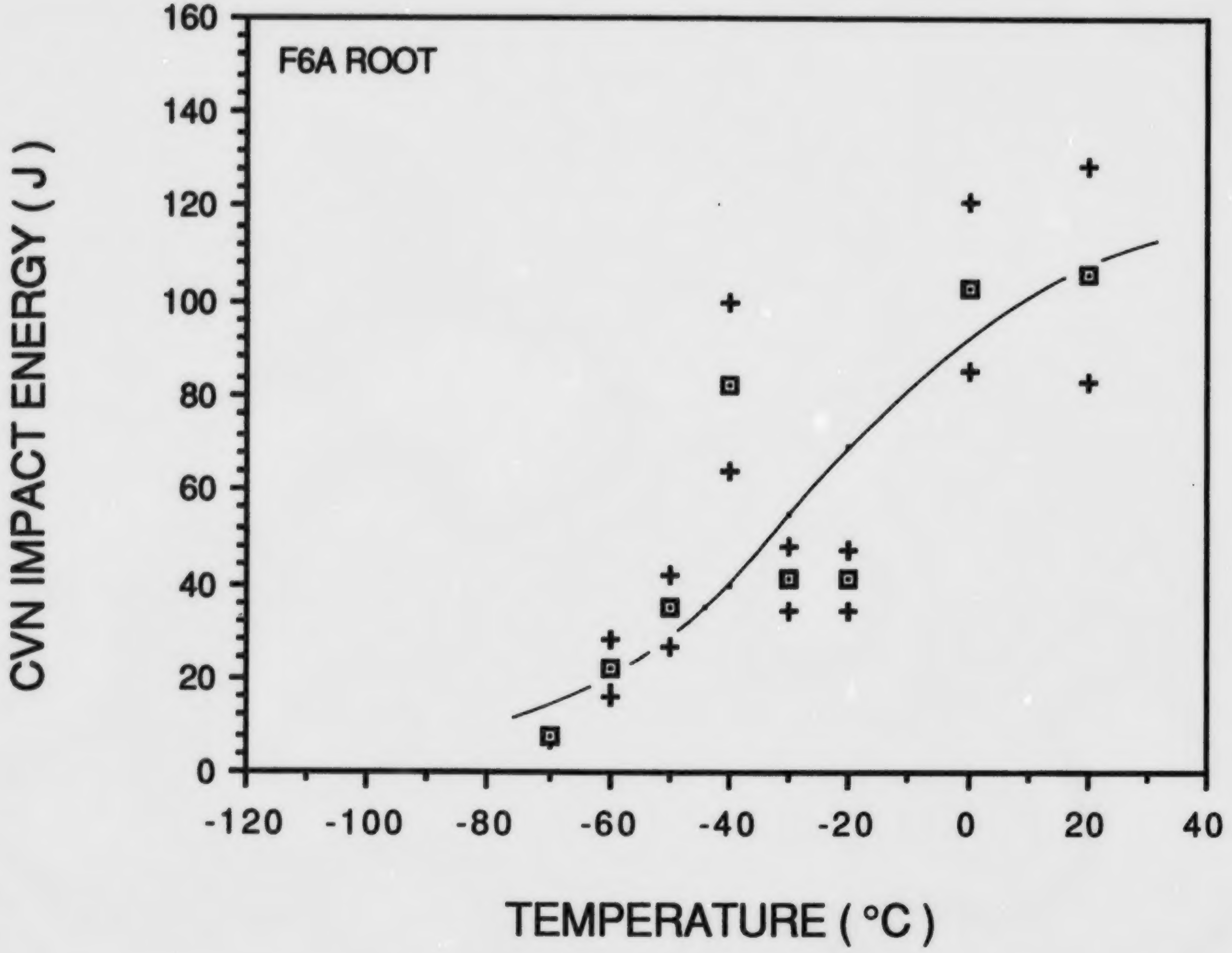

Figure D12: CVN transition curve for root location of stress relieved 2.0 kJ/mm weld in 1G position of Consumable B

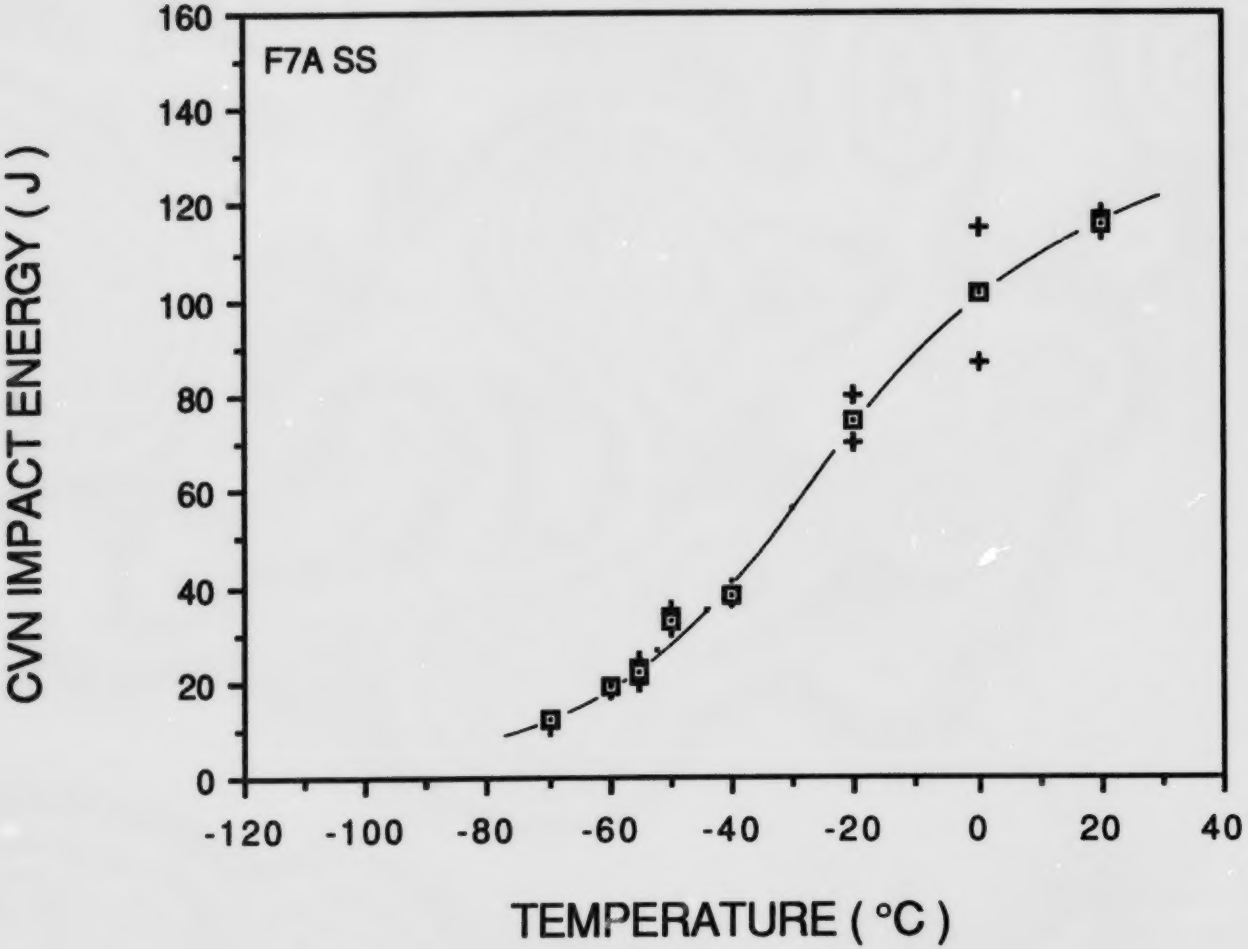

Figure D13: CVN transition curve for subsurface location of stress relieved 2.0 kJ/mm weld in 3G position of Consumable B

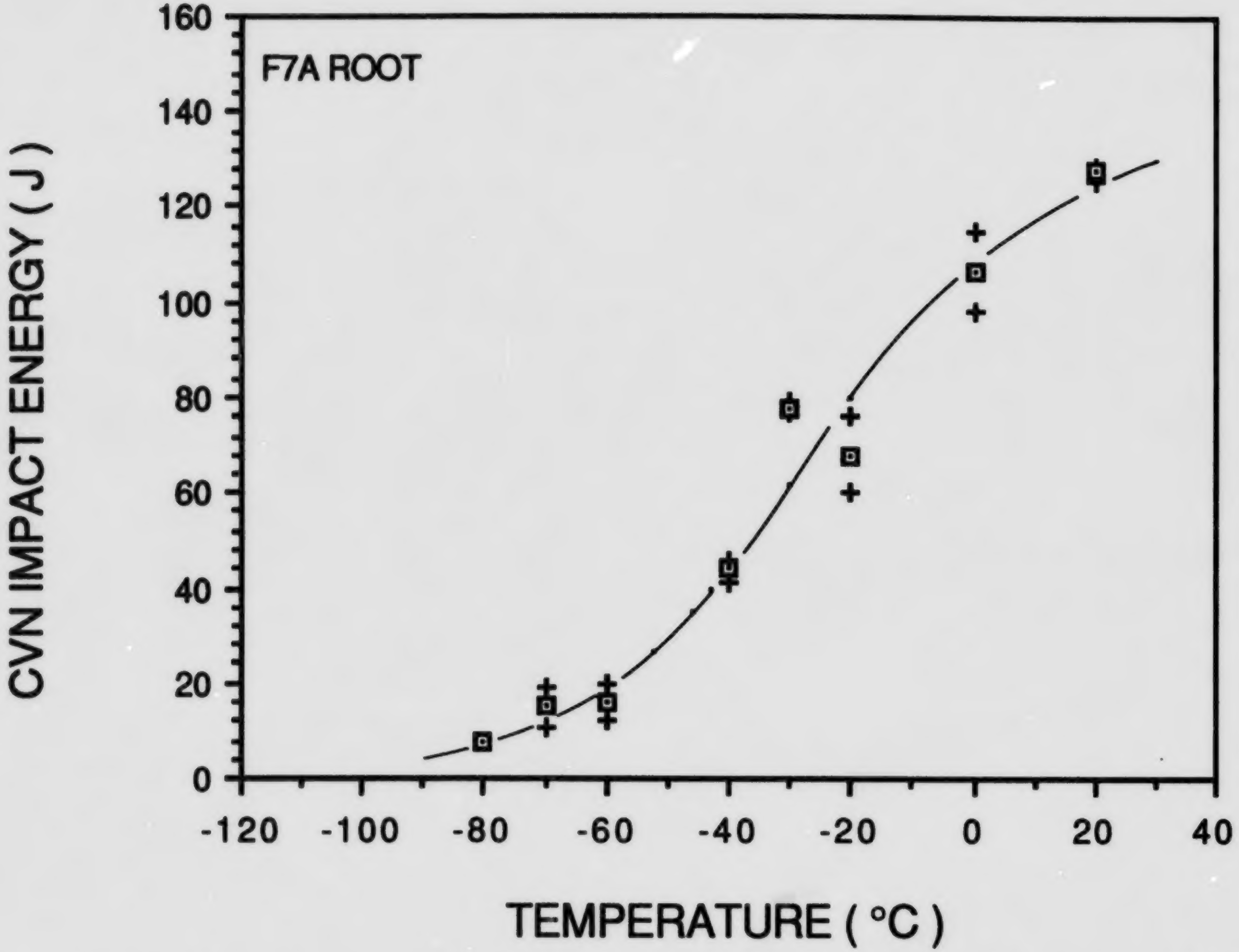

Figure D14: CVN transition curve for root location of stress relieved 2.0 kJ/mm weld in 3G position of Consumable B

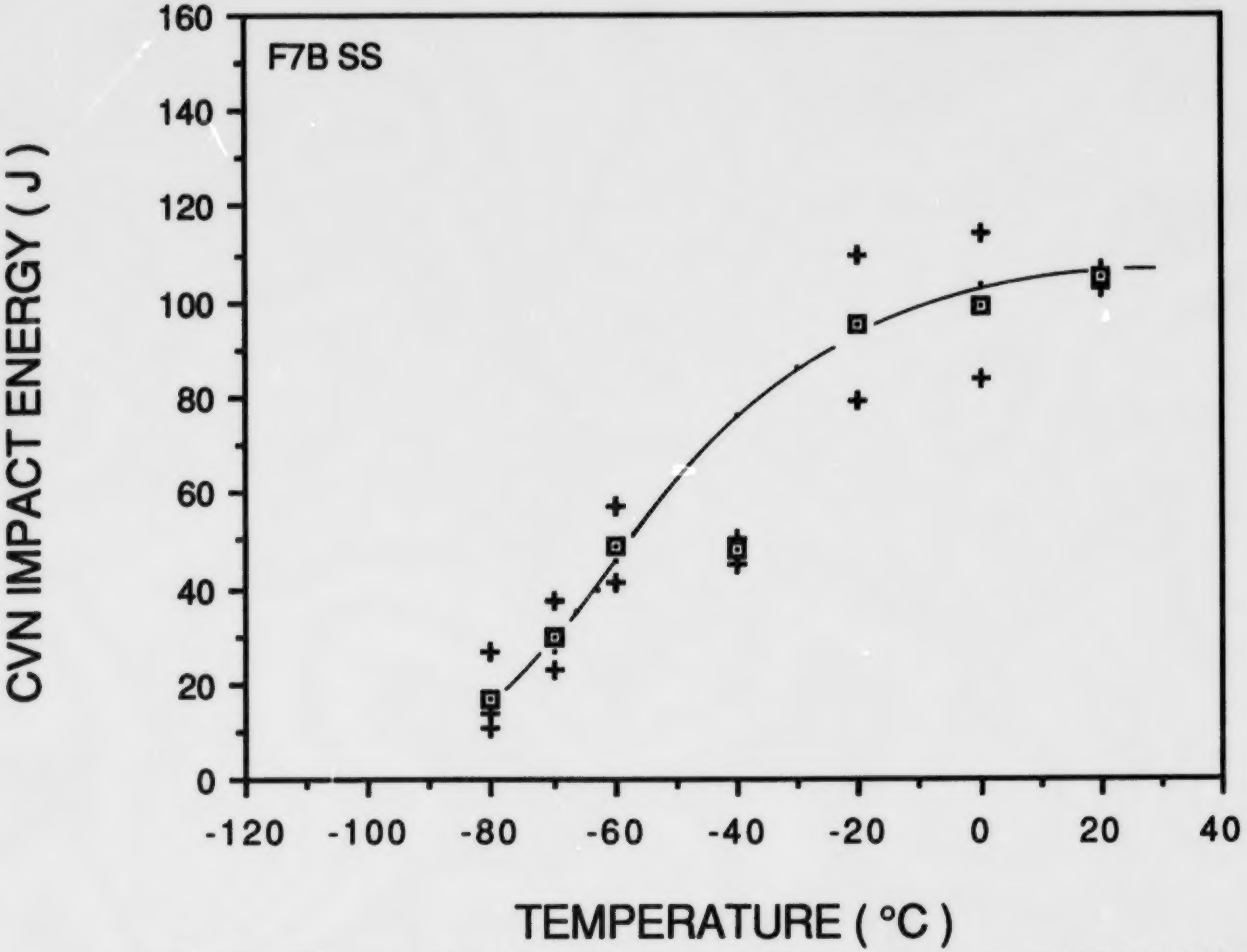

Figure D15: CVN transition curve for subsurface location of as welded 2.0 kJ/mm weld in 3G position of Consumable B

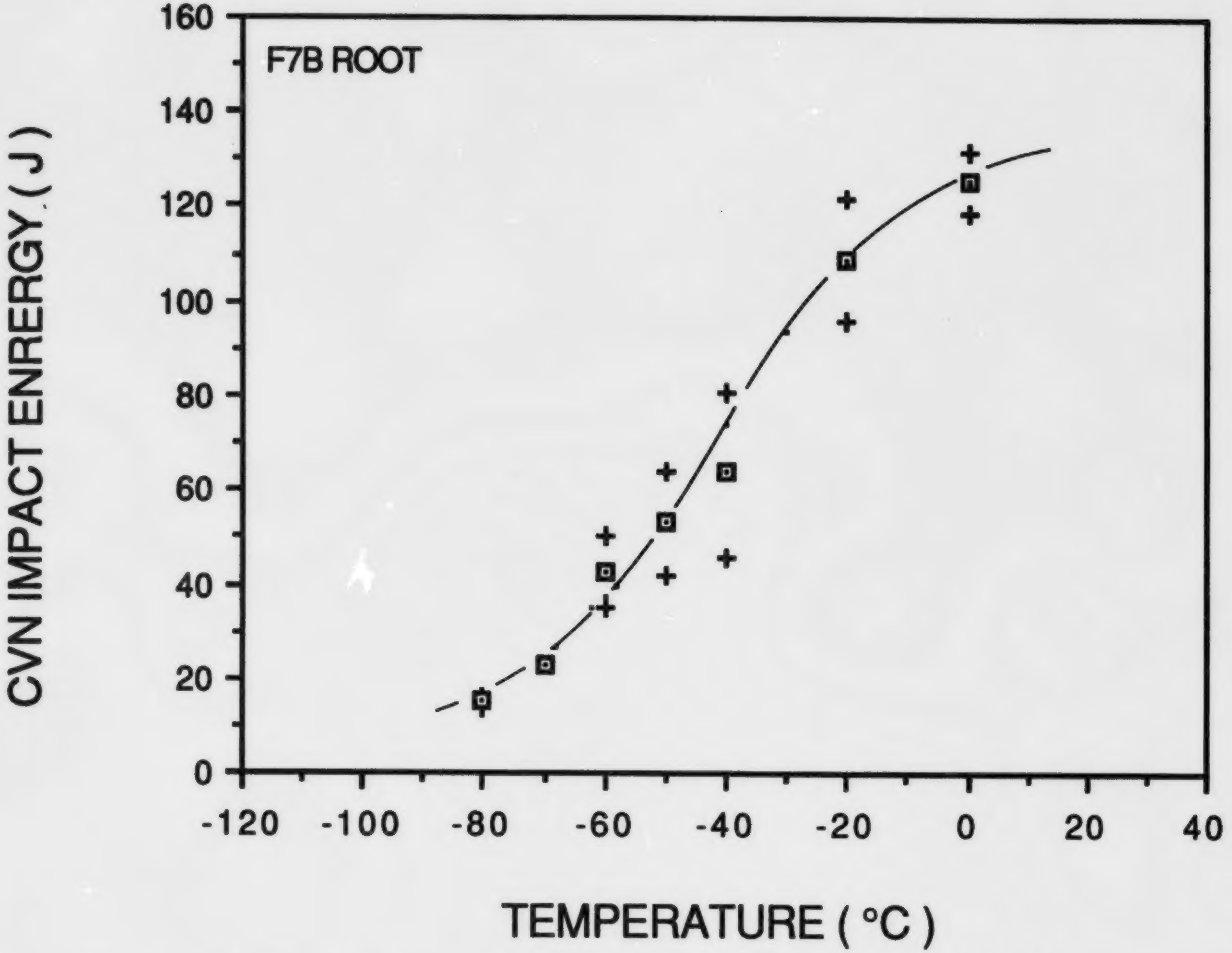

Figure D16: CVN transition curve for root location of as welded 2.0 kJ/mm weld in 3G position of Consumable B

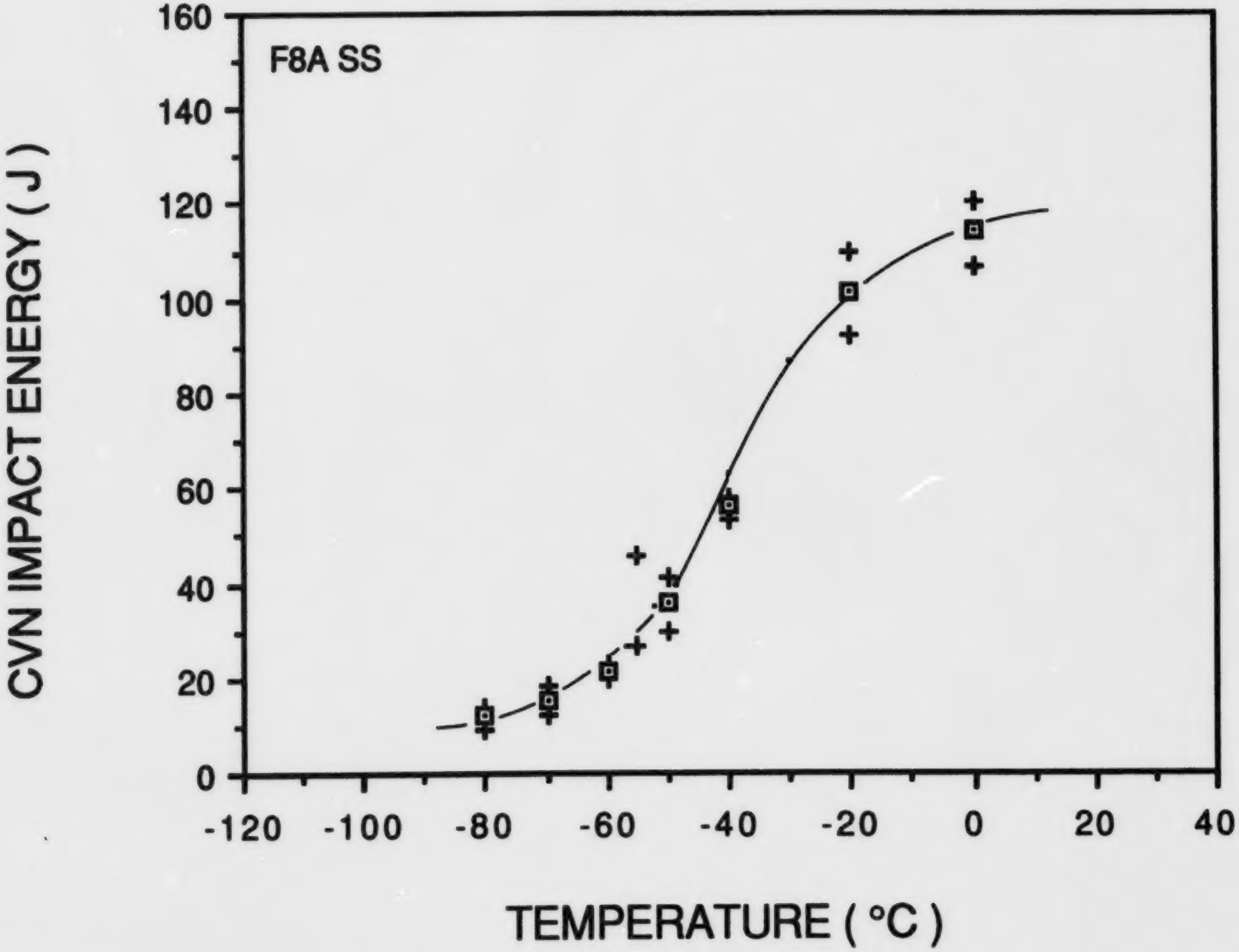

Figure D17: CVN transition curve for subsurface location of stress relieved 2.0 kJ/mm weld in 3G position of Consumable C

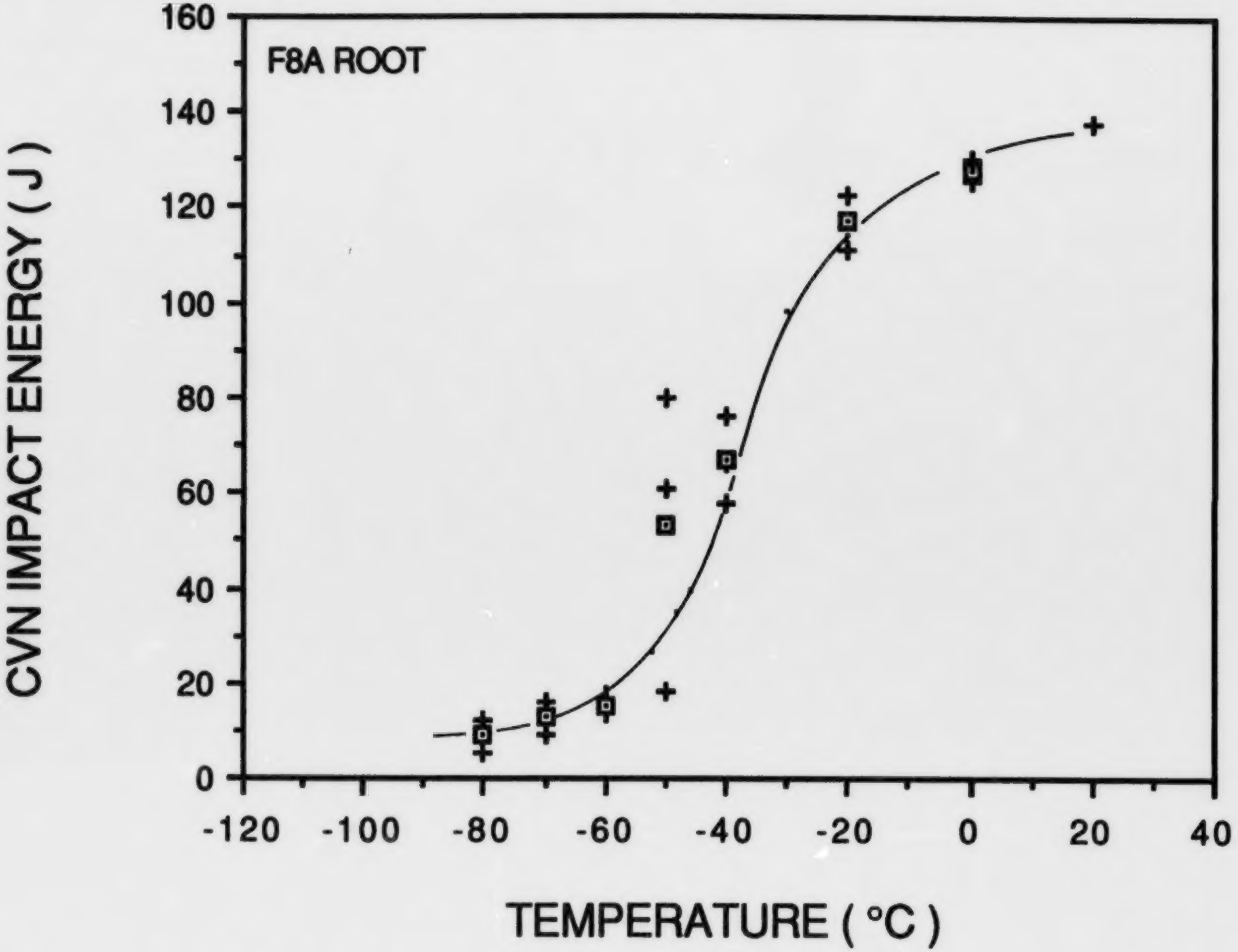

Figure D18: CVN transition curve for root location of stress relieved 2.0 kJ/mm weld in 3G position of Consumable C

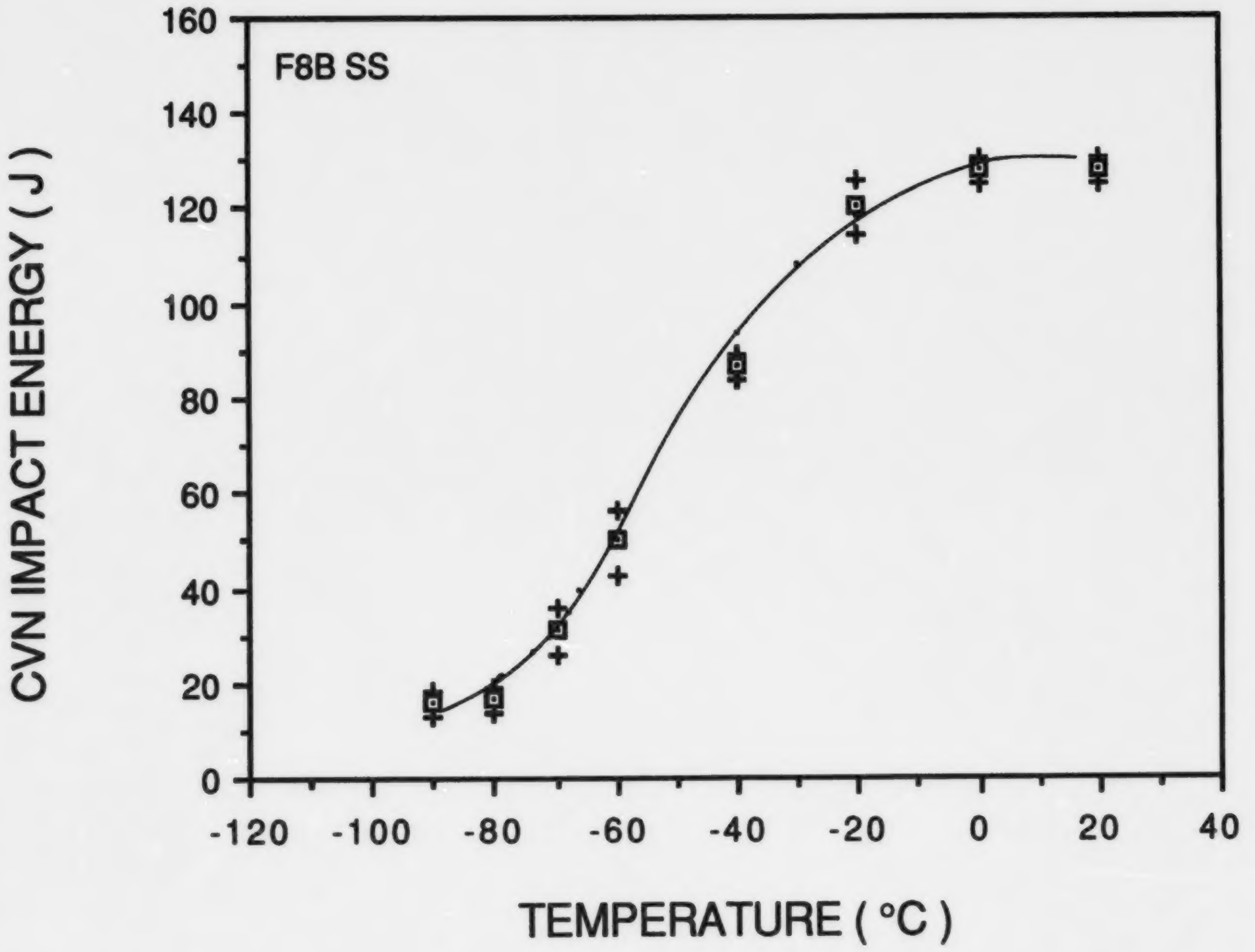

Figure D19: CVN transition curve for subsurface location of as welded 2.0 kJ/mm weld in 3G position of Consumable C

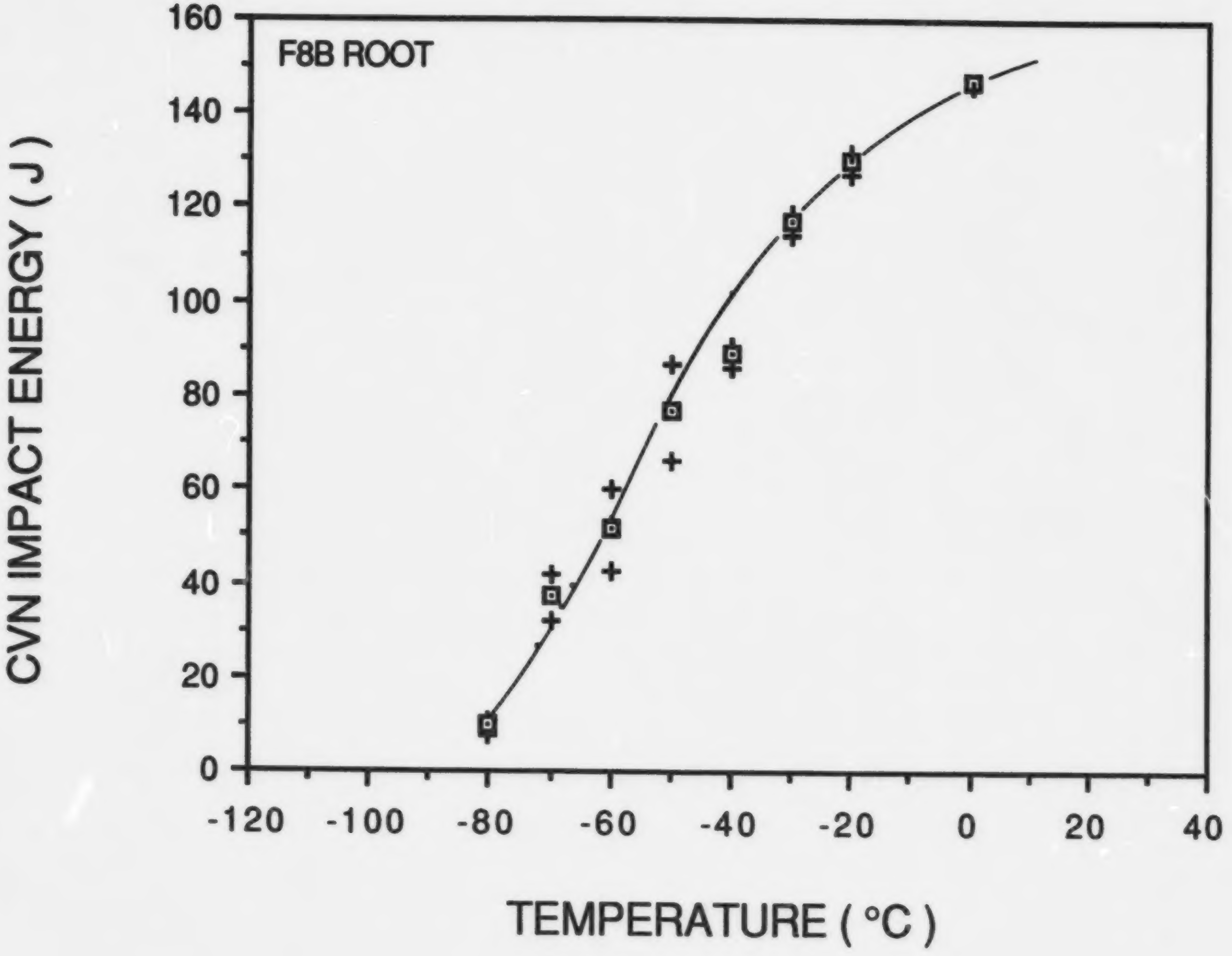

Figure D20: CVN transition curve for root location of as welded 2.0 kJ/mm weld in 3G position of Consumable C

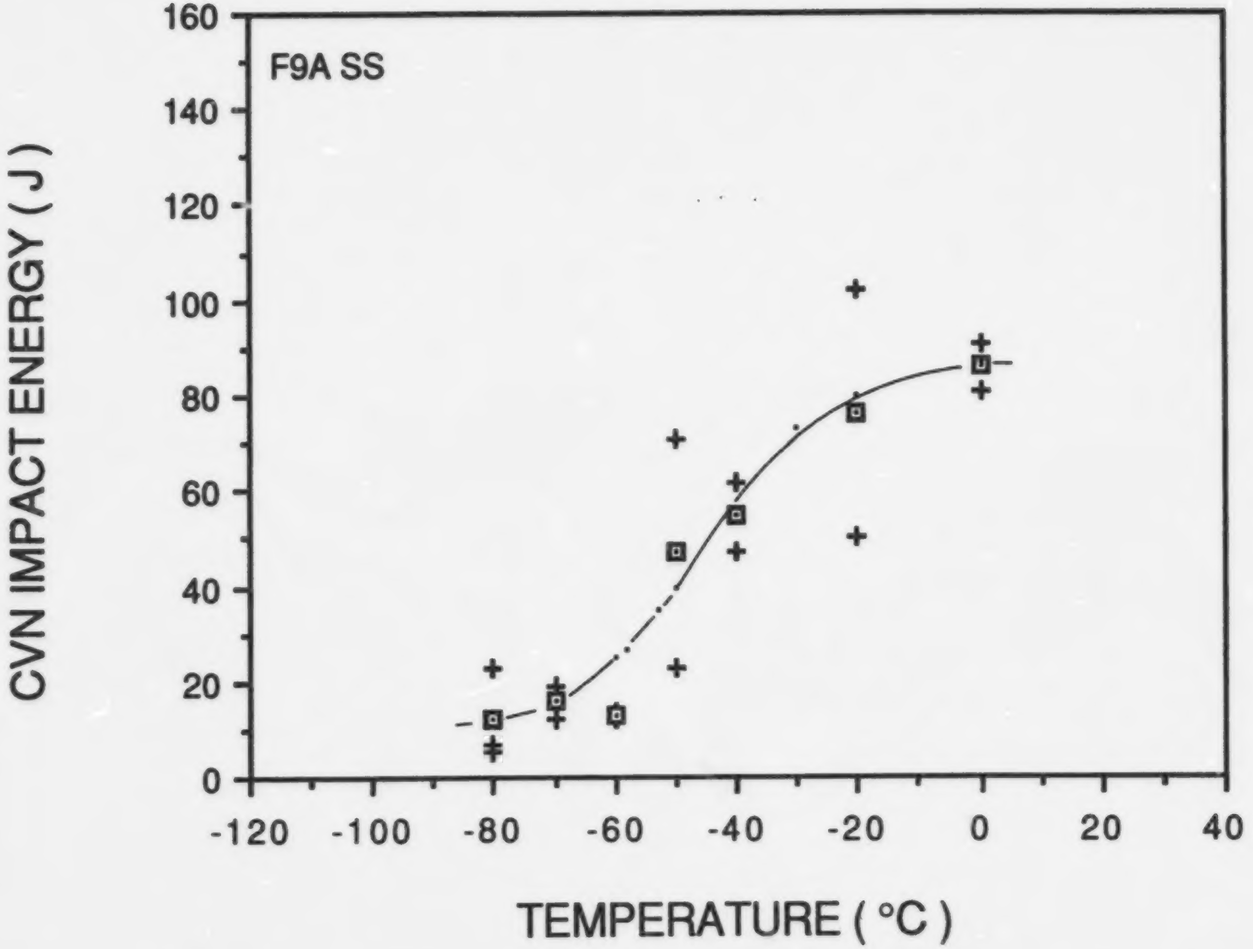

Figure D21: CVN transition curve for subsurface location of stress relieved 2.0 kJ/mm weld in 1G position of Consumable C

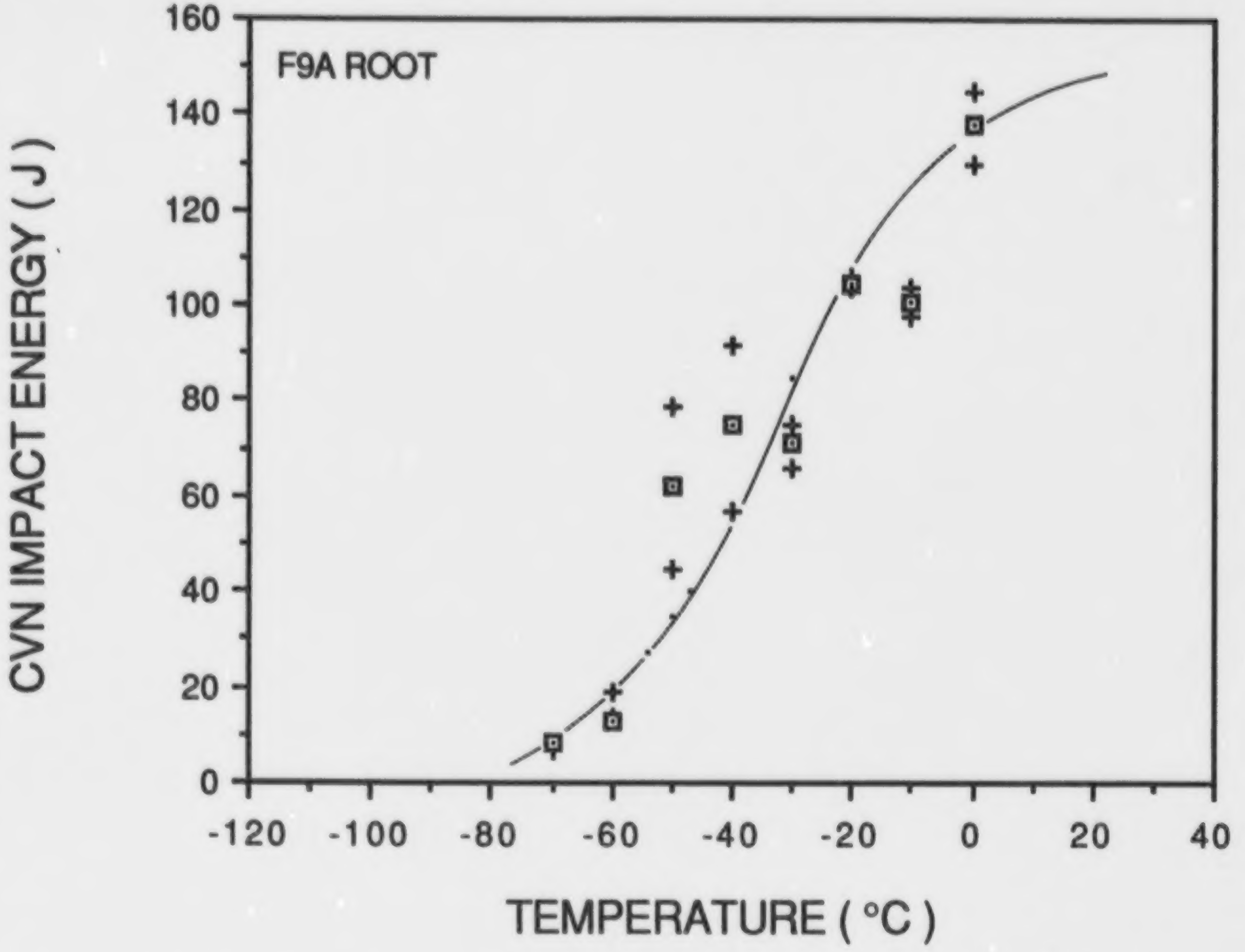

Figure D22: CVN transition curve for root location of stress relieved 2.0 kJ/mm weld in 1G position of Consumable C

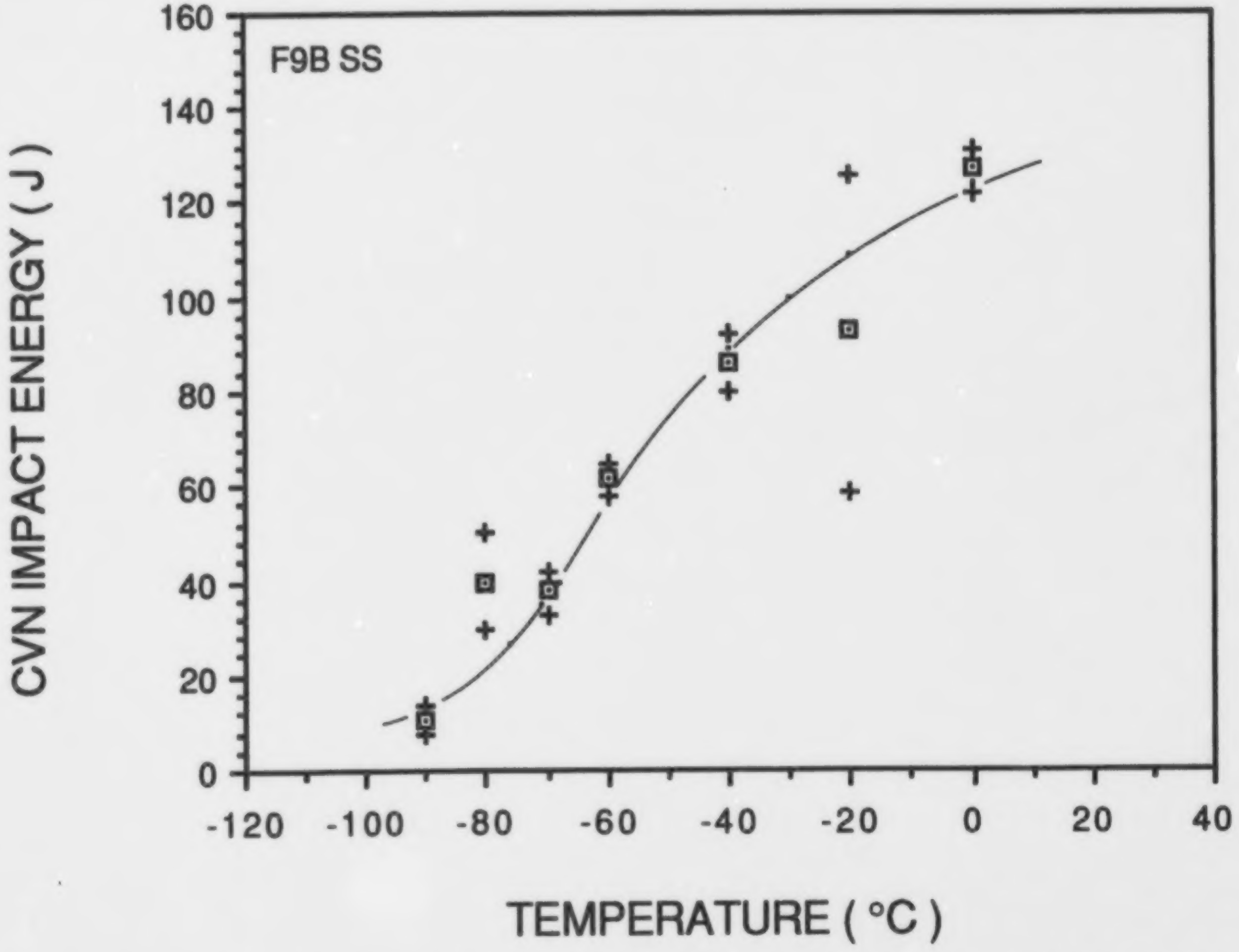

Figure D23: CVN transition curve for subsurface location of as welded 2.0 kJ/mm weld in 1G position of Consumable C

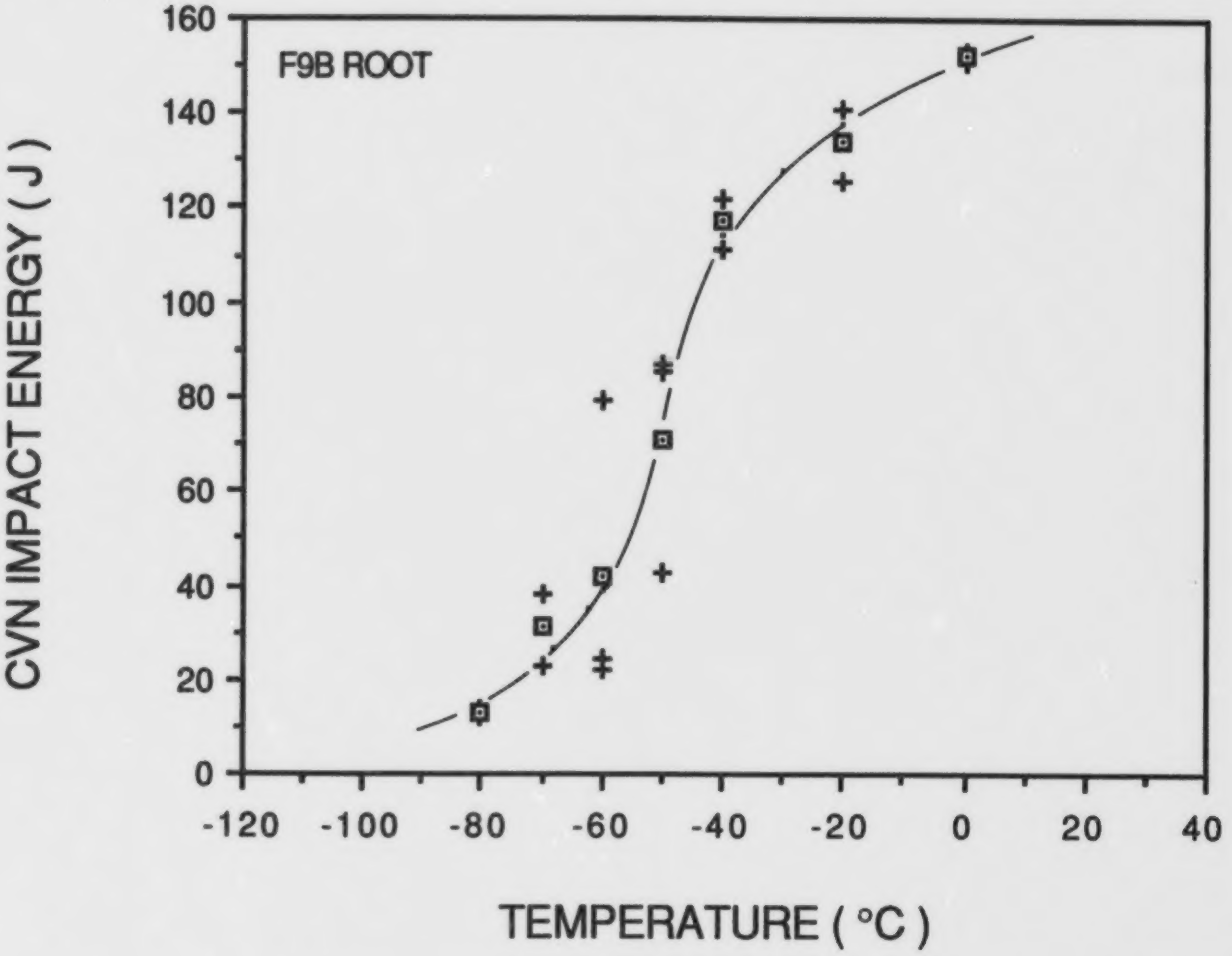

Figure D24: CVN transition curve for root location of as welded 2.0 kJ/mm weld in 1G position of Consumable C

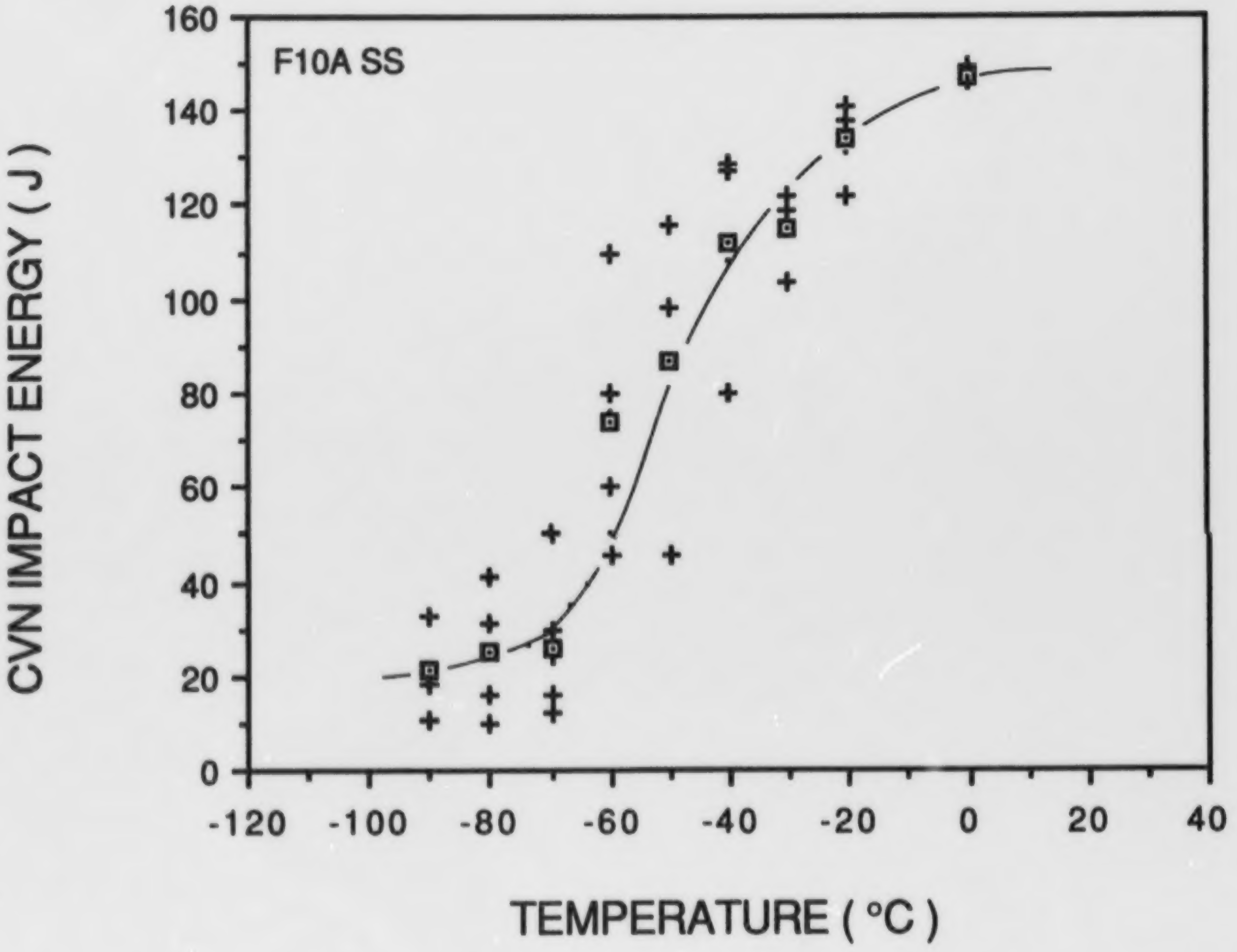

Figure D25: CVN transition curve for subsurface location of low restraint single V weld (as welded 2.0 kJ/mm of Consumable A)

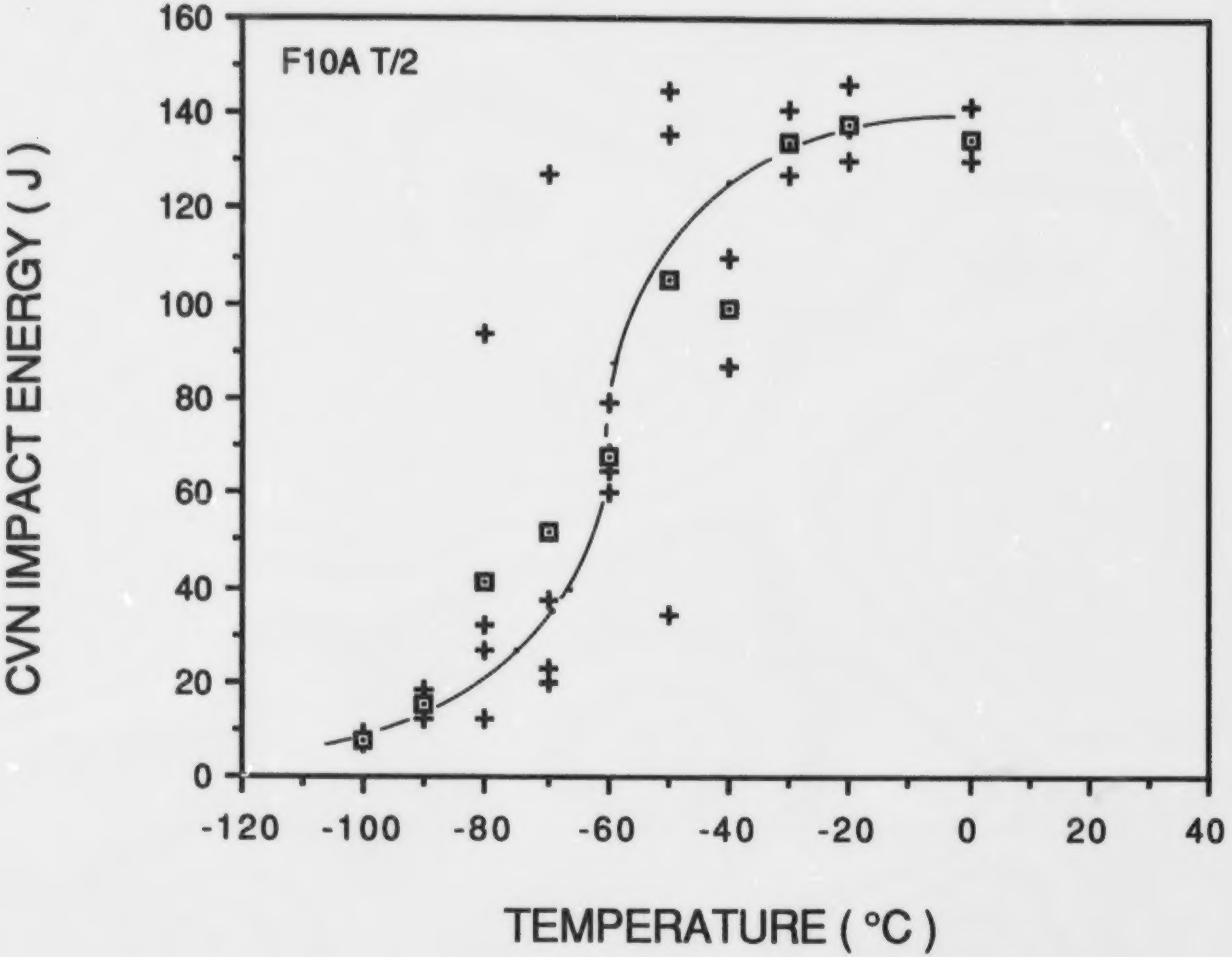

Figure D26: CVN transition curve for T/2 location of low restraint single V weld (as welded 2.0 kJ/mm weld of Consumable A)

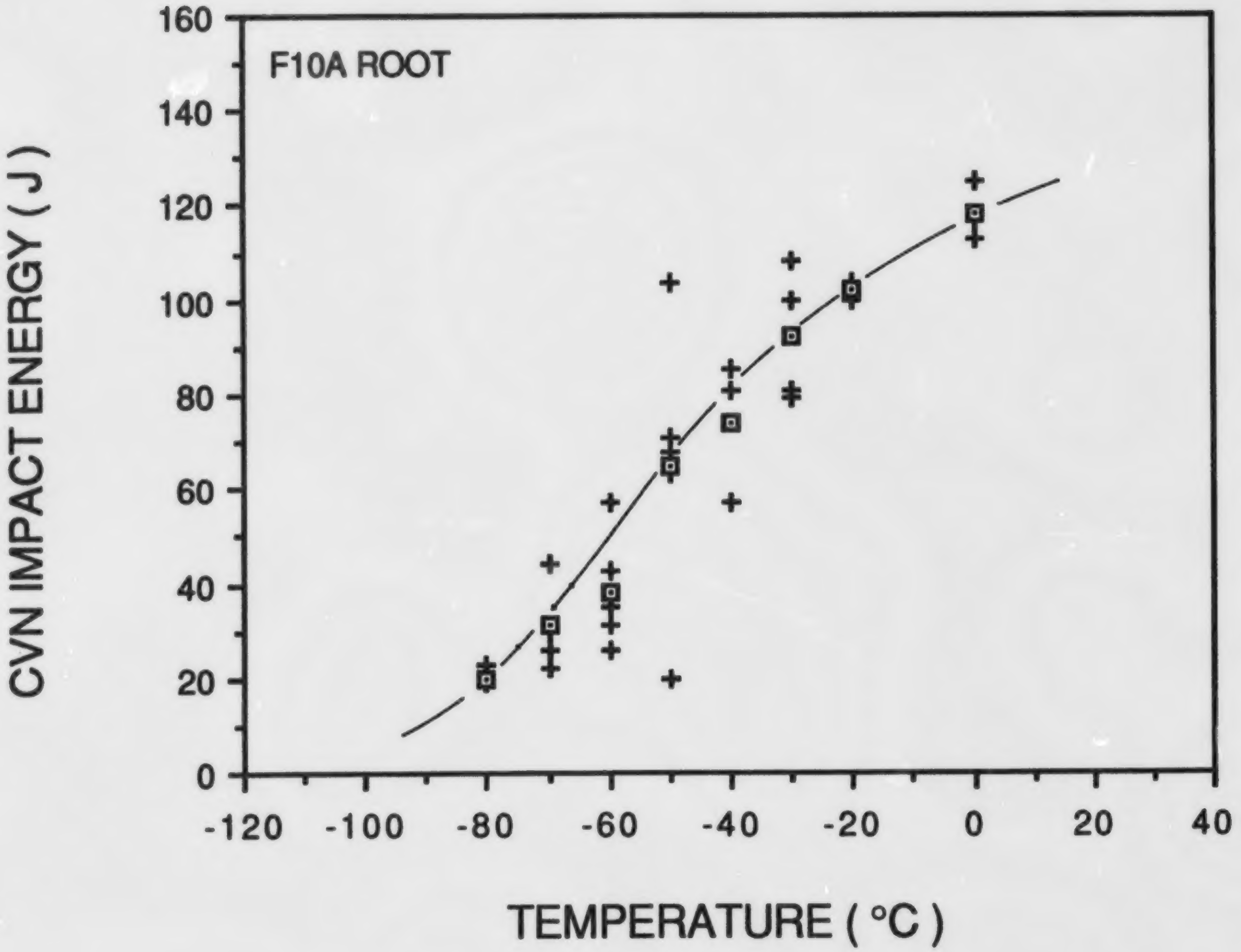

Figure D27: CVN transition curve for root location of low restraint single V weld (as welded 2.0 kJ/mm weld of Consumable A)

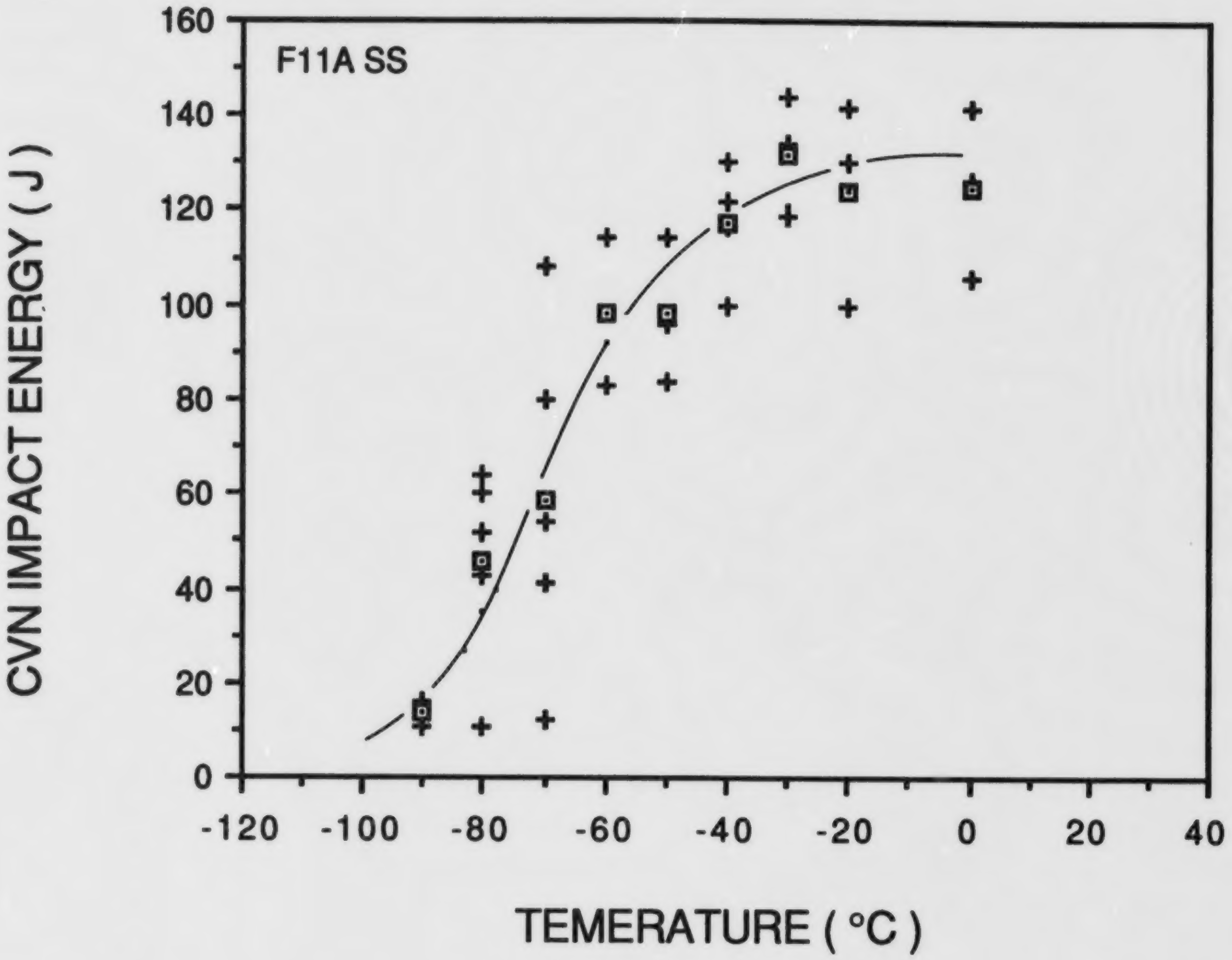

Figure D28: CVN transition curve for subsurface location of high restraint single V weld (as welded 2.0 kJ/mm weld of Consumable A)

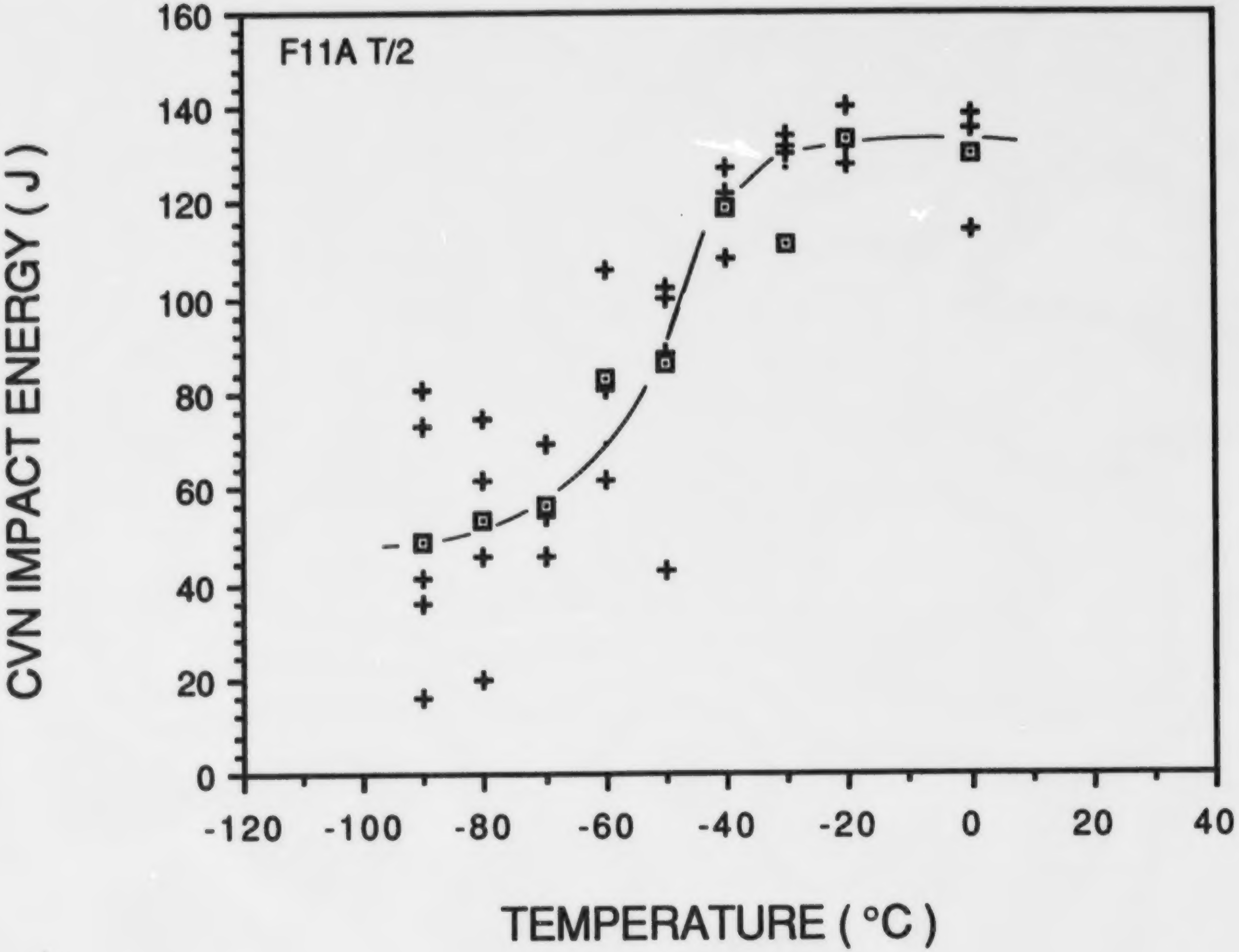

Figure D29: CVN transition curve for T/2 location of high restraint single V weld (as welded 2.0 kJ/mm weld of Consumable A)

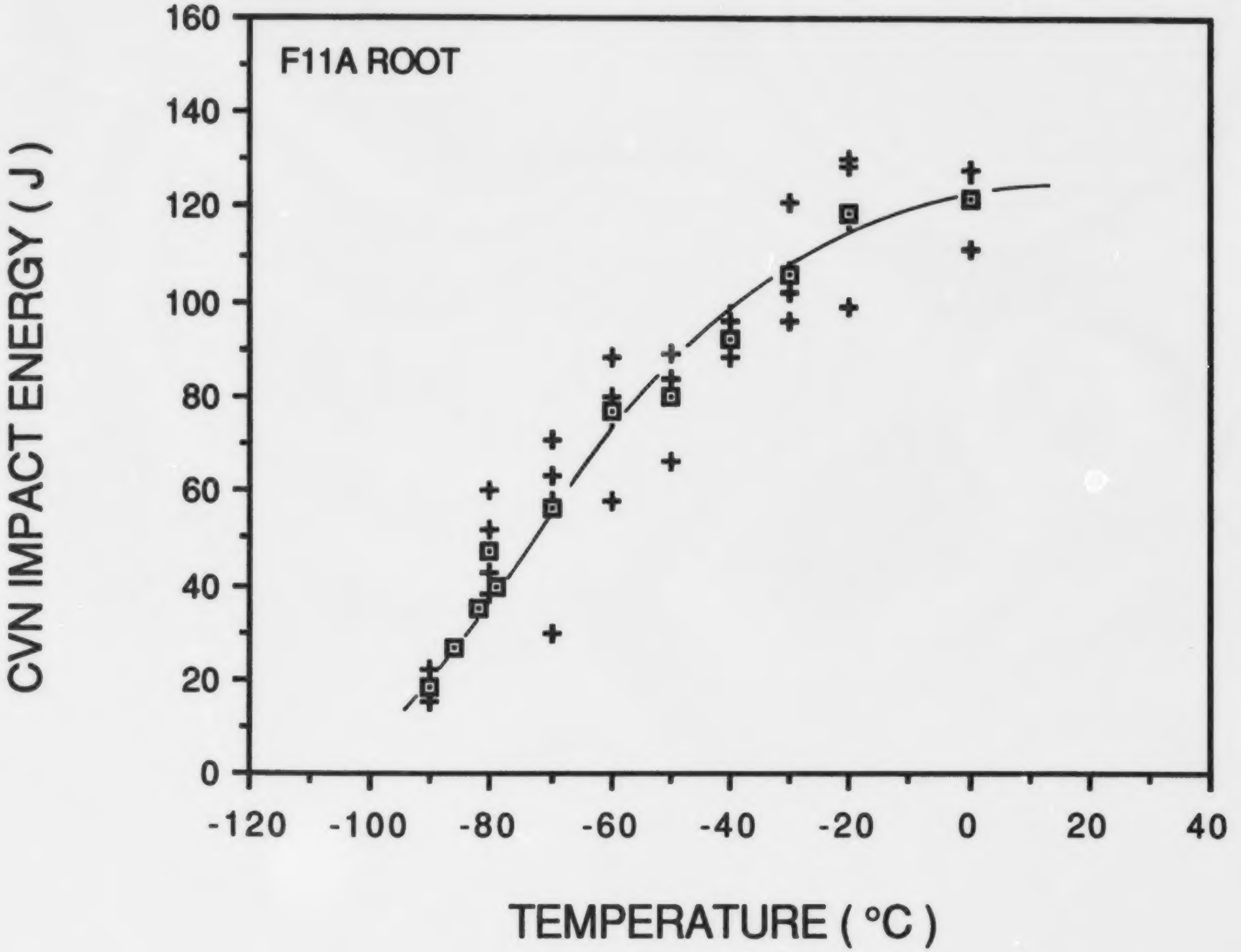

Figure D30: CVN transition curve for root location of high restraint single V weld (as welded 2.0 kJ/mm weld of Consumable A)

APPENDIX E

Data on CTOD Testing

Specimen ID	Temperature (C)	A2 (25%) (IN)	A3 (50%) (IN)	A4 (75%) (IN)	A ave. (IN)	B (IN)	W (IN)	Aave/W	Y	YIELD (KSI)	Vp (IN)	Pmax (LB)	ELASTIC (mm)	PLASTIC (mm)	CTOD (mm)
1F4	-10	1.9310	1.9980	1.9580	1.9617	1.8900	3.7850	0.5183	11.25	81.84	0.0098	38391	0.057	0.063	0.120
1F5	-10	1.9610	1.9900	1.9210	1.9540	1.8840	3.7850	0.5162	11.18	81.84	0.0006	24084	0.025	0.004	0.029
1F6	-10	1.9680	2.0490	1.9680	1.9910	1.8880	3.7830	0.5263	11.56	81.84	0.0381	40750	0.076	0.245	0.321
1F1	-30	1.9490	2.0090	1.9200	1.9593	1.8890	3.7820	0.5181	11.25	81.27	0.0038	32494	0.046	0.025	0.071
1F2	-30	1.9060	1.9960	1.9210	1.9410	1.8880	3.7850	0.5128	11.03	81.27	0.0041	34249	0.049	0.027	0.077
1F3	-30	1.9540	2.0440	1.9570	1.9850	1.8900	3.7860	0.5243	11.48	81.27	0.0044	33198	0.050	0.028	0.078
2F4	-10	1.8010	1.7730	1.8620	1.8120	1.8880	3.7730	0.4803	9.96	74.05	0.0068	39708	0.059	0.050	0.109
2F5	-10	1.8130	1.7790	1.8640	1.8187	1.8880	3.7680	0.4827	10.06	74.05	0.0063	38241	0.056	0.046	0.102
2F6	-10	1.7580	1.7400	1.8800	1.7927	1.8870	3.7790	0.4744	9.78	74.05	0.0064	38863	0.054	0.048	0.102
2F1	-30	1.9450	1.8850	1.8780	1.9027	1.8850	3.7890	0.5022	10.68	75.74	0.0009	28534	0.034	0.008	0.041
2F2	-30	1.8590	1.8370	1.9010	1.8657	1.8810	3.7700	0.4949	10.44	75.74	0.0016	31721	0.041	0.011	0.052
2F3	-30	1.8210	1.8040	1.8780	1.8343	1.8880	3.7670	0.4869	10.18	75.74	0.0094	31739	0.039	0.068	0.106
3F4	-10	1.9070	1.9070	1.9230	1.9390	1.8870	3.7800	0.5130	11.07	75.57	0.0008	22482	0.023	0.004	0.027
3F5	-10	1.9600	2.0210	1.8940	1.9583	1.8890	3.7770	0.5185	11.25	75.57	0.0212	37454	0.066	0.140	0.205
3F6	-10	1.9700	2.0330	1.8890	1.9640	1.8840	3.7770	0.5200	11.33	75.57	0.0188	34725	0.058	0.123	0.181
3F1	-30	1.9230	2.0030	1.9430	1.9563	1.8880	3.7790	0.5177	11.25	79.80	0.0011	24432	0.027	0.007	0.034
3F2	-30	1.9150	2.0010	1.9280	1.9480	1.8860	3.7770	0.5158	11.18	79.60	0.0013	24890	0.027	0.009	0.036
3F3	-30	1.9350	1.9920	1.9050	1.9440	1.8860	3.7780	0.5148	11.14	79.80	0.0053	28589	0.036	0.035	0.071
4F4	-10	1.9070	1.8390	1.8310	1.8590	1.8900	3.7800	0.4918	10.34	74.15	0.0084	38438	0.060	0.060	0.119
4F5	-10	1.8450	1.7530	1.8020	1.8000	1.8920	3.7770	0.4766	9.87	74.15	0.0464	41925	0.064	0.344	0.408
4F6	-10	1.8080	1.7880	1.8380	1.8413	1.8860	3.7820	0.4869	10.18	74.15	0.0028	34088	0.046	0.019	0.064
4F1	-30	1.8590	1.9010	1.9240	1.8947	1.8870	3.7780	0.5015	10.65	76.29	0.0008	28738	0.034	0.004	0.039
4F2	-30	1.8530	1.8520	1.8960	1.8670	1.8890	3.7850	0.4933	10.38	76.29	0.0013	32545	0.042	0.009	0.051
4F3	-30	1.8540	1.8590	1.9030	1.8720	1.8890	3.7840	0.4947	10.44	76.29	0.0131	30952	0.038	0.092	0.131

Table E1

Summary of CTOD Values for F1 - F4

Specimen ID	Temperature (C)	A2 (25%) (IN)	A3 (50%) (IN)	A4 (75%) (IN)	A ave. (IN)	B (IN)	W (IN)	Aave/W	Y	YIELD (KSI)	Vp (IN)	Pmax (LB)	ELASTIC (mm)	PLASTIC (mm)	CTOD (mm)
F5A1	-10	1.7995	1.9140	1.8055	1.8397	1.7790	3.5700	0.515	11.25	81.267	0.0004	28205	0.0414	0.0027	0.0440
F5A2	-30	1.9780	2.0800	1.9880	2.0153	1.8795	3.7680	0.535	11.91	81.267	0.0065	37326	0.0689	0.0408	0.1097
F5A3	-30	1.9940	2.1145	1.9755	2.0280	1.8860	3.7725	0.538	12.04	81.267	0.0457	40915	0.0839	0.2846	0.3686
F5A4	-30	1.9635	2.0265	1.9780	1.9893	1.8765	3.7710	0.528	11.22	81.267	0.0019	32250	0.0458	0.0122	0.0580
F5A5	-10	1.9605	2.0485	1.9950	2.0013	1.8770	3.7670	0.531	11.75	81.267	0.0033	32820	0.0520	0.0206	0.0726
F5A6	-10	2.0055	2.0590	2.0115	2.0253	1.8855	3.7665	0.538	12.04	81.267	0.0019	30476	0.0467	0.0118	0.0585
F6A1	-30	1.9385	2.0330	1.9865	1.9860	1.8885	3.7700	0.527	11.22	75.736	0.0019	29708	0.0412	0.0122	0.0534
F6A2	-30	1.9665	2.0200	1.9530	1.9798	1.8860	3.7755	0.524	11.48	75.736	0.0020	28974	0.0410	0.0129	0.0540
F6A3	-30	1.9745	2.0425	1.8270	1.9480	1.8860	3.7795	0.515	11.14	75.736	0.0004	19380	0.0173	0.0027	0.0199
F6A4	-10	1.9860	2.0285	1.9550	1.9898	1.8855	3.7780	0.527	11.6	75.736	0.0000	23316	0.0271	0.0000	0.0271
F6A5	-10	1.9765	2.0355	1.9800	1.9973	1.8845	3.7720	0.530	11.71	75.736	0.0148	35714	0.0650	0.0933	0.1583
F6A6	-10	1.9310	2.0190	1.9620	1.9707	1.8835	3.7765	0.522	11.4	75.736	0.0002	31550	0.0481	0.0010	0.0492
F7A1	-30	1.7830	1.7060	1.8280	1.7723	1.8805	3.7785	0.469	9.83	75.736	0.0283	47985	0.0796	0.1988	0.2785
F7A2	-30	1.8340	1.7865	1.8040	1.8082	1.8870	3.7690	0.480	9.96	75.736	0.0573	44798	0.0739	0.4208	0.4947
F7A3	-30	1.8115	1.8115	1.8605	1.8278	1.8860	3.7735	0.484	10.09	75.736	0.0108	43443	0.0713	0.0783	0.1496
F7A4	-10	1.8705	1.8655	1.8940	1.8767	1.8885	3.7745	0.497	10.51	75.736	0.0072	40879	0.0683	0.0504	0.1187
F7A5	-10	1.9120	1.8595	1.8605	1.8773	1.8845	3.7775	0.497	10.51	75.736	0.0270	42234	0.0732	0.1890	0.2622
F7A6	-10	1.8550	1.8550	1.8745	1.8615	1.8835	3.7815	0.492	10.34	75.736	0.1142	46520	0.0850	0.8102	0.8952
F7B1	-30	1.9515	2.0450	1.9705	1.9890	1.8845	3.7725	0.527	11.6	75.736	0.0013	28974	0.0420	0.0083	0.0503
F7B2	-30	1.9370	2.0160	1.9385	1.9638	1.8865	3.7720	0.521	11.37	75.736	0.0033	34908	0.0585	0.0216	0.0800
F7B3	-30	1.9410	2.0415	1.9380	1.9735	1.8895	3.7725	0.523	11.44	75.736	0.0160	35750	0.0619	0.1040	0.1658
F7B4	-10	1.9525	2.0155	1.9680	1.9787	1.8835	3.7645	0.526	11.56	75.736	0.0086	36483	0.0663	0.0555	0.1218
F7B5	-10	1.9360	1.9955	1.9265	1.9527	1.8865	3.7665	0.518	11.25	75.736	0.0299	41208	0.0799	0.1966	0.2764
F7B6	-10	1.9550	2.0165	1.9625	1.9780	1.8865	3.7705	0.525	11.52	75.736	0.0631	41831	0.0862	0.4082	0.4944
F8A1	-50	1.8420	1.7500	1.7690	1.7870	1.7770	3.5645	0.501	10.65	76.292	0.0070	35164	0.0616	0.0483	0.1099
2	-50	1.7560	1.7560	1.7965	1.7695	1.7785	3.5695	0.496	10.48	76.292	0.0064	36263	0.0633	0.0449	0.1081
3	-50	1.7815	1.7620	1.7445	1.7627	1.7775	3.5675	0.494	10.41	76.292	0.0000	26007	0.0322	0.0000	0.0322
4	-30	1.9205	1.9235	1.9555	1.9332	1.8895	3.7690	0.513	11.07	76.292	0.0015	32710	0.0482	0.0100	0.0582
5	-30	1.9210	1.9025	1.9230	1.9155	1.8725	3.7660	0.509	10.93	76.292	0.1333	43626	0.0851	0.9029	0.9880
6	-30	1.9145	1.8965	1.9145	1.9085	1.8850	3.7625	0.507	10.85	76.292	0.1134	43113	0.0809	0.7711	0.8520
F8B1	-30	1.9400	2.0175	1.9170	1.9582	1.8840	3.7680	0.520	11.33	79.600	0.0325	42197	0.0810	0.2133	0.2943
2	-30	2.1020	2.2005	2.0955	2.1327	1.8900	3.7745	0.565	13.23	79.600	0.1200	39047	0.0938	0.6880	0.7818
3	-50	1.8230	1.8940	1.8165	1.8445	1.8850	3.7805	0.488	10.21	79.600	0.0105	35018	0.0451	0.0750	0.1201
4	-30	1.9195	1.9935	1.8945	1.9358	1.7805	3.5705	0.542	12.20	79.600	0.0474	43553	0.1182	0.2905	0.4087
5	-50	1.9455	1.9840	1.9055	1.9450	1.8860	3.7730	0.516	11.18	79.600	0.0298	42417	0.0794	0.1979	0.2773
6	-50	1.9355	2.0435	2.0095	1.9962	1.8850	3.7650	0.530	11.71	79.600	0.0246	41355	0.0831	0.1566	0.2396
F9A1	-30	1.9020	1.8490	1.8640	1.8717	1.8850	3.7720	0.496	10.48	76.292	0.0003	30695	0.0382	0.0021	0.0403
2	-30	1.8300	1.7930	1.8865	1.8365	1.8910	3.7795	0.486	10.12	76.292	RUINED	RUINED	RUINED	RUINED	RUINED
3	-30	1.8650	1.8760	1.9010	1.8807	1.8855	3.7795	0.498	10.54	76.292	0.0001	31794	0.0413	0.0007	0.0420
4	-50	1.9200	1.8725	1.8965	1.8963	1.8870	3.7810	0.502	10.68	76.292	0.1456	44908	0.0845	1.0064	1.0909
5	-50	1.8550	1.8175	1.8685	1.8470	1.8895	3.7965	0.487	10.18	76.292	0.0324	44468	0.0748	0.2333	0.3080
6	-50	1.8765	1.8575	1.8265	1.8535	1.8845	3.7325	0.497	10.51	76.292	0.0080	40838	0.0687	0.0560	0.1248
F9B1	-30	1.8920	2.0015	1.9355	1.9430	1.8865	3.7765	0.514	11.11	79.600	0.0878	43150	0.0810	0.5849	0.6659
2	-30	1.9320	2.0150	1.9575	1.9682	1.8855	3.7770	0.521	11.37	79.600	0.0168	38702	0.0683	0.1098	0.1781
3	-30	1.9435	2.0465	1.9980	1.9960	1.8880	3.7740	0.529	11.67	79.600	0.0060	38475	0.0710	0.0383	0.1094
4	-50	1.9870	2.0480	1.9665	2.0005	1.8890	3.7735	0.530	11.71	79.600	0.0000	26996	0.0352	0.0000	0.0352
5	-50	1.9245	2.0390	1.9450	1.9695	1.8845	3.7760	0.522	11.40	79.600	0.0016	30952	0.0440	0.0104	0.0544
6	-50	1.9170	2.0520	1.9550	1.9747	1.7785	3.5705	0.553	12.68	79.600	0.0027	27862	0.0524	0.0157	0.0681

Table E2: Summary of CTOD Values For F5-F9

PROJECT 2522
DATE 25-Jan-88

WELDS SERIES

Specimen ID		Temperature (C)	A2 (25%) (IN)	A3 (50%) (IN)	A4 (75%) (IN)	A ave. (IN)	B (IN)	W (IN)	Aave/W	Y	YIELD (KSI)	Vp (IN)	Pmax (LB)	ELASTIC (mm)	PLASTIC (mm)	CTOD (mm)
F10A	1	-30	2.1135	2.1955	2.0985	2.1358	1.8815	3.7755	0.566	13.28	94.1	0.0124	34304	0.0622	0.0709	0.1332
	2	-30	2.0735	2.1675	2.0835	2.1148	1.8810	3.7720	0.561	13.04	94.1	0.0488	40622	0.0843	0.2833	0.3675
	3	-30	2.1135	2.1810	2.0710	2.1218	1.8745	3.7775	0.562	13.09	94.1	0.0889	38919	0.0784	0.5729	0.6513
	4	-50	2.0535	2.1375	2.0685	2.0865	1.8880	3.7755	0.553	12.64	94.1	0.0080	34688	0.0573	0.0476	0.1049
	5	-50	2.0875	2.1965	2.0990	2.1277	1.8810	3.7830	0.562	13.09	94.1	0.0129	33974	0.0592	0.0746	0.1338
	6	-50	2.0685	2.1925	2.1350	2.1387	1.8880	3.7780	0.566	13.28	94.1	0.0059	33065	0.0574	0.0337	0.0911
F11A	1	-30	2.0625	2.1360	2.0630	2.0872	1.8875	3.7785	0.552	12.64	94.0	0.0058	32794	0.0512	0.0343	0.0855
	2	-30	2.1575	2.3035	2.1610	2.2073	1.8845	3.7725	0.585	14.23	94.0	0.0790	34688	0.0730	0.4254	0.4983
	3*	-50	2.1290	2.1885	2.1310	2.1485	1.8820	3.7505	0.573	13.62	94.0	0.0030	31501	0.0556	0.0168	0.0724
	4	-50	2.0600	2.1610	2.0720	2.0977	1.8755	3.7805	0.555	12.77	94.0	0.0017	23608	0.0274	0.0101	0.0375
	5*	-30	2.0685	2.1705	2.0615	2.1002	1.8805	3.7745	0.556	12.82	94.0	0.0560	39853	0.0785	0.3293	0.4078
	6	-50	2.0455	2.1220	2.0345	2.0673	1.8810	3.7835	0.548	12.37	94.0	0.0001	34468	0.0545	0.0006	0.0551
F10B	7	-30	0.2395	0.2410	0.2415	0.2407	1.8840	1.8915	0.127	3.75	81.27	0.0418	82637	0.0678	0.6838	0.7516
	8	-30	0.2475	0.2760	0.2440	0.2556	1.8760	1.8855	0.136	3.84	81.27	0.0265	80438	0.0669	0.4269	0.4938
	9	-30	0.2725	0.2775	0.2635	0.2712	1.8935	1.8910	0.143	3.93	81.27	0.0200	77362	0.0633	0.3168	0.3801
F11B	7	-30	0.2530	0.2910	0.2475	0.2638	1.8655	1.8385	0.144	3.93	81.27			0.0000	0.0000	0.0000
	8	-30	0.2580	0.2200	0.2535	0.2442	1.8575	1.8520	0.132	3.80	81.27	0.0643	90769	0.0864	1.0428	1.1292
	9	-30	0.2055	0.2075	0.1730	0.1953	1.8505	1.8525	0.105	3.52	81.27	0.0898	90769	0.0745	1.5448	1.6193

Table E3

Summary of CTOD Values For

The Restraint Welds F10-F4

APPENDIX F

Fractographs on Selected CTOD Specimens

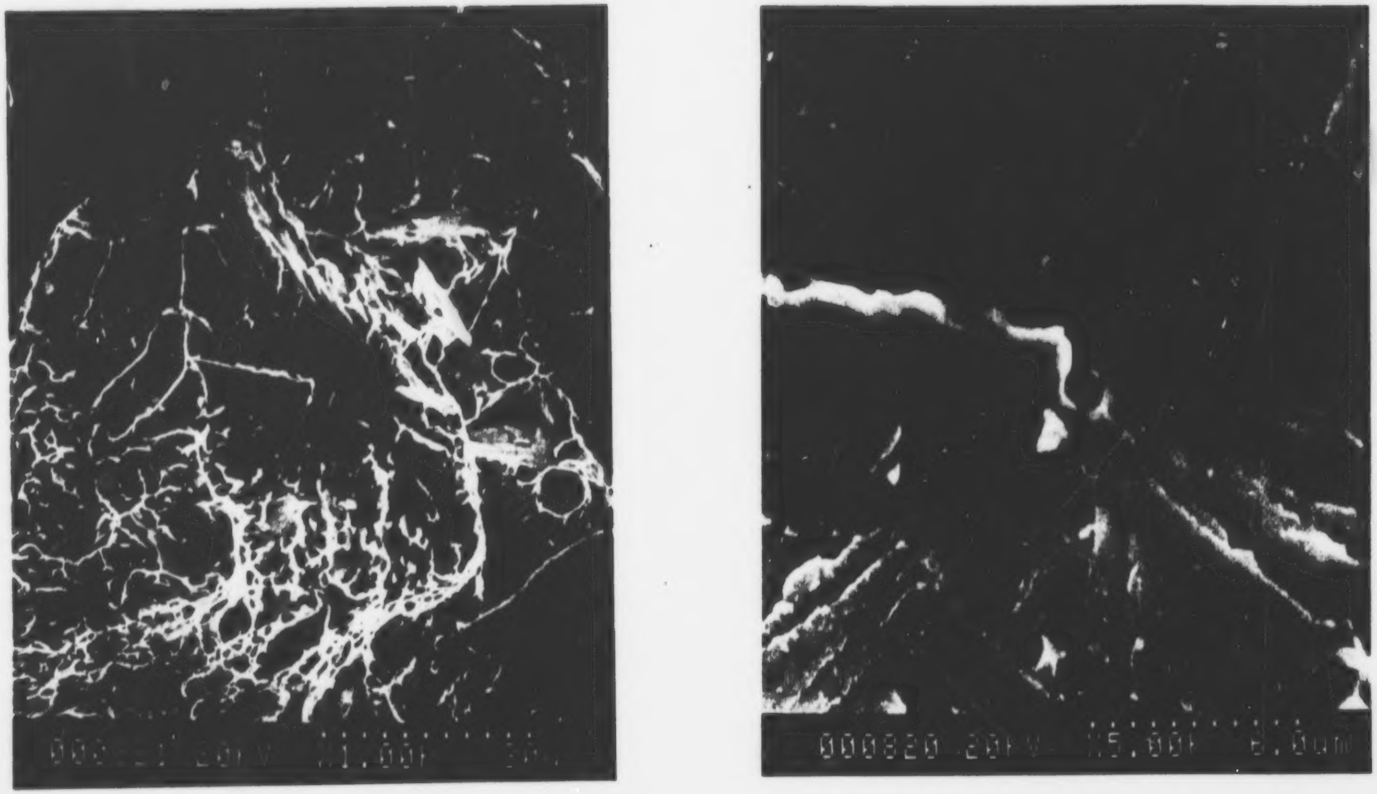

(a) (1000X, Neg. 821)

(b) (500X, Neg. 820)

Figure F1: SEM micrographs show that cleavage fracture emanates from an inclusion (~1 micron) found in as welded 3.0 kJ/mm 1G weld of Consumable A (1F2)

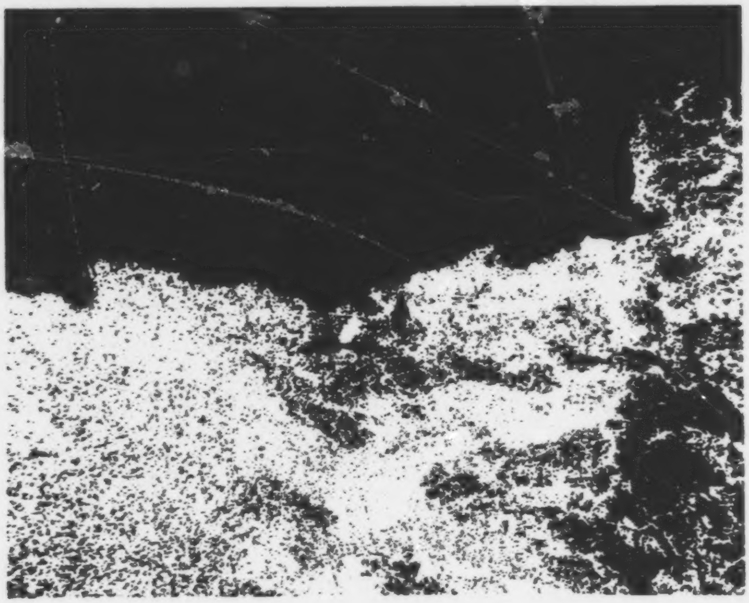

(a) (50X, Neg. 10742)

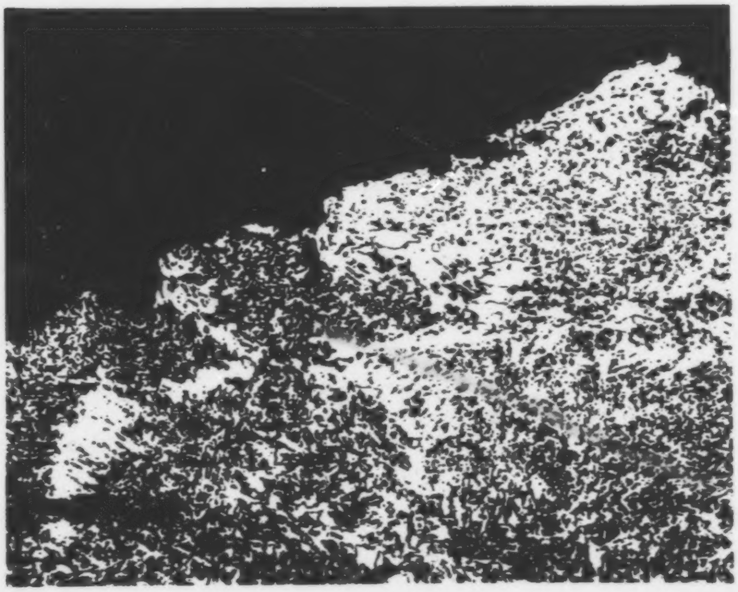

(b) (400X, Neg. 10741)

Figure F2: Optical miccrographs show that the cleavage initiation site is located in the grain boundary ferrite within the columnar region (1F2). The plane of observation is approximately 5μm from the inclusion.

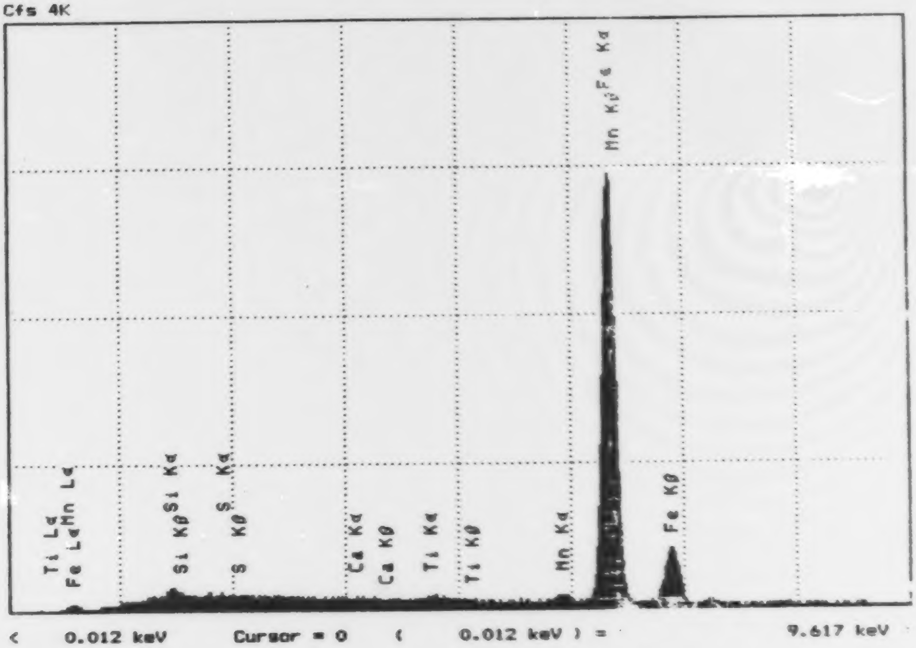

(a) Surrounding matrix

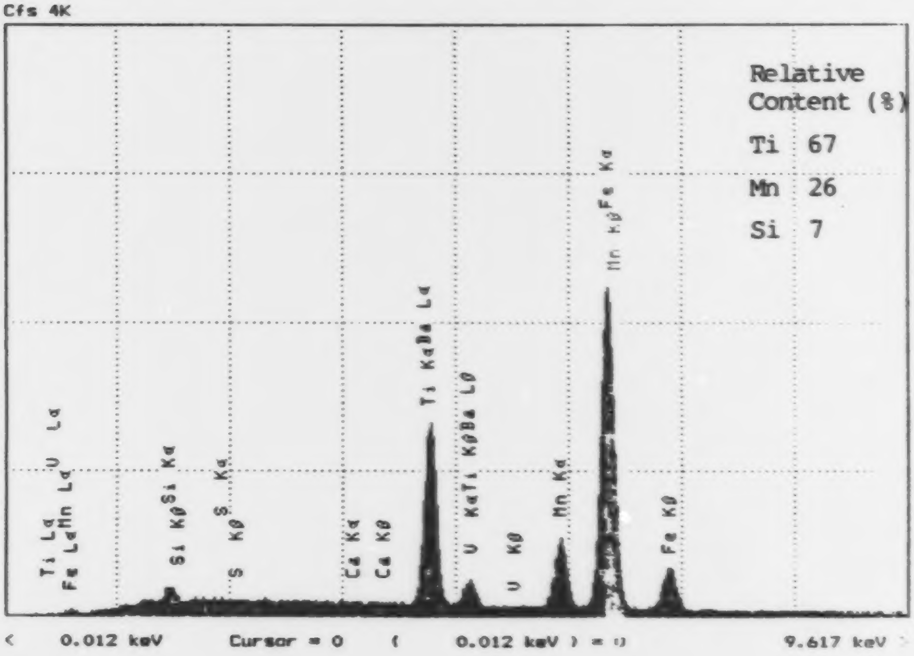

(b) Cleavage initiation site

Figure F3: Difference in EDX spectrums confirms the role of inclusion acting as cleavage initiation site (1F2)

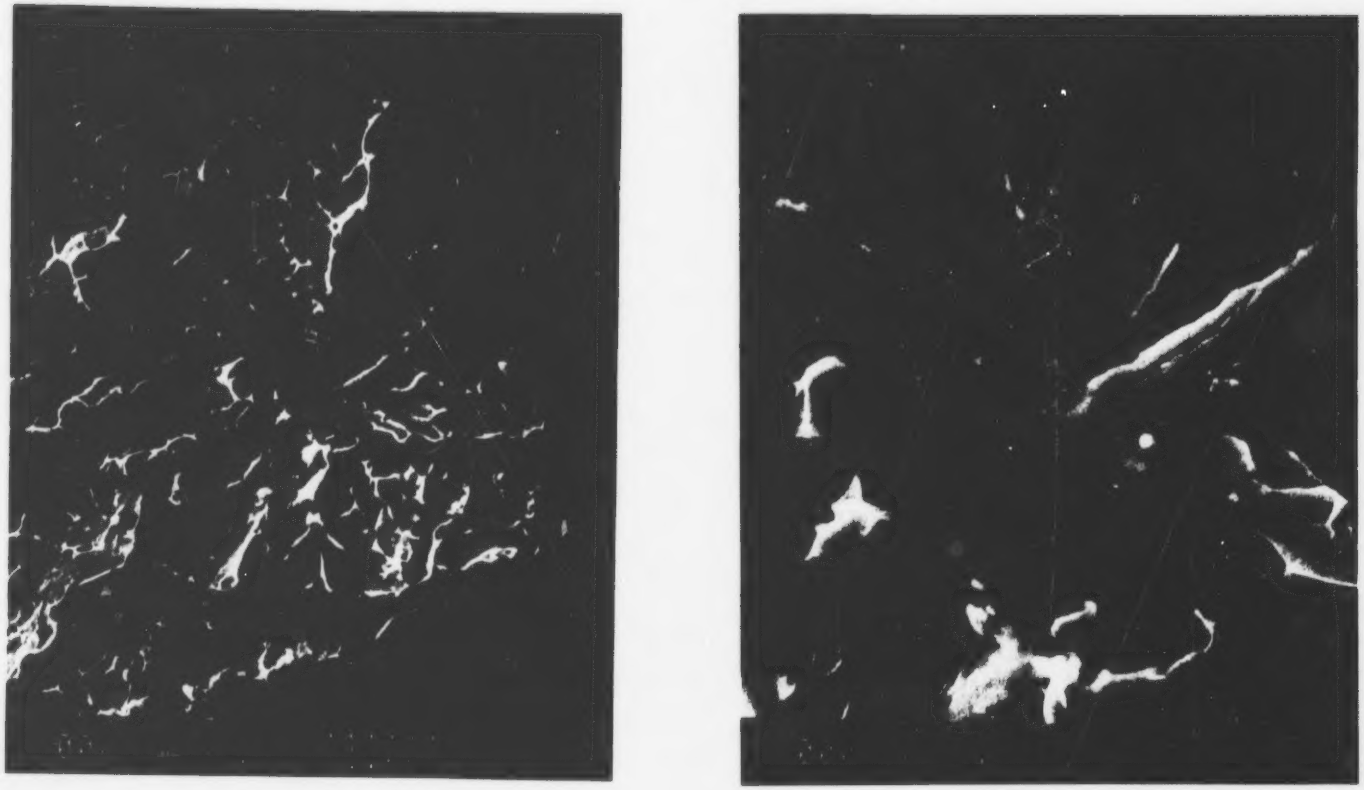

(a) (1000X, Neg. 831)

(b) (5000X, Neg. 830)

Figure F4: SEM micrographs show that cleavage fracture emanates from an inclusion (~1.5 micron) found in as welded 3.0 kJ/mm 1G weld of Consumable A (1F1)

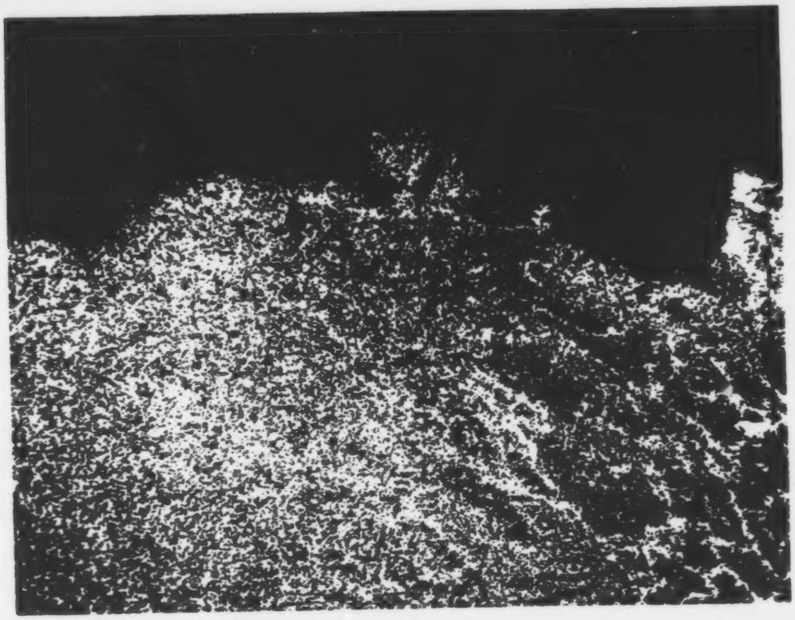

(a) (50X, Neg. 10740)

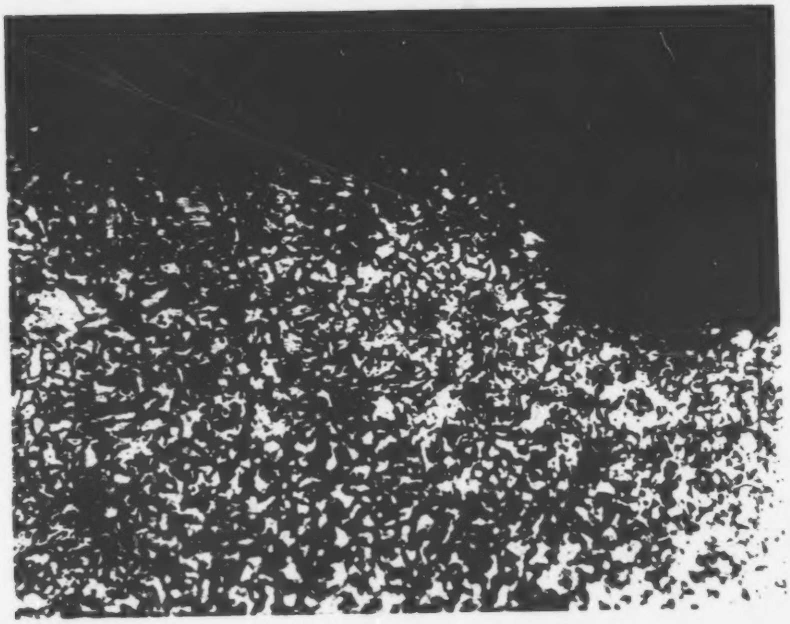

(b) (400X, Neg. 10739)

Figure F5: Optical micrograph indicates that the cleavage initiation site is located in the fine grain reheated zone (1F1).

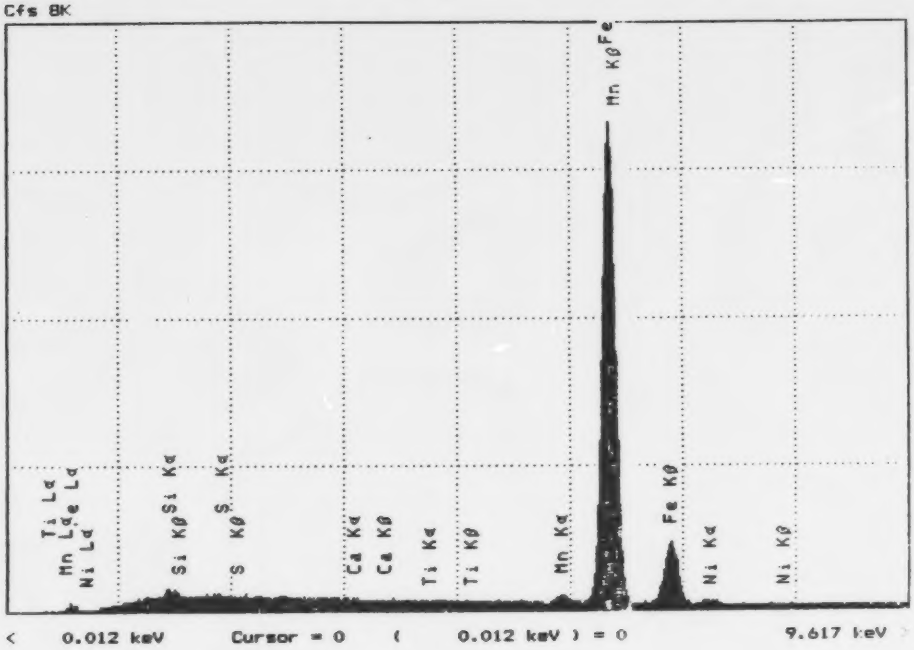

(a) Surrounding matrix

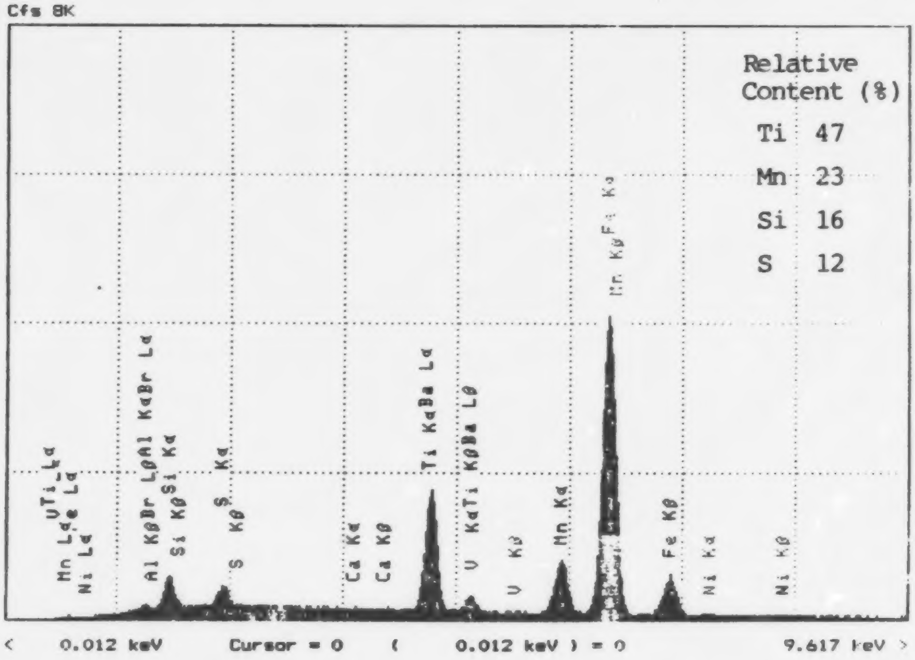

Relative Content (%)

Ti	47
Mn	23
Si	16
S	12

(b) Cleavage initiation site

Figure F6: Difference in EDX spectrums confirms the role of inclusion acting as cleavage initiation site (1F1)

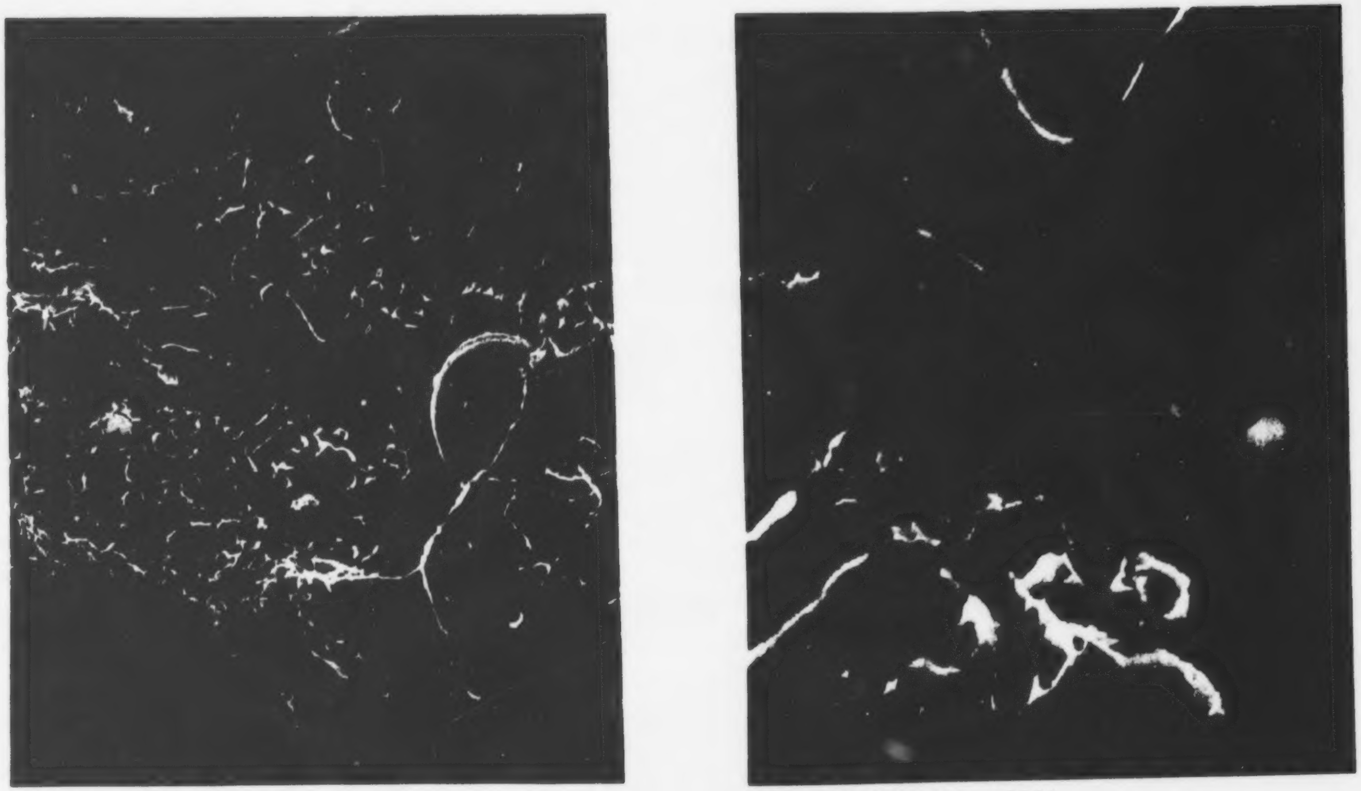

(a) (1000X, Neg. 993)

(b) (5000X, Neg. 992)

Figure F7: SEM micrographs show cleavage river lines emanating from an inclusion (~0.5 micron) found in stress relieved 3.0 kJ/mm 1G weld of Consumable B (2F1). Optical examination of microstructure near the initiation is unsuccessful because of excessive polishing.

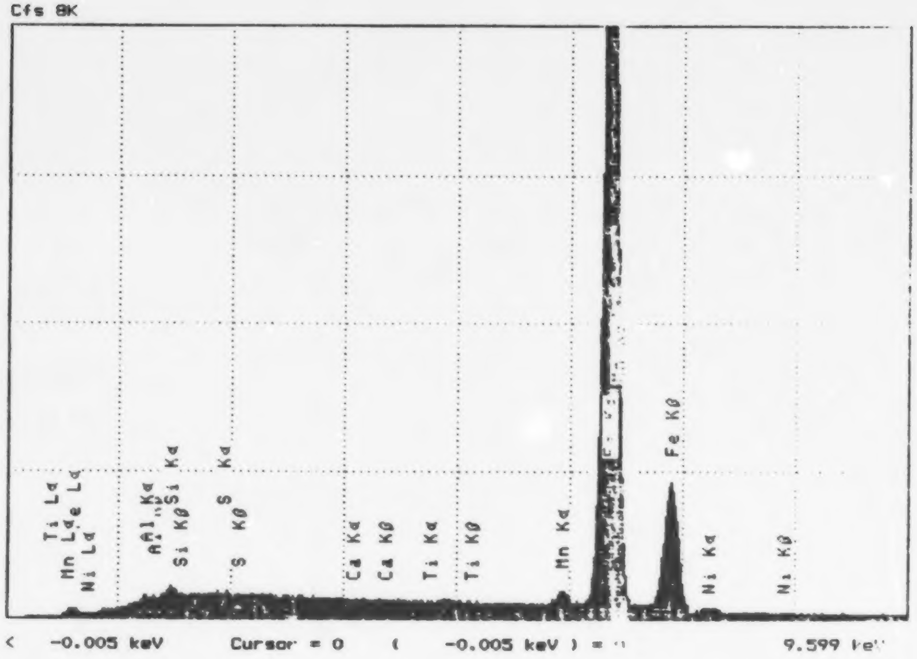

(a) Surrounding matrix

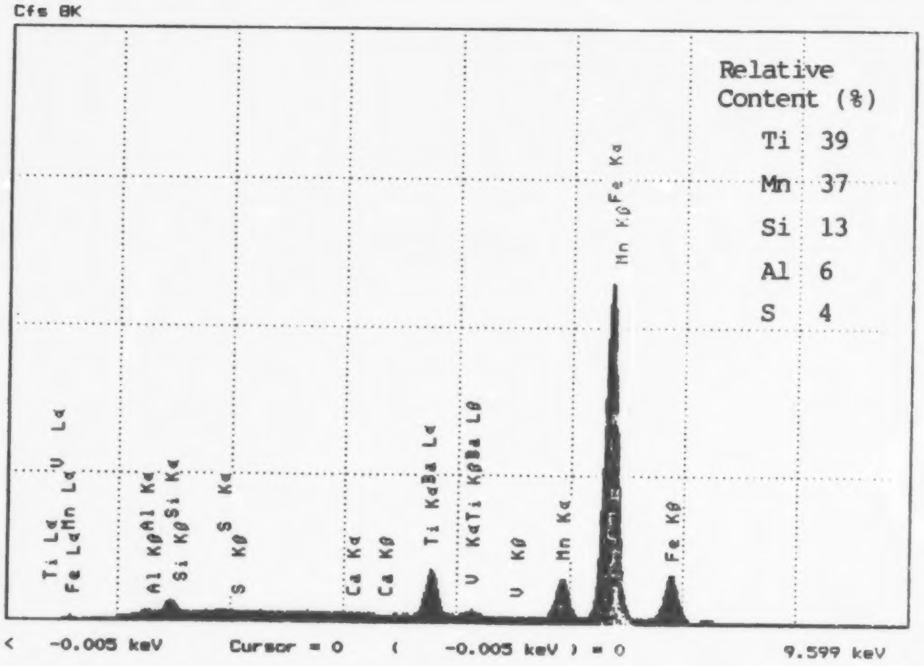

(b) Cleavage initiation site

Figure F8: Difference in EDX spectrums confirms the role of inclusion acting as cleavage initiation site (2F1)

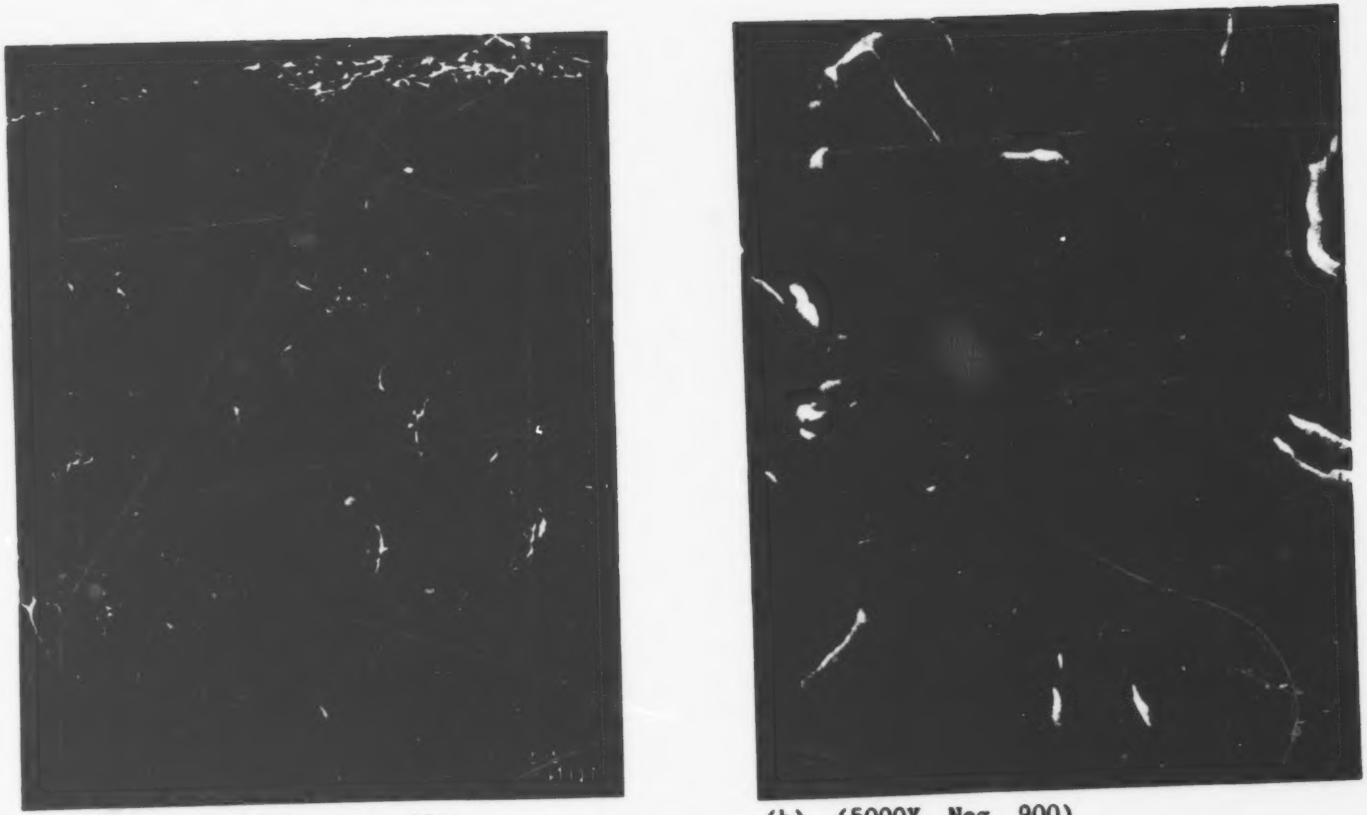

(a) (1000X, Neg. 901)

(b) (5000X, Neg. 900)

Figure F9: SEM micrographs show the cleavage river lines emanating from an inclusion (>0.6 micron) found in stress relieved 3.0 kJ/mm 1G weld of Consumable C (4F1)

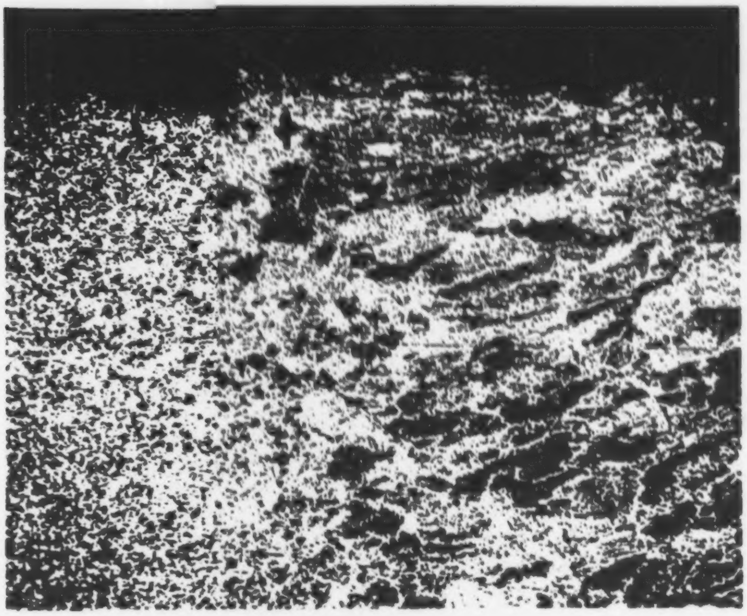

(a) (50X, Neg. 11242)

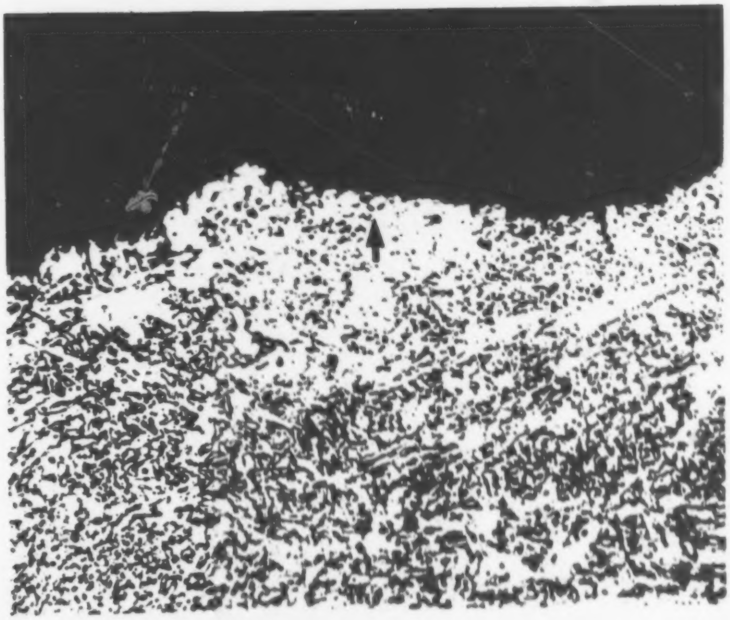

(b) (400X, Neg. 11460)

Figure F10: Optical examination shows the initiation site is located in the coarse grain reheated regions of third root pass of side 1 (4F1). The plane of polishing is approximately 2μm from the inclusion.

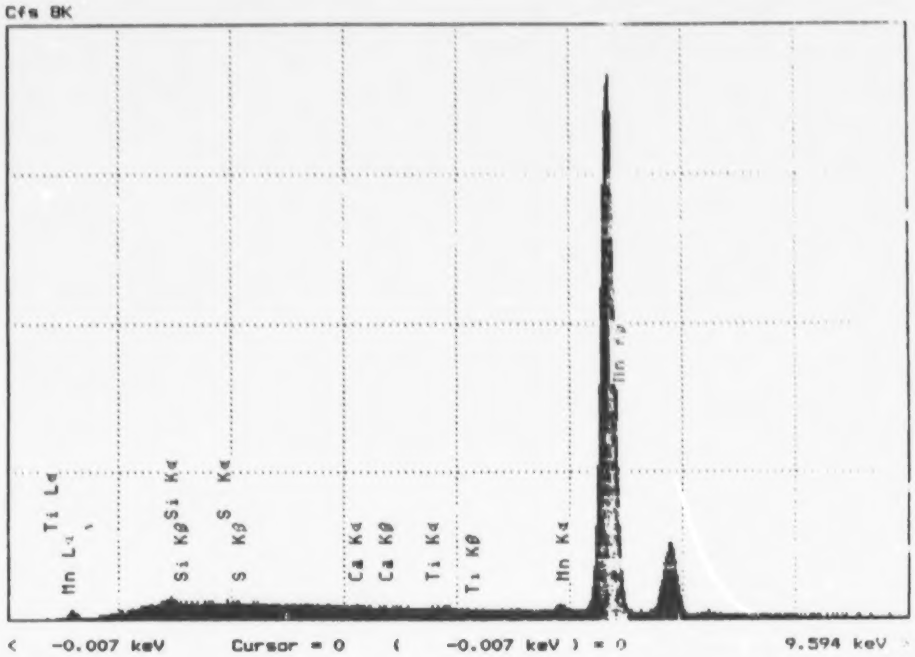

(a) Surrounding matrix

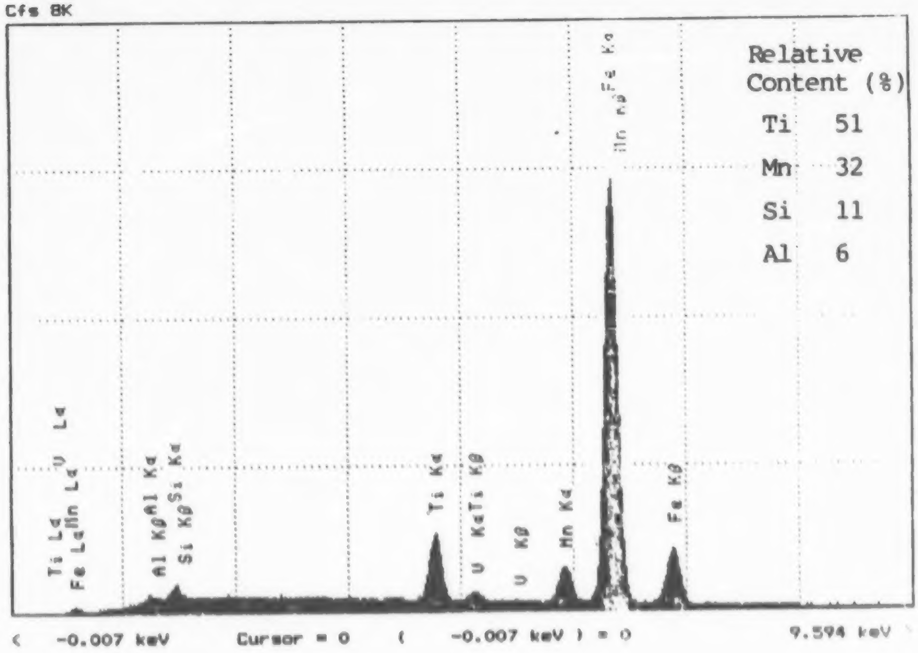

Relative Content (%)	
Ti	51
Mn	32
Si	11
Al	6

(b) Cleavage initiation site

Figure F11: Difference in EDX spectrums confirms the role of inclusions acting as cleavage initiation site (3F1)

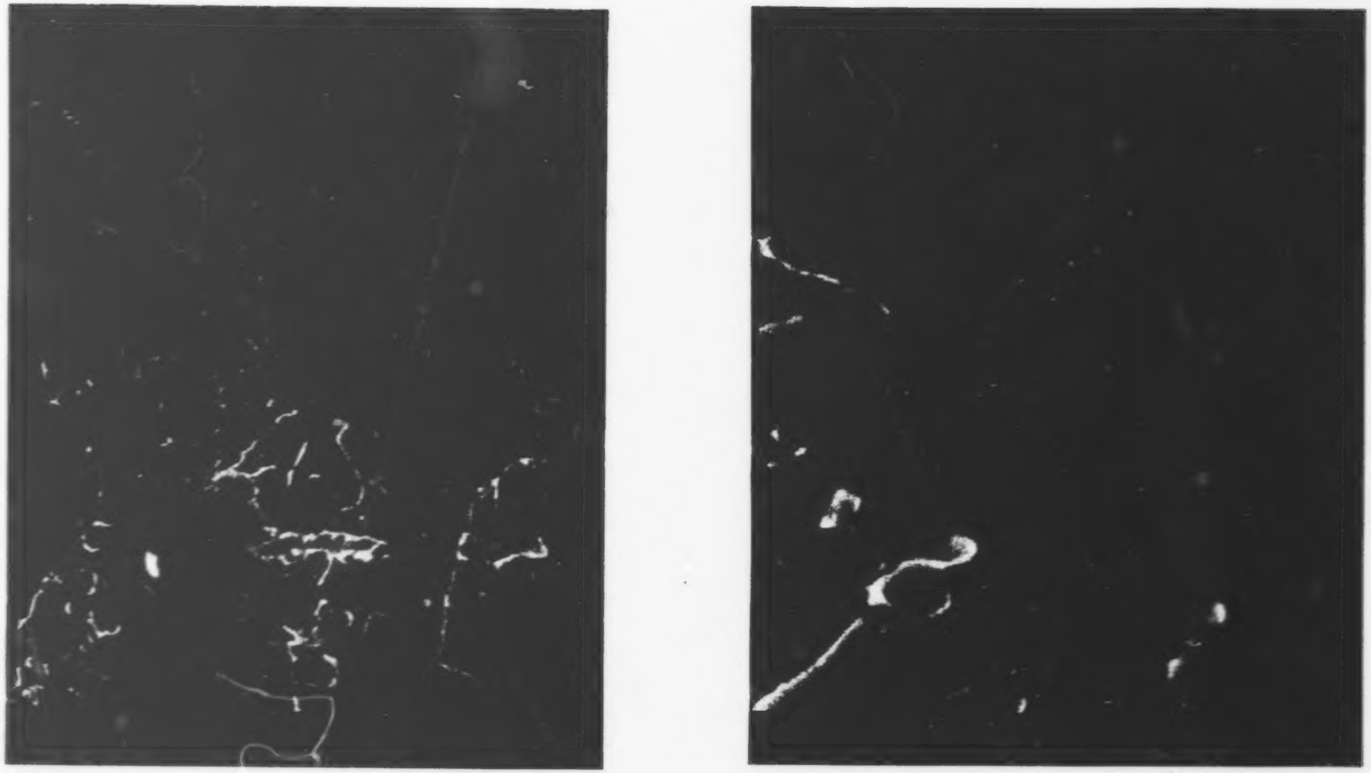

(a) (1000X, Neg. 945)

(b) (5000X, Neg. 944)

Figure F12: SEM micrographs show cleavage river lines emanating from an inclusion (>1.2 micron) found in as welded 3.0 kJ/mm 1G weld of Consumable C (3F1). Optical examination on microstructure near the initiation site is unsuccessful because of excessive polishing.

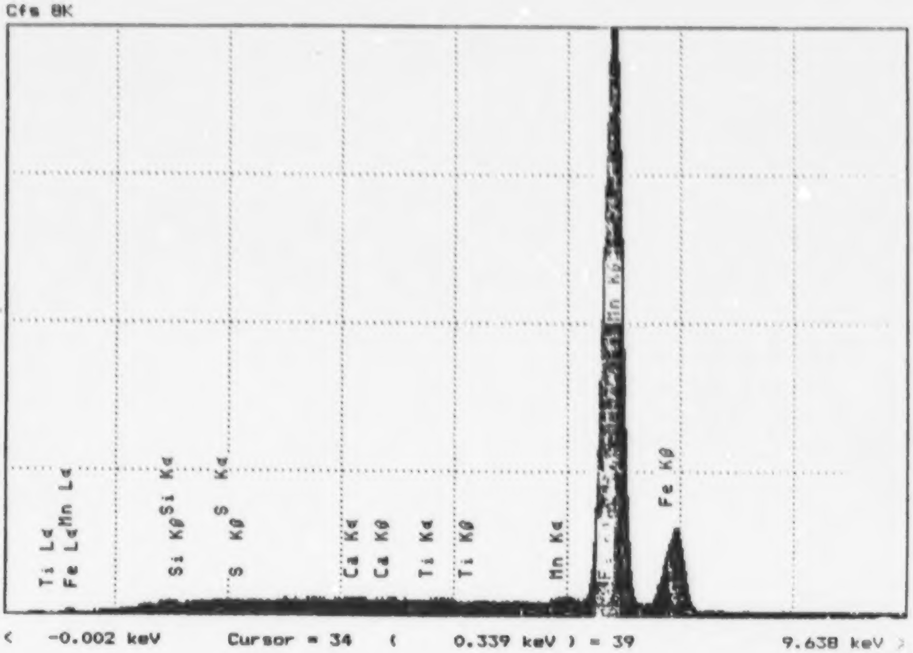

(a) Surrounding matrix

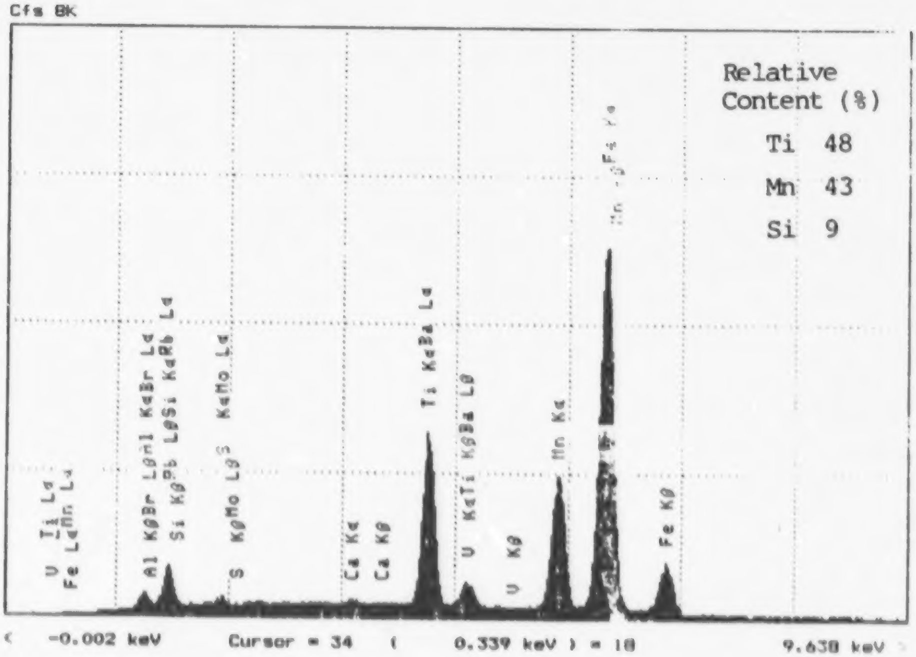

(b) Cleavage initiation site

Figure F13: The difference in EDX spectrums confirms the role of inclusions acting as cleavage initiation site (3F1)

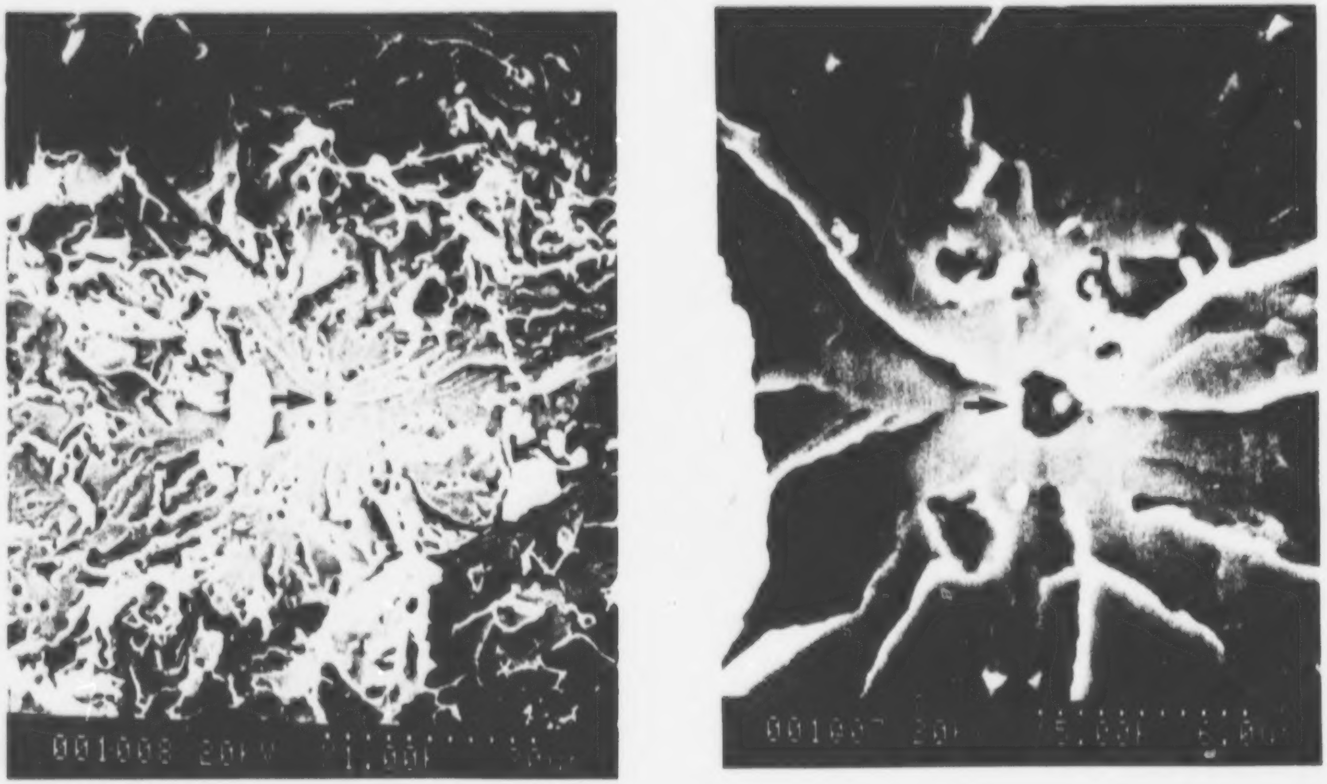

(a) (1000X, Neg. 1008)

(b) (5000X, Neg. 1007)

Figure F14: SEM micrographs show cleavage river lines emanating from a cluster of inclusions. The EDX spectrums are taken at the inclusion denoted by an arrow (F8A3).

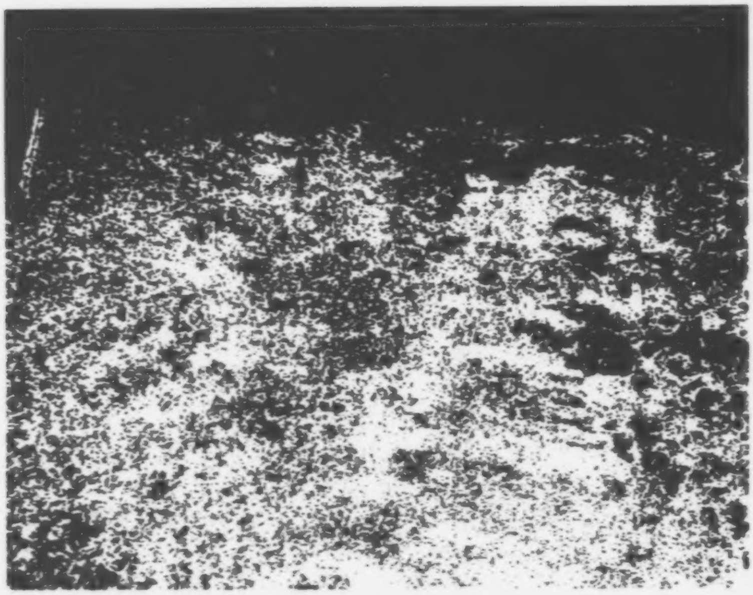

(a) (50X, Neg. 11235)

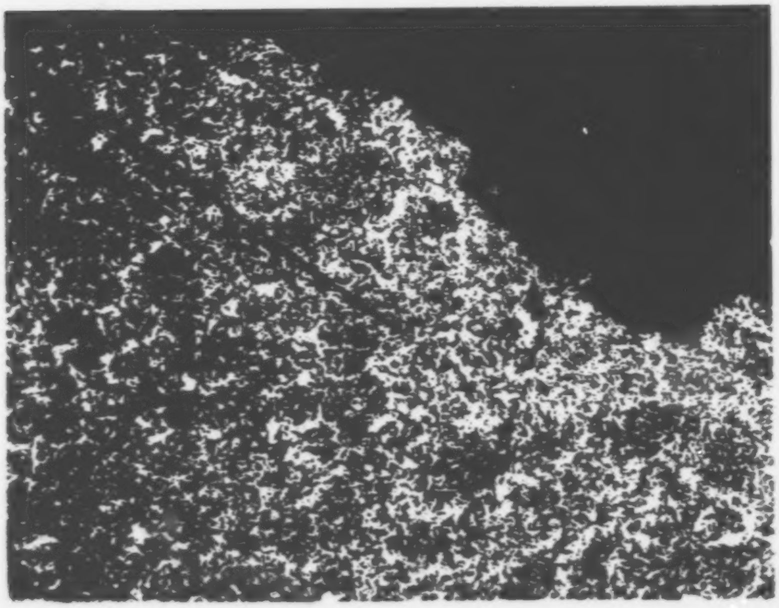

(b) (200X, Neg. 11461)

Figure F15: Optical micrographs show the cleavage initiation site located in the coarse grain reheated region of root pass of side 1 (F8A3)

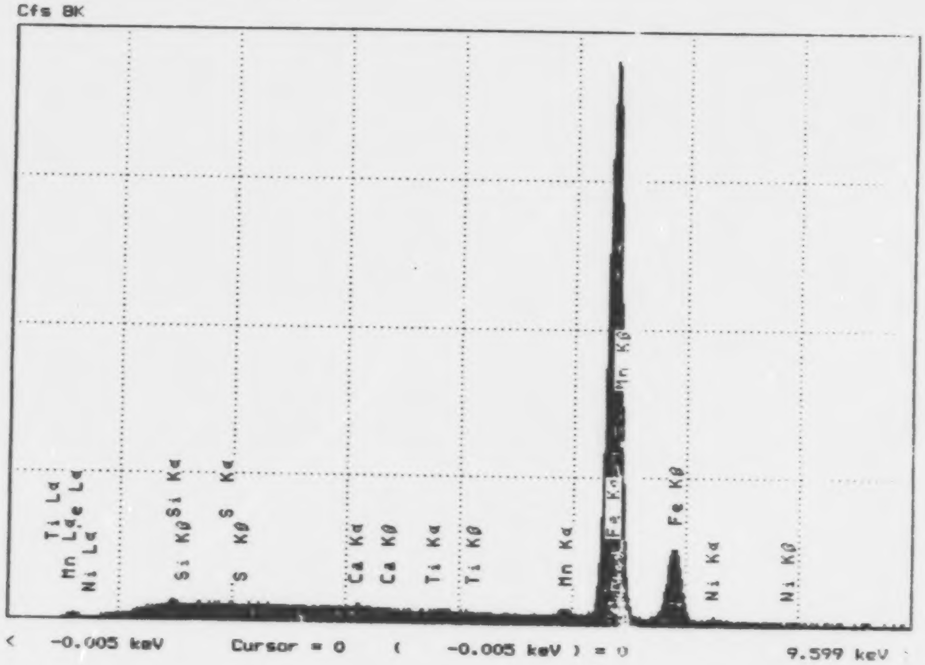

(a) Surrounding matrix

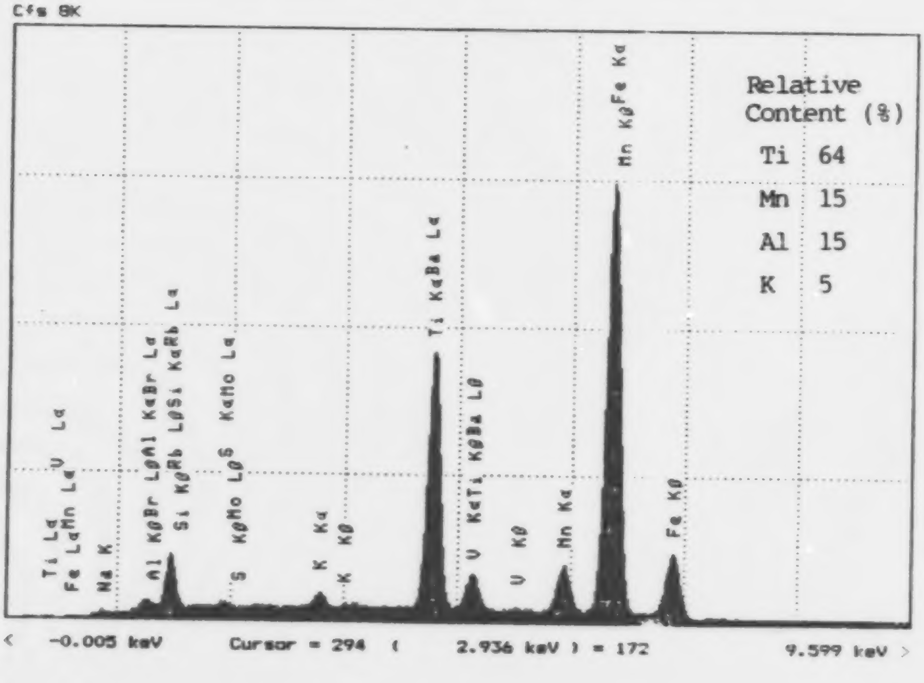

(b) Cleavage initiation site

Figure F16: Difference in EDX spectrums confirms the role of inclusion acting as cleavage initiation site (F8A3)

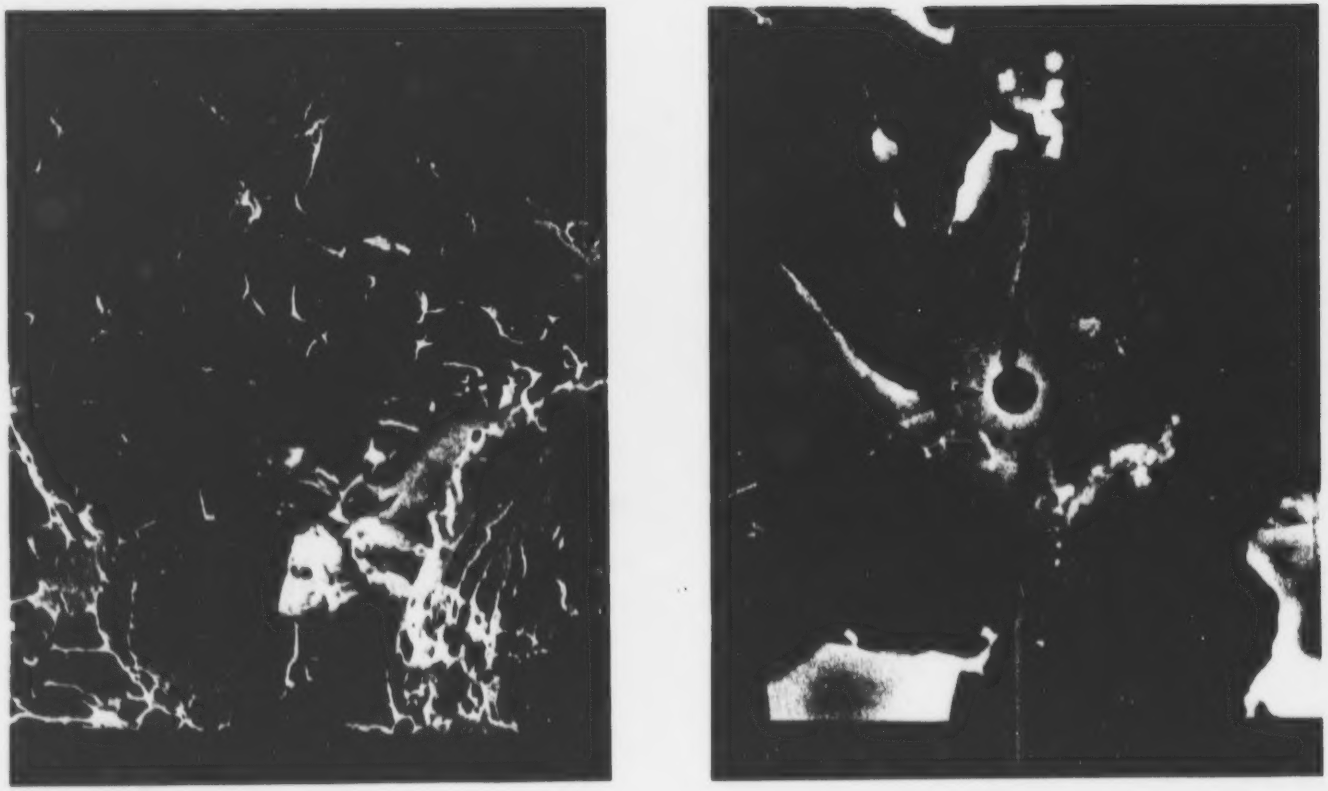

(a) (1000X, Neg. 852)

(b) (5000X, Neg. 851)

Figure F17: SEM micrographs show that cleavage river lines emanating from an inclusion (>1.2 micron) found in as welded 3.0 kJ/mm 1G weld of Consumable C (3F6). Optical examination of microstructure near the cleavage initiation site is unsuccessful due to excessive polishing.

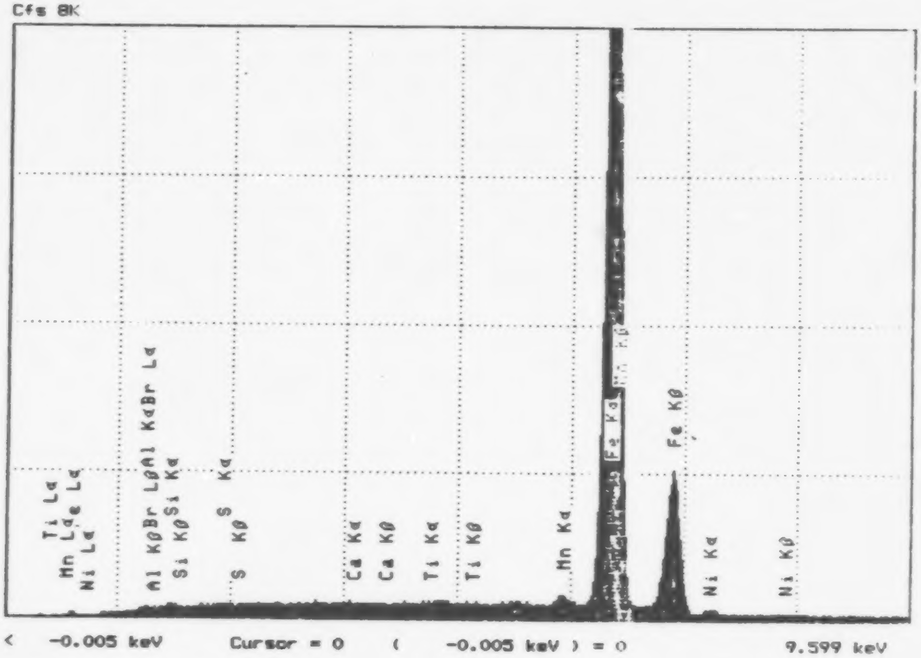

(a) Surrounding matrix

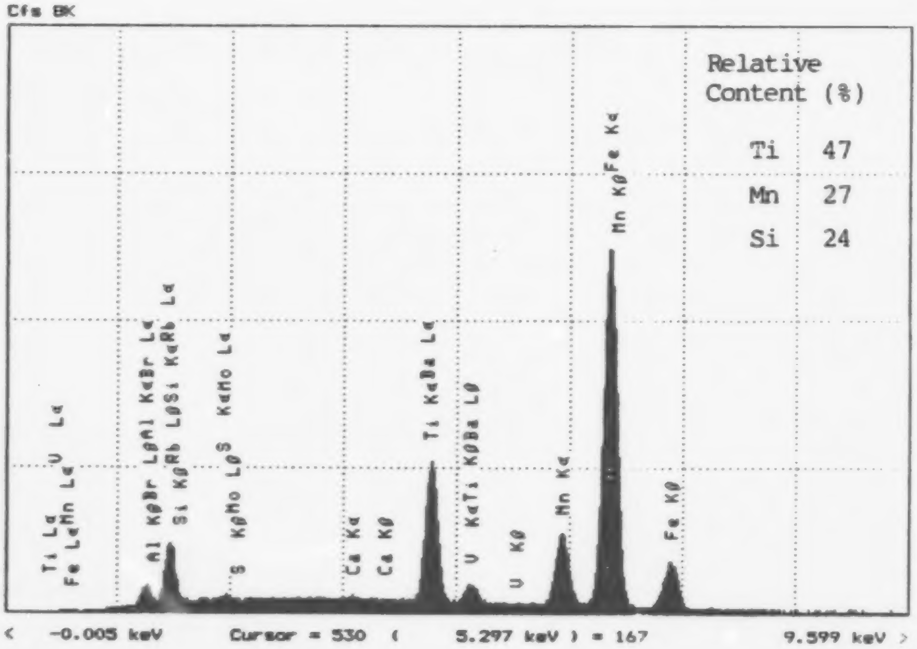

Relative Content (%)

Ti	47
Mn	27
Si	24

(b) Cleavage initiation site

Figure F18: Difference in EDX spectrums confirms the role of inclusion acting as cleavage initiation site (3F6)

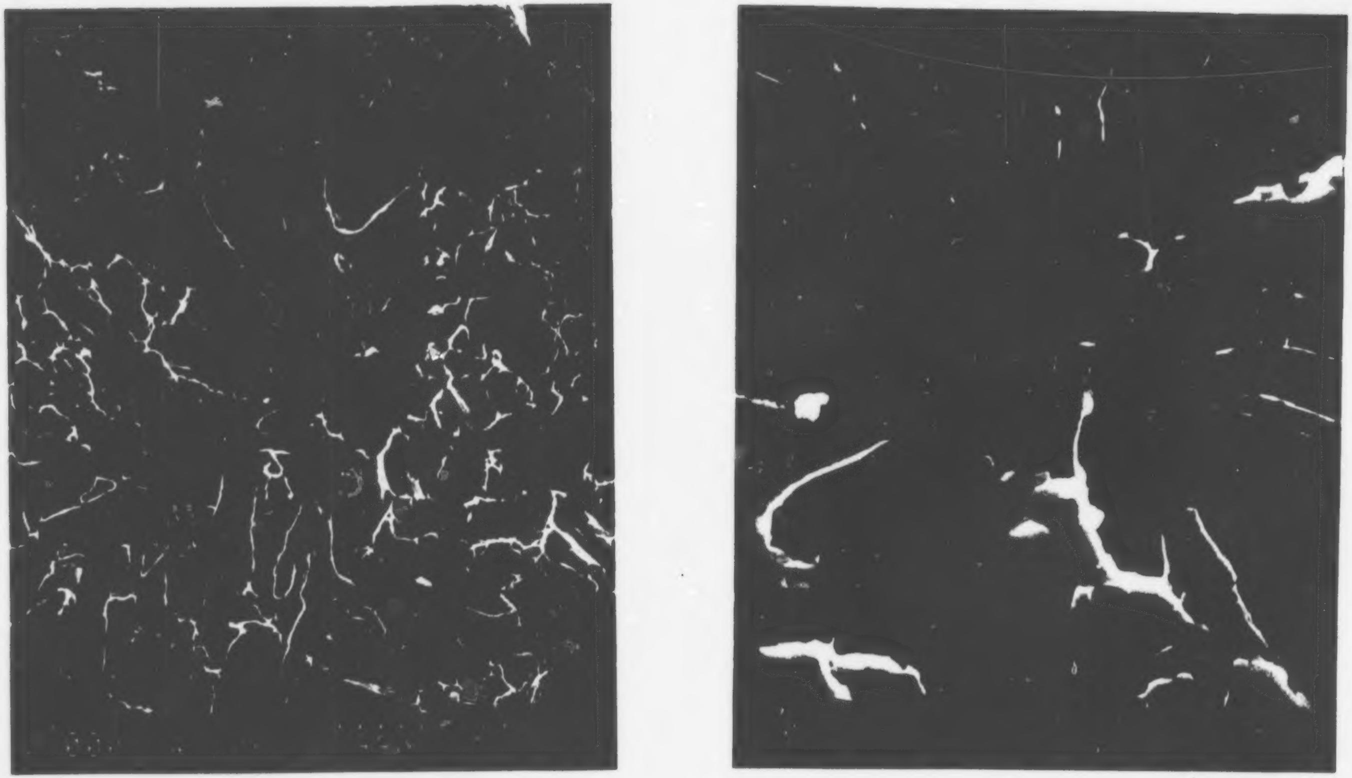

(a) (1000X, Neg. 834)

(b) (5000X, Neg. 833)

Figure F19: SEM micrographs show that cleavage river lines emanating from a large inclusion (>5 micron) found in as welded 3.0 kJ/mm 1G weld of Consumable A (1F4). Optical examination of microstructure near the cleavage initiation site is unsuccessful due to excessive polishing.

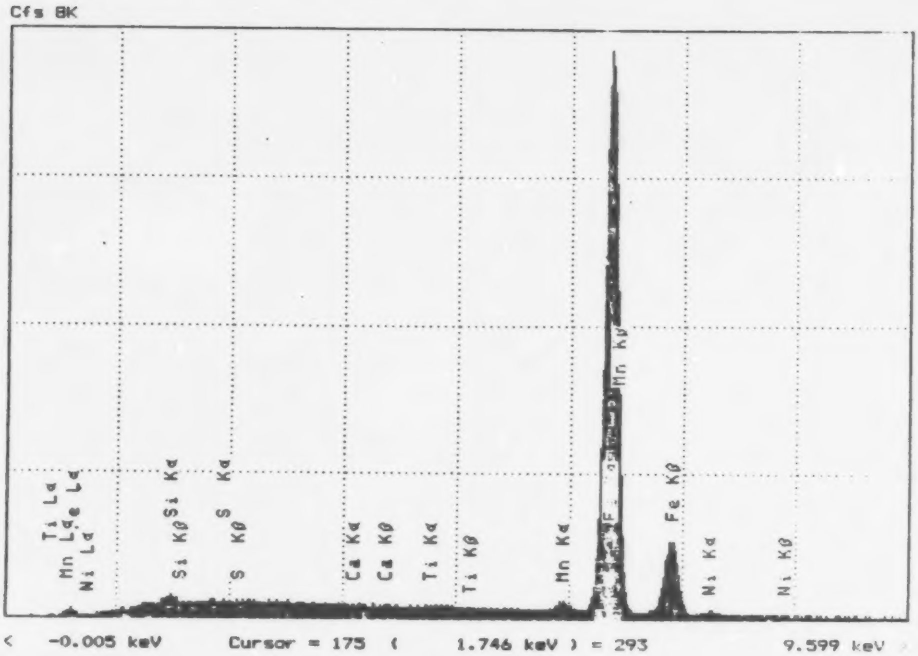

(a) Surrounding matrix

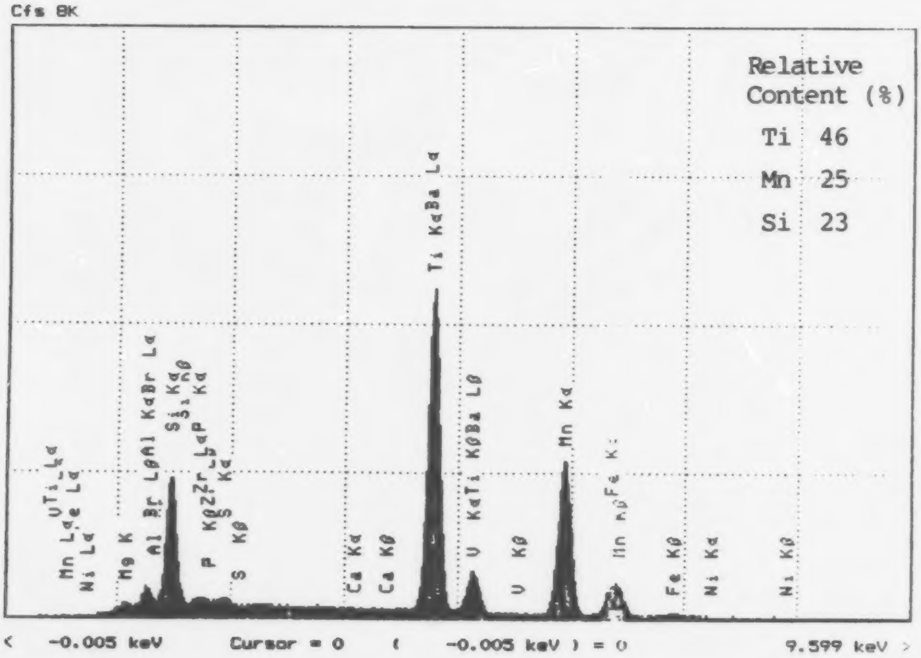

(b) Cleavage initiation site

Figure F20: The difference in EDX spectrums confirms the role of inclusion acting as cleavage initiation site (1F4)

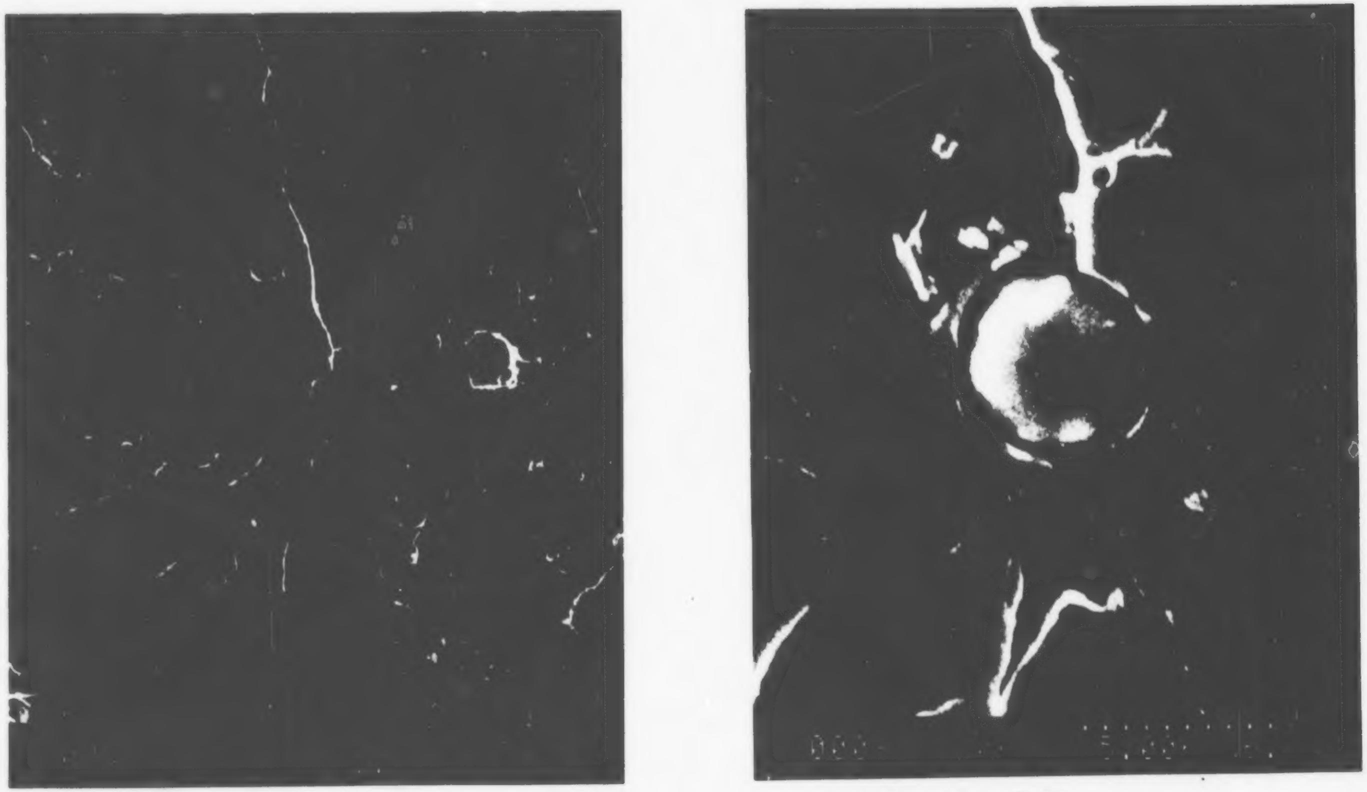

(a) (1000X, Neg. 834)

(b) (5000X, Neg. 833)

Figure F21: SEM micrographs show that cleavage river lines emanating from an inclusion (>1.2 micron) found in as welded 3.0 kJ/mm 1G weld of Consumable A (1F4). Optical examination of microstructure near the cleavage initiation site is unsuccessful due to excessive polishing.

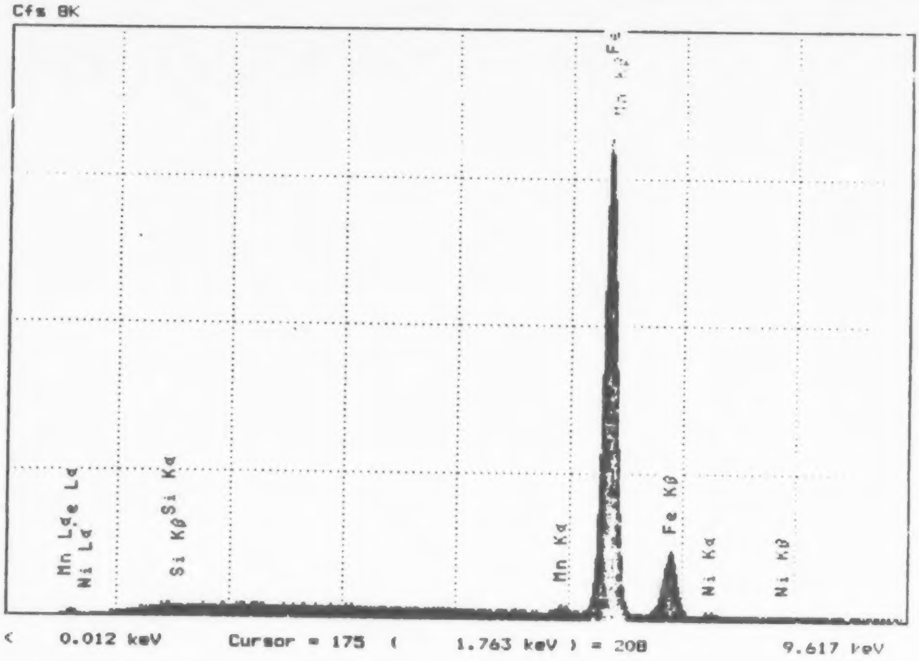

(a) Surrounding matrix

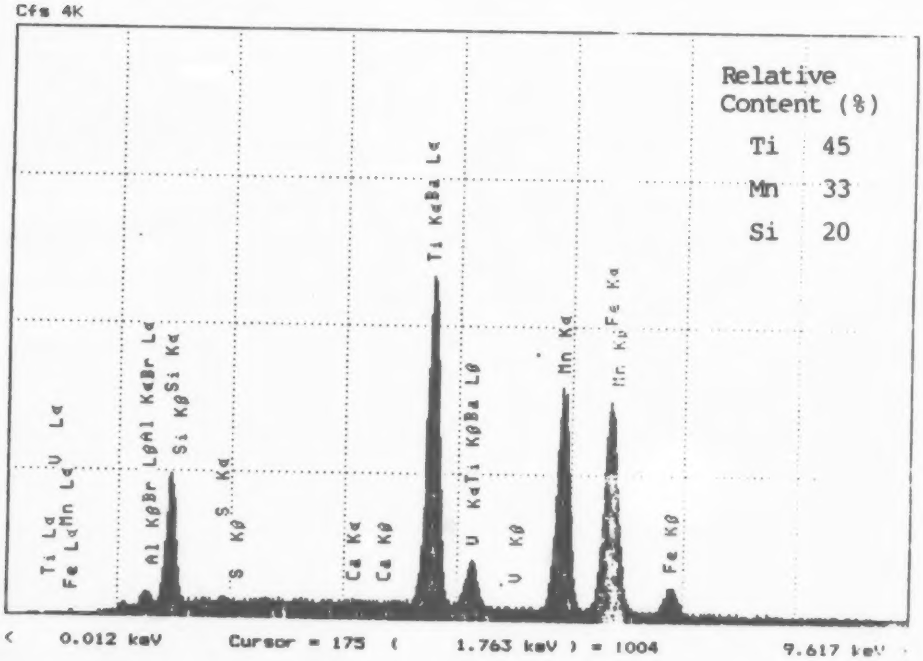

(b) Cleavage initiation site

Figure 22: The difference in EDX spectrums confirms the role of inclusions acting as cleavage initiation site (1F4)

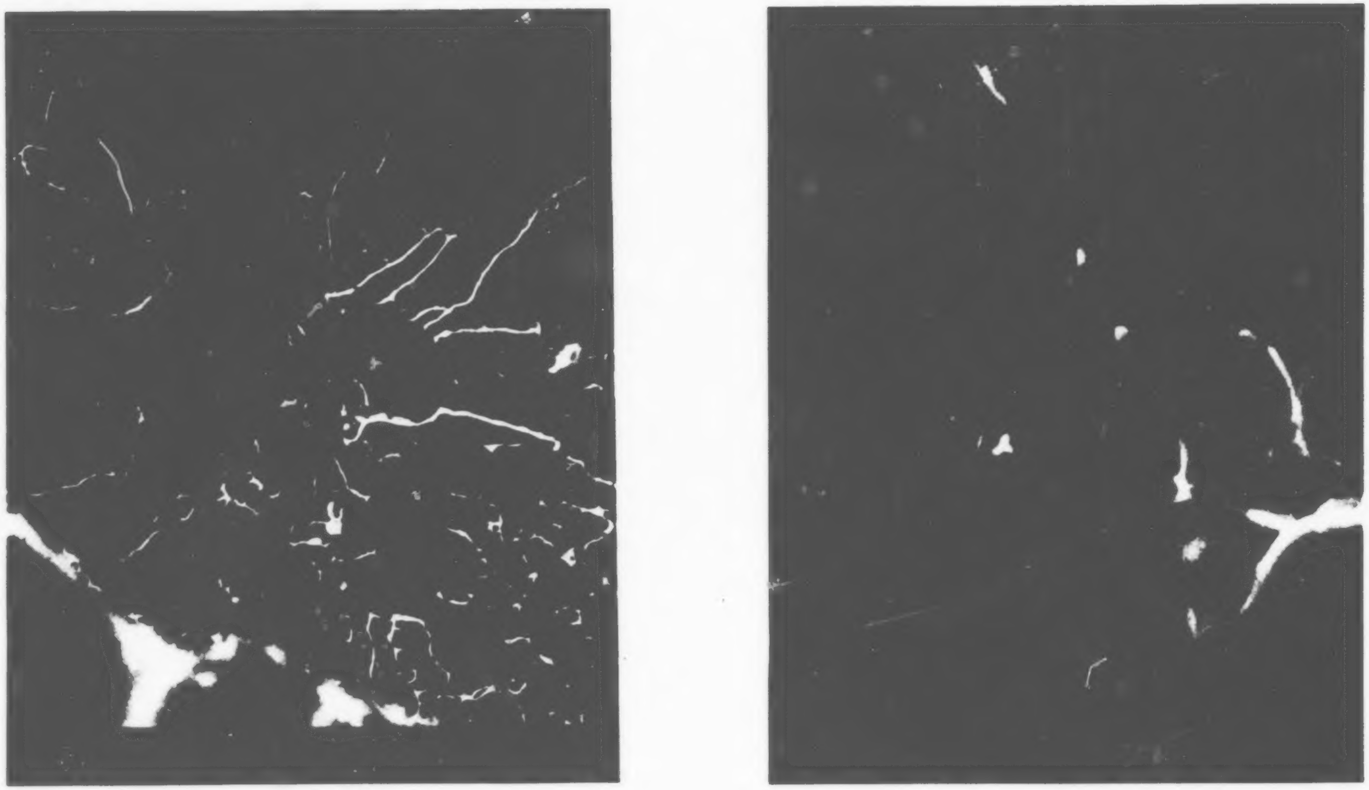

(a) (1000X, Neg. 827)

(b) (5000X, Neg. 826)

Figure F23: SEM micrographs show the cleavage river lines emanating from a cluster of inclusions found in as welded 3.0 kJ/mm 1G weld of Consumable A (1F6).

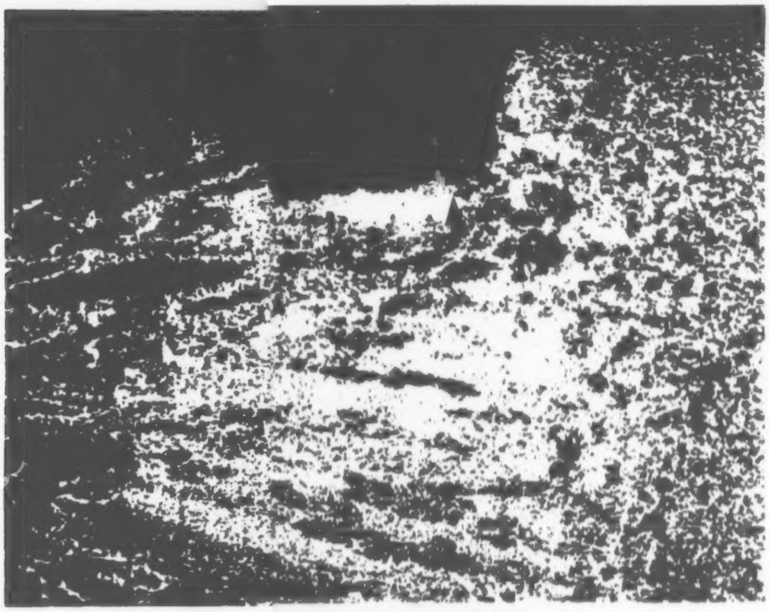

(a) (50X, Neg. 10725)

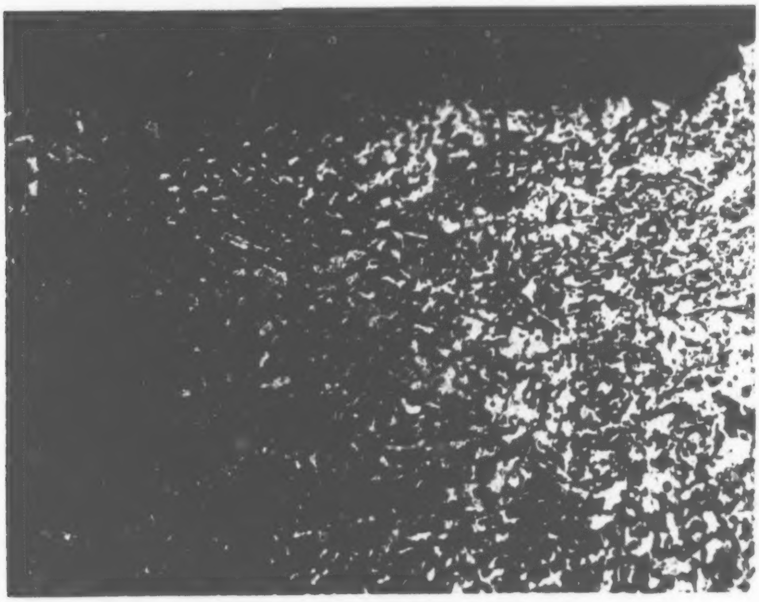

(b) (400X, Neg. 10724)

Figure F24: Optical micrograph indicates that the cleavage initiation site is located near the interface between columnar grains and reheated region.

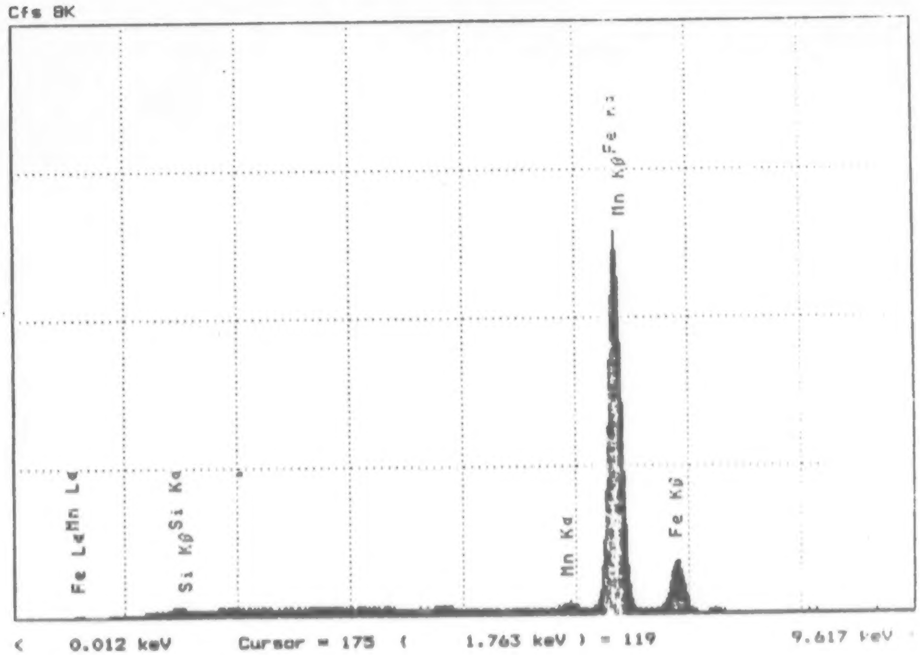

(a) Surrounding matrix

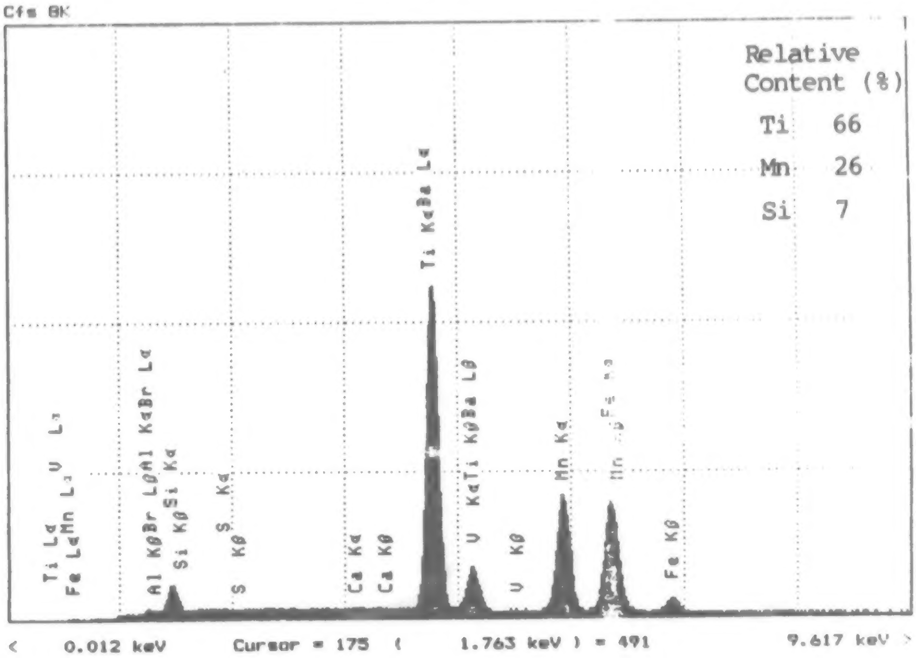

(b) Cleavage initiation site

Figure F25: The difference in EDX spectrums confirms the role of inclusions acting as cleavage initiation site (1F6)